NSRRC
Activity Report
2024

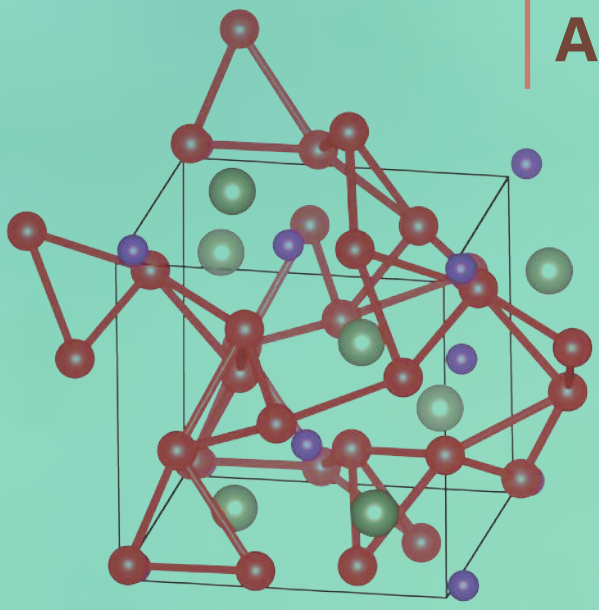

National
Synchrotron Radiation
Research Center

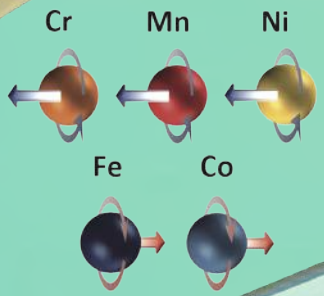

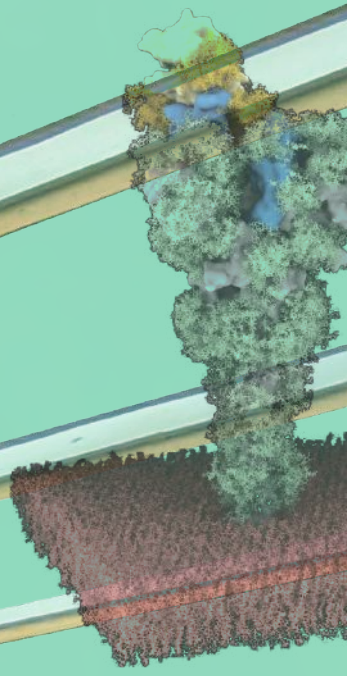

ISSN 1814-7879

About the National Synchrotron Radiation Research Center

Located in Hsinchu Science Park, the National Synchrotron Radiation Research Center (NSRRC) is a non-profit research organization, funded by Taiwan's National Science and Technology Council (NSTC). NSRRC currently operates two synchrotron light sources: the Taiwan Light Source (TLS) and the Taiwan Photon Source (TPS). As of December 2024, NSRRC provides users worldwide with 42 beamlines including two Taiwanese contract beamlines at SPring-8. The TLS, of beam energy 1.5 GeV and circumference 120 m, is the first third-generation synchrotron light source facility established in Asia and the third globally. It comprises 22 beamlines and over 50 experimental stations, and began user operation in 1993. The TPS, of circumference 518.4 m, is equipped with a low-emittance synchrotron storage ring and a booster synchrotron of energy 3 GeV. It has a capacity for about 40 beamlines, with 18 currently open to users. As one of the brightest mid-energy synchrotron light sources in the world, the TPS not only accelerates scientific advancements but also broadens the application of synchrotron radiation across diverse research fields. In 2024, NSRRC's experimental facilities served more than 2,900 users. For more information about the NSRRC, please visit www.nsrrc.org.tw.

NSRRC Activity Report 2024

Table of Contents

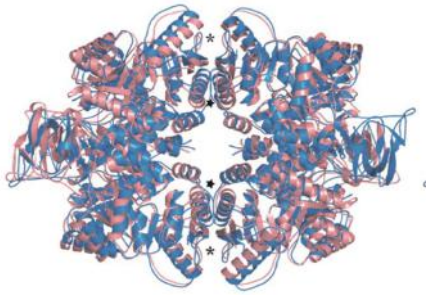

Research Highlights

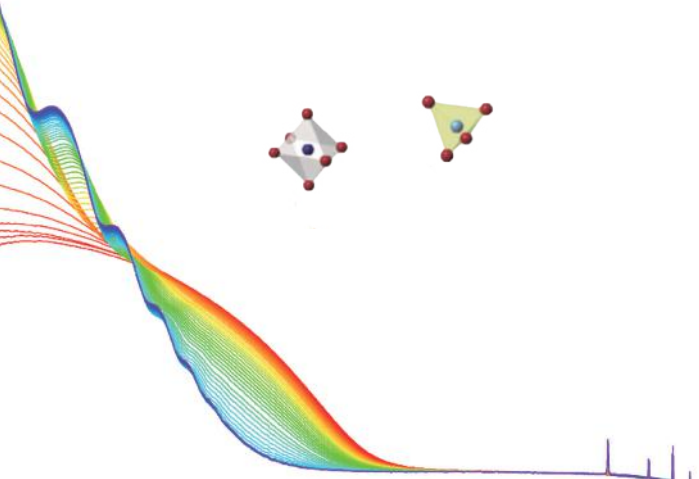

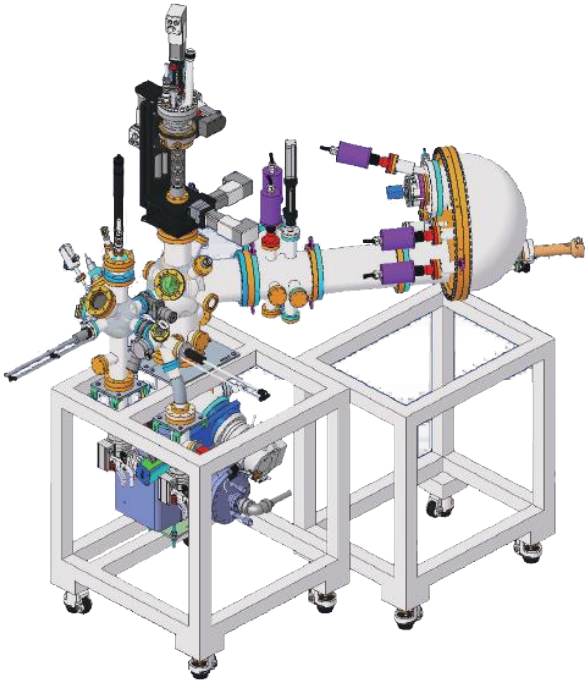

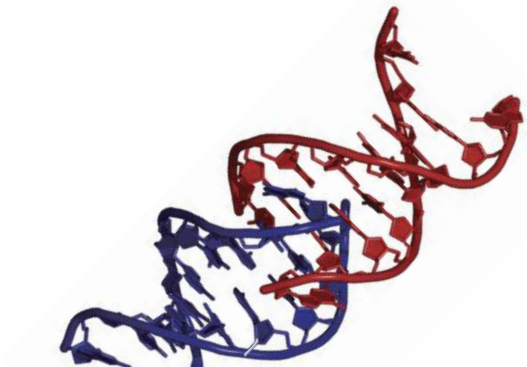

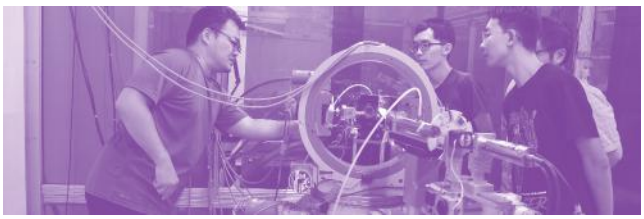

Message from the Director

Reflecting on 2024, I am filled with a sense of pride, gratitude, and motivation for all we've accomplished. As we continue to expand and enhance our research facilities, significant progress has been made, marking a pivotal moment in both our operations and the scientific achievements.

In terms of achievements, 2024 saw our user community reach a new milestone of 2,929 users, with 1,830 experimental runs and 13,861 user visits. These efforts have contributed to the publication of 619 SCI research papers, of which 58% have an impact factor higher than that of *Phys. Rev. Lett*., underscoring the critical role that NSRRC plays in advancing scientific discovery.

In 2024, a series of alarming earthquakes caused beam disruptions at the Taiwan Light Source (TLS) and the Taiwan Photon Source (TPS). After the magnitude 7.1 Hualien earthquake on April 3, our accelerators were restored to normal and stable operation within just a few hours. We are grateful for the support and concerns expressed by other synchrotron radiation facilities during this period. Although these events resulted in a slight decrease in annual availability—99.4% for the TLS and 97.7% for the TPS—the overall performance remains highly satisfactory.

Looking ahead, NSRRC is committed to expanding the capabilities of TPS. Currently, 18 beamlines are operational, with plans to increase to 26 by 2029. This expansion will include a dedicated beamline for industrial applications, fostering deeper collaboration with industry partners. We have also launched a call for letters of interest for new beamlines, and an Infrared Microspectroscopy Beamline has been selected. The addition of this new infrared beamline will further broaden the spectral range of the TPS and strengthen the research in the fields of biomedicine and semiconductors.

As these advancements unfold, we also take time to reflect on the legacy of the TLS. Inaugurated in 1993, TLS is not only an exemplification of Taiwan's ability to develop cutting-edge technologies in ultra-high vacuum technologies, precision magnets, and instrumentation, but also a cornerstone of scientific research in Asia. With over 225,000 user visits and more than 7,000 SCI publications, TLS's impact is undeniable. However, age-related issues are beginning to emerge, with key components experiencing wear and the discontinuation of their production. NSRRC foresaw this situation more than a decade ago, leading to the construction of the TPS, designed to replace and surpass the TLS, particularly in X-ray capabilities. The time for this transition is approaching.

Moreover, while NSRRC has earned international recognition for the high-quality user support, maintaining this expertise with limited manpower has become increasingly challenging. Following a thorough evaluation of economic considerations and user research needs, the Board of Trustees has resolved to operate TLS until the end of 2028, with partial operation possible in 2029 if needed. As TPS beamlines are phased in, TLS beamlines will gradually be scaled down, with all users ultimately transitioning to the TPS.

NSRRC is committed to supporting users throughout this transition. We will continue offering training courses and workshops to help users maximize the potential of the new TPS facilities and broaden their research opportunities. By embracing these changes, we will ensure our user community remains at the forefront of global scientific research.

Looking to the future, NSRRC will continue pushing the boundaries of scientific frontiers, advancing accelerator technologies, and driving innovation in experimental techniques. Our goal is not just to collect data but to transform the data into actionable insights that can help solve the world's fundamental challenges and support industries in overcoming critical issues.

Chia-Hung Hsu
Director

Preface

NSRRC is a research facility that provides powerful light sources and experimental capabilities not readily available in in-house laboratories to facilitate scientific advances and foster innovation. Thanks to the efforts of all users and our hard-working staff, 2024 continues to be a very productive year. To give an overview of the diverse activities that took place throughout this year, the editorial committee has carefully selected a range of research publications using the experimental facilities offered in Taiwan Photon Source (TPS), Taiwan Light Source (TLS), Taiwan Contract Beamlines at SPring-8, and the neutron facilities to illustrate NSRRC's contributions. One thing worth mentioning here is the growth of contributions from TPS. While such a trend is expected due to the construction of TPS phase-III beamlines entering its fourth year, and the continuation of TLS-to-TPS transition, I would like to express my sincere thanks to those efforts that are not necessarily reflected in terms of scientific publications.

In the Research Highlights of this volume, we feature 31 fascinating research topics across sections of Physics and Materials Science, Chemical Science, Soft Matter, Life Science, Energy Science, Environmental and Earth Sciences, and Neutron Science. In Facility Development and Status, we present four articles that explore the operational status and advancements in accelerator technology, including the optimization of the undulator system, performance of the energy-saving initiatives, and the innovative helium phase separator; additionally, two newly opened experimental facilities at the TPS—Soft X-ray Nanoscopy Beamline and Tender X-ray Spectroscopy Beamline—are introduced with detailed descriptions.

Facts and Figures provides a snapshot of NSRRC's operations, offering key statistics on administrative aspects, user engagement, beamline list, major events, and outreach activities. The Appendix includes lists of NSRRC publications resulting from the use of NSRRC beamlines, or related to instrumentation, accelerator facility, and neutron project, as well as student dissertations and theses, further highlighting NSRRC's impact in the science community.

One goal the editorial committee hopes to achieve is to channel research happening at NSRRC to a broader readership. This task is a challenge itself. Enjoy reading.

Der-Hsin Wei
Deputy Director

Research Highlights

Physics and Materials Science

This year has seen groundbreaking research in physics and materials science, leading to advancements in magnetism, quantum materials, high-entropy oxides, and phosphors. These discoveries drive innovations in spintronics, superconducting qubits, and next-generation electronics. One study explores circular dichroism in Ni_3TeO_6, an observed giant X-ray natural circular dichroism effect linked to parity-time symmetry breaking and Berry curvature, revealing the characteristic of altermagnetism and evidence for coupling between spin and chirality. Another study solves a puzzle in ferrimagnetic alloys, demonstrating how Mn-moment switching and Fe-moment increase influence Curie temperature in $Gd_6(Mn_{1-x}Fex)_{23}$. In 2D quantum materials, researchers highlight the potential of ultrathin β-Sn as a 2D topological nodal line semimetal, advancing quantum computing. High-entropy spinel oxide (Fe, Co, Ni, Cr, Mn)$_3O_4$ films exhibit strain-induced crystalline magnetic anisotropy due to Mn 3d orbital changes. Rare-earth phosphor research reveals stable Eu-doped $BaAl_2O_4$ despite non-uniform doping, enhancing LED technology. Lastly, nanometer-thick aluminum films grown *via* molecular beam epitaxy with an Al_2O_3 capping layer demonstrate high crystallinity and stable superconducting properties, which are essential for quantum circuits. These studies exemplify cutting-edge research and shape future technological advancements. (by Cheng-Maw Cheng)

Discovery of Giant X-ray Natural Circular Dichroism in an Antiferromagnet with Time-Reversal Symmetry

A structurally chiral, polar, and collinear antiferromagnet with effective time-reversal symmetry and no net spin moments is shown to exhibit a giant X-ray natural circular dichroism.

Circular dichroism is the difference in the absorption of right- and left-handed circularly polarized (RCP and LCP, respectively) light. It is a valuable spectroscopic tool used for studying the magnetic properties and structural chirality of molecules, proteins, and solids. For example, a typical ferromagnet with a net magnetic moment represents a broken time-reversal symmetry state and shows an X-ray magnetic circular dichroism (XMCD) signal that provides the spin- and orbital-magnetic moments of constituent atoms. Although an antiferromagnet (AFM) is not expected to show an XMCD signal as it does not have a net magnetic moment, some studies have shown that an XMCD signal can be observed in AFM materials with non-collinear or chiral spin structures. More recently, the so-called "altermagnets" with no net spin moments have also shown XMCD, which were understood as originating from broken time-reversal symmetry. In contrast, AFM materials with conserved time-reversal symmetry but broken space inversion symmetry can exhibit X-ray natural circular dichroism (XNCD) without an applied magnetic field.[1,2]

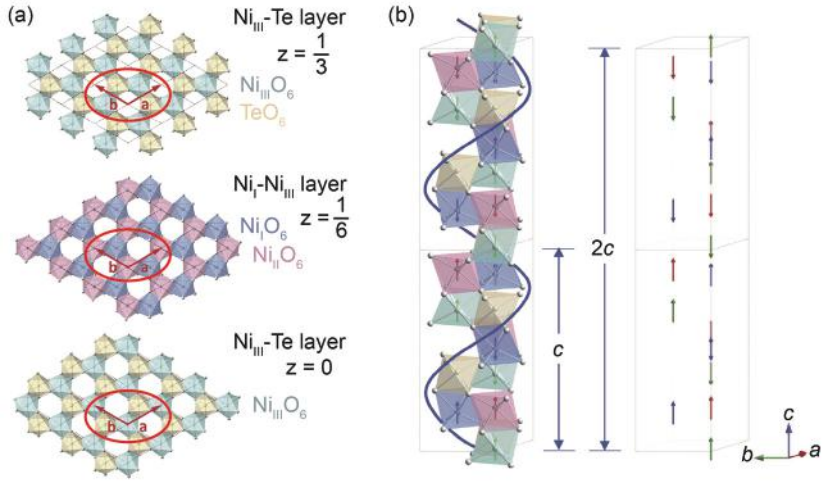

Fig. 1: Crystal and spin structures of Ni_3TeO_6. (a) The crystal structure of Ni_3TeO_6 consists of ferromagnetically coupled Ni_IO_6 and $Ni_{II}O_6$ honeycomb layers alternating with the $Ni_{III}O_6$ and TeO_6 honeycomb layers. (a) and (b) are in-plane unit-cell vectors. The structural unit cell comprises six honeycomb layers stacked along the *c*-axis. (b) Chiral crystal structure of Ni_3TeO_6. The blue helix represents the handedness of the crystal chirality. The spins represented by arrows are aligned along the *c*-axis, showing the collinear antiferromagnetic structure of Ni_3TeO_6.[5] The magnetic unit cell consists of two structural unit cells, that is, 12 honeycomb layers stacking along the *c*-direction. The structural unit-cell length *c* and the magnetic unit-cell length 2*c* are indicated by double-headed arrows. [Reproduced from Ref. 3]

It is known that XNCD originates from the interference between electric-dipole (E1) and electric-quadrupole (E2) transitions.[2] However, its magnitude is orders of magnitude lower than those of typical XMCD signals. In a path-finding study led by Di-Jing Huang (NSRRC) and conducted in collaboration with scientists from Taiwan, the United States, Japan, and Germany, researchers have now discovered a giant XNCD in X-ray absorption spectroscopy (XAS) of a collinear AFM Ni_3TeO_6 that exhibits time-reversal symmetry. The authors used spatially resolved (~1 μm) XAS to study Ni_3TeO_6 that possesses a polar and chiral crystal structure with a collinear magnetic structure.[3] The results also showed that the observed giant XNCD changes its sign between domains of opposite crystal chirality with the magnetic structure keeping time-reversal symmetry.

Nickel tellurite, Ni_3TeO_6, crystallizes in a modified corundum structure and is known to exhibit a large optical rotation associated with chiral and polar domains.[4] The three Ni sites and one Te site in the structure form two kinds of honeycomb layers consisting of edge-shared NiO_6 and TeO_6 octahedra stacked along the *c*-axis, generating the polar crystal structure. The ferromagnetically coupled Ni_IO_6 and $Ni_{II}O_6$ honeycomb layer alternates with the $Ni_{III}O_6$ and TeO_6 honeycomb layer, as shown in **Fig. 1(a)**.

Ni_3TeO_6 shows an AFM transition with a Néel temperature of $T_N = 62$ K, from a paramagnetic state to a commensurate collinear AFM state with Ising anisotropy,[5] as schematically shown in **Fig. 1(b)**. This is confirmed by momentum scans of resonant X-ray magnetic scattering (RXMS) with an incident X-ray beam spot size of ~1 μm, measured as a function of temperature (**Figs. 2(a) and 2(b)**, see next page) at positions A and B, respectively, as shown in **Fig. 3(a)** (see next page). The results show that the intensity of the (0, 0, 1.5) peak appears below T_N and steadily increases with decreasing temperature. These results of temperature-dependent RXMS at the Ni L_3-edge XAS (**Figs. 2(a)–2(c)**)

and magnetic susceptibility measurements (**Fig. 2(d)**) are consistent with the collinear AFM structure of Ni_3TeO_6. The observed AFM transition is marked by a sharp cusp in the parallel-to-*c*-axis component χ|| of the magnetic susceptibility. These results also agree with the results of temperature-dependent X-ray linear dichroism (XLD) measured at **TPS 41A** and plotted in **Fig. 2(c)**.

Ni_3TeO_6 is actually considered to be a unique material, as it exhibits both chirality and polarity. However, because of its polar *R*3 structure, polarity aligns with chirality, and this makes it impossible to observe different polarities within the same chiral domain concurrently. The authors then circumvented this difficulty by carrying out spatially resolved temperature-dependent XAS and XNCD mapping over an area of 90 × 90 μm² with a resolution of ~1 μm in order to characterize the domain structure, as shown in **Figs. 3(a) and 3(c)**. The authors could distinguish two types of chiral domains by performing Ni L_3-edge XAS measurements at **TPS 41A** using circularly polarized X-rays.

Most importantly, the authors observed a relatively large XNCD for two distinct types of domains for temperatures below ≈ T_N, as shown in **Fig. 3(b)**, despite the absence of both an external magnetic field and remanent magnetization. The measured dichroic spectra, *i.e.*, the RCP – LCP difference spectra, show a maximum magnitude of XNCD of approximately 20% of the Ni L_3-edge XAS peak, much larger than the previously reported one of 2%,[6] thus indicating a giant XNCD in Ni_3TeO_6. The observed giant XNCD exhibits a non-linear dependence on the X-ray intensity, showing a positive peak at ω_{RT} + 0.3 eV at position A and a negative peak at ω_{RT} + 0.7 eV at position B. The dichroic maps shown in **Fig. 3(c)** demonstrate a sign change between the domains of opposite chirality. The color contrast between the domains increases with temperature, and it becomes strongest around T_N and invisibly weak at room temperature. The XNCD intensities at A and B plotted as functions of temperature in **Fig. 3(d)** show a clear enhancement below ≈ T_N.

The magnitude of the observed XNCD in Ni_3TeO_6 is comparable to the XMCD of 3*d* transition metals but is much larger than the usual XNCD resulting from the E1–E2 interference. This is indicative of a new mechanism going beyond the E1–E2 interference, likely arising from a uniform "effective magnetic field" active in Ni_3TeO_6. From a symmetry perspective, moving X-ray photons in a chiral crystal structure can induce an effective magnetic field along their propagation direction. The authors propose a theoretical model to explain the giant XNCD, which is attributed to a broken *PT* symmetry, where *P* is the parity and *T* is time reversal. In particular, the authors could show from their model that the XNCD cross-section of L-edge XAS is proportional to the integration of Berry curvature over momentum at a fixed energy.[3] In accordance with the XMCD sum rule, the energy integration of XNCD is proportional to the integration of Berry curvature across the entire momentum space, leading to an orbital moment. Thus, the chiral structure of Ni_3TeO_6 ensures a non-zero average orbital magnetization responsible for the "effective magnetic field" and the giant XNCD. Further, the observed XNCD shows a strong temperature dependency, just like the XMCD from a ferromagnet across its magnetic phase transition, revealing the characteristic of altermagnetism and evidence for coupling between spin and chirality. All these properties of Ni_3TeO_6 establish the first example of a new class of magnetic materials that can exhibit circular dichroism with time-reversal symmetry. (Reported by Ashish Chainani, Jun Okamoto and Di-Jing Huang)

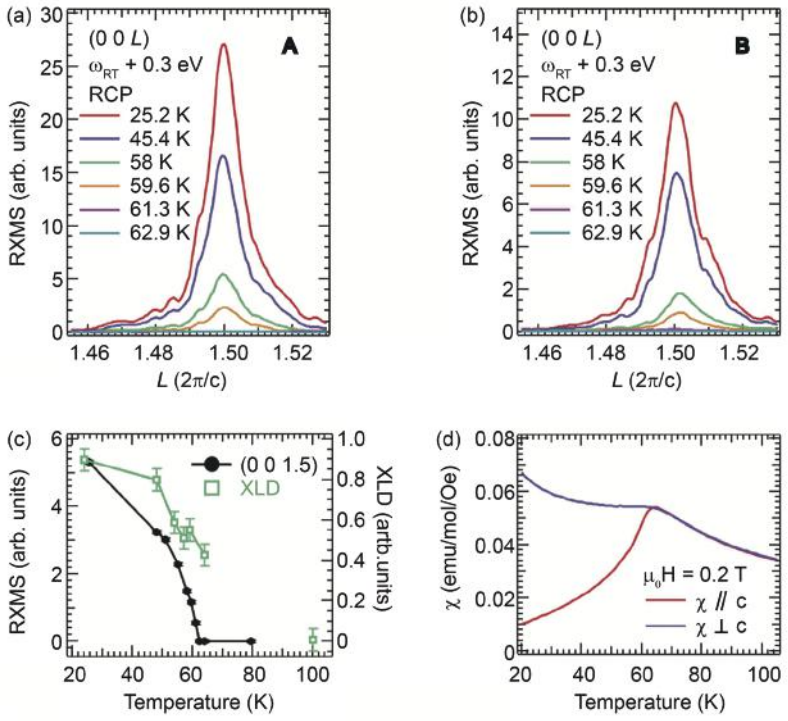

Fig. 2: Magnetic transition of Ni_3TeO_6. (a,b) RXMS intensities at $q^{\rightarrow}$= (00*L*) in the reciprocal space scanned along *L* with RCP at the photon energy of ω_{RT}+0.3 eV as a function of temperature measured at positions A and B, respectively. Here, ω_{RT} is the Ni L_3-edge XAS peak energy, and A and B belong to opposite chiral domains shown in Fig. 3(a). (c) Temperature dependence of XLD and the (0, 0, 1.5) peak of RXMS at the Ni L_3 edge plotted across the Néel transition. (d) DC magnetic susceptibility for magnetic field parallel and perpendicular to the *c* axis taken with μ_0H = 0.2 T. [Reproduced from Ref. 3]

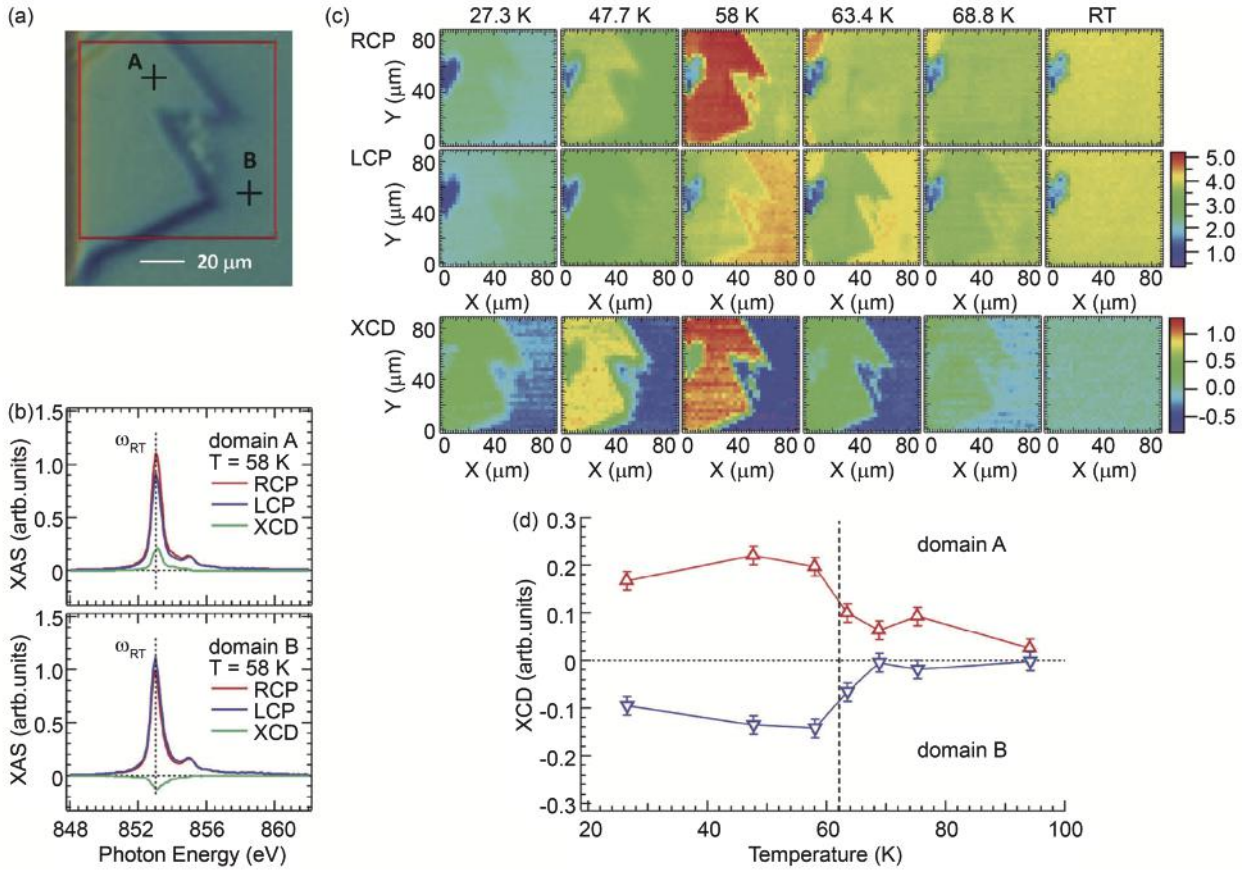

Fig. 3: Temperature-dependent XNCD of Ni_3TeO_6. (a) Image of the Ni_3TeO_6 sample recorded with a polarized-light microscope. Horizontal and vertical edges are parallel to the [0 1 $\bar{1}$ 0] and [2 $\bar{1}$ $\bar{1}$ 0] axes, respectively. The red-square box shows a 90 × 90 μm² area on which the XAS and XCD images were taken. Positions A and B are in two different domains of opposite crystal chirality. (b) XAS spectra taken at positions A and B with RCP and LCP and difference spectra, *i.e.*, X-ray circular dichroism spectra, at 58 K measured by the fluorescence-yield method. Circular dichroism signals at A and B are positive and negative, respectively. (c) XAS images of Ni_3TeO_6 in the 90 × 90 μm² area measured at a photon energy of ω_{RT} + 0.7 eV (photon energy of ω_{RT} at RT) with RCP (top) and LCP (middle) and RCP − LCP difference images (bottom) at various temperatures. (d) XCD intensity normalized to the L_3 XAS peak intensity, defined by 2(RCP − LCP)/(RCP + LCP), at positions A and B plotted against temperature. The dichroism changes its sign between A and B. [Reproduced from Ref. 3]

This report features the work of Jun Okamoto, Di-Jing Huang and their collaborators published in Adv. Mater. ***36****, 2309172 (2024).*

TPS 41A Soft X-ray Scattering

- XAS, XNCD, RXMS
- X-ray Natural Circular Dichroism, Antiferromagnetic Transition, Materials Science, Condensed-matter Physics

References

1. L. Alagna, T. Prosperi, S. Turchini, J. Goulon, A. Rogalev, C. Goulon-Ginet, C. R. Natoli, R. D. Peacock, B. Stewart, Phys. Rev. Lett. **80**, 4799 (1998).
2. J. Goulon, A. Rogalev, F. Wilhelm, N. Jaouen, C. Goulon-Ginet, C. Brouder, J. Phys.: Condens. Matter **15**, S633 (2003).
3. J. Okamoto, R.-P. Wang, Y.-Y. Chu, H.-W. Shiu, A. Singh, H.-Y. Huang, C.-Y. Mou, S. Teh, H.-T. Jeng, K. Du, X. Xu, S.-W. Cheong, C.-H. Du, C.-T. Chen, A. Fujimori, D.-J. Huang, Adv. Mater. **36**, 2309172 (2024).
4. X. Wang, F.-T. Huang, J. Yang, Y. S. Oh, S.-W. Cheong, APL Mater. **3**, 076105 (2015).
5. I. Živković, K. Prša, O. Zaharko, H. Berger, J. Phys.: Condens. Matter **22**, 056002 (2010).
6. A. Ghosh, K.-H. Chen, X.-S. Qiu, S.-H.Hsieh, Y.-C. Shao, C.-H. Du, H.-T. Wang, Y.-Y. Chin, J.-W. Choiu, S. C. Ray, H.-M. Tsai, C.-W. Pao, H.-J. Lin, J.-F. Lee, R. Sankar, F.-C. Chou, W.-F. Pong, Sci. Rep. **8**, 15779 (2018).

Element-Specific Curie Temperatures and Heisenberg Criticality in Ferrimagnetic $Gd_6(Mn_{1-x}Fe_x)_{23}$

Temperature-dependent X-ray magnetic circular dichroism solves a long-standing puzzle of non-monotonic Curie temperatures coupled to monotonic composition-controlled magnetization.

Many rare-earth (R)–transition-metal (M, M') ternary alloys of the type $R_a(M_{1-x}M'_x)_b$ exhibit non-monotonic ferrimagnetic Curie temperatures (T_C) coupled to monotonic composition-controlled magnetization. Its origin has remained an important long-standing puzzle in the absence of studies investigating their temperature (T)-dependent element-specific magnetism. To answer this question, a team of scientists from the NSRRC, Taiwan, and Institut Jean Lamour, France, conducted a systematic study of the ferrimagnetic series $Gd_6(Mn_{1-x}Fe_x)_{23}$, x = 0.0–0.75. The researchers used the experimental techniques of X-ray absorption spectroscopy (XAS), X-ray magnetic circular dichroism (XMCD), and hard X-ray photoemission spectroscopy (HAXPES) in combination with density functional theory calculations, including on-site Coulomb energy (DFT+U), to determine the answer. For the first time, the researchers successfully applied the Kouvel–Fisher analysis method to element-specific T-dependent XMCD data. The study unambiguously revealed distinct sublattice T_C values and 3-D Heisenberg critical behavior of the ferrimagnetic transition in $Gd_6(Mn_{1-x}Fe_x)_{23}$, as well as clarified the origin of non-monotonic ferrimagnetic T_C coupled to monotonic composition-controlled magnetization.[1]

As shown in **Figs. 1(a)–1(f)**, the researchers performed XAS–XMCD measurements at the Dragon beamline **TLS 11A1,** with an applied field of ±1 T for the series $Gd_6(Mn_{1-x}Fe_x)_{23}$, x = 0.0–0.75 after characterization of the crystal structure and ferrimagnetic T_C values obtained from magnetization measurements. **Figures 1(a)–1(c)** show representative XAS spectra for (a) Gd M-edge and (b) Mn L-edge of the parent compound, as well as (c) the Fe L-edge of $Gd_6(Mn_{0.5}Fe_{0.5})_{23}$ measured at T = 29 K. From such measurements of compounds with x = 0.0–0.75, the researchers obtained XMCD spectra, as shown for all x in panels (d) to (f). While the Gd M-edge XMCD spectra for all x indicate a total magnetic moment of ~7 μ_B, the Mn L-edge XMCD shows a small net magnetic moment (~0.4 μ_B), which switches from parallel to antiparallel with respect to the Gd magnetic moments and becomes ~0.05 μ_B on increasing x. By contrast, Fe L-edge XMCD shows that Fe magnetic moments are antiparallel with respect to the Gd magnetic moments for all x and increase systematically from ~0.4 μ_B (for x = 0.2) to 1.4 μ_B (for x = 0.75).

Next, the researchers performed HAXPES measurements at **SP 12U1**, one of the Taiwan-contract Beamlines in SPring-8, for the series and showed that the Gd 3*d* core-level multiple spectra can be analyzed using an intermediate coupling scheme.[2] By contrast, the Fe 2*p* core-level spectra showed single peaks attributed to typical metals, whereas the Mn 2*p* spectra showed a main peak and shoulder, which could be assigned to Mn up-spin and down-spin sites.

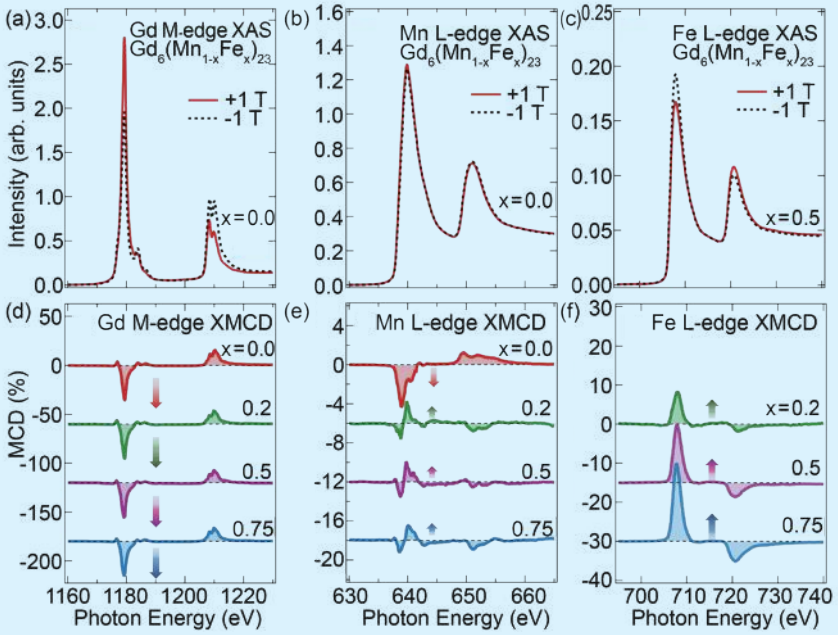

Fig. 1: Representative XAS spectra of $Gd_6(Mn_{1-x}Fe_x)_{23}$ with an applied field of ±1 T for (a) Gd M-edge (x = 0), (b) Mn L-edge (x = 0), and (c) Fe L-edge (x = 0.5) measured at T = 29 K, from which we obtained the XMCD spectra, as shown for all x in panels (d)–(f). XAS–XMCD spectra of (d) Gd M-edge, (e) Mn L-edge, and (f) Fe L-edge of the series $Gd_6(Mn_{1-x}Fe_x)_{23}$ (x = 0, 0.2, 0.5, and 0.75) measured at T = 29 K. Arrows in (d)–(f) show the relative magnitude and orientation of the spins. [Reproduced from Ref. 1]

This observation is consistent with the crystal and magnetic structures of the parent Gd_6Mn_{23}, as obtained from neutron diffraction studies,[3] which indicated two types of Mn "b, d" up-spin sites and two types of Mn "f_1, f_2" down-spin sites, as shown in **Fig. 2(a)**. The Fe and Mn 3*s* core level HAXPES spectra showed exchange splitting, and a Van–Vleck analysis result indicated magnetic moments that are consistent with neutron diffraction results.[2]

Next, the researchers conducted bulk-sensitive HAXPES valence band spectroscopy and compared it with DFT+*U* electronic structure calculations. **Figure 2(b)** shows the comparison between the experimental valence band spectrum and the calculated partial density of states (P-DOS) for Gd 4*f*, Gd 5*d*, Mn 4*s*, and Mn 3*d* and the total DOS for Gd_6Mn_{23} obtained from DFT+*U* calculations with on-site Coulomb energies U_{Mn}^{DFT} = 0.75 eV and U_{Gd}^{DFT} = 6.5 eV. The optimal values of U_{Mn}^{DFT} = 0.75 eV and U_{Gd}^{DFT} = 6.5 eV also yielded magnetic moment values consistent with neutron diffraction results.[3] The crucial role of on-site Coulomb energies in the valence band states of transition metals was further clarified by 2*p*–3*d* resonant-PES.[4] **Figure 2(c)** shows a plot of the valence band P-DOS for Gd 4*f*, Gd 5*d*, Fe 4*s*, and Fe 3*d* and the total DOS for Gd_6Fe_{23} obtained from the DFT+*U* calculations. To compare with experimental data for x = 0.75, the calculated total DOS for $Gd_6(Mn_{0.25}Fe_{0.75})_{23}$ was approximated as a sum of 25% Gd_6Mn_{23} and 75% Gd_6Fe_{23} total DOS, plotted together with the bulk-sensitive HAXPES valence band spectrum in **Fig. 2(d)**. The results indicated a fair match between experimental and calculated results.[1]

The researchers conducted *T*-dependent XMCD and bulk magnetization experiments to determine element-specific T_C values and the nature of the ferrimagnetic transition in $Gd_6(Mn_{1-x}Fe_x)_{23}$.

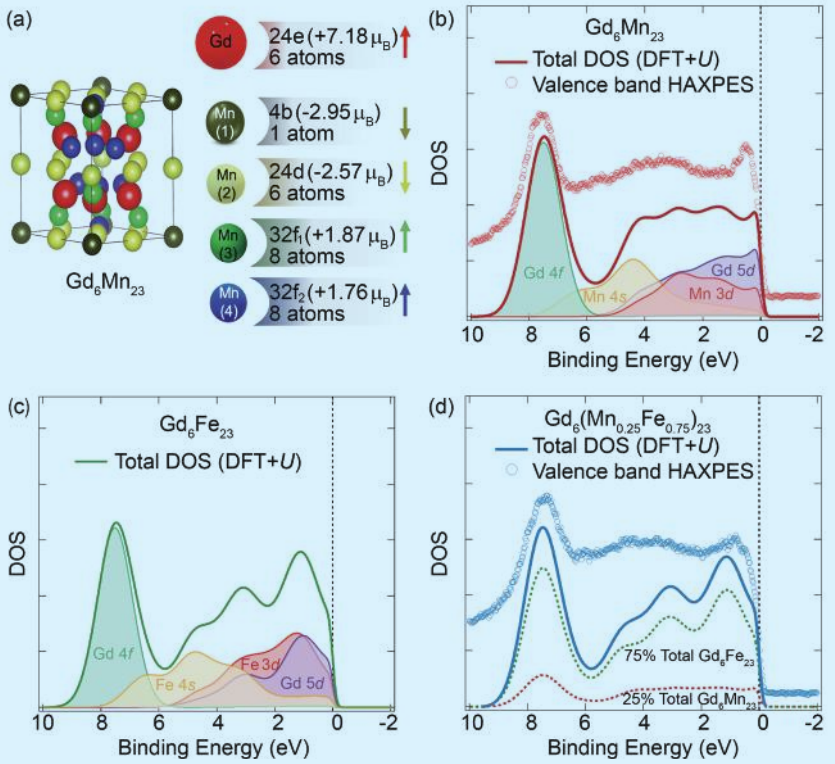

Fig. 2: Crytal structure schematic and comparison of HAXPES valence band with DOS calculations. (a) The crystal structure of Gd_6Mn_{23}, indicating the magnetic moments from the band structure calculations of the Gd site, Mn "b, d" sites, and Mn "f_1, f_2" sites. (b) The P-DOS for Gd 4*f*, Gd 5*d*, Mn 4*s*, and Mn 3*d* and the total DOS for Gd_6Mn_{23} obtained from DFT+*U* calculations with U_{Mn}^{DFT} = 0.75 eV and U_{Gd}^{DFT} = 6.5 eV compared with bulk-sensitive HAXPES valence band spectrum. (c) The valence band P-DOS for Gd 4*f*, Gd 5*d*, Fe 4*s*, and Fe 3*d* and the total DOS for Gd_6Fe_{23} obtained from DFT+*U* calculations. (d) The valence band total DOS for $Gd_6(Mn_{0.25}Fe_{0.75})_{23}$ is approximated by an additive mixture of 25% Gd_6Mn_{23} and 75% Gd_6Fe_{23} total DOS, and it is plotted together with the bulk-sensitive HAXPES valence band spectrum. [Reproduced from Ref. 1]

Figure 3 (see next page) shows the *T*-dependent Gd/Fe XMCD results fitted to a power law for all x. The data revealed that Gd T_C = 273.5 K for x = 0.0 and 0.75 and that it was smaller than the bulk T_C values (489 K for x = 0; 306 K for x = 0.75). In contrast, it decreased to the bulk T_C values of 172 K (for x = 0.2) and 135 K (for x = 0.5) when Gd T_C decreased to below 273.5 K. A scaling analysis (**Fig. 3(b)**) indicated a 3D Heisenberg-type transition for all x values. To confirm the critical behavior, a more rigorous Kouvel–Fisher analysis was performed for all x values, and the results are shown in the bottom row of **Fig. 3**. The *T*-dependent Mn L-edge XMCD could not be measured as it showed weak XMCD intensity. The results confirmed the 3-D Heisenberg critical behavior of the ferrimagnetic transition in $Gd_6(Mn_{1-x}Fe_x)_{23}$.[1]

Finally, a magnetic phase diagram (**Fig. 4**, see next page) based on element-specific T_C values with total magnetization from XMCD and total bulk magnetization measurements (M_{Tot}^{X} and M_{Tot}^{B}, respectively) showed three regions with (i) Mn-sublattice bulk-T_C > Gd-sublattice T_C, (ii) a reduced common-T_C for all sublattices, and (iii) Fe-sublattice bulk-T_C > Gd-sublattice T_C. The results thus revealed that the Mn-moment switching and gradual increase in Fe moment combined to cause non-monotonic T_C values coupled to monotonic magnetization. The study indicates the importance of element-specific T_C values for tuning magnetic properties in $R_a(M_{1-x}M'_x)_b$ ternary alloys. (Reported by Ashish Chainani)

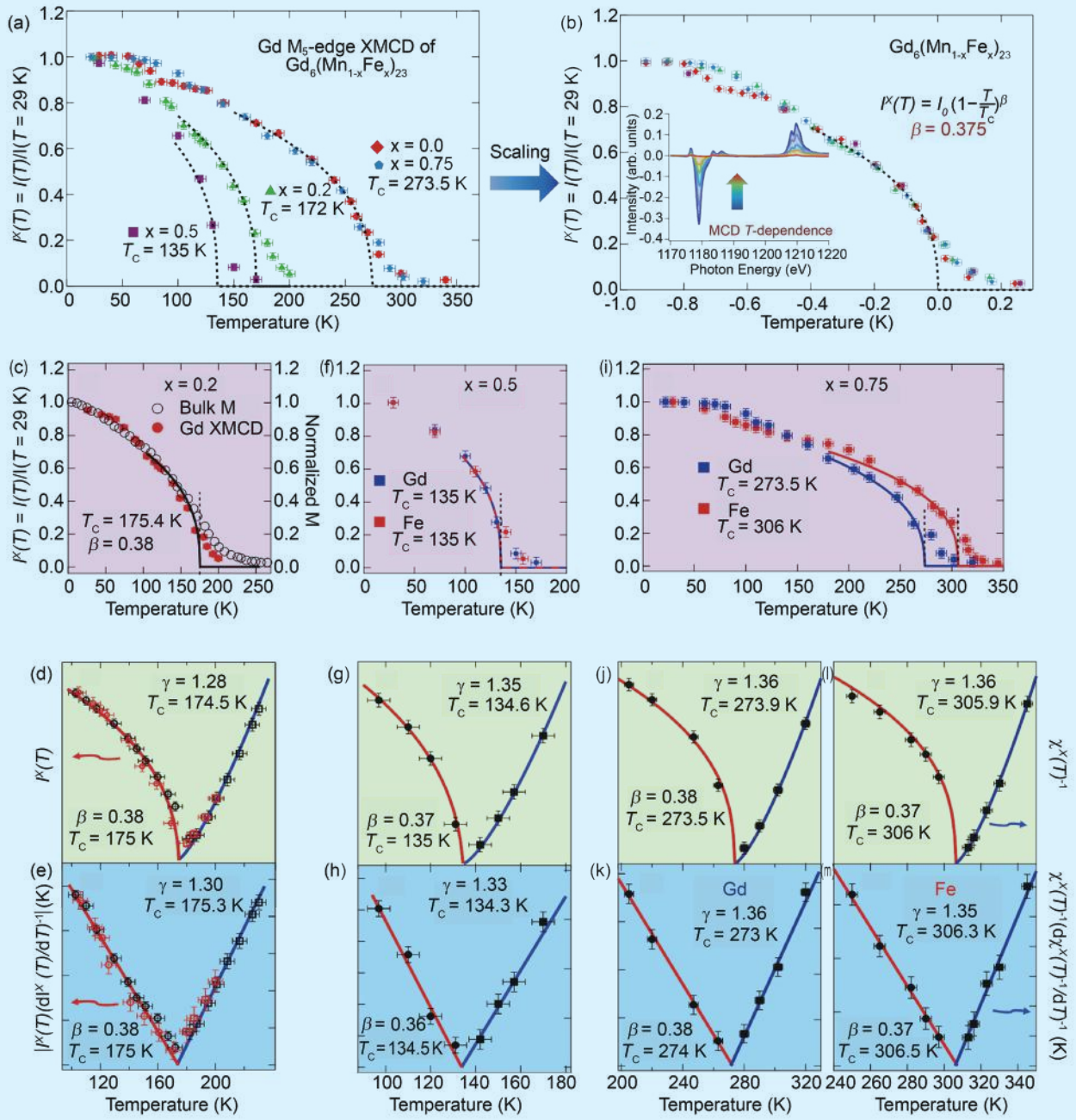

Fig. 3: Element-specific T_C values from power law analyses and Kouvel–Fisher analyses of XMCD. (a) T dependence of the Gd M_5-edge XMCD intensity for $Gd_6(Mn_{1-x}Fe_x)_{23}$, fitted by a power law exponent $\beta = 0.38 \pm 0.01$ (dashed black line). (b) Critical scaling behavior for the $Gd_6(Mn_{1-x}Fe_x)_{23}$ series. The inset shows T dependence of Gd M-edge XMCD intensity for $Gd_6(Mn_{0.25}Fe_{0.75})_{23}$. (c) T dependence of the Gd M_5-edge XMCD intensity and total bulk magnetization ($M^B_{Tot}(T)$) of $Gd_6(Mn_{0.8}Fe_{0.2})_{23}$ fitted by a power law with $\beta = 0.38 \pm 0.01$ (black line). (d) Power-law and (e) Kouvel–Fisher analysis fits for $M^B_{Tot}(T)$ (black empty circles). The Gd M_5-edge XMCD intensity $I^X(T)$ plotted together (red empty circles) also follows the Kouvel–Fisher analysis for $M^B_{Tot}(T)$ near T_C. (f) T dependence of the Gd M_5-edge (blue squares) and Fe L_3-edge (red squares) XMCD intensity for $Gd_6(Mn_{0.5}Fe_{0.5})_{23}$ fitted to a power law with $\beta = 0.37 \pm 0.01$ (dashed blue-red line). (g) Power-law and (h) Kouvel–Fisher analyses for both Gd M_5-edge and Fe L_3-edge XMCD intensities plotted together. (i) T dependence of the Gd M_5-edge (blue squares) and Fe L_3-edge (red squares) XMCD intensity for $Gd_6(Mn_{0.25}Fe_{0.75})_{23}$ fitted by a power law with $\beta = 0.38 \pm 0.01$ (blue and red lines, respectively). (j) Power-law and (k) Kouvel–Fisher analyses for Gd M_5-edge XMCD intensities, and (l) power-law and (m) Kouvel–Fisher analyses for Fe L_3-edge XMCD intensities. The red and blue lines in (d), (e), (g), (h), (j)–(m) are the fits below and above T_C, respectively. All XMCD results were obtained with an applied field of ±1 T. [Reproduced from Ref. 1]

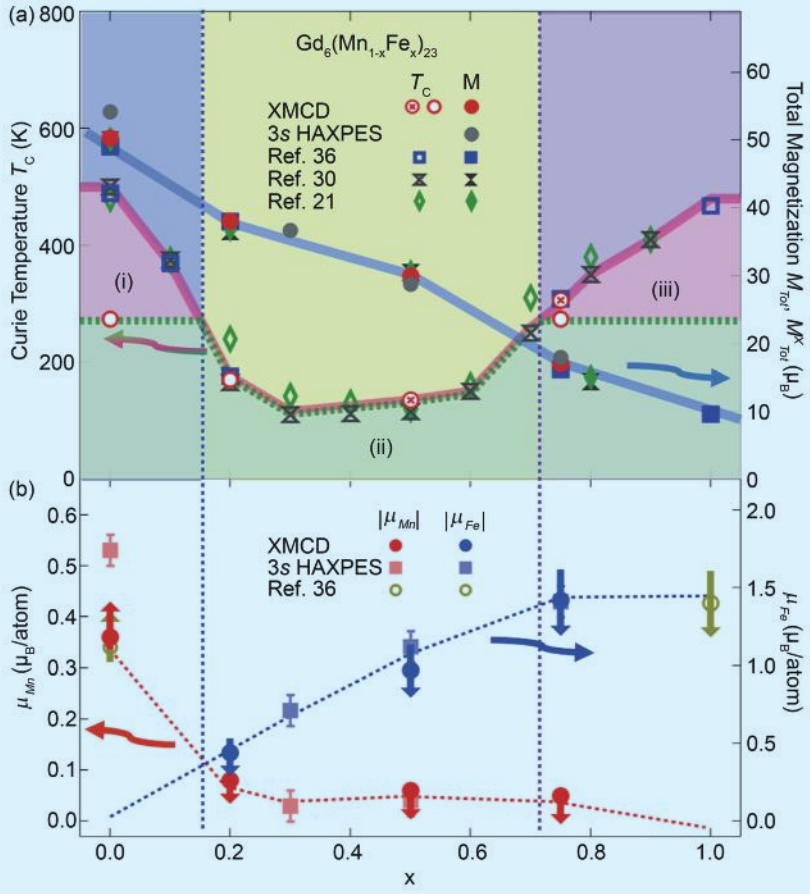

Fig. 4: Magnetic phase diagram of $Gd_6(Mn_{1-x}Fe_x)_{23}$. (a) Summary of element-specific T_C values with XMCD and bulk magnetizations (M^X_{Tot} and M^B_{Tot}) as a function of x. The plots of $T_{C(Gd)}$ (empty red circle ○) and $T_{C(Fe)}$ (red cross circle ⊗) show three regions: (i) For $0.0 < x \leq 0.15$, bulk T_C is determined by the Mn sublattice, and $T_{C(Gd)} = 273.5$ K < bulk T_C. (ii) For $0.15 < x \leq 0.72$, the Gd and Fe sublattices show the same T_C = bulk T_C. (iii) For $0.72 < x \leq 1.0$, the Fe moments determine the bulk T_C, and $T_{C(Gd)} = 273.5$ K < bulk T_C. (b) Summary of Mn and Fe magnetic moments (μ_{Mn}, μ_{Fe}) as a function of x, showing switching of Mn moments for $x \geq 0.2$ plotted with magnetic moments from 3*s* HAXPES analysis. [Reproduced from Ref. 1]

This report features the work of Ashish Chainani and his collaborators published in Commun. Mater. ***5****, 68 (2024) and Physical Review B* ***109****, 035102 (2024).*

TLS 11A1 (Dragon) MCD, XAS
SP 12U1 HAXPES/Photoemission

- XAS, XMCD, HAXPES
- Ferrimagnetic Transition, Materials Science, Condensed-matter Physics

References

1. T. Ly Nguyen, T. Mazet, E. Gaudry, D. Malterre, F.-H. Chang, H.-J. Lin, C.-T. Chen, Y.-C. Tseng, A. Chainani, Commun. Mater. **5**, 68 (2024).
2. T. Ly Nguyen, T. Mazet, D. Malterre, H. J. Lin, M. Yoshimura, Y. F. Liao, H. Ishii, N. Hiraoka, Y. C. Tseng, A. Chainani, Phys. Rev. B **106**, 045144 (2022).
3. A. Delapalme, J. Déportes, R. Lemaire, K. Hardman, W. J. James, J. Appl. Phys. **50**, 1987 (1979).
4. T. Ly Nguyen, C.-C. Yang, C.-H. Wang, Y.-W. Yang, T. Mazet, E. Gaudry , D. Malterre, M. Yoshimura, Y. F. Liao, H. Ishii, N. Hiraoka, H. J. Lin, Y. C. Tseng, A. Chainani, Phys. Rev. B **109**, 035102 (2024).

Unlocking Dual Topological States in the 2D Limit

A promising way enhances the understanding of 2D topological materials and lays the groundwork for future electronic and superconducting applications.

Two-dimensional (2D) quantum materials have gained attention for their exceptional electronic properties, particularly in spintronics and quantum computing. Among them, 2D topological insulators (TIs) are notable for their protected metallic edge states, which exhibit spin-momentum locking and insusceptibility to backscattering from nonmagnetic impurities. These features make them strong candidates for low-power electronic devices and quantum computing. The discovery of topological nodal line semimetals (TNLSMs), which host one-dimensional nodal lines of band degeneracy in the Brillouin zone, has further expanded the landscape of topological materials. However, experimental realization of 2D TNLSMs remains rare despite numerous theoretical predictions. Stanene, the monolayer allotrope of tin (Sn), has emerged as a promising 2D TI because of its sizable topological band gap (~0.3 eV) induced by strong spin–orbit coupling (SOC). Unlike silicene and germanene, which possess much smaller SOC-induced gaps, stanene's robust band inversion enables the quantum spin Hall effect at room temperature. Additionally, stanene's electronic properties can be tuned *via* strain

engineering and substrate interactions, making it a versatile platform for investigating topological phase transitions. In contrast, β-Sn, a metallic allotrope of tin with a body-centered tetragonal structure, exhibits superconducting behavior and has potential applications in topological superconductivity. However, the electronic structure of ultrathin β-Sn films remains largely unexplored, leaving its potential as a 2D TNLSM unexamined.

To advance understanding of 2D TNLSMs, Pin-Jui Hsu and Horng-Tay Jeng, both from National Tsing Hua University, and Cheng-Maw Cheng from the NSRRC investigated the electronic structure of monolayer β-Sn grown on a Cu(111) substrate by using scanning tunneling microscopy (STM), angle-resolved photoemission spectroscopy (ARPES), and density functional theory (DFT) calculations. Their study probed the structural and electronic phase transition from honeycomb stanene (α-Sn) to cubic β-Sn as Sn coverage increased. The transition from a 2D TI to a 2D TNLSM was directly observed, revealing the coexistence of type-I and type-III nodal lines in monolayer β-Sn for the first time. Experimental observations aligned well with DFT calculations, confirming that β-Sn exhibits a nearly freestanding electronic structure on Cu(111), an unexpected behavior in a metal-on-metal system. This suggests that β-Sn/Cu(111) provides an ideal platform for studying intrinsic 2D TNLSM properties. Furthermore, integrating superconducting few-layer Sn with topological nodal line monolayer β-Sn could open new avenues for exploring 2D topological superconductivity and Majorana fermions. Comprehensive ARPES experiments at the **TLS 21B1** beamline were carried out on high-quality α-Sn and β-Sn thin films prepared on Cu(111) using molecular beam epitaxy. A single layer of α-Sn was first grown on a Cu(111) substrate at low temperature. STM and low-energy electron diffraction revealed a honeycomb lattice of stanene with a $p(2\times2)$ supercell. ARPES measurements confirmed the band structure's consistency with reported results. When an equivalent amount of Sn atoms was subsequently deposited onto the stanene/Cu(111) at low temperature, the honeycomb lattice disappeared, and a high-coverage Sn (HC-Sn) cubic β-Sn phase emerged, as observed in the STM images. This structural phase transition from semiconducting honeycomb α-Sn to metallic cubic β-Sn provided a unique opportunity to investigate this topological transition in the band structure of ultrathin β-Sn(001) thin films.

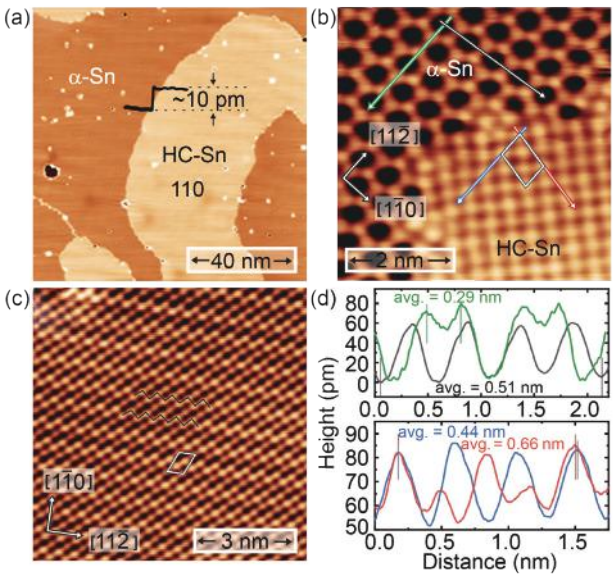

Fig. 1: (a) STM topographic overview of about 0.54 ML Sn grown on Cu(111). (b) Atomically resolved image at the boundary between α-Sn and HC-Sn. The white rhombuses indicate the unit cells of α-Sn ($p(2\times2)$) and HC-Sn. (c) STM image of HC-Sn on a larger scan area with atomic resolution. The periodic zigzag pattern (black zigzag stripes) has been clearly resolved. White rhombus frame denotes the unit cell. (d) Top panel: black and green curves are topographic line profiles taken along the arrow lines on the α-Sn phase along [1 $\bar{1}$ 0] and [1 1 $\bar{2}$] directions, respectively, in (b). Bottom panel: topographic line profiles (red and blue curves) taken along the arrow lines on HC-Sn in (b). [Reproduced from Ref. 1]

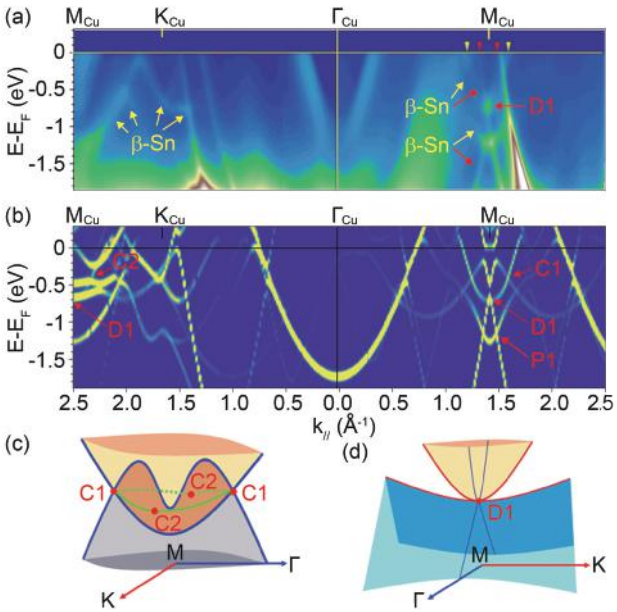

Fig. 2: (a) The band dispersions of single-layer β-Sn/Cu(111) along M_{Cu}-K_{Cu}-Γ_{Cu}-M_{Cu} relative to Cu(111) high-symmetry point direction. (b) The calculated unfolding band structure of freestanding monolayer β-Sn along the high symmetry lines in the BZ of Cu(111). Schematic diagram of type-I (c) and type-III (d) nodal line band crossings. C1 and C2 in (c) and D1 in (d) near the high-symmetry point M_{Cu} are indicated by the red arrows in (a) and (b). [Reproduced from Ref. 1]

STM topographic imaging of Sn thin films grown on Cu(111) at 80 K revealed distinct regions corresponding to α-Sn and β-Sn phases. We identified a honeycomb lattice with a $p(2\times2)$ supercell in the darker regions characteristic of α-Sn, while the brighter regions exhibited a higher-coverage Sn phase with a denser atomic arrangement. DFT calculations confirmed that the interlayer distance between the top β-Sn layer and the first Cu layer was 2.40 Å, consistent with the STM findings. To explore evolution in electronic structure from low-coverage (LC) to high-coverage (HC) Sn phases on Cu(111), ARPES measurements were conducted. Relative to pristine Cu(111), a linear band dispersion with a Dirac point at 0.62 eV binding energy emerged around the M_{Cu} point for β-Sn/Cu(111) shown in **Fig. 2(a)**, indicating an electronic topological transition. Two wave vectors crossing the Fermi level were identified, along with two electron pockets around the M_{Cu} point: one with significant Fermi level crossing and another deeper in the binding energy region. Additional β-Sn-derived bands, which are confirmed as 2D features through photon energy-dependent ARPES experiments, appeared at the K_{Cu} point. DFT band structure calculations were performed for both freestanding monolayer β-Sn and β-Sn/Cu(111). The unfolded band structure of freestanding β-Sn monolayer closely matched ARPES results, particularly around the M_{Cu} and K_{Cu} points. The band-crossing points C1 and D1 near M_{Cu} were identified as type-I and type-III nodal line semimetal features. The C1 crossing formed a closed ring-shaped type-I nodal line, while the D1 crossing exhibited a type-III nodal line characterized by a cone-saddle intersection. These findings confirm that β-Sn/Cu(111) hosts a dual-nodal line semimetal phase, making it an exciting candidate for further exploration of 2D TNLSMs.

Similar to reported 2D nodal line materials such as CuSe, AgSe, and Cu_2Si, monolayer β-Sn possesses mirror reflection symmetry. In three-dimensional TNLSMs, nodal line projections onto surfaces generate drumhead-like flat surface bands protected by topological invariants. However, in 2D TNLSMs, node lines do not directly protect edge states, complicating their observation. Despite this challenge, β-Sn's coexistence of type-I and type-III nodal lines presents an exceptional case for further research. Few experimental realizations of 2D TNLSMs exist due to stringent symmetry and SOC requirements. While theoretical predictions suggest that external perturbations like strain or electric fields can induce a TNLSM phase in some 2D materials, experimental verification remains scarce. The discovery of type-I and type-III gapless nodal line behaviors in β-Sn/Cu(111) marks a significant step forward. These findings, backed by STM–ARPES–DFT investigations, establish monolayer β-Sn as a novel 2D dual-nodal line semimetal, offering a valuable platform for exploring topological superconductivity and other quantum phenomena.

To summarize, by elucidating topological transition and nodal line behavior in ultrathin β-Sn films, this work enhances the understanding of 2D topological materials and lays the groundwork for future electronic and superconducting applications. The unique properties of β-Sn highlight its potential as a novel material for next-generation quantum devices. (Reported by Cheng-Maw Cheng)

This report features the work of Pin-Jui Hsu, Horng-Tay Jeng, Cheng-Maw Cheng and their collaborators published in ACS Nano ***18****, 20990 (2024).*

TLS 21B1 Angle-resolved UPS

- High-resolution ARPES
- Materials Science, Condensed-matter Physics

Reference

1. Y.-S. Lan, C.-J. Chen, S.-H. Kuo, Y.-H. Lin, A. Huang, J.-Y. Huang, P.-J. Hsu, C.-M. Cheng, H.-T. Jeng, ACS Nano **18**, 20990 (2024).

Single-Element-Driven Crystalline Magnetic Anisotropy in the High-Entropy Oxide $(Fe, Co, Ni, Cr, Mn)_3O_4$

X-ray absorption spectroscopy, magnetic circular dichroism, and linear dichroism show that crystalline magnetic anisotropy in $(Fe, Co, Ni, Cr, Mn)_3O_4$ originates from the orbital anisotropy of Mn 3d states due to substrate-induced epitaxial strain.

The design of multicomponent materials or so-called high-entropy alloys and compounds has attracted enormous attention due to their extraordinary ability to tailor functional properties. However, it is not easy to identify the role of each element in terms of their impact on crystal structure and its relation to electronic and magnetic properties in such materials. In a recent study on high-entropy spinel oxide $(Fe, Co, Ni, Cr, Mn)_3O_4$ epitaxial films, Ying-Hao Chu's team (National Tsing Hua University) successfully grew high-quality films with varying strain states, and then carried out a detailed investigation on the crystal structure and magnetic properties, as well as used electron microscopy and synchrotron spectroscopy techniques to determine element-specific properties. The team discovered that the high-entropy oxide (HEO) thin film under compressive strain shows evidence of crystalline magnetic anisotropy that is derived from a single element.[1] Using a combination of X-ray absorption spectroscopy (XAS), X-ray magnetic circular dichroism (XMCD), and X-ray linear dichroism (XLD), the team showed that the observed crystalline magnetic anisotropy originates from orbital occupation changes in Mn 3d states induced by epitaxial strain in the films.

The team first fabricated high-entropy $(Fe, Co, Ni, Cr, Mn)_3O_4$ epitaxial films on single-crystal $MgAl_2O_4$ (MAO) and MgO substrates with a high-quality interface. This resulted in elimination of defects in the HEO film and imposed compressive and tensile strain on HEO films grown on MAO and MgO, respectively. The team then carried out extensive analyses for a detailed understanding of HEO films, including X-ray diffraction (XRD), reciprocal space mapping, Raman spectroscopy, macroscopic magnetic characterization, electron microscopy, and synchrotron spectroscopy. The XRD rocking curves of the HEO (004) peak on MAO and MgO substrates measured at **TLS 17A1** show full width at half maximum (FWHM) of 0.42° and 0.14°, respectively, demonstrating the superior crystallinity of HEO films on these substrates. Reciprocal space mapping (RSM) was then used to show that the HEO film is under an in-plane compressive strain of 0.52% on the MAO substrate, while the HEO film is under an in-plane tensile strain of 0.85% on the MgO substrate. Raman spectroscopy showed four peaks at 527 cm^{-1} ($3F_{2g}$), 588 cm^{-1} ($3F_{2g}$), 648 cm^{-1}, and 700 cm^{-1} (A_{1g}). The wavenumbers of 648 and 700 cm^{-1} indicate the octahedral and tetrahedral centers in HEO. Accordingly, the crystal structure of HEO was classified as a spinel based on results from XRD and Raman spectroscopy. Scanning transmission electron microscopy with electron energy loss spectroscopy further confirmed that the HEO films exhibited a spinel phase.

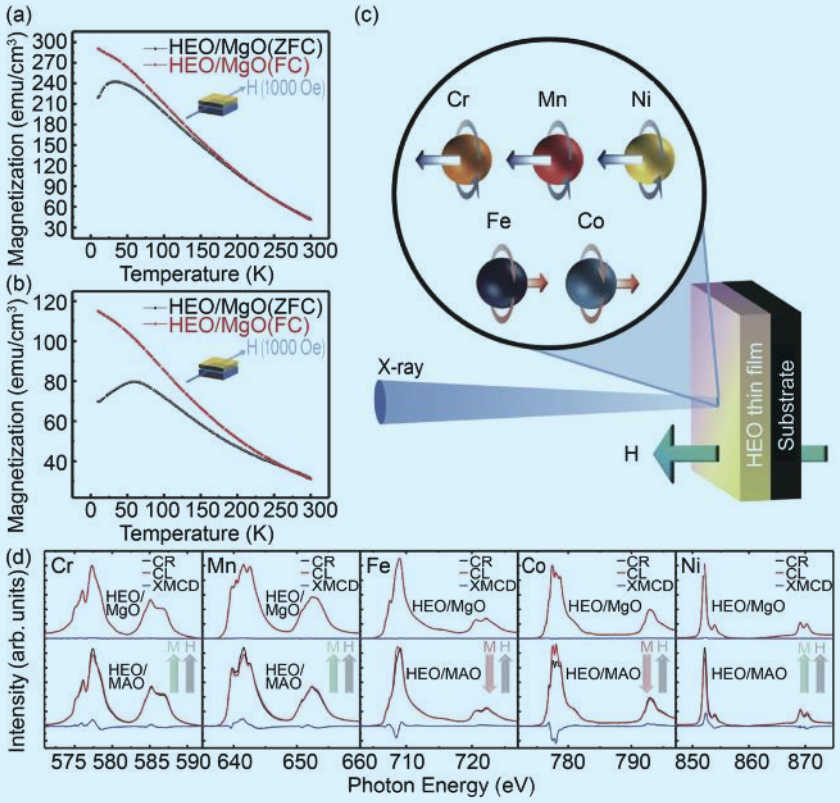

Fig. 1: M(T) and XMCD results. Temperature-dependent magnetization for (a) HEO/MgO and (b) HEO/MAO heterostructures under ZFC and FC processes with a DC magnetic field of 1000 Oe along the in-plane direction. (c) Schematic diagram illustrating the relationship between the applied magnetic field and the direction of the element's magnetic moment. (d) XMCD spectra of each element for the HEO/MgO and HEO/MAO structures. [Reproduced from Ref. 1]

Next, in order to understand the magnetic behavior of HEO films as a function of temperature, zero-field-cooled (ZFC) and field-cooled (FC) magnetization (M_{ZFC} and M_{FC}, respectively) measurements of the HEO/MgO and HEO/MAO heteroepitaxies were carried out as shown in **Figs. 1(a) and 1(b)**. It was found that both samples show a spin-glass-like behavior since considerable deviation was observed between M_{ZFC} and M_{FC} below ~280 K.

The team carried out XMCD measurements at **TPS 45A**, with the samples in a remanence state and the incident X-ray normal to the surface at 200 K, as shown schematically in **Fig. 1(c)**. The samples were magnetized with a field of 3 T normal to the sample surface before they were introduced into the chamber. **Figure 1(d)** shows clear XMCD signals for all five transition metals. For the HEO/MAO structure, a positive XMCD signal at the main absorption peak of the Cr, Mn, Ni L_3 edge spectra was observed. In contrast, Fe and Co spectra showed a negative XMCD signal at the L_3 edge. These results indicate that the spin direction of Cr, Mn, and Ni corresponds to the direction of the applied magnetic field (parallel), and that of Fe and Co is opposite to the applied magnetic field (antiparallel), as shown in **Fig. 1(c)**. In addition, a higher-intensity XMCD signal for the HEO/MAO structure and a lower-intensity XMCD signal for HEO/MgO were observed (**Fig. 1(d)**). The team concluded that because of the strong in-plane shape of its magnetic anisotropy, the magnetic moments of the HEO/MGO structure are aligned in-plane, while the magnetic moments of the HEO/MAO structure are aligned with the out-of-plane direction. This suggests that crystalline magnetic anisotropy dominates over the shape of magnetic anisotropy in the HEO/MAO structure. These results were further confirmed by superconducting quantum interference device (SQUID) magnetometry measurements. The authors also carried out SQUID measurements of HEO/MAO samples with film thicknesses from ~50 nm to over 1 μm and quantified the relationship between anisotropy energy density and film thickness. These results show that the thinner is the HEO film, the greater is the anisotropy energy density (~3×10^6 erg cm^{-3}), indicating that it is more affected by crystalline magnetic anisotropy. It is speculated that this magnetic anisotropy behavior comes from the epitaxial strain imposed by the substrate.

The team then carried out XAS measurements at T = 300 K as shown in **Fig. 2(a)** in order to check the valency and local geometry of the transition-metal ions. **Figure 2(b)** shows a schematic illustrating 3d orbital splitting when transition-metal elements occupy octahedral and tetrahedral sites. By comparing with standard reference samples, we concluded that Cr ions exhibit octahedral coordination with a valency of Cr^{3+}. On the other hand, Mn was found to adopt multiple valence states with Mn^{2+} in tetrahedral coordination and with Mn^{3+} and Mn^{4+} in octahedral coordination. The Mn^{2+} ion exhibits a half-filled 3d orbital, implying that it has a spherically symmetric

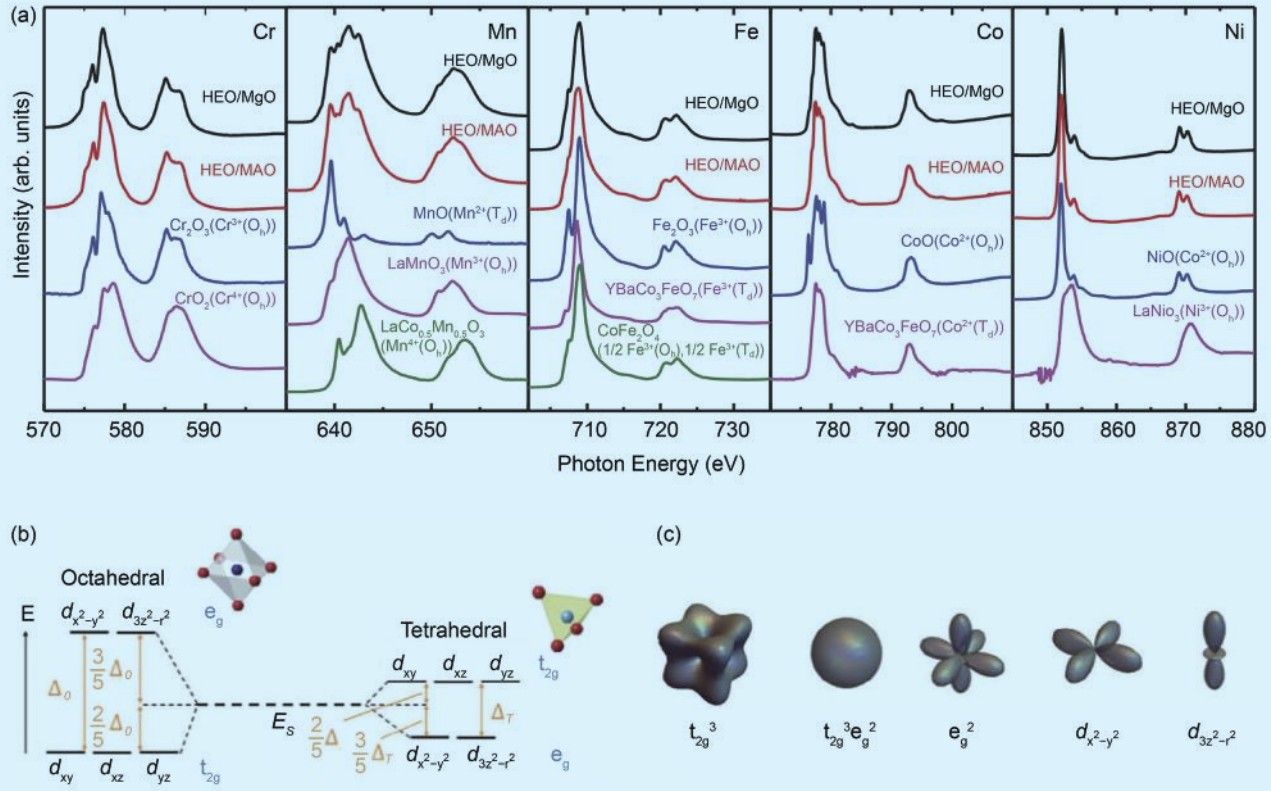

Fig. 2: XAS measurements. (a) XAS spectra of HEO/MgO and HEO/MAO structures. (b) 3D orbital splitting of a transition-metal ion at the octahedral and tetrahedral sites into e_g orbitals (d_{x2-y2}, d_{3z2-r2}) and t_{2g} orbitals (d_{xy}, d_{xz}, d_{yz}). (c) The electron clouds of different occupied orbitals. [Reproduced from Ref. 1]

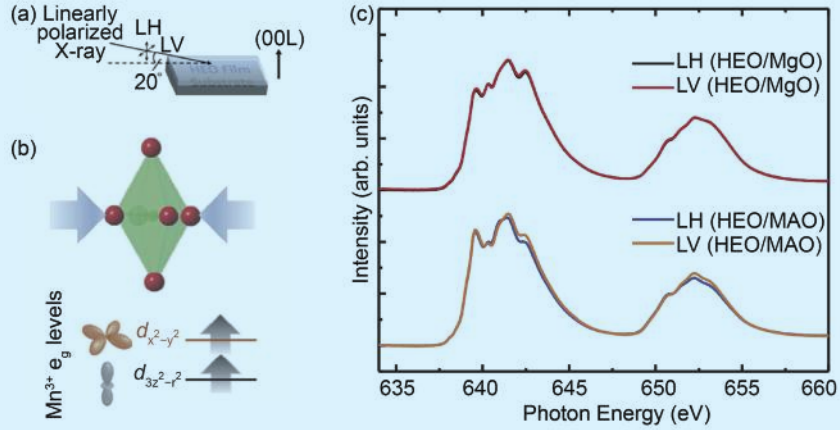

Fig. 3: XLD measurements. (a) Schematic of an XLD measurement. (b) A representation of MnO_6 under compressive strain and the subsequent effect on e_g splitting. (c) Mn $L_{2,3}$ XLD spectrum of the HEO/MgO and HEO/MAO structures. [Reproduced from Ref. 1]

electron cloud shape of $t_{2g}^3e_g^2$, as shown in **Fig. 2(c)**. For Mn^{4+} octahedral coordination, three electrons occupy the d_{xy}, d_{xz}, and d_{yz} orbitals, forming an electron cloud with cubic symmetry in t_{2g}^3, similar to that of Cr^{3+}. Similarly, it was found that Fe atoms show Fe^{3+} valency and adopt a half-filled 3d orbital for octahedral and tetrahedral sites, both corresponding to a spherically symmetric electron cloud shape $t_{2g}^3e_g^2$, while Co atoms show Co^{2+} valency in tetrahedral coordination with a fully occupied e_g but half-filled t_{2g} shell. Therefore, it exhibits an electron cloud with cubic symmetry in $t_{2g}^3e_g^4$. Lastly, Ni atoms exhibit an octahedral Ni^{2+} configuration with a fully occupied t_{2g} shell and half-filled e_g shell, resulting in a $t_{2g}^6e_g^2$ configuration and an electron cloud with cubic symmetry .

Finally, the team employed XLD to probe the asymmetric orbital occupation of Cr, Mn, Fe, Co, and Ni to verify the correlation between strain states and magnetic behavior. In the XLD measurements, linearly polarized X-rays were used with a grazing angle of 20° as depicted in **Fig. 3(a)**. The out-of-plane polarization (LH) absorption of Cr, Fe, Co, and Ni L edge spectra was very similar to the in-plane polarization (LV) absorption of the HEO/MAO structure. It was concluded that because of their symmetrical electron cloud shapes, these four elements should not contribute to orbital anisotropy. On the other hand, **Fig. 3(c)** indicates a discernible difference in the XLD spectrum of the Mn L edge absorption between the HEO/MgO (tensile) and HEO/MAO (compressive) structures. The LH absorption of the Mn L edge spectrum is weaker than that of LV in the HEO/MAO, suggesting a larger number of in-plane empty states in the e_g band. This indicates a higher occupancy of out-of-plane ($3z^2$-r^2) orbitals. This occupancy is primarily influenced by the strain state, which in turn determines the magnetic behavior of the HEO thin film. Since only the Mn^{3+} cation contains four electrons in the 3d orbitals, the crystalline magnetic anisotropy in HEO/MAO is primarily attributed to the higher electron occupancy of ($3z^2$-r^2) orbitals. **Figure 3(b)** depicts a schematic diagram illustrating the splitting of 3d orbitals in octahedral Mn under in-plane compressive strain. Thus, the authors could show that the difference in magnetic anisotropy originates from distortion in Mn^{3+} coordination, which is attributed to the strain applied from the substrate.

In conclusion, this study revealed that Mn^{3+} is the primary driver of crystalline magnetic anisotropy in the spinel HEO $(Fe, Co, Ni, Cr, Mn)_3O_4$ due to strain-modified orbital occupation.[1] This study shows that advanced synchrotron techniques can be fruitfully used to investigate the role of individual elements in influencing the electronic and magnetic properties of HEOs and to provide valuable insights for understanding the fundamental physics of HEOs. (Reported by Ashish Chainani)

This report features the work of Ying-Hao Chu, Chang-Yang Kuo, Yi-Cheng Chen and their collaborators published in Adv. Funct. Mater. ***34****, 2312856 (2024).*

TPS 45A Submicron Soft X-ray Spectroscopy
TLS 17A1 X-ray Powder Diffraction

- XRD, XAS, XMCD, XLD
- Materials Science, Condensed-matter Physics

Reference

1. W.-E. Ke, J.-W. Chen, C.-E. Liu, Y.-C. Ku, C.-F. Chang, P. Shafer, S.-J. Lin, M.-W. Chu, Y.-C. Chen, J.-W. Yeh, C.-Y. Kuo, Y.-H. Chu, Adv. Funct. Mater. **34**, 2312856 (2024).

Visualization of the Distribution of Mixing Enthalpy and Entropy

Mixing enthalpy and entropy can be calculated by using the X-ray nanoprobe to understand the thermodynamic stability, solubility, and miscibility of the materials.

It is well known that high-entropy alloys (HEAs) can be studied by enthalpy and entropy, but have you ever thought about using them to analyze luminescent materials? E-Wen Huang (National Yang Ming Chiao Tung University) and his collaborators present a new approach to mapping thermodynamic parameters through the use of the spatially resolved synchrotron X-ray methods (**TPS 23A** and **TPS 21A**). It demonstrates how the distribution of mixing enthalpy and entropy correlates with the local optical properties of the activator Eu ions in the $BaAl_2O_4$ host lattice. The study clearly demonstrates the use of synchrotron radiation for the combinatorial approach, including X-ray nano-diffraction, X-ray fluorescence (XRF), X-ray absorption spectroscopy (XAS), and X-ray excited optical luminescence (XEOL), to map the valence states and spatial distributions of Eu^{2+} and Eu^{3+} ions. To understand the mechanisms by which the substitution of Eu ions in the host lattice affects the crystal structure and related properties, they quantify mixing enthalpy and entropy to explain the interactions between Eu ions and host elements, particularly Al and Ba. XRF maps (**Fig. 1**) not only provide the elemental distributions, such as those for Ba, Al, and Eu, but they also visualize the valence state distributions of Eu^{2+} and Eu^{3+} ions.

This study provides critical insights into the thermodynamic and structural stability of Eu ions, offering guidance for designing and optimizing phosphor materials with enhanced performance and stability (**Fig. 2**). The results reveal that Eu^{3+} ions aggregate within a specific region, while Eu^{2+} ions occupy the surrounding areas, highlighting distinct distribution patterns. Thermodynamic calculations show that Eu^{3+} ions exhibit favorable interactions with Al, which are characterized by a negative mixing enthalpy ($\Delta H < 0$) and a positive mixing entropy ($\Delta S > 0$), indicating high solubility and increased disorder. Conversely, the mixing behavior of Eu^{3+} ions with Ba is less favorable, as indicated by positive ΔH and ΔS values, which suggest repulsive interactions and greater disorder within

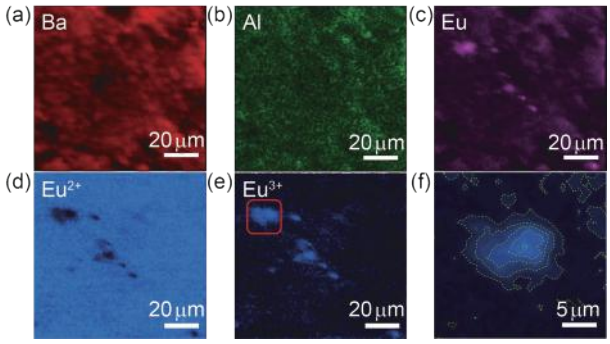

Fig. 1: XRF maps of (a) Ba, (b) Al, (c) Eu, (d) Eu^{2+}, and (e) Eu^{3+} in the Eu-doped $BaAl_2O_4$. (f) The enlarged map of the red square area marked in (e). [Reproduced from Ref. 1]

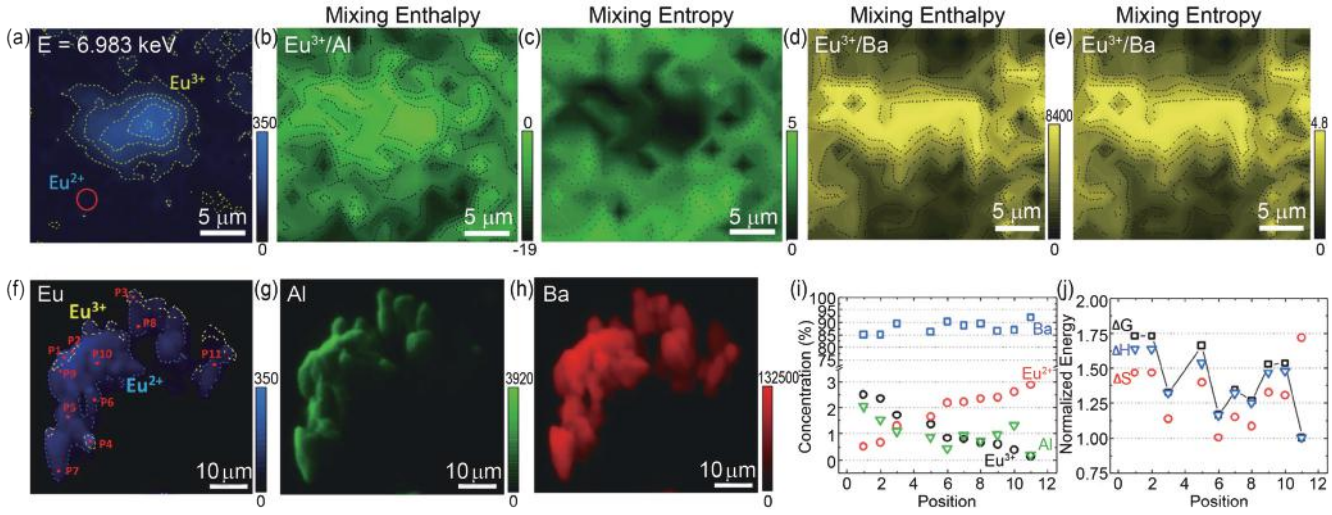

Fig. 2: (a) Distribution of Eu^{2+} and Eu^{3+} ions at X-ray energy of 6.983 keV. (b) Mixing enthalpy and (c) mixing entropy of Eu^{3+} ions and Al elements, respectively. (d) Mixing enthalpy and (e) mixing entropy of Eu^{3+} ions and Ba elements, respectively. (f) Distribution of Eu with 11 selected points for X-ray Laue diffraction. (g) Distribution of Al. (h) Distribution of Ba. (i) Concentration variation of constituent elements at different positions. (j) Gibbs free energy of mixing, mixing enthalpy, and mixing entropy at 11 different positions. [Reproduced from Ref. 1]

the system. The study further confirms that the crystal structure remains stable despite variations in composition, with no significant impact from Eu doping. Furthermore, Eu^{2+} ions display a stronger affinity for Al than Ba, leading to the observed aggregation of Eu^{3+} ions. These findings provide valuable insights into the thermodynamic behavior and structural stability of Eu ions, offering important guidance for the design and optimization of advanced phosphor materials.

The study investigates the effects of X-ray irradiation on $BaAl_2O_4$ doped with Eu^{2+} and Eu^{3+} ions, focusing on emission intensity and color changes (**Fig. 3**). In the XEOL spectrum, the peak at 500 nm corresponds to the Eu^{2+} 4f5d→4f transition, and the peaks at 588, 612, 650, and 698 nm are attributable to Eu^{3+} $^5D_0 \rightarrow {}^7F_i$ transitions. Under X-ray exposure, a significant decrease in Eu^{2+} emission intensity and a minor decrease in Eu^{3+} emission, which are likely due to thermal accumulation that increases non-radiative coupling, are observed. The ratio of Eu^{3+} to Eu^{2+} gradually increases with irradiation time, while X-ray absorption spectra indicate no significant changes in the electronic structure. The CIE chromaticity coordinates shift from (0.032, 0.524) to (0.043, 0.520), indicating a transition from green to white. This change is attributed to an increased presence of electrons in the conduction band, which is facilitated by X-ray-induced electron–electron scattering and phonon-assisted processes. The findings highlight the potential for X-ray dosimetry applications and tunable emission color strategies through defect state engineering in wide-bandgap semiconductors.

In summary, the behavior of Eu ions demonstrates that their aggregation is influenced by their different valence states and thermodynamic factors, providing insights into how rare-earth elements distribute and dissolve. Understanding how Eu ions interact with Al and Ba is important for designing and improving phosphor materials. The study further shows that even when doping is not uniform, the crystal structure maintains its stability, which helps improve the reliability of the doped materials. The assessment of thermodynamic parameters provides key data for understanding how rare-earth materials interact, supporting the development of efficient luminescent materials. This result demonstrates that the photoluminescence of the Eu-doped $BaAl_2O_4$ phosphor can be effectively modulated through the precise control of X-ray irradiation levels.

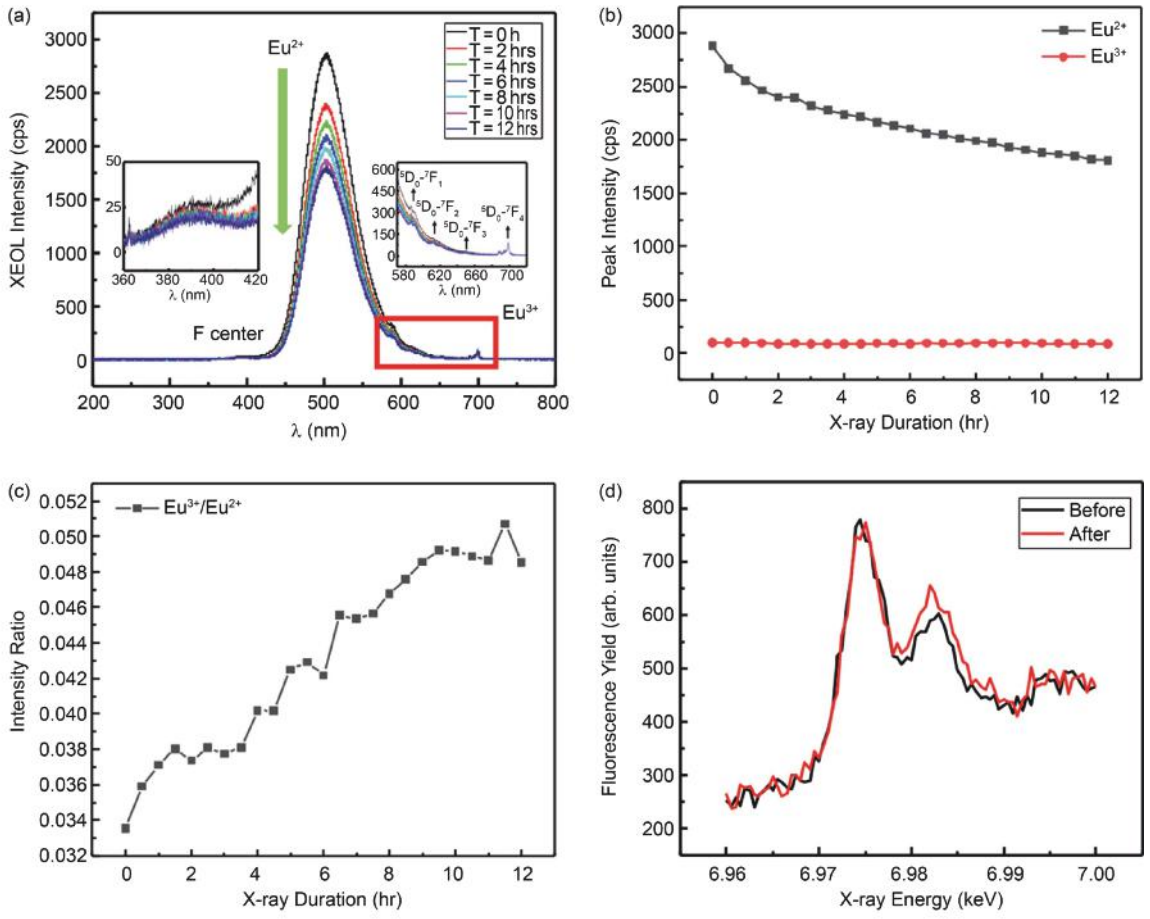

Fig. 3: (a) The XEOL spectrum of Eu^{2+}/Eu^{3+} co-activated ions in $BaAl_2O_4$ phosphor; (b) the intensity variation of Eu^{2+} and Eu^{3+} emission peaks; (c) the intensity ratio of Eu^{2+} and Eu^{3+} emission peaks under X-ray irradiation from 0 to 12 h. (d) The variation of fluorescence yield characterized by X-ray absorption near edge structure before and after X-ray irradiation. [Reproduced from Ref. 1]

Overall, this study offers a theoretical foundation for designing and using rare-earth phosphor materials, focusing on thermodynamics and structural stability and supporting the ongoing development of high-performance white-light LED technologies. (Reported by Bi-Hsuan Lin)

This report features the work of E-Wen Huang and his collaborators published in Appl. Phys. Lett. ***124****, 094105 (2024).*

TPS 21A X-ray Nanodiffraction
TPS 23A X-ray Nanoprobe

- XRF, XEOL, XAS
- Materials Science, Structure, Emission Properties, Applications of High-Entropy Materials

Reference

1. Y.-H. Wu, T.-N. Lam, S.-W. Ke, W.-J. Lee, C.-Y. Lee, B.-Y. Chen, G.-C. Yin, W.-Z. Hsieh, C.-Y. Chiang, M.-T. Tang, B.-H. Lin, E-W. Huang, Appl. Phys. Lett. **124**, 094105 (2024).

Exploring Quantum Materials by Using Synchrotron X-rays

Superconducting qubits composed of aluminum (Al) and aluminum oxide (Al_2O_3) play a pivotal role in advancing quantum information science.

The United Nations proclaimed 2025 as the International Year of Quantum Science and Technology (IYQ). Quantum technology will have a significant impact on human life. Synchrotron facility plays a vital role in the development of science and technology. This article will introduce how synchrotron X-rays can be used for quantum technology. Minghwei Hong (National Taiwan University) and his collaborators investigates the structural and superconducting properties of nanometer-thick aluminum (Al) films grown on sapphire substrates using molecular beam epitaxy (MBE), with an emphasis on the use of an *in situ* deposited aluminum oxide (Al_2O_3) capping layer to maintain the pristine condition of the ultrathin films.

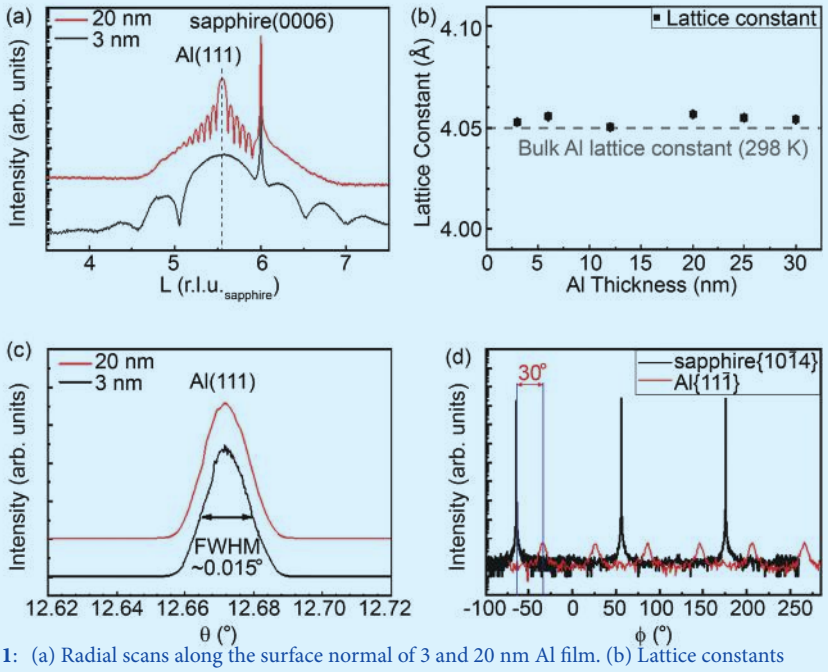

Fig. 1: (a) Radial scans along the surface normal of 3 and 20 nm Al film. (b) Lattice constants derived from inter-planar spacing along surface normal as a function of film thickness. (c) θ-rocking curves of 3 and 20 nm-thick Al films. (d) Azimuthal ϕ-scans across off-normal Al{11$\bar{1}$ and sapphire{10$\bar{1}$4 reflections. [Reproduced from Ref. 1]

This paper aims to describe the key challenges in developing materials for superconducting quantum circuits, where high crystallinity and minimized dielectric losses are essential for enhancing the coherence times. By carefully controlling the growth parameters and implementing the Al_2O_3 capping layer, they achieved high-quality Al films with remarkable crystallinity, abrupt interfaces with adjacent layers, and superconducting properties, which demonstrate potential for applications in quantum information technologies.

Figure 1 demonstrates the high structural quality, crystallographic orientation, and stability of lattice properties in the nanometer-scale Al films. The radial scans along the surface normal, θ-rocking curves, and azimuthal ϕ scans exhibit the structure, crystallographic quality, and the epitaxial alignment of the nanometer-thick Al films. X-ray diffraction (XRD) using synchrotron X-ray (**TLS 17B1** and **TLS 13A1**) can provide the capability for measuring the nanometer-thick Al films.

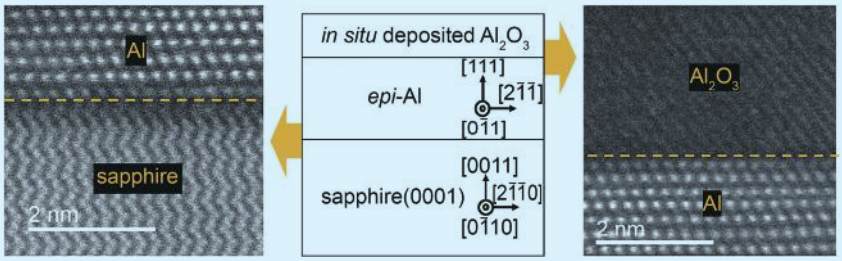

Fig. 2: High-angle annular dark-field scanning transmission electron microscopy (HAADF-STEM) images of cross-sectional views of the MBE-grown *epi*-Al/sapphire heterostructure (left) and the *in situ* deposited Al_2O_3/*epi*-Al heterostructure (right). A schematic representation of the heterostructure (center) shows the orientations of the *epi*-Al film and the sapphire substrate. [Reproduced from Ref. 1]

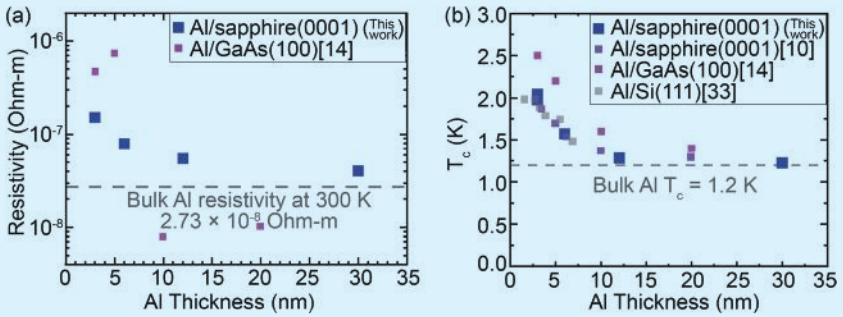

Fig. 3: (a) Resistivity vs. Al film thickness and (b) superconducting critical temperature vs thickness of Al films. [Reproduced from Ref. 1]

Figure 2 exhibits the excellent crystal growth capability of MBE and visually confirms the success of the *in situ* Al_2O_3 capping layer technique in maintaining the pristine, well-ordered structure of ultrathin Al films. These results are prerequisites for the development of reliable, low-dielectric-loss superconducting devices in quantum computing, demonstrating that the perfected growth process can produce the high-quality, stable interfaces required for effective superconducting quantum circuits.

To understand the potential of these ultrathin Al films in superconducting quantum circuits, we illustrate in **Fig. 3** the electrical properties of the nanometer-scale Al films, particularly their resistivity and superconducting critical temperature (T_c), as a function of film thickness. This study successfully demonstrated superconductivity in these nanometer-thick Al films, with T_c varying with the film thickness. T_c ranged from 1.2 K for thicker films up to approximately 2 K for the thinnest films. This variation in T_c with thickness is likely due to quantum confinement effects or modifications in phonon modes, which alter the superconducting properties as the dimensions of the film decrease. These results suggest that these ultrathin Al films could be valuable for applications requiring superconducting materials at scaled dimensions as they maintain superconductivity even at nanometer-scale thicknesses.

In summary, this study provided valuable insights into the growth and superconducting properties of ultrathin epitaxial Al films for quantum computing applications. By employing precise MBE growth techniques and implementation of an *in situ* Al_2O_3 capping layer, Hong and his collaborators successfully demonstrated the potential of these ultrathin films to meet the serious demands of superconducting qubits, such as high crystallinity, abrupt interfaces, and stable superconducting properties at low temperatures. This paper highlights a new direction for fabricating Josephson junctions and microwave resonators, the key components in superconducting qubits for quantum computing. (Reported by Bi-Hsuan Lin)

This report features the work of Minghwei Hong and his collaborators published in J. Appl. Phys. ***136****, 074401 (2024).*

TLS 13A1 X-ray Scattering
TLS 17B1 X-ray Scattering

- XRD, XRR
- Materials Science, Surface, Interface, Superconducting Quantum Circuits

Reference

1. Y. H. G. Lin, C. K. Cheng, L. B. Young, L. S. Chiang, W. S. Chen, K. H. Lai, S. P. Chiu, C. T. Wu, C. T. Liang, J. J. Lin, C. H. Hsu, Y. H. Lin, J. Kwo, M. Hong, J. Appl. Phys. **136**, 074401 (2024).

Chemical Science

The chemical science section of this year's NSRRC Activity Report highlights groundbreaking research leveraging synchrotron-based techniques. Studies span diverse fields, including organic photovoltaics, near-infrared (NIR) optoelectronics, photoresponsive materials, catalytic ammonia synthesis, and astrochemistry. These investigations underscore the critical role of synchrotron radiation in elucidating atomic and molecular phenomena, driving scientific and technological advancements.

A pivotal study on nonfullerene acceptors for organic photovoltaics explores the structure–property–performance relationships of a novel acceptor, CB16. By removing the central thiadiazole unit, researchers achieved an 18.32% power conversion efficiency, surpassing the Y6-based counterparts. Small/wide-angle X-ray scattering provided insights into molecular packing and interactions, setting new benchmarks for simplified acceptor designs to enhance the solar cell efficiency.

In NIR optoelectronics, two studies push organic light-emitting diode (OLED) emission wavelengths beyond 900 nm. One exploits an interfacial energy transfer mechanism to achieve hyperfluorescence at 925 nm and 1022 nm using Pt(II) complex and fluorescent dye bilayers, with implications for telecommunications and bioimaging. The other study investigates chromium-doped materials, revealing that luminescence quenching in $GaInO_3:Cr^{3+}$ arises from hole-type thermal quenching rather than electron transfer—a key insight for improving NIR-emitting materials for sensors and LEDs.

A breakthrough in light-responsive materials features MXenegel, a composite hydrogel integrating MXene nanosheets and azobenzene-based supramolecular complexes. Exhibiting reversible phase transitions under UV and visible light without compromising conductivity, this innovation paves the way for reconfigurable soft electronics. Synchrotron techniques were instrumental in probing the gel's structural transformations.

Catalysis remains a focal point, with a study on ammonia synthesis using carbon-supported ruthenium catalysts. Researchers optimized mesoporous carbon supports to enhance catalytic performance and stability, aligning with renewable-energy initiatives. Synchrotron characterizations of Ru nanoparticle dispersion and electronic promoter interactions revealed the mechanisms mitigating hydrogen poisoning, offering scalable solutions for efficient ammonia production.

Astrochemical research explores molecular ices and doped graphene. One study examines the behavior of 1-propanol ice under interstellar conditions, showing its persistence beyond the melting point without crystallization—key for understanding cosmic dust mantles. Another investigates ethanolamine ice, providing insights into its formation pathways and spectroscopic properties, enriching knowledge of prebiotic chemistry in star-forming regions. A final study on N-doped graphene correlates its photoluminescence properties with astrophysical observations of the Red Rectangle Nebula. Synchrotron radiation played a crucial role in characterizing bonding environments and electronic structures.

Collectively, these studies demonstrate the transformative impact of synchrotron-based research. From renewable energy advancements to unraveling cosmic mysteries, NSRRC continues to foster collaborations that push the boundaries of chemical sciences, contributing to sustainable and innovative solutions. (By Yu-Jong Wu)

Insights into Molecular Packing

Controlling π–π stacking in non-fullerene acceptors could be key to enhancing organic photovoltaic performance.

Organic photovoltaics (OPVs) have emerged as a promising renewable energy technology due to their lightweight, flexible, and scalable nature, making them ideal for next-generation solar energy solutions. A key factor driving the advancement of OPVs is the development of non-fullerene acceptors (NFAs), which have surpassed fullerene-based acceptors in optical absorption, tunability, and efficiency.[1] Among these, Y6-based NFAs stand out as benchmarks, enabling power conversion efficiencies (PCEs) exceeding 18% through their unique A-DA' D-A-type molecular architecture.[2] This structure, featuring a central thiadiazole (Tz) unit and a C-shaped ortho-benzodipyrrole skeleton, supports strong absorption and efficient charge transport. Despite these successes, challenges such as the synthetic complexity of Y6 and its tendency toward aggregation hinder further improvements and limit scalability.

To address these challenges, teams led by Yen-Ju Cheng (National Yang Ming Chiao Tung University) and U-Ser Jeng (NSRRC) are exploring innovative molecular designs aimed at maintaining high performance while minimizing structural complexity and aggregation. This research focused on three carefully designed NFAs—CB16, Y6-16, and SB16—to better understand the relationships between molecular structure, packing behavior, and device performance. As shown in **Fig. 1**, CB16 simplifies the Y6 architecture by removing the central Tz unit while preserving the C-shaped ortho-benzodipyrrole skeleton. This modification is intended to reduce self-aggregation and improve donor–acceptor interactions. Y6-16, a derivative of Y6 with side chains identical to those of CB16, retains the Tz unit and serves as a benchmark for comparison. Additionally, SB16 features an S-shaped para-benzodipyrrole skeleton, offering a direct comparison in molecular geometry. These three NFAs were strategically selected to elucidate how structural modifications influence molecular packing, charge transport, and overall device performance.

Grazing-incidence wide-angle X-ray scattering (GIWAXS) and simultaneous small- and wide-angle X-ray scattering (SWAXS) provided detailed insights into the molecular packing and phase behavior of the NFAs in both neat films and when blended with the donor polymer PM6. **Figure 2** highlights the GIWAXS patterns and corresponding 1D scattering profiles, revealing the key differences in molecular packing among the three NFAs. CB16 exhibits vertically oriented π–π stacking with abundant small nanodomains, facilitating the formation of bicontinuous networks essential for efficient charge transport. This packing arrangement reflects the benefits of removing the Tz unit, which results in reduced aggregation while maintaining robust donor–acceptor interactions. By contrast, SB16 demonstrates large, phase-separated domains with poor π–π stacking due to its S-shaped geometry, resulting in suboptimal performance. Y6-16, while similar to CB16 in packing features, shows

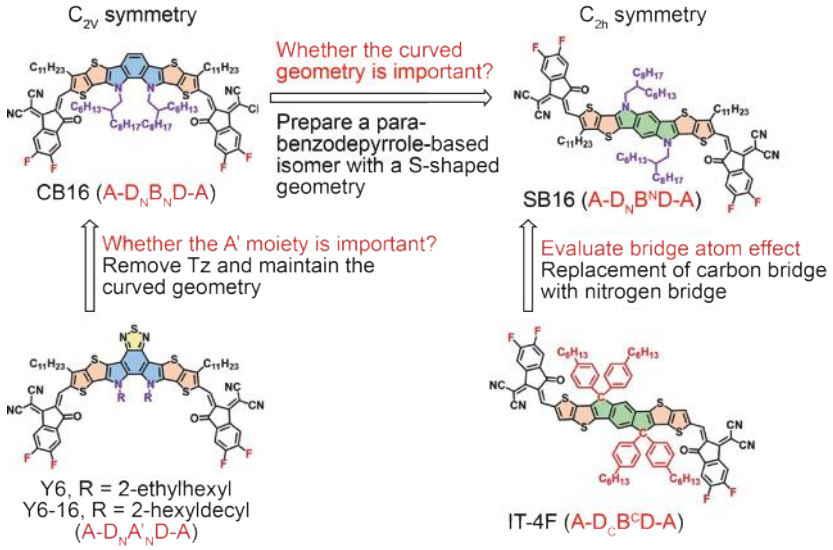

Fig. 1: Chemical structures of Y6, Y6-16, and IT-4F that inspired the design of CB16 and SB16 NFAs. [Reproduced from Ref. 3]

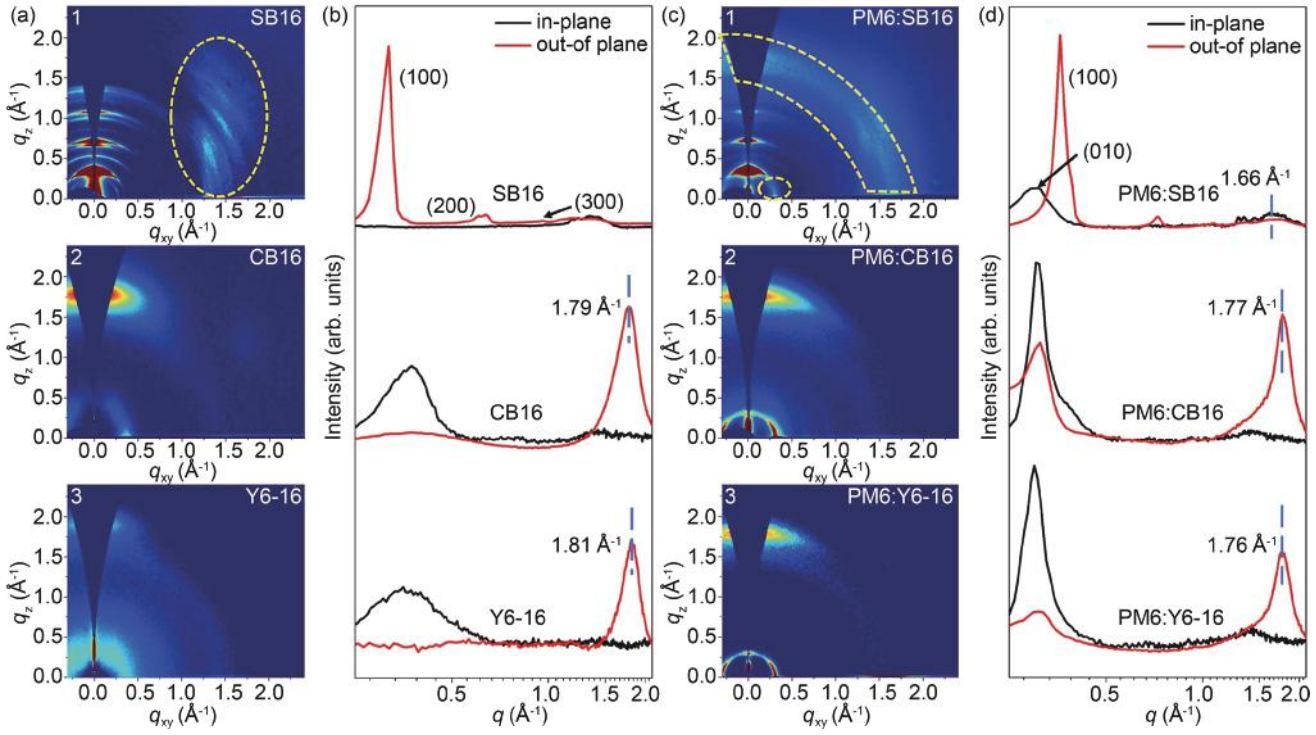

Fig. 2: 2D GIWAXS patterns of the SB16 (a-1), CB16 (a-2), and Y6-16 (a-3) and their blended films PM6:SB16 (c-1), PM6:CB16 (c-2), and PM6:Y6-16 (c-3) and their corresponding 1D scattering profiles along the in-plane and out-of-plane directions for the neat films (b) and blended films (d), respectively. [Reproduced from Ref. 3]

slightly reduced donor–acceptor interactions due to the presence of the Tz unit. In device studies, CB16, when blended with PM6, achieved a remarkable PCE of 18.32% in binary OPV devices, surpassing both those of Y6-16 and SB16. The enhanced performance of CB16 is attributed to its optimized molecular packing, reduced aggregation, and efficient charge transport properties. By removing the Tz unit, CB16 not only simplifies molecular design but also balances structural simplicity with high performance, making it a promising candidate for scalable OPV applications. The contrast in performance between CB16 and SB16 underscores the critical role of molecular geometry, with the C-shaped architecture of CB16 and Y6-16 offering significant advantages over the S-shaped design.

In summary, this study provides insights into the structure–property–performance relationships of NFAs. The C-shaped A-DNBND-A skeleton in CB16 plays a crucial role in promoting efficient π–π stacking, reducing aggregation, and enhancing donor–acceptor interactions. The removal of the Tz unit simplifies synthesis while improving phase separation and charge transport, demonstrating the potential for designing high-performance NFAs with reduced complexity. Furthermore, advanced synchrotron-based characterization techniques such as GIWAXS and SWAXS at **TLS 23A1** proved invaluable for revealing the molecular packing behaviors and guiding rational molecular design. By leveraging rational sample design and state-of-the-art characterization methods, this study not only advances the understanding of NFAs but also paves the way for future innovations in OPVs. The findings emphasize the importance of integrating molecular design, structural analysis, and device optimization to overcome limitations in existing NFAs. (Reported by Hao Ming Chen, National Taiwan University)

This report features the work of Yen-Ju Cheng and U-Ser Jeng published in J. Am. Chem. Soc. ***146****, 833 (2024).*

TLS 23A1 Small/Wide Angle X-ray Scattering

- GIWAXS, GISAXS
- Materials Science, Thin-film Chemistry

References

1. C. Yan, S. Barlow, Z. Wang, H. Yan, A. K. Y. Jen, S. R. Marder, X. Zhan, Nat. Rev. Mater. **3**, 18003 (2018).
2. G. Zhang, F. R. Lin, F. Qi, T. Heumüller, A. Distler, H.-J. Egelhaaf, N. Li, P. C. Y. Chow, C. J. Brabec, A. K.-Y. Jen, H.-L. Yip, Chem. Rev. **122**, 14180 (2022).
3. Y.-J. Xue, Z.-Y. Lai, H.-C. Lu, J.-C. Hong, C.-L. Tsai, C.-L. Huang, K.-H. Huang, C.-F. Lu, Y.-Y. Lai, C.-S. Hsu, J.-M. Lin, J.-W. Chang, S.-Y. Chien, G.-H. Lee, U-Ser Jeng, Y.-J. Cheng, J. Am. Chem. Soc. **146**, 833 (2024).

Advancing the Frontiers of Near-Infrared Optoelectronics

Innovative approaches advance NIR emission technologies by improving their quantum efficiency, energy transfer, and thermal stability.

The field of near-infrared (NIR) optoelectronics has emerged as a critical area of innovation driven by the increasing demand for high-performance materials and devices across diverse applications, from bioimaging and sensing to advanced communication systems. Researchers have actively striven to overcome fundamental challenges such as low quantum efficiencies, energy loss, and thermal instability. The development of novel materials and device architectures has emerged as a cornerstone of progress in this domain. This highlight presents two pioneering studies that exemplify the synergy of materials sciences, photophysics, and engineering in advancing NIR technologies.

Traditional organic light-emitting diodes (OLEDs) in the NIR range have faced challenges related to low external quantum efficiencies (EQEs). This issue is caused by the emission energy gap law, which results in significant nonradiative losses as emission wavelengths extend into the infrared spectrum. This limitation often leads to inefficiencies that hinder the practical implementation of NIR OLEDs in fields such as bioimaging, data communication, and advanced sensing. To overcome these barriers, a collaborative research group led by Yun Chi (City University of Hong Kong, China) and Pi-Tai Chou (National Taiwan University) has introduced an innovative bilayer device architecture incorporating Pt(II) complexes and fluorescent dyes such as BTP-eC9.[1] The components of the architecture are engineered to form a synergistic donor–acceptor system. By leveraging interfacial energy-transfer mechanisms, this architecture achieves hyperfluorescence with peak emissions at 925 nm and EQEs of 2.24%, setting a new benchmark in the field. Additionally, the integration of a transfer printing method preserves the integrity of delicate molecular assemblies, ensuring efficient energy transfer and device stability. A grazing-incidence wide-angle X-ray scattering (GIWAXS) analysis performed at **TLS 13A1** revealed that the Pt(II) complexes in the OLED architecture exhibited highly ordered edge-on π–π stacking, which is crucial for efficient energy transfer. The BTP-eC9 fluorescent dye displayed lamellar-type face-on π–π stacking, which is also important for its function as an energy acceptor and emitter, facilitating the interfacial energy transfer mechanisms. Thus, the Pt(II) complexes act as highly efficient energy donors, transferring triplet-state energy to the singlet-state acceptors (BTP-eC9) *via* a Förster resonance energy transfer (FRET) mechanism, as demonstrated in **Fig. 1**. This process bypasses nonradiative loss channels, enhancing fluorescence intensity. A bilayer architecture with precise control over material interfaces minimizes back energy transfer and maintains structural order. The implementation of transfer printing addresses the challenge of assembling self-organized layers while maintaining their molecular arrangement, demonstrating the potential for large-scale manufacturing. This research not

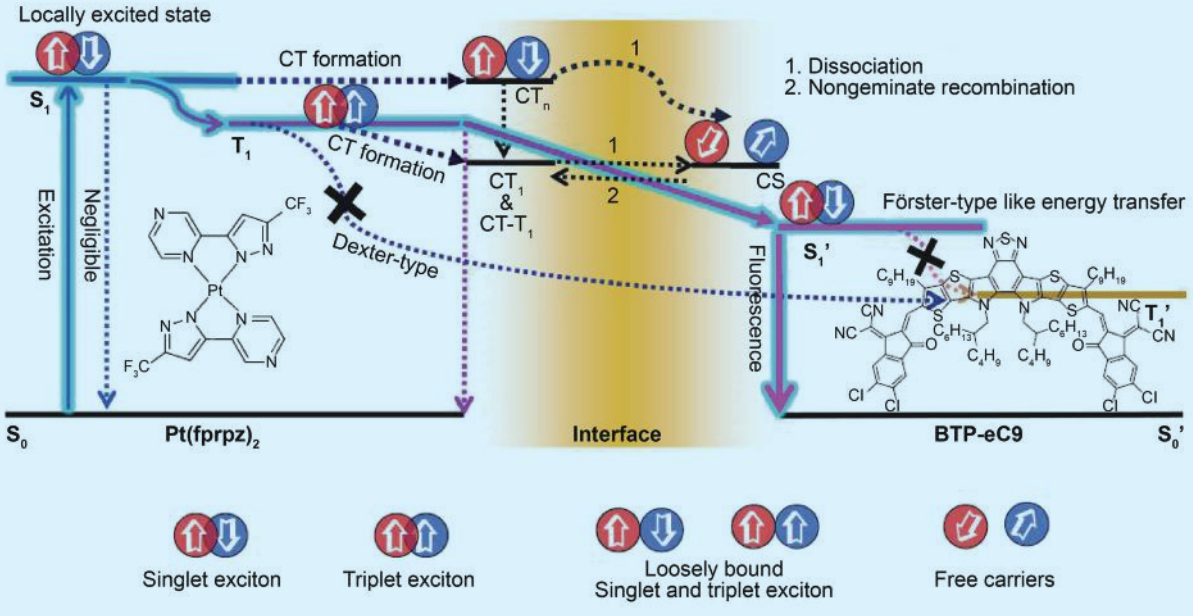

Fig. 1: An overview of the interfacial energy transfer dynamics that underpin NIR OLED functionality: the solid sky-blue pathway illustrates the interfacial energy-transfer process, which facilitates FRET. In this context, the S_0 and S_1 states represent the ground and excited states, respectively, of the singlet manifold, and the T_1 state denotes the triplet state. [Reproduced from Ref. 1]

only demonstrates a leap in device performance but also establishes a robust framework for tackling the inherent limitations imposed by the emission energy gap law.

The second significant research contribution comes from Sebastian Mahlik of the University of Gdansk, Poland, focusing on inorganic materials, specifically, Ga–In oxides doped with Cr^{3+} ions.[2] This study investigates the dual-purpose functionality of these materials as NIR phosphors for light-emitting diodes (LEDs) and ultraviolet photodetectors. The research examines the intricate interplay between radiative and nonradiative processes, emphasizing luminescence-quenching mechanisms. Cr^{3+}-activated materials have attracted significant attention for their ability to emit broadband NIR light, positioning them as ideal candidates for phosphor-converted LEDs. However, traditional interpretations of luminescence quenching often fail to explain the unique thermal behaviors observed in these systems. This study presents a novel perspective by attributing luminescence quenching to hole-based thermal ionization rather than electron transfer to the conduction band—a paradigm shift in understanding transition-metal-doped luminescent materials. High-resolution synchrotron X-ray diffraction (XRD) data, obtained at **TPS 19A**, revealed that Ga–In oxide samples predominantly exhibit a monoclinic β-Ga_2O_3 structure. Increasing indium (In^{3+}) doping levels led to the coexistence of two phases: the monoclinic β-Ga_2O_3 phase and the cubic In_2O_3 phase. This phase separation underscores the limited solubility of In^{3+} in the Ga_2O_3 host lattice and the structural changes induced by In^{3+} substitution. Greater indium concentrations introduced more disorder into the crystal lattice, as evidenced by the broadening of peaks in diffraction patterns and the appearance of mixed phases at higher doping levels. This disorder affected the local crystal field around Cr^{3+} dopants, significantly influencing their optical and photoelectric properties.

The study presents a groundbreaking hole-based thermal quenching mechanism, which challenges the conventional focus on electron transfer. This mechanism accounts for the material's luminescence behavior at elevated temperatures. The $Ga_{1.98-x}In_xO_3$:$0.02Cr^{3+}$ system exhibits tunable NIR emission and efficient photocurrent generation, rendering it suitable for both light emission and detection applications. By combining high-resolution synchrotron XRD with photoluminescence analysis, the research links In-induced structural modifications to enhanced optical performance. The substitution of In^{3+} ions alters the crystal field environment, optimizing energy level alignments for NIR emission and expanding the material's functionality in optoelectronic applications.

Together, these studies provide a comprehensive exploration of the challenges and solutions shaping the future of NIR optoelectronics. The meticulous research on OLEDs emphasizes the importance of molecular precision and device architecture, whereas the insights into Cr^{3+}-activated materials highlight the interplay between structure, energy dynamics, and multifunctionality. By connecting organic and inorganic systems, this compilation highlights the shared principles that underpin success in the field: innovation in material design, rigorous characterization, and a vision for translational impact. (Reported by Yu-Jong Wu)

This report features the work of Yun Chi, Pi-Tai Chou and their collaborators published in Nat. Commun. ***15****, 4664 (2024), and the work of Sebastian Mahlik and his collaborators published in JACS* ***146****, 22807 (2024).*

TPS 19A High-resolution Powder X-ray Diffraction
TLS 13A1 X-ray Scattering

- GIWAXS, XRD
- Materials Science, Inorganic Chemistry, Solid-state Chemistry, Photoluminescence

References

1. C.-M. Hung, S.-F. Wang, W.-C. Chao, J.-L. Li, B.-H. Chen, C.-H. Lu, K.-Y. Tu, S.-D. Yang, W.-Y. Hung, Y. Chi, P.-T. Chou, Nat. Commun. **15**, 4664 (2024).
2. N. Majewska, M.-H. Fang, Sebastian Mahlik, JACS **146**, 22807 (2024).

Light-Activated Gel: Paving the Way for Smarter Electronics

A novel light-responsive gel combining MXene nanosheets with supramolecular complexes was investigated, showcasing reversible phase transitions and enhanced conductivity.

MXenes are a rapidly emerging class of two-dimensional (2D) materials that have garnered significant attention in materials science due to their unique properties and broad applications. First discovered in 2011, MXenes are synthesized by selectively etching out elements from layered transition metal carbides, nitrides, or carbonitrides. MXenes exhibit a unique combination of metallic conductivity, excellent mechanical flexibility, high surface area, and tunable surface chemistry. These attributes make them highly promising for various applications, including energy storage, electromagnetic interference, water purification, and catalysis. The research team led by Jiun-Tai Chen from National Yang Ming Chiao Tung University explored conductive composite gels with multifunctional capabilities. By incorporating inorganic dopants into an organic matrix, the gel's conductivity can be significantly improved while introducing new properties such as thermal responsiveness, light responsiveness, and self-healing abilities.

The research team studied a light-responsive MXene-based composite gel, termed MXenegel, which integrates azobenzene-containing supramolecular complexes with MXene nanosheets (**Fig. 1**).[1] This innovative material exhibits reversible photo-modulated phase behavior, transitioning between liquid and solid states under UV and visible light, respectively, while maintaining its electrical conductivity, making it suitable for traditional solid-state electronics. The motivation behind this research stems from the need for intelligent and eco-friendly electronic components that can adapt to environmental changes and promote sustainability. Traditional solid-state materials often lack compatibility with dynamic substrates, such as human skin, and do not respond to environmental stimuli. The MXenegel addresses these challenges by providing a new charge transport pathway that can sense environmental changes and be reprogrammed or recycled.

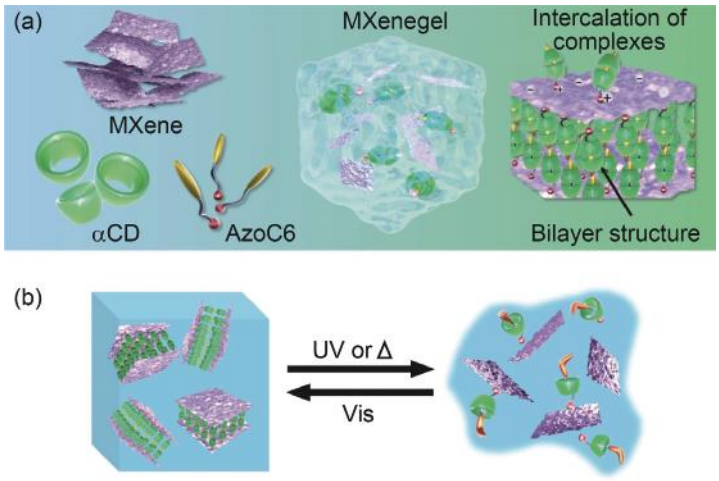

Fig. 1: Schematic illustration of the light-responsive MXenegel. (a) αCD and AzoC6 form a bilayer structure of AzoC6@2αCD supramolecular complexes in MXenes. The positive head ends of the complexes are electrostatically attached to the negatively charged MXene surfaces. (b) Light-responsive sol–gel transition behavior of the MXenegel. [Reproduced from Ref. 1]

Multiple instruments were used in this work, providing spectroscopical and electronic evidence to support the unique behavior of MXenegel. The MXenegel was shown to undergo a gel-to-sol transition upon UV light irradiation, which is attributed to the disassembly of the AzoC6@2αCD inclusions intercalated between the MXene layers. This phase transition is reversible, as the sol-state MXenegel can be converted back to a gel-like structure under visible light irradiation or by keeping it in a dark room at room temperature. Additionally, the X-ray diffraction spectra performed at **TLS 23A1** of the NSRRC played an important role in this research. The small-angle X-ray scattering (SAXS) spectra revealed the microstructural details of MXenegel, confirming the successful formation of the AzoC6@2αCD inclusion complexes and their intercalation between MXene layers (**Fig. 2**).

In summary, this work shows a light-modulated MXenegel with reversible phase transition based on photoresponsive host–guest chemistry. Detailed NMR, 2D-ROESY, XPS, and X-ray scattering analyses obtained from synchrotron facilities revealed the microstructure of the MXenegel. The potential applications of MXenegel in electronic circuitry are diverse and promising. The material could serve as a light-responsive wire in electronic circuits, enabling its integration into solid-state electronics

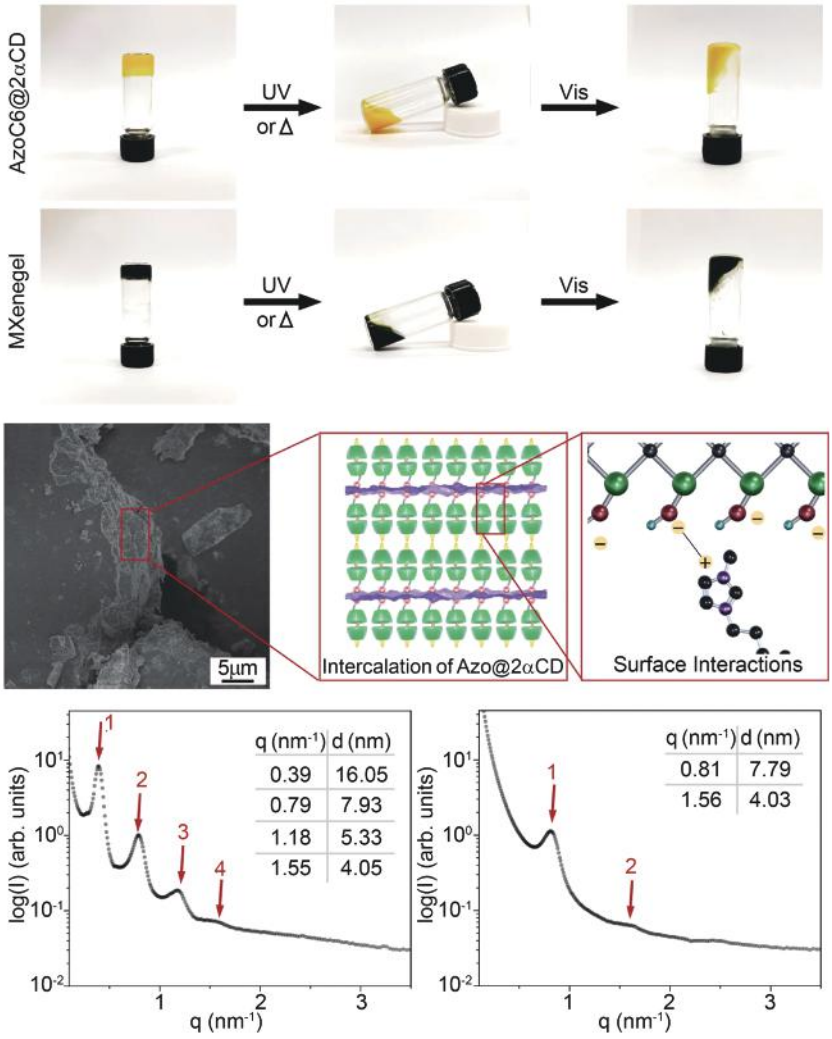

Fig. 2: Light-responsive phase behavior of AzoC6@2αCD and 30 wt% MXenegel under different light irradiations. SEM images of the vacuum-dried MXenegel, in which a cross-sectional view of the MXenegel layers is displayed. The maxima are indicated in the SAXS spectra of AzoC6@2αCD hydrogel and MXenegel. [Reproduced from Ref. 1]

as conductive wires or switches. This material demonstrates a reversible photo-modulated phase behavior, allowing it to function as a photo-controllable switch, which can be utilized to control devices like LEDs. Additionally, MXenegel can be used as a writable and reconfigurable conductive ink, making it suitable for brush printing on various substrates, thus expanding its application in flexible and eco-friendly electronics. (Reported by Yu-Liang Lin, National Yang Ming Chiao Tung University)

This report features the work of Jiun-Tai Chen and his collaborators published in Nat. Commun. ***15****, 916 (2024).*

TLS 23A1 Small/Wide Angle X-ray Scattering

- Supramolecular Complex Scattering
- Materials Science, Chemistry, Surface, Thin-film Technology, Chemical Kinetics

Reference

1. Y.-L. Lin, S. Zheng, C.-C. Chang, L.-R. Lee, J.-T. Chen, Nat. Commun. **15**, 916 (2024).

Versatile Roles of Cesium

Cs-promoted Ru catalysts play a key role in enhancing efficient ammonia synthesis.

Ammonia synthesis is a cornerstone of the global chemical industry as it is essential for fertilizer production and is increasingly recognized as a potential hydrogen carrier for renewable energy applications.[1] However, the conventional Haber–Bosch (HB) process requires high temperatures and pressures, leading to substantial carbon emissions and energy consumption.[2] In the pursuit of more sustainable and energy-efficient catalytic systems, research teams led by Shih-Yuan Chen (National Institute of Advanced Industrial Science and Technology, Japan), Hsin-Yi Tiffany Chen (National Tsing Hua University), Ho-Hsiu Chou (National Tsing Hua University), and Chia-Min Yang (National Tsing Hua University) investigate the impact of carbon support graphitization on the activity and stability of cesium (Cs)-promoted ruthenium (Ru) catalysts for ammonia synthesis. By systematically tuning the graphitization degree of mesoporous carbon plates (MCPs), this study provides fundamental insights into the relationship between carbon support structure, Ru dispersion, and catalytic performance.

The research introduces a series of Ru catalysts supported on MCPs with varying degrees of graphitization, synthesized through controlled carbonization. MCP-1100, which possesses the highest degree of graphitization, emerges as the optimal support, offering superior thermal stability, enhanced electron conductivity, and minimized carbon methanation. **Figure 1(a)** illustrates that higher carbonization temperatures lead to increased graphitic ordering, further validated by high-angle annular dark-field scanning transmission electron microscopy images. These images reveal well-dispersed Ru nanoparticles on MCP-1100 (**Fig. 1(b)**). By contrast, catalysts supported on lower-graphitization-degree MCPs exhibit Ru particle agglomeration, which negatively impacts catalytic efficiency. The catalytic performance evaluation, presented in **Fig. 1(c)**, demonstrates that the Cs-promoted Ru/MCP-1100 catalyst achieves an ammonia synthesis rate of 43 mmol $NH_3 \cdot g^{-1} \cdot h^{-1}$ at 410 °C under ambient pressure, significantly outperforming conventional Fe-based catalysts under the similar conditions. These results indicate a strong correlation between the degree of graphitization and ammonia synthesis rates, with higher graphitization promoting better Ru dispersion and electronic conductivity. The critical role of cesium promotion is further supported by density functional theory (DFT) calculations (**Fig. 1(d)**), which show that CsOH weakens hydrogen adsorption on Ru, facilitating ammonia formation by accelerating hydrogen desorption. This cooperative effect between Ru and Cs enhances catalytic efficiency by promoting the crucial dissociative adsorption of N_2 while preventing catalyst deactivation.

A major highlight of this study is the application of *in situ* X-ray absorption spectroscopy (XAS) at **TLS 01C1** for the Ru K-edge and **TLS 17C1** for the Cs L_3-edge, along with near-ambient-pressure X-ray photoelectron spectroscopy (NAP-XPS) at **TLS 24A1**. These techniques provide real-time insights into the electronic and structural evolution of Ru and Cs species

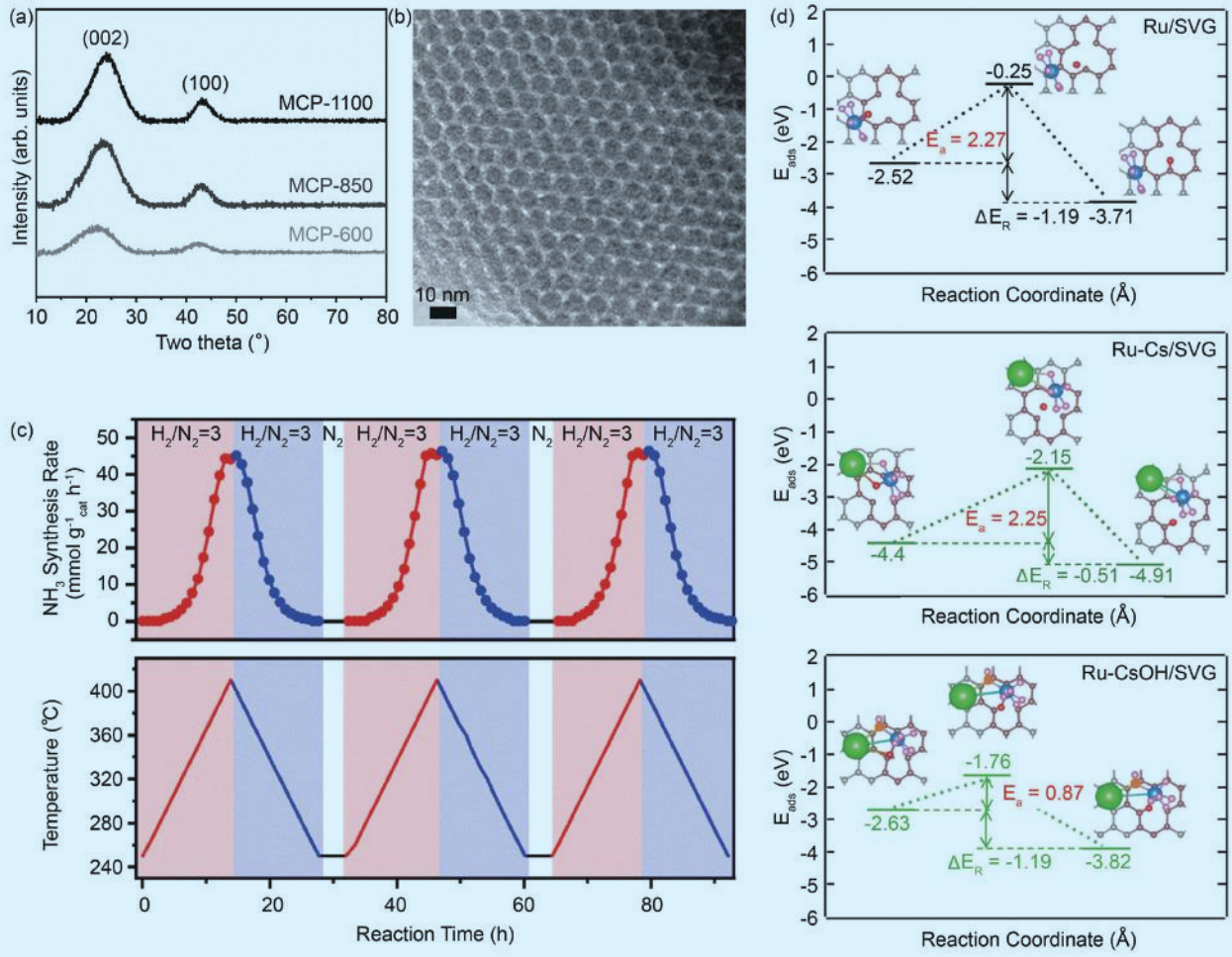

Fig. 1: (a) Wide-angle Powder X-ray Diffraction profiles of MCP-600, MCP-850, and MCP-1100. (b) TEM image of MCP-1100. (c) Temperature dependence of ammonia synthesis rate over 2.5Cs-10Ru/MCP-1100 under intermittent operating conditions. (d) Reaction coordinate diagram of hydrogen spillover from a Ru atom to single-vacancy graphene (SVG) in Ru/SVG, Ru–Cs/SVG, and Ru–CsOH/SVG models with hydrogen saturated at a Ru/H ratio of 1:6. Ea refers to the activation energy for hydrogen spillover from non-spillover models to spillover models through transition states (structures shown on the left, right, and middle in each image, respectively). ΔE_R refers to the reaction energy between non-spillover and spillover models. Blue, Ru; pink, H; red, spilled-over H; green, Cs; orange, O; gray, C atom away from the C point defect; brown, C atom close to the C point defect. [Reproduced from Ref. 3]

under various reaction conditions. **Figure 2** presents *in situ* X-ray absorption near-edge structure (XANES) and NAP-XPS spectra, which reveal a dynamic transformation of cesium species from CsOH to metallic Cs^0 during the reaction. This transformation, facilitated by hydrogen spillover from Ru sites, enhances the electron-donating ability of Ru, reducing hydrogen poisoning and increasing N_2 activation. The XAS and NAP-XPS results confirm that Cs^0 acts as an electronic promoter, effectively modifying the electronic structure of Ru to boost NH_3 synthesis rates.

In summary, this study establishes that Ru nanoparticle size, Cs/Ru ratio, and the degree of graphitization critically influence NH_3 synthesis rates and resistance to carbon methanation. By leveraging *in situ* XAS, NAP-XPS, kinetic analyses, and theoretical modeling, this work provides a real-time mechanistic understanding of how Cr species dynamically enhance Ru's catalytic performance. The findings establish a new design paradigm for next-generation ammonia synthesis catalysts, offering a scalable and energy-efficient alternative to conventional HB catalysts while mitigating carbon emissions. These insights contribute to the ongoing transition toward sustainable and low-carbon chemical manufacturing. (Reported by Hao Ming Chen, National Taiwan University)

This report features the work of Chia-Min Yang, Ho-Hsiu Chou, Hsin-Yi Tiffany Chen and Shih-Yuan Chen published in Appl. Catal. B-Environ. ***346****, 123725 (2024).*

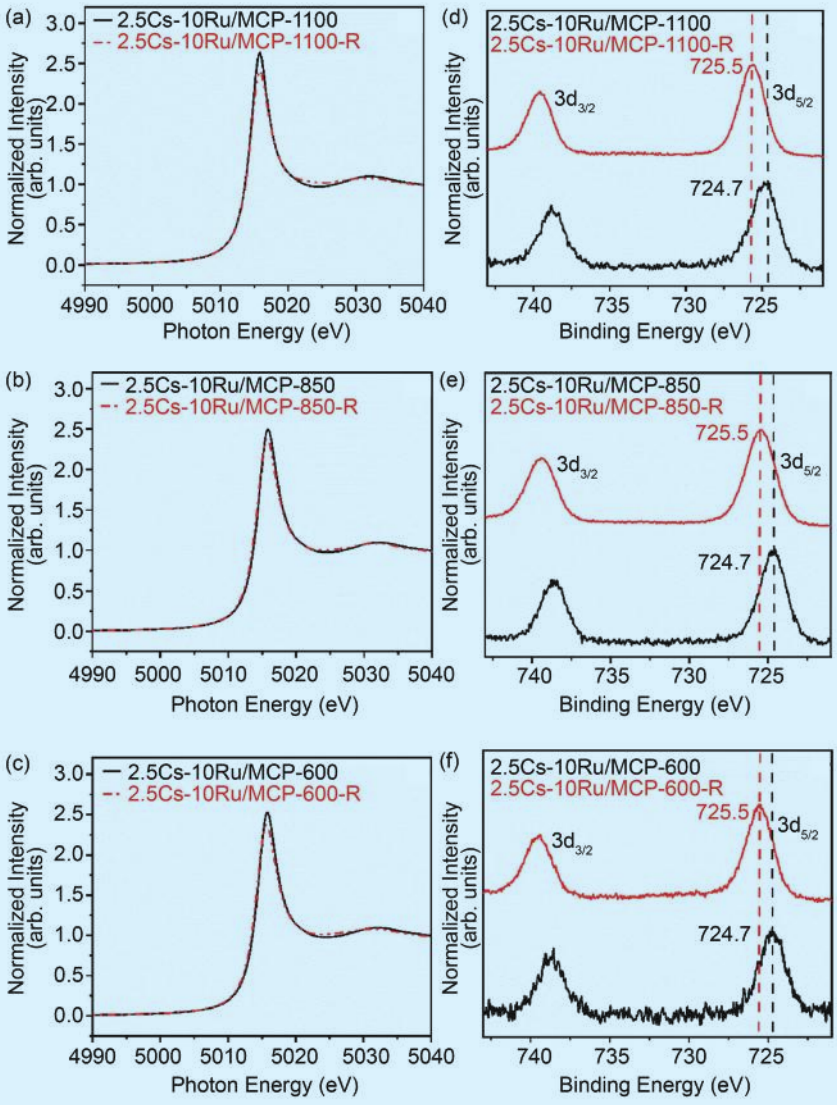

Fig. 2: Results of *in situ* XAS and NAP-XPS measurements. (a–c) XANES spectra at the Cs L_3-edge, and (d–f) NAP-XPS profiles of the Cs 3d region. [Reproduced from Ref. 3]

TLS 01C1 EXAFS
TLS 17C1 EXAFS
TLS 24A1 XPS, UPS, XAS, APXPS

- *In situ* XAS, NAP-XPS
- Materials Science, Ammonia Synthesis

References

1. S. Giddey, S. P. S. Badwal, C. Munnings, M. Dolan, ACS Sustain. Chem. Eng. **5,** 10231 (2017).
2. F. Schüth, R. Palkovits, R. Schlögl, D. S. Su, Energy Environ. Sci. **5**, 6278 (2012).
3. S.-Y. Chen, L.-Y. Wang, K.-C. Chen, C.-H. Yeh, W.-C. Hsiao, H.-Y. Chen, M. Nishi, M. Keller, C.-L. Chang, C.-N. Liao, T. Mochizuki, H.-Y. T. Chen, H.-H. Chou, C.-M. Yang, Appl. Catal. B-Environ. **346**, 123725 (2024).

Illuminating the Cosmic Laboratory with Vacuum Ultraviolet Light

Exploring the origin and evolution of interstellar and circumstellar molecules enhances our understanding of the Universe.

In the vast expanse of the cosmos, scientists are continuously uncovering secrets that bridge the gap between stars and the building blocks of life. Among these pursuits, three recent studies used the vacuum ultraviolet (VUV) beamlines of the Taiwan Light Source (TLS) to illuminate intriguing connections between interstellar chemistry, materials science, and the potential origins of life. These stories unfold like chapters in a grand cosmic narrative, each offering a glimpse into the intricate dance of molecules and light in the universe.

The first story begins with ethanolamine, a simple molecule with profound implications. Known as a precursor to amino acids, ethanolamine has the potential to unveil how the building blocks of life might have formed in the harsh environments of space. A joint research group led by Bhalamurugan Sivaraman from Physical Research Laboratory of India, delved into its mysteries by recreating astrochemical conditions in the laboratory. Using advanced spectroscopy, they probed the spectral fingerprints of this molecule, capturing the behavior of ethanolamine ice as it is warmed from frigid interstellar temperatures.[1] Infrared and VUV spectroscopy provided critical insights, revealing how the molecule interacts with ultraviolet photons and sublimates as it transitions to higher temperatures. The end station connected to **TLS 03A1** employed ultrahigh vacuum chambers to mimic interstellar conditions, with ethanolamine deposited on cryogenically cooled substrates. These setups allowed for precise control of temperature and environment, ensuring that the behavior of the molecule could be observed without interference. Coupled with computational models, this work pieced together plausible pathways for the molecule's formation on cosmic dust grains, providing a roadmap for future discoveries of prebiotic chemistry in the cosmos.

Next, their focus shifted to 1-propanol, a fatty alcohol that holds the potential to shed light on the origins of proto-cell membranes. The tale of 1-propanol is one of resilience, as experiments revealed its unusual stability in the icy realms of the interstellar medium. Despite warming beyond its melting point, this molecule defied expectations, remaining amorphous and adhering to simulated dust grain surfaces.[2] Mid-infrared spectroscopy was again employed to trace the molecular vibrations of 1-propanol across a range of temperatures, while VUV spectroscopy captured its absorption characteristics in the 115–220 nm range, as shown in **Fig.1**. Using a cryostat system with LiF windows and controlled heating rates, researchers meticulously documented the phase transitions and sublimation behavior of 1-propanol. The VUV spectra of 1-propanol were recorded well beyond its melting point of 147 K, demonstrating that the solid-state sample remained amorphous throughout the warming process, from 10 K to 175 K, until sublimation. This represents the first observation of a molecule persisting on a cold substrate beyond its melting point in a UHV chamber. In contrast, 2-propanol, a positional isomer of 1-propanol, exhibits entirely different behavior: it crystallizes at approximately 120 K and sublimates at 150–155 K, prior to reaching its melting point. Mid-infrared spectroscopy was again employed to trace the molecular vibrations of 1-propanol across a range of temperatures, while vacuum ultraviolet spectroscopy captured its absorption characteristics in the 115–220 nm range. Complementing these experiments, molecular dynamics simulations unravelled the microscopic interactions between the alcohol molecules, offering a new perspective on the complexity of icy mantles in space. This surprising discovery challenges conventional ideas about the phase behavior of interstellar ices and expands our understanding of the molecular diversity in space.

Meanwhile, a different kind of light emerged from the depths of the Red Rectangle Nebula—a mysterious blue luminescence (BL). This glow had puzzled scientists for decades, with its origins tied to the enigmatic interplay of polycyclic aromatic hydrocarbons. BL is characterized by

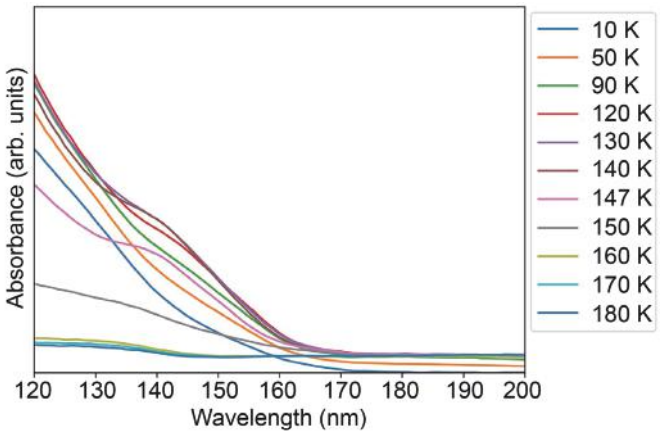

Fig. 1: VUV spectra of 1-propanol ice recorded after deposition at 10 K. The deposited ice was then warmed to higher temperatures and spectra recorded at specific temperatures until sublimation. [Reproduced from Ref. 2]

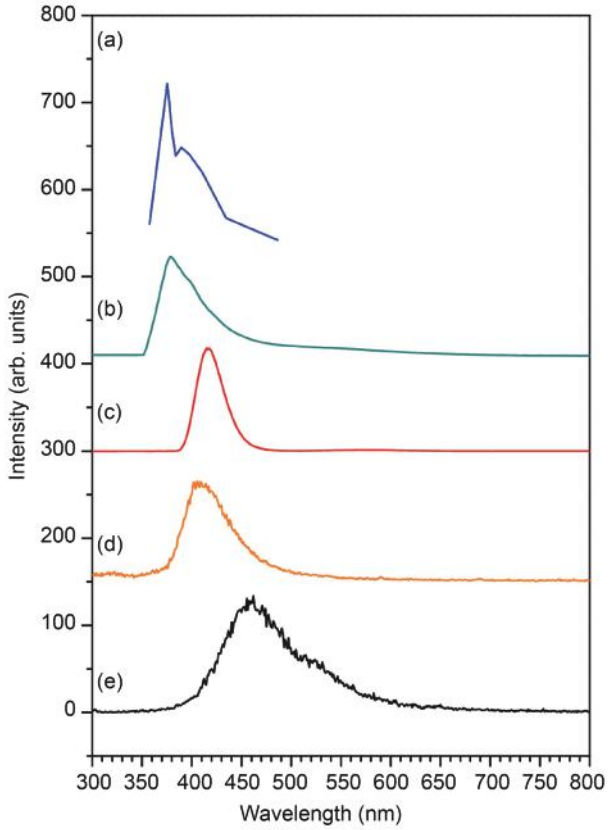

Fig. 2: (a) Blue luminescence recorded in the Red Rectangle Nebula,[4] and PL spectra measured at 10 K upon excitation with 121.6 nm for (b) photochemically N_2-covered graphene, (c) photochemically O_2-covered graphene, (d) commercial N-doped graphene flakes, and (e) commercial graphene oxide flakes. [Reproduced from Ref. 3]

an asymmetrical spectral band peaking around 375–378 nm in the ultraviolet and visible regions. Its discovery in astrophysical environments such as the Red Rectangle Nebula links it to aromatic compounds and quantum effects in interstellar dust. In a breakthrough study,[3] Y.-J. Wu (NSRRC) and his collaborators turned to graphene, a material as versatile as it is remarkable. By doping graphene with nitrogen atoms and exposing it to VUV light, they recreated conditions that echoed the astrophysical environments where BL thrives. The experimental setup involved single-layer graphene films, covered by a few layers of N_2 or O_2 solids and mounted on MgF_2 substrates, which were then cooled to 10 K and exposed to intense VUV light at 121.6 nm at **TLS 21A2**. Photoluminescence spectroscopy revealed a peak at 378 nm, closely matching the BL spectra recorded in the Red Rectangle Nebula, as shown in **Fig. 2**. Further analysis using Raman spectroscopy and X-ray photoelectron spectroscopy identified the structural defects and pyrrolic-N and pyridinic-N groups in the graphene lattice responsible for the luminescence. These defects disrupt the carbon network's symmetry, introducing localized electronic states that emit the characteristic blue light when excited. This study established N-doped graphene as a potential carrier of BL observed in astrophysical environments.

Together, these studies weave a rich tapestry of discovery, connecting laboratory experimentation with the mysteries of the universe. They remind us that the smallest molecules, whether in icy grains or luminous nebulae, hold the power to unlock profound insights into our cosmic origins. As scientists continue to explore these molecular frontiers, the stories of ethanolamine, 1-propanol, and N-doped graphene serve as beacons, guiding us toward a deeper understanding of the molecular universe and our place within it. (Reported by Yu-Jong Wu)

This report features the work of Bhalamurugan Sivaraman and his collaborators published in Astrophys. J. ***975****, 181 (2024) and MNRAS* ***530****, 1027 (2024), and the work of Yu-Jong Wu and his collaborators published in Astrophys. J.* ***977****, 230 (2024).*

TLS 03A1 High-flux VUV Beamline
TLS 21A2 VUV Photochemistry

- Photoabsorption, Photoluminescence
- Astrochemistry, Molecular Science

References

1. R. Ramachandran, M. Sil, P. Gorai, J. K. Meka, P. Sundararajan, J.-I. Lo, S.-L. Chou, Y.-J. Wu, P. Janardhan, B.-M. Cheng, A. Bhardwaj, V. M. Rivilla, N. J. Mason, B. Sivaraman, A. Das, Astrophys. **975**, 181 (2024).
2. R. Ramachandran, A. Hazarika, S. Gupta, S. Nag, J. K. Meka, T. S. Thakur, S. Yashonath, G. Vishwakarma, S.-L. Chou, Y.-J. Wu, P. Janardhan, B. N. Rajasekhar, A. Bhardwaj, N. J. Mason, B. Sivaraman, P. K. Maiti, MNRAS **530**, 1027 (2024).
3. S.-Y. Lin, S.-L. Chou, T.-P. Huang, M.-Y. Lin, H.-F. Chen, P. J. Sarre, C.-M. Tseng, Y.-J. Wu, Astrophys. J. **977**, 230 (2024).
4. U. P. Vijh, A. N. Witt, K. D. Gordon, Astrophys. J. Lett. **606**, L65 (2004).

Soft Matter

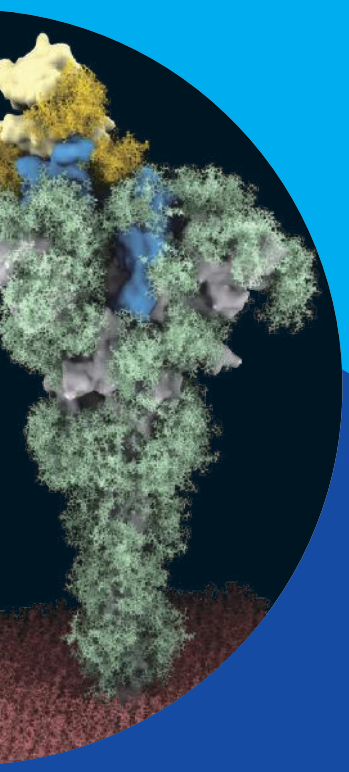

Soft-matter science covers a diverse range of materials, including polymers, colloids, liquid crystals, biomacromolecules, and self-assembled systems. These materials exhibit hierarchical structures and dynamic behaviors that require advanced characterization techniques to unravel their complex properties. Synchrotron radiation provides powerful tools for probing soft matter at multiple length scales, offering high-resolution insights into their structure, interactions, and functional properties.

Several beamlines are dedicated to soft-matter research at the Taiwan Photon Source (TPS) and Taiwan Light Source (TLS). **TPS 13A** biological small-angle X-ray scattering (BioSAXS) enables structural analysis of biomacromolecules in solution. **TPS 44A** quick-scanning X-ray absorption spectroscopy provides element-specific insights into local electronic and atomic structures. **TLS 23A1** small/wide-angle X-ray scattering facilitates the characterization of hierarchical architectures in polymers, biomaterials, and nanostructured systems.

This section presents four recent studies that demonstrate the versatility of synchrotron techniques in soft-matter research. The first study investigated glycoprotein structures by using **TPS 13A** BioSAXS combined with computational modeling to characterize the conformational properties of highly glycosylated proteins. The findings offer insights into glycan-mediated interactions and their role in biological functions. The second study explored centrosome regulation during cell division, focusing on the phase separation of Cep57 and its role in microtubule nucleation. **TPS 13A** BioSAXS helped elucidate the molecular mechanisms governing centrosomal organization and its impact on cellular processes.

The third study examined the aqueous-phase crystallization of metal–organic frameworks, with **TPS 13A** *in situ* SWAXS providing real-time tracking of nucleation and growth mechanisms. The results revealed how biomolecules influence framework formation, shedding light on biomimetic strategies for sustainable material synthesis. The fourth study focused on the stabilization of single platinum atoms within silicate nanochannels for enhanced catalytic efficiency. **TPS 44A** X-ray absorption spectroscopy was used to confirm atomic coordination environments, while **TLS 23A1** and **TPS 13A** were utilized to aid analysis of the hierarchical structure and dispersion of Pt atoms.

These studies exemplify how synchrotron-based techniques enable a deeper understanding of soft-matter systems, providing essential structural and functional insights. The ability to probe nanoscale architectures with high precision continues to drive advances in biomaterials, catalysis, and fundamental science, paving the way for future discoveries and technological applications. (by Orion Shih)

Advancing Glycoprotein Insights: Bridging Glycobiology and Structural Biology

Protein glycosylation is integral in biology; however, quantitative annotation of the structure-function relationship of glycosylation is challenging. This article reports the findings of an interdisciplinary and international team formed to tackle this challenge.

The surfaces of cells and viruses are often coated with a thick layer of sugar (also known as glycans), presenting a challenge for identifying specific proteins or biomolecules within this complex environment. In nature, however, efficient biomolecular interactions take place within this forest of glycans. Most extracellular proteins are post-translationally modified by glycans with varying sizes and complexity. The masking effect of these glycans allows bacteria and viruses to evade recognition and attack by the host immune system.

Structural biology focuses on providing pivotal structural information at an atomic resolution to help to understand the mechanisms governing biological functions. Such an underlying principle is also used by the immune system, where antibodies recognize the structural characteristics of foreign substances, such as antigens, to achieve immune protection. Nevertheless, structural biology encounters two technical challenges when examining the intricate structures of protein glycans. First, glycan molecules have a complex chemical composition, and their biosynthesis lacks a one-to-one template. Second, glycans are highly dynamic, making it challenging to accurately define three-dimensional spatial distributions. Therefore, the intrinsic microscopic compositional and conformational heterogeneity presents a fundamental challenge to the accurate modeling of glycan structures.

The research team led by Shang-Te Danny Hsu (Academia Sinica) tried to solve this problem from the structural understanding of protein glycosylation started in 2018 through a collaboration with Hui-Wen Chang at the National Taiwan University and Kay-Hooi Khoo at Academia Sinica. They used cryo-electron microscopy (cryo-EM) to determine the near-atomic structure of the spike protein of a type I feline infectious peritonitis virus (FIPV).[1] They identified an exceptionally well-defined cryo-EM map enabling the modeling of one of the longest N-glycan structures in the literature. The atomic model of the fully glycosylated FIPV spike protein was built manually using the information derived from mass spectrometry (MS) analysis. Nonetheless, the data analysis and model building are laborious and not very quantitative.

To address these issues, they collaborated with Khoo to develop a robust workflow to quantitatively characterize the N-glycosylation profiles of the spike proteins of SARS-CoV-2 variants.[2] They also determined the cryo-EM structures of the same spike proteins, with an emphasis on recovering structural information of glycans. They further collaborated with Cyril Hanus at the Inserm, France, and Mateusz Sikora at the Max Planck Institute of Biophysics, Germany, to develop the computational tool called GlycoSHIELD[3] to integrate the experimental observables with computational modeling to automate the process of model building of glycoproteins (**Fig. 1**). Such a procedure can be accomplished using a personal computer in minutes rather than using a high-performance computing center for full-blown all-atom molecular dynamics simulations of fully glycosylated spike proteins solvated in an explicit solvent model. Additionally, GlycoSHIELD offers predictive powers for identifying potential receptor binding sites and antigenic targets for therapeutic purposes based on the common characteristic that the less-shielded protein surfaces are generally more likely to be used for host receptor binding and targeted by neutralizing antibodies.

Small-angle X-ray scattering (SAXS) is exceptionally versatile in describing protein structures and dynamics in solution. The research team has benefited tremendously from the support of the biological SAXS **TPS 13A** beamline research team at the NSRRC. In the context of GlycoSHIELD, they used SAXS to characterize two highly glycosylated proteins, namely, the extracellular domains (ECDs) of N-cadherin pertinent to cell–cell adhesion and

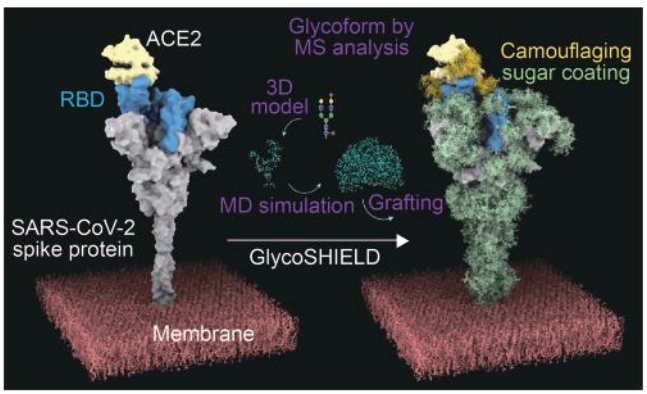

Fig. 1: Schematic overview of the principle of GlycoSHIELD.

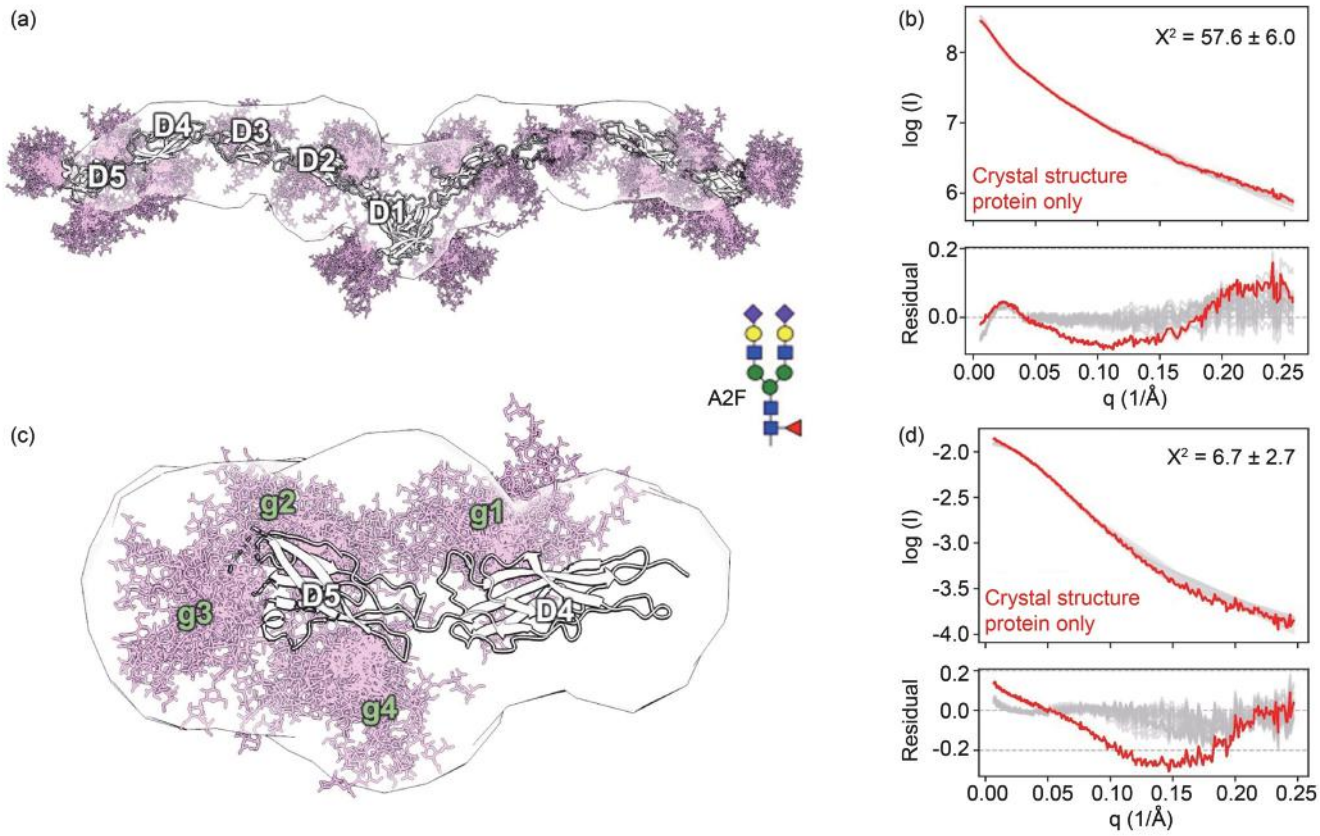

Fig. 2: SAXS analysis of N-cadherin variants. (a) The molecular envelope of N-cadherin ECD 1-5 (D1-D5) in a seagull-like homodimeric assembly. The crystal structure, indicated by a white outline, is modified with a biantennary complex type (A2F) N-glycan in its putative N-glycosylation sites, which are indicated by pink sticks. (b) The experimental SAXS profile is superimposed with the back-calculated SAXS profiles based on the crystal structure (red) and the additional N-glycan structures in 20 different conformations (gray). The residuals are shown below the SAXS profiles. Similar structural representations of the D4 and D5 of N-cadherin are shown in (c), and the corresponding SAXS data analyses are shown in (d). [Reproduced from Ref. 3]

the ECD of the receptor-like protein tyrosine phosphatase (PTPRA), which is crucial for transmitting extracellular signals to trigger intracellular chemical reactions.

N-cadherin is a calcium-binding glycoprotein comprising five folded ECDs (**Fig. 2(a)**). Molecular dynamics simulations have shown that glycosylation is important for maintaining the extension of N-cadherin. However, most of the glycans are removed to solve the crystal structure of N-cadherin, which is an intrinsic issue in protein crystallography. The team used SAXS to demonstrate that the fully glycosylated N-cadherin variants indeed adopt an extended seagull-like dimer structure, which is consistent with the crystallographic finding (**Fig. 2(a)**). By modeling different glycan ensembles onto the putative N-glycosylation sites, they could further improve the agreement between the experimental and back-calculated SAXS profiles based on the atomic ensemble structures. This illustrates how the combination of GlycoSHIELD modeling and experimental SAXS inputs can generate a more realistic glycoprotein conformational ensemble (**Figs. 2(a)–2(d)**).[3]

Structural analysis of highly glycosylated intrinsically disordered proteins represents an even more significant challenge to structural biology. In collaboration with Khoo and his colleagues, they comprehensively profiled the glycosylation of the PTPRA-ECD, which comprises only 120 amino acids with four N-glycosylation sites and over 30 O-glycosylation sites. Using the SAXS data derived from the PTPRA-ECD fused to a dimeric Fc scaffold and GlycoSHIELD, the team generated an ensemble structure with the N- and O-glycans decorating PTPRA-ECD to account for the spatial occupancy by the N- and O-glycans (**Fig. 3**). They further collaborated with Takayuki Uchihashi at Nagoya University in Japan to directly visualize the opening and closing states of the PTPRA-ECD through high-speed molecular force microscopy to confirm the bottlebrush-like molecular envelope of PTPRA-ECD inferred by SAXS. This interdisciplinary exercise underscores the importance of an integrated structural-biology approach to characterize such a highly complex and dynamic system.[4]

The current modeling algorithm of GlycoSHIELD is limited to the steric effect of glycan ensemble structures on the protein of interest. An improved algorithm is required to account for the non-covalent interactions. Furthermore, the compositional heterogeneity of the individual glycosylation sites presents a combinatorial problem of a large number

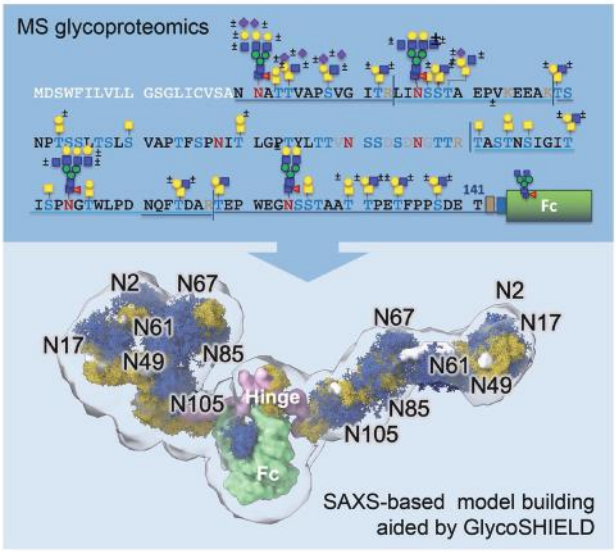

Fig. 3: Integrated structural analysis of the densely N- and O-glycosylated and intrinsically disordered PTPRA-ECD fused to Fc. The representative N- and O-glycoforms derived from MS analysis are shown on the top, and the atomic model of the fully glycosylated protein structure is shown below. The N- and O-glycans are shown in blue and yellow, respectively. The molecular envelope of the Fc-fused PTPRA-ECD is shown on a transparent surface. [Reproduced from Ref. 4]

of overall glycosylation patterns that one should consider when describing the physicochemical properties of the protein of interest at an atomic level. The optimization of GlycoSHIELD's molecular models and experimental observations is necessary to achieve a balance between the computational performance and the completeness of experimental observations while ensuring that the molecular models of glycoproteins comply with the basic laws of physics and chemistry, an area that will require further explorations. (Reported by Shang-Te Danny Hsu, Academia Sinica)

This report features the work of Shang-Te Danny Hsu and his collaborators published in Cell ***187****, 1296 (2024), and the work of Kay-Hooi Khoo and his collaborators published in JACS Au* ***3****, 1864 (2023).*

TPS 13A Biological Small-angle X-ray Scattering

- Biological Small/Wide Angle X-ray Scattering
- Biological Macromolecules, Protein Solution, Life Science

References

1. T. J. Yang, Y. C. Chang, T. P. Ko, P. Draczkowski, Y. C. Chien, Y. C. Chang, K. P. Wu, K. H. Khoo, H. W. Chang, S.-T. D. Hsu, PNAS **117**, 1438 (2020).
2 C. W. Kuo, T. J. Yang, Y. C. Chang, P. Y. Yu, S.-T. D. Hsu, K. H. Khoo, Glycobiology. **32**, 60 (2022).
3. Y. X. Tsai, N. E. Chang, K. Reuter, H. T. Chang, T. J. Yang, S. von Bülow, V. Sehrawat, N. Zerrouki, M. Tuffery, M. Gecht, I. L. Grothaus, L. C. Ciacchi, Y. S. Wang, M. F. Hsu, K. H. Khoo, G. Hummer, S.-T. D. Hsu, C. Hanus, M. Sikora, Cell **187**, 1296 (2024).
4. Y. C. Chien, Y. S. Wang, D. Sridharan, C. W. Kuo, C. T. Chien, T. Uchihashi, K. Kato, T. Angata, T. C. Meng, S.-T. D. Hsu, K. H. Khoo, JACS Au **3**, 1864 (2023).

The Key to Accurate Cell Division: Centrosome Regulation

Cep57 regulates centrosome maturation and microtubule nucleation via phase separation, ensuring accurate cell division.

Liquid–liquid phase separation (LLPS) is a process driven by multivalent interactions among biomolecules, such as proteins and nucleic acids, forming dense, dynamic structures known as biomolecular condensates. Recent evidence supports LLPS as a fundamental organizing principle for membrane-less organelles. The centrosome, consisting of a pair of centrioles surrounded by pericentriolar material (PCM), plays a crucial role in regulating cell division. As cells prepare for mitosis, the centrosome undergoes a maturation process characterized by the expansion of the PCM and an increase in its microtubule nucleation capacity by recruiting centrosomal scaffolding proteins and microtubule nucleation factors. This facilitates the assembly of the mitotic spindle and ensures the precise segregation of chromosomes during mitosis.

Human Cep57 is a coiled-coil scaffold protein located in the inner layer of the PCM and controls the process of centriole duplication and centrosome maturation for faithful cell division. Cep57 truncation mutations are genetically linked to mosaic-variegated aneuploidy syndrome, which features centrosome amplification and aberrant spindle formation. However, the molecular mechanisms by which Cep57 regulates PCM organization and microtubule assembly remain unknown. Phase separation has been implicated in some key centrosomal scaffolds, such as SPD-5 (a human CDK5RAP2 functional homolog) and the Cep63/Cep152 complex. During interphase, Cep57 forms a complex with the middle layer scaffold Cep63 and Cep152, serving as regulators for centrosome maturation. However, it is unclear whether Cep57 undergoes phase separation and how these centrosomal scaffolding components coordinate to organize the centrosome.

To address these questions, the research team led by Hui-Chun Cheng at National Tsing Hua University employed various analytical techniques and successfully demonstrated that Cep57 assembles into micron-sized biomolecular condensates through LLPS driven by multivalent interactions. Blocking multivalent interactions on Cep57 induced centrosome amplification in the cells. Furthermore, Cep57 condensates were found to facilitate microtubule nucleation by concentrating α/β-tubulin in the condensates. Finally, a novel molecular interplay was observed between the centrosomal scaffold, which is the negative regulation of Cep63 on LLPS, and the microtubule nucleation activity of Cep57. The following report briefly presents their results.

Cheng's team observed that overexpression of Cep57 forms spherical puncta in cells and some of them colocalized with microtubules (**Fig. 1(a)**). To study the molecular mechanism of the puncta formation, they purified Cep57 and found that Cep57 is highly soluble in high salt conditions (1 M NaCl) but self-assembles into micron-sized spherical droplets with liquid-like properties when salt was reduced to 200 mM (**Fig. 1(c)**).

As full-length Cep57 is prone to degradation, a Cep57S construct was created, which has similar properties to Cep57 but allows for higher protein quality to perform biochemical and biophysical characterization (**Fig. 1(b)**). To identify the regions responsible for LLPS, the N-terminal and C-terminal fragments of Cep57 were expressed and purified. It was found that both terminals are necessary for condensate formation. As it was observed that the phase separation of Cep57 is salt-dependent, electrostatic interactions were speculated to play a role in phase separation. Mutagenesis analysis revealed a highly conserved K/R motif located in the C-terminal direction from the NTD, which also contributes to the phase separation of Cep57S. The combined data showed that the NTD, CTD, and K/R motifs contribute to the phase separation of Cep57S.

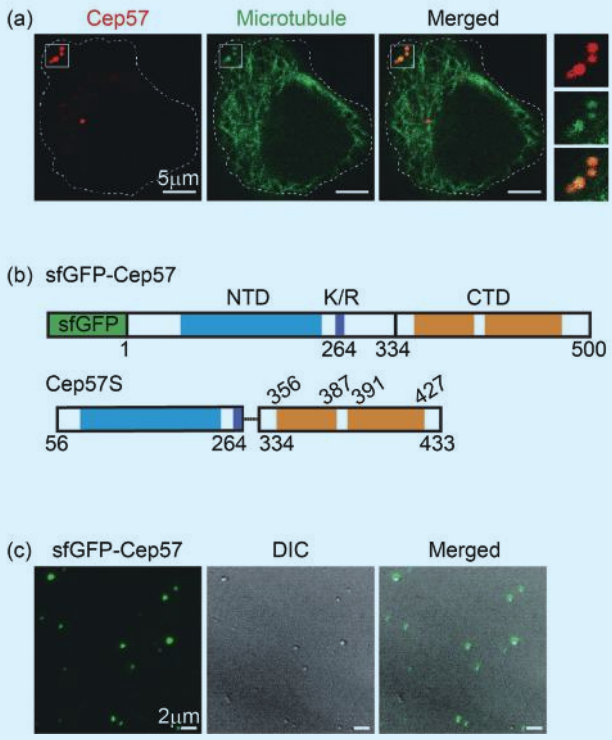

Fig. 1: Human Cep57 undergoes liquid–liquid phase separation under physiological conditions. (a) Confocal images of HeLa cells co-expressing Cep57-mCherry (red) and Neon-MAP4m as the microtubule marker (green) for 16 h. (b) Domain organization of sfGFP-Cep57 and Cep57S. Coiled-coil N-terminal domain (NTD), blue; coiled-coil C-terminal domain (CTD), orange; poly-K/R motif (K/R), dark blue. Cep57S is composed of residues 56 to 264 fused to 334 to 433. (c) TIRF images of sfGFP-Cep57 droplets. The sfGFP-Cep57 (25 nM) were visualized 4 h after condensation in low salt (200 mM NaCl). [Reproduced from Ref. 1].

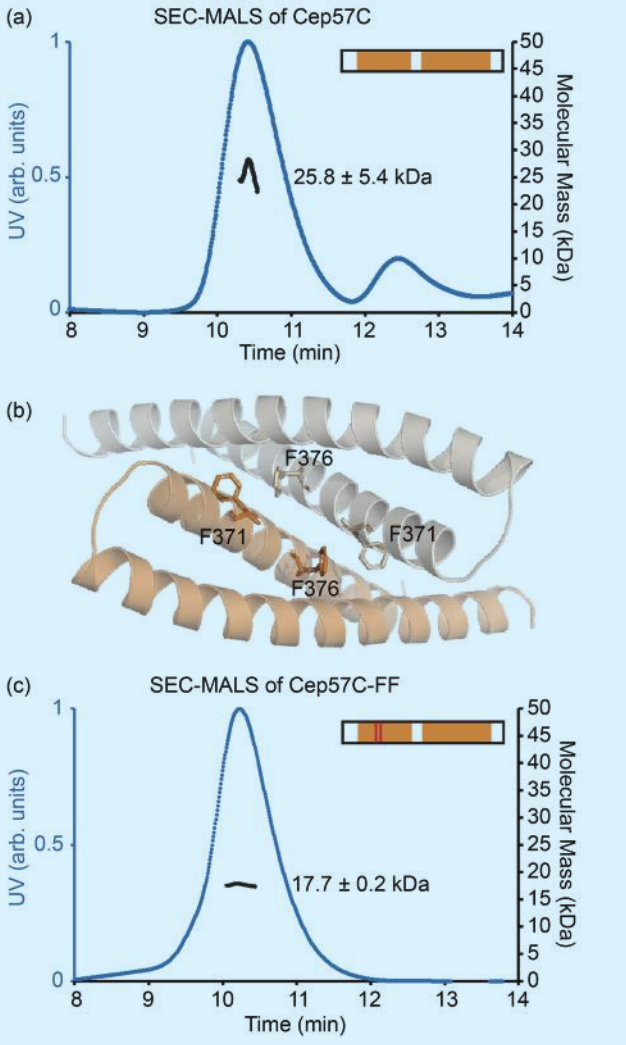

Fig. 2: CTD dimerization facilitates phase separation of Cep57. (a) SEC-MALS profile of Cep57C. The calculated molecular mass for Cep57C is 12.5 kDa. (b) The crystal structure of Cep57C is shown as a dimer. The side chains of F371 and F376 are in stick presentation. (c) SEC-MALS profile of Cep57C-FF. [Reproduced from Ref. 1]

From the SEC-MALS analysis and crystal structure of Cep57C, Cheng's team showed that Cep57C, which adopts a helix-turn-helix fold, forms a symmetric dimer with residues F371 and F376 at the dimer interface (**Figs. 2(a) and 2(b)**). When these two residues were mutated to alanines in the Cep57S-FF mutant, the dimer formation was weakened (**Fig. 2(c)**), and the phase separation ability decreased. Therefore, Cep57C dimerization is essential to promote Cep57 condensation.

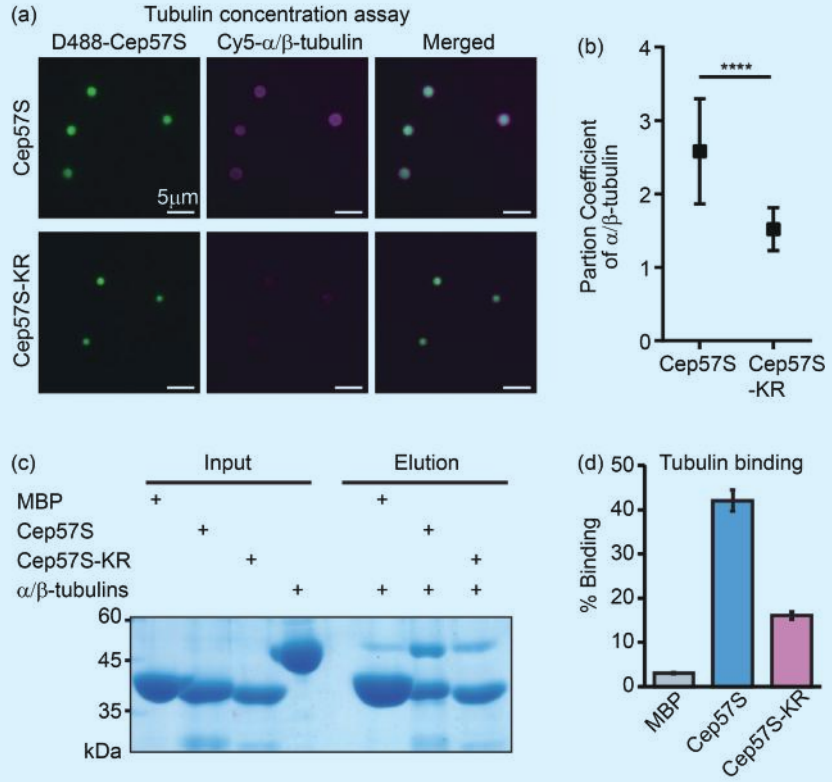

Fig. 3: The Cep57 scaffold concentrates α/β-tubulin for microtubule assembly. (a) D488-Cep57S or D488-Cep57S-KR condensates with Cy5-tubulin dimers in 66 μM nocodazole. Images were taken 20 min after the addition of tubulin. (b) Quantification of the α/β-tubulin partition coefficient to Cep57S (n = 69) or Cep57-KR (n = 76) condensates in experiments from panel (a) pooled from three repeats. [****] $p < 0.0001$. Data represent mean ± SD. (c) His-tag pull-down assay of tubulin with His-Cep57S and His-Cep57S-KR. His-MBP was used as the negative control. Quantification of binding of α/β-tubulin in experiments. The percentage of binding was defined as the intensity of tubulin in the eluent divided by the intensity of the loaded sample (N = 3). (d) Percentage of cells with centrosomal microtubule asters in the microtubule regrowth experiments. HeLa cells were sequentially transfected from left to right with negative control siRNA + empty vector, Cep57 siRNA + empty vector, Cep57 siRNA + Cep57, and Cep57 siRNA + Cep57-KR. Each data point was derived from observations of 100 to 200 cells. [*] $p < 0.05$; [**] $p < 0.01$. N = 3. [Reproduced from Ref. 1]

Cep57S condensates were also found to concentrate α/β-tubulin by about 2.6-fold to promote microtubule polymerization inside the Cep57S condensates (**Figs. 3(a) and 3(c)**). The *in vitro* pull-down assay revealed that the K/R motif is the tubulin binding site. A siRNA rescue experiment with the Cep57S-K/R mutant demonstrated that Cep57 plays a role in centrosomal microtubule organization in a K/R motif-dependent manner (**Figs. 3(c) and 3(d)**).

The research shows that Cep63 prevents the LLPS and microtubule nucleation functions of Cep57S. When Cep57S formed co-condensates with Cep63, the ability to concentrate α/β-tubulin was decreased (**Fig. 4(a)**). Additionally, both the condensate size and partition coefficient of Cep57S decreased as the concentration of Cep63N, the Cep57 binding domain, increased (**Figs. 4(b) and 4(c)**). SAXS measurements taken at the **TPS 13A** beamline showed that the fractal network of Cep57S was diminished by the addition of Cep63N, further suggesting that Cep63 dissolves Cep57S condensates by disrupting the network structure (**Fig. 4(d)**). Collectively, these results

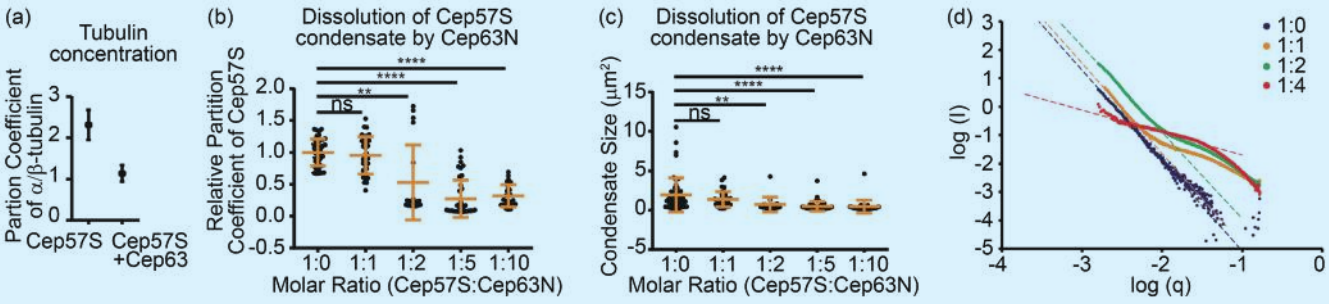

Fig. 4: Cep63 inhibits Cep57's LLPS and function. (a) The partition coefficient of α/β-tubulin in Cep57S or Cep57S–Cep63 condensates. n = 51 (Cep57) and n = 102 (Cep57S–Cep63) pooled from three independent experimental repeats. (b,c) Partition coefficient and size analysis of Cep57S condensates with increasing concentrations of MBP-Cep63N. The concentration of Cep57S was fixed at 2 μM. Data from two independent experiments were pooled for quantification; n = 51 (1:0), n = 34 (1:1), n = 19 (1:2), n = 39 (1:5), and n = 28 (1:10). (d) SAXS profile of Cep57S fixed at 10 μM in the presence of MBP-Cep63N at indicated ratios (Cep57S:MBP-Cep63N). Proteins were incubated at 22 °C for 12 hours before the SAXS experiments. The dotted line represents extrapolation of the linear regression of scattering data in the q range from 0.01 $Å^{-1}$ to 0.002 $Å^{-1}$ or 0.01 $Å^{-1}$ to 0.006 $Å^{-1}$ (for 1:1 only). Slopes for linear regression were –3.2 (1:0), –3.2 (1:1), –3.0 (1:2), and –0.8 (1:4). As MBP-Cep63N increased, the absolute value of the slope decreased, implying that the complexity of the structure decreased. [Reproduced from Ref. 1]

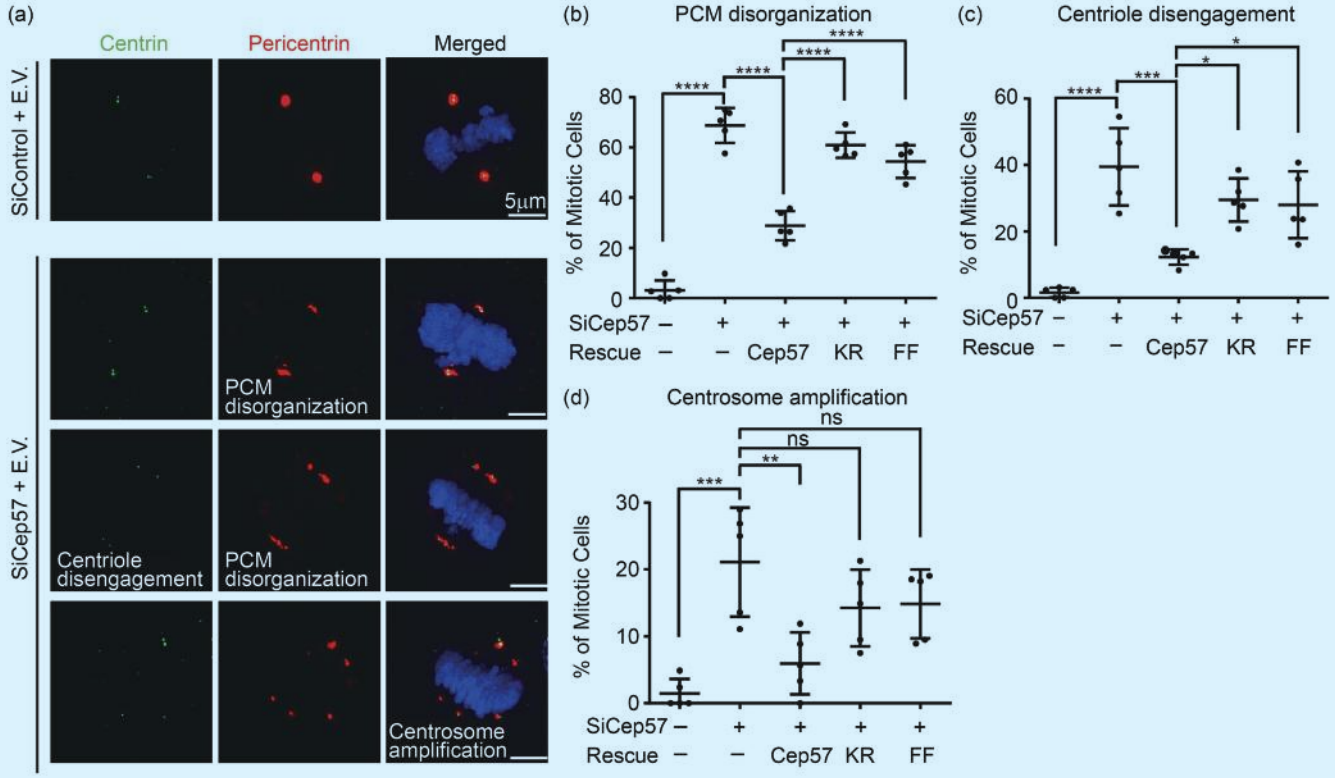

Fig. 5: Multivalent interactions of Cep57 regulate the structure and number of human centrosomes. (a) Fluorescence images of mitotic HeLa cells sequentially transfected with negative control siRNA and mCherry empty vector, or Cep57 siRNA and mCherry empty vector. Centrin, green; pericentrin, red; DNA, blue. (b–d) Percentage of mitotic cells with indicated phenotypes. HeLa cells were sequentially transfected from left to right with negative control siRNA + mCherry empty vector, Cep57 siRNA + mCherry empty vector, Cep57 siRNA + Cep57-mCherry, Cep57 siRNA + Cep57-KR-mCherry, and Cep57 siRNA + Cep57-FF-mCherry, followed by synchronization. Each data point was collected from 30 to 50 mitotic cells. N = 5. [*] $p < 0.05$, [**] $p < 0.01$, [***] $p < 0.001$, and [****] $p < 0.0001$. [Reproduced from Ref. 1]

suggest that modulating LLPS of Cep57 by Cep63 serves as a mechanism to regulate the structural expansion and functional activity of the PCM scaffolding proteins.

Finally, cell assays with Cep57-FF and Cep57-KR mutants were performed to examine the functional significance of Cep57 in centrosome duplication. Depletion of endogenous Cep57 by siRNA results in PCM disorganization, centriole disengagement, and centrosome amplification in the mitotic cells (**Fig. 5**), while introducing siRNA-resistant Cep57 construct rescues these phenotypes. In contrast, Cep57-FF or Cep57-KR mutants failed to rescue these phenotypes. Hence, Cep57 maintains the PCM integrity through multivalent interactions.

Collectively, this study provides crucial insights into the molecular mechanisms by which Cep57 contributes to centrosome organization through LLPS. It highlights the role of Cep57 condensates in promoting microtubule nucleation by concentrating α/β-tubulin and reveals a novel regulatory interaction where Cep63 negatively modulates Cep57's phase separation and microtubule nucleation activity. These findings enhance our understanding of the dynamic assembly of the centrosome, its regulation during cell division, and the potential implications of Cep57

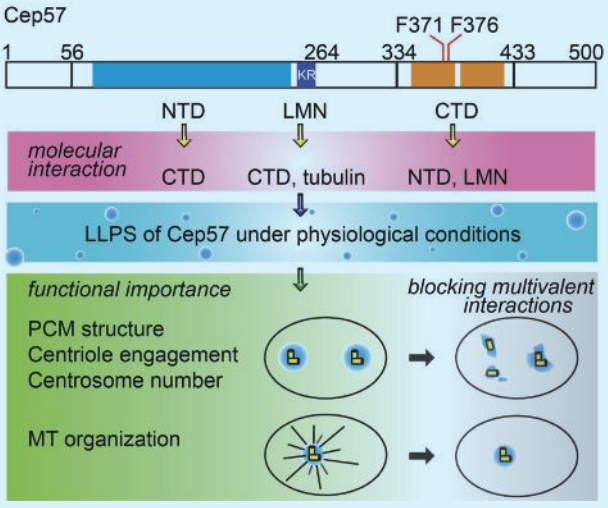

Fig. 6: A model for the assembly of human Cep57 in centrosome regulation. The domain organization of Cep57 is depicted with interactions that drive LLPS under physiological conditions. SiRNA rescue experiments reveal that the multivalent interactions of Cep57 are essential for PCM organization, and the polybasic LMN (LLPS and Microtubule Nucleation) motif facilitates microtubule aster formation. [Reproduced from Ref. 1]

mutations in centrosome-related pathologies, such as mosaic-variegated aneuploidy syndrome. (Reported by Hui-Chun Cheng, National Tsing Hua University)

This report features the work of Hui-Chun Cheng and her collaborators published in PNAS ***121****, e2305260121 (2024).*

TPS 13A Biological Small-angle X-ray Scattering

- Biological Small/Wide Angle X-ray Scattering
- Biological Macromolecules, Structural Biology, Life Science

Reference

1. H. W. Yeh, P. P. Chen, T. C. Yeh, S. L. Lin, Y. T. Chen, W. P. Lin, T. Chen, J. M. Pang, K. T. Lin, L. H.-C. Wang, Y. C. Lin, O. Shih, U. S. Jeng, K. C. Hsia, H. C. Cheng, PNAS **121**, e2305260121 (2024).

Blueprints in a Drop

This research aims to revolutionize the synthesis of metal–organic frameworks (MOFs) in water by unlocking the molecular codes of biomineralization, paving the way for sustainable innovation.

Metal–organic frameworks (MOFs) have emerged as superior materials for sustainable and transformative applications. Composed of metal ions and organic linkers, MOFs possess exceptional porosity and tunability, making them ideal for diverse uses such as energy conversion, catalysis, water harvesting, and biosensing. However, traditional MOF synthesis methods often rely on organic solvents, raising environmental concerns and hindering scalability and bio applications. Water-based methods for producing zirconium-based and zeolitic MOFs offer significant environmental and economic benefits while enabling the incorporation of biomolecules such as DNA and proteins. Fa-Kun Shei (National Central University) and his team focus on improving protein encapsulation efficiency within MOFs, addressing a critical challenge for expanding their practical applications.[1, 2]

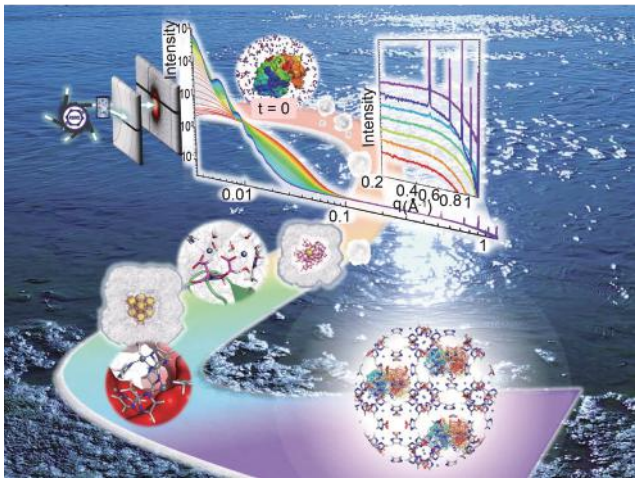

The Protein@ZIF-8 Crystallization Journey

Water's dual role in facilitating proton transfer while suppressing undesired reactions adds complexity to MOF nucleation and crystallization. To address this, Hsiao-Ching Yang's team (Fu Jen Catholic University) has developed a ground-breaking approach to elucidate water's critical role in reaction pathways. Through all-atom molecular dynamics simulations and quantum dynamics calculations, they investigated proton transfer mechanisms and structural evolution during MOF formation, uncovering essential molecular-level insights into factors influencing protein encapsulation. To validate their theoretical findings, Yang collaborated with U-Ser Jeng (NSRRC) and his team at the **TPS 13A** beamline, successfully bridging computation structures with experimental data.[3]

Accordingly, the interdisciplinary to transdisciplinary teamwork led by Shei, Jeng, and Yang launched a collaborative effort to explore the biomimetic nucleation and crystallization journey using ZIF-8, a zeolitic imidazolate framework, as a model system.[3] Through combining advanced techniques such as *in situ* small-/wide-angle X-ray scattering (SWAXS), multiscale simulations, and quantum calculations, the team meticulously tracked the overall process of nucleation and crystallization of ZIF-8 in aqueous solutions in real-time. This complementary approach of all-atom molecular dynamics simulations and experimental observation offered a comprehensive understanding of the molecular blueprint underlying MOF formation, decoding the ZIF-8 nucleation and crystallization process. Their research showed that the process unfolds in three distinct stages:

Stage I: Acidity Flip Proton Transfer Initial Assembly to Amorphous Nuclei. Water in the zinc–water complex is replaced by imidazole ligands, initiating an "acidity flip" that accelerates proton transfer. This shift drives the structural organization of zinc ions into amorphous cluster nuclei; imidazole ligands replace water molecules within zinc–water coordination complexes, forming the first blueprint of the crystalline structure and lead to the assembly of amorphous nuclei—the initial building blocks of the MOF structure. No ordered precursors or diffraction peaks were observed, marking the early aggregation of secondary building units (SBUs) into amorphous nuclei.

Stage II: Transition to Crystalline Nuclei and Ordered Structures. The amorphous nuclei undergo a critical transformation, evolving into ordered nuclei. This stage involves amorphous nuclei being consumed to form ordered mesoscale structures, overcoming energy barriers of approximately 21 kcal/mol in this rate-determining step. The emergence

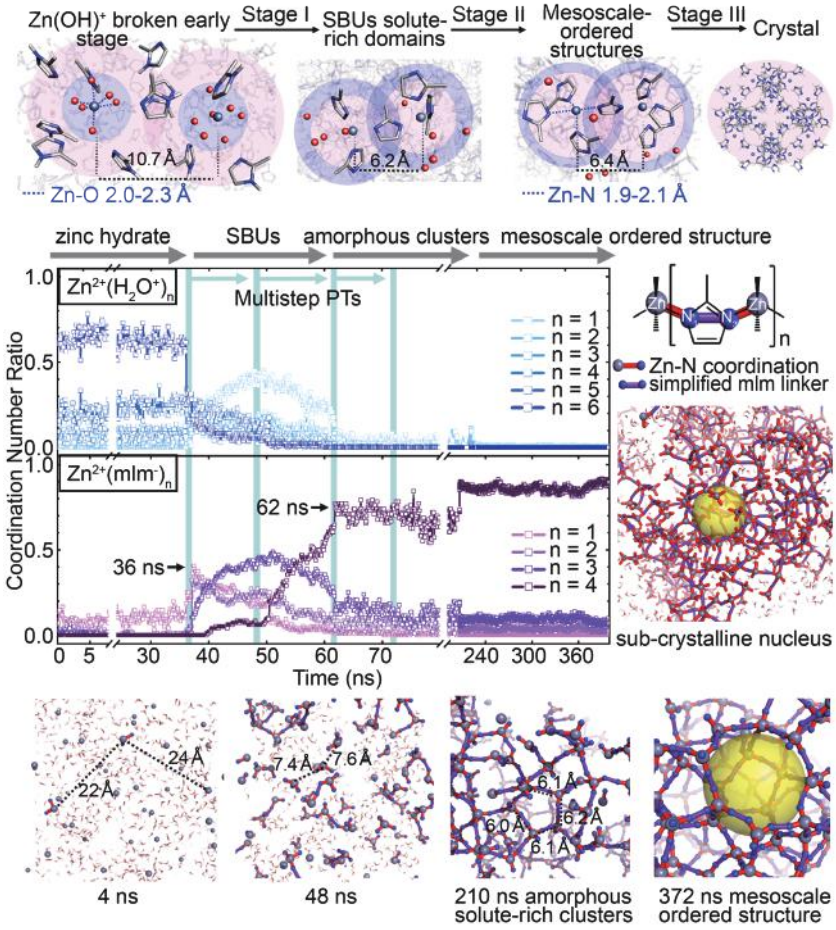

Fig. 1: MD analysis of ZIF-8 reveals a multistep Proton Transfer (PT) mechanism and structural evolution showing key Zn-O (water), Zn-N, and HmIm (N1(H), N3) interactions enabling precise protonation control with SBUs and amorphous clusters forming nucleation sites for crystalline growth in solution. [Reproduced from Ref. 3]

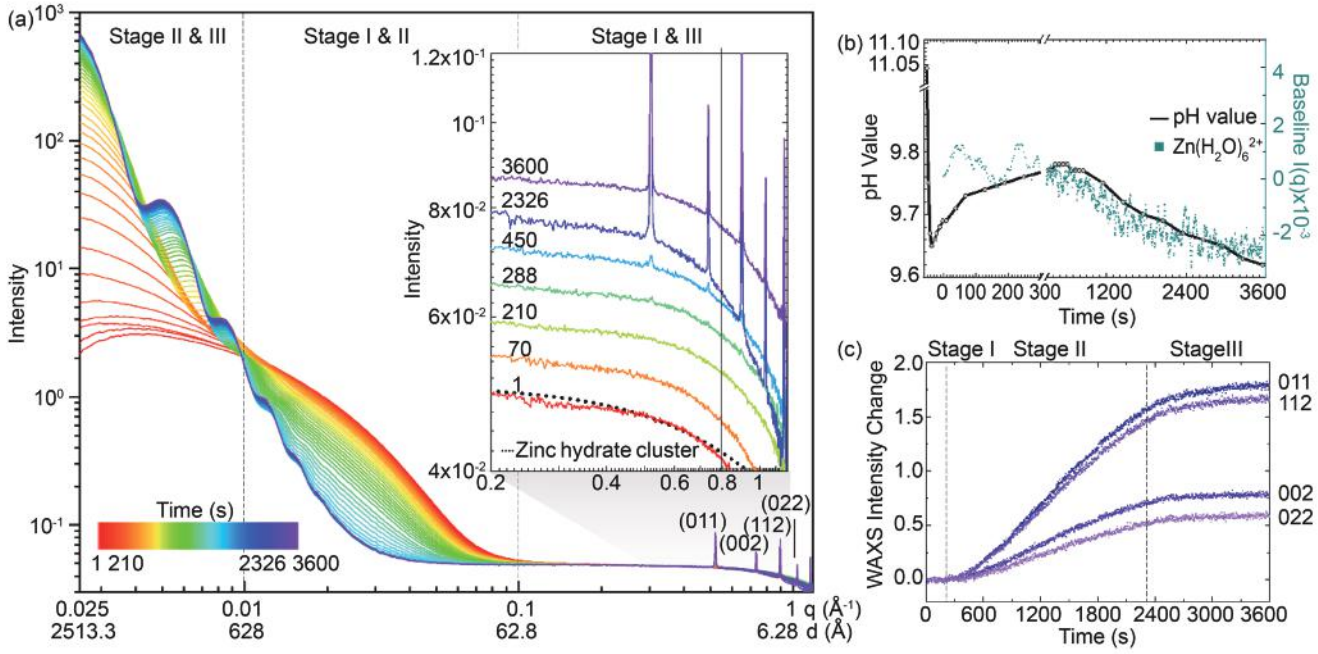

Fig. 2: *In situ* and *operando* SWAXS of ZIF-8 synthesis in aqueous solution for a HmIm/Zn^{2+} molar ratio of 1:57 at 10 °C (a) The *q*-range for scattering extends from 0.0025 to 1.2 $Å^{-1}$, with data acquired every second for a total duration of 3600 seconds. The inset shows an enlarged WAXS region. (b) The scattering profile baseline exhibits a clear dependence on the reaction solution's pH value. (c) The WAXS peaks corresponding to Miller indices (011), (002), (112), and (022) of ZIF-8, which all display correlated time-dependent intensity changes and can be normalized to one reference. [Reproduced from Ref. 3]

of diffraction peaks at specific q-values corresponds to the growth of crystalline nuclei, characterized by the growth of diffraction peaks at q = 0.52, 0.74, 0.90, and 1.04 Å^{-1}, corresponding to the Miller indices (011), (002), (112), and (022), respectively.

Stage III: Formation of Stable Nanoparticles toward Crystals. Stable crystal nanoparticles emerge when molecular interactions between the crystals and the surrounding solution reach temperature-dependent thermal equilibrium. This occurs when the structural dimensions stabilize, corresponding to the completion of the second stage. This appears to involve a temperature-dependent thermal equilibrium of the molecular interaction dynamics at the crystal–solution interface.

Biomolecular Integration in MOF Encapsulation
The results showed an inverse relationship between

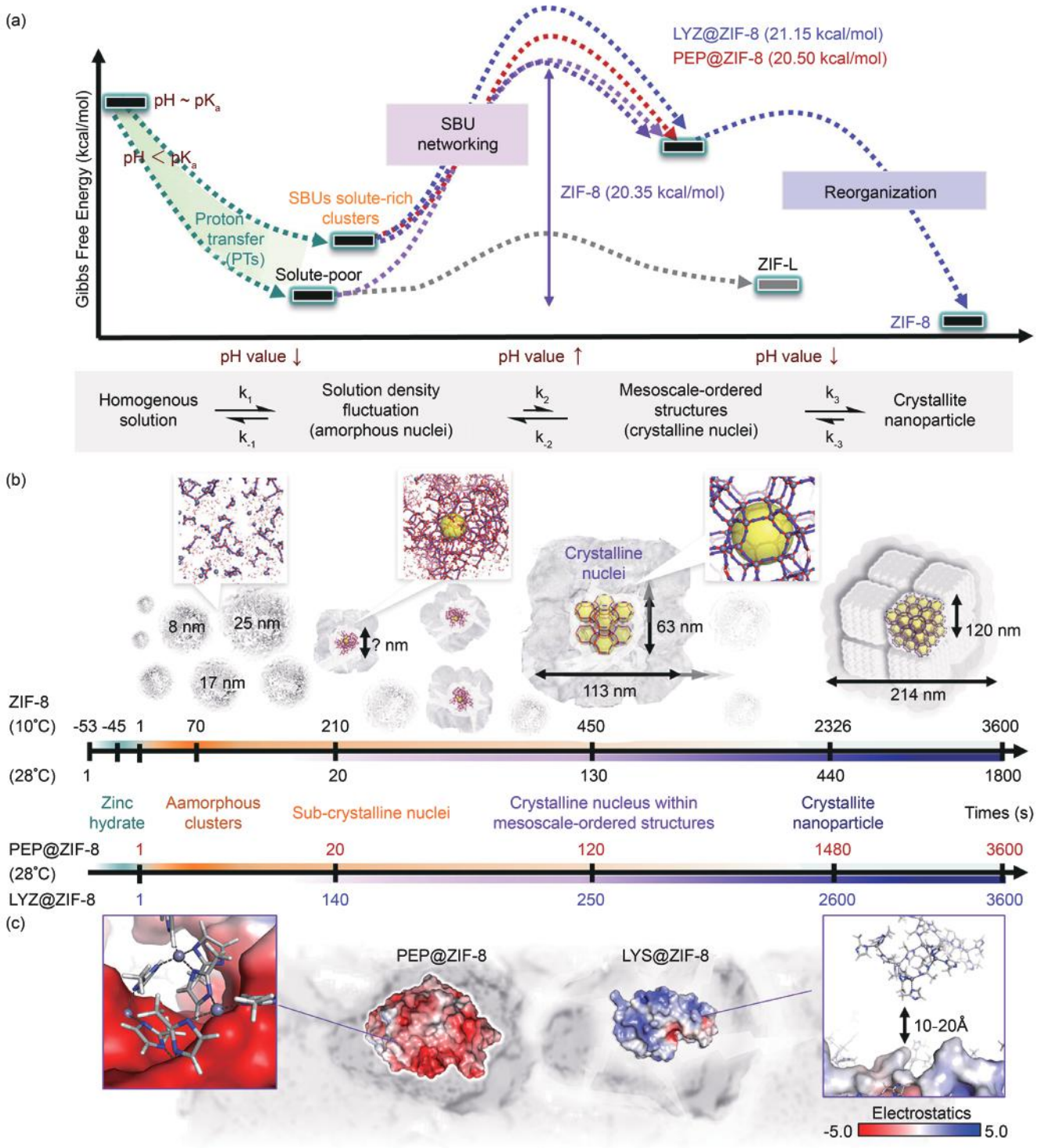

Fig. 3: *In situ* SWAXS reveals ZIF-8 and protein@ZIF-8 synthesis mechanisms. (a) Gibbs free energy landscapes for ZIF-8 systems. (b) Time-resolved nucleation and growth under various conditions. (c) Protein effects: PEP (negative, red) binds strongly, while LYZ (positive, blue) shows poor interaction due to electrostatic repulsion. [Reproduced from Ref. 3]

temperature and particle size. Experimental data showed that as the temperature increased from 10 to 28 °C, the microcrystal size (D 011) decreased from 139 to 80 nm, while the nanoparticle size decreased from 337 to 97 nm. This phenomenon is mainly attributed to the increased nucleation rate at higher temperatures. With the formation of more crystalline nuclei, the available reactants are distributed among more growing particles, resulting in smaller final particle sizes. Further innovation emerged from studying the effects of biomolecules on MOF formation. By incorporating proteins such as pepsin and lysozyme, researchers demonstrated that amino acid proton transfer ability and concentration directly influence the morphology and encapsulation efficiency of biomolecule–MOF composites. This study identified how proteins act as nucleation sites within amorphous MOF structures. These insights not only advance our understanding of biomineralization but also hint at designing proteins as nucleation sites for amorphous MOF growth.

In summary, this transdisciplinary research offers profound insights into the molecular mechanisms of biomimetic mineralization, where biological principles inspire synthetic material design. The findings pave the way for designing tailored MOF systems for applications. By bridging computational modeling simulations and experimental validation, this study provides a comprehensive "blueprint in a drop"—a molecular-level precision for understanding and optimizing MOF formation. By mastering these microscopic processes, the team unlocks more sustainable and innovative applications in fields ranging from energy storage to pharmaceuticals. The journey from a single aqueous drop to a complex crystalline network underscores the profound potential of small beginnings in shaping the advanced materials of the future. (Reported by Hsiao-Ching Yang, Fu Jen Catholic University)

This report features the work of Hsiao-Ching Yang and her collaborators published in ACS Nano ***18****, 25170 (2024).*

TPS 13A Biological Small-angle X-ray Scattering

- *In situ* SWAXS
- Physical Chemistry, Chemical Physics, Computation Chemistry, Materials Science, Aqueous Chemistry

References

1. S.-Y. Chen, W.-S. Lo, Y.-D. Huang, X. Si, F.-S. Liao, S.-W. Lin, B. P. Williams, T.-Q. Sun, H.-W. Lin, Y. An, T. Sun, Y. Ma, H.-C. Yang, L.-Y. Chou, F.-K. Shieh, C.-K. Tsung, Nano Lett. **20**, 6630 (2020).
2. P. K. Lam, T. H. Vo, J.-H. Chen, S.-W. Lin, C.-L. Kuo, J.-J. Liao, K.-Y. Chen, S.-R. Huang, D. Li, Y.-H. Chang, H.-Y. Chen, H.-T. Hsieh, Y.-A. Hsu, H.-K. Tsao, H.-C. Yang, F.-K. Shieh, J. Mater. Chem. A **11**, 24678 (2023).
3. S.-W. Lin, P. K. Lam, C.-T. Wu, K.-H. Su, C.-F. Sung, S.-R. Huang, J.-W. Chang, O. Shih, Y.-Q. Yeh, T. H. Vo, H.-K. Tsao, H.-T. Hsieh, U-S. Jeng, F.-K. Shieh, H.-C. Yang, ACS nano **18**, 25170 (2024).

Unlocking Hydrogen Power with Single-Atom Pt Catalysts

3D hierarchically organized metal single atoms have attracted considerable attention for their high efficiency in various catalytic reactions.

Single-atom catalysts have garnered significant attention because of their exceptional activity and efficiency across a broad spectrum of catalytic reactions.[1] However, developing stable single-atom catalysts and cocatalysts that maintain high performance presents significant challenges, particularly in achieving uniform dispersion, stabilization, and a sufficiently high density of single-atom sites. Currently, the majority of reported single-atom catalysts have predominantly been achieved using two-dimensional substrates lacking steric infrastructures. The dispersion of these single-atom catalysts relies heavily on their adsorption or coordination with substrates, such as carbon blacks or graphene surfaces. These weak interactions struggle to counteract the aggregation of single-atom catalysts into nanoparticles during catalytic reactions, leading to suboptimal performance.

Recent studies have suggested the potential use of metal–organic frameworks (MOFs) to create three-dimensional (3D) hierarchical structures, thus allowing the deployment of catalysts/cocatalysts inside MOF cages through diffusion or onsite reduction. This approach aims to mitigate the aggregation effect of single atoms, thereby sustaining their performance. However, achieving a uniform deposition of single catalysts/cocatalysts throughout the deep inner MOF cages presents a significant challenge.

U-Ser Jeng and his team at the NSRRC recently developed a method that involves embedding single platinum (Pt) atoms within silicate nanochannels for a paired single-atom cocatalyst and catalyst to achieve efficient and stable photocatalytic centers of a high number density in 3D substrates. Using phosphotungstic acids (PTAs) as templates, they achieved a high loading of single Pt atoms (3.0 wt%). Advanced techniques, including X-ray absorption spectroscopy (**TPS 44A**)[2] and electron microscopy, revealed that Pt atoms are stabilized *via* four-oxygen coordination within PTA, effectively reducing the energy-driving aggregation (**Fig. 1**). This system's design relies on controlling the ratio of Pt atoms to PTA. A critical ratio of 3.7 ensures nearly pure single-atom dispersion. At higher ratios, Pt clustering becomes evident. The research team used a three-stage solution synthesis process of template formation, Pt adsorption, and reduction at the air–liquid interface to create this unique structure. *In situ* grazing-incidence small-angle scattering (GISAXS) measurements (**TLS 23A1** and **TPS 13A**)[3,4] and thermogravimetric analyses demonstrated that increasing PTA content enhanced single-atom dispersion, while excessive PTA led to structural deterioration. The resulting Pt–PTA pairs within silicate nanochannels exhibit the outstanding hydrogen evolution reaction (HER) efficiency, achieving a hydrogen production rate of 300 mmol/h/g Pt, which is double that of previous systems. The PTA's empty tungsten d shell facilitates photoexcited electron transfer to Pt, enabling efficient hydrogen reduction. The nanochannels also prevent Pt clustering and sustain long-term performance. This breakthrough establishes a record-high Pt efficiency for HER among polyoxometalate (POM)-based systems. The 3D-ordered structure stabilizes single Pt atoms and creates a synergistic network for enhanced charge transfer. This innovative strategy highlights the potential for developing robust, high-performance single-atom catalysts for energy applications.

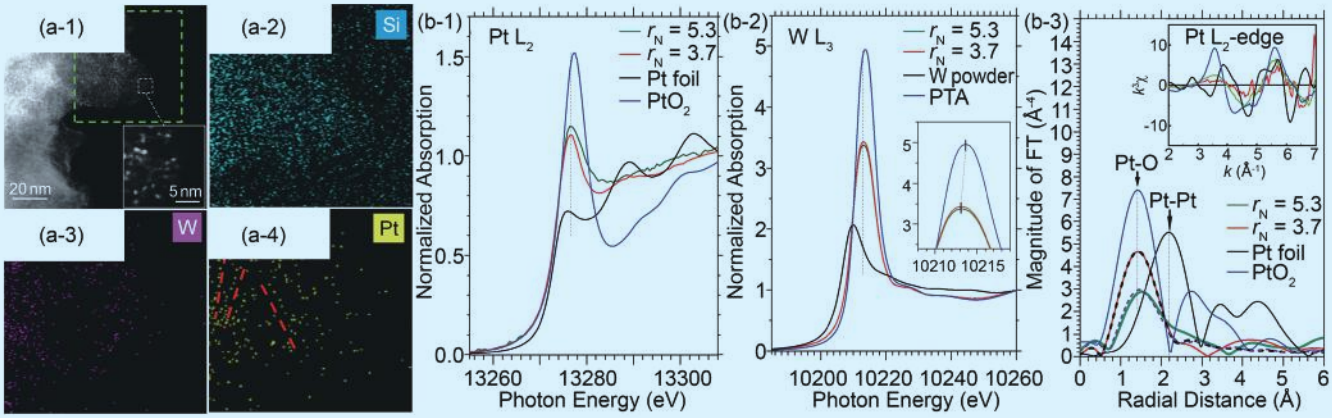

Fig. 1: (a-1) High-angle annular dark field-scanning transmission electron microscopy (HAADF–STEM) image of a typical zone on Pt–PTA within the silicate nanochannels of a low Pt atom/PTA number ratio, r_N, of 5.3; the inset (white square) zooms in on the local details, with the dispersed bright spots contributed by the scattering from heavier elements of Pt and W in the sample. Corresponding energy-dispersive X-ray spectroscopy (EDS) maps of (a-2) Si, (a-3) W, and (a-4) Pt, taken from the sample zone marked by the green dotted frame in (a-1). (b-1–3) X-ray absorption spectra measured at the (b-1) Pt L_2-edge and (b-2) W L_3-edge for the two samples of Pt–PTA within silicate nanochannels, with r_N = 5.3 and 3.7. Also shown are the spectra of Pt foil (measured in transmission mode), PtO_2, and tungsten and PTA powders for comparison. (b-3) Fourier transform of the samples and the references (with no phase corrections). The inset shows the corresponding (same colors) Pt L_2-edge k^3-weight extended X-ray absorption fine structure (EXAFS) spectra. The data with r_N = 3.7 (or 5.3) are respectively fitted with the dotted (or dashed) curve by using a mean first-shell coordination number Nc = 3.88 (or 2.6) and a Pt–O bond length R = 1.93 Å (or 1.96 Å). [Reproduced from Ref. 5]

From the HER and X-ray absorption spectroscopy (XAS) results, Pt single atoms in Pt_1–PTA pair coordination within the arrayed silicate nanochannels outperform Pt nanoparticles with PTA in the same environment by fourfold efficiency (**Fig. 2(a)**, see next page). Such one-to-one Pt_1–PTA pair coordination has many advantages in the photoelectric conversion of HER *via* metal-to-metal charge-transfer excitation. In this process, the WO_3-based PTA (having an empty d shell with tungsten W^{6+} in $5d^0$ configuration) provides photoexcited electrons, with the states of W^{5+} in $5d^1$ configuration to the coordinated Pt_1 for hydrogen reduction. The PTA-4H site provides Pt_1 a stable absorption and four coordinated oxygen atoms for an oxidation state of ca. +2 (as revealed from the XAS and discrete Fourier transform calculation results). The median oxidation state of Pt_1 presumably is favorable for serving as a co-catalyst to accept photoelectrons from PTA and subsequently transfer the electrons to nearby protons for HER. The hydrogen adsorption energy ΔG of Pt (−0.1 eV) is closer to zero than that of PTA (−0.9 eV) in an acidic environment, further enhancing the HER kinetics *via* faster, easier hydrogen desorption after reduction. These advantages render the Pt_1 of the Pt_1–PTA pair an efficient co-catalyst in the photocatalytic HER mechanism. On top of the high HER efficiency within the Pt_1–PTA pair, the 3D network of a high number density of Pt_1–PTA pairs organized *via* the arrayed silicate nanochannels can further synergistically convert near neighbors' photoelectrons available within the network and those contributed by the PTA in the HER solution. Moreover, the nanochannel pore

structure (ca. 2 nm channel pore size) with densely intercalated PTA (ca. 1 nm size) suppresses the clustering of the channel Pt_1 during catalytic reactions for sustainable performance. With all these advantages, this new hierarchical structure achieves a record high Pt efficiency in HER among the POM-based photocatalytic systems. It may be considered an efficient electrode material in photoelectrochemical cells.

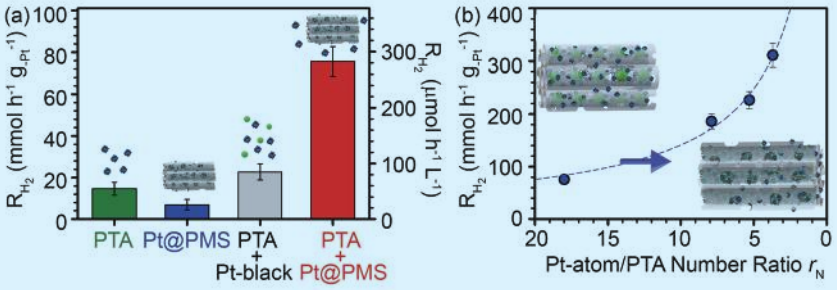

Fig. 2: (a) H_2 production rate measured for a 100 mL solution containing 5 mg of the nanocomposite of Pt–PTA within silicate nanochannels (r_N =18), 1.2 mM PTA, 0.2 M H_2SO_4, and isopropanol (20% vol.). Also shown are the H_2 production rates measured in similar solutions for the nanocomposite, solely PTA, and Pt black (of an equal Pt weight) suspension, in similar PTA solutions, as illustrated by the illustrations. (b) Increase in the H_2 production rate with the reduction of r_N of the nanocomposite with increasingly more Pt_1–PTA pairs; inset illustrations show the corresponding transition of Pt dispersion from nanoparticles (left) to Pt_1 on PTA (right) within the arrayed silicate nanochannels. [Reproduced from Ref. 5]

In summary, the team successfully developed a three-stage synthesis process at the air–liquid interface, enabling precise control over the deposition and dispersion of platinum atoms (Pt_1) within hexagonally packed silicate nanochannels. This approach achieved an efficient Pt_1–PTA configuration, demonstrating record-high performance in HER. The outstanding performance of this structure is attributed to the stable 4H-site coordination, enhanced electron transfer efficiency, high-density Pt_1–PTA pairs, and exceptional anti-clustering properties. Moreover, the integration of synchrotron radiation techniques, such as GISAXS and XAS, played a pivotal role in providing high-sensitivity *in situ* analysis, allowing a detailed understanding of the formation mechanism, structural characteristics, and reaction dynamics of Pt_1–PTA pairs within the nanochannels. These advanced characterization methods offered critical data for the experimental process and provided valuable insights for designing and optimizing 3D single-atom catalysts. This study highlights the potential of combining synchrotron radiation capabilities with advanced synthesis techniques to develop highly stable and efficient single-atom catalysts. It paves the way for innovative applications in photochemical and renewable energy conversion systems. (Reported by Je-Wei Chang)

This report features the work of U-Ser Jeng and his collaborators published in ACS Nano ***18****, 1611 (2024).*

TPS 13A Biological Small-angle X-ray Scattering
TPS 44A Quick-scanning X-ray Absorption Spectroscopy
TLS 23A1 Small/Wide Angle X-ray Scattering

- GISAXS, NEXAFS, WAXS
- Materials Science, Chemistry, Surface, Interface and Thin-film Chemistry, Condensed-matter Physics

References

1. X. F. Yang, A. Wang, B. Qiao, J. Li, J. Liu, T. Zhang, Acc. Chem. Res. **46**, 1740 (2013).
2. C.-W. Pao, J. L. Chen, J. F. Lee, M. C. Che, C. Y. Huang, C. C. Chiu, C. Y. Chang, L. C. Chiang, Y. S. Huang, J. Synchrotron Radiat. **28**, 930 (2021).
3. U.-S. Jeng, C. H. Su, C.-J. Su, K.-F. Liao, W.-T. Chuang, Y.-H. Lai, J.-W. Chang, Y.-J. Chen, Y.-S. Huang, M.-T. Lee, K.-L. Yu, J.-M. Lin, D.-G. Liu, C.-F. Chang, C.-Y. Liu, C.-H. Chang, K. S. Liang, J. Appl. Crystallogr. **43**, 110 (2010).
4. O. Shih, K. F. Liao, Y. Q. Yeh, C. J. Su, C. A. Wang, J. W. Chang, W. R. Wu, C. C. Liang, C. Y. Lin, T. H. Lee, C. H. Chang, L. C. Chiang, C. F. Chang, D. G. Liu, M. H. Lee, C. Y. Liu, T. W. Hsu, B. Mansel, M. C. Ho, C. Y. Shu, F. Lee, E. Yen, T. C. Lin, U. Jeng, J. Appl. Crystallogr. **55**, 340 (2022).
5. J. W. Chang, K. H. Su, C. W. Pao, J. J. Tsai, C. J. Su, J. L. Chen, L. M. Lyu, C. H. Kuo, A. C. Su, H. C. Yang, Y. H. Lai, U. S. Jeng, ACS Nano **18**, 1611 (2024).

Life Science

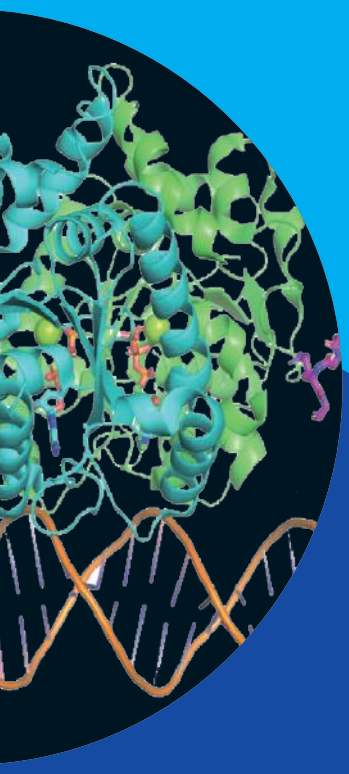

Despite advancements in computational techniques, which were recognized by the 2024 Nobel Prize in Chemistry for groundbreaking work, and cryo-EM methods, synchrotron macromolecular crystallography remains an indispensable tool for revealing the intricate atomic structures of biomolecules. This high-resolution structural information is crucial for understanding the structure–function relationships, as well as for driving various scientific applications, from elucidating complex biological mechanisms to supporting drug development and analyzing bio-samples to unravel unsolved issues in biology.

The NSRRC in Taiwan maintains a robust infrastructure to support this field, featuring three specialized protein beamlines—**TLS 15A1**, **TPS 05A**, and **TPS 07A**—that are accessible to a broad community of users. Starting in 2025, the **TPS 05A** and **TPS 07A** beamlines will undergo an upgrade program, which will enable them to provide more diverse functionalities to meet the evolving needs of users better. Furthermore, the NSRRC offers a diverse array of specialized beamlines, including those for small-angle X-ray scattering (**TPS 13A**), soft X-ray tomography (**TPS 24A**), transmission X-ray microscopy (**TPS 31A**), quick-scanning X-ray absorption spectroscopy (**TPS 44A**), white X-ray (**TLS 01A1**), X-ray microscopy (**TLS 01B1**), and infrared microspectroscopy (**TLS 14A1**), enabling researchers to tackle a broad range of biological problems.

The NSRRC user community enjoyed a banner year in 2024, delivering an array of significant scientific breakthroughs. Consequently, we have selected four exemplary studies conducted at our facilities to feature in this activity report. The first study, conducted by Yuh-Ju Sun and Chwan-Deng Hsiao, examined the distinct molecular systems—ParABS in bacteria and Seg filaments in archaea—used by single-celled organisms to ensure accurate DNA partitioning during cell division, revealing the complex and elegant survival solutions even in the simplest life forms. The second study, conducted by Ming-Hon Hou, investigated using bidirectional bis-intercalating acridine compounds to target DNA junction sites as a potential anticancer strategy because these compounds can cross-link and stabilize DNA junctions, thereby disrupting cellular processes and inhibiting cancer cell proliferation. The third study was by Hui-Chun Cheng, who showed that H_2S modification of PKM2 through cysteine 326 sulfhydration reduces its activity, impairs cancer cell division, and leads to tumor suppression, suggesting blocking this H_2S-mediated PKM2 modification as a promising therapeutic approach for targeting cancer cell metabolism. Finally, the fourth study was by Shiou-Ru Tzeng, who revealed how the adaptor protein NlpI regulates the cell wall endopeptidase MepS to maintain bacterial cell wall integrity by modulating MepS activity and targeting it for degradation. (by Chun-Hsiang Huang)

Two Ancient Solutions to One Modern Problem: DNA Management in Single-Celled Organisms

Single-celled bacteria and archaea use different but equally clever molecular systems to partition their DNA during cell division; bacteria with their ParABS motor system and archaea with their Seg filament system. These microscopic mechanisms show that even the simplest life forms have complex and elegant survival solutions.

One of the most fundamental challenges in microscopic cellular life is ensuring accurate DNA partitioning during cell division. This process, much like dividing a vast library's contents between two new locations, requires intricate coordination and precise organization. To address this important scientific phenomenon, Yuh-Ju Sun (National Tsing Hua University) and Chwan-Deng Hsiao (Academia Sinica) collaborated by using various bioassays and protein crystallography techniques to reveal fascinating details regarding how single-celled organisms (bacteria and archaea) accomplish this crucial task. All crystallographic data were collected at **TLS 15A**, **TPS 05A**, and **TPS 07A** of the NSRRC.

Researchers have uncovered the sophisticated ParABS (*par* stands for partitioning) system in bacteria, consisting of three key components working in harmony. ParA acts as a molecular motor powered by ATP, ParB serves as a versatile DNA-binding protein, and the *parS* sequences function as specific DNA anchoring points.[1] In this study, the *Helicobacter pylori* ParB (*Hp*ParB) protein demonstrates remarkable adaptability, behaving like a skilled librarian who can both locate specific books and organize entire shelves. This versatility is controlled by CTP, which acts as a molecular switch. When CTP is absent, *Hp*ParB focuses on specific DNA sequences (*e.g.*, *parS*), but in its presence, *Hp*ParB can slide freely along DNA (**Fig. 1(a)**).

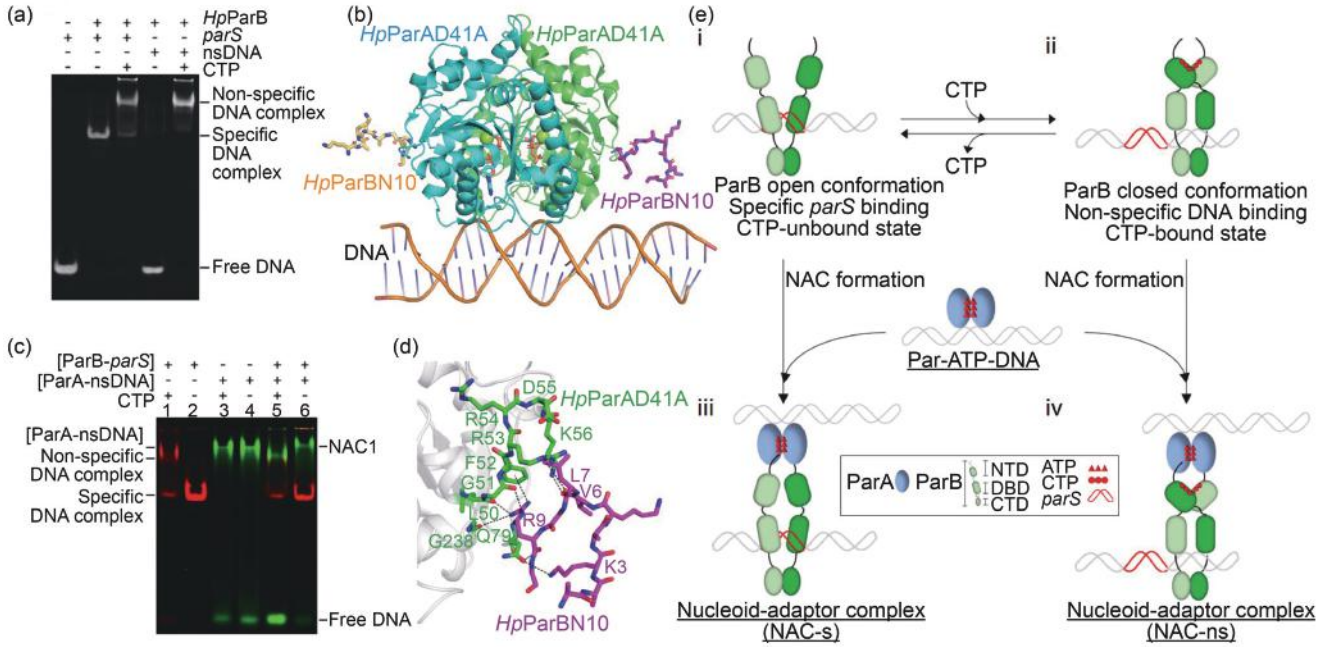

Fig. 1: (a) The electrophoretic mobility shift assay (EMSA) reveals *Hp*ParB's pattern for binding to *parS* and non-specific DNA, both with and without CTP present. (b) The *Hp*ParAD41A–DNA–*Hp*ParBN10 complex structure shows a cyan and green dimer, with orange and magenta *Hp*ParBN10 peptides bound to each monomer, alongside a wheat-colored DNA molecule. (c) EMSA analysis was performed to examine binding interactions between *Hp*ParB–*parS* and *Hp*ParA–nsDNA complexes. Initially, *Hp*ParB and *Hp*ParA were separately incubated with Cy3-labeled *parS* and Cy5-labeled nsDNA, respectively, either with or without CTP. These preformed complexes were then combined and further incubated under CTP-present or CTP-absent conditions before EMSA detection. (d) In the *Hp*ParAD41A–DNA–*Hp*ParBN10 complex, the magenta *Hp*ParBN10 binding site interacts with the grey *Hp*ParAD41A ribbon structure, where green-colored residues form key contacts marked by dashed lines. (e) The ParABS system model shows how green-colored ParB, containing three domains—the N-terminal domain (NTD), the DNA-binding domain (DBD), and the C-terminal domain (CTD)—adopts CTP-regulated open and closed conformations for specific (i) and non-specific (ii) DNA binding. When these Par–DNA complexes interact with purple-blue ParA–ATP–DNA, they form either specific NAC-s (iii) or non-specific NAC-ns (iv) nucleoid–adaptor complexes. [Reproduced from Ref. 1]

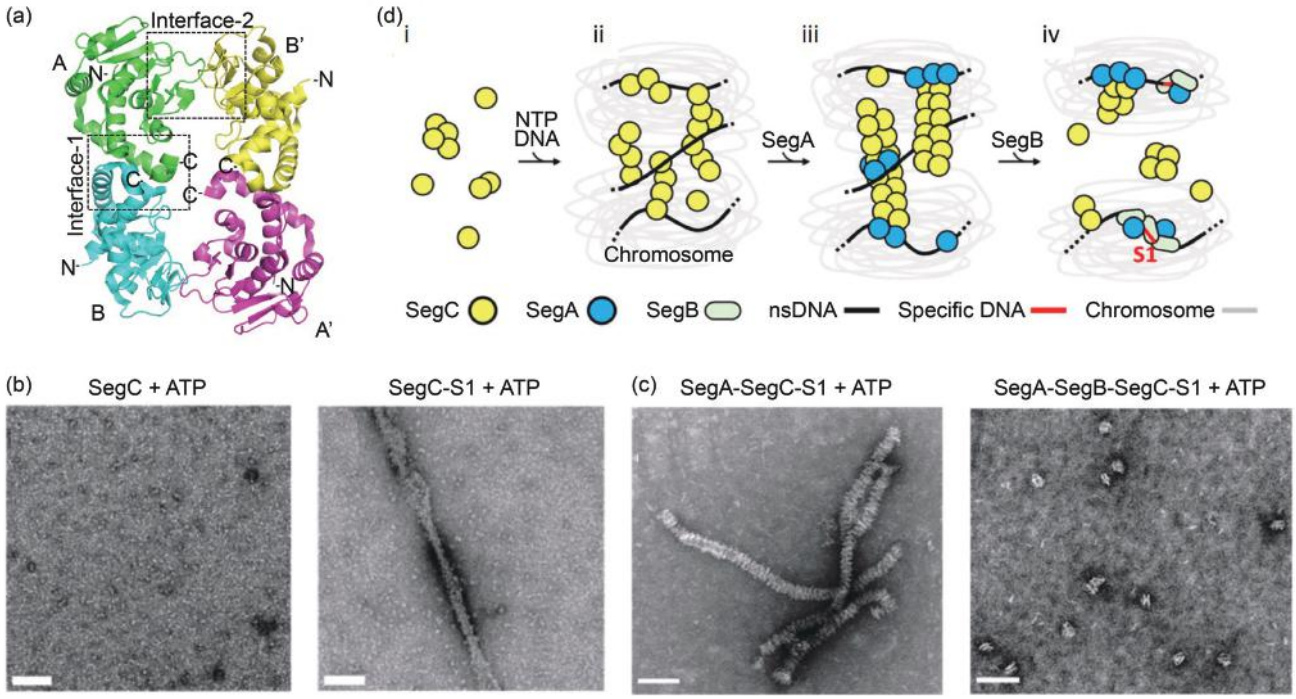

Fig. 2: (a) The SegC tetramer comprises four molecules (A, B, A', B') displayed in green, cyan, magenta, and yellow, respectively, with dimer interfaces marked by dotted squares as Interface-1 and Interface-2. (b) Negative-stain electron microscopy (EM) showing SegC structures with and without DNA and NTP. S1 (site 1) refers to a specific DNA sequence. (c) Negative-stain EM visualization of SegC, SegA, SegB, and DNA interactions. (d) A four-step model for SegC filament function: (i) Random distribution and multimerization of SegC in archaeal cells, (ii) NTP and DNA-dependent filament formation, (iii) SegA-mediated remodeling into higher-order filaments, and (iv) SegB-stimulated SegA ATPase activity leading to filament disassembly. [Reproduced from Ref. 2]

To improve our understanding of this system, researchers employed a clever strategy using a mutant form of *Hp*ParA (*Hp*ParAD41A) that displays a slower turnover rate, similar to using slow-motion photography to capture rapid movements. This approach revealed crucial details about how *Hp*ParA interacts with DNA and uses ATP for energy. *Hp*ParAD41A allowed scientists to observe the step-by-step process of how *Hp*ParA recognizes and binds to DNA, providing unprecedented insights into this fundamental mechanism (**Fig. 1(b)**).

One of the most significant discoveries in the bacterial system involves the formation of the nucleoid–adaptor complex (NAC; this term represents the composition of *Hp*ParA–*Hp*ParB–DNA). The research revealed that *Hp*ParA proteins form dimers when bound to CTP, creating a complex with DNA that can interact with *Hp*ParB through a specialized cation–π interaction. This interaction, particularly between *Hp*ParB's Arg9 and *Hp*ParA's Phe52, proves essential for the entire system's functionality (**Figs. 1(b) –1(d)**).

The bacterial study also unveiled a detailed molecular mechanism where CTP acts as a master regulator. When CTP is absent, ParB maintains an "open" configuration, specifically binding to *parS* sequences and preparing to interact with the ParA–ATP–DNA complex. The introduction of CTP triggers ParB to adopt a "closed" form, enabling it to slide along DNA non-specifically and interact more efficiently with ParA. This CTP-dependent switching mechanism is crucial for promoting ATP hydrolysis by ParA and ensuring proper system function (**Fig. 1(e)**).

Meanwhile, in the ancient world of archaea, researchers have discovered a different but equally fascinating system involving three proteins: SegA, SegB, and the newly identified SegC. Detailed structural analysis revealed that SegC has a unique architectural design that allows it to form both dimers (pairs) and tetramers (groups of four). This molecular architecture, particularly the protein's C-terminal region, proves crucial for its functionality—when researchers removed this tail end, SegC lost its ability to bind DNA and form filaments (**Fig. 2(a)**). The SegC protein shows the remarkable abilities, binding to DNA without sequence specificity and forming thread-like structures (filaments) when it encounters DNA and energy molecules (**Fig. 2(b)**).

The coordination between these components involves SegC working with SegA to form larger filaments in the presence of ATP, while SegB can break these structures apart when needed (**Fig. 2(c)**). The archaeal system's unique feature lies in SegC's ability to break down various energy molecules (NTPs), though the exact role of this capability remains under investigation. The researchers proposed a step-wise process where SegC forms initial filaments, SegA helps

organize these structures, and SegB eventually breaks them down to complete the DNA organization process (**Fig. 2(d)**).

The implications of this research extend far beyond basic science. Understanding these fundamental processes could lead to new strategies for controlling bacterial growth, potentially contributing to antibiotic developments. Furthermore, since archaea are considered ancient relatives of complex organisms, these findings provide valuable insights into how DNA organization evolved over time. (Reported by Chun-Hsiang Huang)

This report features the work of Yuh-Ju Sun and Chwan-Deng Hsiao published in Nucleic Acids Res. ***52****, 7321 (2024) and Nucleic Acids Res.* ***52****, 9966 (2024).*

TPS 05A Protein Microcrystallogrphy
TPS 07A Micro-focus Protein Crystallography
TLS 15A1 Biopharmaceuticals Protein Crystallography

- Protein Crystallography
- Biological Macromolecules, Protein Structures, Life Science

References

1. C.-H. Chu, C.-T. Wu, M.-G. Lin, C.-Y. Yen, Y.-Z. Wu, C.-D. Hsiao, Y.-J. Sun, Nucleic Acids Res. **52**, 7321 (2024).
2. M.-G. Lin, C.-Y. Yen, Y.-Y. Shen, Y.-S. Huang, I. W. Ng, D. Barillà, Y.-J. Sun, C.-D. Hsiao, Nucleic Acids Res. **52**, 9966 (2024).

Targeting DNA Junctions for Anticancer Drug Development

DNA helix–helix junctions form tetraplex base pairs at the junction interface, serving as "hotspots" for bidirectional bis-intercalating agents. This study investigates the structural basis for targeting DNA junctions with acridine bis-intercalators as a potential anticancer strategy.

Biological processes such as recombination or replication can generate DNA juxtaposed helix–helix structures and duplex crossovers.[1,2] These structures require topoisomerases to decatenate the interlinked DNA crossover sites.[3] Within the crossover structures, the base pairs of the duplexes can interact with each other, resulting in novel junctions. Targeting DNA junction sites with bis-intercalating compounds containing bidirectional linkers could inhibit topoisomerase activity, therefore representing an effective anticancer strategy.[4,5] Bidirectional bis-intercalators have the unique ability to insert their chromophores simultaneously into the base pairs of two DNA duplexes. This non-covalent bridging ability of small molecules enables them to cross-link DNA junctions, thereby disrupting biological processes critical for cellular function. However,

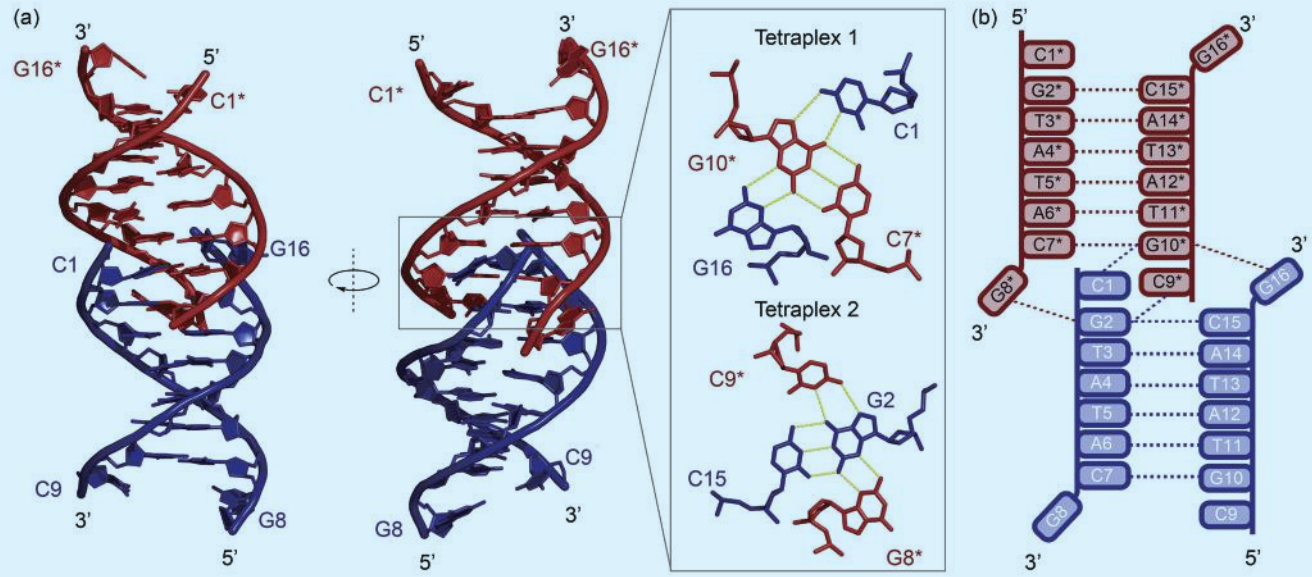

Fig. 1: Structural features of a d(CGTATACG)$_2$ DNA forming junction. (a) Crystal structure assembly of continuous duplexes forming an end-to-end helix–helix junction structure. One DNA duplex is shown in dark blue and the adjacent symmetry-related duplex is in dark red. Asterisks (*) represent residues in the adjacent duplex. Two layered tetraplex base pairings at the junction interface are shown in an enlarged view. (b) Schematic representation of the crystal structure of d(CGTATACG)$_2$, indicating the residues involved in junction formation. [Reproduced from Ref. 6]

the limited structural understanding of DNA junction formation and its interactions with small molecules has hindered the development of these targeted therapies.

The study by Ming-Hon Hou (National Chung Hsing University) and his team sheds light on the structural basis of DNA junction formation and provides valuable insights into targeting DNA junctions with bidirectional bis-intercalators for anticancer drug development.[6] The elucidation of the complex crystal structure required the access to a high-resolution X-ray facility housed at the NSRRC beamline **TLS 15A1**. Hou's team solved the crystal structure of d(CGTATACG)$_2$ DNA, which exhibited a unique duplex–duplex junction (**Fig. 1**). In the central region, the structure showed B-DNA-like right-handed features. Interestingly, the terminal CG base pairs contributed to forming a helix–helix junction with two tetraplex base pairs at the junction interface. Detailed analysis revealed that this structure closely resembles the duplex–duplex contacts in catenated DNA and that the tetraplex interface at the junction site serves as a "hotspot" capable of accommodating external ligands between the two neighboring duplexes.

Next, the team explored the possibility of targeting this junction structure with small-molecule compounds. Yih-Chern Horng (National Changhua University of Education) synthesized two alkyl-linked diaminoacridine compounds, DA4 and DA5 (**Fig. 2(a)**). Both DA4 and DA5 contain acridine chromophores connected by semi-flexible linkers that are four- and five-carbon long, respectively. These two acridine derivatives possess inter-duplex DNA intercalating properties. To investigate the binding mechanism of DA4 and DA5 with DNA, they determined the crystal structures of DA4 and DA5 with the d(CGTATACG)$_2$ sequence in the C222$_1$ and P2$_1$ space groups, respectively, at a resolution of 1.58 Å. As expected, in

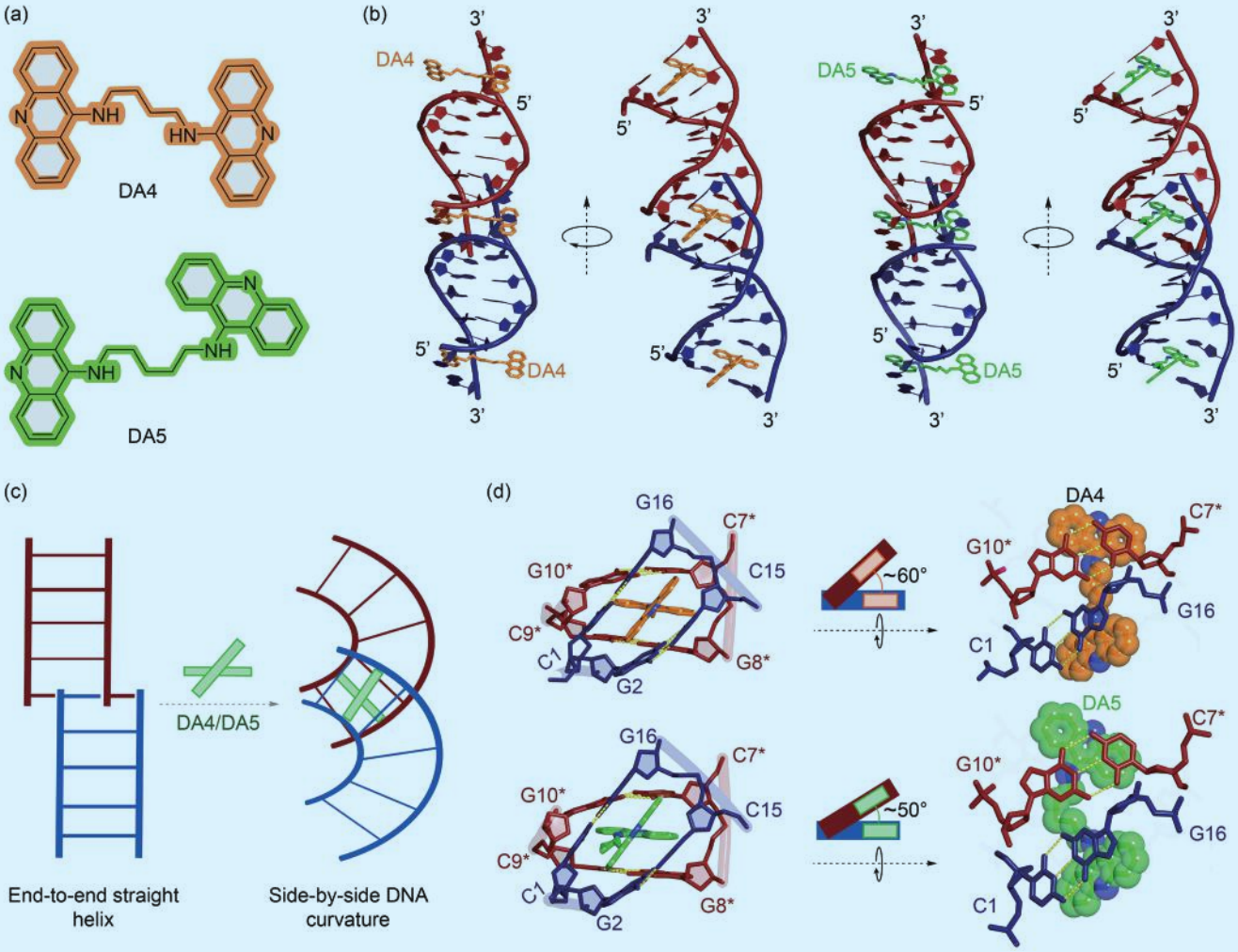

Fig. 2: (a) Chemical structures of the alkyl-linked diaminoacridine bis-intercalators DA4 (orange) and DA5 (green). (b) Crystal structure assembly of DA4–DNA and DA5–DNA complexes showing inter-duplex cross-linking of the DNA duplexes. (c) Schematic diagram showing topological changes in DNA upon intercalation of DA4 or DA5 at the terminal junction site. (d) Magnified view of the intercalation site shows the angled intercalation of DA4 and DA5 at the junction interface in steps C1pG2/C15pG16 in one duplex and C7*pG8*/C9*pG10* in the other adjacent duplex, viewed from the front and top. In DA4, the linker connecting the two acridine moieties is straight, whereas the linker in DA5 has a bent conformation. A single-atom difference in the linker of DA4 and DA5 led to distinct propeller geometries with approximately 60° and 50° between two ligands, respectively. [Reproduced from Ref. 6]

both crystal structures, the intercalation of DA4 or DA5 mediated DNA–DNA contacts and cross-linked adjacent duplexes (**Fig. 2(b)**). Compared to the unliganded native DNA junction structure, DA4 and DA5 induced significant changes in DNA topology, transforming it from an end-to-end straight helix to a side-by-side curved geometry (**Fig. 2(c)**). The cross-linking of DNA duplexes also caused a transition from the B-form to an A-form-like conformation, accompanied by bending and overwinding of the backbone. The different linker lengths and flexibilities of DA4 and DA5 resulted in distinct local structural and stabilizing effects on DNA. In the DA4–DNA complex, the four-carbon linker of DA4 adopted a straight geometry, while the DA5 linker bent toward one of the DNA backbones (**Fig. 2(d)**). This difference in linker flexibility caused the chromophores of DA4 and DA5 to stagger at different angles. In the DA4–DNA complex, the chromophores formed an angle of approximately 60° with the horizontal plane of the acridine ring, while in the DA5–DNA complex, the angle between the two acridine chromophores was approximately 50°. This flexibility of the DA5 linker allowed its chromophores to align more optimally, enabling continuous stacking interactions with DNA base pairs. Consequently, DA5 exhibited more stacking interactions with DNA than DA4. The bent linker and less tilted chromophore of DA5 brought its amino groups closer to the cytosine bases, facilitating a direct water-mediated interaction that likely resulted in a more stable complex with stronger binding. By contrast, the greater distance between the amino group of the DA4 linker and the keto group of cytosine in the DA4–DNA complex led to indirect and weaker water-mediated interactions. These findings suggest that DA5 induces stronger structural changes in DNA than DA4, potentially leading to stronger stabilizing effects. These results were further corroborated through biophysical experiments.

When tested in *in vitro* and *in vivo* models, the two acridine derivatives inhibited topoisomerase II activity, induced G2/M phase accumulation in the cell cycle, triggered apoptosis, and reduced cancer tumor growth, highlighting the anticancer potential of this mode of DNA binding. Notably, the results showed that DA5 exhibited more pronounced anticancer effects than DA4, likely due to its enhanced stability and stronger DNA-binding interactions at the junction. Through investigation of the structural basis for these results, Hou and his team demonstrated how small molecules can precisely target and stabilize DNA junction sites, inhibit topoisomerase activity, and impair cancer cell proliferation. These findings could guide the development of more effective derivatives in future, paving the way for targeting DNA–DNA duplex contacts through bis-intercalation. (Reported by Roshan Satange, National Chung Hsing University)

This report features the work of Ming-Hon Hou and his collaborators published in Nucleic Acids Res. ***52****, 9303 (2024).*

TLS 15A1 Biopharmaceuticals Protein Crystallography

- X-ray Crystallography
- Biological Macromolecules, Cancer, DNA Junctions, Life Science

References

1. M. L. Martínez-Robles, G. Witz, P. Hernández, J. B. Schvartzman, A. Stasiak, D. B. Krimer, Nucleic Acids Res. **37**, 5126 (2009).
2. G. Witz, A. Stasiak, Nucleic Acids Res. **38**, 2119 (2009).
3. Y. Pommier, A. Nussenzweig, S. Takeda, C. Austin, Nat. Rev. Mol. Cell Biol. **23**, 407 (2022).
4. E. Ivens, M. M. D. Cominetti, M. Searcey, Bioorg. Med. Chem. **69**, 116897 (2022).
5. K. T. McQuaid, A. Pipier, C. J. Cardin, D. Monchaud, Nucleic Acids Res. **50**, 12636 (2022).
6. S.-C. Huang, C.-W. Chen, R. Satange, C.-C. Hsieh, C.-C. Chang, S.-C. Wang, C.-L. Peng, T.-L. Chen, M.-H. Chiang, Y.-C. Horng, M.-H. Hou, Nucleic Acids Res. **52**, 9303 (2024).

Breaking Cancer's Energy Code: New Insights into Hydrogen Sulfide and Pyruvate Kinase M2 Regulation

Hydrogen sulfide modifies the pyruvate kinase M2 enzyme at cysteine 326, affecting cancer cell metabolism. Blocking this modification reduces PKM2 activity and impairs cancer cell division, leading to complete tumor suppression.

Cancer cells undergo significant metabolic reprogramming that is primarily characterized by the Warburg effect. In this process, they prefer aerobic glycolysis over oxidative phosphorylation. Although this process is less efficient for ATP production, it provides essential metabolic intermediates for rapid cancer cell proliferation under nutrient-limited conditions.

The glycolytic pathway is regulated by three key enzymes, with the pyruvate kinase M2 (PKM2) playing a crucial role. PKM2, which is predominantly expressed in cancer cells, differs from PKM1's catalytic properties. While PKM1 maintains high activity as a tetramer, PKM2's activity is typically low in cancer cells because of various post-translational modifications, which allow redirection of glucose metabolism toward biomass synthesis.

Recent research has focused on hydrogen sulfide (H_2S), an endogenous gasotransmitter that shows concentration-dependent effects on cancer progression. H_2S primarily functions through protein sulfhydration, a post-translational modification where H_2S forms a persulfide (-SSH) bond on cysteine residues of target proteins.[1] At lower concentrations, H_2S promotes tumor growth through multiple mechanisms, including antiapoptotic effects, DNA repair, and angiogenesis. However, higher concentrations can inhibit cancer cell proliferation.

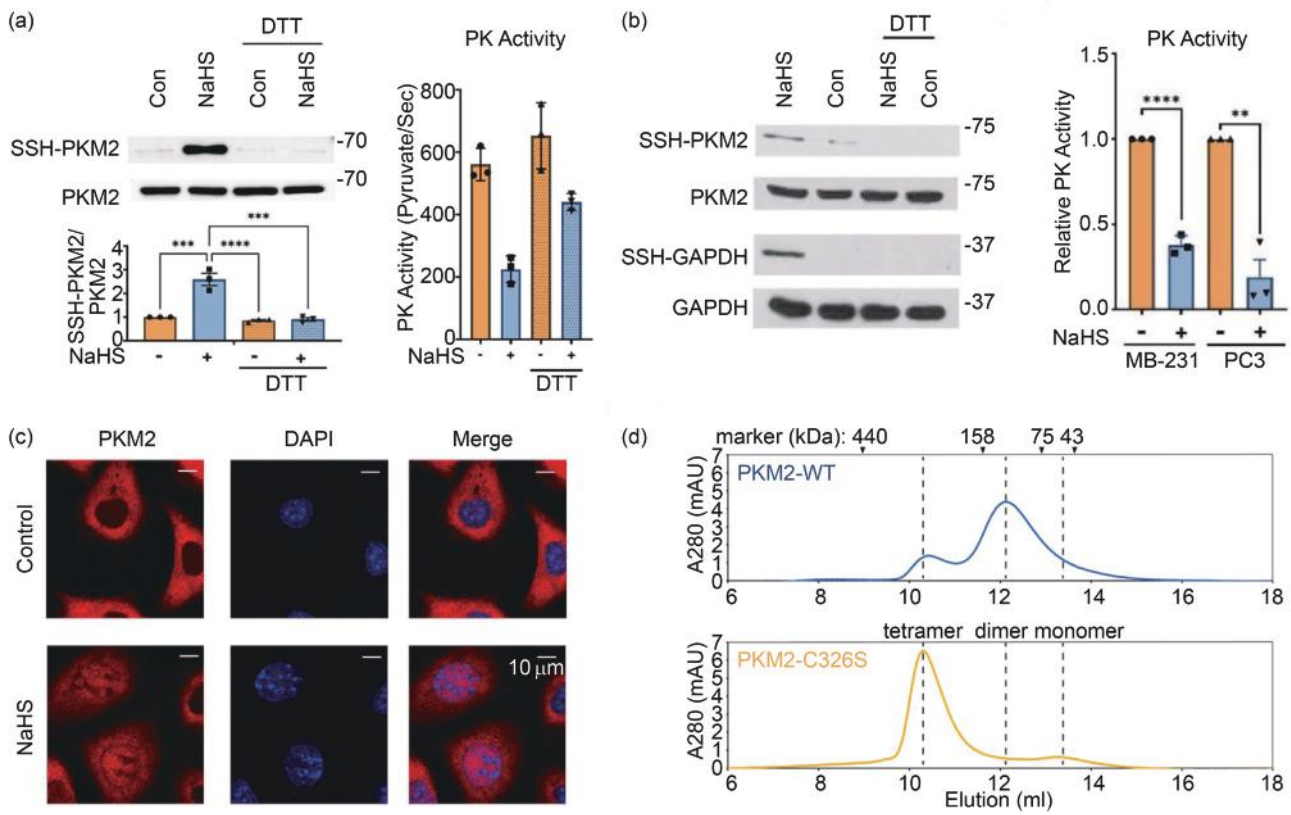

Fig. 1: (a) Results of two main analyses performed in the experimental study. The first part examined PKM2 sulfhydration in MDA-MB-231 cell lysates treated with NaHS and DTT by using a biotin switch assay followed by immunoblotting with an anti-PKM2 antibody. The second part investigated pyruvate kinase activity by measuring pyruvate production in recombinant PKM2 after treatment with NaHS and DTT under ice-cold conditions. (b) Results of the experiment investigating protein sulfhydration and enzymatic activity in two parts. The first part examined PC3 cell lysates treated with NaHS and DTT by using biotin switch assay and immunoblotting to detect sulfhydration of both PKM2 and GAPDH (used as a positive control). The second part focused on measuring pyruvate kinase activity in both MDA-MB-231 and PC3 cell lysates after NaHS treatment, specifically by quantifying pyruvate production. (c) Treatment of MDA-MB-231 cells with NaHS and visualization of PKM2 localization using immunocytochemistry with DAPI nuclear staining (scale: 10 μm). (d) Results of gel filtration analysis of PKM2 proteins (WT and C326S mutant) performed without FBP to examine their oligomeric states. [Reproduced from Ref. 2]

The interplay between H_2S and PKM2 represents a fascinating area of research, particularly given that PKM2 activity can be inhibited by L-cysteine, which serves as the primary source for H_2S production. This intricate connection, which is mediated through protein sulfhydration, reveals a critical regulatory mechanism in cancer cell metabolism. The emerging understanding of how H_2S-mediated protein sulfhydration influences cancer progression has opened promising new avenues for therapeutic interventions that specifically target cancer-specific metabolic pathways. To further explore this novel regulatory mechanism, Lu-Hai Wang (China Medical University), Hui-Chun Cheng (National Tsing Hua University), and Kai-Ti Lin (National Tsing Hua University) launched a collaborative effort to investigate the molecular mechanisms underlying H_2S-mediated PKM2 regulation in cancer cells.

The researchers first investigated the role of H_2S in PKM2 activity through protein sulfhydration. **Figures 1(a) and 1(b)** show that treatment with NaHS, a H_2S donor, induced PKM2 sulfhydration in both breast cancer MDA-MB-231 and prostate cancer PC3 cells; this modification reduced PKM2 enzyme activity, which could be reversed by dithiothreitol (DTT) treatment. Importantly, H_2S caused the dissociation of fructose 1,6-bisphosphate (FBP)-induced PKM2 tetramers into monomers or dimers. This led to enhanced PKM2 nuclear translocation (**Fig. 1(c)**) and increased expression of PKM2-responsive genes, such as cyclin D1 and glutaminase-1; the expression levels of these genes show a positive correlation with tumor growth. When H_2S was depleted using the aminooxyacetic acid inhibitor or by knocking down H_2S-producing enzymes, such as cystathionine β-synthase and cystathionine γ-lyase, both PKM2 sulfhydration and nuclear translocation decreased.

Through mass spectrometry analysis, the researchers identified two sulfhydration sites on recombinant PKM2: cysteines 49 and 326. However, only cysteine 326 was found to be endogenously sulfhydrated in MDA-MB-231 cells. To further study the effects of sulfhydration at this site, they created a mutation replacing cysteine 326 with serine ($PKM2^{C326S}$). This mutation significantly reduced PKM2 sulfhydration and, notably, resulted in increased tetramer formation compared to wild-type PKM2 (**Fig. 1(d)**). Crystal structure analysis revealed that $PKM2^{C326S}$ adopts a unique tetrameric conformation that is different from previously known conformations (**Fig. 2(a)**). The X-ray diffraction data were collected at **TPS 07A** of the NSRRC.

The functional consequences of blocking PKM2 sulfhydration at C326 were substantial. The $PKM2^{C326S}$ mutation increased pyruvate kinase activity and led to significant metabolic changes in cells. Cells expressing $PKM2^{C326S}$ showed increased oxygen consumption rates and enhanced mitochondrial oxidative phosphorylation, while extracellular acidification rates only slightly increased. These cells also showed reduced expression of most PKM2-responsive genes, decreased levels of glycolytic intermediates, and reduced nuclear translocation of PKM2.

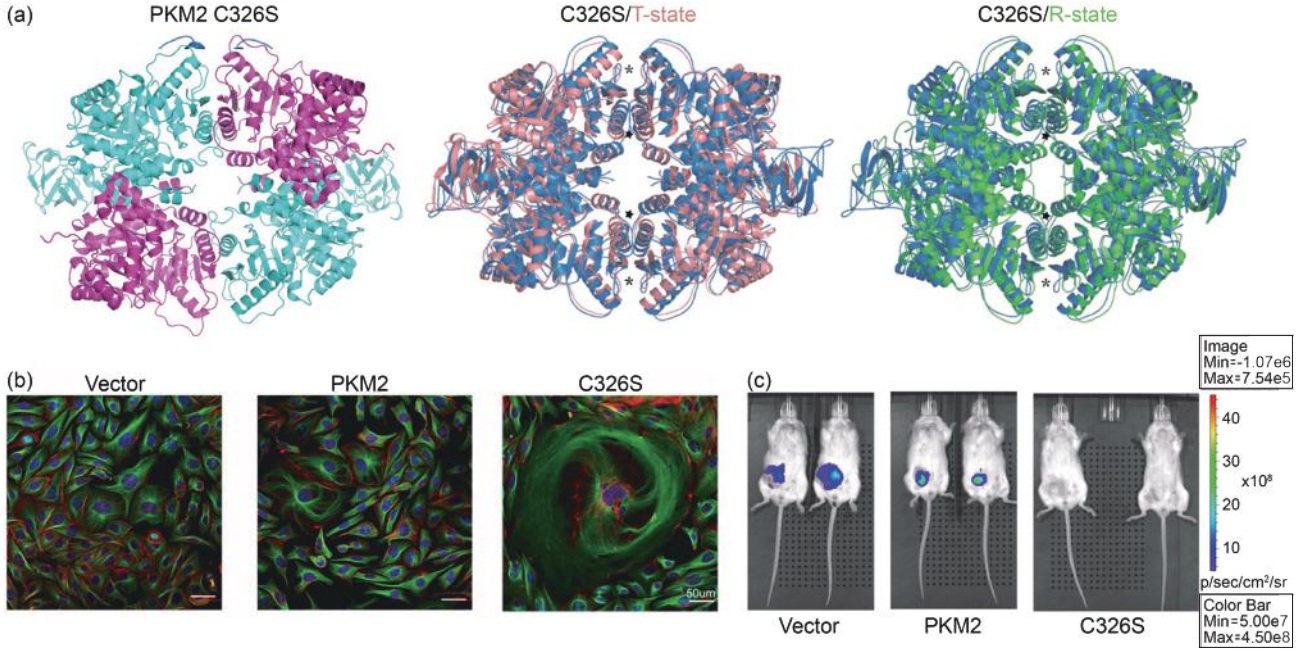

Fig. 2: (a) Structural analysis comparison of the crystal structure of PKM2 C326S mutant with both T-state (phenylalanine-bound) and R-state (FBP/serine-bound) conformations, highlighting key regions: the effector loop and α14-α15 regions, which are indicated by asterisk and star, respectively. The overlaid structures are color-coded as C326S mutant in blue, T-state in pink, and R-state in green to allow for direct comparison of conformational differences between these states. (b) Immunostaining of MDA-MB-231 cells expressing vector, PKM2, or $PKM2^{C326S}$, showing actin (red), α-tubulin (green), and nuclei (DAPI, blue). Images are displayed at 50 μm scale. (c) Bioluminescence imaging of tumor growth in mouse mammary fat pads at week 7 post-implantation of MDA-MB-231 cells expressing different PKM2 variants (vector, wild-type, or C326S). [Reproduced from Ref. 2]

The researchers observed significant negative effects on cancer cell division and proliferation in cells expressing $PKM2^{C326S}$. These cells showed an increased percentage of polyploidy cells and a higher frequency of giant multinucleated cells (**Fig. 2(b)**). Time-lapse microscopy revealed a 1.5-fold increase in cytokinesis failure in $PKM2^{C326S}$-expressing cells. Furthermore, $PKM2^{C326S}$ failed to interact with the spindle checkpoint protein BUb3, and cells showed reduced proliferation rates. Similar effects were observed in cells with H_2S depletion, supporting the specific role of sulfhydration in these processes.

Perhaps most significantly, in a mouse xenograft model, tumor growth was completely suppressed in the $PKM2^{C326S}$ group (**Fig. 2(c)**). While there were no significant differences in mouse body weight between groups, there was a dramatic reduction in tumor bioluminescence signals in the $PKM2^{C326S}$ group, indicating strong anti-tumor effects.

These comprehensive results demonstrate that H_2S-mediated sulfhydration of PKM2 at C326 is a crucial mechanism regulating cancer cell metabolism. Blocking this modification through the $PKM2^{C326S}$ mutation leads to the stabilization of PKM2 tetramers, enhanced oxidative phosphorylation, reduced nuclear translocation and transcriptional activity, impaired cell division, and suppressed tumor growth. These findings suggest that targeting PKM2 sulfhydration could be a promising therapeutic approach for cancer treatment, particularly by rewiring glucose metabolism from aerobic glycolysis to oxidative phosphorylation. The study provides both mechanistic insights into cancer metabolism and potential therapeutic strategies for future drug development.
(Reported by Chun-Hsiang Huang)

This report features the work of Hui-Chun Cheng and her collaborators published in Nat. Commun. ***15****, 7463 (2024).*

TPS 07A Micro-focus Protein Crystallography

- Protein Crystallography
- Biological Macromolecules, Protein Structures, Life Science

References

1. B. D Paul, S. H Synder, Nat. Rev. Mol. Cell Biol. **13**, 499 (2012).
2. R.-H. Wang, P.-R. Chen, Y.-T. Chen, Y.-C. Chen, Y.-H. Chu, C.-C. Chien, P.-C. Chien, S.-Y. Lo, Z.-L. Wang, M.-C. Tsou , S.-Y. Chen, G.-S. Chiu, W.-L. Chen, Y.-H. Wu, L. H.-C. Wang, W.-C. Wang, S.-Y. Lin, H.-J. Kung, L.-H. Wang, H.-C. Cheng, K.-T. Lin, Nat. Commun. **15**, 7463 (2024).

Structure of the Prc–NlpI–MepS Complex: Elucidating the Regulatory Mechanism of Bacterial Cell Walls

This study reveals how the adaptor protein NlpI regulates the activity and cellular levels of the cell wall endopeptidase MepS, which facilitates peptidoglycan remodeling and maintains cell wall integrity during bacterial growth and development.

Peptidoglycan (PG) is vital for protecting bacterial cells from osmotic pressure. It consists of linear glycan strands of alternating *N*-acetylglucosamine (NAG) and *N*-acetylmuramic acid (NAM), linked to short peptide chains. The main cross-linking of the short peptide chains is the 4–3 linkage between D-Ala and meso-diaminopimelic acid (DAP), forming a net-like structure that prevents osmotic rupture. During cell growth, the net-like structure must be cleaved to incorporate new PG strands, a process facilitated by several endopeptidases, including MepS, MepM, and MepH. In *Escherichia coli* (*E. coli*), these three endopeptidases are essential for cell wall expansion and their absence leads to abnormal cell shapes and lysis.

NlpI is an outer membrane-anchored lipoprotein found in Gram-negative bacteria (*e.g.*, *E. coli*) and plays multiple roles in cell division, cell wall metabolism, virulence, and host interactions. It interacts with various hydrolases and associates with the PG synthesis machinery, influencing the stability of cell envelope components. As an adaptor protein, NlpI can bind to three endopeptidases—MepS, MepM, and PBP4—and facilitates the formation of trimeric complexes (*e.g.*, MepS-NlpI-PBP4). In addition, NlpI helps localize these enzymes, connecting PG hydrolysis to expansion. Reconstitution experiments show that NlpI organizes PG multienzyme complexes, suggesting it aids in integrating hydrolases and synthases during PG expansion.

MepS is abundant during the log phase of cell growth but declines in the stationary phase. Its protein levels within the cell are regulated by the periplasmic PDZ-protease Prc (also called tail-specific protease), in complex with the adaptor NlpI. Without NlpI, Prc cannot effectively degrade MepS, highlighting NlpI's crucial role in MepS recruitment. Mutants lacking Prc or NlpI show increased MepS levels, leading to long filaments and growth defects in low-osmolarity conditions.

In 2017, the structure of the Prc-NlpI complex (PDB ID 5WQL) was determined by X-ray crystallography, revealing a symmetric NlpI homodimer attached to two bowl-shaped Prc proteins. NlpI, an adaptor protein with four tetratricopeptide repeats (TPRs), interacts with Prc through TPR2, forming an extensive electrostatic network. The unliganded PDZ domain of Prc has a misaligned conformation, which rearranges upon ligand binding, activating its proteolytic activity (**Fig. 1(a)**).[1] However, two important issues regarding the regulation mechanism of PG expansion have not been resolved, namely how NlpI regulates MepS to affect their activities and how NlpI modulates the protein levels of MepS in the presence of the Prc protease. To investigate the mechanisms underlying these two important issues, Shiou-Ru Tzeng (National Taiwan University) and her collaborators U-Ser Jeng (NSRRC) and Chun-Hsiang Huang (NSRRC) employed various experimental techniques, including nuclear magnetic resonance (NMR), biological small-angle X-ray scattering (BioSAXS), protein crystallography (PX), and other biochemical analysis methods. Specifically, X-ray diffraction and scattering data were acquired using the beamlines **TPS 05A**, **TPS 07A**, and **TPS 13A** at the NSRRC.

To elucidate how NlpI regulates MepS, NMR experiments were performed (**Fig. 1(b)**) and demonstrated that the mature full-length MepS (mMepS) can utilize its intrinsically disordered N-terminal region to interact with the adaptor protein NlpI. The crystal structure of the NlpI–mMepS complex reveals a heterohexameric assembly, where a homodimer of NlpI binds to four MepS molecules (**Fig. 1(c)**). This structural arrangement facilitates the colocalization and cooperative function of multiple MepS molecules, enhancing their avidity for PG binding and hydrolysis. Notably, upon binding to NlpI, the disordered N-terminal region of MepS undergoes a transition to an ordered state (**Fig. 1(d)**), promoting the dimerization of MepS. This structural insight provides a mechanistic understanding of how NlpI regulates the activity of MepS through modulating its oligomerization state and cooperative interactions with the PG substrate.

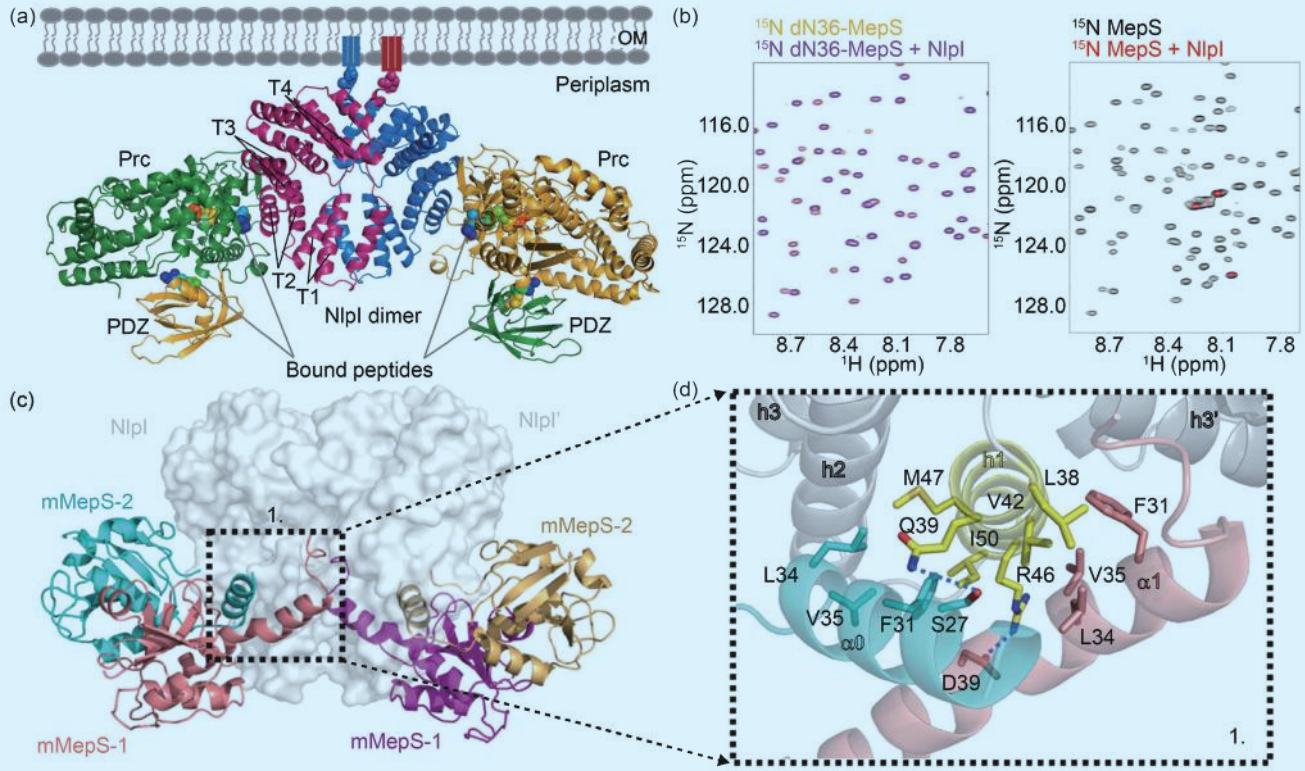

Fig. 1: (a) Overall structure of the NlpI–Prc complex shows a dimeric NlpI bound to two Prc proteins, represented in different colors. The PDZ domain of Prc and the four tetratricopeptide repeats (TPR1–4) of NlpI are labeled. The outer membrane (OM) and lipid anchors are depicted, with the first residues linked to the lipobox cysteine shown as spheres. Four co-crystallized substrate peptides are shown as rainbow-colored spheres. (b) NMR experiments were performed to study the interaction between NlpI and the mMepS proteins. ^{1}H-^{15}N TROSY-HSQC spectra were acquired for the truncated mutant dN36-MepS, which is devoid of the N-terminal 36 residues, and mMepS in the absence and presence of unlabeled NlpI dimer. (c) Overall structure of the NlpI-mMepS complex reveals a dimeric NlpI (grey surface) bound to four mMepS proteins (illustrated in different colors). (d) The interactions between NlpI and mMepS involve specific hydrophobic contacts. [Reproduced from Ref. 1 and Ref. 2]

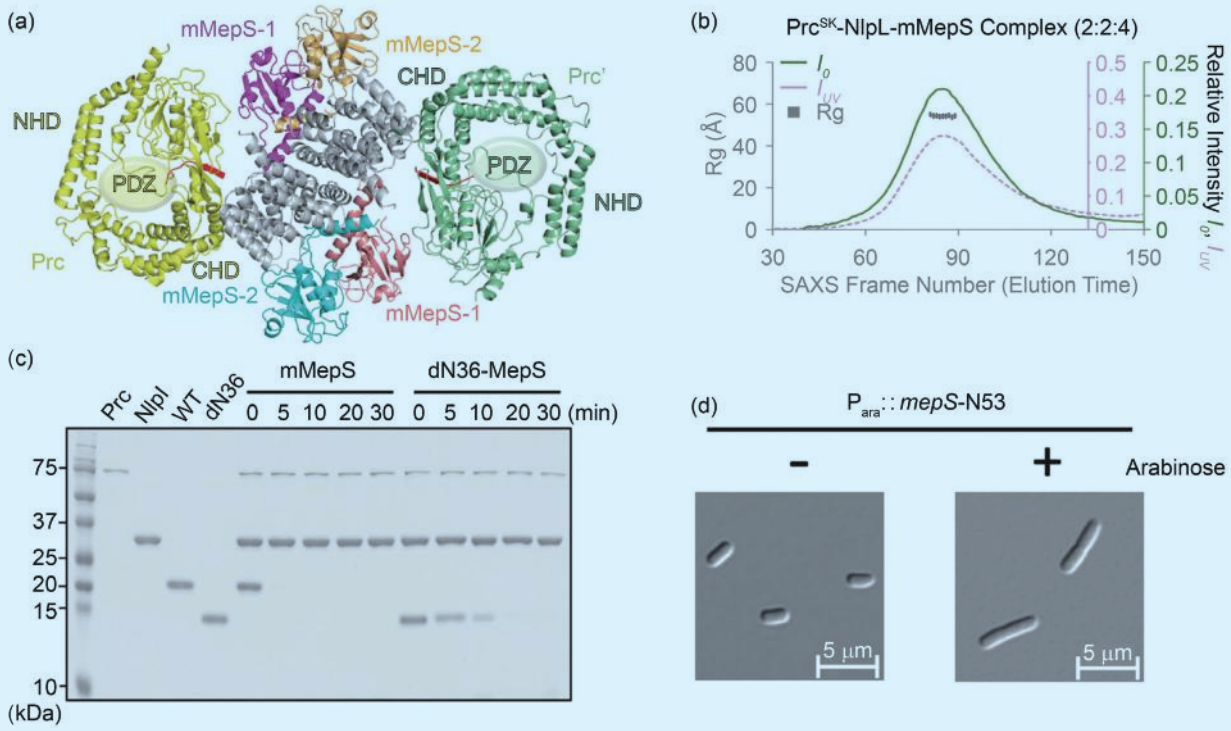

Fig. 2: (a) Overall structure of the Prc–NlpI-mMepS complex is shown, with NlpI in gray, Prc in yellow and pale green, and mMepS1 and mMepS2 in other colors. (b) A size-exclusion chromatogram of the Prc–NlpI–mMepS complex is presented, displaying the radius of gyration (*Rg*), zero-angle scattering intensity (I_0), and absorbance at 280 nm (I_{UV}). (c) *In vitro* degradation assays were conducted to examine the proteolytic activity of the Prc–NlpI system on mMepS and dN36-MepS. (d) The impact of overexpressing MepS-N53 on bacterial cell morphology was visualized using differential interference-contrast (DIC) microscopy. [Reproduced from Ref.1]

To understand how NlpI modulates the protein levels of MepS in the presence of the Prc protease, structural analysis was performed and revealed that the tail-specific protease Prc forms a 2:2:4 hetero-octameric complex with the adaptor protein NlpI and the endopeptidase mMepS (**Fig. 2(a)**). Size exclusion chromatography coupled with small-angle X-ray scattering (SEC-SAXS) experiments confirmed this 2:2:4 stoichiometry, ruling out the possibility that the observed stoichiometry was an artifact of crystal packing (**Fig. 2(b)**). Furthermore, the experimental data showed that the dN36-MepS significantly reduced its interaction with NlpI and decreased the degradation efficiency of mMepS by the Prc–NlpI system (**Fig. 2(c)**). This further confirms the important role of the N-terminal region in the recognition of mMepS by NlpI and the subsequent targeting of mMepS for Prc-mediated degradation. At the cellular level, overexpression of the N-terminal 53 residues of mMepS (MepS-N53) led to a significant change in bacterial morphology, resulting in the formation of long filamentous cells (**Fig. 2(d)**).

This study provides crucial structural insights into how the lipoprotein NlpI recruits and colocalizes the endopeptidase MepS, facilitating enhanced PG hydrolysis during bacterial cell growth. The binding of NlpI induces a disorder-to-order transition in the N-terminal region of MepS, promoting its dimerization and increasing enzymatic activity. Additionally, NlpI plays a pivotal role in targeting MepS for degradation by the protease Prc during the stationary phase, thus regulating the cellular levels of MepS and maintaining cell wall integrity. These findings advance our understanding of the molecular mechanisms underlying bacterial cell wall remodeling and highlight the functional versatility of NlpI in coordinating PG synthesis and degradation. (Reported by Chun-Hsiang Huang, NSRRC)

This report features the work of Shiou-Ru Tzeng and her collaborators published in Nat. Commun. ***15****, 5461 (2024).*

TPS 05A Protein Microcrystallography
TPS 07A Micro-focus Protein Crystallography
- Protein Crystallography
- Biological Macromolecules, Protein Structures, Life Science

TPS 13A Biological Small-angle X-ray Scattering
- BioSAXS
- Structural Transitions of Macromolecules in Solution

References

1. M.-Y. Su, N. Som, C.-Y. Wu, S.-C. Su, Y.-T. Kuo, L.-C. Ke, M.-R. Ho, S.-R. Tzeng, C.-H. Teng, D. Mengin-Lecreulx, M. Reddy, C.-I Chang, Nat. Commun. **8**, 1516 (2017).
2. S. Wang, C.-H. Huang, T.-S. Lin, Y.-Q. Yeh, Y.-S. Fan, S.-W. Wang, H.-C. Tseng, S.-J. Huang, Y.-Y. Chang, U-S. Jeng, C.-I Chang, S.-R. Tzeng, Nat. Commun. **15**, 5461 (2024).

Energy Science

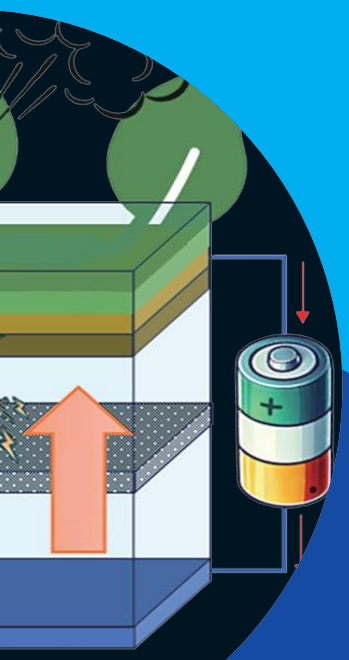

Synchrotron-based techniques remain indispensable in advancing energy storage and catalysis research despite significant progress in computational modeling and emerging *in situ* characterization methods. These techniques provide atomic-level insights into the structural and electronic properties of materials, thus enabling the development of high-performance batteries, electrocatalysts, and photocatalysts. At the NSRRC, several beamlines are dedicated to energy-related research, supporting breakthroughs in sodium ion batteries, zinc–air batteries, photocatalysis, methanol decomposition, and CO_2 electroreduction. Researchers have leveraged X-ray absorption spectroscopy, X-ray photoelectron spectroscopy, and X-ray diffraction to explore material transformations during operation, shedding light on reaction mechanisms and structural stability. **TPS 32A** and **TPS 44A** have been instrumental in characterizing the electronic structure of target materials and have provided crucial insights into defect-engineered nanosheets, which have optimized piezoelectric polarization in the field of sustainable electrocatalysis. **TLS 17C1** has enabled atomic-scale studies of Fe–Co and Ni–Fe bifunctional catalysts, thereby improving oxygen evolution and reduction reactions for zinc–air batteries. **TLS 09A2** and **TLS 24A1** have facilitated research on revealing the role of undercoordinated platinum sites in methanol decomposition. NSRRC's state-of-the-art beamlines continue to support diverse scientific endeavors, enabling fundamental discoveries that drive advancements in sustainable-energy solutions.

In 2024, researchers utilizing NSRRC facilities achieved significant breakthroughs in energy storage and catalytic applications. This report highlights five outstanding contributions that advance battery technology and catalysis for sustainable-energy solutions. The first direction, led by Han-Yi Chen and Ji Liang, addressed a major limitation in current sodium ion transport technology within cathodes. Their work underscored the potential of layered structures, particularly layered metal oxide cathodes with complex elemental compositions, to enhance conductivity, stability, and overall performance. The second direction, headed by Shih-Yuan Lu and Yuan-Yao Li, introduced synergistic binary single-atom catalysts as air cathodes for high-performance and ultrastable zinc–air batteries. This dual-functional system significantly improved the efficiency and rechargeability of zinc–air and aluminum–air batteries, thus paving the way for flexible and sustainable energy storage solutions. For the third direction, Jih-Jen Wu developed dual-vacancy-engineered $ZnIn_2S_4$ nanosheets for hydrogen evolution. This study revealed a novel mechanism where low-frequency-vibration-induced piezoelectric polarization coupled with a static dipole field enhances photocatalytic hydrogen production. For the fourth direction, Meng-Fan Luo investigated undercoordinated Pt sites on the surface of layered $PtTe_2$, elucidating their role in methanol decomposition. This work provided crucial insights into catalytic activity modulation, which can lead to more efficient methanol-to-energy conversion technologies. Finally, Bing Joe Hwang's study introduced a dual single-atom Ni/Cu catalyst that demonstrated highly selective CO_2-to-ethanol conversion. This research represents a major step forward in carbon capture and utilization, offering a promising route for sustainable fuel production. These studies underscore the vital role of NSRRC facilities in advancing battery technology and catalysis, which thereby contributes to the global pursuit of sustainable and efficient energy solutions. (by Hao Ming Chen)

Innovating Sodium-Ion Battery Cathodes: Enhancing Stability and Performance

Layered metal oxide cathode material engineering for sodium ion batteries holds significant potential for alkali-doped P2 and O3 high-capacity layered oxides.

With the rise in the global reliance on renewable energy sources, the demand for cost-effective, scalable energy-storage solutions has increased. Traditional lithium ion batteries (LIBs), while effective, face resource limitations due to lithium's limited supply and mining complexities. By contrast, sodium (Na) is the sixth most abundant element on Earth, making sodium ion batteries (SIBs) a cheaper, highly safe, and more sustainable alternative for large-scale energy-storage applications (**Fig. 1**).[1] The performance of SIBs is considerably influenced by the components of the cathode, anode, and electrolyte. However, achieving the energy densities and performance levels of SIBs comparable to LIBs has been challenging, necessitating extensive research into material compositions, structural arrangements, and electrochemical behaviors of Na ion systems. One of the focal points of recent research on SIBs has been the layered P2 and O3 structures in metal oxide cathode materials, which describe how sodium and transition-metal oxides are arranged within the cathode. In this context, "P" indicates sodium ions positioned at prismatic sites, while "O" indicates those located at octahedral sites based on the stacking sequences of oxide layers. The numbers 2 and 3 represent the number of Na ion layers per unit cell. Recently, most researchers have been exploring the ways to modify the layered structures and develop hybrid models to capitalize on each structure's strengths, aiming to suppress the adverse phase transition of layered oxide cathodes. For instance, inserting or doping alkali or transition-metal cations in the layered structure, designing a multi-element intention known as a high-entropy system, and switching between O3 and P2 phases during operation can, in theory, provide the high specific capacities for efficient energy storage and exhibit excellent cycling stability for reliable performance over multiple charge–discharge cycles. Variations of designs remain an area of active investigation, with potential implications for improving SIB performance. Employing a combination of advanced synchrotron X-ray techniques, including X-ray photoelectron spectroscopy (XPS), X-ray diffraction (XRD), and X-ray absorption spectroscopy (XAS), plays a key role in examining the structural and electrochemical properties of the layered cathode materials. These techniques allow for in-depth analysis of the materials at an atomic and molecular level, providing insights into their structural stability, chemical composition, and electronic behavior.

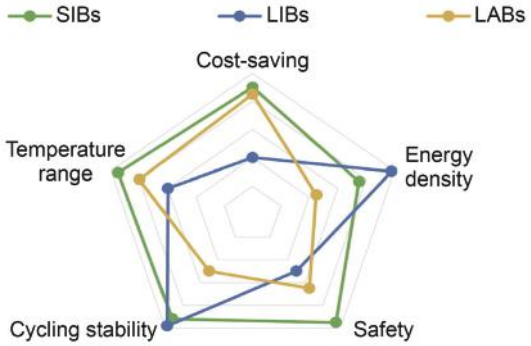

Fig. 1: Comparison of three established rechargeable battery technologies (SIBs, LIBs, and lead–acid batteries (LABs)) in the current market. [Reproduced from Ref. 1]

Most studies have tackled these challenges through innovative cathode material engineering for achieving high energy density and ensuring long-term cycling stability for SIBs. Han-Yi Chen (National Tsing Hua University) focused on a potassium (K)-doped P2-type layered $Na_{0.67}Mg_{1/3-x}Cu_xMn_{2/3}O_2$ oxide cathode, which utilizes alkali-doped configuration to facilitate the movement of Na ions through larger diffusion pathways. This configuration enhances ionic conductivity and improves electrochemical performance.[2] K ions were selected for doping because of their larger ionic radius compared to Na, which thereby serves as a "pillar" that stabilizes the layered structure during Na ion intercalation and deintercalation. In particular, a doping level of $K_{0.05}$ showed the most promising results, achieving the highest specific capacity of 203 mAh/g, which represents a significant improvement compared to the undoped material's capacity of 185 mAh/g. This highlights the effectiveness of K doping in expanding ion diffusion pathways and enhancing material stability. *In situ* XRD analysis conducted at **TLS 01C2** provided insights into structural shifts within the cathode materials, revealing that moderate potassium doping (up to $K_{0.05}$) supports the P2 structure without causing unwanted phase transitions (**Fig. 2**, see next page). XAS analysis of transition-metal K-edges performed at **TPS 44A** and **TLS 17C1** further supported these findings, revealing that potassium doping did not alter the oxidation states of the transition metals. The structural integrity and charge balance were maintained within the material. This result is critical as it demonstrates that potassium serves as a stabilizer without disrupting the essential redox processes in the cathode material.

Another similar research conducted this year by Ji Liang (Tianjin University, China) explored a Li/Ti co-substitution strategy to address structural challenges in O3-type layered oxide cathodes for SIBs.[3] By modifying the local electronic configuration of oxygen in $NaNi_{0.5}Mn_{0.5}O_2$ (NM) with an O3 structure, this approach effectively mitigates phase transitions and enhances structural stability, especially at high voltages, a common problem for layered oxides under high sodium extraction. This is a key development in stabilizing O3-phase materials through the specific elemental substitution. It demonstrates that Li/Ti co-substitution strengthens electrostatic bonding in the transition-metal layer and prevents adverse phase transitions, such as those from O3 to OP2, in a voltage range of 2.0–4.3 V. The Li/Ti-modified $NaLi_{1/9}Ni_{1/3}Mn_{4/9}Ti_{1/9}O2$ (LNMT) cathode achieved impressive electrochemical performance with a capacity of 161.2 mAh g^{-1} at 1C and 80% retention after 100 cycles, underscoring the effectiveness of local electronic regulation in addressing phase instability (**Fig. 3**).

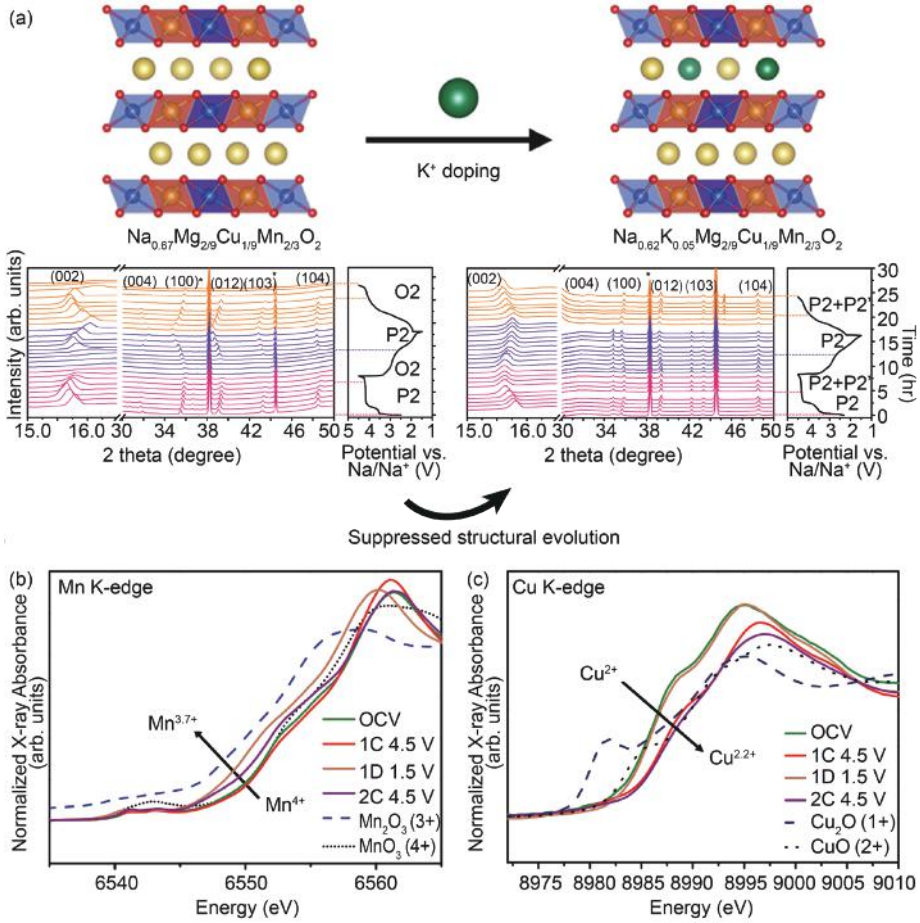

Fig. 2: Schematic K-doped P2 crystal structures and *in situ* XRD patterns of (a) $K_{0.00}$ and $K_{0.05}$. *In situ* XAS spectra of (b) Mn K-edge and (c) Cu K-edge of $K_{0.05}$ during cycling. [Reproduced from Ref. 2]

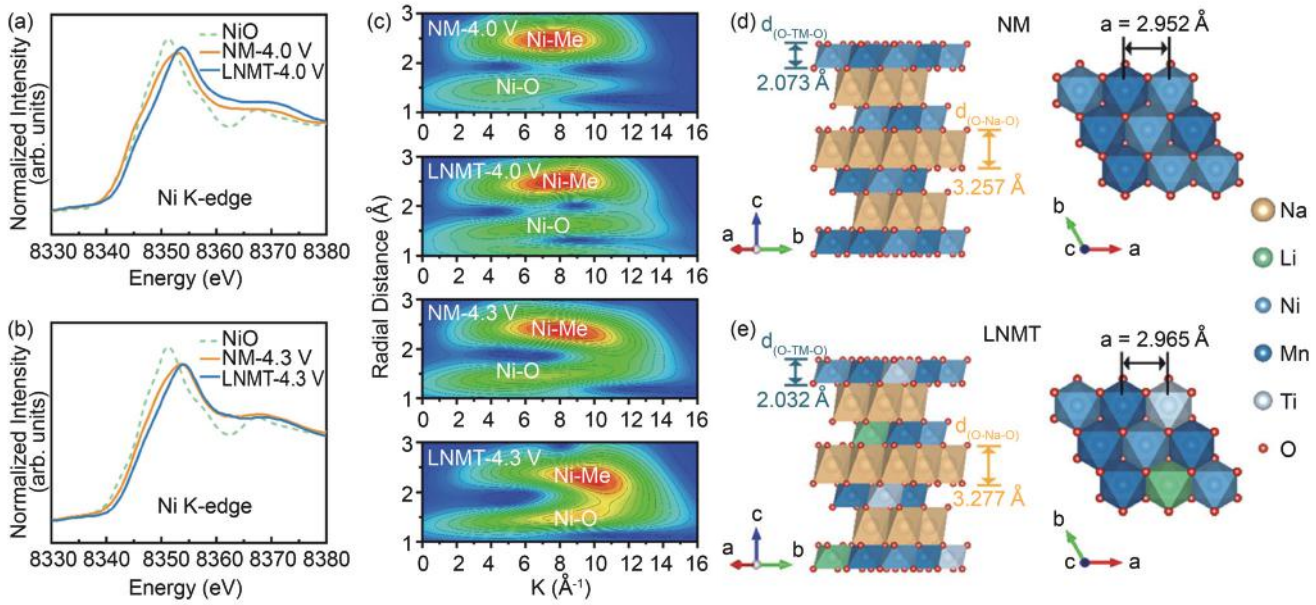

Fig. 3: (a,b) *Ex situ* XANES spectra at Ni K-edge of NM, LNMT, and NiO obtained at different charging conditions. (c) Wavelet transformation diagrams of the NM and LNMT under different voltage states. Schematic crystal structures and detailed lattice parameters of (d) NM and (e) LNMT. [Reproduced from Ref. 3]

XAS analysis conducted at **TPS 32A** revealed that LNMT promotes a stable electronic environment, mitigates drastic structural changes, and supports a more robust charge compensation mechanism. These findings highlight the importance of fine-tuning local electronic and atomic structures in designing high-capacity, high-voltage SIB cathodes. Together, these studies offer key insights into the effects of local structure on the electrochemical behavior of layered oxide cathodes, thereby paving the way for new developments in energy-storage solutions that offer enhanced capacity and cycle life.

In conclusion, while developing high-capacity and long-cycle-life SIBs remains challenging, addressing one of the major limitations of the current sodium ion transport technology in the cathodes highlights the potential of layered structures. Investigating the impact of these layered metal oxide cathodes with complex element compounds could potentially enhance the conductivity, stability, and overall performance. Applying *in situ* synchrotron X-ray techniques is essential for monitoring SIB behavior during operation. These methods provide valuable insights into changes that occur during charge–discharge cycles, enabling researchers to customize materials for improved performance. By combining the strengths of these configurations and leveraging advanced synchrotron X-ray techniques, the research lays the groundwork for more efficient, durable, and economically viable SIBs. (Reported by Chi-Liang Chen)

This report features the work of Han-Yi Chen and her collaborators published in ACS Sustain. Chem. Eng. ***12****, 12795 (2024), and the work of Ji Liang and his collaborators published in ACS Nano* ***18****, 18622 (2024).*

TPS 32A Tender X-ray Absorption Spectroscopy
TPS 44A Quick-scanning X-ray Absorption Spectroscopy
TLS 17C1 EXAFS
TLS 01C2 X-ray Powder Diffraction

- XPS, XRD, XAS
- Energy Science, Chemistry, Materials Science, Condensed Matter

References

1. L. Zhao, T. Zhang, W. Li, T. Li, L. Zhang, X. Zhang, Z. Wa ng, Engineering **24**, 172 (2023).
2. C.-H. Yeh, J.-W. Kang, Y.-L. Chen, H.-J. Chen, H.-H. Chang, W.-H. Lu, S.-Y. Chen, H.-L. Chen, C.-W. Hu, L.-Y. Chueh, Y.-T. F. Pan, H.-Y. Chen, ACS Sustain. Chem. Eng. **12**, 12795 (2024).
3. Q. Wang, G. Yu, B. Luo, W. Ji, Z. Liu, M. Li, Y. Nong, Y. Tian, X. Wang, J. Zhang, C.-L. Chen, C.-K. Chang, Z. Sang, Z. Zhao, R. Zhao, J. Liang, ACS Nano **18**, 18622 (2024).

Breathing Zinc–Air Batteries: Clean, Powerful, and Sustainable Energy Solutions

The development of advanced bifunctional catalysts is essential for attaining high-performance cathodes in rechargeable zinc-air batteries.

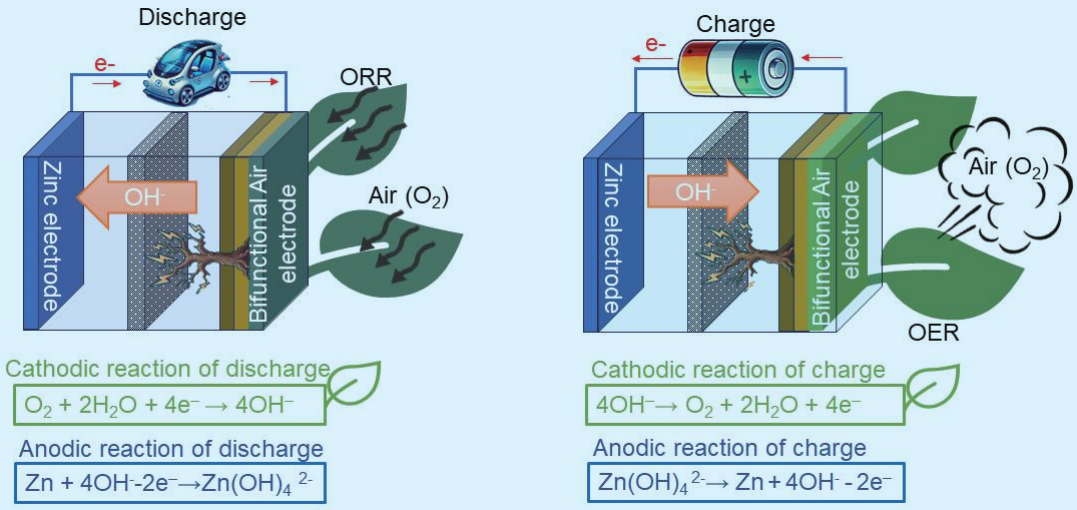

Fig. 1: A schematic configuration of zinc–air batteries and oxygen bifunctional electrocatalysts.

Zinc–air batteries (ZABs), a type of metal–air battery, generate electricity by combining zinc (Zn) with oxygen (O_2) from the air. At their core, these batteries consist of a Zn anode, a porous air cathode, and an electrolyte, which is often a strong alkaline solution. During discharge, zinc oxidizes at the anode, releasing electrons that travel through an external circuit to the cathode. Simultaneously, oxygen molecules from the air reduce at the cathode, combining with water and electrons to form hydroxide ions. These ions react with Zn ions in the electrolyte to form zincates (**Fig. 1**). This process releases energy that powers devices. ZABs are appealing for energy-intensive applications such as electric vehicles, grid energy storage, and portable devices. With a theoretical energy density potentially exceeding 1,000 Wh/kg, ZABs surpass lithium ion batteries. However, challenges in rechargeability and stability have historically hindered their commercial viability. Key limitations of ZABs include the rechargeability of the zinc anode and the sluggish oxygen reduction reaction (ORR) and oxygen evolution reaction (OER) kinetics at the cathode. Repeated charge–discharge cycles can lead to zinc dendrite formation, causing short circuits. In addition, reactions between zinc and the alkaline electrolyte can produce by-products that degrade performance. To address these issues, recent research has focused on improving the electrolyte, cathode catalysts, and zinc anode structure. Promising developments include the use of solid-state electrolytes to minimize side reactions and innovative anode designs to prevent dendrite formation. Particularly, enhancing cathode catalysts to improve ORR and OER efficiency is a critical area of research for bifunctional electrocatalysts. Synchrotron X-ray absorption spectroscopy (XAS), which includes X-ray absorption near edge structure (XANES) and extended X-ray absorption fine structure (EXAFS) analyses, provides the valuable insights. XAS examines the oxidation state, electronic properties, atomic coordination, and bond lengths of

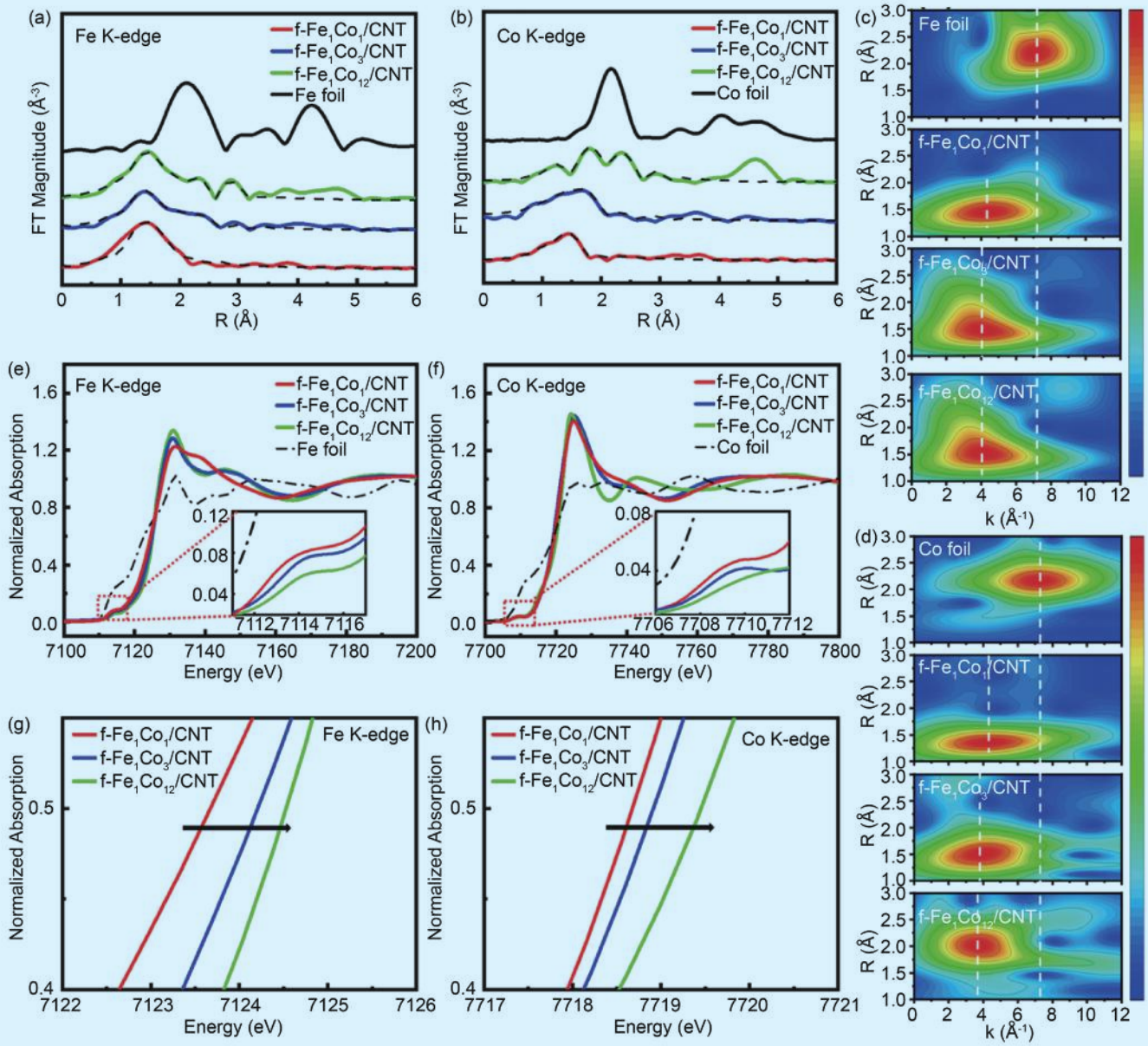

Fig. 2: EXAFS k^2-weighted R-space results for (a) Fe K-edge and (b) Co K-edge, including fitted curves (black dashed lines). (c,d) k^2-weighted WT images for the Fe and Co K-edges. (e,f) XAS spectra, with insets highlighting pre-edge peaks and (g,h) absorption edges. [Reproduced from Ref. 1]

catalyst atoms. This detailed understanding is essential for the rational design of more efficient catalysts by elucidating the relationships between the structure and properties, as it reveals the atomic structure and electronic properties. This analysis also sheds light on how these factors influence catalytic performance through a comprehensive analysis of the underlying mechanisms. Some ZABs have achieved impressive cycling stability and reaction efficiency this year, outperforming traditional and commercial Pt/C + IrO_2 catalysts. Therefore, if these innovations continue, ZABs could emerge as mainstream alternatives to lithium ion batteries in the near future.

Shih-Yuan Lu (National Tsing Hua University) investigated a binary Fe and Co single-atom catalyst (SAC) named f-Fe_1Co_1/CNT. This catalyst, which is synthesized *via* a formamide-assisted solvothermal approach and analyzed using XAS at **TLS 17C1**, anchors Fe and Co single atoms on nitrogen-doped carbon layers supported by carbon nanotubes (CNTs). This design achieves high atom loading and prevents aggregation, significantly enhancing ORR and OER efficiency in alkaline media. The f-Fe_1Co_1/CNT catalyst demonstrates superior ORR and OER activities and achieves the remarkable discharge peak power density and stability when paired with a carbon-paper-composited nickel foam (NF/CP) air cathode. XAS analysis, including EXAFS and wavelet-transform (WT) analysis, confirmed the changes in coordination environments and revealed synergistic activity from Fe and Co atoms, with Fe-N_4 sites identified as the primary active centers. These findings highlight the potential of SACs to achieve high catalytic activity, selectivity, and stability.

Furthermore, this year, noteworthy research conducted by Yuan-Yao Li (National Chung Cheng University) introduced a sophisticated bifunctional catalyst that integrates nickel–iron-layered double hydroxide (NiFe LDH), iron–cobalt dual single atoms (FeSACoSA), and iron–cobalt nanoalloy (FeCoAlloy) within a framework of nitrogen-doped carbon (NC) and CNTs. This combination maximizes the ORR and OER activities by leveraging the synergistic properties of its components, notably, the high density of ORR active sites provided by the FeCo alloy and FeSACoSA and the enhanced durability and OER efficiency contributed by NiFe LDH. The low ORR–OER potential gap of the catalyst and its implementation in a conductive, porous cathode structure deliver the outstanding performance in liquid-state and flexible ZABs. Such ZABs achieve impressive power densities, specific capacities, and cycling stability surpassing commercial benchmarks. **Figure 3** presents the results of XAS analysis conducted at **TLS 17C1**. The Co and Fe K-edge results revealed the presence of metal–metal bonds, confirming both metal-N coordination and the existence of an FeCo alloy within the material. Furthermore, the Ni K-edge spectra exhibited Ni–O and Ni–Ni bonds from NiFe LDH, confirming the successful coating of NiFe LDH on the material. These findings highlight the importance of both single-atom dispersion and synergistic interactions between the different active sites in achieving high catalytic efficiency in these binary SACs.

The development of ZABs highlights the potential of advanced catalyst–cathode configurations. Utilizing synchrotron XAS to analyze catalytic mechanisms can drive further advancements. With continuous improvements in bifunctional catalysts,

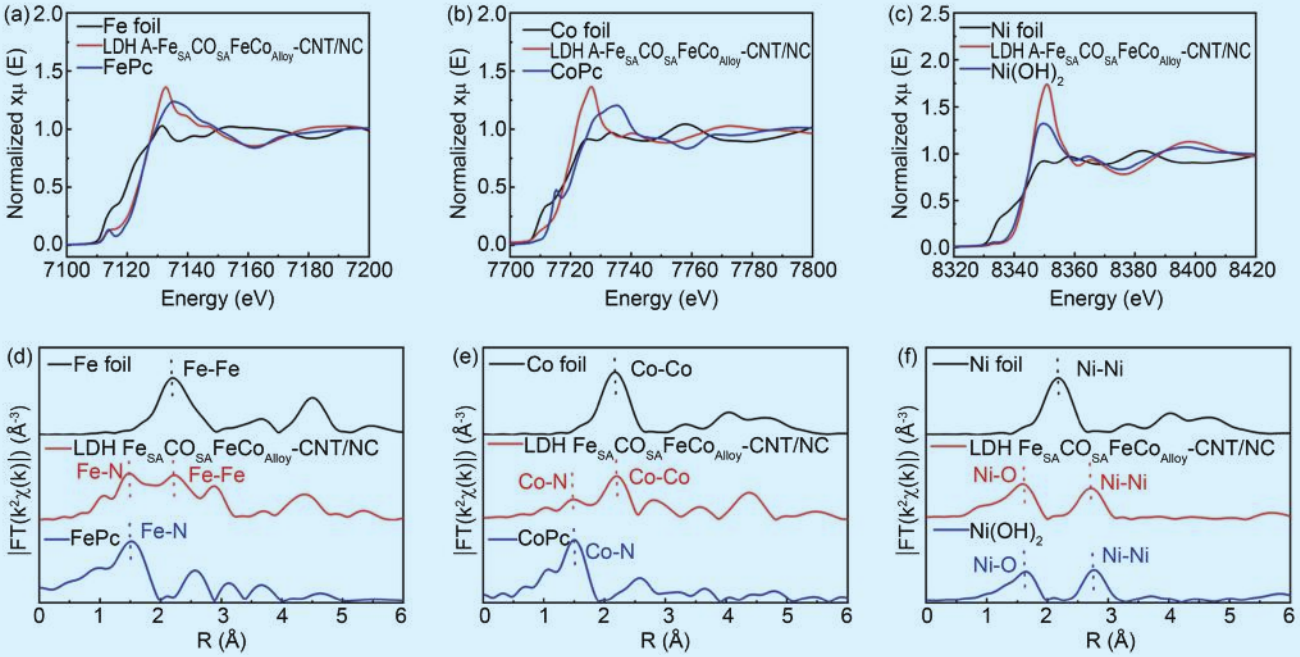

Fig. 3: XAS spectra of NiFe LDH A-FeSACoSA-FeCo Alloy CNT/NC. XANES spectra for (a) Fe K-edge, (b) Co K-edge, and (c) Ni K-edge. Fourier transform EXAFS spectra for (d) Fe K-edge, (e) Co K-edge, and (f) Ni K-edge. [Reproduced from Ref. 2]

ZABs may soon emerge as a viable solution for large-scale energy storage and transportation. Combining high energy density, eco-friendly materials, and reduced costs, ZABs hold promise as a cornerstone of sustainable energy solutions. (Reported by Chi-Liang Chen)

This report features the work of Shih-Yuan Lu and his collaborators published in Energy Storage Mater. ***67****, 103286 (2024), and the work of Yuan-Yao Li and his collaborators published in Nano Energy* ***121****, 109236 (2024).*

TLS 17C1 EXAFS

- XAS, WT
- Materials Science, Chemistry, Condensed-matter Physics

References

1. Y.-C. Ting, C.-C. Cheng, S.-H. Lin, T.-Y. Lin, P.-W. Chen, F.-Y. Yen, S.-I Chang, C.-H. Lee, H.-Y. T. Chen, S.-Y. Lu, Energy Storage Mater. **67**, 103286 (2024).
2. W.-X. Hong, W.-H. Wang, Y.-H. Chang, H. Pourzolfaghar, I-H. Tseng, Y.-Y. Li, Nano Energy **121**, 109236 (2024).

Novel $ZnIn_2S_4$ Combines Piezopotential and Dipole Field for Hydrogen Technique

This study offers an in-depth examination of vacancy engineering in ZIS nanosheets, utilizing piezopotential and dipole fields to optimize photocatalytic performance.

Visible-light-driven photocatalysts often suffer from significant charge recombination due to their limited carrier diffusion lengths, which constrain their practical applications. A common strategy for mitigating this challenge is the development of heterostructure photocatalysts with built-in junction fields to promote charge separation. Alternatively, leveraging the dipole field within the internal bulk phase of photocatalysts has demonstrated considerable effectiveness in enhancing charge separation and transport. This dipole field arises naturally in photocatalysts with non-centrosymmetric crystal structures and can be introduced through the structural modifications. Piezoelectric polarization, a macroscopic built-in potential, is generated in piezoelectric crystals with non-centrosymmetric structures in response to applied mechanical stress. Piezo-photocatalysis synergistically integrates the piezoelectric effect with the light-harvesting capabilities of piezoelectric semiconductors, facilitating the separation and movement of photogenerated charge carriers through the macroscopic built-in potential field.

Jih-Jen Wu (National Cheng Kung University) and his coworkers recently investigated the influence of In- and S-vacancy concentrations on the photocatalytic activity of zinc indium sulfide (ZIS) nanosheets for hydrogen evolution reactions (HERs). Using X-ray absorption spectroscopy (XAS) measurements, including X-ray absorption near edge structure (XANES) and extended X-ray absorption fine structure (EXAFS), conducted at **TPS 32A** and **TPS 44A**,[1] they gained deeper insights into the structural transformations of defective ZIS after hydrazine treatment. For clarity, the unmodified ZIS powder, as well as the modified ZIS powders that had been subjected to hydrazine treatment for 1 hour and 5 hours, are designated as ZIS-0, ZIS-1, and ZIS-5, respectively. **Figure 1(a)** presents the XANES spectra of the ZIS samples at the S K-edge, revealing a notable increase in sulfur vacancies and unoccupied states at sulfur sites following hydrazine treatment. **Figures 1(b) and 1(c)** illustrate the XANES and EXAFS spectra at the Zn K-edge for ZIS-0 and ZIS-5. The reduced coordination number and elevated electron density observed at Zn sites in ZIS-5 compared to ZIS-0 are attributed to the higher concentration of sulfur vacancies in ZIS-5. Similarly, **Figs. 1(d) and 1(e)** display the XANES and EXAFS spectra at the In K-edge for ZIS-0 and ZIS-5. Because of the contrasting trends in electron density changes driven by sulfur and indium vacancies, it was determined that sulfur vacancies have a more pronounced effect on the electron density at the indium sites in ZIS-5 than do indium vacancies, resulting in increased electron density at these sites compared to ZIS-0. Additionally, ZIS-5 exhibits a slightly diminished sulfur coordination environment relative to ZIS-0, which is attributed to a higher sulfur vacancy concentration post-treatment. The atomic arrangement of sulfur and indium vacancies within

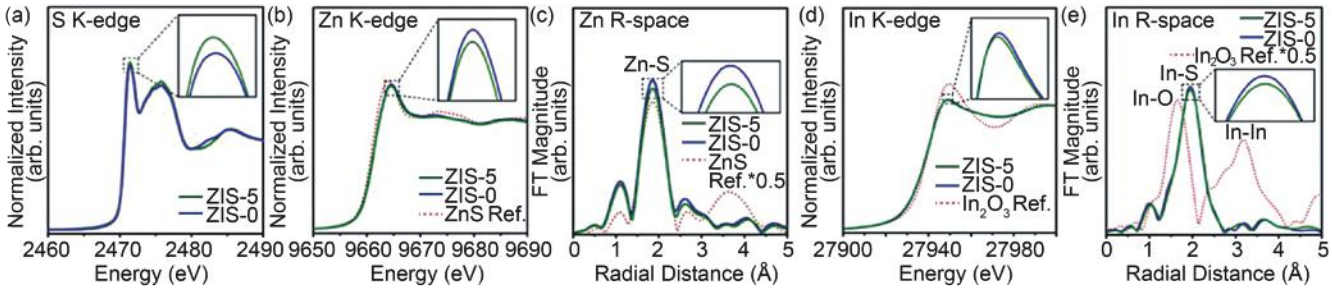

Fig. 1: (a) Normalized S K-edge XANES spectra for ZIS-0 and ZIS-5. (b) Normalized Zn K-edge XANES spectra and (c) Fourier transformed (FT) EXAFS spectra in R-space of ZIS-0, ZIS-5, and ZnS reference. (d) Normalized In K-edge XANES spectra and (e) FT EXAFS spectra in R-space of ZIS-0, ZIS-5, and In_2S_3 reference. [Reproduced from Ref. 1]

the ZIS structure plays a pivotal role in facilitating rapid charge transfer and effective charge separation, ultimately enhancing hydrogen production. This investigation meticulously explores how sulfur and indium vacancies improve charge dynamics and hydrogen evolution rates. By integrating the experimental data with multi-scale simulations, the study demonstrates how these vacancies optimize hydrogen production, offering valuable insights into the mechanisms by which structural vacancies in ZIS influence its electrochemical performance, particularly in hydrogen generation applications.

In summary, defect engineering of ZIS nanosheets with varying levels of indium and sulfur vacancies was successfully realized through hydrazine post-treatment of hydrothermally synthesized ZIS nanosheets. The photocatalytic HER rates show a positive correlation with the combined concentrations of indium and sulfur vacancies in the ZIS nanosheets. This study provides a detailed exploration of vacancy engineering in ZIS nanosheets, leveraging piezoelectric polarization in conjunction with the dipole field to enhance photocatalytic efficiency. (Reported by Yan-Gu Lin)

This report features the work of Jih-Jen Wu and his coworkers published in Adv. Mater. ***36****, 2403228 (2024).*

TPS 32A Tender X-ray Absorption Spectroscopy
TPS 44A Quick-scanning X-ray Absorption Spectroscopy

- XAS
- Materials Science, Chemistry, Condensed-matter Physics, Environmental and Earth Science

Reference

1. W. J. Zhong, M. Y. Hung, Y. T. Kuo, H. K. Tian, C. N. Tsai, C. J. Wu, Y. D. Lin, H. C. Yu, Y. G. Lin, J. J. Wu, Adv. Mater. **36**, 2403228 (2024).

Defect-Engineering for Selective Methanol Decomposition

Undercoordinated Pt sites in $PtTe_2$ are crucial in facilitating methanol decomposition and promoting formaldehyde production.

Two-dimensional transition metal dichalcogenides (TMDs) have garnered significant attentions in catalysis due to their unique electronic properties, high surface area, and tunable surface chemistry. Unlike conventional noble metal catalysts, which exhibit disadvantages such as high costs and susceptibility to poisoning, TMDs are promising alternatives owing to their structural versatility and defect engineering capabilities.[1,2] However, the basal planes of pristine TMDs are often inert, limiting their catalytic utility. Surface defects, particularly chalcogen vacancies, introduce the undercoordinated metal sites that can serve as highly active catalytic centers, significantly altering their chemical reactivity. Among TMDs, platinum telluride ($PtTe_2$) is of particular interest due to its intrinsic metallic nature, which provides superior conductivity compared to semiconducting TMDs such as MoS_2 or WS_2. A research team led by Meng-Fan Luo (National Central University), Jyh-Pin Chou (National Changhua University of Education), and Chun-Liang Lin (National Yang Ming Chiao Tung University) is investigating the catalytic properties of $PtTe_2$ with engineered Te vacancies. Their study focuses on $PtTe_2$, a metallic group-10 TMD, emphasizing the role of undercoordinated Pt (Pt_{uc}) sites at Te vacancies in methanol decomposition, which is a crucial reaction for hydrogen production and direct methanol fuel cells. To explore the catalytic behavior of $PtTe_2$, controlled Ar^+

bombardment was employed to selectively remove surface Te atoms, generating Pt_{uc} sites while maintaining the structural integrity of the underlying Pt lattice. **Figure 1(a)** presents the scanning tunneling microscopy (STM) images before and after ion bombardment, confirming the introduction of single and multi-Te vacancies. **Figure 1(b)** further characterizes the defect structure through synchrotron-based photoelectron spectroscopy (PES), which reveals a shift in the Pt 4f binding energy. This shift indicates a lower oxidation state at Pt_{uc} sites, which enhances their reactivity. To assess the influence of Pt_{uc} concentration on catalytic performance, **Figs. 1(c) and 1(d)** quantify the methanol conversion probability as a function of vacancy density. At low Pt_{uc} concentrations (≤10%), methanol conversion exceeds 90%, with high selectivity toward CH_2O and CH_4. As Pt_{uc} concentration increases (10%–20%), selectivity shifts, favoring C–O bond scission over dehydrogenation, which is further validated by near-ambient-pressure photoelectron spectroscopy (NAP-PES) and near-ambient-pressure mass spectroscopy results.

Methanol adsorption and decomposition were systematically investigated using synchrotron-based *in situ* NAP-PES and near-ambient pressure mass spectrometry (NAP-MS). As shown in **Fig. 2(a)**, the NAP-PES spectra for pristine $PtTe_2$ reveal that methanol does not undergo significant decomposition, confirming its catalytic inertness. In contrast, on defect-rich $PtTe_2$, the spectral intensity of methanol-related species (CH_3OH) decreases with increasing temperature, indicating the progressive methanol conversion. Concomitantly, peaks corresponding to CH_2O (formaldehyde) and CH_x species are observed, which demonstrate that Pt_{uc} sites actively promote methanol dehydrogenation. NAP-MS results further confirm these findings by monitoring the gaseous products formed during the reaction (**Fig. 2(b)**). On Pt_{uc}-enriched $PtTe_2$, CH_2O (formaldehyde) and CH_4 (methane) are the dominant products, whereas only trace amounts of CO and CO_2 are detected.

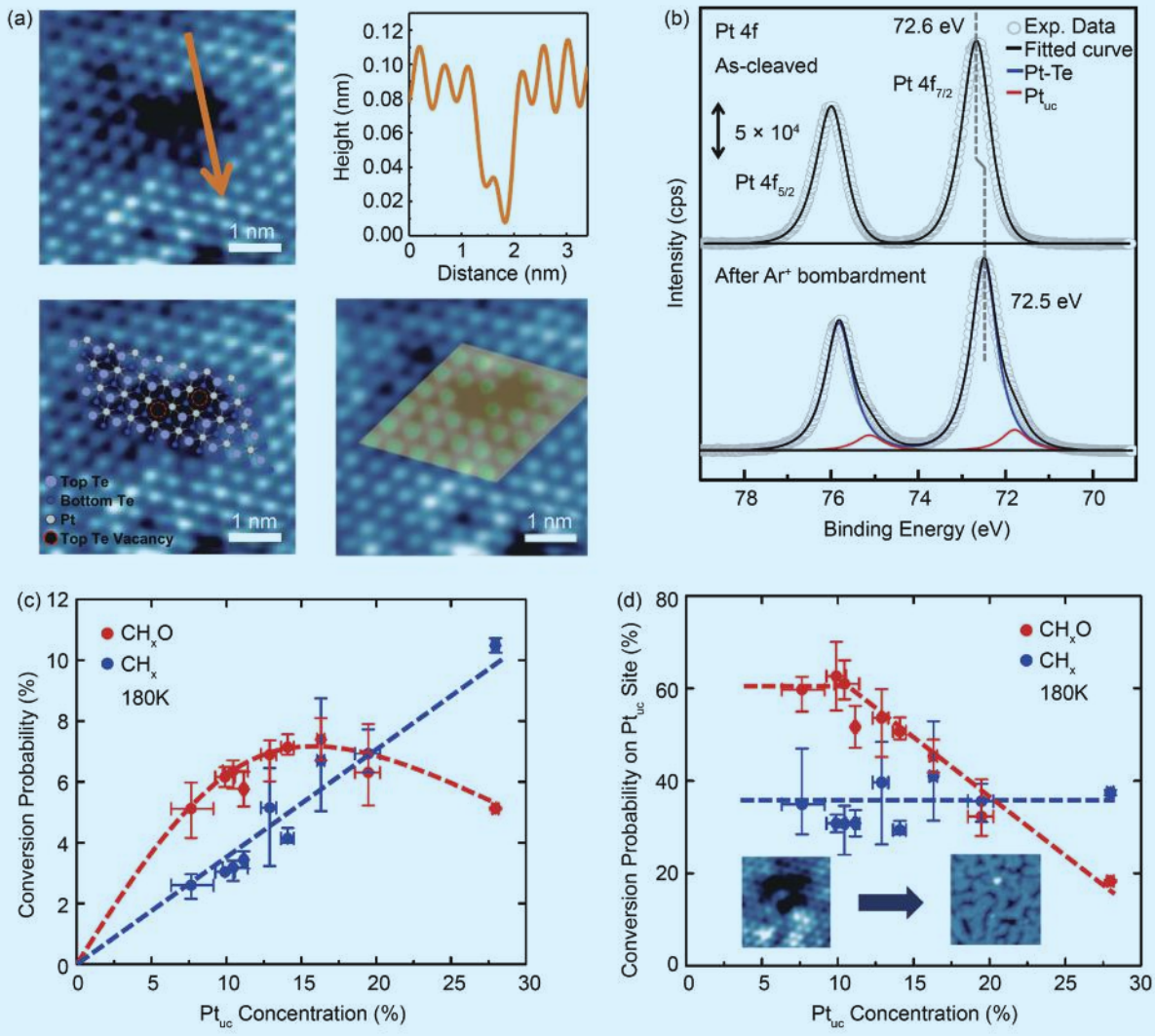

Fig. 1: (a) High-resolution image of two single-Te vacancies, the line profile across a single-Te vacancy, the overlap of the two single-Te vacancies model with the imaged ones and the overlap of the STM image with the DFT-simulated one produced based on the vacancy model. (b) PES spectra of Pt 4 f core level from layered $PtTe_2$ as cleaved and bombarded by Ar^+ (0.5 keV, 3 mins). (c,d) Varied reaction probabilities of methanol adsorbed on a $PtTe_2$ surface with Pt_{uc} sites. Probabilities of conversion to CH_xO^* (red circles) and CH_x^* (blue) of monolayer methanol adsorbed on a $PtTe_2$ surface, and those on Pt_{uc} sites as a function of the concentration of the surface Pt_{uc}. [Reproduced from Ref. 3]

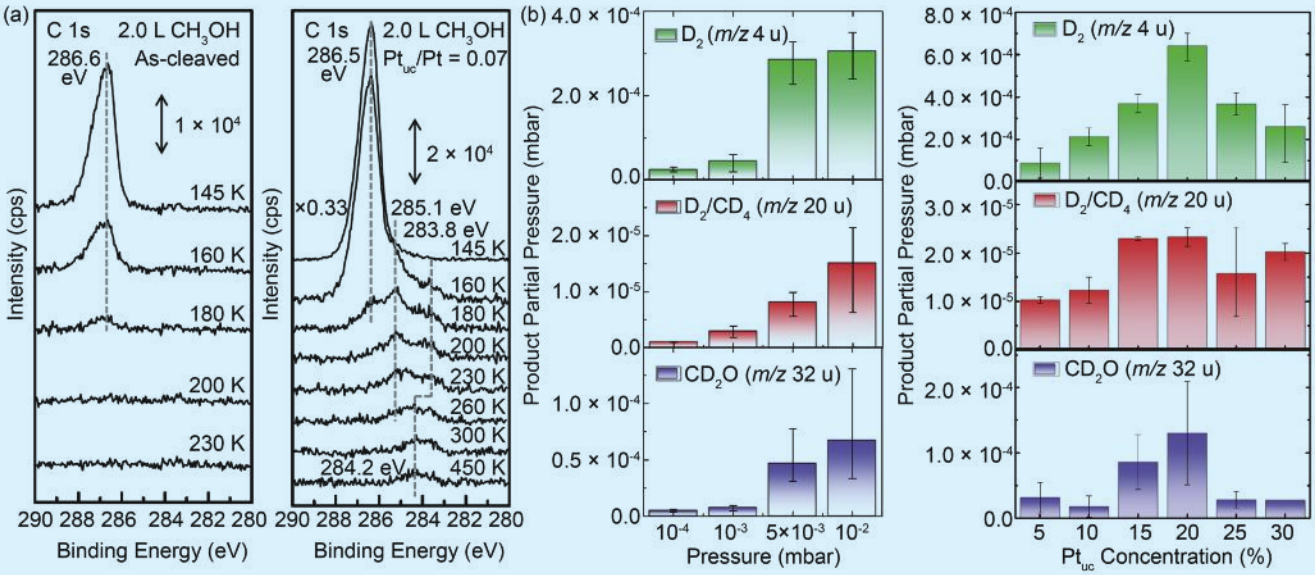

Fig. 2: (a) PES spectra of C 1s core level for methanol adsorbed on as-cleaved and Ar^+-bombarded $PtTe_2$ at 145 K and annealed stepwise to selected temperatures. (b) Production of $D_{2(g)}$ (*m/z* 4 u), $D_2O_{(g)}$ /$CD_{4(g)}$ (*m/z* 20 u), and $CD_2O_{(g)}$ (*m/z* 32 u) from $PtTe_2$ at 300 K, as a function of methanol-d_4 pressure (Pt_{uc}/Pt ratio 0.10) and Pt_{uc} concentration (10^{-2} mbar). [Reproduced from Ref. 3]

This highlights the selective nature of Pt_{uc} sites, which favor formaldehyde formation over complete C–O bond scission, reducing unwanted CO poisoning, which is an issue commonly observed for conventional Pt catalysts. Additionally, the reaction selectivity shifts with increasing Pt_{uc} concentration. At moderate defect densities (~10%), methanol decomposition predominantly follows the dehydrogenation pathway, producing CH_2O and CH_4. However, at higher Pt_{uc} densities (>10%), the C–O bond cleavage pathway becomes more competitive, leading to increased CH_4 and H_2 formation while slightly reducing CH_2O selectivity. This trend is consistent with density functional theory (DFT)-calculated reaction barriers, which suggest that Pt_{uc} sites lower the activation energy for selective dehydrogenation but can also facilitate C–O scission at higher defect concentrations.

In summary, this study establishes $PtTe_2$ with undercoordinated Pt sites as a highly efficient catalyst for methanol decomposition, offering superior activity and selectivity compared to conventional Pt catalysts. The unique triangular coordination and oxidation state variations of Pt_{uc} sites play a crucial role in tuning the reaction pathways. By integrating advanced synchrotron-based PES, *in situ* NAP-PES/NAP-MS at **TLS 09A2** and **TLS 24A1**, and theoretical modeling, this work provides fundamental insights into defect engineering in TMDs. It lays the foundation for designing next-generation catalysts for methanol reforming, hydrogen production, and direct methanol fuel cells. (Reported by Hao Ming Chen, National Taiwan University)

This report features the work of Meng-Fan Luo, Jyh-Pin Chou and Chun-Liang Lin published in Nat. Commun. ***15****, 653 (2024).*

TLS 09A2 Spectroscopy
TLS 24A1 XPS, UPS, XAS, APXPS

- *In situ* NAP-XPS
- Materials Science, Thin-film Chemistry

References

1. G. D'Olimpio, C. Guo, C.-N. Kuo, R. Edla, C. S. Lue, L. Ottaviano, P. Torelli, L. Wang, D. W. Boukhvalov, A. Politano, Adv. Funct. Mater. **30**, 1906556 (2020).
2. Y. Chen, S. Huang, X. Ji, K. Adepalli, K. Yin, X. Ling, X. Wang, J. Xue, M. Dresselhaus, J. Kong, B. Yildiz, ACS Nano, **12**, 2569 (2018).
3. J.-W. Hsueh, L.-H. Kuo, P.-H. Chen, W.-H. Chen, C.-Y. Chuang, C.-N. Kuo, C.-S. Lue, Y.-L. Lai, B.-H. Liu, C.-H. Wang, Y.-J. Hsu, C.-L. Lin, J.-P. Chou, M.-F. Luo, Nat. Commun. **15**, 653 (2024).

Dual-Atom Catalyst for Selective CO_2 Reduction

A dual-atom NiCu catalyst achieves record-high selectivity for CO_2-to-ethanol conversion.

The electrochemical reduction of carbon dioxide (CO_2) into valuable multi-carbon fuels is a promising strategy for mitigating CO_2 emissions while producing sustainable chemical feedstocks.[1] However, achieving high selectivity and efficiency for ethanol production remains a major challenge because of the difficulty of C–C coupling and the competitive formation of C1 products. Copper-based catalysts have demonstrated the potential for facilitating C–C coupling, but their selectivity for ethanol is often low, requiring significant overpotentials.[1,2]

To address these challenges, the teams led by Bing Joe Hwang (National Taiwan University of Science and Technology, NTUST), Wei-Nien Su (NTUST), and Meng-Che Tsai (National University of Tainan) demonstrated a dual single-atom catalyst (SAC) system featuring atomically dispersed Ni and Cu sites (NiCu-SACs/N-C), which synergistically enhance ethanol selectivity and catalytic efficiency. **Figure 1(a)** illustrates the rational design and synthesis of NiCu-SACs/N-C prepared *via* hydrothermally assisted pyrolysis using zeolitic imidazolate frameworks.

The synthetic strategy ensures the atomic dispersion of Ni and Cu in a nitrogen-doped carbon matrix, creating abundant accessible active sites. To further elucidate the role of cooperative dual active sites, control experiments in CO-saturated electrolytes were conducted. The results confirm that Ni sites generate labile CO intermediates, which diffuse to adjacent Cu sites for C–C coupling, thereby forming ethanol. A key highlight of this work is the use of Ni–Cu cooperative heteroactive sites, which uniquely facilitate CO_2 reduction to ethanol with an unprecedented Faradaic efficiency (FE) of 92.2% at −0.6 V vs. reversible hydrogen electrode (RHE) (**Fig. 1(b)**). To the authors' knowledge, this represents the highest selectivity reported to date for direct electrochemical CO_2-to-ethanol conversion. The dual-atom catalyst also exhibits the lowest onset potential for ethanol production at −0.4 V vs. RHE, surpassing the performance of single-atom Cu or Ni catalysts. This exceptional performance is attributed to the cooperative entanglement of adjacent Ni and Cu sites, where CO generated on Ni–N_3 sites is efficiently transferred to Cu–N_4 sites for C–C coupling, ultimately leading to ethanol formation.

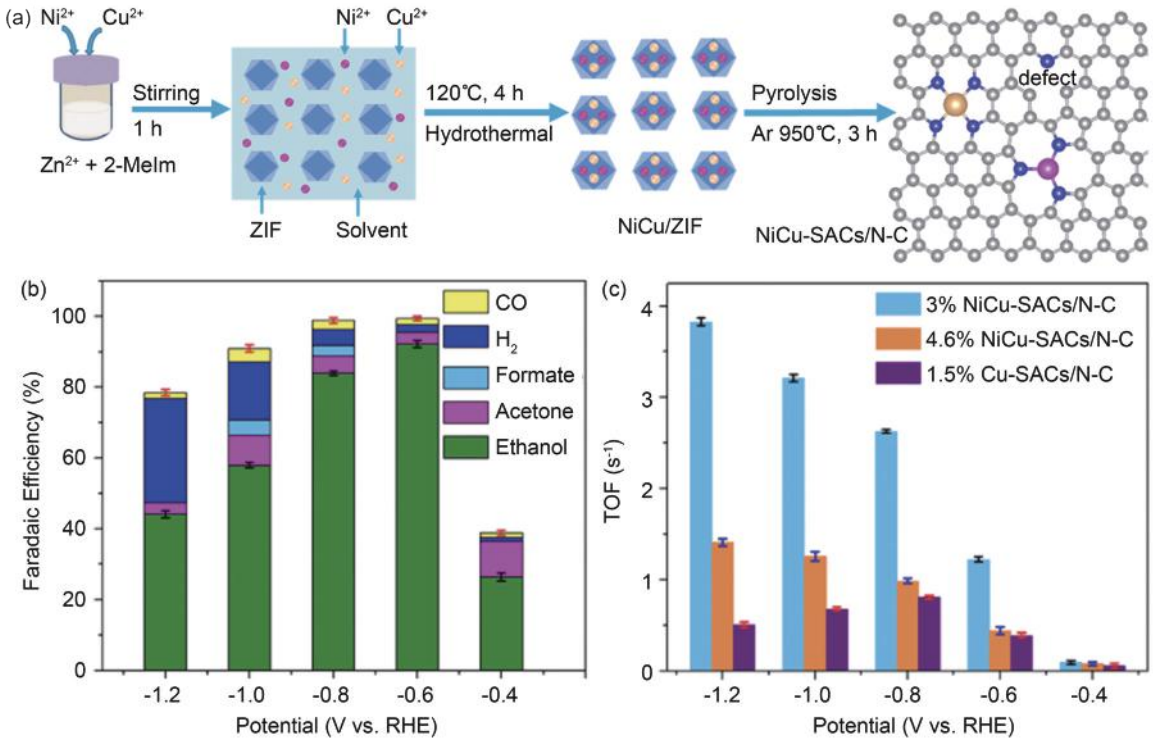

Fig. 1: (a) Schematic representation of the synthesis of dual SACs *via* hydrothermally assisted pyrolysis method. (b) FEs and product distributions over the catalysts of 3% NiCu-SACs/N-C electrodes at different potentials. Error bars indicate the standard deviation. (c) TOF of ethanol over NiCu-SACs/N-C hybrids with different metal loadings, compared with Cu-SACs/N-C at different applied potentials. [Reproduced from Ref. 3]

Figure 1(c) highlights the turnover frequency (TOF) of CO_2-to-ethanol conversion, with the NiCu-SACs/N-C catalyst exhibiting a TOF four times higher than single-atom Cu catalysts. The cooperative synergy between Ni and Cu is also evident in the significantly enhanced electrochemical active surface area and reduced charge transfer resistance (R_{ct}), indicating more efficient electron and mass transport. The computational modeling further supports the experimental findings by demonstrating that the energetically favorable C–C coupling step occurs at the Cu–N_4 sites, which are enhanced by neighboring Ni–N_3 sites. At greater negative potentials, the formation of Cu clusters increases the energy barrier for C–C coupling, leading to a decline in ethanol selectivity. This mechanistic insight explains the volcano-shaped ethanol FE trend observed in the electrochemical studies.

The role of *in situ* X-ray absorption spectroscopy (XAS) is crucial in unraveling the mechanistic insights of this dual-site catalyst. **Figure 2** presents *in situ* extended X-ray absorption fine structure (EXAFS) and X-ray absorption near-edge structure (XANES) analyses. The results reveal a key structural transformation during CO_2 reduction. Notably, while Ni remains in its single-atom Ni–N_3 coordination environment throughout the reaction, Cu undergoes dynamic restructuring, forming potential-induced Cu clusters at high negative potentials. These dynamic Cu clusters play a critical role in modulating catalytic activity, but excessive clustering leads to decreased ethanol selectivity. This observation, which is supported by density functional theory (DFT) calculations, confirms that C–C coupling occurs preferentially on atomically dispersed Cu–N_4 sites rather than Cu clusters, explaining the decline in ethanol FE at highly negative potentials.

In summary, this study establishes NiCu-SACs/N-C as a groundbreaking dual-site catalyst for CO_2-to-ethanol conversion, achieving record-high FE and low onset potential. The findings underscore the importance of cooperative single-atom site engineering and the synergistic role of Ni and Cu in promoting selective C–C coupling. The insights gained from *operando* XAS at **TPS 44A**, electrochemical analysis, and DFT modeling pave the way for designing next-generation electrocatalysts for carbon-neutral fuel production. This work provides a scalable and sustainable strategy for high-selectivity electrochemical CO_2 conversion, contributing to advancements in renewable energy and carbon capture technologies. (Reported by Hao Ming Chen, National Taiwan University)

This report features the work of Bing Joe Hwang, Wei-Nien Su and Meng-Che Tsai published in Appl. Catal. B-Environ. ***358****, 124420 (2024).*

TPS 44A Quick-scanning X-ray Absorption Spectroscopy

- *In situ* XAS
- Materials Science, Electrocatalyst

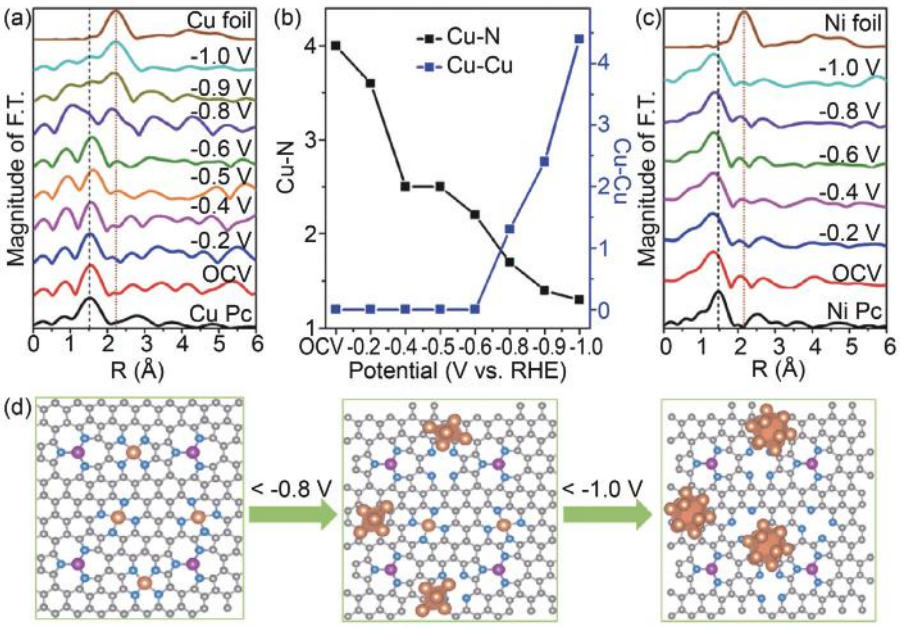

Fig. 2: (a) *In situ* EXAFS spectra and (b) the corresponding average coordination number for Cu–N and Cu–Cu shells of the Cu K-edge for 3% NiCu-SACs/N-C hybrid recorded during the CO_2 electrolysis at different applied potentials in CO_2-saturated 0.5 M $KHCO_3$. Data for CuPc and Cu foil are included for reference. (c) *In operando* EXAFS spectra of Ni K-edge for 3% NiCu-SACs/N-C hybrid recorded during the CO_2 electrolysis at different applied voltages. Data for NiPc and Ni foil are included for reference. (d) The structural models of atomically distributed Ni and Cu sites, as well as the potential-induced dynamic Cu clusters from Cu single atoms, as suggested by *in operando* analysis during the CO_2 electrolysis. [Reproduced from Ref. 3]

References

1. P. Grosse, D. Gao, F. Scholten, I. Sinev, H. Mistry, B. RoldanCuenya, Angew. Chem. Int. Ed. **57**, 6192 (2018).
2. P.-P. Yang, X.-L. Zhang, F.-Y. Gao, Y.-R. Zheng, Z.-Z. Niu, X. Yu, R. Liu, Z.-Z. Wu, S. Qin, L.-P. Chi, Y. Duan, T. Ma, X.-S. Zheng, J.-F. Zhu, H.-J. Wang, M.-R. Gao, S.-H. Yu, J. Am. Chem. Soc. **142**, 6400 (2020).
3. S. A. Chala, K. Lakshmanan, W.-H. Huang, A. W. Kahsay, C.-Y. Chang, F. T. Angerasa, Y.-F. Liao, J.-F. Lee, H. Dai, M.-C. Tsai, W.-N. Su, B. J. Hwang, Appl. Catal. B-Environ. **358**, 124420 (2024).

Environ-mental and Earth Sciences

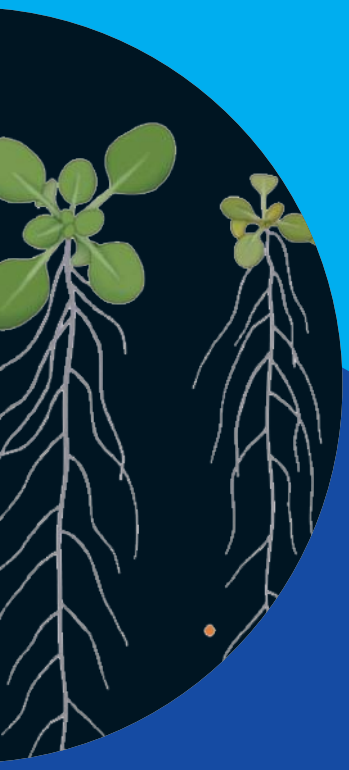

Plants and their environment exhibit complex interactions. Through their relationship with soil, plants absorb nutrients and heavy metals, improving soil quality and fixing carbon. By absorbing and transpiring water, plants regulate the water cycle and purify water. In their interaction with air, plants absorb carbon dioxide for photosynthesis, regulate gas exchange, and reduce air pollution. Plants also form symbiotic relationships with microorganisms to enhance nutrient utilization and disease resistance, while interactions with animals support pollination and seed dispersal. Additionally, plants mitigate the greenhouse effect by absorbing carbon and adapting to extreme climates, thereby maintaining ecological balance. In 2024, research on plant–environment interactions using synchrotron radiation technologies at the NSRRC achieved significant progress.

Plants' ability to absorb and accumulate toxic substances makes them essential indicators for evaluating soil conditions. Understanding their absorption mechanisms is crucial for preventing harmful toxins from entering crops and improving soil health. Shan-Li Wang at National Taiwan University used X-ray absorption near-edge structure (XANES) technology to explore how soil conditions affect molybdenum (Mo) chemical forms and their absorption by rice.

Kuo-Chen Yeh at Academia Sinica applied the X-ray Nanoprobe beamline for X-ray fluorescence (XRF) analysis of *Arabidopsis*, mapping element distribution under varying soil conditions. This provided insights into element absorption and transport mechanisms.

Samir Gamil Mohammad Al-Solaimani at King Abdulaziz University (Saudi Arabia) used XANES and XRF imaging to study the effects of humic acid (HA) on nutrient availability, toxic elements, and plant growth. The results showed that HA improves soil fertility and reduces the absorption of toxic metals, offering practical solutions for enhancing soil and crop health.

Yu-Ting Liu at National Chung Hsing University focused on using plants and their derivatives to remove toxic metals from the environment. They demonstrated that thiol-functionalized biochar (BC) effectively removes hexavalent chromium [Cr(VI)] and uncovered how thermophilic acidic microalgae *Cyanidiales* detoxify trivalent arsenic [As(III)]. These findings highlight BC's effectiveness in Cr(VI) removal and *Cyanidiales*'s efficiency in As(III) detoxification, offering sustainable solutions *via* materials science and bioremediation.

Yu-Min Tzou at National Chung Hsing University investigated phosphorus regulation in soil to promote plant growth. His study examined citric acid adsorption on HA–ferric hydroxide co-precipitates (HAFHCPs) and competition between citric acid and phosphate (P) at different carbon-to-iron (C/Fe) ratios. Results revealed that HAFHCPs regulate phosphorus availability, which is influenced by C/Fe ratios, HA composition, and citric acid presence, as observed by XANES technology. Optimizing phosphorus availability is vital for sustainable phosphorus resource use.

These studies advance our understanding of plant–environment interactions and soil remediation strategies, providing critical insights for ecosystem sustainability. (by Chun-Chieh Wang)

Assessing Soil Conditions Through Plant Accumulation of Toxic Substances

Research reveals how absorption of soil toxins by plants can indicate soil health, guiding effective management and remediation strategies.

Plants can serve as the direct indicators of soil environmental conditions because they readily absorb and accumulate toxic substances from the soil. By studying the mechanisms through which plants accumulate chemical or toxic substances, we may prevent crops from taking up these harmful substances. Additionally, analysis of plants may be used to evaluate the effectiveness of soil remediation. Here, we present the research findings from 2024 conducted at the NSRRC, which focused on how plants accumulate toxic substances from the soil and how this process can be used to assess the effectiveness of soil

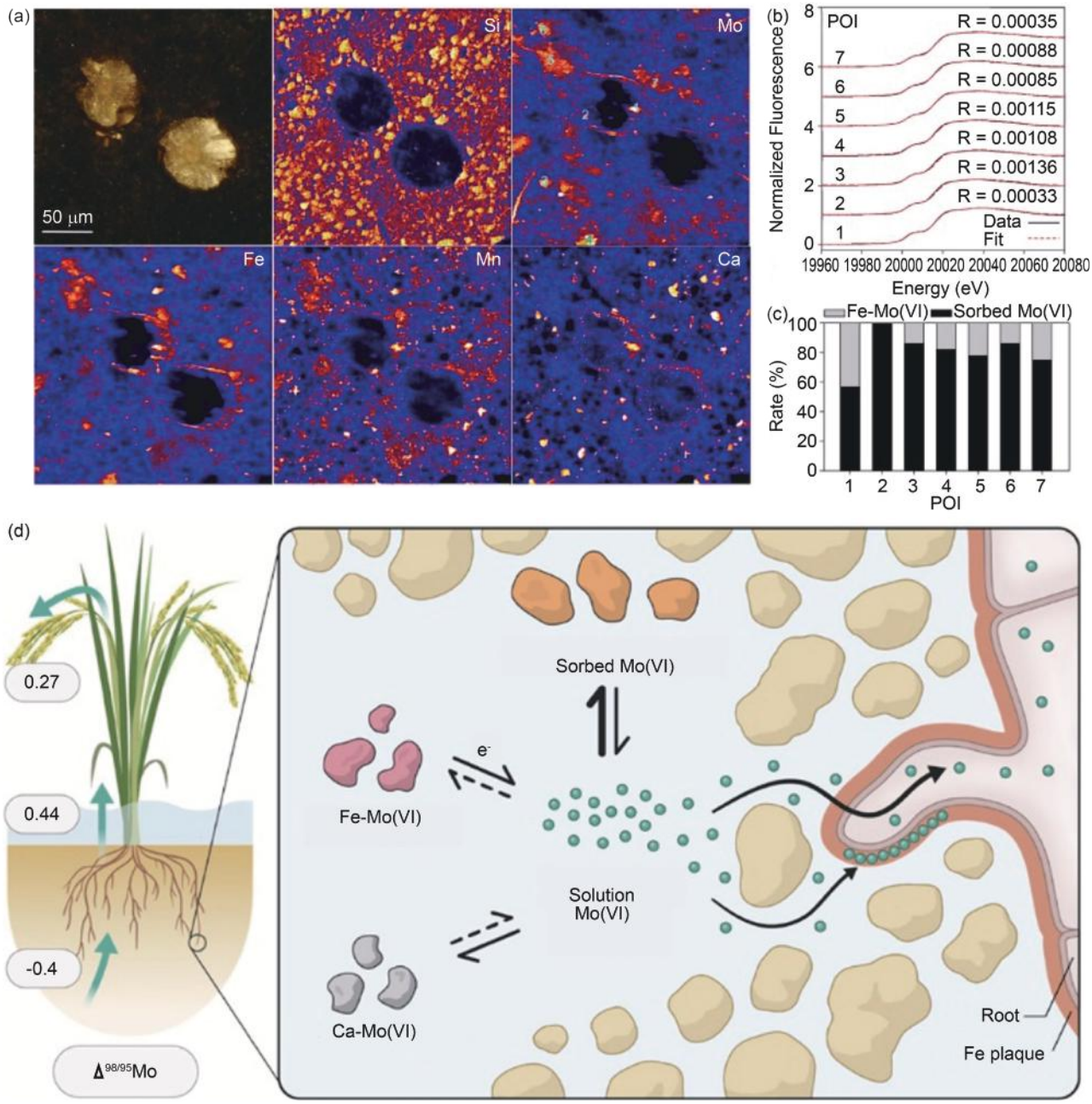

Fig. 1: (a) Microscopic view of rice roots, and spatial distributions of Si, Mo, Fe, Mn, and Ca; (b) μ-XANES spectra and (c) linear combination fits of the points of interest (POIs) indicated in (a). (d) Mechanism of rice uptake of soil molybdenum. [Reproduced from Ref. 1]

modification. With these discoveries, we aim to deepen our understanding of the interactions between plants and soil and to develop more effective soil management and remediation strategies.

Chemical Speciation and Uptake of Molybdenum by Rice

Molybdenum (Mo), a vital micronutrient for organisms, facilitates the metabolism of nitrogen, carbon, and sulfur and is crucial in enzyme catalysis. Although generally present in low concentrations in the Earth's crust, Mo levels can be elevated near industrial areas, potentially contaminating soil and accumulating in crops. This poses the health risks, including livestock poisoning and, in humans, conditions such as infertility and gout-like symptoms.

Rice, a major Mo dietary source for humans, often grows in submerged conditions that enhance Mo solubility and availability. This availability is further influenced by continuous flooding, which contrasts with the reduced Mo uptake seen in alternating wet–dry cycles. Key factors include soil redox processes driven by microbial activity and the dissolution of iron hydroxides, which affect the mobility of Mo compounds.

Shan-Li Wang (National Taiwan University) and his co-workers utilized X-ray absorption near edge structure (XANES) at **TPS 44A** and **TLS 16A1** and other microanalytical techniques to investigate how soil conditions affect Mo chemical forms and uptake in rice (**Fig. 1**). Their findings highlight the strong associations between Mo and Fe in the rice rhizosphere, which are facilitated by Fe plaques on root surfaces. This association promotes Mo dissolution/desorption, which is crucial for root absorption and subsequent transport to plant shoots, though only minimal amounts reach the grains.

The study reveals that Mo can accumulate significantly in rice without apparent toxicity, even in contaminated soils, raising concerns about Mo levels in consumed rice. Advanced studies in soil solution chemistry and Mo speciation provide the deeper insights into the complex dynamics of Mo availability and uptake, influencing the future research directions, particularly in Mo isotope fractionation. This study provides further understanding of the mechanisms affecting Mo's behavior in soil and its broader environmental and health impacts.

Physiology and Molecular Basis of Thallium Toxicity and Accumulation in *Arabidopsis thaliana*

Thallium (Tl) is a heavy metal with extensive applications across several industries, including chemical, pharmaceutical, optical, electronics, energy, and aerospace, as well as in superconducting materials and high-energy physics. Despite its limited annual production—approximately 10 tons globally—industrial processes inadvertently release an estimated 2,000 to 5,000 tons into the environment each year. This can significantly elevate Tl concentrations in contaminated soils, with well above the typical background level of less than 1 mg/kg found in most uncontaminated soils. Recognized for its extreme toxicity, Tl has been classified as a priority pollutant, which necessitates thorough research into its environmental impact, exposure routes, and toxicity.

Tl is particularly concerning because of its ability to be readily absorbed by plants, where it can disrupt potassium (K)-dependent biological processes and accumulate in the edible parts of plants, such as the roots and leaves. This accumulation poses the significant risks of food chain contamination. The model plant *Arabidopsis thaliana* (hereafter Arabidopsis), which is known for its fully sequenced genome, provides an excellent subject for mutagenesis studies aimed at understanding the physiological and molecular impacts of Tl. These studies are crucial for developing strategies to mitigate Tl toxicity and accumulation in plants.

Kuo-Chen Yeh (Academia Sinica) and his co-workers utilized the NSRRC **TPS 23A** X-ray nanoprobe beamline to perform X-ray fluorescence (XRF) analyses on Arabidopsis (**Fig. 2(a)**). These studies reveal that different concentrations of Tl not only inhibit growth and cause leaf chlorosis but also result in Tl accumulation in both roots and shoots, illustrating the plant's transport capabilities and the mechanisms of Tl toxicity.

Further investigations showed that Tl absorption occurs primarily through the roots, moving to the stems with increasing concentrations in the growth media. At peak levels, Tl concentrations reached 1,775 mg/kg in roots and 1,219 mg/kg in shoots. The plant demonstrated a significant transfer factor from roots to aerial parts, but this accumulation adversely affects the growth of both. The similarity in the distribution patterns of Tl and K within Arabidopsis suggests that they might share transport proteins or channels.

In addition to physiological studies, genetic and transcriptomic analyses aim to identify mutants with altered responses to Tl and to explore the genes involved in its uptake and transport. Early transcriptional response studies have identified several Tl-responsive genes associated with oxidative stress, antioxidant defense, K channel activity, and photosynthesis. These findings are integral to understanding Tl's behavior in plants and the potential mechanisms of bioaccumulation (**Fig. 2(b)**), paving the way for future research and mitigation strategies.

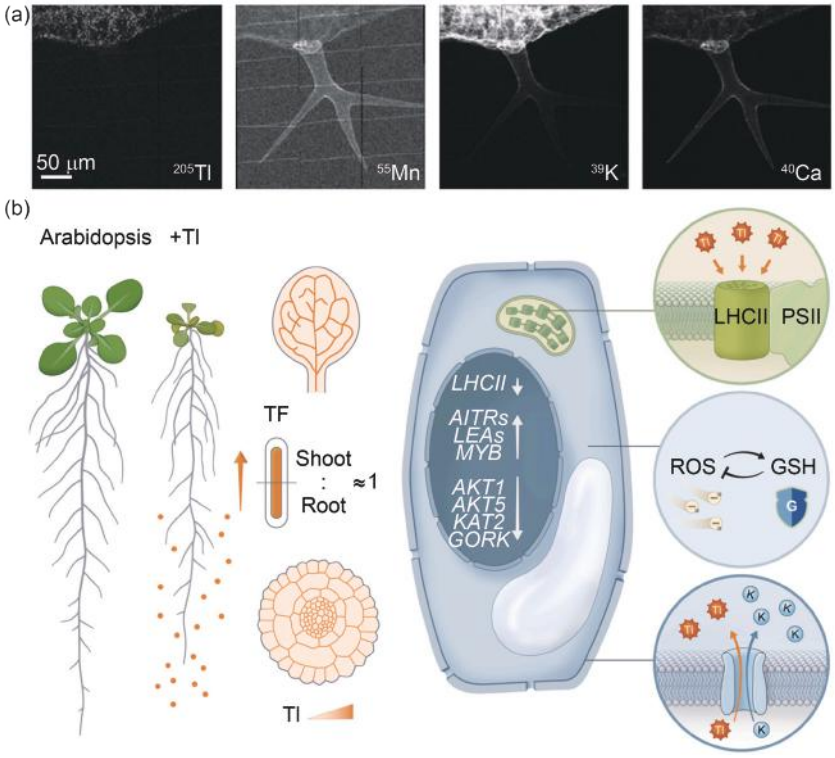

Fig. 2: (a) Synchrotron μ-XRF images of Tl, Mn, K, and Ca distribution in Tl-treated leaves. The elemental signal is shown in white. (b) A schematic representation of the uptake, toxicity, and accumulation of Tl in Arabidopsis plants. [Reproduced from Ref. 2]

Lemongrass and Sage Fertilized with Humic Acid Accumulate Toxins in Soil Treated with Heavy Oil Fly Ash

Saudi Arabia relies on over 40 million tons of heavy oil annually

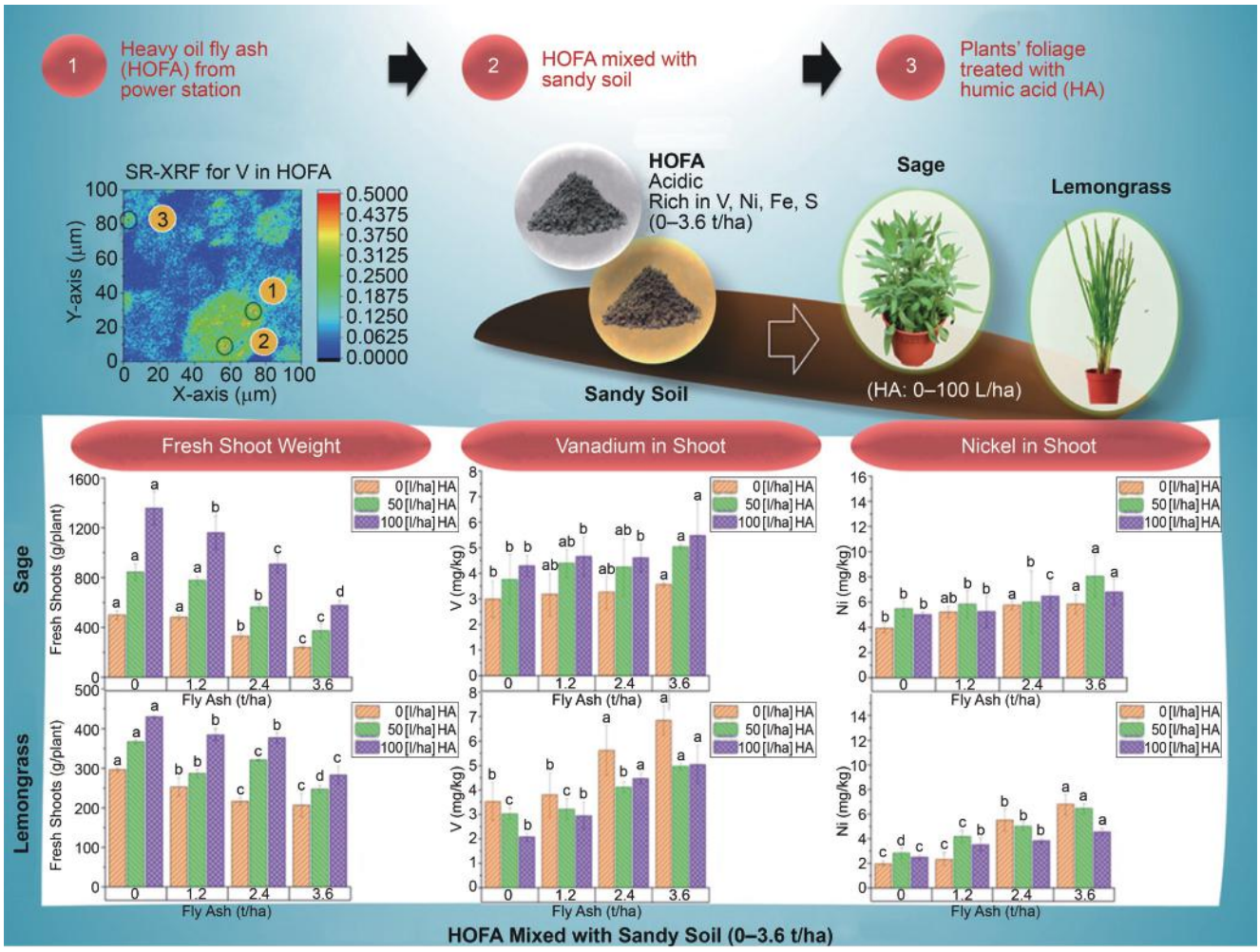

Fig. 3: Evaluating the effect of soil amendment with HOFA using sage and lemongrass as indicators. [Reproduced from Ref. 3)

for electricity and desalination, which contribute to 70% of its energy output, and it consumes about 320 million barrels of oil each year. This process results in the production of roughly 250,000 tons of heavy oil fly ash (HOFA) annually, with the individual facilities like the Rabigh power plant generating around 10,000 tons. Predominantly, HOFA is disposed of in landfills, a method that increases the risk of air, surface water, and groundwater pollution due to its content of unburned carbon and toxic inorganic compounds like vanadium and nickel.

Efforts to manage and mitigate HOFA's environmental risks are crucial. It has found uses in construction as a stabilizing material in cement, concrete blocks, asphalt mixtures, and in synthesizing glass ceramics. Additionally, HOFA serves economical roles in recovering valuable metals and as a water treatment adsorbent. However, its application in agriculture as a soil amendment is less explored because of the high levels of toxic elements it contains, which can harm soil quality and plant growth.

Samir Gamil Mohammad Al-Solaimani (King Abdulaziz University, Saudi Arabia) and his co-workers conducted research using the NSRRC **TPS 23A** beamline, including XRF imaging and XANES analysis. These techniques aided in assessing the impact of varying HOFA doses on sandy soils' nutrient and toxic element profiles and explored the effects of humic acid on plant growth and elemental uptake (**Fig. 3**).

Results indicated a significant presence of vanadium, nickel, iron, and sulfur in HOFA, with lower levels of chromium and manganese and minimal silicon. Notably, about 17.3% of vanadium exhibited high mobility, potentially increasing the environmental risks. Experiments demonstrated that low HOFA doses (1.2 to 3.6 tons per hectare) slightly affected soil pH, electrical conductivity, and element content, while higher doses adversely impacted plant growth. Treatment with humic acid significantly improved plant resilience to HOFA-induced stress.

Among the species tested, common sage showed the superior capability in accumulating elements compared to lemongrass, though both remained below critical toxicity thresholds. The findings suggest that controlled application of HOFA could enhance nutrient levels in low-fertility soils without severely altering their properties, particularly when combined with humic acid. Common sage also displayed potential for phytoremediation in HOFA-treated soils containing nickel and vanadium. These insights confirm the potential of HOFA as a resource for improving soil health in arid environments and offer new strategies for its disposal that are relevant both within Saudi Arabia and globally.

These studies underscore the critical role of plants in monitoring and improving soil health, providing the valuable data that can inform soil management strategies and mitigate pollution. The findings from the NSRRC in 2024 emphasize the complex dynamics of substance accumulation in plants and offer new insights into effective environmental management practices. (Reported by Chun-Chieh Wang)

This report features the work of Shan-Li Wang and his collaborators published in Sci. Total Environ. ***949****, 175141 (2024); the work of Kuo-Chen Yeh and his collaborators published in Ecotox. Environ. Safe.* ***276****, 116290 (2024); and the work of Samir Gamil Al-Solaimani and his collaborators published in Sci. Total Environ.* ***945****, 173998 (2024).*

TPS 23A X-ray Nanoprobe
TPS 44A Quick-scanning X-ray Absorption Spectroscopy
TLS 16A1 Tender X-ray Absorption, Diffraction

- Quick-scanning XAS, XRF, XANES
- Environmental and Earth Sciences, Physics, Materials Science, Chemistry

References

1. P.-T. Yang, Y.-H. Liang, D.-C. Lee, S.-L. Wang, Sci. Total Environ. **949**, 175141 (2024).
2. H.-F. Chang, S.-C. Tseng, M.-T. Tang, S. S.-Y. Hsiao, D.-C. Lee, S.-L. Wang, K.-C. Yeh, Ecotox. Environ. Safe. **276**, 116290 (2024).
3. S. G. Al-Solaimani, A. Al-Qureshi, S. S. Hindi, O. H. Ibrahim, M. A. A. Mousa, Y.-L. Cho, N. E. E. Hassan, Y.-T. Liu, S.-L. Wang, V. Antoniadis, J. Rinklebe, S. M. Shaheen, Sci. Total Environ. **945**, 173998 (2024).

Sustainable Remediation Materials for Toxic-Metal Removal: Insights into Arsenic and Chromium Detoxification Mechanisms

Heavy metal remediation is achieved using an environmentally sustainable approach that involves thiol-functionalized black carbon and thermoacidophilic Cyanidiales.

The remediation of toxic metals, such as chromium (Cr) and arsenic (As), is vital for public health and ecological balance. The 2024 studies at the NSRRC explores the advanced materials and biological pathways for hexavalent Cr(VI) and arsenite [As(III)] removal. Utilizing synchrotron-based techniques, the research highlights thiol-functionalized black carbon for Cr(VI) remediation and thermoacidophilic Cyanidiales for As(III) detoxification, offering effective and sustainable solutions through materials science and bioremediation advancements.

Thiol-Functionalized Black Carbon as Effective and Economical Materials for Cr(VI) Temoval:

Hazardous Cr(VI) continues to raise critical environmental and public health concerns, necessitating the development of effective remediation methods. Yu-Ting Liu (National Chung Hsing University) and her collaborators recently discovered the removal mechanisms of Cr(VI) by modifying black carbon (BC), which is synthesized from rice straw residue and contains thiol groups. This is the first study that alters BC with thiol groups to target Cr(VI) removal. Here, the designated samples were evaluated: i) BC and ii) thiol-functionalized black carbon (S-BC) with BC/thioglycolic acid ratios (g mL^{-1}) of 1:20 (S-BC20), 1:30 (S-BC30), and 1:40 (S-BC40).

The research team conducted X-ray absorption spectroscopy (XAS) at **TLS 17C1** and **TPS 44A** to determine the related Cr speciation on solid samples. The results revealed that Cr species on solid samples primarily transformed from Cr(VI) to Cr(III), as shown in **Fig. 1**. At pH 3.5, over 86.2% of Cr(VI) was reduced to Cr(III), with S-BC retaining only 4.1–6.8% Cr(VI) compared to 13.8% for BC. At pH 5.5, all Cr(VI) was converted to Cr(III) on both materials. Finally, at pH 7.5, S-BC retained no Cr(VI), while BC retained 13.2% Cr(VI).

Sorption isotherms confirmed that S-BC40 demonstrated high Cr(VI) sorption capacities—201.2, 145.8, and 106.6 mg g^{-1} at pH 3.5, 5.5, and 7.5—exceeding BC sorption capacities by 2.0–2.3 times. Notably, S-BC40 converted all sorbed Cr into Cr(III) at pH ≥ 5.5, forming $Cr(OH)_3$ and organic Cr(III) complexes. These findings highlight thiol functionalization as a promising strategy for effective Cr(VI) remediation and waste reutilization.

Accumulation and Bio-Oxidation of Arsenite Mediated by Thermoacidophilic Cyanidiales:

As contamination from geogenic and anthropogenic sources poses a critical environmental and public health threat due to the high toxicity and mobility of As(III). Liu and her team unveiled the molecular mechanisms of As(III) removal by thermoacidophilic microalga Cyanidiales. This red alga, thriving in acidic, metal-rich environments, exhibits unique detoxification characteristics ideal for As remediation. This pioneering study evaluated As(III) removal by *Cyanidium caldarium* (Cc) and *Galdieria partita* (Gp) across a pH range of 2.0–7.0.

The team employed transmission X-ray microscopy (TXM) at **TLS 01B1** to reveal the related As distribution on Cyanidiales, as shown in **Fig. 2** (see next page). 3D tomography revealed that As present on Cc was distributed both near their surface and internally, particularly at pH 5.0, which suggests intracellular tolerance mechanisms. In contrast, Gp relied on surface-level As immobilization. These findings indicate that Cc is more resilient to As stress, particularly at pH ≤ 5.0 due to its superior intracellular detoxification capacity.

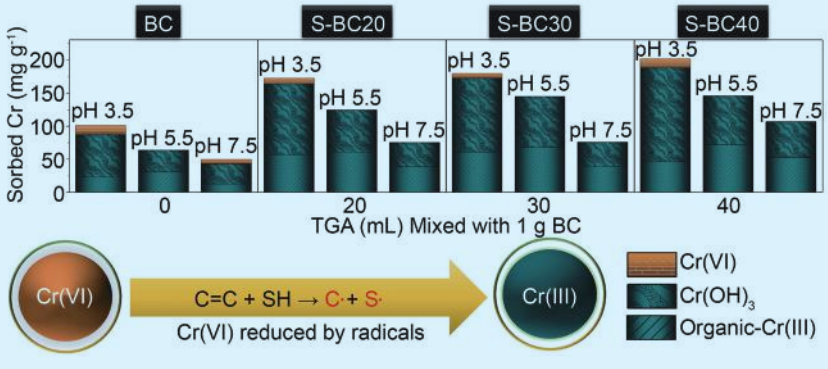

Fig. 1: Proposed removal mechanisms for Cr(VI) by thiol-functionalized black carbon. [Reproduced from Ref. 1]

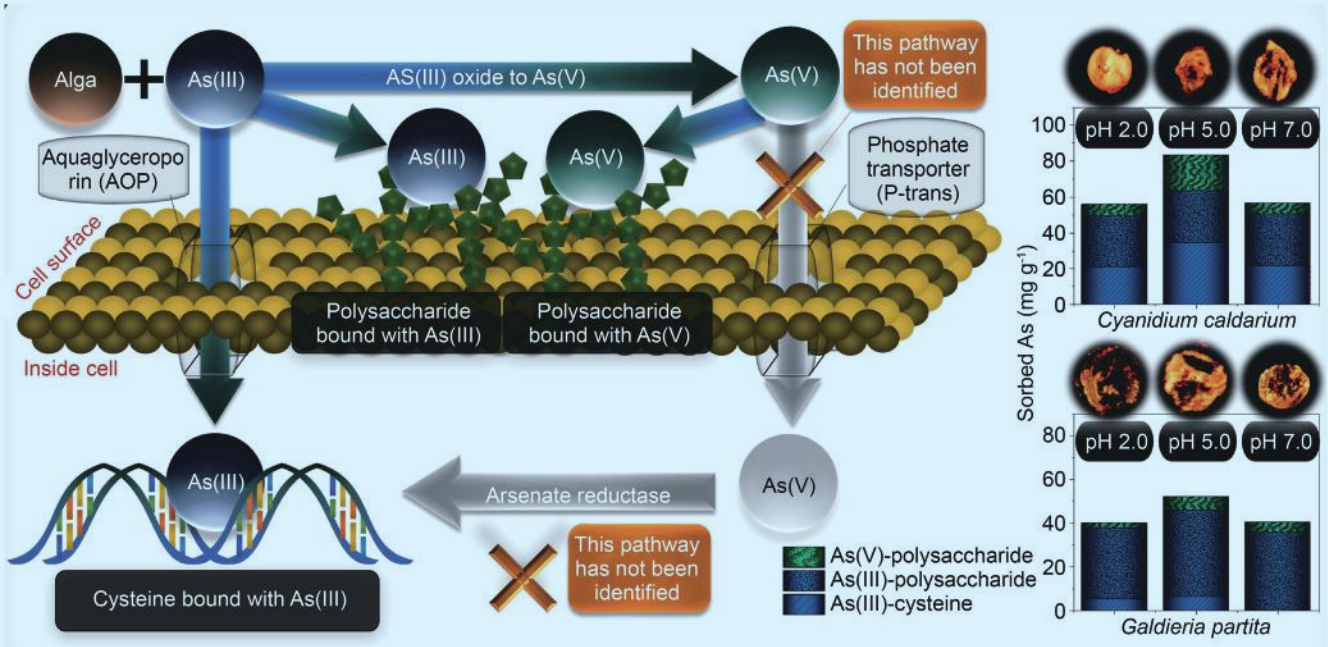

Fig. 2: Proposed mechanisms for As(III) removal by Cyanidiales. [Reproduced from Ref. 2]

The team conducted XAS analysis at **TLS 17C1** and **TPS 44A** to determine the related As speciation on Cyanidiales. As species were identified as arsenate [As(V)]-polysaccharide, As(III)-polysaccharide, and As(III)-cysteine, as illustrated in **Fig. 2**. At pH 5.0, Cc showed the highest sorption capacity that was dominated by As(III)-cysteine, while Gp retained mainly As(III)-polysaccharide. At pH 2.0 and 7.0, Cc exhibited balanced As(III)-polysaccharide and As(III)-cysteine with minimal As(V). These results highlight Cyanidiales' reliance on surface complexation and intracellular sequestration, with Cc exhibiting superior detoxification capacity.

To study As interactions in Cyanidiales, the team conducted synchrotron-based Fourier transform infrared spectroscope at **TLS 14A1** to examine the changes in functional groups and protein secondary structures under As(III) exposure. The results show that α-helix/β-strand ratios correlated with sorbed As levels. However, Gp exhibited a negative correlation between α-helix/β-strand ratios and sorbed As levels, indicating structural fragility. In contrast, Cc displayed positive correlations at pH ≤ 5.0, reflecting strong protein adaptation. Notably, Cc exhibited fewer unordered structures, suggesting intracellular protein proliferation as a key response to As toxicity, further highlighting its superior resilience.

Cc demonstrated superior sorption capacity, achieving 83.2 mg g^{-1} at pH 5.0. Cc outperformed Gp across all tested conditions, driven by mechanisms such as As(III) oxidation, surface complexation with polysaccharides, and intracellular formation of As(III)–cysteine complexes, as shown in **Fig. 2**. These findings highlight Cyanidiales' ability to transform and immobilize As, paving the way for innovative and effective detoxification strategies.

In summary, this report showcases two sustainable approaches for heavy-metal remediation: i) thiol-functionalized BC for Cr(VI) removal and ii) thermoacidophilic Cyanidiales for As(III) removal. Leveraging NSRRC's synchrotron-based techniques, both methods demonstrated high levels of toxic-metal removal, offering promising solutions to environmental contamination. (Reported by Yen-Lin Cho, National Sun Yat-sen University, and Kamonchanok Huangmee, National Chung Hsing University)

This report features the work of Yu-Ting Liu and her collaborators published in J. Environ. Manage. ***360****, 121074 (2024) and Bioresource Technol.* ***406****, 130912 (2024).*

TPS 44A Quick-scanning X-ray Absorption Spectroscopy
TLS 01B1 X-ray Microscopy
TLS 14A1 IR Microscopy
TLS 17C1 EXAFS

- TXM, FT-IR, EXAFS, XAS
- Environmental and Earth Sciences, Biological Science, Chemistry

References

1. K. Huangmee, L.-C. Hsu, Y.-M. Tzou, Y.-L. Cho, C.-H. Liao, H.-Y. Teah, Y.-T. Liu, J. Environ. Manage. **360**, 121074 (2024).
2. Y.-L. Cho, Y.-M. Tzou, A. Assakinah, N.A.T. Than, H. S. Yoon, S.I. Park, C.-C. Wang, Y.-C. Lee, L.-C. Hsu, P.-Y. Huang, S.-L. Liu, Y.-T. Liu, Bioresource Technol. **406,** 130912 (2024).

Citric Acid Enhances Phosphate Release from Humic Acid-Iron Hydroxide Coprecipitates

The presence of citric acids could mildly obstruct the structural development of the Fe domain in humic acid–iron hydroxide coprecipitates, as shown by X-ray absorption spectroscopy techniques.

Recent research led by Yu-Min Tzou (National Chung Hsing University) and his team has demonstrated the sorption of citric acid onto two humic acid–iron hydroxide coprecipitates (HAFHCPs), as well as the mutual effects of citric acid and phosphate (P) sorption on these HAFHCPs at different C/Fe ratios. Their findings show that as the C/Fe ratio increases to 0.5, the maximum sorption capacity (MSC) of citric acid on HAFHCP-Y50 and HAFHCP-A50 decreases by 9.1–16.7% (**Fig. 1**). In addition, the citric acid sorption capacity of HAFHCP containing humic acid was extracted from volcanic soil of Yangmingshan (HAFHCP-YHA) is approximately 92% of that of HAFHCP containing the Sigma-Aldrich humic acid (HAFHCP-AHA). This trend is likely due to competition for sorption sites on iron hydroxide (FH) surfaces between YHA and citric acid, which is driven in part by the electrostatic repulsion between negatively charged HA and citric acid at pH 5.5.

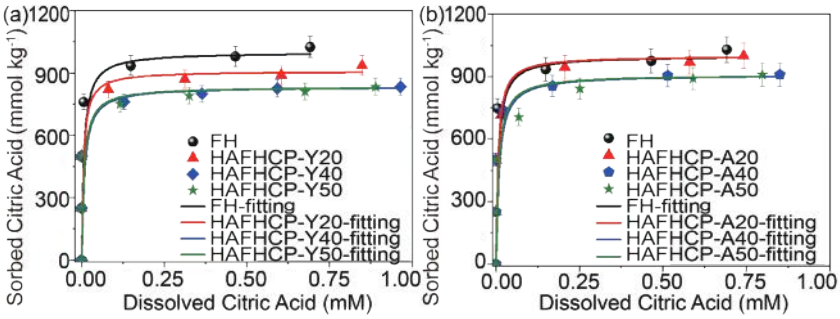

Fig. 1: Citric acid sorption isotherms for iron hydroxide (FH) and HAFHCP containing (a) YHA and (b) AHA with initial C/Fe ratios of 0.2, 0.4, and 0.5 (HAFHCP-Y20, Y40, Y50, A20, A40, and A50) fitted with the Langmuir isotherm model (solid lines). [Reproduced from Ref. 1]

Using X-ray absorption spectroscopy (XAS) at **TLS 16A1**, Tzou and coworkers observed through Fe K-edge X-ray absorption fine structure (EXAFS) analysis that the k^3-weighted $\chi(k)$ data for iron hydroxide (FH) and FH with sorbed citric acid were largely similar. However, slight differences emerged at $k \approx 5.0$, 7.5, and 8.5 $Å^{-1}$ between free HAFHCP-Y50/A50 and HAFHCP-Y50/A50 with sorbed citric acid. These findings suggest that citric acid impedes the structural development of Fe domains in HAFHCP, increasing dissolved Fe content and reducing the sorption capacity for citric acid (**Fig. 1**). A previous study by Tzou and his colleagues showed that HAFHCP-Y50 likely contains a relatively homogeneous distribution of C and Fe domains. In contrast, HAFHCP-A50 appears to have a ferrihydrite core with humic acid growing on its surface and possesses fewer polar functional groups. This arrangement results in greater Fe dissolution when citric acid is sorbed.

Understanding how HAFHCPs influence P availability is critical, particularly when organic acids and P coexist. To explore this, three experimental systems were developed to assess the cross-competitive sorption of P and citric acid on FH and HAFHCPs. Across all three systems, P sorption onto FH, HAFHCP-YHA, and HAFHCP-AHA followed the same order: P–C > S > C–P (**Fig. 3**, see next page). In the P–C, S, and C–P systems, P sorption on FH, HAFHCP-Y50, and HAFHCP-A50 differed significantly, having a decreasing trend of 1669–1780, 1245–1365, and 1018–1132 mmol kg^{-1}, respectively (**Fig. 3**). Notably, in the C–P system, pre-sorbed citric acid reduced P sorption by 50% compared with the MSC of P on FH (2250 mmol kg^{-1}) likely because of citric acid acting as a diffusion barrier for P. In

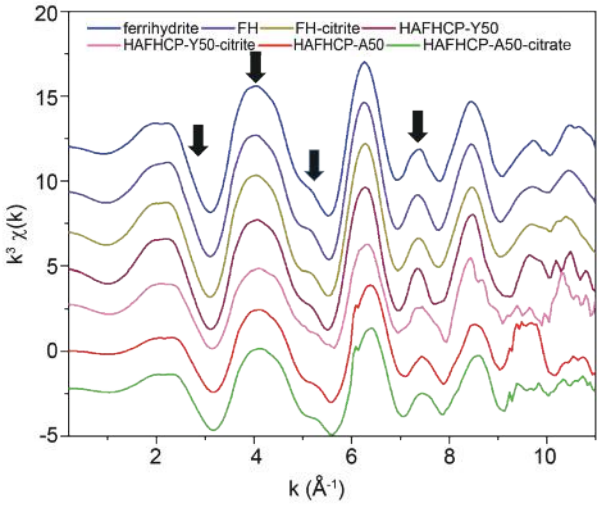

Fig. 2: Fe K-edge EXAFS spectra after sorption of citric acid on FH, HAFHCP-Y50, and HAFHCP-A50. Initial amounts of added citric acid were 0 and 2500 mmol kg^{-1}. [Reproduced from Ref. 1]

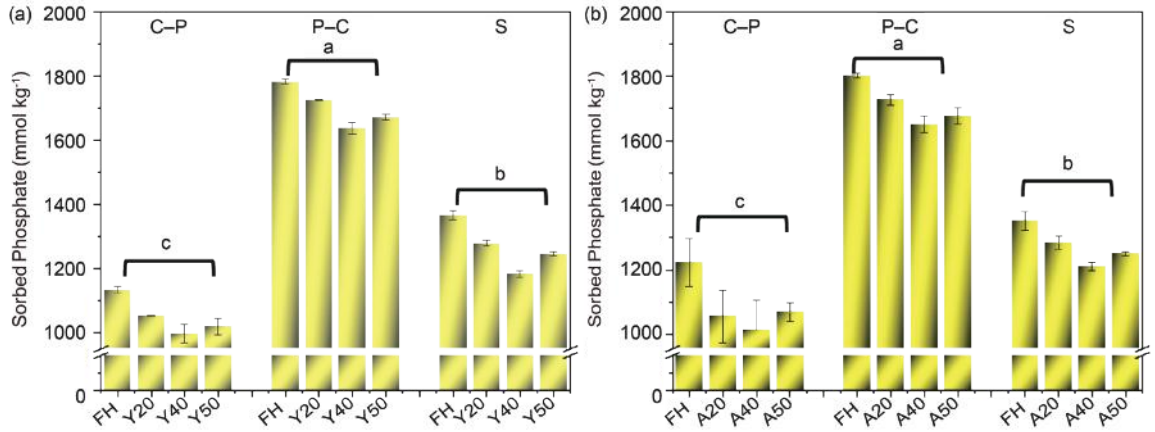

Fig. 3: The P sorption capacity for FH and HAFHCP containing (a) YHA and (b) AHA with initial C/Fe ratios of 0.2, 0.4, and 0.5 (HAFHCP-Y20, Y40, Y50, A20, A40, and A50) on cross-competitive sorption systems of C–P, P–C, and S. The order of addition for the different sorption systems are as follows: (1) For the C–P system, 1000 mmol kg^{-1} of citric acid was first added into FH/HAFHCP suspensions for 42 h, and then 2250 mmol kg^{-1} of P was added and allowed to react for another 42 h. (2) For the P–C system, 2250 mmol kg^{-1} of P was added and allowed to react with FH/HAFHCP for 42 h prior to the addition of 1000 mmol kg^{-1} of citric acid. The mixtures were then allowed to react for another 42 h. (3) In the S system, both P and citric acid were added simultaneously and allowed to react for 42 h. Statistical analysis was performed using one-way analysis of variance followed by Fisher's least-significant-difference (LSD) multiple-comparisons test at a significance level of $P < 0.05$. Significant differences between groups are denoted by different letters (a, b, c), as determined by Fisher's protected LSD test at a significance level of $P = 0.05$. [Reproduced from Ref. 1]

contrast, in the P–C system (where P was pre-sorbed), the presence of citric acid reduced P sorption by approximately 20%. Such effects may result from dissolved Fe functioning as a bridging agent between citric acid and P. Overall, these results indicate that citric acid strongly enhances P release in the C–P system.

In summary, this study emphasizes the role of HAFHCPs in the cross-competitive sorption of citric acid and P. The findings show that factors such as C/Fe ratios, the organic composition of humic acids, and the presence of citric acids (as observed through XAS) are key to understanding P availability. Consequently, the implementation of soil management strategies that foster favorable conditions for P availability is crucial for the sustainable utilization of P resources. (Reported by Kai-Yue Chen, National Chiayi University)

This report features the work of Yu-Min Tzou and his collaborators published in Environ. Res. ***240****, 117517 (2024).*

TLS 16A1 Tender X-ray Absorption, Diffraction

- EXAFS
- Environmental and Earth Sciences, Chemistry

Reference

1. M. M. M. Ahmed, K.-Y. Chen, F.-Y. Tsao, Y.-C. Hsieh, Y.-T. Liu, Y.-M. Tzou, Environ. Res. **240**, 117517 (2024).

Neutron Science

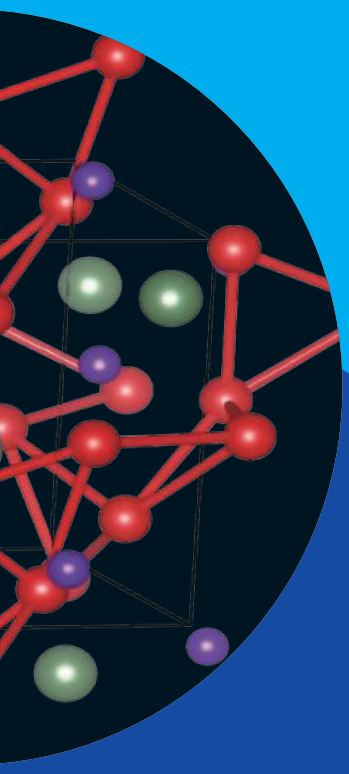

Recent research conducted at the Australian Nuclear Science and Technology Organization (ANSTO) has employed neutron scattering techniques to explore the properties of various materials, yielding critical insights into their behavior and potential applications. One investigation examined the hyperkagome antiferromagnet Mn_3RhSi using low- and high-energy inelastic neutron scattering to analyze its magnetic excitations. Led by Shin-ichi Shamoto, the research team determined that, despite the manganese magnetic moment being approximately 5 μB, only 2.6 μB orders below the Néel temperature of 190 K, suggesting substantial fluctuations attributable to geometric spin frustration. The calculated effective exchange interaction predicts a transition temperature aligning closely with the observed magnetic short-range order temperature of 720 K. Additionally, the study characterized the magnon dispersion, revealing an unusual form that results in a minimal magnon contribution to the electronic specific heat at low temperatures, underscoring the efficacy of neutron scattering in clarifying the magnetic properties of complex materials.

Another study utilized neutron reflectometry at ANSTO's **SPATZ** instrument to assess the thermal stability of non-fullerene organic solar cells (OSCs). Tzu-Yen Huang and colleagues investigated the morphology of bulk heterojunctions (BHJs) comprising PffBT4T-2OD as the donor and ITIC as the acceptor under thermal annealing. Their results revealed that the vertical morphology of the BHJ layers is initially well-mixed; however, annealing above 150°C triggers interface diffusion, predominantly due to ITIC molecule aggregation within the blends. This research highlights the critical need to address the thermal instability of acceptor materials like ITIC to improve the performance and longevity of OSCs.

The third investigation utilized neutron powder diffraction at ANSTO's **ECHIDNA** and **WOMBAT** instruments to explore the tunability of magnetic properties in the oxygen-deficient double perovskite $YBaCuFeO_5$ (YBCFO). Chao-Hung Du and his team demonstrated that introducing small amounts of Fe/Cu self-doping effectively modulates magnetic transition temperatures and the nature of magnetic order. Notably, a mere 1% iron addition increased the lower magnetic transition temperature (T_{n2}) by 65 K. This study offers a viable approach to tailoring YBCFO's magnetic properties by simultaneously inducing lattice effects and adjusting the Cu/Fe distribution.

Magnetic Excitation in the Hyperkagome Antiferromagnet Mn_3RhSi

Low- and high-energy inelastic neutron scattering measurements of a hyperkagome antiferromagnet revealed little magnetic specific heat capacity contribution in the enhanced electronic specific heat γ term.

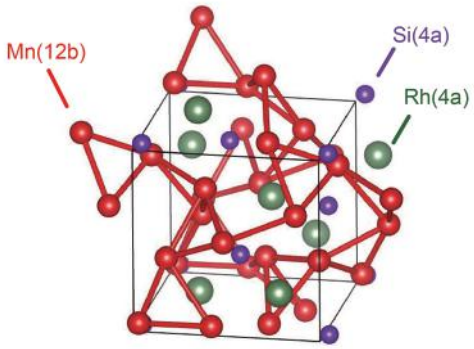

Fig. 1: Mn_3RhSi cubic crystal structure with a lattice parameter of a = 6.467 Å at 293 K. The red bond network is a hyperkagome lattice of the Mn site (12b), where the Mn–Mn bond distance ranges from 2.66 to 2.76 Å. [Reproduced from Ref. 3]

The hyperkagome antiferromagnetic semimetal Mn_3RhSi lacks spatial inversion symmetry in its β-Mn-type crystal structure (**Fig. 1**). The material exhibits intriguing magnetic behavior in which magnetic diffuse scattering due to magnetic short-range order is observed in the paramagnetic state up to 720 K, approximately 500 K higher than its Néel temperature of 190 K. The hyperkagome lattice is also found in well-studied β-Mn, which is a known spin liquid candidate and is a heavy Fermion 3*d* material with an electronic specific heat coefficient (γ) of about 70 mJ/MnK^2.[1] In ordered β-Mn-type alloys, a quantum critical behavior is observed in the enhanced γ term.[2] Here, the team of Shin-ichi Shamoto (Comprehensive Research Organization for Science and Society, Japan) studied the magnetic excitation of Mn_3RhSi by low- and high-energy inelastic neutron scattering measurements to elucidate the magnetic contribution to the enhanced γ term. Their research results provided the fluctuating magnetic moment size and the magnetic specific heat capacity at low temperatures for Mn_3RhSi.

In this study, the team measured a 1.65 g Mn_3RhSi single crystal and observed one magnon mode up to the maximum energy, as shown in **Fig. 2**. The observed intensity in **Fig. 3(a)** revealed that the magnitude of the magnetic moment of Mn 3d^5 was approximately 5 μ_B and is almost localized. The magnetic moment of the long-range order state below the Néel point was only 2.6 μ_B at 4 K,[4] indicating that most of the magnetic moment fluctuates without being ordered. This fluctuation is thought to be due to the geometrical spin frustration of the hyperkagome lattice. Interestingly, by using a magnetic moment of 2.6 μ_B and the Néel temperature (190 K), the effective exchange interaction can be estimated, yielding a predicted transition temperature of 700 K from the magnetic moment of 5 μ_B based on classical mean field approximation theory. The predicted temperature is very close to the temperature of the magnetic short-range order temperature 720 K mentioned above. The ability to measure low- and high-energy spin fluctuations even with a small crystal has allowed us to better understand mysterious magnetic materials.

Figure 3(b) shows the magnon dispersion of the low-energy mode in Mn_3RhSi. The solid line is fit using the equation $E = E_{top} \sin^{\alpha}(\pi h)$, where the best fit was obtained with E_{top} = 39.5(3) meV and α = 0.53(3). The peculiar dispersion leads to the magnon specific heat capacity of $C_{mag} = dU/dT \propto (T/E_{top})^{3/\alpha}$. As for the electronic specific heat coefficient γ of Mn_3RhSi, the magnon heat capacity becomes small at low temperatures because of the large exponent of ~$(T/E_{top})^6$, resulting in little magnon effect on the T-linear electronic specific heat. The team confirmed that the magnon dispersion continues to the low-energy region below 1 meV at **SIKA** without an appreciable spin gap. The combination of the low- and high-energy inelastic

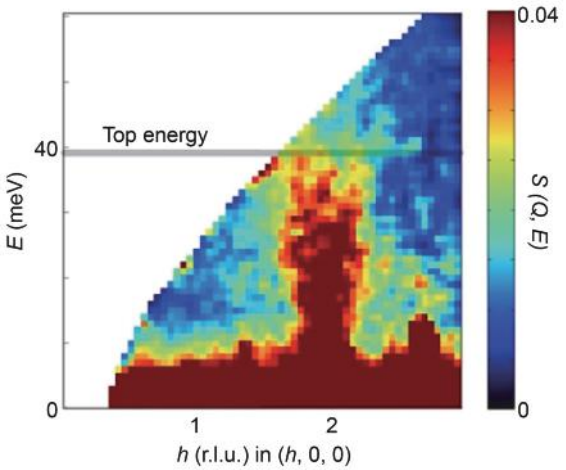

Fig. 2: Dynamical structure factor divided by the Bose factor $(Q, E)/\{n(E) + 1\}$ in the low-Q region measured with E_i = 95 meV. The single-crystal scattering intensity at T = 6 K is averaged vertically in the range of $-0.2 < k < 0.2$ and $-0.2 < l < 0.2$ (r.l.u.). The horizontal scattering plane is $[h, 0, 0]$-$[0, k, k]$. The top energy of the low-energy magnon mode is shown by a solid line. [Reproduced from Ref. 3]

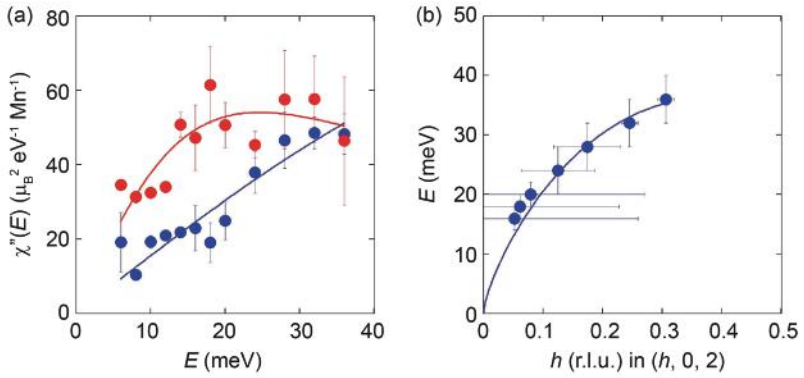

Fig. 3: (a) The dynamical spin susceptibilities are plotted as a function of energy at $T = 6$ K (blue open circles) and 200 K (red closed circles). (b) Magnon dispersion observed at $T = 6$ K. Solid lines are used to aid with visual inspection. [Reproduced from Ref. 3]

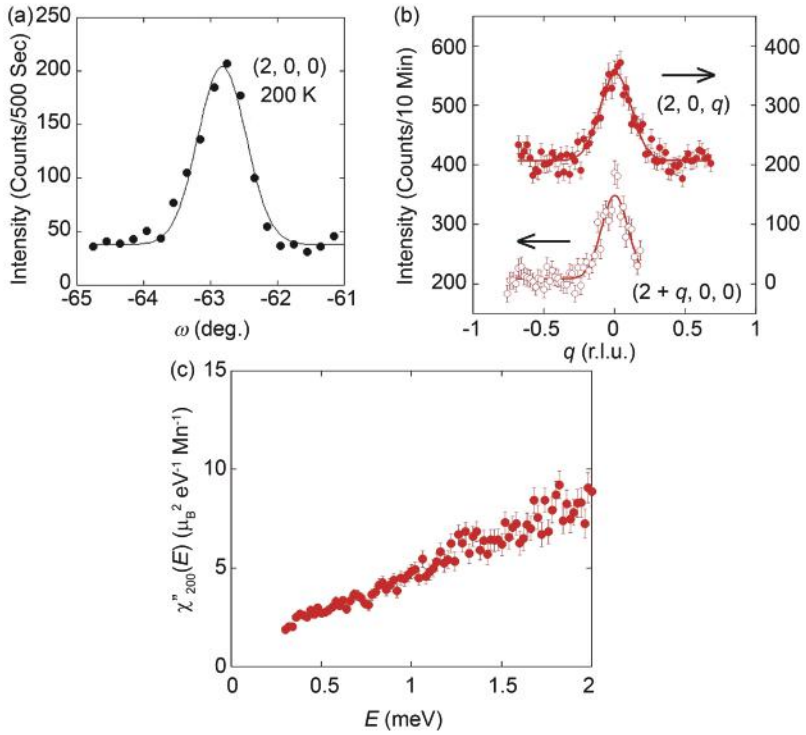

Fig. 4: (a) ω-scan at (2, 0, 0) of the Mn_3RhSi crystal. (b) The constant-energy q-scan in (2 + q, 0, 0) (open circles) and (2, 0, q) (closed circles) of $E = 1$ meV at $T = 200$ K. The horizontal scattering plane is [h, 0, 0]-[0, 0, l]. (c) Low-energy Q-integrated local dynamical spin susceptibility $\chi_{200}(E)$ at Q = (2, 0, 0) measured at $T = 200$ K. [Reproduced from Ref. 3]

neutron scattering measurements of a hyperkagome antiferromagnet revealed how magnetic excitation can contribute to the magnetic specific heat capacity in the enhanced electronic specific heat γ term. (Reported by Shin-ichi Shamoto, Comprehensive Research Organization for Science and Society, Japan)

This report features the work of Shin-ichi Shamoto and his collaborators published in Phys. Rev. Research ***6****, 033303 (2024).*

ANSTO SIKA – Cold Neutron Triple-axis Spectrometer

- Neutron Inelastic Scattering
- Materials Science, Condensed-matter Physics

References

1. H. Nakamura, K. Yoshimoto, M. Shiga, M. Nishi, K. Kakurai, J. Phys.: Condens. Matter **9**, 4701 (1997).
2. H. Yamauchi, D. P. Sari, Y. Yasui, T. Sakakura, H. Kimura, A. Nakao, T. Ohhara, T. Honda, K. Kodama, N. Igawa, K. Ikeda, K. Iida, D. Ueta, T. Yokoo, M. D. Frontzek, S. Chi, J. A. Fernandez-Baca, K. M. Kojima, D. Arseneau, G. Morris, B. Hitti, Y. Cai, A. Berlie, I. Watanabe, P.-T. Hsu, Y.-S. Chen, M. K. Lee, A. E. Hall, G. Balakrishnan, L.-J. Chang, S. Shamoto, Phys. Rev. Research **6**, 013144 (2024).
3. S. Shamoto, H. Yamauchi, K. Iida, K. Ikeuchi, K. Kaneko, Y.-S. Chen, S. Yano, P.-T. Hsu, M. K. Lee, A. E. Hall, B. Geetha, L.-J. Chang, Phys. Rev. Research **6**, 033303 (2024).
4. H. Yamauchi, D. P. Sari, I. Watanabe, Y. Yasui, L.-J. Chang, K. Kondo, T. U. Ito, M. Ishikado, M. Hagihara, M. D. Frontzek, S. Chi, J. A. Fernandez-Baca, J. S. Lord, A. Berlie, A. Kotani, S. Mori, S. Shamoto, Commun. Mater. **1**, 43 (2020).

The Non-Fullerene Acceptor ITIC Induced the Morphology of Bulk Heterojunctions Through Thermal Annealing

The key component affecting the thermal stability of non-fullerene organic solar cells is explored.

The nanomorphology of bulk heterojunctions (BHJs) is a critical factor influencing the performance of non-fullerene organic solar cells (OSCs). Thermal annealing is widely used in enhancing device performance by reorganizing the donor and acceptor phases within BHJs. A team led by Tzu-Yen Huang (NSRRC) and Yan-Ling Yang (National Taiwan University of Science and Technology) systematically examined the vertical morphology of BHJ blend films, which utilized poly[(5,6-difluoro-2,1,3-benzothiadiazol-4,7-diyl)-alt-(3,3‴-di(2-octyldodecyl)-2,2′;5′,2″;5″,2‴-quaterthiophen-5,5‴-diyl)] (PffBT4T-2OD) polymer as the donor and 3,9-bis(2-methylene-(3-(1,1-dicyanomethylene)-indanone))-5,5,11,11-tetrakis(4-hexylphenyl)-dithieno[2,3-d:2′,3′-d′]-s-indaceno[1,2-b:5,6-b′]dithiophene (ITIC) as the acceptor through thermal annealing.

The team made use of the neutron reflectometry (NR) instrument (**SPATZ**) at the Australian Nuclear Science and Technology Organisation (ANSTO) to study the blend morphology of BHJ thin films. **Figures 1(a) and 1(c)** illustrate the NR patterns and scattering length density (SLD) profiles of PffBT4T-2OD:ITIC BHJs with various blend ratios deposited on quartz-coated glass substrates. The SLD values of PffBT4T-2OD monomers and ITIC molecules were calculated to be 0.65 and 1.44×10^{-6} Å^{-2}, respectively. The NR curves of the 1:9 ratio revealed distinct Kiessig fringes spanning a Q-range of 0.02 to 0.10 Å^{-1}, indicating high-quality thin films. As the ratio of PffBT4T-2OD is increased, the clear fringes are preserved, demonstrating good film quality across different blend ratios. The fringes of the BHJ layer (9:1 ratio) became less defined due to the proximity of the SLD value of PffBT4T-2OD to that of the atmosphere, which reduced contrast. For all samples, the quartz layer on the glass substrate exhibited a consistent thickness of about 200 Å with a roughness of 13 Å. The SLD value of different BHJ layers ranged from 1.39 $\times 10^{-6}$ Å^{-2} (1:9 ratio) to 0.70 $\times 10^{-6}$ Å^{-2} (9:1 ratio). These findings suggest that the vertical morphology of the BHJ layers is well-mixed, without distinct phase segregation.

Thermal annealing is a common method for optimizing phase separation in a BHJ layer, facilitating the formation of the desired morphologies for efficient charge transport. To avoid surpassing the recrystallization temperature of ITIC at 170°C, the thermal treatment was carried out incrementally, with annealing temperatures reaching up to 150°C. **Figures 1(b) and 1(d)** present the NR patterns and the SLD profiles of the PffBT4T-2OD:ITIC BHJ layers (5:5 blend ratio) deposited on Si wafers, which were subjected to annealing at temperatures ranging from 90 to 150°C. The pristine PffBT4T-2OD:ITIC BHJ layers exhibit fringes in the Q-range of 0.010 to 0.040 Å^{-1}, indicating the formation of smooth and uniform thin films. At an annealing temperature of 130°C, the fringes remain intact, signifying that

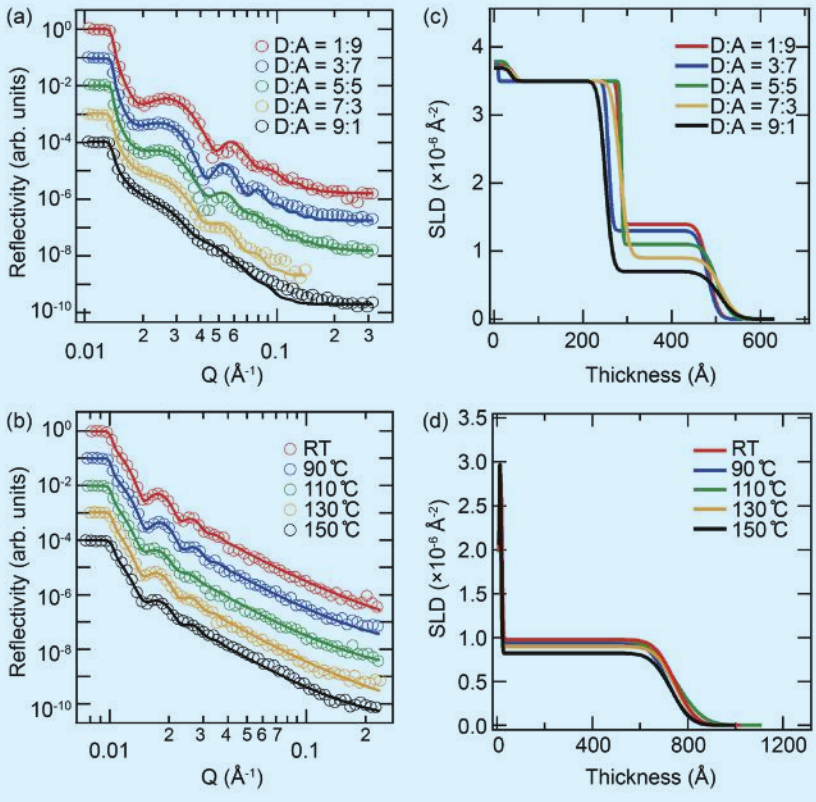

Fig. 1: (a) NR profiles and (c) corresponding SLD profiles of PffBT4T-2OD:ITIC BHJ films with different donor/acceptor ratios (1:9, 3:7, 5:5, 7:3, and 9:1) on the quartz-coated glass substrates. The individual data points and solid lines represent the experimental data and fitting results, respectively. The NR curves have been offset for clarity. (b) NR profiles and (d) corresponding SLD profiles of PffBT4T-2OD:ITIC (5:5) BHJ films on the Si wafers annealed from RT to 150°C. [Reproduced from Ref. 1]

the interface of the film is maintained. The corresponding SLD value ($0.96 \pm 0.05 \times 10^{-6}$ Å^{-2}) of the PffBT4T-2OD:ITIC BHJ layer also remains unchanged at this temperature. At 150°C, the fringes near Q = 0.025 Å^{-1} become indistinct, suggesting an increased diffusive interface between the air and the film, accompanied by a decrease in the SLD value to 0.81×10^{-6} Å^{-2}. These results indicate that interface diffusion of the PffBT4T-2OD:ITIC BHJ layers is initiated after annealing at 150°C.

To understand the phase behavior of BHJ blends, the individual donor and acceptor materials were examined under the same annealing conditions. The NR curves and SLD profiles of pristine PffBT4T-2OD films on the Si wafer with different annealing temperatures are shown in **Figs. 2(a) and 2(c)**. The fringes remain unchanged as the annealing temperature increases. The SLD profiles show that a thickness of 614 ± 9 Å and surface roughness of 30 ± 1 Å are retained after thermal treatment. These results suggest that even when the annealing temperature exceeds 90°C, the highly active side chains of PffBT4T-2OD do not induce significant vertical morphological changes in the films. On the other hand, **Figs. 2(b) and 2(d)** display the NR patterns and SLD profiles of pure ITIC thin films. The fringes are observed within the Q-range of 0.01 to 0.03 Å^{-1} for temperatures between 90 and 130°C. The corresponding film thickness and roughness are about 554 ± 10 and 106 ± 9 Å, respectively. The NR patterns become less distinct after thermal annealing at 150°C. In addition, there is little change in the position of the Kiessig fringes, indicating that there is little change in the ITIC film thickness. The thickness was set to 555 Å with limits of ±5 Å, and then the SLD value and interfacial roughness were fitted. The SLD value decreased to 0.75 $\times 10^{-6}$ Å^{-2} along with an increase in roughness to 139 Å. These results suggest that interface diffusion begins at 150°C, likely driven by intrinsic agglomeration of the ITIC molecules rather than by interactions with the substrate. Additionally, even brief annealing at this temperature appears to induce ITIC nanocrystal reorganization, leading to variations in the vertical morphology of the thin film.

In summary, the study demonstrated the diffusive interfaces of the PffBT4T-2OD:ITIC BHJ thin films emerging when the annealing temperature exceeds 150°C primarily because of ITIC aggregation within the blends. Thermal annealing serves as a critical post-treatment process for removing residual solvent and optimizing phase distribution in BHJ thin films. Within a brief annealing period, the morphology of PffBT4T-2OD:ITIC BHJs are influenced by ITIC nanoclusters. The findings suggest that the initial unfavorable mixing contributes to the instability of ITIC molecules during annealing, adversely affecting power conversion efficiency and device stability. It is essential to consider thermal instability and processing conditions for the enhanced performance of OSCs for promising BHJs incorporating ITIC-based small molecules. (Reported by Tzu-Yen Huang)

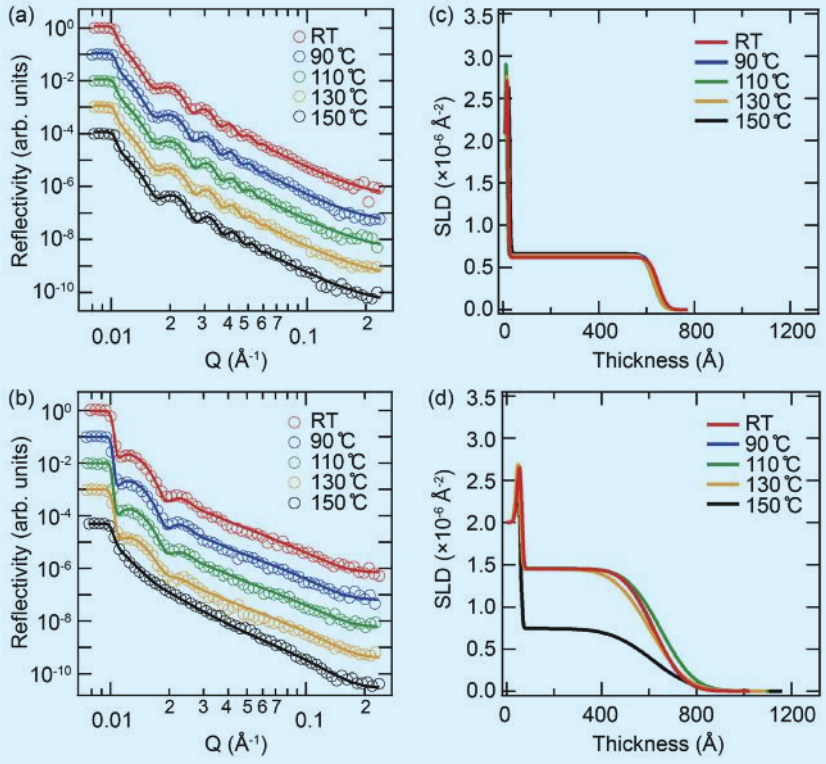

Fig. 2: NR curves and the corresponding SLD profiles for pristine (a,c) PffBT4T-2OD and (b,d) ITIC films on the Si wafers annealed from RT to 150°C. [Reproduced from Ref. 1]

This report features the work of Tzu-Yen Huang and his collaborators published in ACS Appl. Nano Mater. 7, 17588 (2024).

ANSTO SPATZ – Neutron Reflectometer

- NR
- Polymers, Morphology, Interfaces, Thin Films

Reference

1. T. Y. Huang, A. P. Le Brun, B. Sochor, C. M. Wu, Y. Bulut, P. Müller-Buschbaum, S. V. Roth, Y. L. Yang, ACS Appl. Nano Mater. **7**, 17588 (2024).

Effective Modulation of the Magnetic Properties of $YBaCuFeO_5$

Very low concentrations of Cu/Fe self-doping can effectively change the magnetic properties of $YBaCuFeO_5$.

Multiferroic materials, in which ferroelectricity and magnetic ordering coexist, have been actively studied with interests in fundamental and applied sciences. Several decades of investigations reveal that the incommensurate orientation-modulated spin structures, such as spiral and cycloidal, are good candidates for hosting ferroelectricity. In such materials, termed type II ferroelectrics, the electrical polarization is coupled with the magnetic structures triggered by the Dzyaloshinskii–Moriya interaction or magnetic frustration. Nevertheless, the magnetic ordering temperature T_N and ferroelectric Curie temperature T_C are generally well below the ambient temperature and are unfavorable for daily-life applications. While pursuing multiferroic materials with high T_c, the oxygen-deficient double perovskite, $YBaCuFeO_5$ (YBCFO), arouses wide attention. YBCFO possesses the layered structure of $MM'O_9$ bipyramids (**Fig. 1(a)**), and Cu/Fe resides within the double pyramids. The Cu/Fe spins undergo antiferromagnetic transition to a commensurate, collinear antiferromagnetic order characterized by the propagation vector of k_{c1} = (1/2, 1/2, 1/2) at T_{N1}. Below the second magnetic phase-transition temperature T_{N2}, the spin structure transits into an incommensurate chiral structure, with propagation vector k_i = (1/2, 1/2, 1/2 ± δ).[1] The reported values of T_{N1} and T_{N2} are inconsistent in the literature, and the differences are as large as several tens of degrees. Such differences are unlikely due to the experimental errors but imply a tunable magnetic property of the compound. It is demonstrated that T_{N2} is successfully tuned by chemical substitution and a post-sintering cooling rate.[2,3] Chemical substitution can tune the lattice, change the interlayer distances, and subsequently alter the strength of interlayer interactions. Increasing the cooling rate or quenching the sample after the sintering has been proven to be an effective way of controlling the Cu/Fe distribution within the bipyramids. Theoretical studies show that disorder in the Cu/Fe distribution is crucial for the onset of commensurate to incommensurate magnetic transition (CM–ICM). At the same time, the CM phase persists down to low temperature without transiting into the ICM phase in the sample with highly ordered cation distribution.[4]

Magnetic transition temperatures are correlated with the degree of disorder. T_{N2} increases while T_{N1} is slightly suppressed when the Cu/Fe distribution is more disordered. Therefore, the ICM order temperature can be enhanced by tuning the Cu/Fe distribution. In the noncentrosymmetric *P*4*mm* structure, the bipyramids are occupied by one Fe and one Cu, with ordered arrangement. The in-plane nearest-neighbor interactions are strongly antiferromagnetic despite the Cu/Fe distribution; therefore, the spins order into the checkerboard arrangement in the ab-plane.

Meanwhile, the interplane interactions alternate the sign along the c-axis and are ferromagnetic within the bipyramids and antiferromagnetic between bipyramids, resulting in the [+--+] ground state characterized by the propagation vector of k_{c1} = (1/2, 1/2, 1/2). By increasing the post-annealing cooling speed or quenching, disorder is introduced. Fe–Fe and Cu–Cu pairs could occupy the bipyramid sites locally. Theoretical works suggest that the Fe–Fe pairs occupying the bipyramid impurities serve as "impurities", introducing antiferromagnetic interactions to the matrix of ferromagnetic coupling. When the concentration is sufficiently high and the temperature is sufficiently low, the incommensurate spiral structure sets in.

Chao-Hung Du (Tamkang University) proposed an alternative way to tune the magnetic properties of YBCFO by directly modifying the B site. By introducing additional Fe/Cu to the B sites, the local Fe/Cu arrangement could be changed to avoid the potential effects of the foreign

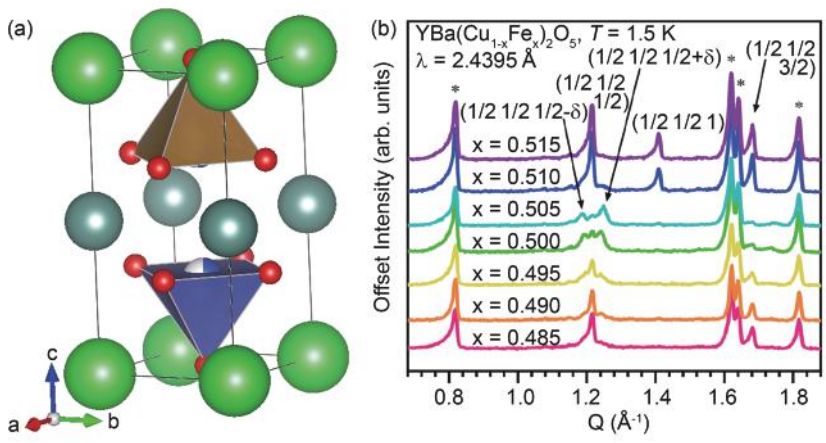

Fig. 1: (a) Crystal structure of YBCFO. (b) NPD patterns of selected $YBa(Cu_{1-x}Fe_x)_2O_5$ samples. The asterisks indicate the nuclear reflections, and the Miller indexes of magnetic peaks are labeled. [Reproduced from Ref. 6]

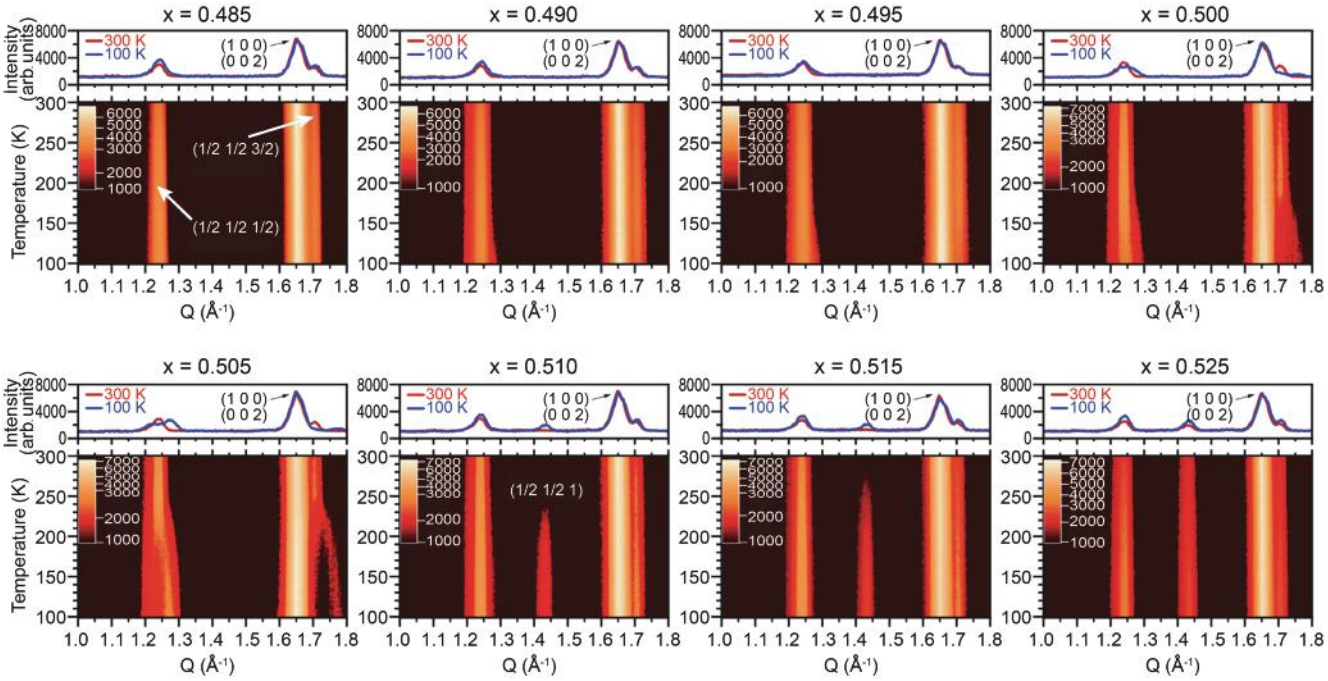

Fig. 2: Two-dimensional contours of eight $YBa(Cu_{1-x}Fe_x)_2O_5$ samples with distinct Cu/Fe ratios illustrate the temperature dependence of NPD patterns measured from 100 to 300 K. These figures focus on the low-Q region where the magnetic reflections appear NPD-pronounced. [Reproduced from Ref. 6]

element dopants. Polycrystalline $YBa(Cu_{1-x}Fe_x)_2O_5$ with x ranging between 0.485 and 0.525 were synthesized. **Figure 1(b)** shows the neutron powder diffraction (NPD) patterns collected at 1.5 K, employing the high-resolution neutron powder diffractometer, **ECHIDNA**. The patterns reveal various magnetic structures. The thermal evolution of magnetic structures was studied on the high-intensity neutron powder diffractometer, **WOMBAT**. **Figure 2** displays the temperature evolution of the magnetic structures of $YBa(Cu_{1-x}Fe_x)_2O_5$ and is summarized in the phase diagram shown in **Fig. 3**. The k_{c1} and k_{icm} magnetic phases coexisted at 1.5 K in the x = 0.500 sample. Noticeably, the incommensurate phase was most pronounced in the x = 0.505 sample, and the associated peaks were weaker because the iron content increased above 0.505. Compared to the parent YBCFO sample, T_{N2} was enhanced by 65 K by adding merely 1% iron. When the iron content was reduced from x = 0.505, the CM–ICM transition temperature, T_{N2}, gradually decreased, suggesting that the impurity bond density was gradually reduced. By contrast, the k_{icm} phase diminished much more quickly, and there were only extremely weak peaks of k_{icm} in the NPD of x = 0.510 and 0.515 samples. In samples with high iron content (x = 0.510 and 0.515), a new commensurate magnetic phase k_{c2} = (1/2, 1/2, 1) emerged. In the k_{c2} phase, the checkerboard arrangement was preserved in the ab-plane, and the sequence of spin arrangement along the c-axis was [+-+-], contrary to [+--+] in the k_{c1} phase. The additional iron content likely introduced excessive antiferromagnetically coupled Fe–Fe pairs to the bipyramid layers and destroyed the delicate balance for the emergence of the incommensurate spiral structure. The coexistence of k_{c1}, k_{c2}, and k_{icm} phases was observed in isostructural $NdBaCuFeO_5$ as magnetic texturing due to the partial ordering of Fe/Cu[5] and is similar to the behavior of highly ordered YBCFO.[4]

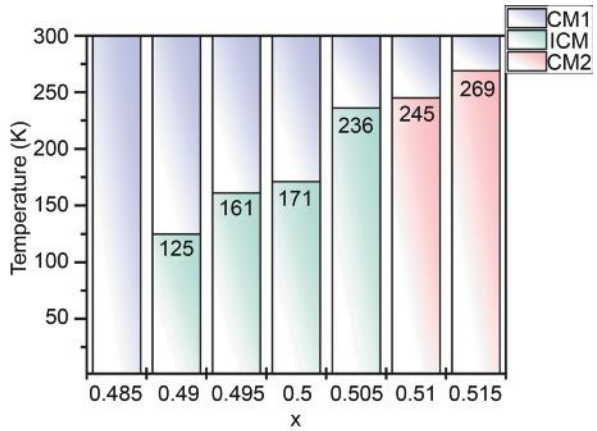

Fig. 3: Phase diagram of $YBa(Cu_{1-x}Fe_x)_2O_5$. [Reproduced from Ref. 6]

The magnetic properties of the oxygen-deficient double perovskite YBCFO can be tuned by A-site doping by adjusting the crystal structure to affect the magnetic coupling strength. By controlling the post-sintering cooling rate, the cation distribution on the B sites where the magnetic species Cu/Fe resides was determined. The current work proposed a more effective route that can simultaneously introduce the lattice effect and tune the Cu/Fe distribution. (Reported by Chin-Wei Wang)

*This report features the work of Chao-Hung Du and his collaborators published in Phys. Rev. Mater. **8**, 054404 (2024).*

ANSTO ECHIDNA – High Resolution Powder Diffractometer
ANSTO WOMBAT – High-Intensity Powder Diffractometer

- NPD
- Materials Science, Chemistry, Condensed-matter Physics

References

1. Y. C. Lai, C. H. Du, C. H. Lai, Y. H. Liang, C. W. Wang, K. C. Rule, H. C. Wu, H. D. Yang, W. T. Chen, G. J. Shu, F. C. Chou, J. Phys.: Condens. Matter **29**, 145801 (2017).
2. A. Romaguera, X. Zhang, O. Fabelo, F. Fauth, J. Blasco, J. L. García-Muñoz, Phys. Rev. Res. **4**, 043188 (2022).
3. T. Shang, E. Canévet, M. Morin, D. Sheptyakov, M. T. Fernández-Díaz, E. Pomjakushina, M. Medarde, Sci. Adv. **4**, eaau6386 (2018).
4. A. Romaguera, X. Zhang, R. Li, O. Fabelo, J. L. García-Muñoz, EPJ Web of Conferences **286**, 05005 (2023).
5. M. Pissas, J. M. M. M. **432**, 224 (2017).
6. C. H. Lai, C. W. Wang, H. C. Wu, Y. H. Kiang, A. J. Studer, W. T. Chen, C. H. Du, Phys. Rev. Mater. **8**, 054404 (2024).

Inelastic Neutron Scattering Reveals Strong Electron–Phonon Interactions Driving Ultrahigh *zT* Values

Through inelastic neutron scattering, strong electron–phonon interactions in Sb–Bi codoped GeTe crystals are revealed, unlock ultrahigh zT values. This breakthrough redefines thermoelectric innovation and accelerates the development of materials such as PbTe, SnTe, and SnSe.

Imagine a world where we can recover and utilize heat that would normally be lost. This includes the heat produced by automobile engines, the warmth radiating from industrial machines, and even the heat generated during physical exercise. The possibility of turning this heat into usable electricity could radically change how we consume energy. This is the promise of thermoelectric materials, which have the remarkable ability to convert thermal energy into electrical energy.[1] The range of potential applications is extensive—everything from making vehicles more fuel-efficient to developing more energy-efficient homes and appliances.

A significant advancement in the understanding and improvement of thermoelectric materials was achieved through the research conducted by Yang-Yuan Chen and his team at the Institute of Physics, Academia Sinica. By utilizing the powerful **SIKA** Cold Neutron Triple-axis Spectrometer at the Australian Nuclear Science and Technology Organisation (ANSTO),[2] Chen and his team discovered a novel mechanism in thermoelectric materials: the presence of ultrahigh *zT*, which serves as a figure of merit for thermoelectric performance driven by strong electron–phonon (EP) interactions and a low-dimensional Fermi surface. These discoveries offer new possibilities for enhancing thermoelectric performance, paving the way for applications that may revolutionize how we capture and use energy in our everyday lives.

Thermoelectric materials are designed to capture heat and convert it into electrical energy. However, they face a challenge: the heat usually travels through the material in a way that reduces its efficiency in generating electricity. The *zT* value is a key metric that indicates the efficiency of a thermoelectric material; the higher the *zT*, the better the material can convert heat into electrical power. By studying the intricate interactions between electrons (which carry electricity) and phonons (which transport heat), Chen's team identified a method to develop a material with an exceptionally high *zT*, enabling it to convert heat into electricity with remarkable efficiency.

The discovery is based on EP interactions, which occur at the atomic level, as shown in **Figs. 1(a) and 1(b)**. In many thermoelectric materials, heat dissipates too quickly because of weak coupling between electrons and phonons. However, in the materials studied by Chen's team, the strong EP interaction allows efficient electrical conduction while maintaining a temperature gradient that drives the thermoelectric process. Such as behavior leads to an ultrahigh *zT*, which is a game-changer in the thermoelectric field.

Moreover, Chen and his team found that the low-dimensional Fermi surface of the material—essentially, the arrangement of the electrons within the material—further enhances its thermoelectric properties. A low-dimensional Fermi surface allows electrons to travel with less resistance, which in turn improves the material's ability to generate electrical energy from heat, as shown in **Figs. 1 (c) and 1(d)**. This is a crucial insight for developing new thermoelectric materials suitable for real-world applications.

Further investigation into Sb–Bi codoped GeTe by Chen's team, using the SIKA Cold Neutron Triple-axis Spectrometer, revealed even more remarkable findings as shown in **Figs. 1(e) and 1(f)**. They found a strong Kohn anomaly in the phonon dispersion of this material, which indicates the strong electron-phonon interaction. This anomaly occurs when the Fermi surfaces of the material exhibit significant nesting, which implies that the two parallel Fermi surfaces overlap significantly. This nesting enhances the EP interactions, which are crucial for thermoelectric efficiency. The Sb–Bi codoped GeTe material exhibited a distinctive Kohn anomaly that was absent in the pristine GeTe, suggesting that codoping with Sb and Bi strengthens the EP interaction, thereby improving the material's thermoelectric properties.

The Kohn anomaly plays a pivotal role in enhancing the thermoelectric efficiency of materials. In Sb–Bi codoped GeTe, the anomaly occurs because the Fermi level is slightly below the D maximum of the material, resulting in an electronic structure that behaves in a one-dimensional manner. This feature allows electrons to move more efficiently along a single axis, which contributes to improved thermoelectric performance. The strong EP interactions in Sb–Bi codoped GeTe result in superior heat-to-electricity conversion, leading to a material with a higher zT value.

How does this discovery impact our daily lives? Consider the substantial energy we waste. In the modern world, nearly everyone has experienced some form of energy loss, whether from excessive heat in homes, industries, or vehicles. For example, in a typical car engine, a considerable portion of the energy from the fuel is lost as heat. Imagine if a car could capture even a small portion of that wasted heat and convert it into electricity to power its electronic systems or improve fuel efficiency. Thermoelectric materials with ultrahigh zT values could facilitate this, creating more efficient vehicles that require less fuel and produce lower emissions.

Similarly, industries generate enormous amounts of heat during the production processes. Factories could use thermoelectric materials to capture and convert this waste heat into usable electricity, thus powering their operations or reducing the need for external energy sources. This approach could lead to more sustainable manufacturing practices, reduce energy consumption, and lower costs for businesses, ultimately benefiting consumers as well.

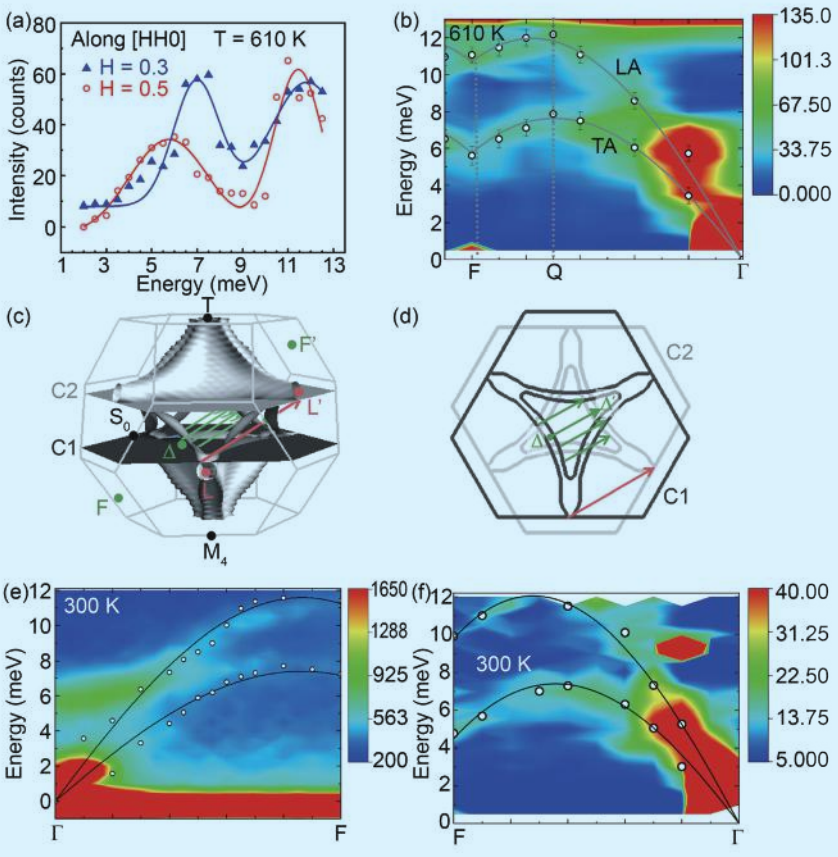

Fig. 1: Relationship between phonon dispersion and density of states. (a) Phonon excitation spectra measured in constant-Q scans along the crystallographic [HH0] direction at 610 K, with H = 0.3 represented by filled triangles and H = 0.5 represented by open circles. (b) Phonon dispersion of $(Ge_{0.86}Sb_{0.08}Bi_{0.06})Te$ at 610 K, measured along the crystallographic [110] direction. (c) Calculated Fermi surface of p-type GeTe at the Fermi energy, E_{x0}. (d) The two corresponding 2D cross-sections (C1 and C2) of the Fermi surface. The short green arrows and the long red arrows indicate the wave vector difference Dk between the initial and final states due to the electronic transition in the [110] direction (G-F direction). Images of (c) and (d) were prepared using FermiSurfer. (e) Phonon dispersion of pristine GeTe at 300 K. (f) Phonon dispersion of Sb–Bi codoped GeTe at 300 K. [Reproduced from Ref. 3]

Thermoelectric materials have the potential to revolutionize energy consumption in our daily lives. In household appliances such as refrigerators, air conditioners, and heating systems, these materials could recycle heat generated during their operation, either by directly converting it into electricity or by improving efficiency. This advancement would enhance energy efficiency of everyday appliances, reduce reliance on external power sources, and lower electricity expenses.

In the renewable-energy sector, thermoelectric materials with ultrahigh *zT* values could also play a vital role. Although solar panels are proficient at capturing sunlight, they frequently lose excess heat. By integrating thermoelectric materials into solar panels, we could recover and convert this wasted heat into additional electricity, further boosting the overall efficiency of solar energy systems.

The research conducted by Chen's team, supported by the advanced technology of the **SIKA** Cold Neutron Triple-axis Spectrometer, paves the way for the development of more efficient thermoelectric materials. By understanding how electrons and phonons interact on a microscopic level, we are progressing toward a future where energy is used more efficiently, waste is minimized, and a greater number of devices can be powered by everyday heat. The implications of this research are profound, offering the potential to improve energy efficiency across transportation, industrial production, and daily appliances, all while contributing to a more sustainable and energy-conscious society. (Reported by Chun-Ming Wu)

This report features the work of Yang-Yuan Chen and his collaborators published in Energy Environ. Sci. ***17****, 1904 (2024).*

ANSTO SIKA – Cold Neutron Triple-axis Spectrometer

- Inelastic Neutron Scattering
- Thermal Electric Materials, Ultrahigh *zT*, Condensed Matter, Energy Materials, Quantum Physics

References

1. G. J. Snyder, E. S. Toberer, Nat. Mater. **7**, 105 (2008).
2. C.-M. Wu, G. Deng, J.S. Gardner, P. Vorderwisch, W.-H. Li, S. Yano, J.-C. Peng, E. Imamovic, JINST **11**, 10009 (2016).
3. V. K. Ranganayakulu, T.-H. Wang, C.-L. Chen, A. Huang, M.-H. Ma, C.-M. Wu, W.-H. Tsai, T.-L. Hung, M.-N. Ou, H.-T. Jeng, C.-H. Lee, K.-H. Chen, W.-H. Li, M. K. Brod, G. J. Snyder, Y.-Y. Chen, Energ. Environ. Sci. **17**, 1904 (2024).

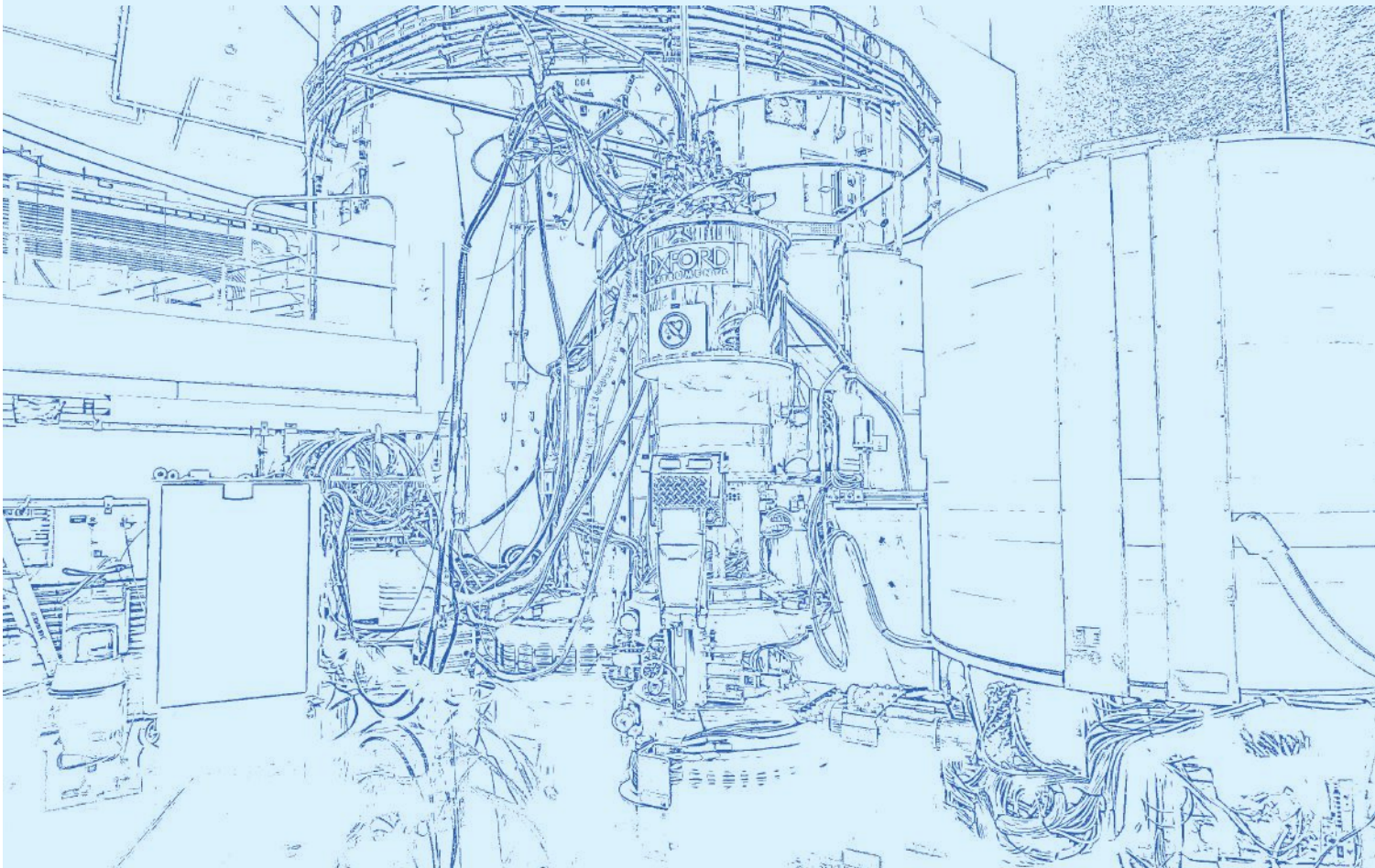

Facility Development and Status

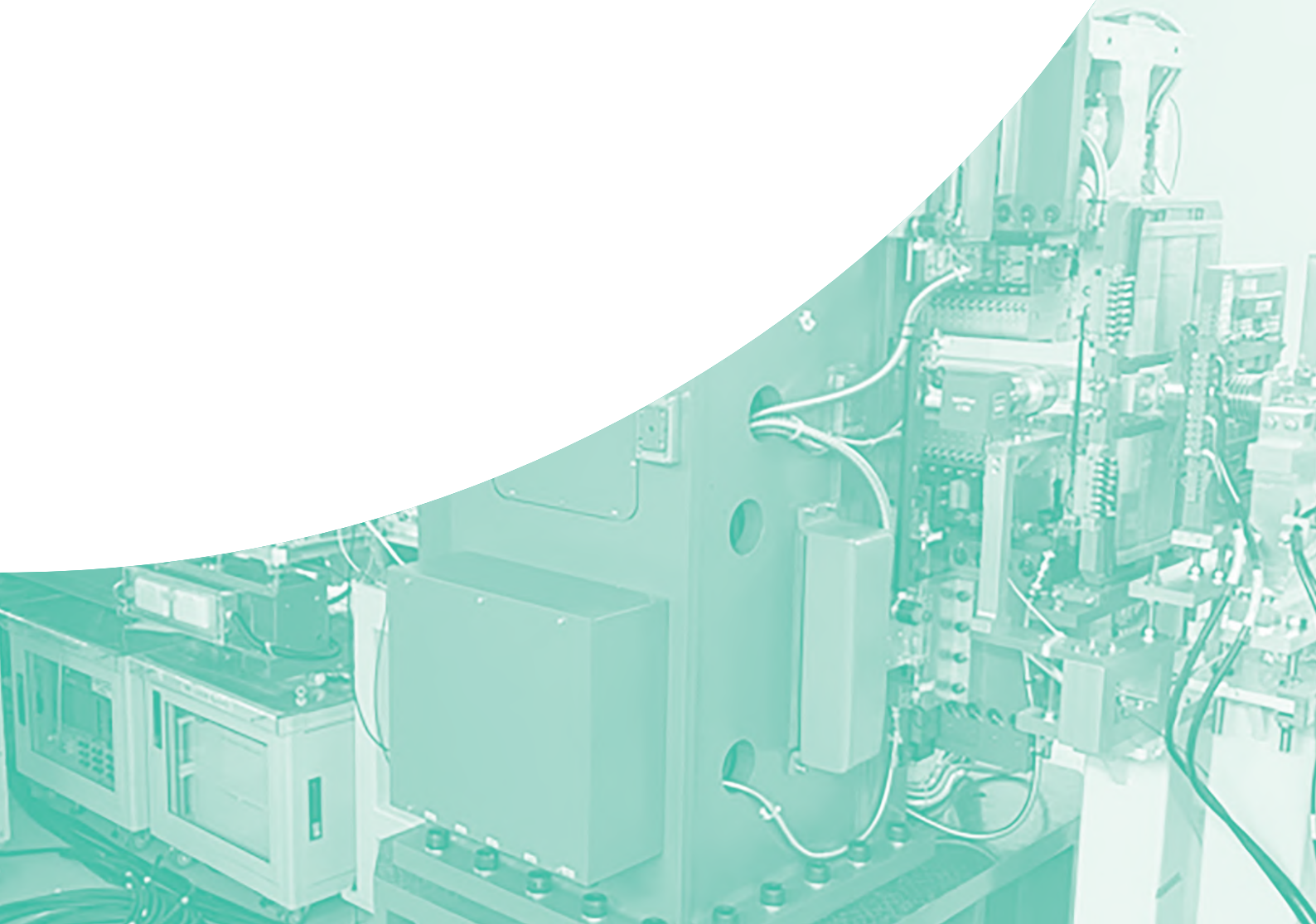

Status of TLS and TPS Accelerators

Taiwan Light Source (TLS)

Machine Parameters of the TLS

The Taiwan Light Source (TLS) celebrated its 30th anniversary of its first operation in 2023. Since its commissioning in 1993, TLS has invited experimental proposals and opened its facilities to users, initially featuring three soft X-ray beamlines: HSGM, LSGM, and Seya. The original TLS design was based on a triple bend achromatic lattice with a beam energy of 1.3 GeV and a beam current of 200 mA. Following several phases of upgrades, the accelerator has now achieved a beam energy of 1.5 GeV, a maximum stored beam current of 360 mA, top-up injection capabilities, a superconducting radio-frequency (SRF) cavity, a liquid-helium cryogenic system, superconducting wigglers (SCWs), and advanced feedback systems for orbit and bunch-to-bunch stability. Many of these advancements were pioneering and unique in the low-energy synchrotron community. The key parameters of TLS are presented in **Table 1**.

Table 1: Main parameters of the TLS storage ring.

Beam Energy (GeV)	1.5
Number of Buckets	200
Current (mA)	360
Horizontal Emittance (nm-rad.)	22
Vertical Emittance (pm-rad.)	88
Tunes (ν_x/ν_y)	7.303/4.175
Lifetime (hour)	> 6

The storage ring, which is designed with sixfold symmetry, features four room-temperature undulators, one wiggler, and five SCWs, giving resulting in the most densely packed SCW configuration in the community for the TLS. SCWs enable the generation of high-energy photons to support X-ray users. The specifications of the insertion devices are listed in **Table 2**.

Table 2: Main parameters of the insertion devices used in the TLS.

	W200	U50	U90	EPU56	SWLS	SW60	IASWA	IASWB	IASWC
Type	Hybrid	Hybrid	Hybrid	Pure	SC	SC	SC	SC	SC
Period length (mm)	200	50	90	56	250	60	61	61	61
Photon energy (eV)	800–15k	60–1.5k	5–500	80–1.4k	2k–38k	5k–20k	5k–20k	5k–23k	5k–20k

Statistics of TLS Machine Operation

During the initial top-up injection phase, the stored beam current was limited to 200 mA in early 2005 because of the constraints of the radio frequency system capabilities and beam stability. Following the installation of the SRF module and the upgrade of the feedback system, TLS gradually increased the stored beam current to 360 mA after 2010. **Figure 1** presents the performance metrics of TLS operations from 2011 to 2024. Availability is defined as the ratio of actual user time to scheduled user time; mean time between failures (MTBF) is defined as the ratio of scheduled user time to the number of system faults; and the beam stability index is evaluated based on photon intensity variation in the diagnostic beamline, maintained within 0.1%.

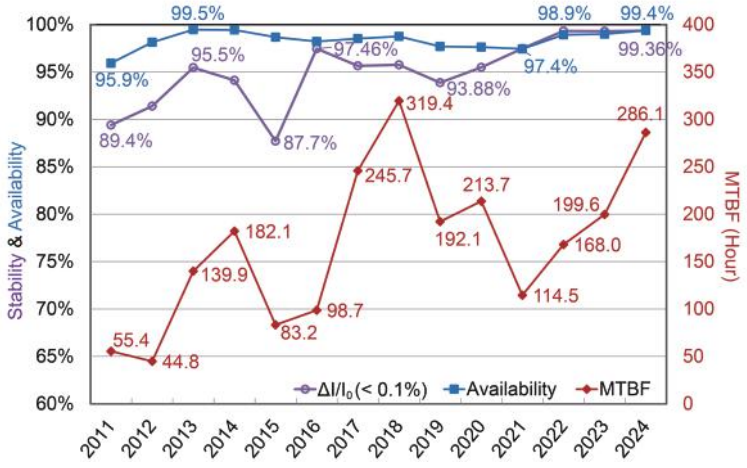

Fig. 1: Annual beam stability index of 0.1%, availability, and MTBF of the TLS.

In 2024, the annual availability of the TLS reached 99.4%, with scheduled user time totaling 4,578 hours, a second-highest MTBF of 286.1 hours, and a beam stability of 99.36%. After switching of the pulsed klystron supplier from Thales to Canon in 2023, the operational reliability and stability of the TLS linear accelerator system have significantly improved in 2024.

Downtime and Failure Analysis of the TLS

In 2024, there were 15 beam trips and a total of 28.35 hours of downtime. The SRF system, which provides high power to the stored beam and operates at 4.5 K, is complex and requires a strict interlock protection system. This system accounted for the largest portion of the annual downtime with a fast recovery time. The contributions from each subsystem of the TLS facility are shown in **Figs. 2 and 3**. The primary causes of downtime were force majeure and unknown events, including earthquakes and voltage drops at the power station. The second-most common cause of downtime was related to the instrumentation and control group (I&C), including issues such as FOFB, failures in the power supply of the 500 MHz master clock RF amplifier, and ILC failures. Alternative solutions for replacing failed and aging systems are currently being evaluated.

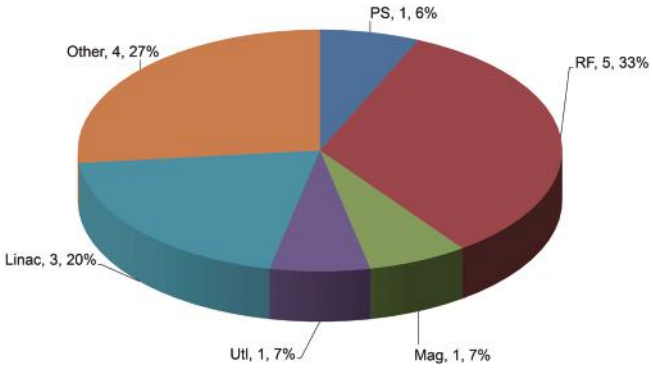

Fig. 2: Proportions of beam trips for the TLS accelerators in 2024 (15 trip events in total). RF stands for radio frequency; PS stands for power supply; and I&C stands for instrumentation & control. "Other" includes 1 earthquake, 1 voltage drop caused by Taiwan Power Company (TPC), and 2 unknown partial beam losses.

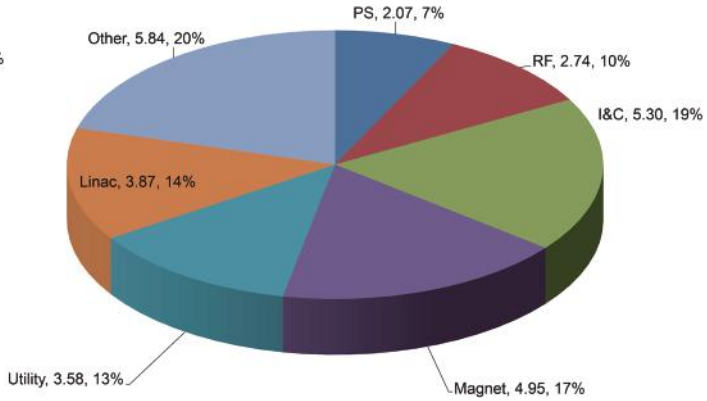

Fig. 3: Downtime distribution for the TLS accelerators in 2024 (totaling 28.35 hours). The major failure times were as follows: other, 5.84 hours; I&C, 5.3 hours; magnet, 4.95 hours; and Linac, 3.87 hours.

Taiwan Photon Source (TPS)

Machine Parameters of the TPS

The Taiwan Photon Source (TPS) has been operational for eight years, having officially been opened to users in 2016. The TPS storage ring incorporates a strong focusing double bend achromatic lattice, which features low emittance, top-up injection, SRF module operation, long straight sections, and high stability. The major parameters of the TPS storage ring for current operation are listed in **Table 3**. The TPS accelerators consist of concentric storage rings and booster rings within the same tunnel, a design choice made considering the limited space on the campus and energy conservation.

Table 3: Main parameters of the TPS storage ring.

Beam Energy (GeV)	3
Circumference (m)	518.4
Current (mA)	500
Number of Buckets	864
Beam Emittance ($\varepsilon_x/\varepsilon_y$) (nm-rad.)	1.6/0.016
Momentum Compaction (α_1/α_2)	0.0024/0.0021
Tunes (ν_x/ν_y)	26.15/14.23
Lifetime (hour)	> 8

Statistics of TPS Machine Operation

The TPS began operations for users in the last quarter of 2016, with a beam current of 300 mA, which increased to 400 mA in December 2017. The system continued to operate regularly until it reached 450 mA on the last day of 2020. In 2021, the stored beam current reached an operating current of 500 mA. The COVID-19 pandemic caused delays in the delivery of several key components for the Phase-II and Phase-III beamlines. Despite these challenges, through dedicated collaboration between vendors and NSRRC staff, 18 beamlines were available for user operation in 2024.

Figure 4 on the next page shows the scheduled and delivered user times and availability on a quarter-to-quarter basis since 2017. The scheduled user time in 2024 was 4,890 hours. Because of frequent earthquakes in Hualien from April to May, a total of 8 beam trips and a recovery time of 12.01 hours were recorded. As shown in **Fig. 5** on the next page, the annual availabilities with and without seismic induction statistics were 97.7% and 97.92%, and MTBF of 163 hours and 221.2 hours, respectively.

Downtime and Failure Analysis of the TPS

In 2024, there were 29 beam trips and a total downtime of 113.36 hours. With the 8 beam trips caused by earthquakes excluded, the contributions of each subsystem within the TPS facility to these beam trips and downtime are illustrated in **Figs. 6 and 7**. The subsystems most frequently involved in beam trips and downtime are the SRF and LINAC systems. The higher failure rate of the SRF system is attributed to sensor aging and solid-state module damage resulting from prolonged operation at a high current of 500 mA. For the LINAC system, the primary issue is the long recovery time caused by klystron failure. Nevertheless, excluding trips caused by earthquakes, the overall reliability of these subsystems has significantly improved in recent years, enabling stable operation and extending the MTBF. (Reported by Hung-Jen Tsai)

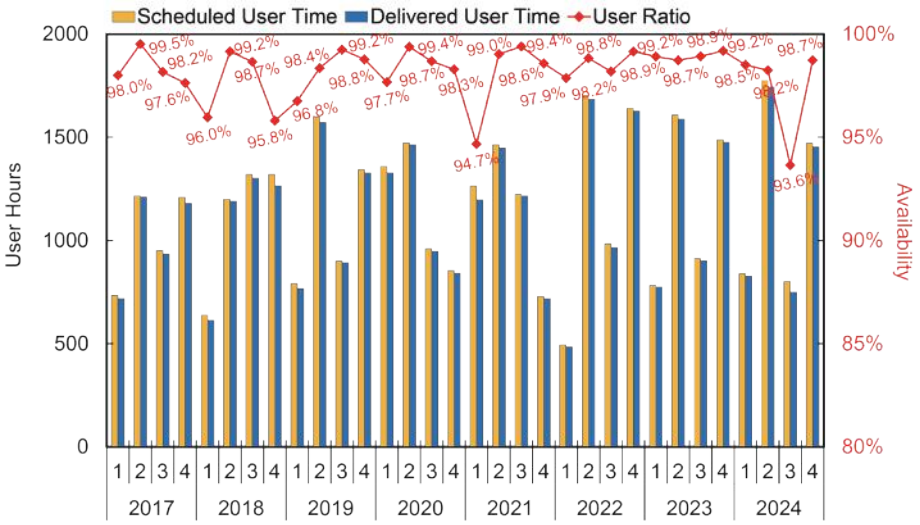

Fig. 4: User time and beam availability of the TPS from 2017 onward.

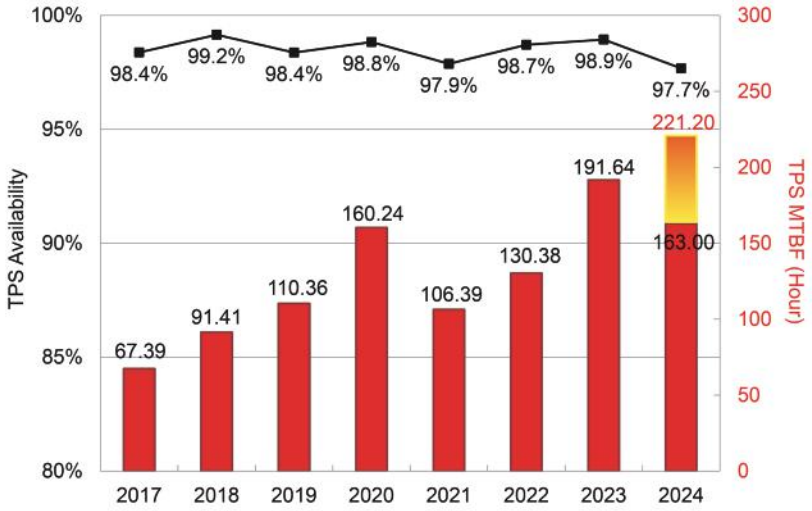

Fig. 5: MTBF and beam trip statistics of the TPS from 2017 onward. In 2024, the MTBF with and without seismic induction statistics was 163 hours and 221.2 hours, respectively.

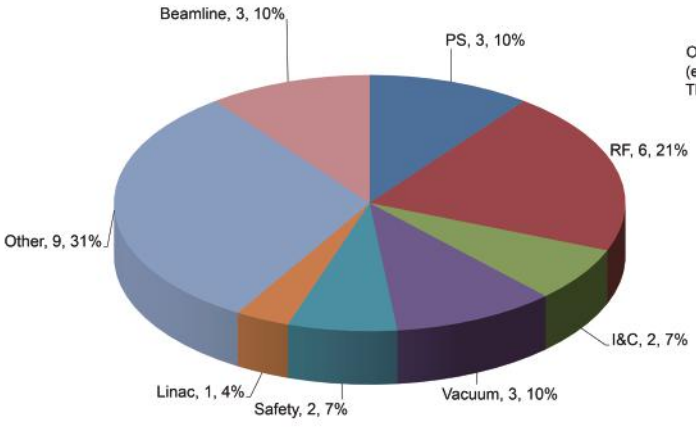

Fig. 6: Proportions of beam trips of the TPS accelerators in 2024. There were 29 trip events in total. "Other" includes 8 earthquake events and 1 TPC voltage drop.

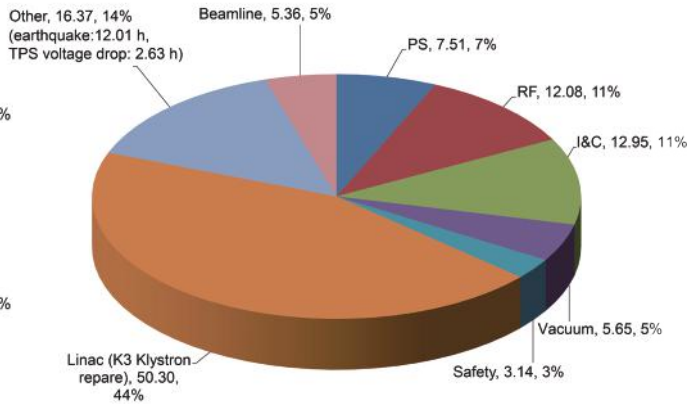

Fig. 7: Proportions of downtime in the TPS accelerators in 2024 (totaling 113.36 hours). The major failure times were as follows: Linac, 50.3 hours; other, 16.37 hours; I&C, 12.95 hours; and RF, 12.08 hours.

Elliptically Polarized Undulator Coupling Correction at the Taiwan Photon Source

Introduction

Five APPLE-II types of elliptically polarized undulators (EPUs) are installed in the Taiwan Photon Source (TPS) to produce elliptically polarized light, namely, EPU46-45, EPU48A-41, EPU48B-41, EPU168-39, and EPU66-27. An APPLE-II-type EPU comprises four identical quadrants of magnet arrays. By enabling the translation of two diagonal quadrants parallel to the magnetic axis while keeping the other two fixed, adjustments can be made to vary the strength of the horizontal and vertical magnetic field components (B_x and B_y), consequently influencing the ellipticity of the electron beam. Because of manufacturing imperfections in the EPU, it generates a skew quadrupole component that varies at different gaps and phases. The residual skew quadrupole component couple horizontal betatron motion and dispersion to the vertical plane and then results in changes in beam size. When the electron beam encounters the residual skew quadrupole component of the EPU and subsequently traverses a region where vertical acceptance is minimal around the entire ring, there is a risk of beam scraping and loss.

To mitigate the coupling effects from the EPU and to maintain vertical beam size, each EPU is equipped with a pair of skew quadrupole magnets, named upstream skew quadrupole (USQ) and downstream skew quadrupole (DSQ), located at the entrance and exit of the EPU, respectively. This type of coupling correction is similar to the three-magnet bump used for orbit correction.[1] Since the residual skew quadrupole of the EPU varies with gaps and phases, a 2D coupling feed-forward table that accounts for gap and phase for both USQ and DSQ is needed to compensate for the residual skew quadrupole from the EPU and to maintain the beam size. To build such a 2D coupling feed-forward table, an indicator beam loss monitor (BLM) is used to monitor the variations in the beam size. This method is fast and sensitive. If the beam size exceeds the vertical acceptance level, then the beam will be scraped and lost. Conversely, if the beam size remains smaller within the vertical acceptance, then the electron beam will not be scraped.

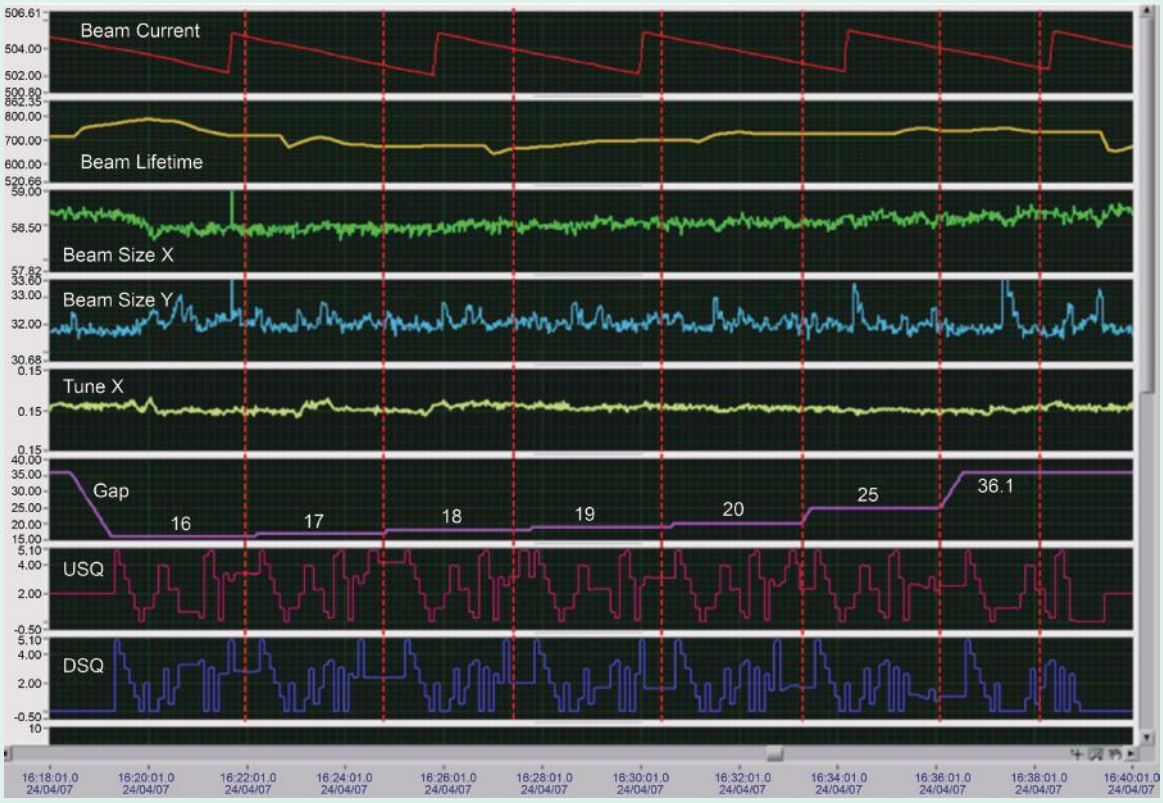

Fig. 1: Optimization process for EPU66-27 coupling feed-forward table by Bayesian optimization.

Coupling Feed-Forward Table

To counteract the undesired coupling effects caused by the residual skew quadrupole component of the EPU, it is essential to construct a 2D coupling feed-forward table based on the gap and phase of the EPU. For this purpose, an automatic measurement program that uses two nested loops to automatically adjust the gap and phase of the EPU has been developed. At each step of the gap and phase, the currents for the USQ and DSQ of the EPU are optimized to minimize the BLM reading using Bayesian optimization. The procedures for building the EPU coupling feed-forward table are outlined as follows:

1. The gaps of all EPUs are ensured to be minimized to their lowest settings to provide appropriate vertical acceptance, while the TPS is operated in top-up injection mode with a beam current of 500 mA.
2. Two nested loops are used to gradually adjust the gap and phase of the EPU to a specific setting and thus modify one gap or phase at a time.
3. For each gap and phase setting, the program automatically adjusts the currents of the USQ and DSQ of the EPU to minimize the BLM reading. The optimization should occur outside of injection periods.
4. Once the minimum BLM reading is achieved, the USQ and DSQ currents corresponding to that gap and phase setting are recorded by the program.
5. This process for each subsequent gap and phase is repeated, with the skew quadrupole currents adjusted and recorded at each step of gap and phase.

This procedure effectively builds the coupling feed-forward table, minimizing the coupling effects across all gap and phase settings of the EPUs. A shell script is then used to convert the 2D feed-forward table into a waveform format to enable the soft IOC to read it and perform interpolation. This allows the soft IOC to adjust the currents of the USQ and DSQ at 200 Hz when the EPU gap or phase varies.

Figure 1 shows the optimization process of the EPU66-27 coupling feed-forward table through Bayesian optimization. The optimization process is described as follows:
The program reduces the gap to 16 mm and the phase to 0 mm. In the beginning, 10 sets of initial points are given (the different sets of USQ and DSQ currents and their associated BLM reading). On the basis of these initial measured points, the Bayesian optimization algorithm varies the USQ and DSQ currents to minimize the BLM reading.

Verification of Coupling Correction by Closest-Tune Approach

After the creation of the 2D coupling feed-forward table, it is important to verify the performance of the coupling correction. The closest-tune approach[2] was applied to check whether the minimum gap (tune-split) between the two normal modes was minimized after the correction had been applied. This was achieved by simultaneously scanning the currents of 36 defocusing quadrupoles (referred to as QS1) from -0.49 to -0.88 A relative to their nominal values, with a step size of 0.01 A. These 36 quadrupoles are located on both sides of the 18 short straight sections. At each step, the turn-by-turn data for 7000 turns from 172 beam position monitors were recorded and converted into betatron tunes using fast Fourier transform. A pulsed pinger magnet was used to excite betatron oscillations to ensure that all 172 BPMs were synchronized with the trigger event initiated by the pinger magnet, allowing the TbT signals to be recorded in sync with the revolution period.

The betatron tunes of the two normal modes were plotted against the QS1 currents relative to their nominal values. The normal mode (eigenmode) tunes can be expressed in terms of uncoupled betatron tunes (ν_x, ν_y) and the coupling strength by using the following equation:

$$\nu_{\pm} = \frac{\nu_x + \nu_y - l}{2} \pm \frac{1}{2}\sqrt{\Delta^2 + G_{1,-1,l}^2}$$

, where $\Delta = \nu_x - \nu_y - l$, and $G_{1,-1,l}$ represents the minimum separation between the normal mode tunes. The integer parts of the betatron tunes for the TPS storage ring are 26 and 14 for the horizontal and vertical planes, respectively, resulting in $l = 12$. The minimum gap $G_{1,-1,l}$ between these two normal modes represents the coupling strength.

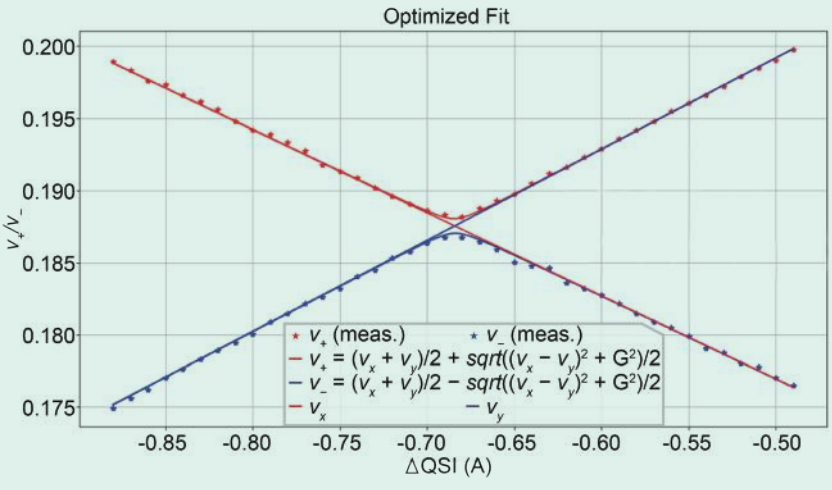

Fig. 2: Measured betatron tunes of two normal modes *versus* the currents of the quadrupole QS1 relative to their nominal values for all EPU ID gaps that are open.

Figure 2 shows the measured betatron tunes of normal modes against the currents of the quadrupole QS1 relative to their nominal values when gaps of all EPU IDs are open. The tune-split $G_{1,-1,l}$ between the two normal modes is 0.001.

Figure 3 shows the measured betatron tunes of normal modes against the currents of the quadrupole QS1 relative to their nominal values when the EPU66-27 gap is closed to 18 mm without coupling correction. The tune-split $G_{1,-1,l}$ between the two normal modes is 0.0046.

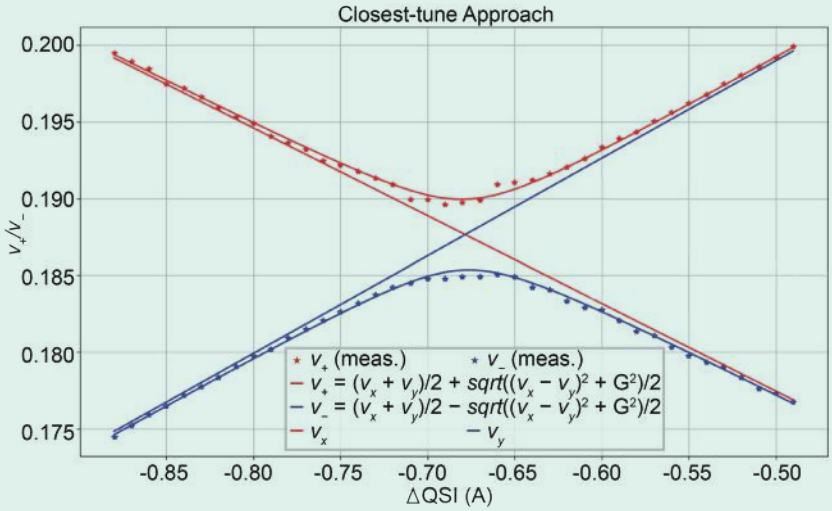

Fig. 3: Measured betatron tunes of two normal modes *versus* the currents of the quadrupole QS1 relative to their nominal values when the EPU66-27 gap is closed to 18 mm.

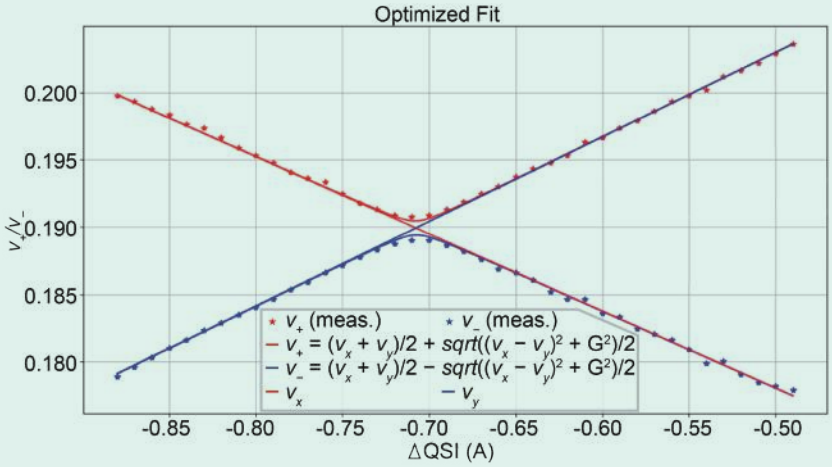

Fig. 4: Measured betatron tunes of two normal modes *versus* the currents of the quadrupole QS1 relative to their nominal values when the EPU66-27 gap is closed to 18 mm after coupling correction by USQ and DSQ.

Figure 4 shows the measured betatron tunes of normal modes against the currents of the quadrupole QS1 relative to their nominal values when the EPU66-27 gap is closed to 18 mm after coupling correction by USQ and DSQ. The tune-split $G_{1,-1,l}$ between the two normal modes is reduced from 0.0046 to 0.001.

Conclusion

Manufacturing imperfections in the EPUs inevitably result in the formation of a residual skew quadrupole component. To mitigate the coupling effects caused by the EPUs and to maintain the vertical beam size, each EPU is equipped with a pair of skew quadrupole magnets. This report demonstrates the feasibility of constructing a 2D coupling feed-forward table based on the gap and phase of EPUs to compensate for the coupling effects using Bayesian optimization. After building this 2D table, the closest-tune approach was employed to verify its performance by checking whether the minimum gap between the two normal modes (tune-split) was minimized after the correction had been applied. (Reported by Mau-Sen Chiu)

References

1. L. Emery, Proc. PAC'**05**, 805 (2005).
2. S. Y. Lee, Accelerator Physics, 4th edition, Singapore: World Scientific (2021).

The Path to Sustainability: Energy-Saving Achievements and Future Plans of the NSRRC

The concentration of carbon dioxide in the atmosphere rose from 280 ppm before the Industrial Revolution to 420 ppm. Fortunately, humanity has recognized the climate change problem caused by this issue and has been actively transitioning energy systems. This includes using low-carbon natural-gas power generation as a transitional step and introducing zero-carbon renewable energy sources.

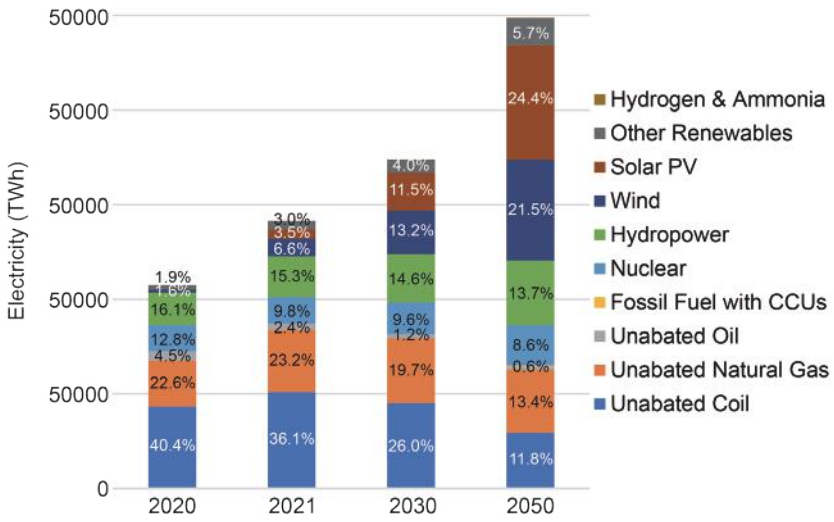

Fig. 1: Global power generation by energy type and percentage.[1]

The International Energy Agency compiled data on global power generation for 2020 and 2021 and predicted the energy mix for 2030 and 2050. As shown in **Fig. 1**, while energy demand continues to rise, the share of fossil fuels is expected to drop from 67.5% in 2020 to 25.8% in 2050. Meanwhile, renewable energy is projected to increase from 19.7% to 65.2%,[1] meaning that in 30 years, the roles of renewable and fossil energy will reverse.

Figure 2 illustrates the power usage and share of major facilities and buildings of the NSRRC in summer. The two accelerators, TLS and TPS, are the largest power consumers, with a combined usage of 4,341 kW. This accounts for 45.3% of the NSRRC total power consumption. The top three subsystems of the accelerators in terms of energy usage are the magnet power supply, radio-frequency (RF) systems, and cryogenic systems. Other major power consumers include the utility systems (3,241 kW, 33.8%), building electricity usage (1,378 kW, 14.4%), and beamlines and laboratories (629 kW, 6.6%).

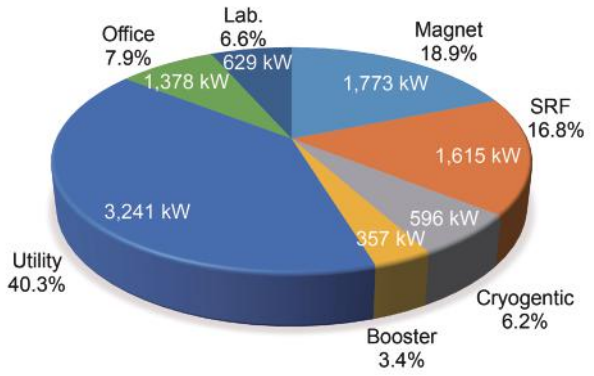

Fig. 2: Power usage and share by major facilities and buildings in summer 2021 at the NSRRC. [Reproduced from Ref. 2]

Using the ISO 14064-1 standard, we record the direct carbon emissions and indirect emissions from purchased electricity of the NSRRC, excluding indirect emissions from employee commuting, business trips, supplier transportation, or service provisions. The annual carbon emissions are about 35,265 tons of CO_2 equivalent, with 95.5% stemming from purchased electricity. The remaining 4.5% comes from kitchen liquid petroleum gas burning, emergency generator operation, official vehicle emissions, refrigerant leaks from air conditioning systems, and experimental processes. Therefore, reducing electricity use is key to decreasing carbon emissions.

From previous energy-flow statistics, it is clear that the accelerators are the most significant power consumers. However, before implementing energy-saving measures, we must consider whether the chosen technologies can affect reliability, safety, investment costs, and economic returns from lower electricity bills. Despite these challenges, recent breakthroughs have been made, such as the energy-efficient operation of booster ring dipole magnets and the implementation of solid-state RF systems in the TPS. Other advancements, such as using permanent magnets, have improved accelerator performance while saving energy, promising further progress.

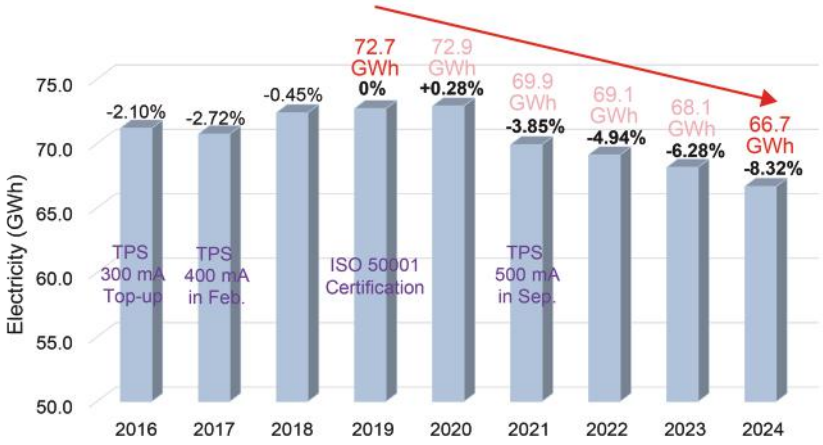

Fig. 3: Yearly electricity usage statistics for the NSRRC. [Reproduced from Ref. 2]

The second-largest power consumer is the utility system. During the construction of the TPS, energy-saving features like variable-frequency drives for pumps, air-conditioning fans, and air compressors were planned. The NSRRC recently implemented an energy management system, earning ISO 50001 certification. This recognition highlights the energy-saving efforts of the NSRRC and supports the development of new techniques, including:

A. Optimizing Chiller Operations: Chillers are the core of air conditioning and accelerator cooling systems and the most energy-intensive machines. Connecting the cooling systems with chilled water pipelines across the TLS and TPS allows chillers to be centrally managed for optimal operation and energy efficiency.

B. Heat Pump Energy Recovery: Waste heat from various equipment and air-conditioning systems can be recovered using heat pumps. This recovered heat can reheat dehumidified cool air to provide the dry, room-temperature air, reducing energy consumption from electric heaters by 70%.

C. Upgrading to light-emitting diode (LED) in the TPS Experimental Hall: Previously, this area used 384 metal halide lamps, each rated at 400 W. These have been replaced with 153 W LED lights, leveraging improvements in LED lighting technology.

Despite the addition of new equipment and record-high accelerator operation hours, our net electricity usage has decreased yearly thanks to collective efforts. As shown in **Fig. 3**, starting from the TPS's official launch in 2016, and using 2019 as the baseline, the annual electricity consumption of the NSRRC dropped from 72.7 GWh (about 7% of Hsinchu City's household electricity usage) to 66.7 GWh in 2024. This reduction saves at least 6.0 GWh annually, equivalent to TWD 26.5 million in electricity costs. Additionally, the NSRRC has installed solar panels with a total capacity of 1,187 kWp on building roofs, generating about 1.5 GWh of renewable energy yearly—2.1% of our annual electricity usage. Although the electricity generated is sold to the Taiwan Power Company and cannot be counted toward energy savings or carbon reductions, it provides considerable revenue for the NSRRC.

Saving energy protects the environment and addresses practical concerns such as rising electricity costs and potential carbon fees. From July 2022 to present, electricity rates have increased by 74.8%, and this year's summer rates were extended for an additional month. Energy costs have also been driven up by the war in Ukraine, and carbon fees may be introduced in the future. Under this stress, the NSRRC will continue to implement energy-saving measures such as:

A. Detecting pipeline leaks
B. Optimizing operational parameters of mechanical equipment
C. Recovering heat energy
D. Replacing outdated equipment
E. Improving building energy efficiency[3]
F. Maintaining heat exchangers
G. Generating renewable energy
H. Utilizing electrical energy or ice storage systems

By taking these actions, we aim to fulfill our corporate social responsibility and accelerate the transition to green energy. (Reported by Wen-Shuo Chan and Chin-Kang Yang)

References

1. The International Energy Agency, World Energy Outlook 2024, October (2024). https://www.iea.org/reports/world-energy-outlook-2024
2. W. S. Chan, "Towards a green accelerator: implementing energy-saving practices at NSRRC" in Proc. IPAC'**24**, May (2024). https://accelconf.web.cern.ch/ipac2024/pdf/WEZN1_talk.pdf
3. J. C. Chang, W. S. Chan, Proc. IPAC'**23**, 209 (2023).

Design and Fabrication of a 4 K Helium Phase Separator

Liquid helium (LHe) is transported from the cryogenic system to superconducting devices through multi-channel transfer lines. However, unavoidable heat loss during transmission causes the LHe to transition into a two-phase flow, which can significantly impact the performance of cryostats in superconducting or other devices not continuously filled with LHe. Helium phase separators were developed at the NSRRC to re-condense the two-phase helium flow from a liquid-helium transfer line and ensure a stable supply of LHe to users.[1,2]

A G-M cryocooler (Sumitomo, model RDK415D) with a cooling capacity of 1.5 W at 4.2 K was integrated into the phase separator to re-condense and liquefy helium while storing it in a 100 L vessel. Practical improvements to reduce the heat load on the helium phase separator were also discussed and implemented.

Figure 1 depicts the configuration of the helium phase separator.[3,4] The second-stage cold head of the cryocooler, which provides a maximum cooling capacity of 1.5 W at 4.2 K, is connected to an oxygen-free copper condenser mounted at the top of the 100 L LHe vessel. To minimize heat transfer through radiation and convection, the LHe vessel is wrapped in multi-layer insulation (MLI) and housed within a vacuum vessel.

The vessel is supported by four G-10 fiberglass-epoxy rods installed at its base, with the opposite ends secured to the outer vessel to bear the weight of the LHe. Three transfer pipes at the top of the vessel act as inlets and outlets for LHe and as a vent for gaseous helium. Vacuum barriers are placed between the transfer pipes and the outer vessel to mitigate conductive heat loss from room temperature.

A thermal shield made of 30 layers of MLI is connected to the first-stage cold head of the 4 K cryocooler. Positioned between the outer vessel and the LHe vessel, this shield blocks radiative heat loss. Additionally, a thermal bridge made of copper connects the thermal shield to the cryogenic valves, further reducing conductive heat loss. The thermal shield and bridge are constructed of copper, while the outer vessel, LHe vessel, and transfer pipes are made of stainless steel, ensuring durability and effective thermal isolation.

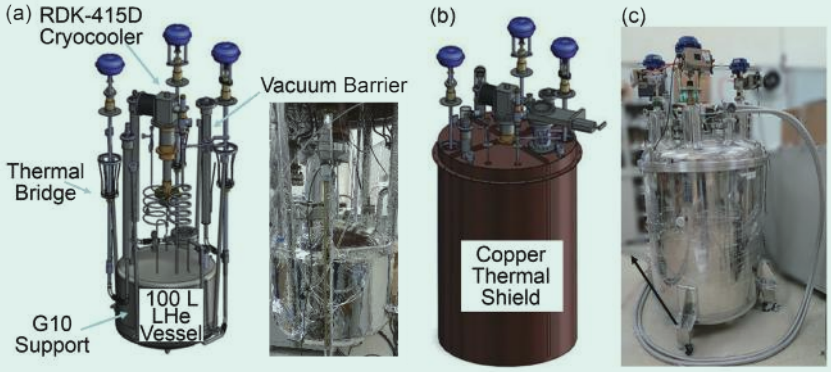

Fig. 1: Configuration of the helium phase separator. (a) Components after removal of the thermal shield; (b) outer vessel removed to reveal the thermal shield; (c) prototype of the helium phase separator. [Reproduced from Ref. 3]

Figure 2 illustrates the piping and instrumentation diagram of the helium phase separator, outlining its operational process. In the first step, the thermal shield was cooled to below 80 K using the first-stage cold head of the cryocooler. Helium gas from the bundle entered the LHe vessel through the pre-cooler, where its temperature was initially reduced. Further cooling occurred *via* heat exchange in the condenser, which was thermally connected to the second-stage cold head of the cryocooler, which brought the helium to its liquefaction temperature.

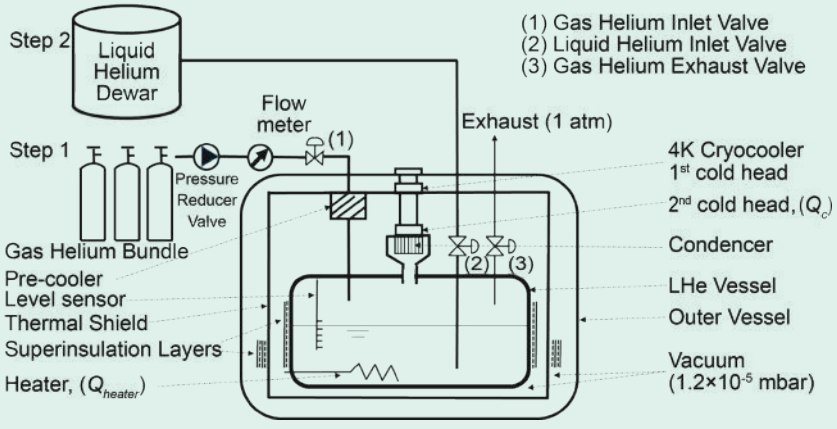

Fig. 2: Configuration of the experiment. Step 1: the separator was cooled with the cryocooler. Step 2: the LHe vessel was filled with LHe; the inner heater was then activated to ensure stable operation in this closed system. [Reproduced from Ref. 3]

The pressure in the LHe vessel was maintained at approximately 1.67 bar-a, and key temperatures, including those of the thermal shield, LHe vessel, condenser, and cold head, were monitored. This was done to confirm that the condenser temperature had reached or dropped below the helium liquefaction temperature of 4.8 K at 1.67 bar-a. Achieving this condition ensured helium liquefaction and confirmed that the separator's heat load was within the cryocooler's cooling capacity. This step established the initial cooling and liquefaction process critical for the subsequent liquid-helium operations.

In the second step, LHe was transferred from the dewar to the LHe vessel under the established operating conditions. During the transfer, a portion of the LHe was naturally consumed and vented to the atmosphere through the exhaust valve, which remained open to allow for pressure regulation.

Once the desired operating level of LHe in the LHe vessel was reached, all inlet and exhaust valves were closed, converting the system into a closed configuration. To maintain stable operating conditions, a heater installed in the LHe vessel was activated. The heater's power was precisely adjusted to stabilize both the LHe level and the internal pressure of the vessel. This heating power played a critical role in determining the overall heat load of the system, providing the valuable data for evaluating the thermal performance and efficiency of the helium phase separator.

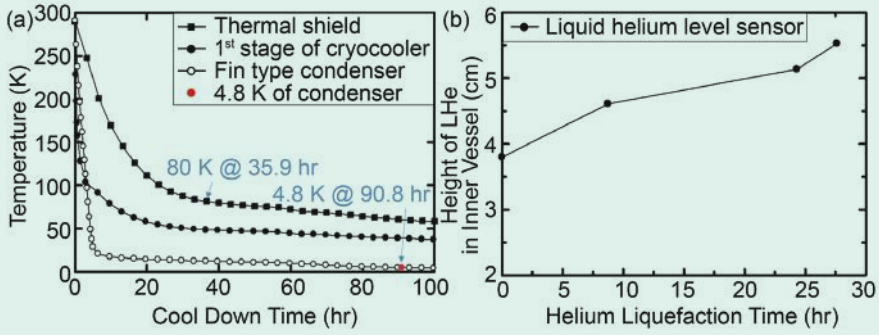

Fig. 3: Experimental results. (a) Cooling-down curve; (b) helium liquefaction rate. [Reproduced from Ref. 3]

Table 1: Thermal parameters.

m	T_e	h_e	T_1	h_1	Q_1	h_{2G}	h_{2L}	Q_S	Q_L	Q_{2nd}	Q_{1st}
(g/s)	(K)	(J/g)	(K)	(J/g)	(W)	(J/g)	(J/g)	(W)	(W)	(W)	(W)
0.0026	295	1532	54	281	3.25	14.06	-1.34	0.69	0.04	0.73	13.8

Helium liquefaction: **Figure 3(a)** illustrates the cooling process of the helium phase separator. The temperature of the thermal shield dropped below 80 K after approximately 35.9 hours. The condenser temperature reached the liquefaction point of 4.8 K at 1.67 bar-a after approximately 90.8 hours, as indicated by the red point in **Fig. 3(a)**. This marked the initiation of the helium liquefaction process. **Figure 3(b)** shows the measured helium liquefaction rate, which was approximately 1.4 cm/day, equivalent to approximately 1.8 L/day. The associated thermal parameters were calculated based on data obtained from the *Helium Material Handbook* and relevant thermodynamic principles, as summarized in **Table 1**. These data provide insights into the thermal efficiency and performance of the separator during its operational cycle.

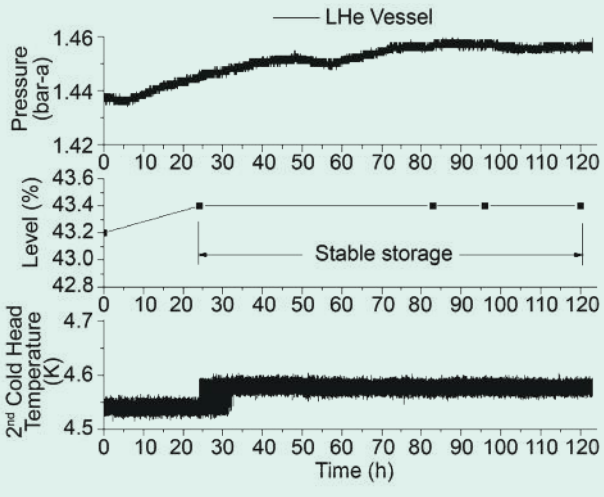

Fig. 4: LHe filling and stable storage. [Reproduced from Ref. 3]

LHe storage: **Figure 4** illustrates the storage process of LHe. The LHe level was maintained at 43.4% by activating the internal heater, which was operated at a power of 0.337 W. The internal pressure was stabilized at 1.46 bar-a ± 0.015 bar throughout the storage period. During this process, the condenser effectively re-condensed the

Table 2: Experimental measurements.

Q_{heat} (W)	LHe vessel pressure (bar-a)	Level (%)	First cold-head temperature (K)	Second cold-head temperature (K)	Q_c (W)	Q_{load} (W)
0.337	1.46	43.4	35.6	4.59	1.892	1.555

vaporized helium, maintaining a steady state. This stability was sustained for a duration of 96 hours, demonstrating that the heat load of the separator was consistently below the cooling capacity of the cryocooler. This ensured efficient and reliable operation of the helium phase separator during the storage phase.

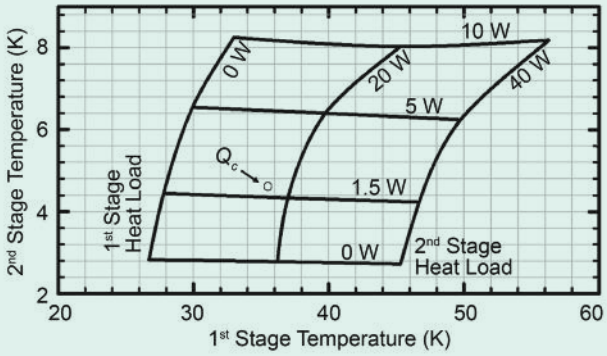

Fig. 5: RDK-415D cold-head load map (60 Hz). [Reproduced from Ref. 5]

The experimental data are summarized in **Table 2**. The results indicate that the cooling capacity of the second-stage cold head (Q_c) was approximately 1.892 W,[5] as derived from the cryocooler load map shown in **Fig. 5**. The electrical power of the heater (Q_{heat}) was measured to be 0.337 W. Using the equation $Q_{load} = Q_c - Q_{heat}$, we calculated the heat load of the LHe vessel Q_{load} , to be 1.555 W. This analysis highlights the effectiveness of the cryocooler in maintaining thermal stability while accounting for the heat input from the heater.

During the transmission process, LHe was prone to vaporization due to the heat, leading to the formation of a two-phase fluid within the transmission pipeline. This phenomenon significantly reduced transmission efficiency, hampering the delivery of sufficient LHe and causing instability in user systems.

To address this challenge, the cryogenics group developed a cryogenic freezer re-condensing LHe phase separator. The primary function of this system was to re-condense the two-phase fluid in the pipeline and re-liquefy the separated low-temperature helium gas. The output from the phase separator was high-purity LHe, which effectively minimized the dryness of the LHe in the transmission pipeline, improving the overall stability of the cryogenics system.

The successfully developed re-condensation LHe phase separator could be coupled with a 4 K cryogenic cryocooler to enable zero-boiling operations to condense low-temperature helium. The special design of the radiation isolation baffle further reduced the heat load. In addition to condensing low-temperature helium and storing LHe, the system could convert normal-temperature helium (295 K) into LHe (4 K), functioning as a small-scale liquid-helium production machine.

The system's net cooling capacity was approximately 0.337 W at 4.59 K, with a LHe production rate of approximately 1.8 L per day. The total heat loss was measured at approximately 1.555 W at 4.59 K, showcasing the system's efficient performance. (Reported by Wen-Rong Liao and Chin-Kang Yang)

References

1. H. H. Tsai, F. Z. Hsiao, H. C. Li, M. C. Lin, C. Wang, W. R. Liao, T. F. Lin, W. S. Chiou, S. H. Chang, P. S. D. Chuang, Cryogenics **77**, 59 (2016).
2. P. S. D. Chuang, W. R. Liao, H. H. Tsai, F. Z. Hsiao, H. C. Li, S. H. Chang, W. S. Chiou, T. F. Lin, Proc. IPAC'**16**, 1212 (2016).
3. W. R. Liao, H. C. Li, P. S. D. Chuang, F. Z. Hsiao, H. H. Tsai, W. S. Chiou, S. H. Chang, T. F. Lin, Cryogenics **96**, 108 (2018).
4. W. R. Liao, P. S. Chuang, F. Z. Hsiao, H. H. Tsai, H. C. Li, W. S. Chiou, Liquid Generator, R.O.C. Patent No. I614472, (2018). https://tiponet.tipo.gov.tw/S092_OUT/out
5. Sumitomo Heavy Industries, RDK-415D 4K Cryocooler Series, September (2020). https://shicryogenics.com/wp-content/uploads/2020/09/RDK-415D_Capacity_Map.pdf

Commissioning of Soft X-ray Nanoscopy Beamline at the Taiwan Photon Source

Commissioning of a soft X-ray nanoscopy beamline at the Taiwan Photon Source 27A (**TPS 27A**) is currently underway. Powered by an elliptically polarized undulator, EPU66, and a newly designed active-mirror plane-grating monochromator (AMPGM), the **TPS 27A** beamline is capable of delivering a photon beam with high energy-resolving power at a constant beam size.[1] Here, we report the commissioning status of beamline **TPS 27A** and its two microscopy endstations: the scanning transmission X-ray microscope (STXM) and photoelectron microscope (photoelectron-related imaging and nano-spectroscopy, PRINS). The STXM endstation is partially opened to users as of the end of 2024, and the PRINS endstation is expected to reach the same status by late 2025.

I. Beamline TPS 27A and 27A1 STXM Endstation

The **TPS 27A** Soft Nanoscopy beamline is designed to deliver a high resolving power and photon flux across a broad photon energy range. To achieve this, a specially developed in-house AMPGM monochromator system with three plane gratings has been implemented. This design supports an energy range from 90 to 3000 eV, with the three gratings covering specific subranges: 90–320 eV, 280–1060 eV, and 1000–3000 eV. Additionally, with the EPU66 undulator system, the photon polarization can be tuned to horizontal, vertical, left-circular, and right-circular states. The beamline is currently in the commissioning stage, which is conducted at the **TPS 27A1** STXM endstation. The first X-ray absorption spectroscopy (XAS) of nitrogen gas has been successfully demonstrated, as shown in **Fig. 1**. The nitrogen K-edge absorption spectroscopy results reveal five distinct vibrational levels in the N1s → $1\pi_g^*$ transition. Fitting analysis indicates that the full width at half maximum (FWHM) for Gaussian and Lorentzian components are 32 and 110 meV, respectively. This corresponds to a resolving power of 12,500 at 400 eV, which aligns well with the expected performance. Currently, the commissioning of the 280–1060 eV energy range is nearly complete. Testing for the 90–320 eV range is planned for the first half of 2025, followed by the testing of the 1000–3000 eV range in the second half of the year.

The **TPS 27A1** endstation is designed to perform XAS-related chemical mapping in transmission mode. Its core components include the Zone Plate (ZP) and scanning stages. The STXM endstation is equipped with multiple scanning systems, including stepping motors, piezo walking stages, and piezo actuators with a laser interferometer feedback system. These systems together maintain the relative position between the ZP and the sample, ensuring nanometer-level positioning performance during energy changes and scans, as illustrated in **Fig. 2**. Due to the fundamental properties of ZPs, where the focal length is proportional to the photon energy, the system is carefully designed and fine-tuned to maintain the imaging area with less than 1 μm lateral movement across the photon energy range of 280–1060 eV.

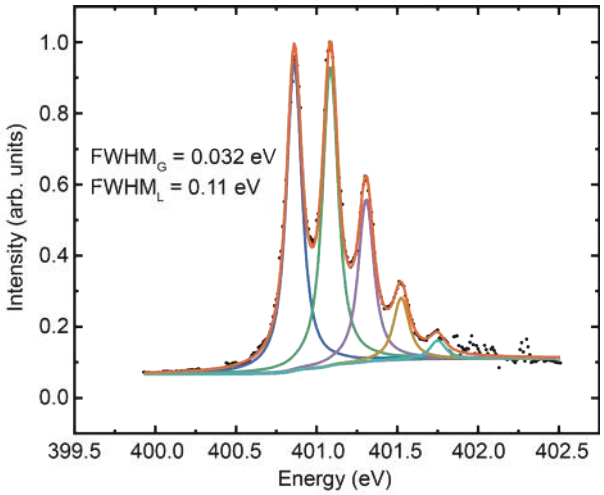

Fig. 1: Nitrogen K-edge absorption spectrum, showing five distinct vibrational levels in the N1s → $1\pi_g^*$ transition. The fitted curve highlights the high-resolution capability of the beamline.

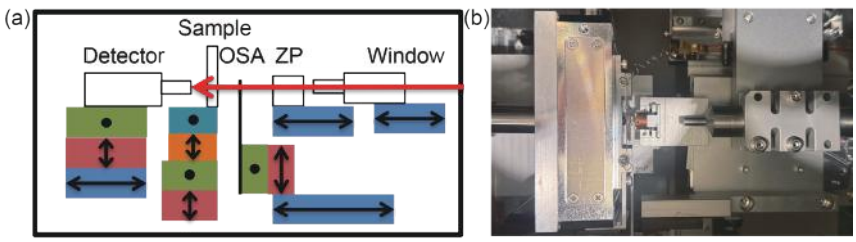

Fig. 2: (a) Schematic representation of the STXM endstation, illustrating the multiple scanning stages, including stepping motors, piezo walking stages, and piezo actuators. (b) Top-view photograph of the STXM endstation, showing the physical layout of the ZP and scanning stages. These components function together to maintain nanometer-level positioning accuracy during energy changes and scans.

Chemical mapping using the spectroscopy capabilities of the STXM endstation is illustrated in **Fig. 3**. The sample consists of Cu nanoparticles (NPs) doped into g-C_3N_4. The STXM elemental mapping, as presented in **Fig. 3(a)**, was conducted at the Cu L-edge and N K-edge. The green region corresponds to the nitrogen signal, while the red region represents the copper signal. These signals were obtained by calculating the difference between the π^* C-N-C peak and the pre-edge for nitrogen, and the Cu main peak and the pre-edge for copper. The corresponding spectra from the Cu L-edge and N K-edge are shown in **Figs. 3(b) and 3(c)**, respectively. The spectrum shown in **Fig. 3(b)** was acquired from the red regions in the elemental map, which highlight the copper signal. Similarly, the spectrum in **Fig. 3(c)** was obtained from the green regions, which represent the nitrogen signal. These results demonstrate the powerful capabilities of STXM in combining high-resolution microscopy with detailed spectroscopic analysis.

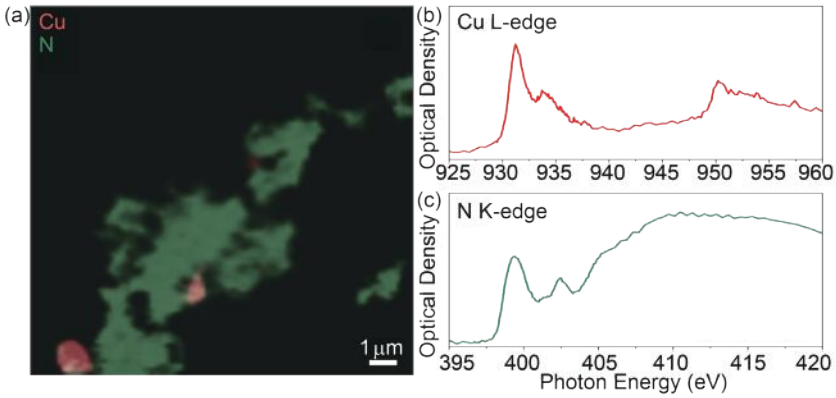

Fig. 3: (a) Elemental mapping of Fe and N for Cu NP/g-C_3N_4. (b,c) Corresponding XAS spectra obtained from the red and green regions, respectively.

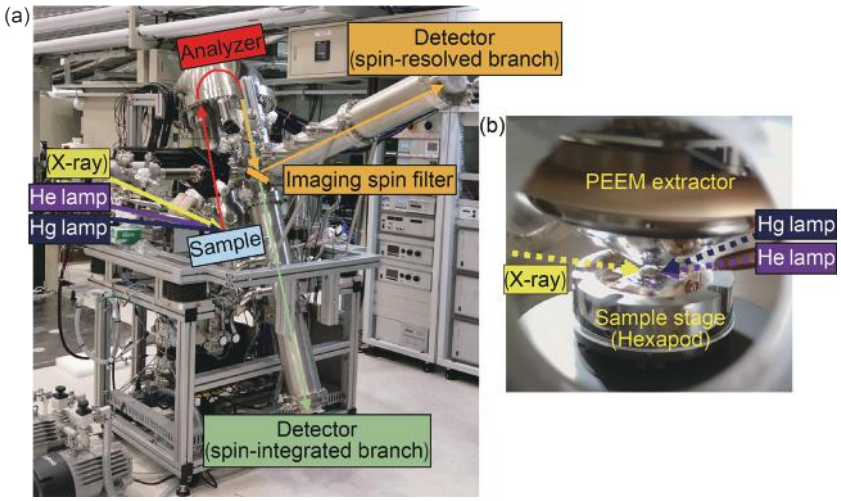

Fig. 4: (a) Configuration of the photoelectron microscope system at the **TPS 27A2**. The beam paths of photoelectrons are indicated by green arrows for the spin-integrated branch or by orange ones for the spin-resolved branch. (b) Image taken close to the hexapod sample stage, extractor lens, and the capillary of the helium discharge lamp. [Reproduced from Ref. 2]

This year, the STXM endstation successfully achieved its first light, marking a significant milestone in its development. Through the current data and commissioning results, we have successfully demonstrated the powerful capabilities of the STXM endstation in delivering high-quality nanoscale imaging and chemical mapping. These achievements validate the endstation's readiness to support the advanced research across diverse scientific fields. This cutting-edge STXM endstation is the result of a collaborative effort between the Department of Physics at Tamkang University and the NSRRC, exemplifying the strength of cross-institutional collaboration in driving scientific innovation. To celebrate this milestone, the Opening Ceremony for the **TPS 27A1** Nanoscopy Beamline and STXM Endstation was held in late December 2024. Moving forward, commissioning efforts will continue in 2025 to further expand the operational energy range and enable more advanced experimental methodologies.

II. TPS 27A2 PRINS Endstation

The **TPS 27A2** endstation aims to perform photoelectron-related imaging and nano-spectroscopy, and its core is a photoelectron momentum microscope (MM) system, which is capable of obtaining direct-space imaging, momentum-space imaging, and photoelectron spectroscopy with position sensitivity.[1] The off-line commissioning utilizing both ultraviolet (UV) He discharge lamp and Hg arc lamp has been initiated from mid-2022, and the off-line commissioning results have been reported in early 2024.[2]

The MM system configuration is shown in **Fig. 4**. All light sources, including the soft X-rays and UV lamps, are incident at an angle of 22° relative to the sample surface. The excited photoelectrons are extracted by the extractor lens and projected onto 2D detectors either along the spin-integrated branch or the spin-resolved branch when an imaging spin filter is introduced.

The spatial resolution of direct-space images was tested by analyzing the intensity profile measured on a standard checkerboard-patterned specimen illuminated by the Hg lamp, and the results are shown in **Fig. 5**. The largest field of view (FoV) is approximately 700 μm (**Fig. 5(a)**), and the

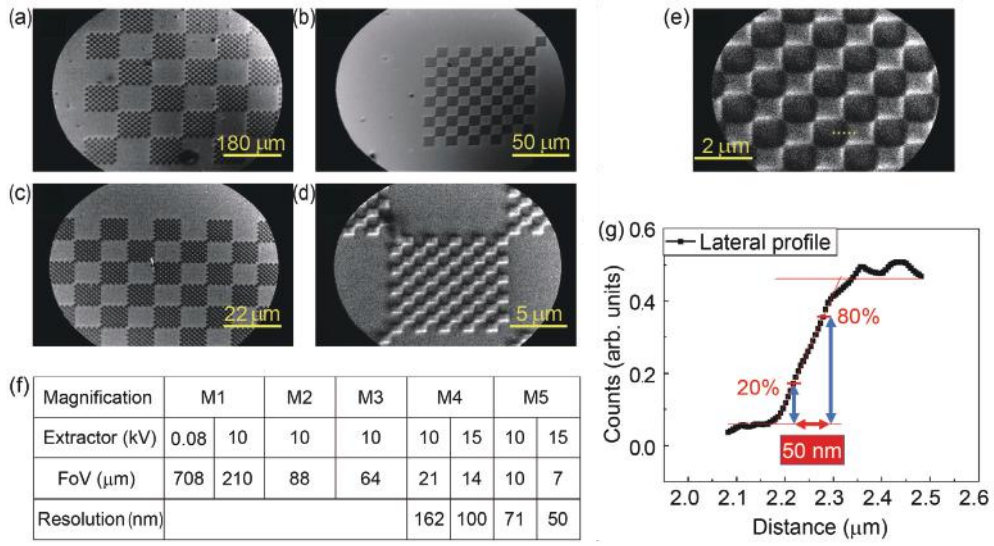

(f)

Magnification	M1		M2	M3	M4		M5	
Extractor (kV)	0.08	10	10	10	10	15	10	15
FoV (μm)	708	210	88	64	21	14	10	7
Resolution (nm)					162	100	71	50

Fig. 5: (a–e) Direct-space photoelectron images of a checkerboard-patterned sample with different FoVs illuminated by the Hg lamp. (f) Table of imaging magnification settings, corresponding FoVs, and resolution. (g) Intensity profile along the edge of the Au patterns marked as a dashed line in (e). [Reproduced from Ref. 2]

smallest FoV is approximately 7 μm (**Fig. 5(e)**). Various magnification settings and the corresponding FoVs are listed in the table of **Fig. 5(f)**. The spatial resolution was estimated to be 50 nm by analyzing the intensity profile shown in **Fig. 5(g)** along the edge of the Au patterns, as indicated by a dashed line in **Fig. 5(e)**.

The momentum-space imaging was tested on a Au(111) single-crystal surface by He(I) radiation (21.2 eV), and the results are summarized in **Fig. 6**. A series of momentum-space images exceeding the first Brillouin zone taken at different binding energies are recorded and shown in **Fig. 6(a)**. After stacking all constant-energy contours together to construct a 3D dataset (k_x, k_y, E_B), which is shown in **Fig. 6(b)**, the electronic band structure along any high-symmetry directions can be obtained simultaneously.

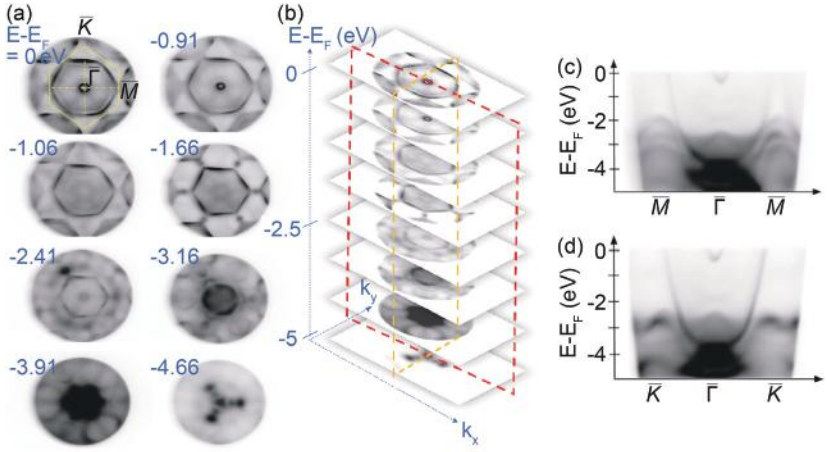

Fig. 6: (a) Momentum-space images recorded at different binding energies obtained from a Au(111) surface at 300 K illuminated by He(I) radiation. (b) Stacking of a series of momentum images with various binding energies, forming a 3D dataset of (k_x, k_y, E_B). (c,d) Slice of the 3D dataset along high-symmetry points of M-Γ-M and K- Γ -K, respectively. [Reproduced from Ref. 2]

In early 2025, more capabilities can be explored using soft X-rays covered by the **TPS 27A** beamline, including the imaging based on XAS, X-ray photoelectron spectroscopy, and X-ray magnetic circular/linear dichroism, which can provide additional element-resolved and magnetization-resolved information. (Reported by Hung-Wei Shiu and Tzu-Hung Chuang)

References

1. H.-W. Shiu, T.-H. Chuang, C.-M. Cheng, C.-H. Chen, Y.-J. Hsu, D.-H. Wei, J. Electron Spectrosc. Relat. Phenom. **266**, 147363 (2023).
2. T.-H. Chuang, C.-C. Hsu, W.-S. Chiu, J.-S. Jhuang, I-C. Yeh, R.-S. Chen, S. Gwo, D.-H. Wei, J. Synchrotron Rad. **31**, 195 (2024).

Tender X-ray Spectroscopy Beamline at the Taiwan Photon Source

A tender X-ray beamline, **TPS 32A**, which is part of Phase III of the Taiwan Photon Source (TPS) construction project, has officially opened to users for the 2024-2 cycle. The techniques involve X-ray absorption spectroscopy (XAS) and hard X-ray photoelectron spectroscopy (HAXPES), which are essential tools for investigating material properties at atomic and electronic levels. The **TPS 32A** beamline offers a photon energy range of 1.7–11 keV and delivers a photon flux of 10^{12} photons per second at 6 keV. It has two back-to-back double-crystal monochromators (DCMs) that include both Si (111) DCM and InSb (111) DCM configurations. These DCMs enable switching between configurations to meet user requirements.[1,2] This design ensures enhanced flexibility, particularly for research teams conducting silicon (Si) element measurements. This beamline can measure elemental XAS spectra, including the K-edges of elements from Si to Zn, as well as the L-edges of second-row and third-row transition metals. Additionally, the use of Kirkpatrick–Baez (K–B) focusing mirrors enables the beam to be reduced to a micron-scale spot size, supporting micro-XAS with spatial resolution. These capabilities address the needs of fundamental research and advanced technological innovation, providing cutting-edge experimental facilities and research resources to academia and industry while opening new scientific frontiers.

The **TPS 32A** beamline integrates HAXPES and XAS techniques, providing users with detailed information on the conduction and valence band electronic structures of materials. As shown in **Fig. 1**, it is divided into four experimental stations: the HAXPES endstation at the focal point, the tender XAS endstation, the hard-XAS endstation, and the micro-XAS endstation.

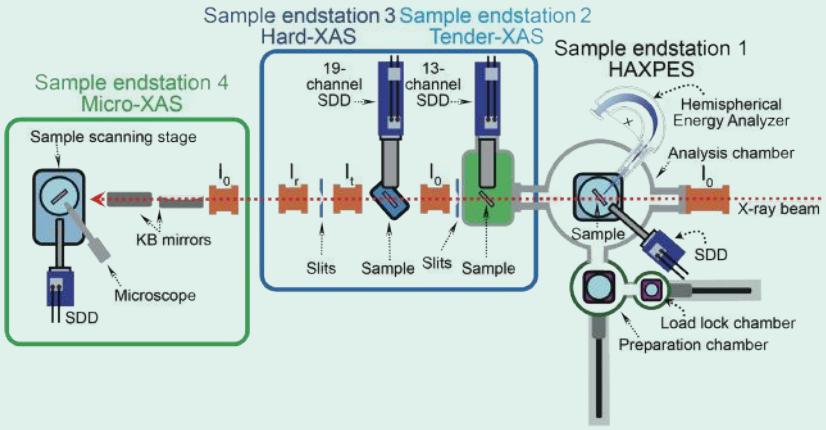

Fig. 1: Layout of the TPS 32A endstations.

The HAXPES endstation, as illustrated in **Fig. 2**, includes a load-lock chamber, a preparation chamber, and an analysis chamber. These chambers maintain ultra-high vacuum conditions exceeding 10^{-10} Torr. The analysis chamber, which is equipped with a high-performance energy analyzer, can detect photoelectron energies up to 6 keV. By adjusting the incident synchrotron tender X-ray with special photon energies, researchers can access deeper core levels and vary the probing depth of the photoelectron spectra. This capability allows for a comprehensive analysis of the valence band composition and electronic structures of surfaces, heterointerfaces, and bulk regions. In addition, a 7-channel silicon drift detector (7ch-SDD) will be installed in this vacuum chamber to facilitate XAS measurements using the partial fluorescence yield (PFY) mode. This setup enables users to investigate the electronic structure of materials both below (occupied states, HAXPES) and above (unoccupied states, XAS) the Fermi level (E_F) at the same location on the material.

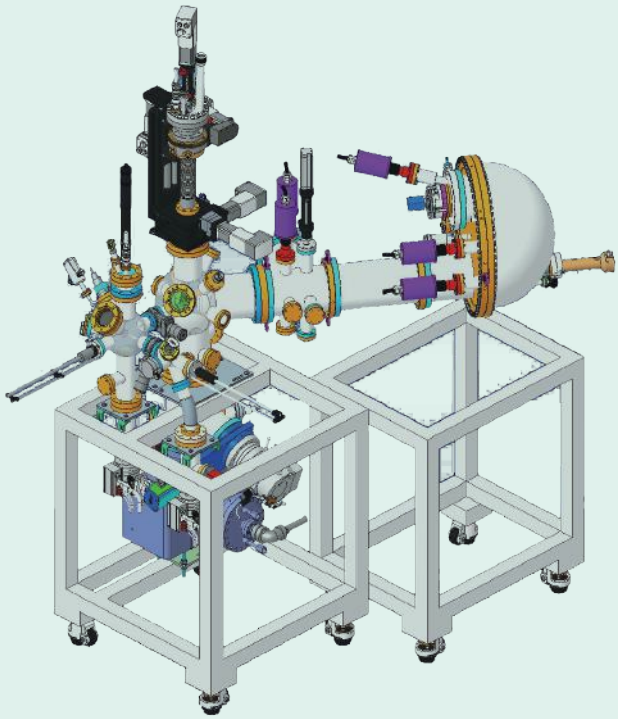

Fig. 2: Schematic drawing of the HAXPES endstation.

Tender XAS endstation is specifically designed for a tender X-ray photon energy range of 1.7–5 keV. The analysis chamber can function in either helium or vacuum mode to minimize photon absorption losses in air at low energies. A load-lock chamber minimizes the time required to stabilize the environment during sample changes. Additionally, a 13-channel silicon drift detector (13ch-SDD) is installed for PFY detection of low-concentration samples, along with simultaneous total electron yield (TEY) measurements. This endstation is designed for measuring the K-edges of silicon, phosphorus, sulfur, and chlorine, along with the L-edges of 4d and 5d transition metals.

The hard-XAS endstation, which covers an energy range of 5–11 keV, is designed for operation under ambient conditions for measuring the L-edges of lanthanides and the K-edges of 3d transition metals. It is equipped with a 19-channel silicon drift detector (19ch-SDD) for PFY mode detection of dilute samples, with sensitivity down to a few ppm. Transmission mode measurements use a grid ion chamber, which offers fast response, a broad linear range, and low background noise. The endstation also supports fly-scan mode, significantly reducing spectral measurement time. For example, Fe K-edge EXAFS scans covering a 1 keV range take approximately 20 seconds in transmission mode and 5 minutes in fluorescence mode.

The endstation is equipped with various *in situ* reaction setups, including electrocatalytic and thermocatalytic reactors and sample cooling systems. Studies of catalytic reactions focus on three main aspects: changes in the catalyst's electronic structure, the formation of intermediates, and the identification of final products. To systematically address these aspects, an advanced electrochemical flow cell integrating XAS, Raman spectroscopy, and gas chromatography–mass spectrometry (GC–MS) has been developed:

XAS: High sensitivity to changes in the electronic structure of the catalyst.
Raman spectroscopy: Effective for detecting reaction intermediates.
GC–MS: Excels in identifying and quantifying final reaction products.

Samples were dispersed on gas diffusion electrodes (GDEs) to facilitate XAS measurements. GDEs feature numerous micro-gas channels to enhance gas diffusion to the catalytic layer. Raman signals are collected through a quartz window, and the final products are analyzed using GC–MS. This setup enables comprehensive studies of catalytic reactions, providing detailed insights into electronic structures, intermediates, and final products to enhance the understanding of reaction mechanisms. This configuration not only enhances the understanding of catalytic processes but also contributes to the development of more efficient catalytic systems.

For thermal catalytic studies, the endstation supports *in situ* measurements at temperatures ranging from room temperature to 1000°C. Samples are placed in capillaries, and reaction gases are introduced through mass flow controllers to allow real-time analysis using XAS, Raman spectroscopy, and GC–MS. This integrated setup, as illustrated in **Fig. 3**, enables a comprehensive understanding of thermal catalytic processes. It allows researchers to investigate the dynamic changes in catalytic materials under the realistic operating conditions. These capabilities are essential for advancing research in fields such as energy conversion, environmental catalysis, and chemical production.

To enhance the efficiency of routine solid-state sample measurements and to minimize errors caused by user unfamiliarity with the operation, the **TPS 32A** has

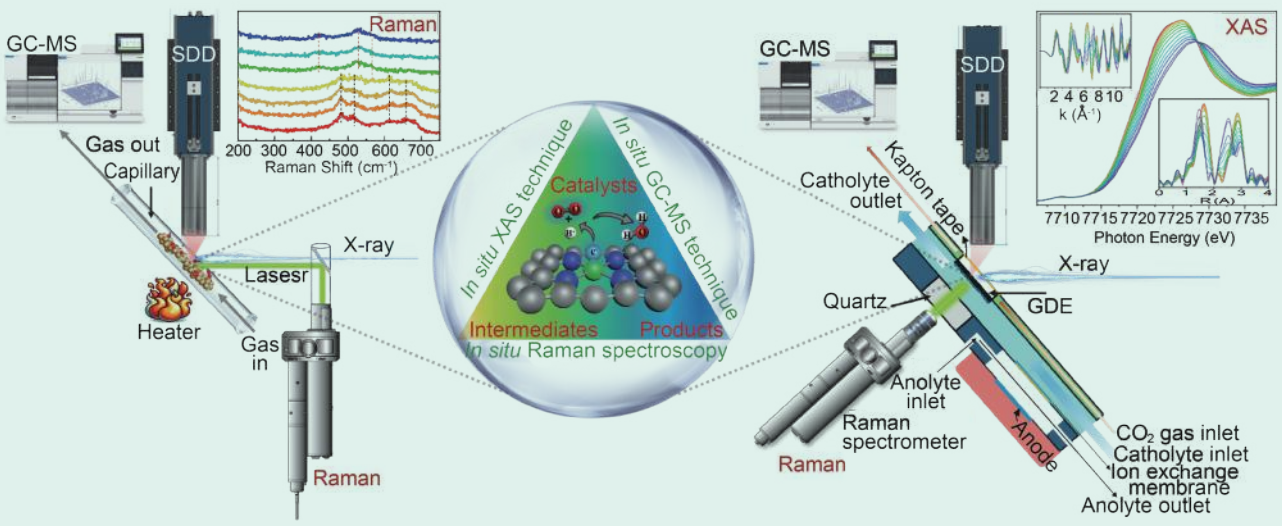

Fig. 3: Schematic drawing of the reaction cell.

developed an automated beamline alignment and sample measurement system. This system improves measurement efficiency and reduces user workload. The automated system comprises the following five subsystems, as shown in **Fig. 4**.

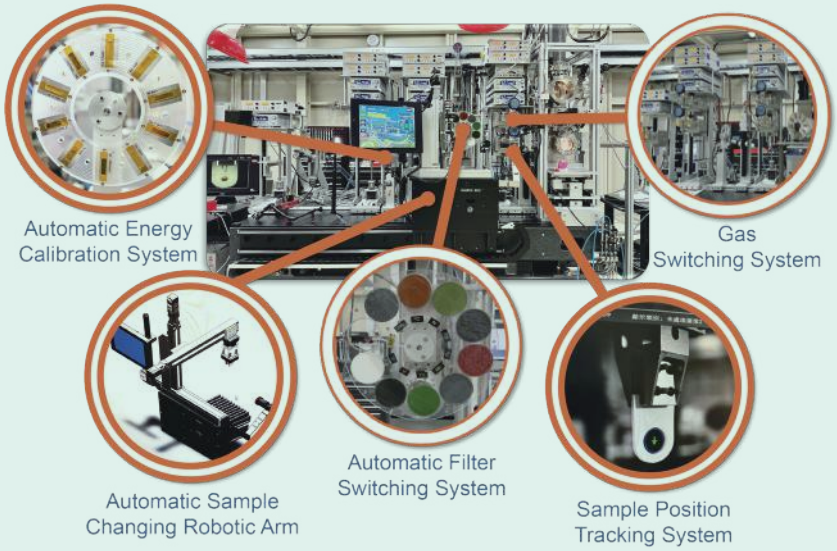

Fig. 4: TPS 32A automation architecture diagram.

1. Automatic filter switching system: This system automatically replaces filters for different elements based on measurement requirements, effectively reducing interference from elastic scattering signals. It also helps reduce the occurrence of replacement errors and reduces the frequency of user access to the hutch, thereby improving experimental efficiency.
2. Gas switching system: This system offers two gas-switching options, namely, for high-and low-energy configurations. It automatically selects the appropriate gas settings based on experimental needs, simplifying the operation process.
3. Automatic sample changer with robotic arm: This robotic arm system can automatically load and unload samples, accommodating up to 100 samples in a single operation. Without manual intervention, it completes sample changes and automated measurements, significantly reducing the time lost due to the frequent user access to the hutch.
4. Sample-position-tracking imaging system: This system accurately tracks the position of the sample, ensuring precise alignment of the X-ray beam with the sample during every measurement. The system automatically moves the beam spot to the sample's center and scans the fluorescence signal intensity to ensure that the beam spot is positioned at the optimal signal strength location.
5. Automatic energy calibration system: This system automatically switches calibration foils for different elements, enabling automatic beamline energy calibration without manual adjustments. It simplifies the beamline alignment process and enhances operational efficiency when measuring multiple elements.

These subsystems function in coordination to provide users with an efficient and user-friendly experimental environment, allowing them to focus more on data processing and the analysis of scientific questions.

The micro-XAS endstation, the fourth on the beamline, is positioned at its end. It is equipped with K–B focusing mirrors at its entrance, which focus the X-ray beam to a spot smaller than 10 microns. The endstation is also equipped with a 7ch-SDD for fluorescence mode detection and includes an optical microscope for sample observation. This setup enables detailed micro-X-ray fluorescence analysis, providing spatially resolved elemental distribution information and facilitating micro-XAS measurements in regions of interest, ultimately offering micron-scale insights into unoccupied electronic states and atomic structures. Micro-XAS offers significant advantages in the fields of energy materials, environmental sciences, and archaeology since it provides high-spatial-resolution analysis of chemical and structural properties.

This report highlights the development of the **TPS 32A** tender X-ray absorption spectroscopy beamline and its endstations. Because of the successful commissioning of the beamline optics and endstations, this beamline has been effectively opened for user access. By incorporating automation and integrating advanced *in situ* analysis techniques, the beamline provides a user-friendly platform for exploring the cutting-edge scientific questions. By the end of 2024, the **TPS 32A** had invited 12 research teams and opened 30% user time for the Proposal Evaluation Committee (PEC) in 2024-2 cycle, resulting in 12 publications. In 2025, **TPS 32A** will open 50% for the PEC cycle and focus on advancing the development and commissioning of the micro-XAS and HAXPES endstations. (Reported by Ying-Rui Lu)

References

1. D.-G. Liu, M.-H. Lee, Y.-R. Lu, J.-F. Lee, C.-L. Chen, J. Synchrotron Rad. **28**, 1202 (2021).
2. D.-G Liu, M.-H Lee, Y.-R Lu, C.-C. Liang, C.-F. Chang, J.-L. Tu, J.-F. Lee, C.-L. Chen, J. Vogel, M. Sacchi, S. Iacobucci, J. Phys.: Conf. Ser. **2380**, 012041 (2022).

Facts and Figures

Organization

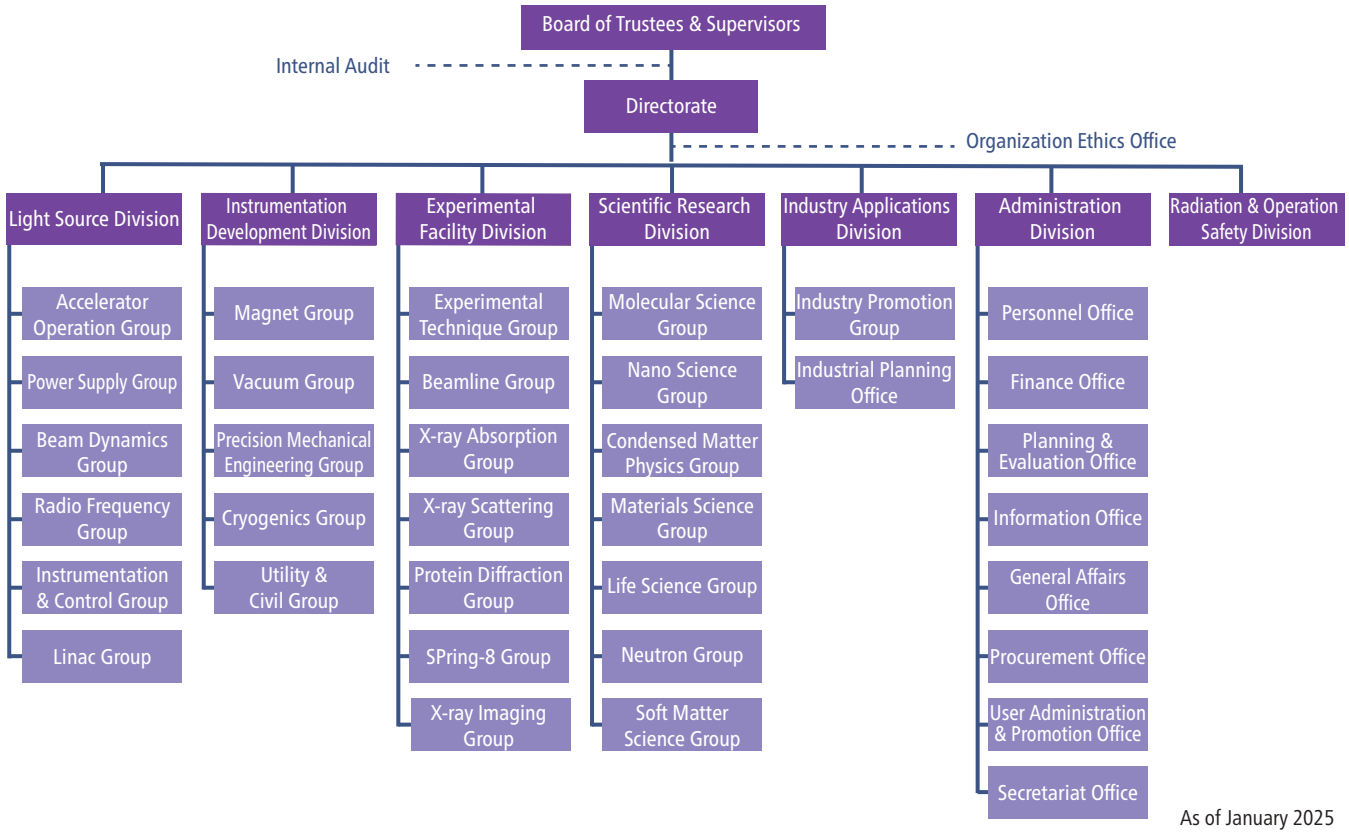

As of January 2025

Board of Trustees & Supervisors 2024.2–2027.2

Board of Trustees

- Minn-Tsong Lin (Acting Chair), National Science and Technology Council (2024.3-2024.5)
- Tzong-Chyuan Chen (Acting Chair & Chair), National Science and Technology Council (2024.5-2024.7)
- Chen-Kang Su (Acting Chair & Chair), National Science and Technology Council (2024.7-)
- Chien-Te Chen, Academia Sinica
- Jen-Sue Chen, National Cheng Kung University
- Yu-Ju Chen, Academia Sinica
- Mei-Yin Chou, Academia Sinica
- Bon-Chu Chung, Academia Sinica
- Ray Hua Horng, National Yang Ming Chiao Tung University
- Bing-Joe Hwang, National Taiwan University of Science and Technology
- Mann-Ching Sherry Ku, Good Management Consulting Inc.
- Yuan-Tseh Lee, Academia Sinica
- Ting-Hua Lu, National Taiwan Normal University
- Meng-Fan Luo, National Central University
- Yuen-Ron Shen, Academia Sinica
- Huey-Kang Sytwu, National Health Research Institutes
- Samuel C. C. Ting, Academia Sinica

Supervisory Board

- Jia Shin Lin (Executive Supervisor), National Science and Technology Council
- Dar-Bin Shieh, National Cheng Kung University
- Wen-Ching Wang, National Tsing Hua University

User Executive Committee 2024

- Hao Ming Chen (Chair), National Taiwan University
- Dun-Yen Kang (Vice Chair), National Taiwan University
- Cheng-Maw Cheng, NSRRC
- Chia-Chen Chung, National Tsing Hua University
- E-Wen Huang, National Yang Ming Chiao Tung University
- Hung-Wei Shiu, NSRRC
- Shan-Li Wang, National Taiwan University
- Yane-Shih Wang, Academia Sinica
- Hsin-Jay Wu, National Yang Ming Chiao Tung University
- Yu-Hao Wu, National Yang Ming Chiao Tung University

Neutron User Executive Committee 2024

- Chao-Hung Du (Chair), Tamkang University
- Wei-Tin Chen (Vice Chair), National Taiwan University
- Yi-Fan Chen, National Central University
- Cheng-Maw Cheng, NSRRC
- Yu-Chun Chuang, NSRRC
- En-Pei Liu, National Taiwan University
- Chieh-Tsung Lo, National Cheng Kung University
- Pai-Chun Wei, National Cheng Kung University
- Chun-Chuen Yang, National Central University

Manpower

As of January 2025, the NSRRC workforce comprises 418 staff members. The following pie charts show the manpower distributions by profession and by educational background.

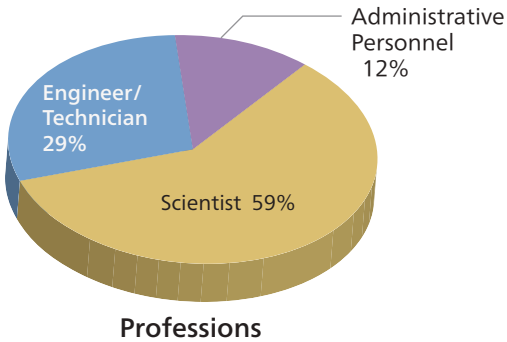

Professions

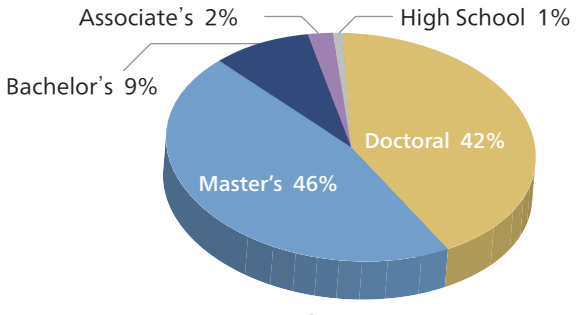

Education

Budget

The total budget for fiscal year 2024 was USD 64.72 million (based on exchange rate: 1 USD = 32.11 TWD). In terms of the budget in TWD, its original currency, there was an increase of 5.4% over the prior year. Fiscal year 2024 budget covered the operating expenses associated with the following categories: TLS accelerator maintenance, TLS BL/endstation/ID/scientific research, utility facilities, administration & salaries, TPS BL/endstation/ID/scientific research, TPS accelerator maintenance, and neutron experimental facility.

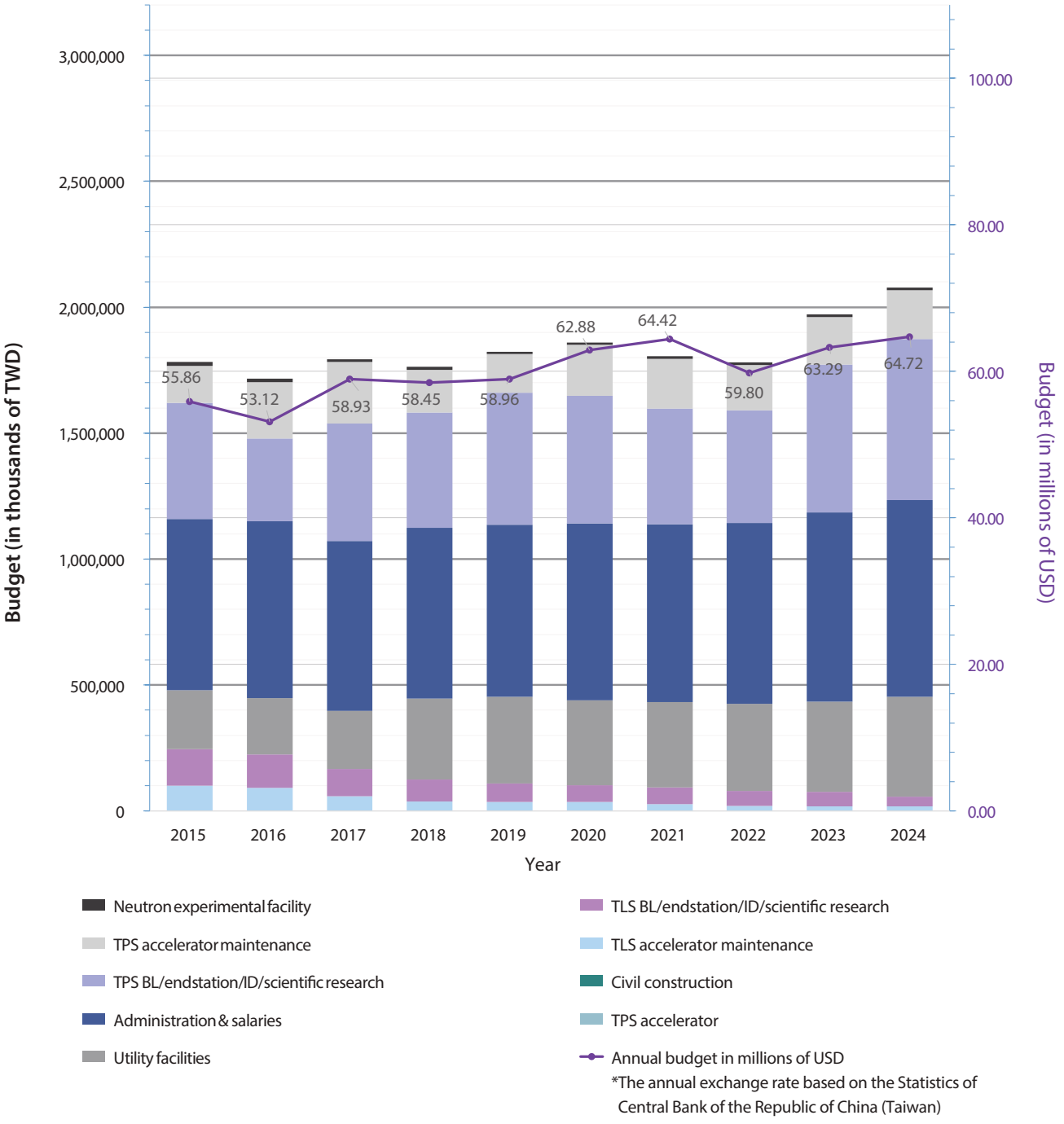

User Statistics

From 1994 to 2024, the total number of beamlines available to general users has increased from 3 to 42, comprising 22 TLS beamlines, 2 Taiwanese beamlines at SPring-8, and 18 newly opened TPS beamlines (see Beamline Status on page 117).

During the year 2024, the User Administration & Promotion Office (UAO) issued 1,054 new user cards and provided services to 2,929 users from 153 affiliations (including 279 users from 89 foreign institutions) to use the above-mentioned 42 NSRRC beamlines. Altogether, 687 proposals led by 413 principal investigators and involving 1,830 experimental runs and 13,861 user runs (visits) were performed.

The overall NSRRC beamtime allocated to users, excluding beamline commissioning, maintenance and training courses, was 6,133.5 shifts for TPS, 10,879 for TLS, and 867 for SPring-8. Each shift consists of eight consecutive hours.

In the year 2024, the UAO processed 220 user subventions for experiments at SPring-8. Another 25 user subventions, which were funded by the National Science and Technology Council, were given to Taiwan neutron users to conduct experiments at neutron facilities worldwide.

In total, 171 master's theses and 31 doctoral dissertations utilizing NSRRC facilities were completed in 2024 (see Appendix). Operational data on beamlines/experimental endstations and users are summarized in the following figures.

Number of users 2004–2024

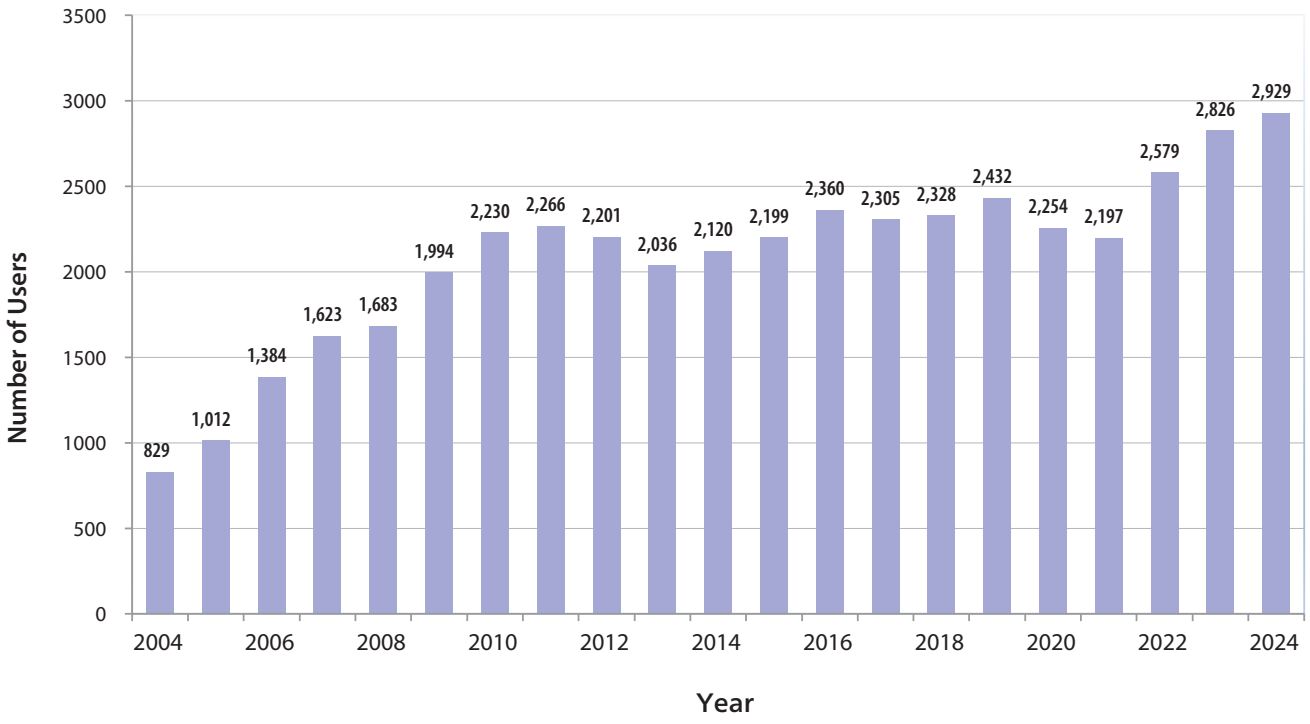

Geographic distribution of users and their numbers

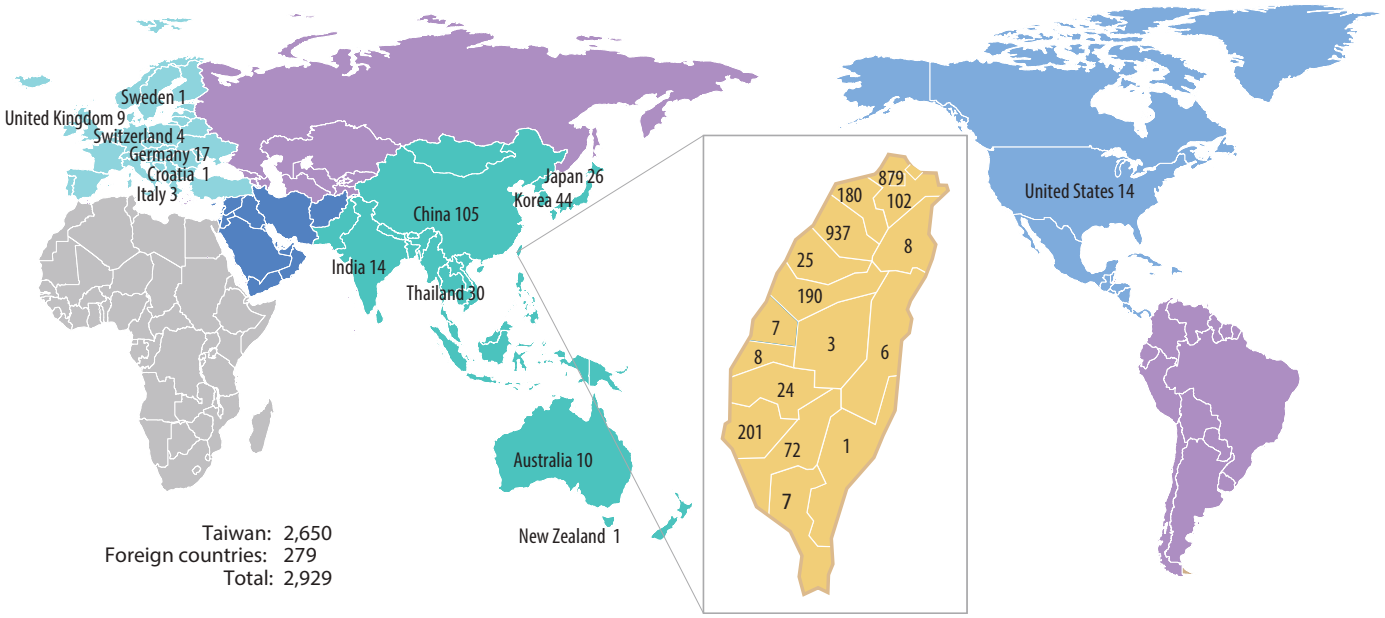

Taiwan: 2,650
Foreign countries: 279
Total: 2,929

Note: The geographic categories of the users are based on the locations of their affiliations.

Distribution of beamtime used by domestic affiliations 2024

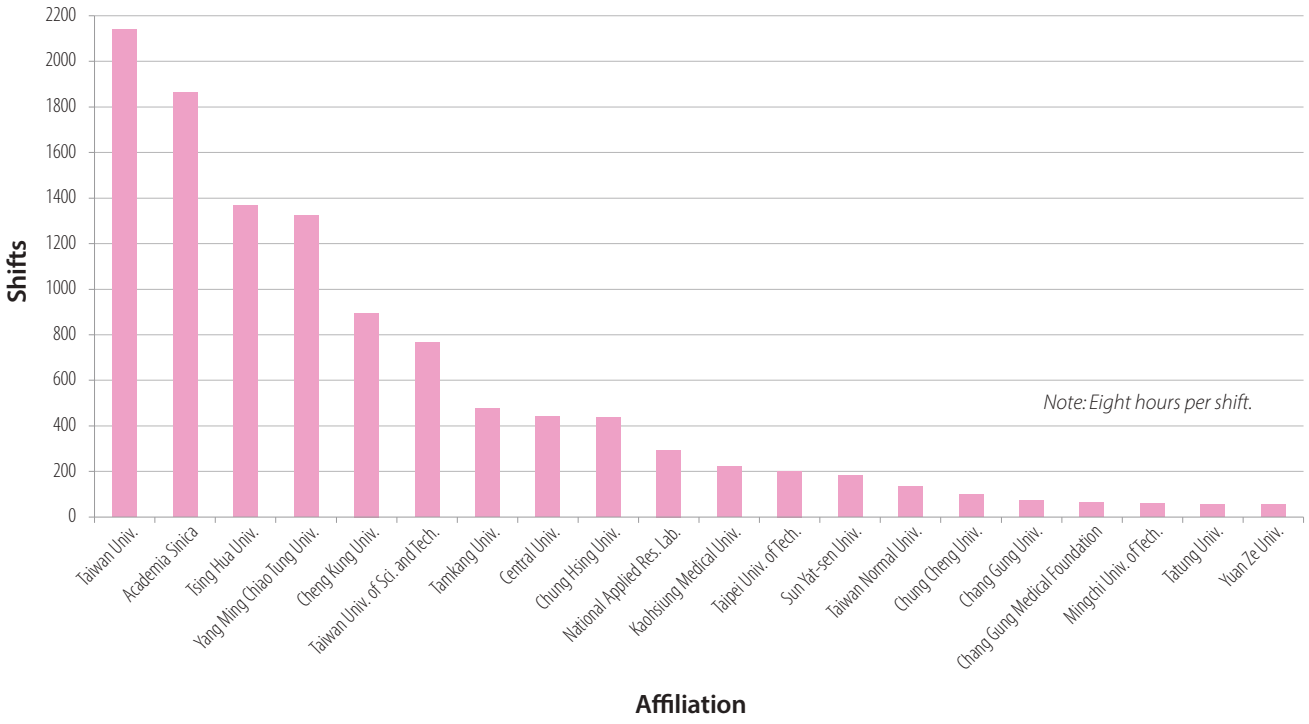

Number of IR/VUV proposals 2004-2024

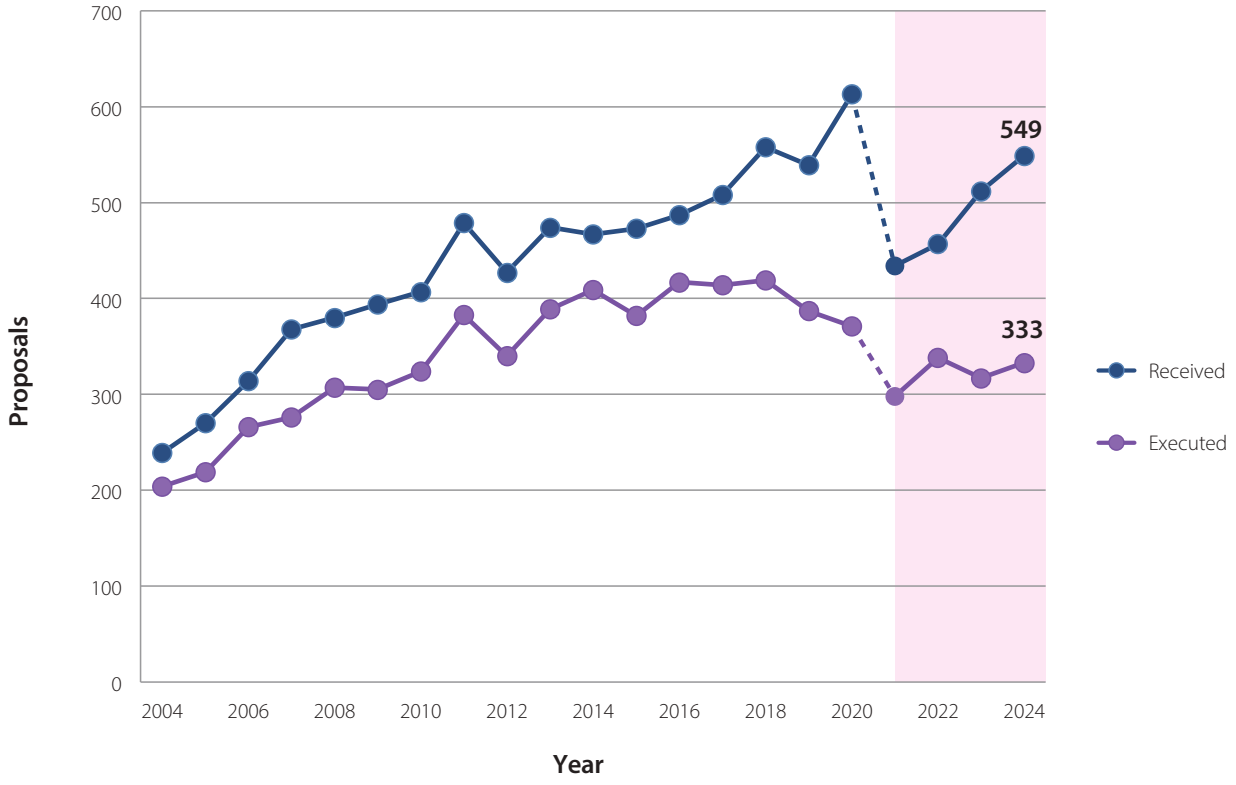

Number of X-ray proposals 2004-2024

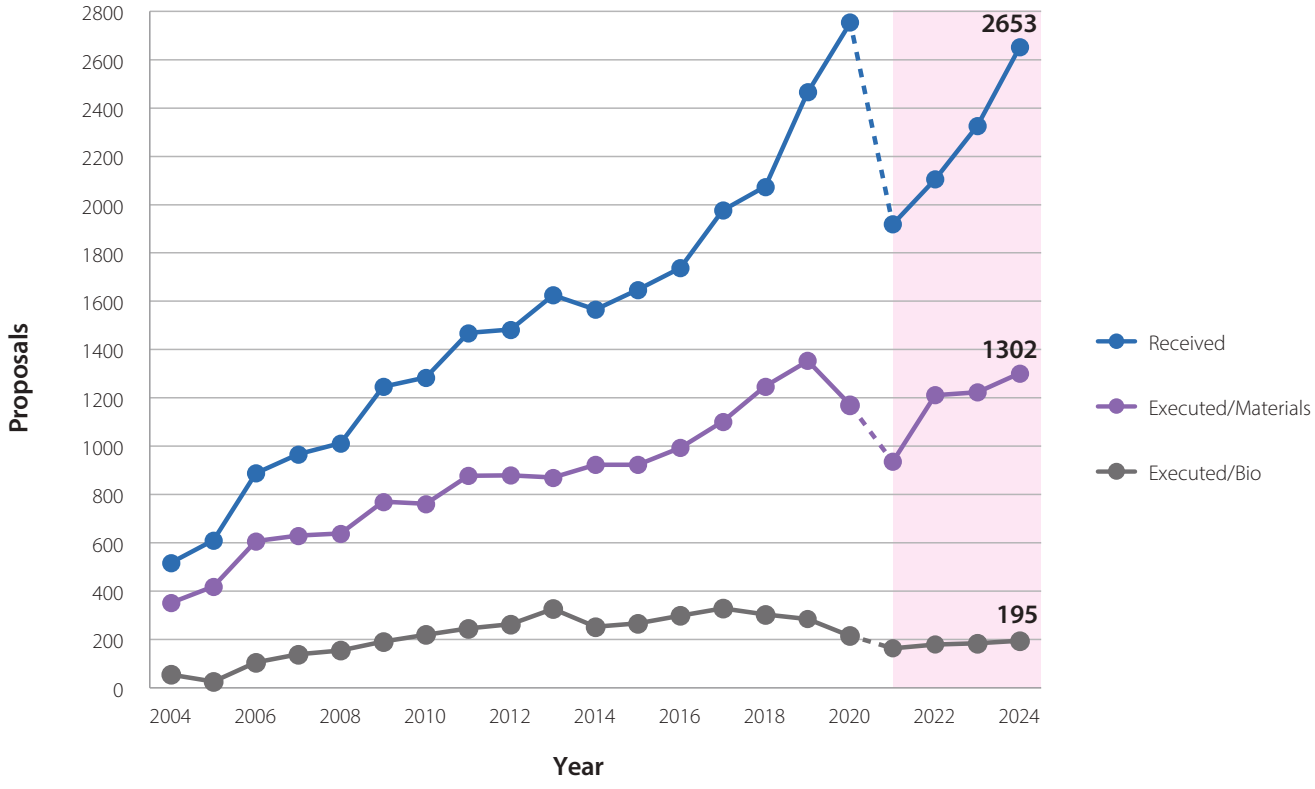

Note: From 2021 onward, NSRRC has changed from 3 calls for proposals per year to 2. This is reflected in a significant decrease in the number of proposals summed up during the year.

Proposal distribution by research fields 2024

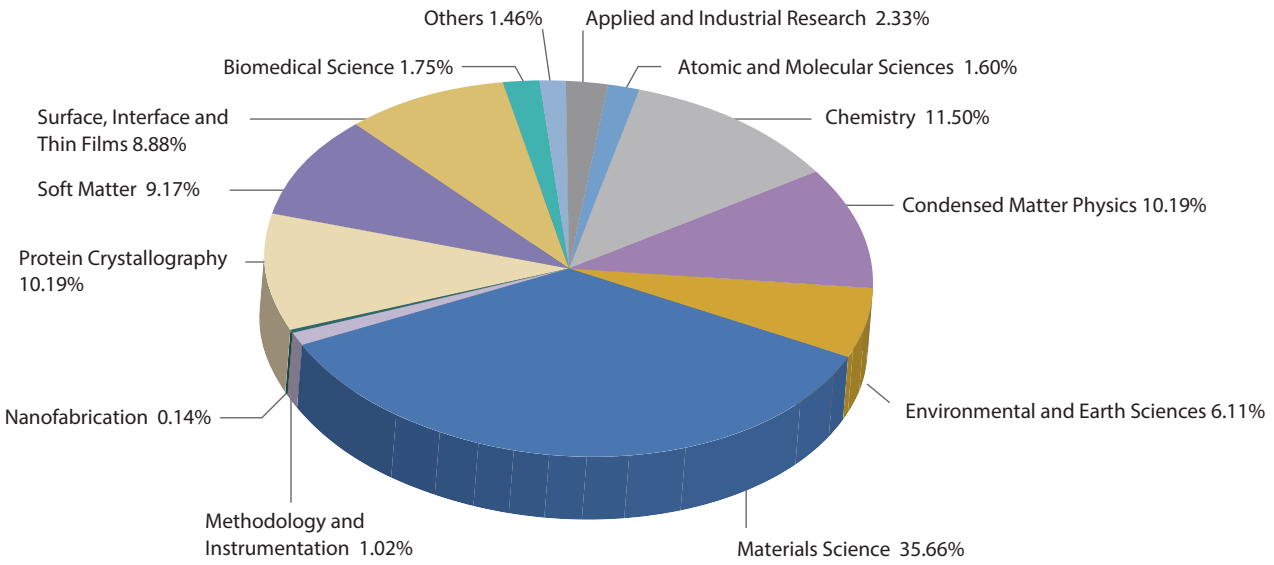

Publications

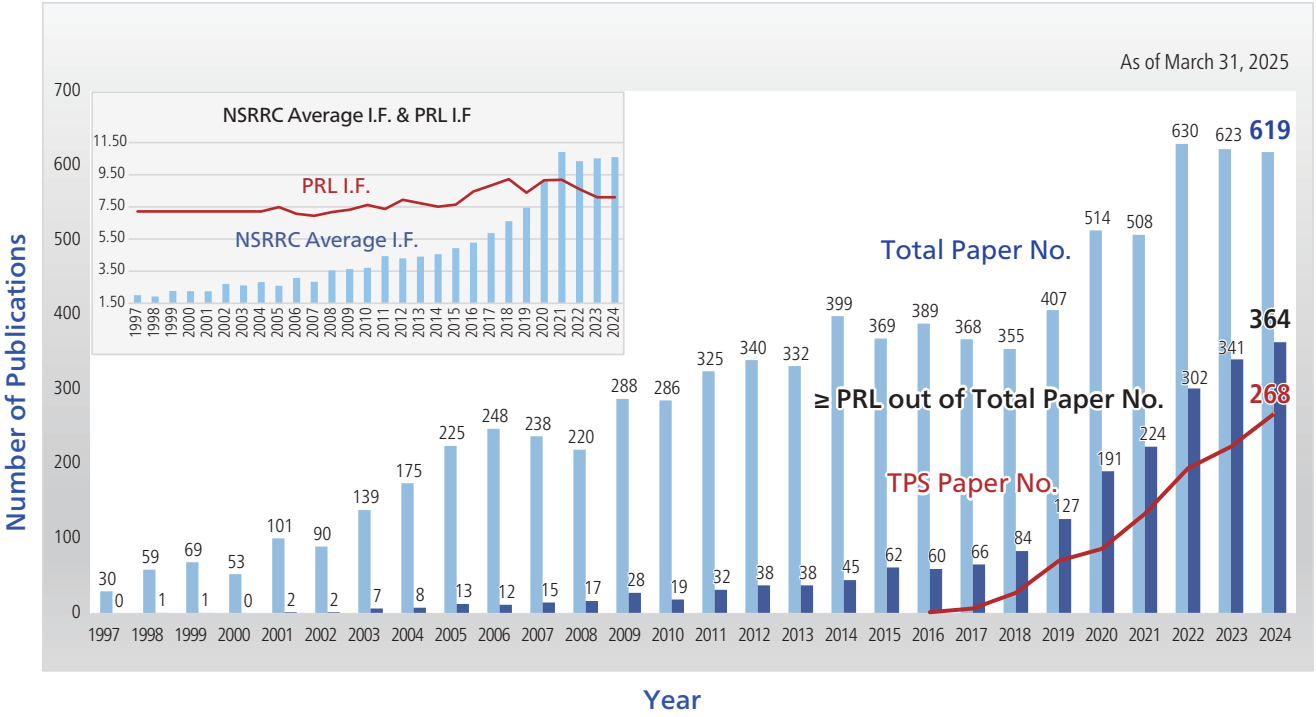

Notes: 1. The Impact Factor (I.F.) for the latest year's publications is based on the current year's release by Journal Citation Report (JCR). For earlier publications, the I.F. is based on the data of the corresponding JCR year.

2. The total number of papers comprises the SCI publications that utilized TLS, TPS, and Taiwan-contract beamlines at SPring-8.

3. PRL refers to Physical Review Letters, the world's premier physics journal, and is mentioned as an index in the graph accordingly.

Beamline Status

Beamlines at the Taiwan Photon Source

No.	Beamline	Mono type	Energy range (eV)	Res. power (E/ΔE)	Endstation / Status	Spokesperson E-mail	Tel. ext.
02A	Brain Imaging	Channel-cut DCM	4k–25k	7,000	in operation	Hwu, Yeu-Kuang phhwu@sinica.edu.tw	3268
05A	Protein Microcrystallography	DCM	5.7k–20k	4,500	in operation	Chao, Frodo frodo@nsrrc.org.tw	2051
07A	Micro-focus Protein Crystallography	DCM	5.7k–20k	4,500	in operation	Chao, Frodo frodo@nsrrc.org.tw	2071
09A	Temporally Coherent X-ray Diffraction	DCM	5.6k–25k	7,000	09A1 in operation	Weng, Shih-Chang weng.sc@nsrrc.org.tw	2091
		HRM	~14.4k	~10^8			
		DCM	8k–10k	7,000	09A2 in operation	Liao, Yen-Fa liao.yenfa@nsrrc.org.tw	
13A	Biological Small-angle X-ray Scattering	DCM	4k–23k	7,000	in operation	Jeng, U-Ser usjeng@nsrrc.org.tw	2131
		DMM	7k–15k	100			
		4BCC	4k–15k	10,000			
15A	Micro-crystal X-ray Diffraction	DCM	9k–35k	7,000	in operation	Wu, Lai-Chin wu.lc@nsrrc.org.tw	2151
		DMM (3%)	9k–25k	333			
		DMM (5%)	9k–25k	200			
19A	High-resolution Powder X-ray Diffraction	DCM	10k–40k	7,000	in operation	Chuang, Yu-Chun chuang.yc@nsrrc.org.tw	2191
21A	X-ray Nanodiffraction	White Beam	5k–30k	7,000	in operation	Chiang, Ching-Yu chiang.cy@nsrrc.org.tw	2211
		4BCM	7k–25k				
23A	X-ray Nanoprobe	HDCM	4k–15k	7,000	in operation	Lin, Bi-Hsuan bihsuan@nsrrc.org.tw	2231
24A	Soft X-ray Tomography	PGM	260–2.6k	2,000	in operation	Lin, Zi-Jing lin.zj@nsrrc.org.tw	2242
25A	Coherent X-ray Scattering	DCM	5.56k–20k	7,000	25A1 in operation	Lin, Jhih-Min lin.jm@nsrrc.org.tw	2251
					25A2 in operation	Huang, Yu-Shan jade@nsrrc.org.tw	
27A	Soft X-ray Nanoscopy	AM-PGM	90–3k	5,000–25,000	27A1 in operation	Hsu, Yao-Jane yjhsu@nsrrc.org.tw	2271
					27A2 commissioning	Wei, Der-Hsin dhw@nsrrc.org.tw	2272
31A	Projection X-ray Microscopy	DCM	5k–30k	7,000	in operation	Yin, Gung-Chian gcyin@nsrrc.org.tw	2312
		DMM	5k–30k	200			
32A	Tender X-ray Absorption Spectroscopy	DCM	1.7k–11k	7,000	in operation	Chen, Chi-Liang chen.cl@nsrrc.org.tw	2321

No.	Beamline	Mono type	Energy range (eV)	Res. power (E/ΔE)	Endstation / Status	Spokesperson E-mail	Tel. ext.
39A	Nanometer Angle-resolved Photoemission Spectroscopy	AM-PGM	20–650	100,000	39A1 in operation 39A2 construction	Cheng, Cheng-Maw makalu@nsrrc.org.tw	2391
41A	Soft X-ray Scattering	AGM	0.4k–1.2k	26,500	in operation	Huang, Di-Jing djhuang@nsrrc.org.tw	2411
44A	Quick-scanning X-ray Absorption Spectroscopy	Quick-mono	4.5k–34k	7,000	in operation	Pao, Chih-Wen pao.cw@nsrrc.org.tw	2441
45A	Submicron Soft X-ray Spectroscopy	AGM	0.28k–1.5k		45A	(BL) Tsai, Huang-Ming tsai.hm@nsrrc.org.tw	7356
				21,500 @510 eV	45A1 in operation	(ES) Chang, Chun-Fu chun-fu.chang@cpfs.mpg.de	2451
				20,000 @860 eV	45A2 in operation	(ES) Chiou, Jau-Wern jwchiou@nuk.edu.tw	2452

Beamlines at the Taiwan Light Source

No.	Beamline	Mono type	Energy range (eV)	Res. power (E/ΔE)	Status	Spokesperson E-mail	Tel. ext.
01A1	SWLS – White X-ray (PRT 75%)	none	> 5k	N/A	in operation	Hwu, Yeu-Kuang phhwu@sinica.edu.tw	1011
01B1	SWLS – X-ray Microscopy	DCM	8k	1,000	in operation	Wang, Chun-Chieh wang.jay@nsrrc.org.tw	1012
01C1	SWLS – EXAFS	DCM	6k–33k	7,000	in operation	Chan, Ting-Shan chan.ts@nsrrc.org.tw	1013
01C2	SWLS – X-ray Powder Diffraction				in operation	Chuang, Yu-Chun chuang.yc@nsrrc.org.tw	1013
03A1	BM – (HF-CGM) – Photoabsorption/ Photoluminescence	CGM	4–40	50,000	in operation	Wu, Yu-Jong yjwu@nsrrc.org.tw	1031
05B1	EPU – Soft X-ray Chemistry	SGM	60–1.5k	20,000	in operation	Liu, Chen-Lin Liu.CL@nsrrc.org.tw	1050
07A1	Industrial Application	DCM	5k–23k	7,000	in operation	Tang, Mau-Tsu mautsu@nsrrc.org.tw	1071
08A1	BM – (L-SGM) XPS, UPS	SGM	15–200	20,000	in operation	Lin, Ping-Hui lin.pinghui@nsrrc.org.tw	1081
08B1	BM – AGM	AGM	0.3k–1k	10,000	in operation	Chainani, Ashish Atma chainani.ash@nsrrc.org.tw	1082
09A1	U50 – SPEM	SGM	60–1.5k	15,000	in operation	Chen, Chia-Hao chchen@nsrrc.org.tw	1101
09A2	U50 – Spectroscopy				in operation	Hsu, Yao-Jane yjhsu@nsrrc.org.tw	1102
11A1	BM – (Dragon) MCD, XAS (PRT 75%)	SGM	8–1.5k	15,000	in operation	Chainani, Ashish Atma chainani.ash@nsrrc.org.tw	1111
13A1	SW60 – X-ray Scattering	ACCM	12k–14k	1,000	in operation	Lee, Ming-Tao mtlee@nsrrc.org.tw	1131

No.	Beamline	Mono type	Energy range (eV)	Res. power (E/ΔE)	Status	Spokesperson E-mail	Tel. ext.
13B2	Beamline of Interdisciplinary Energy Researches	DCM	5k–20k	7,000	in operation	Chuang, Wei-Tsung weitsung@nsrrc.org.tw Chan, Ting-Shan chan.ts@nsrrc.org.tw	1132
14A1	BM – IR Microscopy	FTIR	0.05–0.5 (400–4,000 cm^{-1})	3,200–32,000	in operation	Lee, Yao-Chang yclee@nsrrc.org.tw	1141
15A1	IASW – Biopharmaceuticals Protein Crystallography	DCM	5k–20k	7,000	in operation	Chao, Frodo frodo@nsrrc.org.tw	1151
16A1	BM – Tender X-ray Absorption, Diffraction	DCM	2k–8k	7,000	in operation	Chan, Ting-Shan chan.ts@nsrrc.org.tw	1161
17B1	W200 – X-ray Scattering	DCM	4k–15k	7,000	in operation	Lin, Yan-Gu lin.yg@nsrrc.org.tw	1172
17C1	W200 – EXAFS	DCM	4k–15k	7,000	in operation	Chan, Ting-Shan chan.ts@nsrrc.org.tw	1173
20A1	BM – (H-SGM) XAS	SGM	70–1.2k	10,000	in operation	Haw, Shu-Chih ho.kelman@nsrrc.org.tw	1201
21A1	U90 – (White Light) Chemical Dynamics (PRT 75%)	none	4–500	50	in operation	Lee, Shih-Huang shlee@nsrrc.org.tw	1211
21A2	U90 – (White Light) Photochemistry				in operation	Wu, Yu-Jong yjwu@nsrrc.org.tw	1210
21B1	U90 – (CGM) Angle-resolved UPS	CGM	4–100	10^5	in operation	Cheng, Cheng-Maw makalu@nsrrc.org.tw	1212
21B2	U90 – Gas Phase				in operation	Cheng, Cheng-Maw makalu@nsrrc.org.tw	1212
23A1	IASW – Small/Wide Angle X-ray Scattering	DCM	5k–23k	7,000	in operation	Jeng, U-Ser usjeng@nsrrc.org.tw	1231
		DMM	6–15k	100			
24A1	BM – (WR-SGM) XPS, UPS, XAS, APXPS	SGM	15–1.5k	15,000	in operation	Wang, Chia-Hsin wang.ch@nsrrc.org.tw	1241

Beamlines at SPring-8, Japan

No.	Beamline	Mono type	Energy range (eV)	Res. power (E/ΔE)	Status	Spokesperson E-mail
SP 12B1	BM – Materials X-ray Study	DCM	5k–100k	7,000	in operation	Ishii, Hirofumi h_ishii@spring8.or.jp
SP 12U1	U32 – Inelastic X-ray Scattering	DCM	5k–30k	10^4–10^6	in operation	Hiraoka, Nozomu hiraoka@spring8.or.jp
	HAXPES/Photoemission	HRM	6k–14.4k	300,000		

Neutron Instrument at ACNS, ANSTO, Australia

Instrument	Incident energy (meV)	Energy res. (meV)	Status	Contact
SIKA – Cold Neutron Triple-axis Spectrometer	2.6–25	0.026–2	in operation	Yano, Shin-ichiro yano.shin@nsrrc.org.tw

4BCC: 4-Bounce Crystal Collimator
4BCM: 4-Bounce Channel-cut Monochromator
ACCM: Asymmetrically-cut Curved Crystal Monochromator
AGM: Active Grating Monochromator
APXPS: Ambient-Pressure X-ray Photoelectron Spectroscopy
BM: Bending Magnet
CGM: Cylindrical Grating Monochromator
DCM: Double Crystal Monochromator
DM: Diamond Crystal Monochromator
DMM: Double Multilayer Monochromator
EPU: Elliptically Polarized Undulator
EXAFS: Extended X-ray Absorption Fine Structure
FTIR: Fourier Transform Infrared Spectroscopy
HAXPES: Hard X-ray Photoelectron Spectroscopy
H-SGM: High Energy Spherical Grating Monochromator
HDCM: Horizontal Double Crystal Monochromator
HF-CGM: High Flux Cylindrical Grating Monochromator
HRM: High Resolution Crystal Monochromator
IASW: In-Achromatic Superconducting Wiggler
IR: Infrared Radiation
L-SGM: Low Energy Spherical Grating Monochromator
MCD: Magnetic Circular Dichroism
NIM: Normal Incidence Monochromator
PEEM: Photo-Emission Electron Microscope
PGM: Plane Grating Monochromator
PRT: Participating Research Team
QCM: Quadruple Crystal Monochromator
SGM: Spherical Grating Monochromator
SPEM: Scanning Photoemission Electron Microscope
SW60: Superconducting Wiggler-60 mm
SWLS: Superconducting Wavelength Shifter
U32: Undulator-32 mm
U50: Undulator-50 mm
U90: Undulator-90 mm
UPS: Ultraviolet Photoelectron Spectroscopy
W200: Wiggler-200 mm
WR-SGM: Wide-Range Spherical Grating Monochromator
XAS: X-ray Absorption Spectroscopy
XPS: X-ray Photoelectron Spectroscopy
XRD: X-ray Diffraction

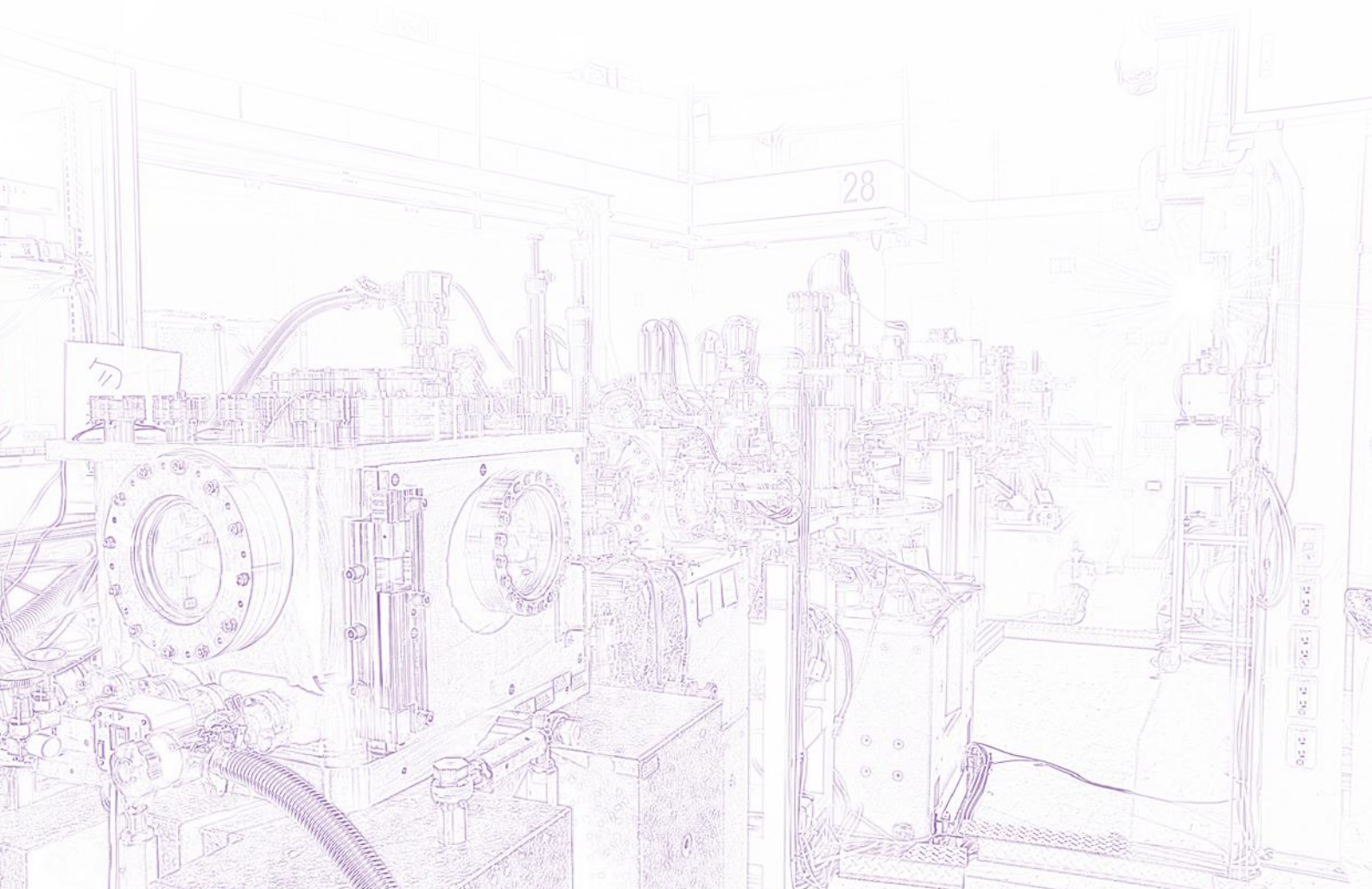

Major Events

NSRRC Board Meetings

The NSRRC Board of Trustees (BOT; see page 110 for details) was established in 2003, and each BOT serves a three-year term. The BOT is responsible for ensuring that the NSRRC serves its purpose as an integral member of the scientific community.

The seventh NSRRC BOT, chaired by Prof. Minn-Tsong Lin, held its tenth and last meeting on February 21. In this meeting, the NSRRC management gave status reports on NSRRC operations and recent achievements. The BOT reviewed the 2023 Final Accounts, work performance, and future plan of the TLS.

The eighth NSRRC BOT was approved by the Executive Yuan on January 30, with the term starting on February 29 and Prof. Minn-Tsong Lin serving as Acting Chair. The first Supervisory Board Meeting was held on March 22, and the first BOT Meeting and the second Supervisory Board Meeting was held on April 25. In the meeting, the goal of the operation termination plan of the TLS at the end of 2028 was decided; however, the possibility of its low-load operation was retained.

The National Science and Technology Council (NSTC) appointed Vice Minister Tzong-Chyuan Chen as Acting Chair of the eighth NSRRC BOT, effective from May 20 onward. On August 27, the Executive Yuan approved Vice Minister Chen-Kang Su of the NSTC as the chair of the eighth NSRRC BOT.

The second BOT Meeting and the third Supervisory Board Meeting was held on July 30. NSRRC management briefed participants on the current operation status, and the BOT members discussed the 2025 Budget Estimate as well as revisions to the internal regulations. On September 27, the first Executive BOT Meeting was held, and the revisions to the internal personnel regulations were discussed.

The third meeting of the year took place on December 10, together with the fourth Supervisory Board Meeting. In the meeting, the new internal audit team member list was approved; the sixth Science Advisory Committee was established, of which the tenure runs from January 1, 2025 to December 31, 2028.

The first BOT Meeting and the second Supervisory Board Meeting was held on April 25. In the photo, from left to right in the front row were BOT members: Ray Hua Horng, Yuan-Tseh Lee, Minn-Tsong Lin (Acting Chair), Mei-Yin Chou, and Bon-Chu Chung. From left to right in the back row were: Jia Shin Lin (Executive Supervisor), Yu-Ju Chen, Huey-Kang Sytwu, Meng-Fan Luo, Mann-Ching Sherry Ku, Yao-Jane Hsu (NSRRC Secretary General), and Chia-Hung Hsu (NSRRC Director).

NSRRC Presented Biomedical Technologies at BIO Asia-Taiwan

NSRRC participated in the BIO Asia-Taiwan International Conference & Exhibition (BIO Asia-Taiwan) at the Taipei Nangang Exhibition Center from July 24 to 27, as part of the Biotechnology-Application Industry-Academia Alliance organized by the College of Life Science at National Tsing Hua University. At the exhibition, NSRRC highlighted the application of synchrotron radiation-based experimental technologies in the biomedical field with main focuses. The first included advanced analysis services, such as core facility support for protein crystallography, structural and compositional analysis of liposomes and exosomes, and the development of drug delivery systems. The second emphasized the practical application of NSRRC's research, featuring innovations like ultra-miniature spectroscopic chips, infrared wax adsorption kinetics for rapid cancer screening, and computed tomography for shadow line alignment. NSRRC staff engaged with numerous enterprises at the exhibition and received positive feedback on the innovations and contributions of the facility.

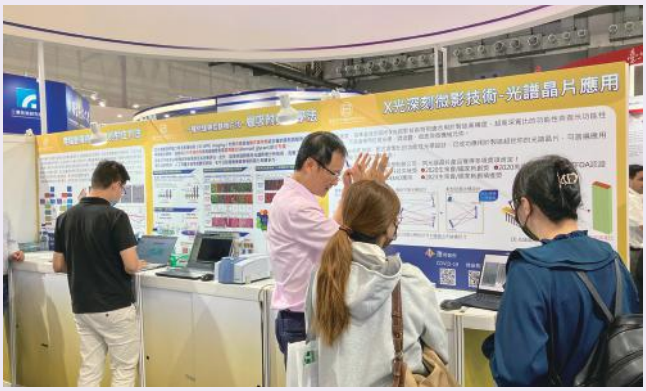

NSRRC highlighted the application of synchrotron radiation-based experimental technologies in the biomedical field at the BIO Asia-Taiwan.

The Annual Open House

The annual NSRRC Open House took place on October 6, attracting 350 adults and children for a fun-filled day of science activities. The event featured an exciting chemical magic performance by the Center for Science Education from Tamkang University, along with interesting science stations at the Taiwan Photon Source (TPS) and engaging science game booths.

Ten science stations were set up along the TPS ring, where "Light Scientists" guided participants through the wonders of how TPS light is used to explore everything in the world, from nanostructures to steel buildings. The demonstrations and hands-on activities offered a glimpse into the critical role of "light" in our everyday lives. Additionally, game booths from the Li Hongming Foundation, NTHU's THz Optics & Photonics Center, and the National Taiwan Science Education Center contributed to the lively atmosphere throughout the event.

The NSRRC remains dedicated to advancing scientific research while bringing science closer to the public. Through entertainment and educational activities, the NSRRC continues to foster a broader understanding and spark public interest.




The NSRRC Open House attracted 350 adults and children to visit the science stations at the TPS.

NSRRC Presented Innovative Technologies at FUTEX 2024

The "Future Tech Pavilion (FUTEX)" at the Taiwan Innotech Expo 2024, held from October 17 to 19 at the Taipei World Trade Center Exhibition Hall 1, was co-organized by NSTC, the Ministry of Education, the Ministry of Health and Welfare, and Academia Sinica. FUTEX spotlighted technological trends expected to shape the next three to ten years, featuring six key exhibition areas: "AIoT & Smart Applications," "Electronics & Optoelectronics," "Evolutionary Materials & Chemicals," "Biotech, New Drugs & Medical Devices," "Net Zero," and "Humanity & Technology." In addition, the highly anticipated "AI Theme Area" and "Healthy Taiwan Theme Area" delivered specialized knowledge in an engaging and accessible format.

This year, NSRRC spotlighted a range of cutting-edge technologies at FUTEX, with a focus on innovative technologies and practical applications. The ten featured technologies included:

1. Solid-State RF Power Amplifiers (presented by Fu-Tsai Chung)
2. The Precise Archer in the Accelerator (presented by Chyi-Shyan Fann)
3. From Lab to Application: Magnetron Sputtering Preparation of Non-Evaporable Getter (NEG) Films (presented by Chin Shueh)
4. The Large Helium Gas Cryogenic Purification System (presented by Huang-Hsiu Tsai)
5. The Liquid Helium Phase Separator with Condenser (presented by Huang-Hsiu Tsai)
6. The Multi-Channel Cryogen Fluid Transfer Line (presented by Huang-Hsiu Tsai)
7. Fast Cancer Screening (presented by Yao-Chang Lee)
8. High-Efficiency Micron-Scale X-ray Computed Tomography (presented by Gung-Chian Yin)
9. Refining at 1600°C: Advanced Synchrotron X-ray Insights into Blast Furnace Ironmaking and the Path to Net-Zero Carbon Emissions (presented by Shi-Wei Chen)
10. Tango Partner: Green Ammonia Plus, Carbon Emissions Minus (presented by Yan-Gu Lin)

Through exhibitions, NSRRC demonstrated its leadership in scientific research and industrial innovation, underscoring its role in driving technological breakthroughs and future advancements.

NSRRC scientists introduced synchrotron radiation technologies to the visitors at FUTEX 2024.

Prof. Ru-Shi Liu of National Taiwan University Received the 2024 NSRRC Outstanding Paper Award

This year, Prof. Ru-Shi Liu from the Department of Chemistry at National Taiwan University was honored with the fourth "Outstanding Paper Award" established by the NSRRC. This esteemed accolade, highly regarded within Taiwan's research community, includes a trophy and a prize of TWD$300,000. Prof. Liu's research team was recognized for their groundbreaking work on "luminescent energy transfer pathways of near-infrared light-emitting diodes" using synchrotron-based light sources, impressing the award's review committee. After a rigorous evaluation process, Prof. Liu's publication was chosen as the standout entry.

The 2024 NSRRC Outstanding Paper Award was presented to Prof. Ru-Shi Liu.

Dr. Der-Hsin Wei, Deputy Director of the NSRRC, chaired the review meetings for the award, inviting a panel of distinguished experts and researchers to assess impactful publications from the past eight years that employed NSRRC's facilities. Prof. Liu's research revealed significant applications in various fields, including optoelectronic technology, security and anti-counterfeiting, agricultural technology, and biomedical imaging. Since its publication in 2018, the team's work has been cited more than 300 times, establishing it as an influential paper in its field. The innovative technology developed has been successfully transferred to Everlight Electronics Co., Ltd., a prominent light-emitting diode (LED) manufacturer in Taiwan, making this a well-deserved recognition for Prof. Liu.

With long-term support from the NSTC, Prof. Liu has dedicated his research to the formulation, synthesis, analysis, and applications of core technologies in materials chemistry, including "photon-to-photon conversion," "photon-to-electron conversion," and "photon-to-heat conversion." His inventions have found applications across various industries of optoelectronics, green energy, biomedicine, and nano-materials, leading to several patents and technology transfer. Notably, Prof. Liu was the pioneer in developing Taiwan's first red LED, laying the groundwork for the country's LED industry.

Throughout his career, Prof. Liu has garnered numerous awards for his exceptional contributions to academic and industrial advancements. His honors include the Excellent Young Person Prize (1989), National Invention Award – Silver Medal from Intellectual Property Office (1995), Young Chemists Award (1998), Z. Hsu Scientific Paper Award (2011) and Z. Hsu Chair Professor Award (2019) from the Far Eastern Y. Z. Hsu Science and Technology Memorial Foundation, Outstanding Research Award from National Science Council (2012, 2017), Hou Chin-Tui Award (2018), TECO Award in Chemical Engineering/ Materials (2019), Academic Award of the Ministry of Education (2020), FutureTech Awards (2021, 2024), Outstanding Paper Award from Chemical Society (2021), and recognition as a Highly Cited Researcher by Clarivate Analytics (2018 to 2021, 2023). The NSRRC's "Outstanding Paper Award" is a testament to Liu's significant impact on both academia and industry.

The award ceremony, originally scheduled to take place during the 30th Users' Meeting & Workshops, was canceled due to government announcements regarding the suspension of work and classes in Hsinchu City on the event date. Nevertheless, the award winner of the year was still announced, and the trophy will be presented at the next Users' Meeting.

Background of the Outstanding Paper Award

Academician Chien-Te Chen was honored with the prestigious Presidential Science Prize in 2017. To encourage more scientists to engage in technological developments in synchrotron-based accelerators, as well as scientific research, Chen donated both the trophy and the monetary award to the NSRRC. His goal is to support Taiwan's synchrotron radiation facilities and inspire scientists to excel in research and make magnificent contributions to the field of science. To uphold Chen's vision, NSRRC used the donated monetary award to install rooftop solar panels. The gross profit generated by solar electricity is used to fund the Outstanding Paper Award.

The objective of the NSRRC Outstanding Paper Award is to advance scientific research in synchrotron-based light sources in Taiwan and encourage researchers in the academic community to develop the technology in accelerators, beamline engineering fields, as well as to publish papers in high-impact international journals by utilizing NSRRC light source facilities. The award is given for papers published in three specific fields: applied science, life science, and natural science. Applications and reviews for each of the three fields are processed every three years in sequential, rotating order.

NSRRC's Industry Applications Division Received the Technology Management Award from CSMOT

The Industry Applications Division of the NSRRC was honored with the 2024 Technology Management Award (Academic and Research Team Category) by the Chinese Society for Management of Technology (CSMOT) on December 6 at Yuan Ze University. This recognition is for the division's exceptional planning, promotion, and execution of the "Industrial Application Service Platforms for the Synchrotron Radiation Facility."

A key mission of the NSRRC is conducting cutting-edge basic and applied research in synchrotron radiation. The Industrial Application Group has been part of its structure since its early founding, and in 2021, the Industry Applications Division was established to meet the growing industrial demand for synchrotron light sources. The division includes the Industrial Planning Office and the Industry Promotion Group, which focus on developing strategies and executing industrial application projects, respectively.

The division integrates NSRRC's research and development capabilities and is developing platforms in such sectors as semiconductors, energy, and accelerator technologies. Its goal is to connect academic research with industry applications, using large-scale accelerator light source technology to address industrial bottlenecks, develop innovative technologies, and boost Taiwan's global competitiveness.

Founded in 1990, CSMOT brings together experts in technology management to foster collaboration between industry, government, and academia. The Technology Management Award, the society's highest honor, annually recognizes individuals and teams for their outstanding contributions to the field and encourages the practical application of academic research in Taiwan's technology management.

NSRRC Industry Applications Division received the Technology Management Award from CSMOT.

Opening Ceremony of the TPS 27A1 Soft X-ray Nanoscopy Beamline & STXM Endstation

The group photo was taken after the plaque was unveiled at the TPS 27A1 Soft X-ray Nanoscopy Beamline and STXM Endstation.

The Taiwan Photon Source (TPS) 27A1 Soft X-ray Nanoscopy Beamline and Scanning Transmission X-ray Microscopy (STXM) Endstation, developed through years of dedicated effort, is now ready to provide high-quality soft X-ray sources and nanoscale chemical imaging capabilities. The opening ceremony of the TPS 27A1 Nanoscopy Beamline and STXM Endstation, organized by the Department of Physics at Tamkang University (TKU) and the NSRRC, took place on December 20 at the NSRRC.

The ceremony began with welcome remarks by Director Chia-Hung Hsu of the NSRRC. The guests of honor from TKU, led by the Chairperson of its Board of Trustees, along with the NSRRC executive team, delivered speeches and unveiled the endstation plaque. The beamline staff then demonstrated the features and core techniques of the endstation to the participants. After the ceremony, attendees proceeded to the lobby for light refreshments and continued their discussions.

This state-of-the-art STXM endstation, collaboratively designed and constructed by the Department of Physics at TKU and the NSRRC, with support from the National Science and Technology Council, highlights the successful outcomes of cross-institutional collaboration. This cutting-edge facility is expected to empower researchers both domestically and internationally in multidisciplinary fields, such as energy, semiconductors, magnetism, and environmental science, aiming to advance scientific research in Taiwan.

MOUs and Collaboration

In 2024, NSRRC focused on the further expansion and extension of our scientific research and development activities. The NSRRC is committed to making the power of synchrotron light sources available to more cross-field applications, building new experimental equipment, developing new capabilities, and nurturing scientific talents. With the continuous sharing of new technologies and by supporting scientific research activities, the NSRRC has, from its foundation, sought opportunities for local and international collaboration to build on previous successes and to encourage new partnerships that contribute to scientific progress. The NSRRC has formalized relationships with a number of institutions and universities by establishing bilateral collaboration and signing the Memoranda of Understanding (MOU). These initiatives are important for accelerating the pace of growth in research and development that is beneficial to all scientists and people around the world.

NSRRC renewed the letter of intent with National Experimental High School at Hsinchu Science Park.

The NSRRC has forged alliances with a range of partners who offer complementary skills, research experiences, and activities. In 2024, the NSRRC had MOUs and collaboration agreements with the following international synchrotron facilities and research institutes in four aspects.

1. Contract beamlines/endstations

- **TPS 02A** Brain Imaging Beamline with Academia Sinica and National Tsing Hua University
- **TPS 13A** Bio-SAXS Beamline with Academia Sinica
- **TPS 27A** STXM/Ptychography Endstation with Tamkang University
- **TPS 39A** nanoARPES Endstation with Taiwan Consortium of Emergent Crystalline Materials
- **TPS 45A1** NSRRC-MPI Beamline with Max-Planck-Institute for Chemical Physics of Solids
- **TPS 45A2** TKU Endstation with Tamkang University

2. International collaboration on beamline/endstation operation and maintenance

- Two Taiwan contract beamlines—**SP 12B** and **SP 12U** at SPring-8, Japan
- Cold neutron triple-axis spectrometer—**SIKA** at ANSTO, Australia

3. Collaborations with research institutes and universities

- Taiwan:
  Academia Sinica,
  National Atomic Research Institute,
  National Center for High-performance Computing,
  National Central University,
  National Cheng Kung University,
  National Chung Cheng University,
  National Chung Hsing University,
  National Experimental High School at Hsinchu Science Park,
  National Health Research Institute,
  National Museum of Natural Science,
  National Pingtung University of Science & Technology,
  National Sun Yat-sen University,
  National Taiwan University,
  National Taiwan University of Science and Technology,
  National Tsing Hua University,
  National Yang Ming Chiao Tung University,
  Tamkang University,
  Tunghai University
- Asia and Oceania: IVPP/CAS, IAS/Wuhan University, Soochow University, NFPSS, IPR/Osaka University,

ISSP/University of Tokyo, JASRI, RIKEN SPring-8, KEK, Okayama University, Tohoku University, PAL, POSTECH, SLRI, ThEP, SSLS, Alagappa University, ANSTO, AS
- Europe: ALBA, Arinax, DESY, JINR, DLS, MPG, ESRF, SOLEIL, CELLS, DESY, MAX IV, HZB, Global Phasing Ltd, ELI Beamlines, EMBL, Elettra, ESS, CSIC, SOLARIS
- America: ALS, ANL, APS, CHESS, NSLS-II, SLAC, Western University, CNPEM, LSU
- User Agreement: APS, BESSY II, BNL, LBNL, NSLS, ORNL

4. Joint graduate programs with Taiwanese universities
- Structural Biology PhD Program with National Tsing Hua University, Academia Sinica, National Health Research Institutes
- International PhD Program for Science—Synchrotron Radiation & Neutron Beam Application with National Sun Yat-sen University
- Science and Technology of Synchrotron Light Source with Graduate Institute of Applied Science and Technology, National Taiwan University of Science and Technology

Conferences, Forums, and Symposia

Synchrotron Radiation Forum at the 2024 PS Annual Meeting

The 2024 Annual Meeting of the Physical Society (PS) of Taiwan took place at National Central University from January 24 to 26. Dr. Tzu-Hung Chuang of the NSRRC organized the satellite meeting entitled "The emergent opportunity for scientific research on sustainable energy materials by high-brilliance synchrotron light sources" as the NSRRC forum on the first day. Sustainable energy has become one of the most prominent fields of research and development in recent years. After the launch of the new high-brightness synchrotron light source, with the support of the National Science and Technology Council and the joint efforts of NSRRC colleagues and users, TPS has achieved fruitful research results using various energy materials. During the PS Annual Meeting, which gathered almost all Taiwanese physicists, the NSRRC seized the opportunity to present and discuss the new scientific research opportunities that synchrotron radiation can bring to the energy materials field. The forum was conducted in the form of invited talks. Focusing on different energy materials, six experts from related fields were invited, including four NSRRC users and two scientists from the NSRRC, to share and discuss the recent research findings and measurement techniques in each subfield. The forum attracted nearly 100 participants.

The Synchrotron Radiation Forum was held at the 2024 PS Annual Meeting in Taoyuan.

Synchrotron Radiation and Neutron Research Forum at the 2024 MCPST Annual Meeting

The 2024 International Conference on Modern Challenges in Polymer Science and Technology (MCPST) was held on January 24 and 25 at National Cheng Kung University. On the second day of the conference, Dr. Wei-Tsung Chuang of the NSRRC held the Synchrotron Radiation and Neutron Research Forum. As energy-related studies have become one of the most popular themes among interdisciplinary research, the forum's topic was set as "New opportunities for metal-organic polymer catalysts" this year. Through this topic, the organizers aimed to attract users from the polymer field who are involved in the synthesis of organic systems, conjugated polymers, or macromolecular frameworks. The forum was presented by the following NSRRC scientists: Drs. U-Ser Jeng, Chun-Ming Wu, Chih-Wen Pao, and Yu-Chun Chuang, each providing explanations for useful experimental techniques. Several users were invited to share recent research findings, including Prof. Lai Ying-Huang from Tunghai University, Prof. Chen Yi-Hong from Wuhan University, and Prof. Guo Jun-Hong from Yang

Ming Chiao Tung University. Through exchanges and discussion in the forum, NSRRC sought to attract potential users to become experimental practitioners in the future.

The Synchrotron Radiation and Neutron Research Forum was held at the 2024 MCPST Annual Meeting.

Synchrotron Light Source Forum at the 2024 Chemistry National Meeting

The 2024 Chemistry National Meeting was hosted by Tamkang University from March 29 to 31. On the second afternoon of the meeting, NSRRC held the NSRRC forum entitled "Applications of Synchrotron Light Source in Chemistry." Four NSRRC scientists, Drs. Jeng-Lung Chen, Yu-Chun Chuang, Lee-Jene Lai and Shu-Chih Haw, made presentations on the advantages of and opportunities for synchrotron-radiation techniques in chemical research, including X-ray absorption spectroscopy, synchrotron powder diffraction, and X-ray tomography. Further, four users shared their experiences of using synchrotron-based techniques in their studies regarding the symmetry-mode analysis of Hg-containing double perovskites, energy storage applications, bioinspired catalysis and bioconjugated protein structural dynamics, and electrochemical oxygen evolution reaction. This forum provided an opportunity for discussions on potential future research and collaboration directions.

The NSRRC forum of Applications of Synchrotron Light Source in Chemistry was held at the 2024 Chemistry National Meeting.

Asian Forum for Accelerators and Detectors 2024 (AFAD2024)

The Asian Forum for Accelerators and Detectors (AFAD) in 2024 was hosted by the NSRRC from April 17 to 19 in Hsinchu. AFADs are held annually under the guidance of the Asian Committee for Future Accelerators to strengthen collaboration between accelerator laboratories across Asia and Oceania in the development of accelerator-related technologies and their applications. The forum organizers invited leading experts and scholars in the fields of particle accelerators and detectors, both domestically and internationally, to share their recent research and development in their facilities. The event facilitated extensive face-to-face exchanges between domestic researchers, young scholars, and international experts on key technologies for them to stay updated on the latest developments in particle accelerators and detectors.

The major topics discussed in the forum included accelerators and their related technologies for photon science; detector technology development; accelerator technologies for industrial and medical applications; innovative accelerator techniques; accelerator and its related technologies for hadron (neutron) science; network and computing; and cryogenics, cryomodule, and superconducting technology for accelerators. The forum was held in a hybrid format, both in person and online, with a total of 174 participants.

AFAD2024 was held at the NSRRC in April.

Hard X-ray Emission Spectroscopy Technical Forum

The Hard X-ray Emission Spectroscopy Technical Forum was held to give information on hard X-ray emission spectroscopy techniques at the TLS 13B2, TPS 38A, and TPS 47A beamlines. NSRRC scientists gave presentations on the construction and progress of the TPS 38A hard X-ray emission spectroscopy optics and shared recent experiment results using X-ray emission spectroscopy at the Taiwan contract beamlines at SPring-8 conducted under the Interdisciplinary Program in energy. In the forum, distinguished speakers were invited to share their insights on future promising research directions, including Prof. Way-Faung Pong from Tamkang University, Prof. Hao Ming Chen from National Taiwan University, Prof. Chun-Chuen Yang from National Central University, and Prof. Jin-Ming Chen from National Yang Ming Chiao Tung University. The organizers invited several young and promising users to participate in the forum, with the hope of gathering users and research topics during the beamline construction phase, fostering collaboration and discussions for future research.

The Hard X-ray Emission Spectroscopy Technical Forum presented the latest hard X-ray emission spectroscopy techniques at the NSRRC.

Third Joint International Symposium of the NSRRC and IPR Osaka University

The 3rd Joint International Symposium of the NSRRC and IPR Osaka University was held in May 2024.

The 3rd Joint International Symposium of the NSRRC and Institute for Protein Research (IPR) of Osaka University—Establishment of the Structural Biology Network in Asia and Oceania was held on May 21 and 22 at the NSRRC. This was the third symposium in the series, with the first and second held in 2015 and 2017, respectively. The third symposium, originally scheduled for 2020, was delayed due to the pandemic and thus took place in 2024. The symposium featured seven international speakers (five from Japan, one from Korea, and

one from Thailand) and six domestic speakers, who shared the updates on their protein crystallography facilities and research findings. A site tour to the latest experimental stations at the TPS was also arranged. This symposium contributed to the establishment of future collaborations and regional connections. Both former and current directors of the Institute for Protein Research at Osaka University participated in the event, and a discussion was held with the director and deputy director of the NSRRC, further strengthening mutual understanding and support for collaboration.

The XIX International Small-Angle Scattering Conference (SAS2024)

The XIX International Small-Angle Scattering Conference (SAS2024), organized by the NSRRC, was held from November 3 to 8 at the Taipei International Convention Center (TICC) in Taiwan. Held every three years since 1965, the SAS conference has become one of the most significant large-scale events for interdisciplinary researchers in the global small-angle scattering community.

SAS2024 brought together nearly 500 scientists and students from around the world, with around 200 talks and more than 200 poster presentations. The conference showcased recent advances and highlighted the broad impact of small-angle scattering techniques on established and emerging scientific fields. In conjunction with SAS2024, a special issue of the Journal of Applied Crystallography will be published as the SAS2024 Conference Proceedings, featuring the latest research contributions from registered conference participants.

The conference also included a site tour to the TPS and TLS, where participants witnessed the high-quality synchrotron light capabilities and recently developed small-angle scattering techniques that serve specialized research needs in structural biology, biomedical science, materials science, and the semiconductor industry.

Notably, the program featured the Sow-Hsin Chen Distinguished Lectureship to honor Academician Chen's pioneering contribution to nuclear science and technology in Taiwan. Additionally, the 2024 Taiwan Neutron Science Society Annual Meeting and Neutron Scattering Workshop, held concurrently at the same venue, aimed to advance neutron scattering techniques and enhance Taiwan's international visibility in the scattering community. At the event's conclusion, the conference baton was passed to MAX IV and ESS, the joint hosts of SAS2027 in Lund, Sweden.

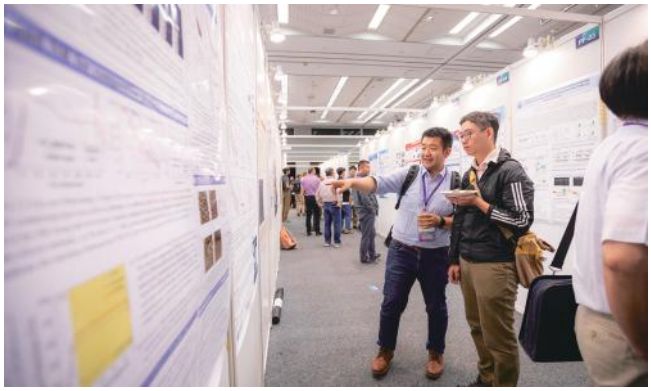

SAS2024 brought together nearly 500 scientists and students from around the world.

Synchrotron X-ray and Neutron Science and Applications Forum at the 2024 MRS-T International Meeting

The 2024 Materials Research Society of Taiwan (MRS-T) Annual Meeting took place at National Chung Hsing University on November 15 and 16. The NSRRC, as a co-organizer, held the "Synchrotron Radiation and Materials Forum" on the afternoon of November 16. Dr. Yan-Gu Lin of the NSRRC invited three distinguished domestic scholars to share their research results using synchrotron light sources. Additionally, four NSRRC scientists introduced the applications of advanced technologies at TPS beamlines in materials science, presenting the latest research trends and potential applications to the attendees.

Furthermore, Dr. Lin also promoted the scientific applications of TPS experimental facilities at the seminar organized for principal investigators in materials science during the MRS-T Annual Meeting. He presented cutting-edge experimental techniques and synchrotron radiation analytical methods, and he cordially invited the researchers and scholars in the fields to conduct experiments at the NSRRC.

Researchers and students attended the Synchrotron X-ray and Neutron Science and Applications Forum at the 2024 MRS-T International Meeting.

Training Courses

NSYSU-NSRRC Joint Summer School on Small-Angle Scattering

The NSYSU-NSRRC Joint Summer School on Small-Angle Scattering was held from July 17 to 28, with focuses on small-angle X-ray scattering (SAXS) and small-angle neutron scattering (SANS). The Summer School provided a platform for junior scientists, engineers of industrial applications, and senior undergraduate and graduate students to exchange scientific ideas, share knowledge, and collaborate. A total of 90 participants gathered at the NSRRC for the program.

The Summer School included not only an introduction to basic concepts, technologies, and applications of SAXS but also hands-on experiments at the NSRRC. Through two weeks of instruction and interaction, participants gained a solid understanding of basic quantum scattering principles, fundamental calculations of two-point spatial correlation functions, and the use of related software for data analysis.

The Summer School attracted participants from various fields, including physics, chemistry, chemical engineering, materials science, and biotechnology, making it a diverse and wide-ranging program. The program was well-balanced, emphasizing both lecturer instruction and participant interaction, fostering a deeper understanding of small-angle scattering across different disciplines and its application in relevant research fields. Through discussions, hands-on practice, group presentations, and outdoor activities, the program strengthened the connections and knowledge exchange between researchers and participants from different fields. The discussions explored the applications of SAXS and its complementary role in other areas of research, such as the analysis of microstructure and molecular forces in such fields as material physics, soft matter science, polymer physics, and biomedical materials.

During the hands-on training sessions, participants operated SAXS experimental stations in groups, collecting and analyzing SAXS data, thereby achieving immediate practical benefits from their learning. At the conclusion of the course, a group-based problem-solving competition was held, allowing participants to present their learning outcomes. Finally, participants were encouraged to continue their research by using NSRRC experimental facilities, paving the way for long-term connection to the synchrotron radiation research and development.

Through the Summer School, it was observed that these domestic participants were on par with their international counterparts, highlighting the importance of continuing to develop and cultivate SAXS techniques in Taiwan. This would ensure Taiwan's academic research competitiveness in relevant fields and provide a strong talent pool for the construction, operation, and maintenance of related facilities in the future.

The NSYSU-NSRRC Joint Summer School emphasized SAXS and SANS.

Summer Internship

The summer internship program has been one of NSRRC's cornerstones for educational outreach, targeting undergraduate students, primarily those in their second to fourth years, since 2013. The program provides systematic instruction on synchrotron-related scientific knowledge and hands-on training at TLS and TPS beamlines. A total of 32 students were accepted into the 2024 Summer Internship program held from July 1 to 31.

The objective of the summer internship was to promote synchrotron-related sciences at the undergraduate level.

This year, the internship program specifically encouraged students to engage in discussions and to share their learning experiences. We were pleased to see that students not only worked diligently in their studies but also actively exchanged knowledge and insights gained from their hands-on experiences. They even assisted participants at other experimental stations, shared their findings, and, at the conclusion of the program, exchanged contact information.

This internship program was a resounding success. It trained over 30 undergraduate students in synchrotron technologies and experimental techniques while also fostering valuable connections between NSRRC and universities. It played a key role in NSRRC's future talent development and in strengthening ties with leading researchers.

Focal-Plane Array Infrared Microspectrocopy Training Course

The Focal-Plane Array Infrared Microspectrocopy Training Course was held on July 11 and 12 at the NSRRC. There were 31 resident physicians, industry professionals, university laboratory assistants, graduate students, and undergraduate students in the training course. The participants were users and potential users from diverse fields, ranging from biomedical sciences, earth and environmental sciences, space science, electrochemistry, and biomaterials and nanomaterials to archaeology.

The training course aimed to provide synchrotron radiation knowledge on Fourier transform infrared spectroscopy, safety operating procedures at the experimental stations, various measurement techniques in infrared spectroscopy, infrared imaging construction techniques, spectroscopic data processing and analysis, and the use of image processing application programs. Participants gained hands-on experience at the infrared microspectroscopy endstation and its experimental facilities, enabling them to understand the spectral information provided by infrared microscopy and the design of experiments to address the scientific issues that they might encounter in the future.

Users and potential users of NSRRC infrared beamlines participated in the Focal-Plane Array Infrared Microspectrocopy Training Course and practiced analyzing data at TLS 14A1.

Summer School on Free Electron Lasers

The Summer School on Free Electron Lasers (FEL) 2024 was held at the NSRRC from July 15 to 19. A total of 26 students participated in the 5-day program. The FEL are widely recognized by the international accelerator community as one of the most important light sources for the future. To train scientists dedicated to FEL science and technology, the school offered extensive knowledge of this emerging technology and its applications in electronics, biomedical science, physics, chemistry, and materials science.

During the summer school, renowned international FEL experts and domestic scientists who conduct research in this field or have conducted experiments using FEL were invited to give lectures in English. This course was designed to help students gain a deeper understanding of FEL; spark their interest in FEL, accelerator technologies, scientific experiments and applications; and make them aware of the demand for this crucial fourth-generation light source. This course trained domestic students, fostering the development of accelerator technology research and applications and addressing the need for talent in industry, medicine, and research.

Summer School on FEL aimed to cultivate scientists in FEL accelerator technologies.

Protein Crystallography Training Courses I and II

The Protein Crystallography Training Courses were held from July 22 to 26 and from July 29 to August 2. Each course consisted of 18 first-year master or PhD students, newly hired postdoctoral fellows, and research assistants, who were from 28 different laboratories. The goal of the training courses was to disseminate experimental techniques of macromolecular crystallography to researchers and students with an interest in using this specific method to further the scope of their research. The courses provided lecture programs and hands-on training, which covered a broad spectrum of topics on synchrotron-based protein crystallography, ranging from the crystallization of proteins, data collection strategy, phasing techniques, and radiation damage on protein crystals to the structure determination of proteins. The knowledge and skills that the students acquired from the courses broadened their perspectives on their research and were essential for experiments in biotechnology and pharmaceuticals.

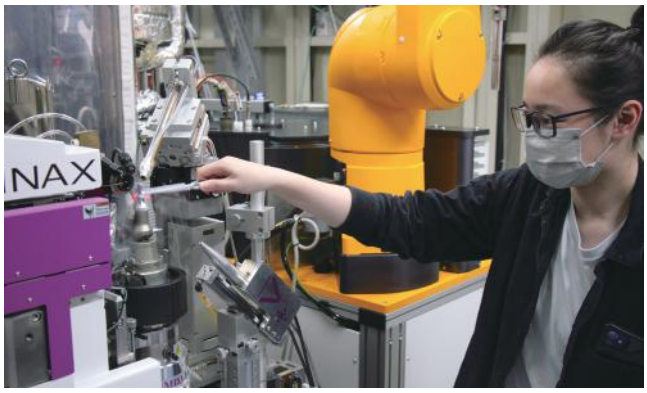

Protein Crystallography Training Courses offered hands-on sessions to practice growing crystals, collecting data, and analyzing diffraction data.

Training Course on the Data Analysis of X-ray Absorption Spectroscopy

The Training Course on the Data Analysis of X-ray Absorption Spectroscopy was designed to deepen participants' understanding of data acquisition and analysis. The course was held at the NSRRC on August 6 and had 74 attendees. NSRRC scientists gave lectures on the experimental principle and the setup and application of X-ray absorption fine-structure (XANES) data collection. Two common software packages used for data acquisition and the analysis of X-ray absorption spectra, Athena and Artemis, were explained, and the wavelet analysis of XANES simulation using the FDMNES code was also demonstrated.

There were 74 users and potential users participating in the Training Course on the Data Analysis of X-ray Absorption Spectroscopy.

NAPXPS/XPS Training Course

In response to the enthusiastic demand for near ambient pressure X-ray photoelectron spectroscopy (NAPXPS), NSRRC organized the NAPXPS/XPS Training Course on August 9. The course included lectures as well as hands-on training in spectrum analysis, and due to time constraints, the number of participants was limited. A total of 33 students and principal investigators attended, consisting of 28 registered participants and five auditors.

During the course, participants raised numerous questions and were eager to apply the techniques to address their research topics. Some principal investigator participants expressed strong interest in conducting experiments at the NSRRC in the future. As a result, this training not only promoted XPS technology but also offered an opportunity to broaden the user base for NSRRC's scientific services.

The NAPXPS/XPS Training Course was attended by 33 students and researchers.

Training Course on X-ray Thin-Film Scattering

The Training Course on X-ray Thin-Film Scattering was held from August 13 to 16 with the aim of providing background knowledge on X-ray thin-film scattering and hands-on training on experimental operations at TPS 09A. The course was designed for new members in the research laboratories to facilitate the application of X-ray scattering in thin-film system research.

This training course consisted of theoretical instruction on the first two days and hands-on practice on the last two days. A total of 40 participants were admitted for the theoretical sessions, and 20 slots were available for the in-house practice for X-ray diffraction experiments. In total, 53 participants (including auditors) from 10 universities and research institutions in Taiwan attended the course.

In previous years, the course focused mainly on TPS 09A. However, this year, a special presentation given by Dr. Jun-Yu Chen was included to introduce the application and research of TPS 25A in thin-film systems, offering participants an additional research perspective.

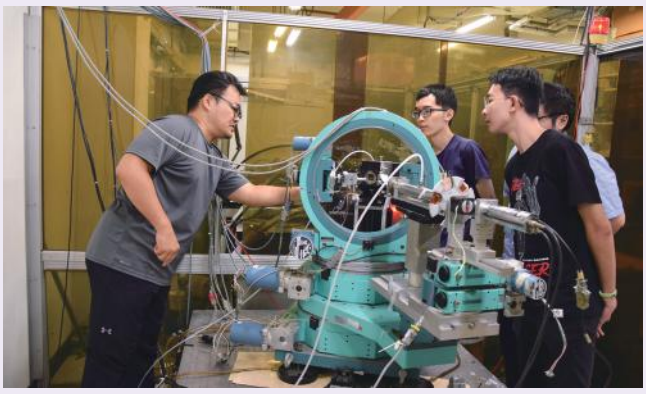

Participants attended the lectures, followed by hands-on training at TPS 09A as part of the Training Course on X-ray Thin-Film Scattering.

2024 Autumn School for Micro-Sized Single-Crystal Diffraction and High Pressure Techniques

The Autumn School for Micro-Sized Single-Crystal Diffraction and High Pressure Techniques was held for the first time in 2024. The training course introduced crystallography theory, the operation of single-crystal and high-pressure experimental equipment, and hands-on training for single-crystal data analysis software at the TPS 15A beamline. A total of 67 participants attended the course, including 14 instructors and 53 students, from diverse fields, such as physics, chemistry, materials science, condensed matter physics, and earth sciences.

Most participants had limited knowledge of crystallography, and some had no practical experience in data collection or crystal structure analysis. After attending the autumn school, students expressed a strong interest in becoming users and conducting experiments at the NSRRC.

The Autumn School for Micro-Sized Single-Crystal Diffraction and High Pressure Techniques was held for the first time in 2024.

Learning Opportunities for NEHS Students

NSRRC began to provide learning opportunities for the National Experimental High School (NEHS) at Hsinchu Science Park in 2019. In 2020, NEHS selected 23 second-year high school students to participate in experiments with NSRRC scientists. The students first took thematic classes on radiation safety and research and science related to synchrotron radiation, and then they began thematic studies in a group with NSRRC scientists for an academic year.

This year, eight research teams at the NSRRC provided students with nine scientific research topics, including enhancing photocatalytic effects by modifying TiO_2 nanoparticles with two-dimensional material quantum dots; application of projection X-ray microscopy and transmission X-ray microscopy in paleontological fossils, and the internal three-dimensional structure of materials; preparation of protein crystals and exploration of crystal structures; versatile membrane proteins in genes and applications in drug deliveries; lipid micelle in genes and applications in drug deliveries; single-crystal analysis of wave-particle duality and the photoelectric effect; developing materials for single-photon sources; crystals growth and structural analysis by using X-ray diffraction; and studies of structures and properties of biomolecules in aqueous solutions.

The learning opportunities helped to sow the seeds of knowledge in brilliant high school students, providing them with opportunities to explore a national research center.

Appendix

List of Publications

Publications (including conference proceedings) listed here are based on the results obtained from facilities associated with the NSRRC

Notes:

1. Asterisks (*) indicate corresponding authors. Their Chinese names are shown in parentheses if applicable.
2. Publications are sorted by endstation and listed in alphabetic order according to the last name of the first author.
3. Publications using more than one beamline are listed in corresponding beamline sections.
4. Publications marked ◎ are selected to report in the sections of Research Highlights.

Experiments Performed at NSRRC Beamlines

TPS 05A Protein Microcrystallography

- C.-W. M. Chang, S.-C. Wang, C.-H. Wang, A. H. Pang, C.-H. Yang, Y.-K. Chang, W.-J. Wu, and M.-D. Tsai*(蔡明道), "*A Unified View on Enzyme Catalysis by Cryo-EM Study of a DNA Topoisomerase*", Commun. Chem. **7**, 45 (2024).
- H.-H. Chang, L.-C. Lee, Tsu Hsu, Y.-H. Peng, C.-H. Huang, T.-K. Yeh, C.-T. Lu, Z.-T. Huang, C.-C. Hsueh, F.-C. Kung, L.-M. Lin, Y.-C. Huang, Y.-H. Wang, L.-H. Li, Y.-C. Tang, L. Chang, C.-C. Hsieh, W.-T. Jiaang*(蔣維棠), C.-C. Kuo*(郭靜娟), and S.-Y. Wu*(伍素瑩), "*Development of Potent and Selective Inhibitors of Methylenetetrahydrofolate Dehydrogenase 2 for Targeting Acute Myeloid Leukemia: SAR, Structural Insights, and Biological Characterization*", J. Med. Chem. **67**, 21106 (2024).
- C.-C. Chen*(陳純琪), X. Li, J. Min, Z. Zeng, Z. Ning, H. He, X. Long, D. Niu, R. Peng, X. Liu, Y. Yang, J.-W. Huang, and R.-T. Guo*(郭瑞庭), "*Complete Decomposition of Poly(Ethylene Terephthalate) by Crude PET Hydrolytic Enzyme Produced in Pichia Pastoris*", Chem. Eng. J. **481**, 148418 (2024).
- C.-C. Chen, H. Li, J.-W. Huang, and R.-T. Guo*(郭瑞庭), "*Structural and Molecular Insights of Two Unique Enzymes Involved in the Biosynthesis of a Natural Halogenated Nitrile*", FEBS J. **291**, 5123 (2024).
- X. Chen, A. Mohapatra, H. T. V. Nguyen, L. Schimanski, T. K. Tan, P. Rijal, C.-P. Chen, S.-H. Cheng, W.-H. Lee, Y.-C. Chou, A. R. Townsend, C. Ma, and K.-Y. A. Huang*(黃冠穎), "*The Presence of Broadly Neutralizing Anti-SARS-CoV-2 RBD Antibodies Elicited by Primary Series and Booster Dose of COVID-19 Vaccine*", PLoS Pathog. **20**, e1012246 (2024).
- W. T. Chiang, Y.-K. Chang, W.-H. Hui, S.-W. Chang, C.-Y. Liao, Y.-C. Chang, C.-J. Chen, W.-C. Wang, C.-C. Lai, C.-H. Wang, S.-Y. Luo, Y.-P. Huang, S.-H. Chou, T.-L. Horng, M.-H. Hou, S. P. Muench, R.-S. Chen, M.-D. Tsai* (蔡明道), and N.-J. Hu*(胡念仁), "*Structural Basis and Synergism of ATP and Na^+ Activation in Bacterial K^+ Uptake System KtrAB*", Nat. Commun. **15**, 3850 (2024).
- C.-C. Cho, C.-Y. Fei, B.-C. Jiang, W.-Z. Yang, and H. S. Yuan*(袁小玲), "*Molecular Mechanisms for DNA Methylation Defects Induced by ICF Syndrome-linked Mutations in DNMT3B*", Protein Sci. **33**, e5131 (2024).
- ◦ C.-H. Chu, C.-T. Wu, M.-G. Lin, C.-Y. Yen, Y.-Z. Wu, C.-D. Hsiao*(蕭傳鐙), and Y.-J. Sun*(孫玉珠), "*Insights into the Molecular Mechanism of ParABS System in Chromosome Partition by HpParA and HpParB*", Nucleic Acids Res. **52**, 7321 (2024).
- C. Cui, L.-J. Yang, Z.-W. Liu, X. Shu, W.-W. Zhang, Y. Gao, Y.-X. Wang, T. Wang, C.-C. Chen, R.-T. Guo*(郭瑞庭), and S.-S. Gao*(高書山), "*Substrate Specificity of a Branch of Aromatic Dioxygenases Determined by Three Distinct Motifs*", Nat. Commun. **15**, 7682 (2024).
- L. Dai, H. Li, S. Dai, Q. Zhang, H. Zheng, Y. Hu, R.-T. Guo*(郭瑞庭), and C.-C. Chen*(陳純琪), "*Structural and Functional Insights into the Self-sufficient Flavin-dependent Halogenase*", Int. J. Biol. Macromol. **260**, 129312 (2024).
- J.-Y. Hong, S.-C. Lin, K. Kehn-Hall, K.-M. Zhang, S.-Y. Luo, H.-Y. Wu, S.-Y. Chang, and M.-H. Hou*(侯明宏), "*Targeting Protein-protein Interaction Interfaces with Antiviral N Protein Inhibitor in SARS-CoV-2*", Biophys. J. **123**, 478 (2024).
- Y.-C. Hsieh, H.-H. Guan, C.-C. Lin, T.-Y. Huang, P. Chuankhayan, N.-C. Chen, N.-H. Wang, P.-L. Hu, Y.-C. Tsai, Y.-C. Huang, M. Yoshimura, P.-J. Lin, Y.-H. Hsieh*(謝義簧), and C.-J. Chen*(陳俊榮), "*Structure-based High-efficiency Homogeneous Antibody Platform by Endoglycosidase Sz Provides Insights into Its Transglycosylation Mechanism*", JACS Au **4**, 2130 (2024).
- C.-H. Lai, K.-T. Ko, P.-J. Fan, T.-A. Yu, C.-F. Chang, P. Draczkowski, and S.-T. D. Hsu*(徐尚德), "*Structural Insight into the ZFAND1-p97 Interaction Involved in Stress Granule Clearance*", J. Biol. Chem. **300**, 107230 (2024).
- C.-C. Lee*(李政忠), W.-C. Kuo, Y.-W. Chang, S.-F. Hsu, C.-H. Wu, Y.-W. Chen, J.-J. Chang*(張瑞仁), and A. H.-J. Wang*(王惠鈞), "*Structure-based Development of a Canine TNF-α-specific Antibody Using Adalimumab as a Template*", Protein Sci. **33**, e4873 (2024).
- H.-Y. Li, H.-Y. Lin, S.-K. Chang, Y.-T. Chiu, C.-C. Hou, T.-P. Ko, K.-F. Huang, D.-M. Niu*(牛道明), and W.-C. Cheng*(鄭偉杰), "*Mechanistic Insights into Dibasic Iminosugars as pH-selective Pharmacological Chaperones to Stabilize Human α-galactosidase*", JACS Au **4**, 908 (2024).
- ◦ M.-G. Lin, C.-Y. Yen, Y.-Y. Shen, Y.-S. Huang, I. W. Ng, D. Barillà, Y.-J. Sun* (孫玉珠), and C.-D. Hsiao*(蕭傳鐙), "*Unraveling the Structure and Function of a Novel SegC Protein Interacting with the SegAB Chromosome Segregation Complex in Archaea*", Nucleic Acids Res. **52**, 9966 (2024).
- S.-M. Lin, H.-T. Huang, P.-J. Fang, C.-F. Chang, R. Satange, C.-K. Chang, S.-H. Chou, S. Neidle*, and M.-H. Hou*(侯明宏), "*Structural Basis of Water-mediated cis Watson-cric k/Hoogsteen Base-pair Formation in Non-CpG Methylation*", Nucleic Acids Res. **52**, 8566 (2024).
- M. Liu, Y. Yang, J.-W. Huang, L. Dai, Y. Zheng, S. Cheng, H. He, C.-C. Chen* (陳純琪), and R.-T. Guo*(郭瑞庭), "*Structural Insights into a Novel Nonheme Iron-dependent Oxygenase in Selenoneine Biosynthesis*", Int. J. Biol. Macromol. **256**, 128428 (2024).
- Y.-C. Lou, C.-F. Tu, C.-C. Chou, H.-H. Yeh, C.-Y. Chien, S. Sadotra, C. Chen, R.-B. Yang*(楊瑞彬), and C.-H. Hsu*(徐駿森), "*Structural Insights into the Role of N-terminal Integrity in PhoSL for Core-fucosylated N-glycan Recognition*", Int. J. Biol. Macromol. **255**, 128309 (2024).
- C. Y. Mok, H. Y. Chu, W. W. L. Lam, and S. W. N. Au*(區詠娥), "*Structural Insights into the Assembly Pathway of the Helicobacter Pylori CagT4SS Outer Membrane Core Complex*", Structure **32**, 1725 (2024).
- C.-H. Peng, T.-L. Hwang, S.-C. Hung, H.-J. Tu, Y.-T. Tseng, T. E. Lin, C.-C. Lee, Y.-C. Tseng, C.-Y. Ko, S.-C. Yen, K.-C. Hsu, S.-L. Pan, and W.-C. HuangFu*(皇甫維君), "*Identification, Biological Evaluation, and Crystallographic Analysis of Coumestrol as a Novel Dual-specificity Tyrosine-phosphorylation-regulated Kinase 1A Inhibitor*", Int. J. Biol. Macromol. **282**, 136860 (2024).
- S. Tang, C.-H. Huang, T.-P. Ko, K.-F. Lin, Y.-C. Chang, P.-Y. Lin, L. Sun, and C.-Y. Chen*(陳青諭), "*Dual Dimeric Interactions in the Nucleic Acid-binding Protein Sac10b Lead to Multiple Bridging of double-stranded DNA*", Heliyon **10**, e31630 (2024).
- L. T. Tran, C. Akıl, Y. Senju, and R. C. Robinson*, "*The Eukaryotic-like Characteristics of Small GTPase, Roadblock and TRAPPC3 Proteins from Asgard Archaea*", Commun. Biol. **7**, 273 (2024).
- J.-C. Tsou, C.-J. Tsou, C.-H. Wang, A.-L. A. Ko, Y.-H. Wang, H.-H. Liang, J.-C. Sun, K.-F. Huang, T.-P. Ko, S.-Y. Lin, and Y.-S. Wang*(王彥士), "*Site-specific Histidine Aza-michael Addition in Proteins Enabled by a Ferritin-based Metalloenzyme*", J. Am. Chem. Soc. **146**, 33309 (2024).
- ◦ S. Wang, C.-H. Huang, T.-S. Lin, Y.-Q. Yeh, Y.-S. Fan, S.-W. Wang, H.-C. Tseng, S.-J. Huang, Y.-Y. Chang, U.-S. Jeng, C.-I. Chang, and S.-R. Tzeng* (曾秀如), "*Structural Basis for Recruitment of Peptidoglycan Endopeptidase MepS by Lipoprotein Nlpl*", Nat. Commun. **15**, 5461 (2024).
- Y. Wu, Y. Yang, G. Lu, W.-L. Xiang, T.-Y. Sun, K.-W. Chen, X. Lv, Y.-F. Gui, R.-Q. Zeng, Y.-K. Du, C.-H. Fu, J.-W. Huang, C.-C. Chen, R.-T. Guo*(郭瑞庭), and L.-J. Yu*(余龍江), "*Unleashing the Power of Evolution in Xylanase Engineering: Investigating the Role of Distal Mutation Regulation*", J. Agr. Food Chem. **72**, 18201 (2024).
- L.-C. Ye, S.-Y. Chow, S.-C. Chang, C.-H. Kuo, Y.-L. Wang, Y.-J. Wei, G.-C. Lee, S.-H. Liaw, W.-M. Chen*(陳文明), and S.-C. Chen*(陳勝嘉), "*Structural and Mutational Analyses of Trehalose Synthase from Deinococcus radiodurans*

Reveal the Interconversion of Maltose-trehalose Mechanism", J. Agr. Food Chem. **72**, 18649 (2024).
- T.-J. Ye, K.-M. Fung, I.-M. Lee, T.-P. Ko, C.-Y. Lin, C.-L. Wong, I.-F. Tu, T.-Y. Huang, F.-L. Yang, Y.-P. Chang, J.-T. Wang, T.-L. Lin, K.-F. Huang*(黃開發), and S.-H. Wu*(吳世雄), "*Klebsiella Pneumoniae K2 Capsular Polysaccharide Degradation by a Bacteriophage Depolymerase Does Not Require Trimer Formation*", mBio **15**, 03519-23 (2024).
- R. Yekta, X. Xiong, J. Li, B. S. Heater, M. M. Lee, and M. K. Chan*(陳文博), "*Mechanoresponsive Protein Crystals for NADH Recycling in Multicycle Enzyme Reactions*", J. Am. Chem. Soc. **146**, 18817 (2024).

TPS 07A Micro-focus Protein Crystallography

- C.-C. Chao*(趙啟超), S.-R. Tzeng, M.-C. Chiang, H.-W. Hsueh, W.-J. Hsieh, Y.-C. Chao, M.-F. Cheng, Y.-H. Lin, M.-Y. Su, C.-H. Huang, Y.-S. Wang, M.-F. Hsieh, P.-H. Tseng, and S.-T. Hsieh*(謝松蒼), "*Diflunisal Versus Tafamidis on Neuropathy and Cardiomyopathy in Hereditary Transthyretin Amyloidosis*", Ann. Clin. Transl. Neurol. **11**, 2426 (2024).
- C.-C. Chen*(陳純琪), X. Li, J. Min, Z. Zeng, Z. Ning, H. He, X. Long, D. Niu, R. Peng, X. Liu, Y. Yang, J.-W. Huang, and R.-T. Guo*(郭瑞庭), "*Complete Decomposition of Poly(Ethylene Terephthalate) by Crude PET Hydrolytic Enzyme Produced in Pichia Pastoris*", Chem. Eng. J. **481**, 148418 (2024).
- C.-C. Chen, H. Li, J.-W. Huang, and R.-T. Guo*(郭瑞庭), "*Structural and Molecular Insights of Two Unique Enzymes Involved in the Biosynthesis of a Natural Halogenated Nitrile*", FEBS J. **291**, 5123 (2024).
- P.-Y. Chen, Y.-C. Chen, P.-P. Chen, K.-T. Lin, K. Sargsyan, C.-P. Hsu, W.-L. Wang, K.-C. Hsia, and S.-Y. Ting*(陳詩允), "*A Whole-cell Platform for Discovering Synthetic Cell Adhesionmolecules in Bacteria*", Nat. Commun. **15**, 6568 (2024).
- J.-Y. Hong, S.-C. Lin, K. Kehn-Hall, K.-M. Zhang, S.-Y. Luo, H.-Y. Wu, S.-Y. Chang, and M.-H. Hou*(侯明宏), "*Targeting Protein-protein Interaction Interfaces with Antiviral N Protein Inhibitor in SARS-CoV-2*", Biophys. J. **123**, 478 (2024).
- M.-H. Hou, C.-J. Chen, C.-S. Yang, Y.-C. Wang, and Y. Chen*(陳曄), "*Structural and Functional Characterization of Cyclic Pyrimidine-regulated Anti-phage System*", Nat. Commun. **15**, 5634 (2024).
- Y.-C. Hsieh, H.-H. Guan, C.-C. Lin, T.-Y. Huang, P. Chuankhayan, N.-C. Chen, N.-H. Wang, P.-L. Hu, Y.-C. Tsai, Y.-C. Huang, M. Yoshimura, P.-J. Lin, Y.-H. Hsieh*(謝義簧), and C.-J. Chen*(陳俊榮), "*Structure-based High-efficiency Homogeneous Antibody Platform by Endoglycosidase Sz Provides Insights into Its Transglycosylation Mechanism*", JACS Au **4**, 2130 (2024).
- Y. Kuan, H.-F. Chu, P.-H. Hsu, K.-C. Hsu, T.-H. Lin, C.-H. Huang*(黃駿翔), and W.-Y. Chen*(陳威儀), "*Disulfiram Inhibits Coronaviral Main Protease by Conjugating to Its Substrate Entry Site*", Int. J. Biol. Macromol. **276**, 133955 (2024).
- C.-C. Lee*(李政忠), W.-C. Kuo, Y.-W. Chang, S.-F. Hsu, C.-H. Wu, Y.-W. Chen, J.-J. Chang*(張瑞仁), and A. H.-J. Wang*(王惠鈞), "*Structure-based Development of a Canine TNF-α-specific Antibody Using Adalimumab as a Template*", Protein Sci. **33**, e4873 (2024).
  - M.-G. Lin, C.-Y. Yen, Y.-Y. Shen, Y.-S. Huang, I. W. Ng, D. Barillà, Y.-J. Sun* (孫玉珠), and C.-D. Hsiao*(蕭傳鐙), "*Unraveling the Structure and Function of a Novel SegC Protein Interacting with the SegAB Chromosome Segregation Complex in Archaea*", Nucleic Acids Res. **52**, 9966 (2024).
- J.-C. Tsou, C.-J. Tsou, C.-H. Wang, A.-L. A. Ko, Y.-H. Wang, H.-H. Liang, J.-C. Sun, K.-F. Huang, T.-P. Ko, S.-Y. Lin, and Y.-S. Wang*(王彥士), "*Site-specific Histidine Aza-michael Addition in Proteins Enabled by a Ferritin-based Metalloenzyme*", J. Am. Chem. Soc. **146**, 33309 (2024).
  - R.-H. Wang, P.-R. Chen, Y.-T. Chen, Y.-C. Chen, Y.-H. Chu, C.-C. Chien, P.-C. Chien, S.-Y. Lo, Z.-L. Wang, M.-C. Tsou, S.-Y. Chen, G.-S. Chiu, W.-L. Chen, Y.-H. Wu, L.-H. Ching, W.-C. Wang, S.-Y. Lin, H.-J. Kung, L.-H. Wang* (王陸海), H.-C. Cheng*(鄭惠春), and K.-T. Lin*(林愷悌), "*Hydrogen Sulfide Coordinates Glucose Metabolism Switch Through Destabilizing Tetrameric Pyruvate Kinase M2*", Nat. Commun. **15**, 7463 (2024).
  - S. Wang, C.-H. Huang, T.-S. Lin, Y.-Q. Yeh, Y.-S. Fan, S.-W. Wang, H.-C. Tseng, S.-J. Huang, Y.-Y. Chang, U.-S. Jeng, C.-I. Chang, and S.-R. Tzeng* (曾秀如), "*Structural Basis for Recruitment of Peptidoglycan Endopeptidase MepS by Lipoprotein NlpI*", Nat. Commun. **15**, 5461 (2024).
- Z.-Z. Wang, J. Weng, J. Qi, X.-X. Fu, B.-B. Xing, Y. Hu, C.-H. Huang, C.-Y. Chen, and Z. Wei*(魏子貢), "*Structure-guided Discovery of Novel dUTPase Inhibitors with Anti-nocardia Activity by Computational Design*", J. Enzym. Inhib. Med. Chem. **39**, 2411573 (2024).
- Y. Wu, Y. Yang, G. Lu, W.-L. Xiang, T.-Y. Sun, K.-W. Chen, X. Lv, Y.-F. Gui, R.-Q. Zeng, Y.-K. Du, C.-H. Fu, J.-W. Huang, C.-C. Chen, R.-T. Guo*(郭瑞庭), and L.-J. Yu*(余龍江), "*Unleashing the Power of Evolution in Xylanase Engineering: Investigating the Role of Distal Mutation Regulation*", J. Agr. Food Chem. **72**, 18201 (2024).

TPS 09A Temporally Coherent X-ray Diffraction

- S. Abbas, B. Jarwal, T.-T. Ho, S. M. Valiyaveettil, C.-R. Hsing, T.-L. Chou, C.-M. Wei, L.-C. Chen*(林麗瓊), and K.-H. Chen*(陳貴賢), "*Synergistic Effect of Indium Doping on Thermoelectric Performance of Cubic GeTe-based Thin Films*", Mater. Today Phys. **49**, 101581 (2024).
- C.-S. Cai, W.-Y. Lai, P.-H. Liu, T.-C. Chou, R.-Y. Liu, C.-M. Lin, S. Gwo, and W.-T. Hsu*(徐瑋廷), "*Ultralow Auger-assisted Interlayer Exciton Annihilation in WS_2/WSe_2 Moiré Heterobilayers*", Nano Lett. **24**, 2773 (2024).
- S.-L. Chen, T.-S. Wu, H.-L. Huang, S.-F. Chen, Y.-L. Soo, H.-T. Jeng, and H.-H. Hung*(洪雪行), "*Polarized X-ray Diffraction Anomalous Near-edge Structure Study on the Orbital Physics of Thin WSe_2 Layers*", J. Appl. Crystallogr. **57**, 344 (2024).
- H.-C. Chu, C.-M. Hung, H.-C. Huang, S.-C. Weng, B.-H. Lin, S. Yang, Y.-H. Wu, K.-H. Chang, J.-J. Shyue, P.-T. Chou*(周必泰), and C.-M. Jiang*(姜昌明), "*Hydrogen Plasma Treatment Compensates for the Intrinsic Defects in $Cs_2AgBiBr_6$ Thin Films*", J. Phys. Chem. C **128**, 20441 (2024).
- M. N. Duong, Y.-X. Chen, W.-Y. Tzeng, T. Amrillah, S. Yang, C.-E. Liu, D. Z. Dimitrov, S.-C. Haw, C.-H. Hsu, J.-M. Chen*(陳錦明), J.-Y. Lin, K.-H. Wu, C.-W. Luo, C.-T. Chen, C.-Y. Kuo*(郭昌洋), and J.-Y. Juang*(莊振益), "*Orbital Ordering and Ultrafast Carrier Dynamics Anisotropies in Orientation-engineered Orthorhombic $YMnO_3$ Films*", APL Mater. **12**, 021117 (2024).
- S. Hegde, V. Sridhar, R. S. Chen, and S. Chattopadhyay*(薛特), "*Gradient Dion-Jacobson Phase Stable Quasi-2D Perovskite@Graphene Hybrid for High Responsivity Photodetectors*", Adv. Opt. Mater. **12**, 2400232 (2024).
- C.-H. Huang, C. S. Gantepogu, P.-J. Chen, T.-H. Wu, W.-R. Liu, K.-H. Lin, C.-L. Chen, T.-K. Lee, M.-J. Wang*(王明杰), and M.-K. Wu, "*Substrate Charge Transfer Induced Ferromagnetism in MnSe/$SrTiO_3$ Ultrathin Films*", Nanomaterials **14**, 1355 (2024).
- D. C. Kakarla*, Y.-H. Ku, H. C. Wu, C. C. Chen, M. Y. Hsu, T. R. Hu, J.-Y. Lin, N. Puri, M.-J. Hsieh, C. W. Wang, W.-H. Li, Dhanasekhar C, A. Tiwari, C. H. Lu, K. J. You, T. W. Kuo, K. J. Fan, Y. C. Chang, and H. D. Yang* (楊弘敦), "*Exploring New Members of Magnetoelectric Materials in CuO-$CuCl_2$-SeO_2 System*", Mater. Today Phys. **46**, 101527 (2024).
- U. Kar, E. C.-H. Lu, A. K. Singh, P. V. S. Reddy, Y. Han, X. Li, C.-T. Cheng, S. Yang, C.-Y. Lin, I.-C. Cheng, C.-H. Hsu, D. Hsieh, W.-C. Lee, G.-Y. Guo* (郭光宇), and W.-L. Lee*(李偉立), "*Nonlinear and Nonreciprocal Transport Effects in Untwinned Thin Films of Ferromagnetic Weyl Metal $SrRuO_3$*", Phys. Rev. X **14**, 011022 (2024).
- C. Li, J. Wang*(王佳), J. Zhao, G. Gao, K.-H. Wu, B.-J. Su, J.-M. Chen, Y. Xi, Z. Huang, Y. Qiao, and F. Li*(李福偉), "*Construction of Synergistic Co/CoO Interface to Enhance Hydrogenation Activity of Ethyl Lactate to 1,2-propanediol*", Chem.-Asian J. **19**, e202301103 (2024).
- C. E. Liu, C. N. Wu, J. Falke, C. F. Chang, C.-Y. Kuo, S. Yang, J. Y. Juang, C. Koz, U. Schwarz, C. T. Chen, L. H. Tjeng, and S. G. Altendorf*, "*In Situ X-ray Absorption and Photoelectron Spectroscopy on Epitaxial Fe_xTe Thin Films with a Wide Range of Fe/Te Compositions*", Phys. Rev. B **110**, 245139 (2024).
- Y.-C. Liu, B.-C. Chen, C.-C. Wei, S.-Z. Ho, Y.-D. Liou, P. Kaur, Rahul, Y.-C. Chen, and J.-C. Yang*(楊展其), "*Thickness-dependent Ferroelectricity in Freestanding $Hf_{0.5}Zr_{0.5}O_2$ Membranes*", ACS Appl. Electron. Mater. **6**, 8617 (2024).
- N. N. Quyen, W.-Y. Tzeng, C.-E. Hsu, I.-A. Lin, W.-H. Chen, H.-H. Jia, S.-C. Wang, C.-E. Liu, Y.-S. Chen, W.-L. Chen, T.-L. Chou, I.-T. Wang, C.-N. Kuo, C.-L. Lin, C.-T. Wu, P.-H. Lin, S.-C. Weng, C.-M. Cheng, C.-Y. Kuo, C.-M. Tu, M.-W. Chu, Y.-M. Chang, C. S. Lue*(呂欽山), H.-C. Hsueh*(薛宏中), and C.-W. Luo*(羅志偉), "*Three-dimensional Ultrafast Charge-density-wave Dynamics in CuTe*", Nat. Commun. **15**, 2386 (2024).
- S. Y. Tsai, P.-H. Tseng, C. C. Chen, C.-M. Huang, H.-W. Yen, Y.-S. Chen, K.-L. Lin, R. Niu, Y.-S. Lai, and F.-H. Ko*(柯富祥), "*Lattice Boundary Enhancement on Thermoelectric Behaviors of Heavily Boron-doped Silicon for Energy Harvesting: Electrical versus Thermal Conductivity*", Adv. Mater. Interfaces **11**, 2400536 (2024).
- P.-H. Tseng, Y.-S. Lai*(賴宇紳), M.-Y. Li, C.-M. Huang, S.-Y. Tsai, K. Y.-J. Hsu, and F.-H. Ko*(柯富祥), "*Sustainable Solar-powered Hydrogen Generation with a Silicon Nanopillar Device with a Low Carbon Footprint*", Int. J. Hydrogen Energ. **68**, 1322 (2024).
- C.-C. Wang and C.-H. Lee*(李志浩), "*Wafer-scale Epitaxial Molybdenum Disulfide Ultrathin Film on Sapphire Prepared by Low-energy Reactive Magnetron Sputtering*", Appl. Surf. Sci. **659**, 159889 (2024).
- W.-L. Wei, C.-Y. Lin, T.-C. Huang, Y.-C. Li, Y.-H. Wu, C.-Y. Lee, B.-Y. Chen, G.-C. Yin, M.-T. Tang, W.-C. Chou, F.-Y. Lo*(駱芳鈺), and B.-H. Lin*

(林碧軒), "*Structural and Optical Properties of Eu-doped ZnO Epitaxial Thin Films Grown by Pulsed-laser Deposition*", APL Mater. **12**, 111112 (2024).

TPS 13A Biological Small-angle X-ray Scattering

- C.-Y. Chang, G.-M. Manesi, W.-E. Wang, Y.-C. Hung, A. Avgeropoulos, and R.-M. Ho*(何榮銘), "*Frank-Kasper-like Network Phase from Self-assembly of High-χ star-block Copolymers*", Sci. Adv. **10**, eado4786 (2024).
- J.-W. Chang, K.-H. Su, C.-W. Pao, J.-J. Tsai, C.-J. Su, J.-L. Chen, L.-M. Lyu, C.-H. Kuo, A.-C. Su, H.-C. Yang*(楊小青), Y.-H. Lai*(賴英煌), and U.-S. Jeng* (鄭有舜), "*Arrayed Pt Single Atoms via Phosphotungstic Acids Intercalated in Silicate Nanochannels for Efficient Hydrogen Evolution Reactions*", ACS Nano **18**, 1611 (2024).
- Y.-J. Chang, K.-T. Lin, O. Shih, C.-H. Yang, C.-Y. Chuang, M.-H. Fang, W.-B. Lai, Y.-C. Lee, H.-C. Kuo, S.-C. Hung, C.-K. -K., U.-S. Jeng, and Y.-R. Chen* (陳韻如), "*Sulfated Disaccharide Protects Membrane and DNA Damages from Arginine-rich Dipeptide Repeats in ALS*", Sci. Adv. **10**, eadj0347 (2024).
- C.-C. Chen, Y.-R. Huang, Y. T. Chan, H.-Y. Lin, H.-J. Lin, C.-D. Hsiao, T.-P. Ko, T.-W. Lin, Y.-H. Lan, H.-Y. Lin, and H.-Y. Chang*(張欣暘), "*A Distinct Dimer Configuration of a Diatom Get3 Forming a Tetrameric Complex with Its Tail-anchored Membrane Cargo*", BMC Biol. **22**, 136 (2024).
- H. Cheng, R. K. Devi, K.-Y. Huang, M. Ganesan, S. K. Ravi, and C. C. Lin* (林群哲), "*Highly Biocompatible Antibacterial Hydrogel for Wearable Sensing of Macro and Microscale Human Body Motions*", Small **20**, 2401201 (2024).
- W.-C. Chiu, Y.-H. Cheng, J.-H. Lin, C.-H. Tung, T. Nishimura, C.-Y. Chen, T. Isono*, T. Satoh, and H.-L. Chen*(陳信龍), "*Tuning the Complex Spherical Phase of Sugar-based Block Co-oligomer via Single-monomer-mediated Composition Variation*", Macromolecules **57**, 6076 (2024).
- Y.-H. Chiu, T.-Y. Huang, K.-T. Lin, K.-C. Wan, Y.-H. Huang, Y.-P. Yang, C.-T. He, H.-Y. Wei, T.-C. Hsu, C.-J. Su, C.-A. Wang, Y.-C. Huang, J. Ruan, U.-S. Jeng, and B. B. Y. Hsu*(徐邦昱), "*Optimizing Dynamic Degrees of Freedom of Solution-processed Semiconducting Polymers to form Long-range Order*", MRS Commun. **14**, 1395 (2024).
- K.-C. Chu, C.-H. Yeh, J.-M. Lin, C.-Y. Chen, C.-Y. Cheng, Y.-Q. Yeh, Y.-S. Huang, and Y.-W. Tsai*(蔡一葦), "*Using Convolutional Neural Network Denoising to Reduce Ambiguity in X-ray Coherent Diffraction Imaging*", J. Synchrotron Radiat. **31**, 1340 (2024).
- W.-T. Chuang*(莊偉綜), S.-P. Chen, Y.-B. Tsai, Y.-S. Sun, J.-M. Lin, C.-Y. Chen, Y.-W. Tsai, C.-M. Chou, Y.-C. Hung*(洪毓珏), T.-W. Chen, W.-E. Wang, C.-C. Huang, P.-D. Hong*(洪伯達), U.-S. Jeng, and Y.-W. Chiang, "*Spontaneous Photonic Jammed Packing of Core-shell Colloids in Conductive Aqueous Inks for Non-iridescent Structural Coloration*", ACS Appl. Mater. Interfaces **16**, 52856 (2024).
- T. T. K. Cuc, C.-H. Hung, T.-C. Wu, P. Q. Nhien, T. M. Khang, B. T. B. Hue, W.-T. Chuang, and H.-C. Lin*(林宏洲), "*Force-activated Ratiometric Fluorescence Switching of Tensile Mechano-fluorophoric Polyurethane Elastomers with Enhanced Toughnesses Improved by Mechanically Interlocked [c2] Daisy Chain Rotaxanes*", Chem. Eng. J. **485**, 149694 (2024).
- M. H. Elsayed, M. Abdellah, A. Z. Alhakemy, I. M. A. Mekhemer, A. E. A. Aboubakr, B.-H. Chen, A. Sabbah, K.-H. Lin, W.-S. Chiu, S.-J. Lin, C.-Y. Chu, C.-H. Lu, S.-D. Yang, M. G. Mohamed, S.-W. Kuo, C.-H. Hung, L.-C. Chen, K.-H. Chen, and H.-H. Chou*(周鶴修), "*Overcoming Small-bandgap Charge Recombination in Visible and NIR-light-driven Hydrogen Evolution by Engineering the Polymer Photocatalyst Structure*", Nat. Commun. **15**, 707 (2024).
- P.-C. Han, C.-H. Chuang, S.-W. Lin, X. Xiang, Z. Wang*(王早銘), M. Kuzumoto, S. Tokuda, T. Tateishi, A. Legrand, M. Y. Tsang, H.-C. Yang, K. C.-W. Wu*(吳嘉文)., K. Urayama, D.-Y. Kang*(康敦彥), and S. Furukawa* (古川修平), "*Phase-transformable Metal-organic Polyhedra for Membrane Processing and Switchable Gas Separation*", Nat. Commun. **15**, 9523 (2024).
- S.-H. Hong, C.-C. Hsu, T.-H. Liu, T.-C. Lee, S.-H. Tung, H.-L. Chen, J. Yu* (游佳欣), and C.-L. Liu*(劉振良), "*Extremely Large Seebeck Coefficient of Gelatin Methacryloyl (GelMA)-based Thermogalvanic Cells by the Dual Effect of Ion-induced Crystallization and Nanochannel Control*", Mater. Today Energy **42**, 101546 (2024).
- C.-C. Hsu, Y.-T. Lin, S.-H. Hong, U.-S. Jeng, H.-L. Chen, J. Yu, and C.-L. Liu*(劉振良), "*3D Printed Gelatin Methacrylate Hydrogel-based Wearable Thermoelectric Generators*", Adv. Sustain. Syst. **8**, 2400039 (2024).
- T.-F. Huang, J.-J. Liu, Z.-Y. Lai, J.-W. Chang, Y.-R. Zhuang, Z.-C. Jiang, C.-L. Chang, W.-C. Lin, Y.-H. Chen, Y.-H. Wu, Y.-E. Sun, T.-A. Luo, Y.-K. Chen, J.-C. Yen, H.-K. Hsu, B.-H. Chen, L.-Y. Ting, C.-Y. Lu, Y.-T. Lin, L.-Y. Hsu, T.-L. Wu, S.-D. Yang, A.-C. Su, U.-S. Jeng*(鄭有舜), and H.-H. Chou* (周鶴修), "*Performance and Solution Structures of Side-chain-bridged Oligo (Ethylene Glycol) Polymer Photocatalysts for Enhanced Hydrogen Evolution under Natural Light Illumination*", Small **20**, 2304743 (2024).
- B. A. Junisu, Y.-S. Sun*(孫亞賢), C. M. Septani, and O. Shih, "*$CsPbBr_3$ Nanocrystals Prepared Using Block Copolymer Micelles for LEDs*", ACS Appl. Nano Mater. **7**, 27745 (2024).
- S. Kenny, C.-H. Lai, T.-S. Chiang, K. Brown, C. S. Hewitt, A. D. Krabill, H.-T. Chang, Y.-S. Wang, D. P. Flaherty, S.-T. D. Hsu*(徐尚德), and C. Das*, "*Altered Protein Dynamics and a More Reactive Catalytic Cysteine in a Neurodegeneration-associated UCHL1 Mutant*", J. Mol. Biol. **436**, 168438 (2024).
- L.-C. Lee, K.-T. Huang, Y.-T. Lin, U.-S. Jeng, C.-H. Wang, S.-H. Tung, C.-J. Huang*(黃俊仁), and C.-L. Liu*(劉振良), "*A pH-sensitive Stretchable Zwitterionic Hydrogel with Bipolar Thermoelectricity*", Small **20**, 2311811 (2024).
- J. M. Liao, S.-T. Hong, Y.-T. Wang, Y.-A. Cheng, K.-W. Ho, S.-I. Toh, O. Shih, U.-S. Jeng, P.-C. Lyu, I.-C. Hu, M.-Y. Huang, C.-Y. Chang*(張晉源), and T.-L. Cheng*(鄭添祿), "*Integrating Molecular Dynamics simulation with Small- and Wide-angle X-ray Scattering to Unravel the Flexibility, Antigen-blocking, and Protease-restoring Functions in a Hindrance-based Pro-antibody*", Protein Sci. **33**, e5124 (2024).
- H.-Y. Lin, B.-J. Zhong, H.-J. Liu, Y.-K. Wu, C.-H. Peng, and C.-L. Wang* (王建隆), "*Optimal Compositions in the NDI: Pyrene Charge-transfer Complexes Revealed by Thermal Analysis and Structural Characterizations*", Cryst. Growth Des. **24**, 2833 (2024).
- P.-H. Lin, G.-W. Wu, Y.-H. Lin, J.-R. Huang, U.-S. Jeng, W.-M. Liu*(劉維民), and J.-R. Huang*(黃介嶸), "*TDP-43 Amyloid Fibril Formation via Phase Separation-related and -Unrelated Pathways*", ACS Chem. Neurosci. **15**, 3767 (2024).
- S.-W. Lin, P. K. Lam, C.-T. Wu, K.-H. Su, C.-F. Sung, S.-R. Huang, J.-W. Chang, O. Shih, Y.-Q. Yeh, T. H. Vo, H.-K. Tsao, H.-T. Hsieh, U.-S. Jeng* (鄭有舜), F.-K. Shieh*(謝發坤), and H.-C. Yang*(楊小青), "*Decoding the Biomimetic Mineralization of Metal-organic Frameworks in Water*", ACS Nano **18**, 25170 (2024).
- T.-C. Lin, O. Shih, T.-Y. Tsai, Y.-Q. Yeh, K.-F. Liao, B. W. Mansel, Y.-J. Shiu, C.-F. Chang, A.-C. Su, Y.-R. Chen*(陳韻如), and U.-S. Jeng*(鄭有舜), "*Binding Structures of SERF1a with NT17-polyQ Peptides of Huntingtin Exon 1 Revealed by SEC-SWAXS, NMR and Molecular Simulation*", IUCrJ **11**, 849 (2024).
- Y.-T. Lin, C.-C. Hsu, S.-H. Hong, L.-C. Lee, U.-S. Jeng, H.-L. Chen, S.-H. Tung, and C.-L. Liu*(劉振良), "*Highly Conductive Triple Network Hydrogel Thermoelectrochemical Cells with Low-grade Heat Harvesting*", J. Power Sources **609**, 234647 (2024).
- M. N. Pham, C.-J. Su, Y.-C. Huang, K.-T. Lin, T.-Y. Huang, Y.-Y. Lai, C.-A. Wang, Y.-K. Liaw, T.-H. Lin, K.-C. Wan, C.-T. He, Y.-H. Huang, Y.-P. Yang, H.-Y. Wei, U.-S. Jeng, J. Ruan, C. Luo, Y. Huang, G. C. Bazan, and B. B. Y. Hsu*(徐邦昱), "*Forming Long-range Order of Semiconducting Polymers through Liquid-phase Directional Molecular Assemblies*", Macromolecules **57**, 3544 (2024).
- S. F. Solari, A. Wieczorek, T. Marcato, M. Wörle, F. Krumeich, Y.-T. Li, Y.-C. Chiu, S. Siol*, S. B. Shivarudraiah*, and C.-J. Shih*(施智仁), "*Stabilization of Quantum-confined Anisotropic $CsPbI_3$ Nanoplatelets by Solid-phase Metal Iodide Crude Reaction for Color-pure Red Emission*", Adv. Opt. Mater. **12**, 2401048 (2024).
- M. K. Sriramoju, K.-T. Ko, and S.-T. D. Hsu*(徐尚德), "*Tying a True Topological Protein Knot by Cyclization*", Biochem. Biophy. Res. Co. **696**, 149470 (2024).
- Y.-S. Sun*(孫亞賢), W.-Y. Hu, P. Chung, K.-W. Wu, O. Shih, and W.-T. Chuang, "*Poly(ethylene oxide) Crystallization and Gelation in Butanol Studied by In Situ SAXS/WAXD*", Macromolecules **57**, 3304 (2024).
- Y.-S. Sun*(孫亞賢), K.-W. Wu, and O. Shih, "*Tuning Perovskite Nanocrystal Synthesis via Amphiphilic Block Copolymer Templates and Solvent Interactions*", ACS Appl. Mater. Interfaces **16**, 62664 (2024).
- C.-L. Tsai, J.-W. Chang, K.-Y. Cheng, Y.-J. Lan, Y.-C. Hsu, Q.-D. Lin, T.-Y. Chen, O. Shih, C.-H. Lin, P.-H. Chiang, M. Simenas, V. Kalendra, Y.-W. Chiang*(江昀緯), C.-H. Chen*(陳俊顯), U.-S. Jeng*(鄭有舜), and S.-K. Wang*(王聖凱), "*Comprehensive Characterization of Polyproline Trihelix Macrocyclic Nanoscaffolds for Predictive Ligand Positioning*", Nanoscale Adv. **6**, 947 (2024).
- Y.-X. Tsai, N.-E. Chang, K. Reuter, H.-T. Chang, T.-J. Yang, S. von Bulow, V. Sehrawat, N. Zerrouki, M. Tuffery, M. Gecht, I. L. Grothaus, L. C. Ciacchi, Y.-S. Wang, M.-F. Hsu, K.-H. Khoo, G. Hummer, S.-T. D. Hsu*(徐尚德), C. Hanus*, and M. Sikora*, "*Rapid Simulation of Glycoprotein Structures by Grafting and Steric Exclusion of Glycan Conformer Libraries*", Cell **187**, 1296 (2024).
- S. Wang, C.-H. Huang, T.-S. Lin, Y.-Q. Yeh, Y.-S. Fan, S.-W. Wang, H.-C. Tseng, S.-J. Huang, Y.-Y. Chang, U.-S. Jeng, C.-I. Chang, and S.-R. Tzeng*

(曾秀如), "*Structural Basis for Recruitment of Peptidoglycan Endopeptidase MepS by Lipoprotein NlpI*", Nat. Commun. **15**, 5461 (2024).

- Y.-J. Xue, Z.-Y. Lai, H.-C. Lu, J.-C. Hong, C.-L. Tsai, C.-L. Huang, K.-H. Huang, C.-F. Lu, Y.-Y. Lai, C.-S. Hsu, J.-M. Lin, J.-W. Chang, S.-Y. Chien, G.-H. Lee, U.-S. Jeng*(鄭有舜), and Y.-J. Cheng*(鄭彥如), "*Unraveling the Structure-property-performance Relationships of Fused-ring Nonfullerene Acceptors: Toward a C-shaped Ortho-benzodipyrrole-based Acceptor for Highly Efficient Organic Photovoltaics*", J. Am. Chem. Soc. **146**, 833 (2024).
- H.-W. Yeh, P.-P. Chen, T.-C. Yeh, S.-L. Lin, Y.-T. Chen, W.-P. Lin, Ting Chen, J. M. Pang, K.-T. Lin, L. H-C. Wang, Y.-C. Lin, O. Shih, U.-S. Jeng, K.-C. Hsia, and H.-C. Cheng*(鄭惠春), "*Cep57 Regulates Human Centrosomes through Multivalent Interactions*", P. Natl. Acad. Sci. USA **121**, e2305260121 (2024).

TPS 19A High-resolution Powder X-ray Diffraction

- J. A. V. Bilo, C.-K. Chang, Y.-C. Chuang, and M.-H. Fang*(方牧懷), "*Coprecipitation Strategy for Halide-based Solid-state Electrolytes and Atmospheric-dependent In Situ Analysis*", ACS Appl. Mater. Interfaces **16**, 27394 (2024).
- C.-C. Bill, C.-K. Chang, S.-Y. Chien, and C.R. Kao*(高振宏), "*Low-temperature Phase Equilibria of the Ternary Cu-In-Sn System at In-rich Corner*", Materialia **36**, 102154 (2024).
- L.-X. Chang, P. Rajamanickam, L.-C. Hsu, C.-K. Chang, Y.-C. Chuang, J.-L. Chen, L.-C. Hsu, and C.-Y. Wang*(王誠佑), "*Metal-organic Framework-derived Carbon-supported High-entropy Alloy Nanoparticles Applied in Ammonia Borane Hydrolytic Dehydrogenation*", J. Catal. **437**, 115663 (2024).
- P.-S. Chang, B.-H. Chen, Y.-C. Lin, W.-T. Dai, G. Kumar, Y.-G. Lin, and M. H. Huang*(黃暄益), "*Growth of Size-tunable Ag_2O Polyhedra and Revelation of Their Bulk and Surface Lattices*", Small **20**, 2401558 (2024).
- Y. H. Chang, A. Pal*, P. T. W. Yen, C. W. Wang, S. Giri, G. R. Blake, J. Gainza, M.-J. Hsieh, J.-Y. Lin, C. Y. Huang, Y. J. Chen, T. W. Kuo, A. Tiwari, D. C. Kakarla, and H. D. Yang*(楊弘敦), "*Field-induced Transformation of Complex Spin Ordering and Magnetodielectric and Magnetoelastic Coupling in $MnGeTeO_6$*", Phys. Rev. B **110**, 064405 (2024).
- Y.-C. Chang, L.-M. Lyu, R.-S. Tsai, R.-H. Juang, S.-H. Yu, C.-S. Li, J.-L. Chen, and C.-H. Kuo*(郭俊宏), "*Pt-1,1´-Bi(2-naphthol) Nanostructures for Electrochemical H_2 Evolution in Alkaline Media*", ACS Appl. Nano Mater. **7**, 11890 (2024).
- J.-H. Chen*(陳經函), T. P. Chhetri, A. T. Grant, X. Bai, Q. Zhang, C.-K. Chang, D. P. Young, I. Dubenko, S. Talapatra, N. Ali, and S. Stadler, "*Controlling Phase Transitions in MnNiGe Using Thermal Quenching and Hydrostatic Pressure*", J. Phys. D- Appl. Phys. **57**, 205003 (2024).
- B. D. Dandena, D.-S. Tsai, S.-H. Wu, W.-N. Su*(蘇威年), and B. J. Hwang*(黃炳照), "*Roles of Cation-doped Li-argyrodite Electrolytes on the Efficiency of All-solid-state-lithium Batteries*", Energy Storage Mater. **69**, 103305 (2024).
- Z. Guo, W. Jiang*(姜薇薇), C.-Z. Liao, C.-K. Chang, C. Zou, W. Ding, Y.-M. Kang*, and J. Zhang*(張吉亮), "*Heterogeneous Conversion Reaction of Hexagonal NiO Anode toward Its Reversible Electrochemical Cycling for Li-ion Batteries*", J. Power Sources **615**, 235081 (2024).
- I. Habib, C.-W. Pao, Y.-C. Chuang, and W.-F. Liaw*(廖文峯), "*Dinitrosyl Iron Complex-derived Nanosized Zerovalent Iron (NZVI) as a Template for the Fe-Co Cracked NZVI: An Electrocatalyst for the Oxygen Evolution Reaction*", Inorg. Chem. **63**, 784 (2024).
- A. G. Hailemariam, Z. Syum, T. T. Mamo, M. Qorbani*, C.-R. Hsing*(邢正蓉), A. Sabbah, S. Quadir, K. S. Bayikadi, H.-L. Wu*(吳恆良), C.-M. Wei, L.-C. Chen*(林麗瓊), and K.-H. Chen*(陳貴賢), "*Oxygen-incorporated Lithium-rich Iron Sulfide Cathodes for Li-ion Batteries with Boosted Material Stability and Electrochemical Performance*", Chem. Mater. **36**, 9370 (2024).
- L. Han*(韓麗麗), C. Sun, H.-T. Wang*(王孝祖), W.-X. Lin, J.-L. Chen, C.-W. Pao, Y.-C. Chuang, C.-H. Wang, J. Zhou, J. Wang, W.-F. Pong, and H. L. Xin*(忻獲麟), "*Interrogation of 3d Transition Bimetallic Nanocrystal Nucleation and Growth Using In Situ Electron Microscope and Synchrotron Xray Techniques*", Nano Lett. **24**, 7645 (2024).
- P.-C. Han, C.-H. Chuang, S.-W. Lin, X. Xiang, Z. Wang*(王早銘), M. Kuzumoto, S. Tokuda, T. Tateishi, A. Legrand, M. Y. Tsang, H.-C. Yang, K. C.-W. Wu*(吳嘉文)., K. Urayama, D.-Y. Kang*(康敦彥), and S. Furukawa*(谷川修平), "*Phase-transformable Metal-organic Polyhedra for Membrane Processing and Switchable Gas Separation*", Nat. Commun. **15**, 9523 (2024).
- R. F. H. Hernandha, B. Umesh, J. Patra, C.-Y. Chen, J. Li, and J.-K. Chang*(張仍奎), "*Core-shell Si@SiOC Particles Synthesized Using Supercritical Carbon Dioxide Fluid for Superior Li-ion Storage Performance*", Adv. Sci. **11**, 2401350 (2024).
- Y.-Y. Hsieh, Y.-C. Chuang, and H.-Y. Tuan*(段興宇), "*Unraveling Dual Mechanisms in Quasi-layered Bi_2O_2Se via Defect Modulation for High-performance Aqueous Zn-Ion Batteries*", Adv. Funct. Mater. **34**, 2406975 (2024).
- F. H. Hsu*(許峰豪), S. Y. Hsu, R. Subramani, T. C. Cheng, B. H. Chen, J. L. Chen, J. M. Chen*(陳錦明), and K. T. Lu*(盧桂子), "*The Ion Behavior and Storage Mechanism of 2D MoO_3 Layer Structure in an Air-stable Hydrated Eutectic Electrolyte for Aluminum-ion Energy Storage*", J. Energy Storage **84**, 110693 (2024).
- Z. Huangfu, T. Yang, S. Ma, K. Wang, K. Shih, W. Yang, and C. Liao*(廖長忠), "*High Valency of Charge Compensator (Mo^{6+}) to Substitute Ti Site in REE Doped Zirconolite (REE=Nd, Sm, Gd, Ho and Yb): Solid Solubility, Phase Evolution and Structural Analysis*", Ceram. Int. **50**, 26351 (2024).
- B. Jarwal, S. Abbas, T.-L. Chou, S. M. Vailyaveettil, A. Kumar, S. Quadir, T.-T. Ho, D. P. Wong, L.-C. Chen*(林麗瓊), and K.-H. Chen*(陳貴賢), "*Boosting Thermoelectric Performance in Nanocrystalline Ternary Skutterudite Thin Films through Metallic $CoTe_2$ Integration*", ACS Appl. Mater. Interfaces **16**, 14770 (2024).
- B.-H. Kao, Y.-F. Zeng, Y.-C. Lee, C.-W. Pao, J.-L. Chen, Y.-C. Chuang, H.-S. Sheu, F.-T. Tsai*(蔡富浔), and W.-F. Liaw*(廖文峯), "*Unveiled the Structure-selectivity Relationship for Carbon Dioxide Reduction Triggered by Bi-doped Cu-based Nanocatalysts*", Small **20**, 2307910 (2024).
- H. Li, S.-C. Huang, S.-Y. Chen, J. Wu, H.-Y. Chen*(陳翰儀), and C.-J. Tsai*(蔡哲正), "*Effect of Fe and Zn Co-doping on $LiCoPO_4$ Cathode Materials for High-voltage Lithium-ion Batteries*", J. Colloid Interf. Sci. **669**, 117 (2024).
- M.-W. Liao, T.-K. Chin, X.-F. Luo, Y.-C. Chuang, and T.-P. Perng*(彭宗平), "*Formation Characteristics of Pt-Ni Alloy Nanoparticles Fabricated by Nanolamination of Atomic Layer Deposition in Hydrogen*", Small **20**, 2404943 (2024).
- Y. Liu, J. A. McLeod, L.-Y. Chang, C.-K. Chang, Y. Jiang, Z. Wang, A. Lefebvre, X. Chen, and L. Liu*(劉儷佳)., "*The Effect of Annealing Temperature on the Site Occupancy and the Persistent Luminescence of Mn^{2+}-doped Magnesium Germanate*", Mater. Today Comm. **38**, 108080 (2024).
- D. Lu, J. Zhang, H. Zhao, M. Pi, X. Ye, Z. Liu, X. Wang, X. Zhang, Z. Pan, S.-Y. Hsu, C.-K. Chang, J.-M. Chen, Z. Hu, and Y. Long*(龍有文), "*Robust Crystal Phase Separation with Distinct Charge, Orbital, and Spin Orders in $AgMn_7O_{12}$*", Inorg. Chem. **63**, 3191 (2024).
- L.-M. Lyu, H.-J. Li, R.-S. Tsai, C.-F. Chen, Y.-C. Chang, Y.-C. Chuang, C.-S. Li, J.-L. Chen, T.-W. Chiu*(邱德威), and C.-H. Kuo*(郭俊宏), "*In Operando X-ray Spectroscopic and DFT Studies Revealing Improved H_2 Evolution by the Synergistic Ni-Co Electron Effect in the Alkaline Condition*", ACS Appl. Mater. Interfaces **16**, 27329 (2024).
- S. Ma, K.-M. Leung, C. Liao*(廖長忠), C.-K. Chang, Y. Zhou, S. Chen, X. Zhao, Q. Zhao, and K. Shih*(施凱閔), "*Green Conversion of Waste Alkaline Battery Material to Zeolitic Imidazolate Framework-8 and Its Iodine Capture Mechanism*", J. Hazard. Mater. **469**, 133612 (2024).
- N. Majewska, M.-H. Fang, and S. Mahlik*, "*Photoelectric Studies as the Key to Understanding the Nonradiative Processes in Chromium Activated NIR Materials*", J. Am. Chem. Soc. **146**, 22807 (2024).
- T. Natarajan, S. Arumugam, Y.-F. Tsai, A. Abou-taleb, and S. S.-F. Yu*(俞聖法), "*Unveiling the Enhanced Electrochemical CO_2 Conversion: The Role of 3D Porous BiOCl with Defects and CTAB-mediated Nanosheets*", J. CO2 Util. **85**, 102888 (2024).
- R. Subramani, S.-Y. Hsu, Y.-C. Chuang, L.-C. Hsu, K.-T. Lu*(盧桂子), and J.-M. Chen*(陳錦明), "*Fe-MIL-101 Metal Organic Framework Integrated Solid Polymer Electrolytes for High-performance Solid-state Lithium Metal Batteries*", J. Mater. Chem. A **12**, 7132 (2024).
- B. W. Taklu, W.-N. Su*(蘇威年), J.-C. Chiou, C.-Y. Chang, Y. Nikodimos, K. Lakshmanan, T. M. Hagos, G. G. Serbessa, G. B. Desta, T. M. Tekaligne, S. A. Ahmed, S.-C. Yang, S.-H. Wu, and B. J. Hwang*(黃炳照), "*Mechanistic Study on Artificial Stabilization of Lithium Metal Anode via Thermal Pyrolysis of Ammonium Fluoride in Lithium Metal Batteries*", ACS Appl. Mater. Interfaces **16**, 17422 (2024).
- Y. Tian, Z. Tao, C. Liu, M. Sun, C. Chang, Q. Gu*(顧勤奮), L. Li*(李良春), and J. Shang*(尚進), "*Adjusting Gate-opening Behavior in a Rigid Cage-type "Molecular Trapdoor" Metal-organic Framework via Anion Modulation*", Chem. Eng. J. **486**, 150293 (2024).
- Y. Tian, Z. Tao, M. Sun, T. Wang, L. Li*(李良春), Q. Gu*(顧勤奮), and J. Shang*(尚進), "*Tunable Gas Admission via a "Molecular Trapdoor" Mechanism in a Flexible Cationic Metal-organic Framework Featuring 1D Channels*", Small **20**, 2400064 (2024).
- Y.-F. Tsai, P.-C. Wei*(魏百駿), N.-T. Tsou, Y.-C. Chao, H.-W. Yen, J.-Y. Lin, K.-K. Wang, and H.-J. Wu*(吳欣潔), "*Grand Herringbone Architecture Securing the High Thermoelectric Performance of GeTe*", Mater. Today Phys. **41**, 101329 (2024).

- Y.-F. Tsai, Y.-C. Chao, C.-R. Hsing, K.-K. Wang, Y.-H. Tung, C.-C. Yang, S.-W. Chen, G. J. Snyder, H.-W. Yen, C.-M. Wei*(魏金明), P.-C. Wei*(魏百駿), and H.-J. Wu*(吳欣潔), "*From Stoichiometric to Off-stoichiometric GeTe: Phase Diagram Reconstruction and Thermoelectric Performance Reassessment*", Acta Mater. **265**, 119644 (2024).
- Y.-T. Tsai, T. Lesniewski, N. Majewska, M. Kaminski, J. Barzowska, E.-P. Liu, W.-T. Chen, S. Mahlik*, and M.-H. Fang*(方牧懷), "*Pressure/Temperature-assisted Crystallographic Engineering-A Strategy for Developing the Infrared Phosphors*", Chem. Eng. J. **490**, 151596 (2024).
- C.-C. Wang*(王志傑), Y.-C. Chung, C.-Y. Shin, Y.-C. Wu, G.-H. Lee, S.-Y. Chien, B.-H. Chen, and Y.-C. Chuang*(莊裕鈞), "*Structural Diversity and Dimensionality of Three Cu(II)-dpdsC<sub<5O5^{2-} Coordination Polymers Controlled by the Coordination Sphere of Cu(II) Centers and the Coordination Modes of $C_5O_5^{2-}$ (dpds=4,4'-dipyridyldisulfide)*", ACS Omega **9**, 40920 (2024).
- P.-C. Wei*(魏百駿), C.-R. Hsing, C.-C. Yang, Y.-H. Tung, H.-J. Wu, W.-T. Yen, Y.-C. Lai, J.-J. Lee, C.-W. Wang, H.-C. Wu, H.-D. Yang, V. Singaravelu, X. Miao, A. Giugni, J.-K. Hu, J.-H. Fu, V. Tung, J. He, C.-M. Wei*(魏金明), and J.-H. He*(何志浩), "*Liquid-like Thermal Conductivity in Solid Materials: Dynamic Behavior of Silver Ions in Argyrodites*", Nano Energy **122**, 109324 (2024).
- P.-C. Wei*(魏百駿), N. Aktar, J.-K. Hu, C.-C. Wu, Y.-H. Tung, C.-C. Yang, and A. Giugni, "*Unveiling the Ultralow in-plane Thermal Conductivity in 2D Organic-inorganic Hybrid Perovskite $(EA)_2PbI_4$ Single Crystals*", J. Mater. Chem. A **12**, 27686 (2024).
- L. Yao, J. Chen, Z. Wang, Y.-C. Chuang, L.-Y. Chang, and T.-K. Sham*(岑俊江), "*An Amorphous-to-anatase Phase Transition Study of TiO_2 Nanotubes by Temperature-Dependent Synchrotron-based In Situ X-ray Diffraction*", J. Phys. Chem. Lett. **15**, 10349 (2024).
- W.-T. Yen and H.-J. Wu*(吳欣潔), "*Asymmetric Homogeneity and Transport Properties of Isotropic Copper-based Ternary Chalcogenides*", ACS Appl. Energy Mater. **7**, 5285 (2024).
- S. Zhang, F. Zhao, L.-Y. Chang, Y.-C. Chuang, Z. Zhang, Y. Zhu, X. Hao, J. Fu, J. Chen, J. Luo, M. Li, Y. Gao, Y. Huang, T.-K. Sham, M. D. Gu*(谷猛), Y. Zhang*, G. King*, and X. Sun*(孫學良), "*Amorphous Oxyhalide Matters for Achieving Lithium Superionic Conduction*", J. Am. Chem. Soc. **146**, 2977 (2024).

TPS 21A X-ray Nanodiffraction

- K. S. Bayikadi, S. Imam, W.-S. Tee, S. Kavirajan, C.-Y. Chang, A. Sabbah, F.-Y. Fu, T.-R. Liu, C.-Y. Chiang, D. Shukla, C.-T. Wu, L.-C. Chen, M.-Y. Chou, K.-H. Chen*(陳貴賢), and R. Sankar*, "*Ultra-low Lattice Thermal Conductivity Driven High Thermoelectric Figure of Merit in Sb/W Co-doped GeTe*", J. Mater. Chem. A **12**, 30892 (2024).
- L. Chen, D. Ren, X. Hou, J. Zhang, Y. Wu, Y. Wang, C. Hu, P. Duan*(段培高), C. Li, C.-Y. Chiang, C. He*(何熾), and Q. Lu*(陸強), "*Asymmetric Oxygen Vacancy-enriched Mn_2O_3@CeO_2 for NO Oxidation with Excellent Low-temperature Activity and Boosted SO_2-resistance*", Appl. Catal. B-Environ. **340**, 123202 (2024).
- S. Hegde, V. Sridhar, R. S. Chen, and S. Chattopadhyay*(薛特), "*Gradient Dion-Jacobson Phase Stable Quasi-2D Perovskite@Graphene Hybrid for High Responsivity Photodetectors*", Adv. Opt. Mater. **12**, 2400232 (2024).
- L.-P. Huang, S.-F. Yeh, Y.-P. Liu, W.-C. Lin, M.-C. Lin, I.-Y. Tsao, C.-Y. Chiang*(蔣慶有), A.-Y. Lo*(駱安亞), and W.-H. Hung*(洪緯璿), "*Reversible High Entropy Oxide Anode: Interfacial Electrocatalysis for Enhanced Capacity and Stability of $LiNi_{0.8}Co_{0.1}Mn_{0.1}O_2$ Lithium-ion Batteries*", J. Power Sources **606**, 234289 (2024).
- Z. Jia, H. Shen*(沈昊), J. Kou, T. Zhang, Z. Wang, W. Tang*(唐偉), M. Doeff, C.-Y. Chiang, and K. Chen*(陳凱), "*Solid Electrolyte Bimodal Grain Structures for Improved Cycling Performance*", Adv. Mater. **36**, 2309019 (2024).
- J. Kou and K. Chen*(陳凱), "*PYXIS: an Integrated Software Package for Synchrotron Micro/Nanodiffraction Data Analysis*", J. Appl. Crystallogr. **57**, 539 (2024).
- J. Kou, K. Chen*(陳凱), S. Huang, C. Zhai, C.-Y. Chiang, S. Wang, Z. Li, and Y.-D. Wang*(王沿東), "*Mapping Stress Heterogeneity in Single-crystal Superalloys by Novel Submicron-resolved X-ray Diffraction*", Mater. Res. Lett. **12**, 450 (2024).
- S.-H. Kuo, Y.-C. Chen*(陳怡誠), Y.-C. Wang, W.-Z. Hsieh, C.-Y. Chiang, C.-M. Cheng, L.-H. Chen, K.-P. Chen, Y.-H. Tu, J.-Y. Lin, and Y.-H. Chu*(朱英豪), "*Superconductive MgB_2 Intercalated Muscovite with Dynamically Tunable Stress*", ACS Omega **9**, 39856 (2024).
- L.-R. Lee, P.-H. Fan, Y.-F. Chen, M.-H. Chang, Y.-C. Liu, C.-C. Chang, and J.-T. Chen*(陳俊太), "*Structurally Defined Amphiphilic AAO Membranes Using UV-assisted Thiol-yne Chemistry: Applications in Anti-counterfeiting and Electronics*", ACS Appl. Mater. Interfaces **16**, 48073 (2024).
- B. Li, W. Xu, W.-Z. Hsieh, D. Liu, Y. Xiang, Q. Lian, H. Li, S. R. P. Silva*, W. Zhang*(張偉), and Y. Zhao*(趙一新), "*Elucidating the Impact of Buried Interface Engineering on Perovskite Properties and Stability in Inverted Perovskite Solar Cells*", J. Phys. Chem. Lett. **15**, 12274 (2024).
- C.-T. Li, C.-Y. Chiang, C.-T. Chiu, M.-L. Yu, A.-Y. Lo, W.-C. Lin, H. Lee, Y.-T. Lu, H.-C. Wu, and W.-H. Hung*(洪緯璿), "*High-entropy Selenide Catalyst for Degradation of Organic Pollutants*", J. Electroanal. Chem. **957**, 118106 (2024).
- C.-H. Liao, C.-Y. Chiang, K. Iputera, S.-F. Hu*(胡淑芬), and R.-S. Liu*(劉如熹), "*Homogeneous Catalytic Process of a Heterogeneous Ru Catalyst in Li-O_2 via X-ray Nanodiffraction Observation*", ACS Appl. Mater. Interfaces **16**, 8783 (2024).
- V. Sridhar, M. Rameez, P. Selvarasu, D. S. Tomar, S. Hegde, R. S. Chen, C. T. Wu, C. H. Hung, and S. Chattopadhyay*(薛特), "*Mega Broadband Photoresponsivity in Degradation-controlled Super-halide PF_6 Substituted Perovskite@graphene Hybrid Photodetectors*", Mater. Today Phys. **40**, 101294 (2024).
- S. Y. Tsai, P.-H. Tseng, C. C. Chen, C.-M. Huang, H.-W. Yen, Y.-S. Chen, K.-L. Lin, R. Niu, Y.-S. Lai, and F.-H. Ko*(柯富祥), "*Lattice Boundary Enhancement on Thermoelectric Behaviors of Heavily Boron-doped Silicon for Energy Harvesting: Electrical versus Thermal Conductivity*", Adv. Mater. Interfaces **11**, 2400536 (2024).
- C.-C. Wang and C.-H. Lee*(李志浩), "*Wafer-scale Epitaxial Molybdenum Disulfide Ultrathin Film on Sapphire Prepared by Low-energy Reactive Magnetron Sputtering*", Appl. Surf. Sci. **659**, 159889 (2024).
- S. Wang*(王世霞), Y. Wang, T. Liu, L. Wang, Y. Huang, and Y. Lu*(陸楊), "*Irreversible Pressure Effect on Phase Transitions and Bandgap Narrowing of Layered MoO_3*", Mater. Today Adv. **21**, 100476 (2024).
- Y.-H. Wu, T.-N. Lam, S.-W. Ke, W.-J. Lee, C.-Y. Lee, B.-Y. Chen, G.-C. Yin, W.-Z. Hsieh, C.-Y. Chiang, M.-T. Tang, B.-H. Lin*(林碧軒), and E.-W. Huang*(黃爾文), "*Mixing Entropy and Enthalpy Effects on Europium Ions in Eu-doped $BaAl_2O_4$*", Appl. Phys. Lett. **124**, 094105 (2024).

TPS 23A X-ray Nanoprobe

- S. G. Al-Solaimani, A. Al-Qureshi, S. S. Hindi, O. H. Ibrahim, M. A. A. Mousa, Y.-L. Cho, N. E. E. Hassan, Y.-T. Liu, S.-L. Wang, V. Antoniadis, J. Rinklebe*, and S. M. Shaheen*, "*Speciation, Phytoavailability, and Accumulation of Toxic Elements and Sulfur by Humic Acid-fertilized Lemongrass and Common Sage in a Sandy Soil Treated with Heavy Oil Fly Ash: A Trial for Management of Power Stations Wastes*", Sci. Total Environ. **945**, 173998 (2024).
- A.-C. Chang, Y.-S. Wu, W.-C. Chen, Y.-H. Weng, B.-H. Lin, C.-C. Chueh, Y.-C. Lin*(林彥丞), and W.-C. Chen*(陳文章), "*Modulating the Photoresponsivity of Perovskite Photodetectors through Interfacial Engineering of Self-assembled Monolayers*", Adv. Opt. Mater. **12**, 2301789 (2024).
- H.-F. Chang, S.-C. Tseng, M.-T. Tang, S. S.-Y. Hsiao, D.-C. Lee, S.-L. Wang, and K.-C. Yeh*(葉國楨), "*Physiology and Molecular Basis of Thallium Toxicity and Accumulation in Arabidopsis Thaliana*", Ecotox. Environ. Safe. **276**, 116290 (2024).
- C.-H. Chen, M.-H. Yu, Y.-Y. Wang, Y.-C. Tseng, I.-H. Chao, I.-C. Ni, B.-H. Lin, Y.-J. Lu, and C.-C. Chueh*(闕居振), "*Enhancing the Performance of 2D Tin-based Pure Red Perovskite Light-emitting Diodes through the Synergistic Effect of Natural Antioxidants and Cyclic Molecular Additives*", Small **20**, 2307774 (2024).
- S. P. Chiniwar, Y.-C. Hsieh, C.-H. Shih, C.-Y. Teng, J.-L. Yang, C. Hu, B.-H. Lin, M.-T. Tang, and Y.-C. Tseng*(曾院介), "*Ferroelectric Enhancement in a TiN/$Hf_{1-x}Zr_xO_2$/W Device with Controlled Oxidation of the Bottom Electrode*", ACS Appl. Electron. Mater. **6**, 1078 (2024).
- H.-C. Chu, C.-M. Hung, H.-C. Huang, S.-C. Weng, B.-H. Lin, S. Yang, Y.-H. Wu, K.-H. Chang, J.-J. Shyue, P.-T. Chou*(周必泰), and C.-M. Jiang*(姜昌明), "*Hydrogen Plasma Treatment Compensates for the Intrinsic Defects in $Cs_2AgBiBr_6$ Thin Films*", J. Phys. Chem. C **128**, 20441 (2024).
- C.-W. Hsu, S.-K. Yu, M.-Y. Shen, Ender Ercan, Y.-J. Wang, B.-H. Lin, H.-C. Wu*(吳亘承), Y.-C. Lin*(林彥丞), C.-L. Liu*(劉振良), and W.-C. Chen*(陳文章), "*Spider Silk/Hemin Biobased Electrets for Organic Phototransistor Memory: a Comprehensive Study on Solution Process Engineering*", Adv. Funct. Mater. **34**, 2314907 (2024).
- Y.-J. Hu, C.-W. Hsu, Y.-H. Weng, B.-H. Lin, C.-L. Liu, Y.-C. Lin*(林彥丞), Y.-Y. Yu*(游洋雁), and W.-C. Chen*(陳文章), "*Hydrogen-bonded Supramolecular Electrets Comprising Block Copolymers and Amino-functionalized Porphyrin for Low-power-consumption Phototransistors*", Polymer **312**, 127668 (2024).
- C.-Y. Huang, S.-C. Tseng*(曾紹欽), W.-C. Chen, G.-C. Yin, B.-Y. Chen, K.-H. Chen, L.-C. Chen*(林麗瓊), and C.-Y. Chen*(陳政營), "*Visualization of*

Anion Vacancy Defect Annihilation in CZTSe Solar Cells by Hydrogen-assisted Selenization with In Operando X-ray Nanoprobe Studies", ACS Appl. Mater. Interfaces **16**, 64656 (2024).

- T.-C. Huang, S.-W. Ke, Y.-H. Wu, E.-R. Wang, W.-L. Wei, C.-Y. Lee, B.-Y. Chen, G.-C. Yin, H.-W. Chang, M.-T. Tang, and B.-H. Lin*(林碧軒), "*Combination of XEOL, TR-XEOL and HB-T Interferometer at the TPS 23A X-ray Nanoprobe for Exploring Quantum Materials*", J. Synchrotron Radiat. **31**, 252 (2024).
- Ankit Kadian*, V. Manikandan, C. L. Chen, C. L. Dong, and S. Annapoorni*, "*Synergistically Enhanced Photocatalytic Properties of Co_3O_4-G/GO Nanocomposites: Unravelling Their Interactions and Charge-transfer Dynamics Using XAS*", Dalton T. **53**, 13550 (2024).
- S.-F. Kao, M.-H. Yu, J.-C. Chen, H.-W. Yu, H.-Y. Yu, B.-H. Lin, I.-C. Ni, Y.-P. Li*(李奕霈), and C.-C. Chueh*(闕居振), "*Unraveling Differences in the Effects of Ammonium/Amine-based Additives on the Performance and Stability of Inverted Perovskite Solar Cells*", Small Methods **8**, 2400039 (2024).
- Y.-C. Li, T.-C. Huang, Y.-H. Wu, W.-L. Wei, T.-S. Wu, L.-Y. Chang, C.-Y. Lee, B.-Y. Chen, G.-C. Yin, M.-T. Tang, and B.-H. Lin*(林碧軒), "*Hard X-ray Nanoprobe to Study the Emission Properties of Ce-doped YAG Wafer by Using XEOL and TR-XEOL*", Opt. Mater. **156**, 116031 (2024).
- Y.-C. Neu, Y.-S. Lin, Y.-H. Weng, W.-C. Chen, C.-L. Liu, B.-H. Lin, Y.-C. Lin*(林彥丞), and W.-C. Chen*(陳文章), "*Reversible Molecular Conformation Transitions of Smectic Liquid Crystals for Light/Bias-gated Transistor Memory*", ACS Appl. Mater. Interfaces **16**, 7500 (2024).
- S. Sathish, T. A. Kumaravelu, C.-J. Yang, R. R. Jayapalan, R. Nirmala, C.-L. Dong, B.-H. Lin, and R. Navamathavan*, "*Enhancing Supercapacitor Performance with Biomass-derived Activated Carbon Interlinked CoS_2 Embedded Graphitic Carbon Nitride*", J. Alloy. Compd. **985**, 174076 (2024).
- S. Saurabh, T.-C. Huang, Y.-T. Li, Y.-C. Li, W.-L. Wei, Y.-H. Wu, C.-Y. Lee, B.-Y. Chen, G.-C. Yin, M.-T. Tang, Y.-C. Chiu*(邱昱誠), and B.-H. Lin*(林碧軒), "*Charge Carrier Recombination Studies of Tm-doped $CsPbBr_3$ by Temperature-dependent PL and TR-PL*", Opt. Mater. **156**, 115929 (2024).
- K. N. Shitaw, M. A. Weret, Y. Nikodimos, T. M. Tekaligne, S.-K. Jiang, C.-J. Huang, B.-H. Lin, S.-H. Wu, W.-N. Su*(蘇威年), and B. J. Hwang*(黃炳照), "*Fundamental Phenomena in Anode-free Coin Cells and Pouch Cells Configured with Imide Salt-based Ether Electrolytes*", Mater. Today Energy **39**, 101461 (2024).
- C.-Y. Sung, W.-C. Chen, C.-L. Liu, B.-H. Lin, Y.-C. Lin*(林彥丞), and W.-C. Chen*(陳文章), "*Ultrafast Quasi-2D/3D Perovskite Photodetectors Conferred Using Interfacial Engineering of Self-assembled Monolayers*", Adv. Opt. Mater. **12**, 2303241 (2024).
- W.-L. Wei, C.-Y. Lin, T.-C. Huang, Y.-C. Li, Y.-H. Wu, C.-Y. Lee, B.-Y. Chen, G.-C. Yin, M.-T. Tang, W.-C. Chou, F.-Y. Lo*(駱芳鈺), and B.-H. Lin*(林碧軒), "*Structural and Optical Properties of Eu-doped ZnO Epitaxial Thin Films Grown by Pulsed-laser Deposition*", APL Mater. **12**, 111112 (2024).
- Y.-H. Wu, T.-N. Lam, S.-W. Ke, W.-J. Lee, C.-Y. Lee, B.-Y. Chen, G.-C. Yin, W.-Z. Hsieh, C.-Y. Chiang, M.-T. Tang, B.-H. Lin*(林碧軒), and E.-W. Huang*(黃爾文), "*Mixing Entropy and Enthalpy Effects on Europium Ions in Eu-doped $BaAl_2O_4$*", Appl. Phys. Lett. **124**, 094105 (2024).
- Y.-S. Wu, A.-C. Chang, W.-C. Chen, E. Ercan, Y.-H. Weng, B.-H. Lin, C.-L. Liu, Y.-C. Lin*(林彥丞), and W.-C. Chen*(陳文章), "*High-performance Synaptic Phototransistor Using a Photoactive Self-assembled Layer toward Ultralow Energy Consumption*", Adv. Opt. Mater. **12**, 2302040 (2024).
- Z.-L. Yan, J.-Y. Chang, C. Tsao, M.-X. Fang, B.-H. Lin, J.-H. Tsai, M.-H. Chen, R.-J. Jeng*(鄭如忠), and C.-C. Kuo*(郭霽慶), "*Mitigating Thermal Burden and Enhancing Minor Phase Emission Energy Transfer in Perovskite by Introducing Dopamine-mediated Silver Nanoparticles*", Chem. Eng. J. **498**, 155835 (2024).
- Y.-T. Yang, Y.-H. Shih, Q.-G. Chen, C.-H. Chen, M.-H. Yu, C.-H. Nieh, B.-H. Lin, W.-C. Chen, W.-Y. Lee*(李文亞), and C.-C. Chueh*(闕居振), "*Revealing the Potential of Perovskite Transistors for Dual-modulated Synaptic Behavior through Heterojunction Design*", ACS Energ. Lett. **9**, 4564 (2024).
- M.-H. Yu, Xingyu Liu, H.-W. Yu, S.-F. Kao, C.-H. Chen, Y.-C. Tseng, I.-C. Ni, B.-H. Lin, Yang Wang*(王漾), and C.-C. Chueh*(闕居振), "*Impact of Self-assembled Monolayer Structural Design on Perovskite Phase Regulation, Hole-selective Contact, and Energy Loss in Inverted Perovskite Solar Cells*", Nano Energy **132**, 110405 (2024).

TPS 24A Soft X-ray Tomography

- C.-C. Hsieh, Z.-J. Lin, and L.-J. Lai*(賴麗珍), "*Minimizing Ice Contamination During Specimen Preparation for Cryo-soft X-ray Tomography and Cryo-electron Tomography*", J. Struct. Biol.-X **10**, 100113 (2024).
- W.-L. Huang, C.-L. Chen, Z.-J. Lin, C.-C. Hsieh, M. D.-S. Hua, C.-C. Cheng, T.-H. Cheng, L.-J. Lai*(賴麗珍), and C.-R. Chang*(張壯榮), "*Soft X-ray Tomography Analysis of Mitochondria Dynamics in Saccharomyces Cerevisiae*", Biol. Direct **19**, 126 (2024).
- Y.-S. Yu, Y.-Y. Liang, C.-C. Hsieh, Z.-J. Lin, P.-H. Cheng, C.-C. Cheng, S.-P. Chen, L.-J. Lai*(賴麗珍), and K. C.-W. Wu*(吳嘉文), "*Downsizing and Soft X-ray Tomography for Cellular Uptake of Interpenetrated Metal-organic Frameworks*", J. Mater. Chem. B **12**, 6079 (2024).

TPS 25A Coherent X-ray Scattering

- S. N. Afraj, B.-H. Jiang, Y.-W. Su, C.-H. Yang, H.-S. Shih, A. Velusamy, J.-S. Ni, Y. Ezhumalai, T.-Y. Su, C.-L. Liu, S. Yau, C.-P. Chen*(陳志平), and M.-C. Chen*(陳銘洲), "*Dicyclopentadithienothiophene-based Non-fullerene Acceptors for Ternary Blend Organic Photovoltaics*", J. Mater. Chem. C **12**, 2247 (2024).
- C.-W. Chang, C.-T. Wu, T.-Y. Lo, Y. Chen, C.-T. Chang, H.-R. Chen, C.-C. Chang, L.-R. Lee, Y.-H. Tseng, and J.-T. Chen*(陳俊太), "*Alkaline-responsive, Self-healable, and Conductive Copolymer Composites with Enhanced Mechanical Properties Tailored for Wearable Tech*", Small **20**, 2402472 (2024).
- K. Chen, C. Lee, C.-Y. Chen, T. Satoh, T. Isono*, and H.-L. Chen*(陳信龍), "*Phase Behavior of Sugar-based Block Co-oligomer Modulated by Molecular Chirality*", Giant **19**, 100308 (2024).
- W.-C. Chen, Y.-C. Lin, Z.-S. Syu, Y.-S. Wu, K.-W. Lin, C.-L. Liu, C.-C. Kuo*(郭霽慶), and W.-C. Chen*(陳文章), "*Surface Ligand Engineering of Perovskite Quantum Dots for N-type and Stretchable Photosynaptic Transistor with an Ultralow Energy Consumption*", Chem. Eng. J. **494**, 152897 (2024).
- P.-H. Chiu, C.-T. Hu, S.-K. Chia, L.-Y. Su*(蘇莉芸), P.-T. Chen, Z.-Y. Liu, C.-Y. Lin, C.-C. Hsieh, C.-A. Dai*(戴子安), and L. Wang*(王立義), "*Synergistic Enhancement of Stability and Performance for Perovskite Solar Cells Using Fluorinated Benzoic Acids as Additives*", Solar RRL **8**, 2300902 (2024).
- W.-C. Chiu, Y.-H. Cheng, J.-H. Lin, C.-H. Tung, T. Nishimura, C.-Y. Chen, T. Isono*, T. Satoh, and H.-L. Chen*(陳信龍), "*Tuning the Complex Spherical Phase of Sugar-based Block Co-oligomer via Single-monomer-mediated Composition Variation*", Macromolecules **57**, 6076 (2024).
- C.-A. Chou, S.-C. Fang, P.-S. Lin, W.-N. Wu, S.-H. Hong, J.-M. Lin, K.-T. Wong*(汪根欉), and C.-L. Liu*(劉振良), "*Tuning Thermoelectric Performance with N-annulated Perylene-based Small Molecules and Single-walled Carbon Nanotube Nanocomposite Films*", Mater. Today Chem. **38**, 102129 (2024).
- K.-C. Chu, C.-H. Yeh, J.-M. Lin, C.-Y. Chen, C.-Y. Cheng, Y.-Q. Yeh, Y.-S. Huang, and Y.-W. Tsai*(蔡一葦), "*Using Convolutional Neural Network Denoising to Reduce Ambiguity in X-ray Coherent Diffraction Imaging*", J. Synchrotron Radiat. **31**, 1340 (2024).
- T.-C. Chuang, S. Nagarajan, C.-C. Su, L.-T. Lee*(李立鼎), and E. M. Woo*(吳逸謨), "*Universality in Interior Periodic Assembly of Banded D-(−)-poly(3-hydroxybutyrate) Justified with the Iridescence Test*", CrystEngComm **26**, 1209 (2024).
- W.-T. Chuang*(莊偉綜), S.-P. Chen, Y.-B. Tsai, Y.-S. Sun, J.-M. Lin, C.-Y. Chen, Y.-W. Tsai, C.-M. Chou, Y.-C. Hung*(洪毓玨), T.-W. Chen, W.-E. Wang, C.-C. Huang, P.-D. Hong*(洪伯達), U.-S. Jeng, and Y.-W. Chiang, "*Spontaneous Photonic Jammed Packing of Core-shell Colloids in Conductive Aqueous Inks for Non-iridescent Structural Coloration*", ACS Appl. Mater. Interfaces **16**, 52856 (2024).
- J.-F. Ding, K. Yamanaka, S.-H. Hong, G.-L. Chen, W.-N. Wu, J.-M. Lin, S.-H. Tung, I. Osaka*(尾坂格), and C.-L. Liu*(劉振良), "*Controlling the Thermoelectric Performance of Doped Naphthobisthiadiazole-based Donor-acceptor Conjugated Polymers through Backbone Engineering*", Adv. Sci. **11**, 2410046 (2024).
- Y.-J. Hsiao, Z.-E. Huang, A. Sahare, M.-Z. Chen, Y.-H. Lin, and H.-L. Chen*(陳信龍), "*Accessing the Frank-kasper Phase of Block Copolymer via Selective Incorporation of Metal Salt*", Macromolecules **57**, 10657 (2024).
- C.-C. Hsu, Y.-T. Lin, S.-H. Hong, U.-S. Jeng, H.-L. Chen, J. Yu, and C.-L. Liu*(劉振良), "*3D Printed Gelatin Methacrylate Hydrogel-based Wearable Thermoelectric Generators*", Adv. Sustain. Syst. **8**, 2400039 (2024).
- J.-H. Huang, X.-F. Luo, T.-Y. Kuo, Y.-H. Lai, P. C. Rath, C.-W. Huang, M.-H. Lin, A.-Y. Hou, J. Li, Y.-S. Su, W.-W. Wu*(吳文偉), and J.-K. Chang*(張仍奎), "*Dual-salt Aqueous Electrolyte for Enhancing Charge-storage Properties of VO_2 Polymorphic Cathodes for Zn-ion Batteries*", Chem. Eng. J. **497**, 154609 (2024).
- Y.-H. Huang, Y. Chang, C.-J. Huang, J.-M. Lin, S.-H. Tung, G.-W. Jang, and C.-L. Liu*(劉振良), "*Electrospun Biomass Polyethylene Furanoate Nonwoven Substrates for Flexible Thermoelectric Generators*", Polymer **312**, 127619 (2024).

- C.-H. Kuan, Y.-C. Chen, S. Narra, C.-F. Chang, Y.-W. Tsai, J.-M. Lin, G.-R. Chen, and E. W.-G. Diau*(刁維光), "*Quadruple-cation Wide-bandgap Mixed-halide Tin Perovskite Solar Cells*", ACS Energ. Lett. **9**, 2351 (2024).
- C.-H. Kuan, T.-S. Liao, S. Narra, Y.-W. Tsai, J.-M. Lin, G.-R. Chen, and E. W.-G. Diau*(刁維光), "*Co-cation Engineering via Mixing of Acetamidinium and Rubidium in $FASnI_3$ for Tin Perovskite Solar Cells to Attain 14.5% Efficiency*", J. Phys. Chem. Lett. **15**, 7763 (2024).
- C.-H. Kuan, S. N. Afraj, Y.-L. Huang, A. Velusamy, C.-L. Liu, T.-Y. Su, X. Jiang, J.-M. Lin, M.-C. Chen*(陳銘洲), and E. W.-G. Diau*(刁維光), "*Functionalized Thienopyrazines on NiOx Film as Self-assembled Monolayer for Efficient Tin-perovskite Solar Cells Using a Two-step Method*", Angew. Chem. Int. Edit. **63**, e202407228 (2024).
- C.-Y. Lin, B.-H. Jiang, P.-J. Weng, Y. Hsuan Lin, Y.-W. Su, H.-S. Shih, Z.-E. Shi, Y.-R. Lin, J. Vailassery, S.-S. Sun, C.-P. Chen*(陳志平), and Y. J. Chang*(張源杰), "*Enhancing Open-circuit Voltage and Suppression of Energy Loss in Ternary Organic Photovoltaics Utilizing Carbazole/Bicarbazole-based Guest Donors*", Chem. Eng. J. **494**, 153183 (2024).
- I.-M. Lin, C.-Y. Yang, Y.-M. Wang, W.-E. Wang, Y.-C. Hung, E. L. Thomas, and Y.-W. Chiang*(蔣酉旺), "*Flexible Block Copolymer Metamaterials Featuring Hollow Ordered Nanonetworks with Ultra-high Porosity and Surface-to-volume Ratio*", Small **20**, 2307487 (2024).
- M.-H. Lin, M. G. Mohamed, C.-J. Lin, Y.-J. Sheng, S.-W. Kuo*(郭紹偉), and C.-L. Liu*(劉振良), "*Achieving High zT with Carbon Nanotube/Conjugated Microporous Polymer Thermoelectric Nanohybrids by Meticulous Molecular Geometry Design*", Adv. Funct. Mater. **34**, 2406165 (2024).
- P.-S. Lin, J.-M. Lin, S.-H. Tung, T. Higashihara*(東原知哉), and C.-L. Liu*(劉振良), "*Synergistic Interactions in Sequential Process Doping of Polymer/Single-walled Carbon Nanotube Nanocomposites for Enhanced n-type Thermoelectric Performance*", Small **20**, 2306166 (2024).
- S. Nagarajan, T.-C. Chuang, M.-H. Hao, W.-T. Chuang, J.-M. Lin, and E. M. Woo*(吳逸謨), "*Unveiling the Secrets of Unusual Long-pitch Periodic Assembly of Poly ($_L$-Lactide) Ring-banded Spherulites*", Mater. Today Chem. **35**, 101878 (2024).
- S. Nagarajan, W.-T. Chuang, J.-M. Lin, C.-Y. Chen, and E. M. Woo*(吳逸謨), "*Periodic Assembly Complexity Beneath the Surface: Formation by Corrugated-grating Lamellae in Poly(Octamethylene Terephthalate)*", Mater. Today Chem. **41**, 102312 (2024).
- W.-C. Shih, M. Matsuda, K. Konno, P.-S. Lin, T. Higashihara*(東原知哉), and C.-L. Liu*(劉振良), "*Tailored Thermoelectric Performance of Poly(Phenylene Butadiynylene)s/Carbon Nanotubes Nanocomposites Towards Wearable Thermoelectric Generator Application*", Compos. Pt. B-Eng. **286**, 111779 (2024).
- Y.-S. Sun*(孫亞賢), Y.-Q. Jian, S.-T. Yang, H.-F. Wang, B. A. Junisu, C.-Y. Chen, and J.-M. Lin, "*Epitaxial Growth of Surface Perforations on Parallel Cylinders in Terraced Films of Block Copolymer/Homopolymer Blends*", Langmuir **40**, 7680 (2024).
- C.-C. Tseng, K.-C. Wang, P.-S. Lin, C. Chang, L.-L. Yeh, S.-H. Tung, C.-L. Liu*(劉振良), and Y.-J. Cheng*(鄭彥如), "*Intrinsically Stretchable Organic Thermoelectric Polymers Enabled by Incorporating Fused-ring Conjugated Breakers*", Small **20**, 2401966 (2024).
- A. Velusamy, Y.-Y. Chen, M.-H. Lin, S. N. Afraj, J.-H. Liu, M.-C. Chen*(陳銘洲), and C.-L. Liu*(劉振良), "*Diselenophene-dithioalkylthiophene Based Quinoidal Small Molecules for Ambipolar Organic Field Effect Transistors*", Adv. Sci. **11**, 2305361 (2024).
- E. M. Woo*(吳逸謨), C.-H. Lin, S. Nagarajan, and C.-C. Su, "*Microbeam X-ray and Scanning Electron Microscopic Analyses on Sector-banded Spherulites of Poly(p-dioxanone) Justified with Pixelated Iridescence*", Polymers **16**, 2736 (2024).
- S.-K. Wu, H.-J. Wang, S.-W. Hsiao*(蕭聖偉), J.-S. Huang, W.-C. Chou*(周武清), C.-S. Yang*(楊祝壽), S.-J. Chang, C.-H. Wu, and Y.-C. Huang, "*Control of Lateral Epitaxial Nanothin β-In_2Se_3 Grown by Molecular Beam Epitaxy: Implications in Fabricating of Next-generation Transistors*", ACS Appl. Nano Mater. **7**, 20445 (2024).
- W.-N. Wu, Q.-B. Zheng, and C.-L. Liu*(劉振良), "*Recent Progress in P-type Doped Conjugated Polymer-based Thermoelectric Thin Films*", Synthetic Met. **307**, 117682 (2024).
- X. Xia, L. Mei, R. Sun, S. Li, C.-Y. Chen, J.-M. Lin, J. Min*(閔杰), H. Chen*(陳紅征), X.-K. Chen*(陳先凱), and X. Lu*(路新慧), "*Uncovering the Crystalline Packing Advantages of Asymmetric Y-series Acceptors for Efficient Additive-insensitive and Intrinsically Stable Organic Solar Cells*", Adv. Energy Mater. **14**, 2303785 (2024).
- Y. Xiang, W.-T. Chuang, and Y.-W. Chiang*(蔣酉旺), "*Synergistic Effects of Dry-brush Compatibility and Shear Stress on Rapid Alignment of Lamellar Microstructures for Block Copolymer Reflectors*", Giant **17**, 100225 (2024).
- Y.-J. Xue, Z.-Y. Lai, H.-C. Lu, J.-C. Hong, C.-L. Tsai, C.-L. Huang, K.-H. Huang, C.-F. Lu, Y.-Y. Lai, C.-S. Hsu, J.-M. Lin, J.-W. Chang, S.-Y. Chien, G.-H. Lee, U.-S. Jeng*(鄭有舜), and Y.-J. Cheng*(鄭彥如), "*Unraveling the Structure-property-performance Relationships of Fused-ring Nonfullerene Acceptors: Toward a C-shaped Ortho-benzodipyrrole-based Acceptor for Highly Efficient Organic Photovoltaics*", J. Am. Chem. Soc. **146**, 833 (2024).
- Q.-B. Zheng, C.-C. Tseng, M.-H. Lin, J.-M. Lin, S.-H. Tung, Y.-J. Cheng*(鄭彥如), and C.-L. Liu*(劉振良), "*High-performance Ladder-type Conjugated Polymer/Carbon Nanotube Nanocomposites Blended with Elastomers for Stretchable Thermoelectric Thin Films*", J. Mater. Chem. C **12**, 7446 (2024).

TPS 27A Soft X-ray Nanoscopy

- T.-H. Chuang*(莊子弘), C.-C. Hsu, W.-S. Chiu, J.-S. Jhuang, I.-C. Yeh, R.-S. Chen, S. Gwo, and D.-H. Wei*(魏德新), "*Performance of a Photoelectron Momentum Microscope in Direct- and Momentum-space Imaging with Ultraviolet Photon Sources*", J. Synchrotron Radiat. **31**, 195 (2024).

TPS 31A Projection X-ray Microscopy and Transmission X-ray Microscope

- L.-J. Chen, T.-C. Yu, B.-H. Huang, K.-C. Tso, Y.-F. Song, G.-C. Yin, J.-S. Yang*(楊家欣), and P.-W. Wu*(吳樸偉), "*Synthesis of Novel Chitosan/Sodium Hyaluronate/Iridium Hydrogel Nanocomposite for Wound Healing Application*", Int. J. Biol. Macromol. **270**, 132351 (2024).
- K.-T. Liu, P.-W. Wang, H.-Y. Hsieh, H.-C. Pan, H.-J. Chin, C.-W. Lin, Y.-J. Huang, Y.-C. Liao, Y.-C. Tsai, S.-R. Liu, I.-C. Su, Y.-F. Song, G.-C. Yin, K.-C. Wu, E.-Y. Chuang, Y.-J. R. Fan*(范育睿) and J. Yu*(游佳欣), "*Site-specific Thrombus Formation: Advancements in Photothrombosis-on-a-chip Technology*", Lab Chip **24**, 3422 (2024).
- Y.-F. Song*(宋艷芳), C.-C. Chiu, B.-Y. Chen, L.-C. Chiang, C.-Y. Lee, M.-H. Lee, C.-Y. Liu, C.-F. Chang, M.-Y. Hsu, S.-W. Lin, Y.-S. Tseng, S.-T. Lo, H.-C. Chan, W.-L. Chen, Li Lo, C.-C. Chen, and G.-C. Yin*(殷廣鈐), "*Projection X-Ray Microscopy and Transmission X-Ray Microscopy at the Taiwan Photon Source*", Synchrotron Rad. News **37**, 26 (2024).

TPS 32A Tender X-ray Absorption Spectroscopy

- C.-B. Chang, Y.-Y. Tseng, Y.-R. Lu, Y.-C. Yang, and H.-Y. Tuan*(段興宇), "*High Entropy Induced Local Charge Enhancement Promotes Frank-van der Merwe Growth for Dendrite-free Potassium Metal Batteries*", Adv. Funct. Mater. **34**, 2411193 (2024).
- C.-Y. Cheng, Y.-M. Shen, W.-H. Huang, C.-C. Chang, C.-C. Tsai, C.-J. Lin, Y.-G. Lin, Y.-R. Lu, C.-L. Dong, W.-N. Su, S.-Y. Chen, K. Kumar, H.-Y. Chen, C.-J. Tsai, and C.-L. Chen*(陳啟亮), "*Electronic and Atomic Structural Properties Associated with Enhanced Photodegradation Activity in Mo-doped TiO_2 Nanoparticles*", Langmuir **40**, 19506 (2024).
- M. Han, Y. Luo, L. Xu, W. Chen*(陳維), C. Li, Y.-C. Huang, Y. Wu, Y. Jiang, W. Wu, R. Wang, Y.-R. Lu, Y. Zou*(鄒雨芹), and S. Wang*(王雙印), "*Oxygen Vacancy Boosts Nitrogen-centered Radical Coupling Initiated by Primary Amine Electrooxidation*", J. Am. Chem. Soc. **146**, 33893 (2024).
- Y.-C. Huang, Y. Wu, Y.-R. Lu, J.-L. Chen, H.-J. Lin, C.-T. Chen, C.-L. Chen, C. Jing, J. Zhou, L. Zhang, Y. Wang, W.-C. Chou*(周武清), S. Wang*(王雙印), Z. Hu*(胡志偉), and C.-L. Dong*(董崇禮), "*Direct Identification of O-O Bond Formation through Three-step Oxidation During Water Splitting by Operando Soft X-ray Absorption Spectroscopy*", Adv. Sci. **11**, 2401236 (2024).
- A. R. Jadhav, X. Liu, P. Silambarasan, V. Kanade, Y. Liu, T. T. T. Nga, T. Yang, M. T. Kim, Y. Han, T. Kim, X. Shao, C. Zhi, C.-L. Dong, and H. Lee*, "*Stable and Efficient Chlorine Evolution Reaction with Atomically Dispersed Ru on Surface Tensile Strained TiO_2*", Appl. Catal. B-Environ. **359**, 124456 (2024).
- Y.-C. Lin*(林裕川), S. Rajagopal, P.-T. Chou, P.-Y. Peng, Y.-R. Lu, C.-L. Chen, M.-H. Tsai, and C.-H. Wang, "*Crafting a Methanation-resistant, Reverse Water-gas Shift-active Nickel Catalyst with Significant Nanoparticle Dimensions Using the Molten Salt Approach*", ACS Sustain. Chem. Eng. **12**, 14771 (2024).
- J. Prameswari, P.-T. Chou, M.-Y. Hung, P.-Y. Peng, Y.-R. Lu, C.-L. Chen, H.-K. Tian*(田弘康), and Y.-C. Lin*(林裕川), "*Boosted Reverse Water-gas Shift Activity via Exsolved Cu and Ni in Silicalite-1*", Chem. Commun. **60**, 14244 (2024).
- J. Shi, W. Chen*(陳維), Y. Wu, Y. Zhu, C. Xie, Y. Jiang, Y.-C. Huang, C.-L. Dong, and Y. Zou*(鄒雨芹), "*Sulfur Filling Activates Vacancy-induced C-C Bond Cleavage in Polyol Electrooxidation*", Natl. Sci. Rev **11**, nwae271 (2024).
- Q. Wang, G. Yu, B. Luo, W. Ji, Z. Liu, M. Li, Y. Nong, Y. Tian, X. Wang*(王小瑋), J. Zhang*(張佳峰), C.-L. Chen, C.-K. Chang, Z. Sang, Z. Zhao, R. Zhao*

(趙瑞瑞), and J. Liang*(梁驥), "*Suppression of Adverse Phase Transition of Layered Oxide Cathode via Local Electronic Structure Regulation for High-capacity Sodium-ion Batteries*", ACS Nano **18**, 18622 (2024).

- S. Wang, F. Li, J. Zhao, Y. Zeng, Y. Li, Z.-Y. Lin, T.-J. Lee, S. Liu, X. Ren, W. Wang, Y. Chen, S.-F. Hung, Y.-R. Lu, Y. Cui, X. Yang, X. Li*(李旭寧), Y. Huang*(黃延強), and B. Liu*(劉彬), "*Manipulating C-C Coupling Pathway in Electrochemical CO_2 Reduction for Selective Ethylene and Ethanol Production over Single-atom Alloy Catalyst*", Nat. Commun. **15**, 10247 (2024).
- S. Zhao, X. Wu, J. Zhang, C. Li, Z. Cui, W. Hu*(胡衛華), R. Ma*(馬汝廣), and C. Li*(李長明), "*Biomass-derived Porous Carbon with Single-atomic Cobalt Toward High-performance Aqueous Zinc-sulfur Batteries at Room Temperature*", J. Energy Chem. **95**, 325 (2024).
- W.-J. Zhong, M.-Y. Hung, Y.-T. Kuo, H.-K. Tian*(田弘康), C.-N. Tsai, C.-J. Wu, Y.-D. Lin, H.-C. Yu, Y.-G. Lin, and J.-J. Wu*(吳季珍), "*Dual-vacancy-engineered $ZnIn_2S_4$ Nanosheets for Harnessing Low-frequency Vibration Induced Piezoelectric Polarization Coupled with Static Dipole Field to Enhance Photocatalytic H_2 Evolution*", Adv. Mater. **36**, 2403228 (2024).
- E. Zhou, H. Jin, H. Lv, Y. Xie, Y. Lu, Y.-R. Lu, T.-S. Chan, C. Wang, W. Yan, J. Zhang, H. Ji*(季恒星), X. Wu*(武曉君), and X. Duan*(段鑲鋒), "*Solid-state Electrocatalysis in Heteroatom-doped Alloy Anode Enables Ultrafast Charge Lithium-ion Batteries*", J. Am. Chem. Soc. **146**, 20700 (2024).
- H. Zou, S. Shu, W. Yang, Y.-C. Chu, M. Cheng, H. Dong, H. Liu, F. Li, J. Hu, Z. Wang, W. Liu, H. M. Chen, and L. Duan*(段樂樂), "*Steering Acidic Oxygen Reduction Selectivity of Single-atom Catalysts through the Second Sphere Effect*", Nat. Commun. **15**, 10818 (2024).

TPS 41A Soft X-ray Scattering

- D. Jost*, H.-Y. Huang, M. Rossi, A. Singh, D.-J. Huang, Y. Lee, H. Zheng, J. F. Mitchell, B. Moritz, Z.-X. Shen, T. P. Devereaux, and W.-S. Lee*(李偉生), "*Low Temperature Dynamic Polaron Liquid in a Manganite Exhibiting Colossal Magnetoresistance*", Phys. Rev. Lett. **132**, 186502 (2024).
- Yongjian Li, Xinyu Zhu, Chenxi Wei, Youyou Fang, Xinyu Wang, Yizhi Zhai, Wenlong Kang, Lai Chen, Duanyun Cao, Meng Wang, Yun Lu, Qing Huang, Yuefeng Su*(蘇岳鋒), Hong Yuan*(袁洪), Ning Li*(李寧), and Feng Wu, "*Unraveling the Chemical and Structural Evolution of Novel Li-rich Layered/Rocksalt Intergrown Cathode for Li-ion Batteries*", Chin. Chem. Lett. **35**, 109536 (2024).
- J. Okamoto, R.-P. Wang, Y.-Y. Chu, H.-W. Shiu, A. Singh, H.-Y. Huang, C.-Y. Mou, S. Teh, H.-T. Jeng, K. Du, X. Xu, S.-W. Cheong, C.-H. Du, C.-T. Chen, A. Fujimori*(藤森淳), and D.-J. Huang*(黃迪靖), "*Giant X-ray Circular Dichroism in a Time-reversal Invariant Antiferromagnet*", Adv. Mater. **36**, 2309172 (2024).
- S. Zhang, Q. Li, C. Zou, H.-Y. Huang, A. Singh, H. Yan, X. Zhou, D.-J. Huang, and Y. Peng*(彭瑩瑩), "*Emergence of Charge Order in Extremely Underdoped $Bi_2Sr_{2-x}La_xCuO_{6+\delta}$*", Phys. Rev. B **110**, 125108 (2024).

TPS 44A Quick-scanning X-ray Absorption Spectroscopy

- S. Abbas, B. Jarwal, T.-T. Ho, S. M. Valiyaveettil, C.-R. Hsing, T.-L. Chou, C.-M. Wei, L.-C. Chen*(林麗瓊), and K.-H. Chen*(陳貴賢), "*Synergistic Effect of Indium Doping on Thermoelectric Performance of Cubic GeTe-based Thin Films*", Mater. Today Phys. **49**, 101581 (2024).
- D. B. Adam, W.-H. Huang, M.-C. Tsai*(蔡孟哲), W.-N. Su*(蘇威年), and B. J. Hwang*(黃炳照), "*Atomically Dispersed Ruthenium Single-atom Alloy Catalysts Enabling Efficient Iodide Oxidation Reaction Electrolysis in Acidic Media*", Int. J. Hydrogen Energ. **91**, 548 (2024).
- T. Abraha Berhe*, W.-N. Su*(蘇威年), and B. J. Hwang*(黃炳照), "*Halide Perovskites' Multifunctional Properties: Coordination Engineering, Coordination Chemistry, Electronic Interactions and Energy Applications beyond Photovoltaics*", Inorganics **12**, 182 (2024).
- D. Bhalothia, H.-Y. Liu, S.-H. Chen, Y.-T. Tseng, W. Li, S. Dai, K.-W. Wang*(王冠文), and T.-Y. Chen*(陳燦耀), "*The Sub-nanometer In_2O Clusters on Ag Nanoparticles with Highly Selective Electrochemical CO_2 Reduction to Formate*", Chem. Eng. J. **481**, 148295 (2024).
- D. Bhalothia, A. Beniwal, C. Yan, K.-C. Wang, C.-H. Wang, and T.-Y. Chen*(陳燦耀), "*Potential Synergy Between Pt_2Ni_4 Atomic-clusters, Oxygen Vacancies and Adjacent Pd Nanoparticles Outperforms Commercial Pt Nanocatalyst in Alkaline Fuel Cells*", Chem. Eng. J. **483**, 149421 (2024).
- J. A. V. Bilo, C.-K. Chang, Y.-C. Chuang, and M.-H. Fang*(方牧懷)., "*Coprecipitation Strategy for Halide-based Solid-state Electrolytes and Atmospheric-dependent In Situ Analysis*", ACS Appl. Mater. Interfaces **16**, 27394 (2024).
- B. Boro, P. Koley*, A. Boruah, T. Hosseinnejad, J. M. Lee, C.-C. Chang, C.-W. Pao, S. Bhargava, and J. Mondal*, "*Deciphering Reactivity Factors of Cu(II)-Pd(0) Engaged in Porous Organic Polymer toward Catalytic Hydrogenolysis of 5-hydroxymethylfurfural to 2,5-dimethylfuran*", ACS Sustain. Chem. Eng. **12**, 14200 (2024).
- A. Boruah, B. Boro, R. Paul, C.-C. Chang, S. Mandal, A. Shrotri, C.-W. Pao, B. K. Mai*, and J. Mondal*, "*Site-selective Zn-metalation in Poly-triphenyl Amine-based Porous Organic Polymer for Solid-gas Phase CO_2 Photoreduction*", ACS Appl. Mater. Interfaces **16**, 34437 (2024).
- S. A. Chala*, K. Lakshmanan, W.-H. Huang, A. W. Kahsay, C.-Y. Chang, F. T. Angerasa, Y.-F. Liao, J.-F. Lee, H. Dai, M.-C. Tsai*(蔡孟哲), W.-N. Su*(蘇威年), and B. J. Hwang*(黃炳照), "*Cooperative Dual Single Atom Ni/Cu Catalyst for Highly Selective CO_2-to-ethanol Reduction*", Appl. Catal. B-Environ. **358**, 124420 (2024).
- C.-C. Chang, Y.-C. Chen, K.-C. Wu, H. N. Priyadarshini, L.-Y. Lee, J.-L. Chen, C.-R. Lee, C.-W. Pao*(包志文), and D.-Y. Wang*(王迪彥), "*Subnanometer-sized CuO_x Clusters on TiO_2 as Active Photocatalysts for Ammonia Production from Photocatalytic Nitration Reduction Reaction*", ChemCatChem **16**, e202400596 (2024).
- C.-Y. Chang, W.-H. Huang, M.-C. Tsai, C.-W. Pao, M. Yoshimura, N. Hiraoka, C.-L. Chen*(陳啟亮), B. J. Hwang*(黃炳照), and W.-N. Su*(蘇威年), "*Turning Natural Copper Phthalocyanine into High-loading Single-atom Catalysts Using an Electrochemically-generated Template and Cationic Substitution*", Mater. Today Nano **25**, 100466 (2024).
- J.-W. Chang, K.-H. Su, C.-W. Pao, J.-J. Tsai, C.-J. Su, J.-L. Chen, L.-M. Lyu, C.-H. Kuo, A.-C. Su, H.-C. Yang*(楊小青), Y.-H. Lai*(賴英煌), and U.-S. Jeng*(鄭有舜), "*Arrayed Pt Single Atoms via Phosphotungstic Acids Intercalated in Silicate Nanochannels for Efficient Hydrogen Evolution Reactions*", ACS Nano **18**, 1611 (2024).
- L.-X. Chang, P. Rajamanickam, L.-C. Hsu, C.-K. Chang, Y.-C. Chuang, J.-L. Chen, L.-C. Hsu, and C.-Y. Wang*(王誠佑), "*Metal-organic Framework-derived Carbon-supported High-entropy Alloy Nanoparticles Applied in Ammonia Borane Hydrolytic Dehydrogenation*", J. Catal. **437**, 115663 (2024).
- P.-S. Chang, B.-H. Chen, Y.-C. Lin, W.-T. Dai, G. Kumar, Y.-G. Lin, and M. H. Huang*(黃暄益), "*Growth of Size-tunable Ag_2O Polyhedra and Revelation of Their Bulk and Surface Lattices*", Small **20**, 2401558 (2024).
- Y.-C. Chang, L.-M. Lyu, R.-S. Tsai, R.-H. Juang, S.-H. Yu, C.-S. Li, J.-L. Chen, and C.-H. Kuo*(郭俊宏), "*Pt-1,1′-Bi(2-naphthol) Nanostructures for Electrochemical H_2 Evolution in Alkaline Media*", ACS Appl. Nano Mater. **7**, 11890 (2024).
- C. Chen, H. Huang, Y. Chen, Z. Zhang, H. Fu, H. Li, W.-H. Huang*(黃偉翔), F. Lai, N. Zhang*(張楠), and T. Liu*(劉天西), "*Interface-engineered Cu/Cu_2In Metallic Aerogels for Efficient Electrochemical CO_2 Reduction*", ACS Mater. Lett. **6**, 756 (2024).
- C.-S. Chen*(陳敬勳), T.-C. Chen, J. H. Wu, H.-C. Wu, C.-M. Yang, T.-C. Yang, and C.-W. Pao, "*Enhancing Methane Formation in Carbon Dioxide Hydrogenation on Nickel Clusters with Zirconium Additives: Exploring Active Sites, Reaction Pathways, and Catalytic Mechanisms*", Chem. Eng. J. **489**, 151198 (2024).
- D. Chen, T. Gao, Z. Wei, M. Wang, Y. Ma, D. Xiao*(肖東東), C. Cao, C.-Y. Lee, P. Liu, D. Wang, S. Zhao, H.-T. Wang*(王孝祖), and L. Han*(韓麗麗), "*WS_2 Moiré Superlattices Supporting Au Nanoclusters and Isolated Ru to Boost Hydrogen Production*", Adv. Mater. **36**, 2410537 (2024).
- G. Chen, Y. Zhu, Y. Ying, Y. Yao, Z. Hu, D. Zu, Z. Lin, C.-W. Pao, Y.-C. Zhang, L. Li, Y. Zhu, and H. Huang*(黃海濤), "*Isolated Active Sites in Perovskite Lattice for Efficient Production of Hydrogen Peroxide*", Matter **7**, P2265 (2024).
- P.-W. Chen, C.-C. Cheng, Y.-C. Ting, T.-Y. Lin, F.-Y. Yen, G.-R. Li, and S.-Y. Lu*(呂世源), "*Single-atom Decorated Hollow Mesoporous Carbon Spheres Composited with Free-standing Carbon Cloth Supported Cobalt Sulfide Nanowire Arrays as High-performance Sulfur Host for Lithium-sulfur Batteries*", J. Taiwan Inst. Chem. Eng. **164**, 105699 (2024).
- X. Chen, N. Yu, Y. Song, T. Liu, H. Xu, D. Guan, Z. Li, W.-H. Huang, Z. Shao, F. Ciucci*, and M. Ni*(倪萌), "*Synergistic Bulk and Surface Engineering for Expeditious and Durable Reversible Protonic Ceramic Electrochemical Cells Air Electrode*", Adv. Mater. **36**, 2403998 (2024).
- Y. Chen, C. Chen, W.-H. Huang*(黃偉翔), C.-W. Pao, C.-C. Chang, T. Mao, J. Wang, H. Fu, F. Lai, N. Zhang*(張楠), and T. Liu*(劉天西), "*Charge Redistribution in High-entropy Perovskite Oxide Porous Nanotubes Boosts Nitrate Electroreduction to Ammonia*", ACS Nano **18**, 20530 (2024).
- Y.-A. Chen, Y. Nakayasu, Y.-C. Lin, J.-C. Kao, K.-C. Hsiao, Q.-T. Le, K.-D. Chang, M.-C. Wu, J.-P. Chou, C.-W. Pao, T.-F. M. Chang, M. Sone, C.-Y. Chen*(陳君怡), Y.-C. Lo*(羅友杰), Y.-G. Lin*(林彥谷), A. Yamakata*(山方啓), and Y.-J. Hsu*(徐雍鎣), "*Double-hollow Au@CdS Yolk@Shell Nanostructures as Superior Plasmonic Photocatalysts for Solar Hydrogen Production*", Adv.

Funct. Mater. **34**, 2402392 (2024).
- C.-C. Cheng, Y.-C. Ting, F.-Y. Yen, G.-R. Li, C.-H. Lee, K.-A. Lee, S.-I. Chang, H.-Y. T. Chen*(陳馨怡), and S.-Y. Lu*(呂世源), "*Synergistic Mo and W Single Atoms Co-doped Surface Hydroxylated NiFe Oxide as Bifunctional Electrocatalysts for Overall Water Splitting*", Appl. Catal. B-Environ. **358**, 124356 (2024).
- M. Cheng, D. Bhalothia, G.-H. Huang, P. K. Saravanan, Y. Wu, A. Beniwal, P.-C. Chen, X. Tu*, and T.-Y. Chen*(陳燦耀), "*Sub-millisecond Pulsed Laser Engineering of CuO_x-decorated Pd Nanoparticles for Enhanced Catalytic CO_2 Hydrogenation*", Catal. Today **441**, 114891 (2024).
- C.-W. Chiang*(江建緯), Y.-H. Chou, C.-H. Chou, H.-C. Chen, J.-L. Chen, L.-C. Hsu, W.-H. Huang, H.-L. Li, and Y.-H. Liu, "*Bioinspired Photoredox Oxidation of Alcohols with Copper-containing Galactose Oxidase Analog*", Eur. J. Inorg. Chem. **27**, e202300516 (2024).
- Y.-L. Cho, Y.-M. Tzou, A. Assakinah, N. A. T. Than, H. S. Yoon, S. I. Park, C.-C. Wang, Y.-C. Lee, L.-C. Hsu, P.-Y. Huang, S.-L. Liu, and Y.-T. Liu*(劉雨庭), "*Accumulation and Bio-oxidation of Arsenite Mediated by Thermoacidophilic Cyanidiales: Innate Potential Biomaterials toward Arsenic Remediation*", Bioresource Technol. **406**, 130912 (2024).
- Y. Chong, T. Chen, B. Zhou, Y. Li, W.-H. Huang, C.-L. Chen, J. Wei, K. Yan, Y. Qiu*(邱勇才), G. Chen*(陳光需), and D. Ye, "*Multistep Quenching of a Rust-derived Catalyst for Enhanced Volatile Organic Compound Catalytic Oxidation*", ACS Catalysis **14**, 7201 (2024).
- Y.-C. Chu, K.-H. Chen, C.-W. Tung, H.-C. Chen, J. Wang*(王佳麗), T.-R. Kuo*(郭聰榮), C.-S. Hsu, K.-H. Lin, L. D. Tsai, and H. M. Chen*(陳浩銘), "*Dynamic (Sub)surface-oxygen Enables Highly Efficient Carbonyl-coupling for Electrochemical Carbon Dioxide Reduction*", Adv. Mater. **36**, 2400640 (2024).
- J. Dai, Z. Shen, Y. Chen, M. Li, V. K. Peterson, J. Tang, X. Wang, Y. Li, D. Guan, C. Zhou, H. Sun, Z. Hu, W.-H. Huang, C.-W. Pao, C.-T. Chen, Y. Zhu*(朱印龍), W. Zhou, and Z. Shao*(邵宗平), "*A Complex Oxide Containing Inherent Peroxide Ions for Catalyzing Oxygen Evolution Reactions in Acid*", J. Am. Chem. Soc. **146**, 33663 (2024).
- A. Das*, C. Latouche, S. Jobic, E. Gautron, A. Merabet, M. Zajac, A. Shibui, P. Krüger, W.-H. Huang, C.-L. Chen, A. Kandasami, and C. Bittencourt, "*Stabilization of High-pressure Phase of CdO by Nanoparticle Formation in $Cd_xZn_{1-x}O$ Thin Films*", Acta Mater. **267**, 119744 (2024).
- L. Deng, H. Chen, S.-F. Hung, Y. Zhang, H. Yu, H.-Y. Chen, L. Li, and S. Peng*(彭生杰), "*Lewis Acid-mediated Interfacial Water Supply for Sustainable Proton Exchange Membrane Water Electrolysis*", J. Am. Chem. Soc. **146**, 35438 (2024).
- L. Deng, S.-F. Hung, S. Liu, S. Zhao, Z.-Y. Lin, C. Zhang, Y. Zhang, A.-Y. Wang, H.-Y. Chen, J. Peng, R. Ma, L. Jiao, F. Hu, L. Li, and S. Peng*(彭生杰), "*Accelerated Proton Transfer in Asymmetric Active Units for Sustainable Acidic Oxygen Evolution Reaction*", J. Am. Chem. Soc. **146**, 23146 (2024).
- T. Dey, A. Rajput, G. Jhaa, B. M. Matsagar, N. C.-R. Chen, N. Kumar, R. Salunkhe, K. C.-W. Wu, B. Chakraborty*, and S. Dutta*, "*Rapid Electronic Transport Channel of Co-P with Mo in a Heterostructure Embedded with P, N Dual Doped Porous Carbon for Electrocatalytic Oxygen and Hydrogen Evolution*", ChemNanoMat **10**, e202400089 (2024).
- H. Fu, Z. Huang, T. Zhu*(朱挺), L. Guan, C.-W. Pao, W.-H. Huang*(黃偉翔), N. Zhang*(張楠), and T. Liu*(劉天西), "*Low-coordinated Pd-Pb Sites in Porous Pd_3Pb Metallene Aerogels Promote Polyalcohol Electrochemical Oxidation*", ACS Mater. Lett. **6**, 4801 (2024).
- I. Habib, C.-W. Pao, Y.-C. Chuang, and W.-F. Liaw*(廖文峯), "*Dinitrosyl Iron Complex-derived Nanosized Zerovalent Iron (NZVI) as a Template for the Fe-Co Cracked NZVI: An Electrocatalyst for the Oxygen Evolution Reaction*", Inorg. Chem. **63**, 784 (2024).
- A. G. Hailemariam, Z. Syum, T. T. Mamo, M. Qorbani*, C.-R. Hsing*(邢正蓉), A. Sabbah, S. Quadir, K. S. Bayikadi, H.-L. Wu*(吳恆良), C.-M. Wei, L.-C. Chen*(林麗瓊), and K.-H. Chen*(陳貴賢), "*Oxygen-incorporated Lithium-rich Iron Sulfide Cathodes for Li-ion Batteries with Boosted Material Stability and Electrochemical Performance*", Chem. Mater. **36**, 9370 (2024).
- L. Han*(韓麗麗), C. Sun, H.-T. Wang*(王孝祖), W.-X. Lin, J.-L. Chen, C.-W. Pao, Y.-C. Chuang, C.-H. Wang, J. Zhou, J. Wang, W.-F. Pong, and H. L. Xin*(忻獲麟), "*Interrogation of 3d Transition Bimetallic Nanocrystal Nucleation and Growth Using In Situ Electron Microscope and Synchrotron Xray Techniques*", Nano Lett. **24**, 7645 (2024).
- M. Han, Y. Luo, L. Xu, W. Chen*(陳維), C. Li, Y.-C. Huang, Y. Wu, Y. Jiang, W. Wu, R. Wang, Y.-R. Lu, Y. Zou*(鄒雨芹), and S. Wang*(王雙印), "*Oxygen Vacancy Boosts Nitrogen-centered Radical Coupling Initiated by Primary Amine Electrooxidation*", J. Am. Chem. Soc. **146**, 33893 (2024).
- Y. Hao, S.-F. Hung, C. Tian, L. Wang, Y.-Y. Chen, S. Zhao, K.-S. Peng, C. Zhang, Y. Zhang, C.-H. Kuo, H.-Y. Chen, and S. Peng*(彭生杰), "*Polarized Ultrathin BN Induced Dynamic Electron Interactions for Enhancing Acidic Oxygen Evolution*", Angew. Chem. Int. Edit. **63**, e202402018 (2024).
- Y. Hao, S.-F. Hung, L. Wang, L. Deng, W.-J. Zeng, C. Zhang, Z.-Y. Lin, C.-H. Kuo, Y. Wang, Y. Zhang, H.-Y. Chen, F. Hu, L. Li, and S. Peng*(彭生杰), "*Designing Neighboring-site Activation of Single Atom via Tunnel Ions for Boosting Acidic Oxygen Evolution*", Nat. Commun. **15**, 8015 (2024).
- S.-H. Hsieh, S. Ghosh, Y.-H. Liang, H.-T. Wang, C.-H. Du*(杜昭宏), J.-W. Chiou, C.-M. Wu, C.-W. Wang, Y.-C. Shao, J.-L. Chen, C.-W. Pao, H.-M. Tsai, T.-S. Chan, W.-B. Wu, H.-J. Lin, J.-F. Lee, A. Kandasami, and W.-F. Pong*(彭維鋒), "*Correlation Between Noncollinear Spin Orientation and Lattice Distortion in $Ni_{0.4}Mn_{0.6}TiO_3$*", Phys. Rev. Mater. **8**, 124410 (2024).
- F. H. Hsu*(許峰豪), S. Y. Hsu, R. Subramani, T. C. Cheng, B. H. Chen, J. L. Chen, J. M. Chen*(陳錦明), and K. T. Lu*(盧桂子), "*The Ion Behavior and Storage Mechanism of 2D MoO_3 Layer Structure in an Air-stable Hydrated Eutectic Electrolyte for Aluminum-ion Energy Storage*", J. Energy Storage **84**, 110693 (2024).
- H. Hu, K. Ma, Y. Yang, N. Jin, L. Zhang*(張林杰), J. Qian, and L. Han*(韓麗麗), "*Ni Clusters Immobilized on Oxygen-rich Siloxene Nanosheets for Efficient Electrocatalytic Oxygen Reduction toward H_2O_2 Synthesis*", Dalton T. **53**, 4823 (2024).
- H. Huang, C. Chen, C.-C. Chang, F. Lai, S. Liu, H. Fu, Y. Chen, H. Li, W.-H. Huang*(黃偉翔), N. Zhang*(張楠), and T. Liu*(劉天西), "*Crystal-phase-engineered High-entropy Alloy Aerogels for Enhanced Ethylamine Electrosynthesis from Acetonitrile*", Adv. Mater. **36**, 2314142 (2024).
- J.-F. Huang*(黃景帆), W.-J. Hsieh, and J.-L. Chen, "*Carbon-promoted Pt-single Atoms Anchored on RuO_2 Nanorods to Boost Electrochemical Hydrogen Evolution*", ACS Appl. Mater. Interfaces **16**, 27504 (2024).
- P.-Y. Huang, Y.-Y. Zhang, P.-C. Tsai, R.-J. Chung, Y.-T. Tsai, M.-K. Leung, S.-Y. Lin*(林時彥), and M.-H. Fang*(方牧懷), "*Interfacial Engineering of Quantum Dots-metal-organic Framework Composite Toward Efficient Charge Transport for a Short-wave Infrared Photodetector*", Adv. Opt. Mater. **12**, 2302062 (2024).
- T.-F. Huang, Y.-R. Zhuang, C.-L. Chang, C.-L. Huang, W.-C. Lin, Z.-C. Jiang, L.-Y. Ting, I. M. A. Mekhemer, Y.-E. Sun, P. Kidkhunthod, J.-L. Chen, Y.-C. Huang, H.-K. Hsu, Y.-T. Tseng, Y.-H. Wu, B.-H. Li, S.-D. Yang, Y.-J. Cheng, and H.-H. Chou*(周鶴修), "*Indanone-based Conjugated Polymers Enabling Ultrafast Electron Transfer for Visible Light-driven Hydrogen Evolution from Water*", J. Mater. Chem. A **12**, 3633 (2024).
- Y.-C. Huang, Y. Wu, Y.-R. Lu, J.-L. Chen, H.-J. Lin, C.-T. Chen, C.-L. Chen, C. Jing, J. Zhou, L. Zhang, Y. Wang, W.-C. Chou*(周武清), S. Wang*(王雙印), Z. Hu*(胡志偉), and C.-L. Dong*(董崇禮), "*Direct Identification of O-O Bond Formation through Three-step Oxidation During Water Splitting by Operando Soft X-ray Absorption Spectroscopy*", Adv. Sci. **11**, 2401236 (2024).
- Z. Huang, Y. Wang, J. Xia, S. Hu, N. Chen, T. Ding, C. Zhan, C.-W. Pao, Z. Hu, W.-H. Huang, T. Shi, X. Meng, Y. Xu*(徐勇), L. Cao*(曹亮), and X. Huang*(黃小青), "*Atom-glue Stabilized Pt-based Intermetallic Nanoparticles*", Sci. Adv. **10**, eadq6727 (2024).
- K. Huangmee, L.-C. Hsu, Y.-M. Tzou, Y.-L. Cho, C.-H. Liao, H. Y. Teah, and Y.-T. Liu*(劉雨庭), "*Thiol-functionalized Black Carbon as Effective and Economical Materials for Cr(VI) Removal: Simultaneous Sorption and Reduction*", J. Environ. Manage. **360**, 121074 (2024).
- A. R. Jadhav, X. Liu, P. Silambarasan, V. Kanade, Y. Liu, T. T. T. Nga, T. Yang, M. T. Kim, Y. Han, T. Kim, X. Shao, C. Zhi, C.-L. Dong, and H. Lee*, "*Stable and Efficient Chlorine Evolution Reaction with Atomically Dispersed Ru on Surface Tensile Strained TiO_2*", Appl. Catal. B-Environ. **359**, 124456 (2024).
- K.-S. Jhang, Y.-C. Yang, Y.-R. Lu, K.-Y. Hsiao, M.-Y. Lu, and H.-Y. Tuan*(段興宇), "*Harnessing Berthollide Configuration Entropy for Expedited K^+ Storages*", Adv. Funct. Mater. **34**, 2411082 (2024).
- P.-S. Jhu, C.-W. Chang, C.-C. Cheng, Y.-C. Ting, T.-Y. Lin, F.-Y. Yen, P.-W. Chen, and S.-Y. Lu*(呂世源), "*Non-precious High Entropy Alloys and Highly Alkali-resistant Composite Membranes Based High Performance Anion Exchange Membrane Water Electrolyzers*", Nano Energy **126**, 109703 (2024).
- Y. Jiang, T.-Y. Chen, J.-L. Chen, Y. Liu, X. Yuan, J. Yan, Q. Sun, Z. Xu, D. Zhang, X. Wang, C. Meng, X. Guo, L. Ren*(任利敏), L. Liu*(劉玲梅), and R. Y.-Y. Lin, "*Heterostructured Bimetallic MOF-on-MOF Architectures for Efficient Oxygen Evolution Reaction*", Adv. Mater. **36**, 2306910 (2024).
- Y. Jiang, W. Cheng, J.-L. Chen, Y. Liu, L. Liu, Z. Xu, N. Ma*(麻娜娜), R. Y.-Y. Lin, L. Ren*(任利敏), and C. Meng, "*Facile Synthesis of Dual-MOF Ultrathin Nanosheets Supported on Layered Double Hydroxides Heterostructure: Electron Modulation Strategy for Enhanced Electrocatalytic Water Splitting*", Appl. Catal. B-Environ. **361**, 124662 (2024).
- C. Jing, L. Li, Y.-Y. Chin, C.-W. Pao, W.-H. Huang, M. Liu, J. Zhou, T. Yuan, X. Zhou, Y. Wang, C.-T. Chen, D.-W. Li*(李大偉), J.-Q. Wang, Z. Hu*(胡志偉), and L. Zhang*(張林娟), "*Balance Between Fe^{IV}–Ni^{IV} Synergy and Lattice*

Oxygen Contribution for Accelerating Water Oxidation", ACS Nano **18**, 14496 (2024).

- J.-C. Kao, T.-Y. Teng, H.-W. Lin, F.-G. Tseng, L.-Y. Ting, D. Bhalothia, H.-H. Chou, Y.-C. Lo, J.-P. Chou*(周至品), and T.-Y. Chen*(陳燦耀), "*Single Atom Ag Bonding Between PF3T Nanocluster and TiO_2 Leads the Ultra-stable Visible-light-driven Photocatalytic H_2 Production*", Small **20**, 2403176 (2024).
- V. Krishnamoorthy, P. Sabhapathy*, P. Raghunath, C.-Y. Huang, A. Sabbah, M. K. Hussien, Z. Syum, S. Muthusamy, M.-C. Lin, H.-L. Wu, R.-S. Chen*(陳瑞山), K.-H. Chen*(陳貴賢), and L.-C. Chen*(林麗瓊), "*Synergistic Electronic Interaction of Nitrogen Coordinated Fe-Sn Double-atom Sites: An Efficient Electrocatalyst for Oxygen Reduction Reaction*", Small Methods **8**, 2301674 (2024).
- T.-W. Lee and C. Chen*(陳佳吟), "*Humic Acid Changes Effect of Naturally Occurring Oxidants on the Environmental Transformation of Molybdenum Disulfide Nanosheets*", J. Environ. Manage. **368**, 122190 (2024).
- Y. Li, C.-K. Peng, Y. Sun*(孫蘊洞), L. D. N. Sui, Y.-C. Chang, S.-Y. Chen, Y. Zhou*(周英棠), Y.-G. Lin*(林彥谷), and J.-M. Lee*, "*Operando Elucidation of Hydrogen Production Mechanisms on Sub-nanometric High-entropy Metallenes*", Nat. Commun. **15**, 10222 (2024).
- Y. Li*(李云華), S. Zheng, Y. He, S. Yang, W.-H. Huang, C.-W. Pao, Z. Hu, and X. Huang*(黃小青), "*Masked Second-shell Sulfur Coordinating Atomically Dispersed Pd on Tin Oxide Boosts the Direct Synthesis of Hydrogen Peroxide*", Chem. Eng. J. **500**, 157297 (2024).
- Yongjian Li, Xinyu Zhu, Chenxi Wei, Youyou Fang, Xinyu Wang, Yizhi Zhai, Wenlong Kang, Lai Chen, Duanyun Cao, Meng Wang, Yun Lu, Qing Huang, Yuefeng Su*(蘇岳鋒), Hong Yuan*(袁洪), Ning Li*(李寧), and Feng Wu, "*Unraveling the Chemical and Structural Evolution of Novel Li-rich Layered/Rocksalt Intergrown Cathode for Li-ion Batteries*", Chin. Chem. Lett. **35**, 109536 (2024).
- K.-W. Liao, H.-Y. Chen, W.-H. Wei, G.-C. Chen, I. Yamanaka, B.-T. Liu, T.-F. Hong, T.-C. Chiang, H.-C. Huang*(黃信智), and C.-H. Wang*(王丞浩), "*Novel Ruthenium-based Catalysts with Atomic Dispersion for Oxygen Evolution Reaction in Water Electrolysis*", Mater. Today Chem. **35**, 101857 (2024).
- J. Lin, S. Zhao, J. Yang, W.-H. Huang, C.-L. Chen, T. Chen, Y. Zhao, G. Chen*(陳光需), Y. Qiu*(丘勇才), and L. Gu, "*Hydrogen Spillover Induced PtCo/CoO_x Interfaces with Enhanced Catalytic Activity for CO Oxidation at Low Temperatures in Humid Conditions*", Small **20**, 2309181 (2024).
- T.-Y. Lin*(林姿瑩), C.-F. Hsieh, A. Kanai, T. Yashiro, W.-J. Zeng, J.-J. Ma, S.-F. Hung, and M. Sugiyama, "*Radiation Resistant Chalcopyrite CIGS Solar Cells: Proton Damage Shielding with Cs Treatment and Defect Healing via Heat-light Soaking*", J. Mater. Chem. A **12**, 7536 (2024).
- Q. Liu, W. Xu, H. Huang, H. Shou, J. Low, Y. Dai, W. Gong, Y. Li, D. Duan, W. Zhang, Y. Jiang, G. Zhang, D. Cao, K. Wei, R. Long*(龍冉), S. Chen, L. Song, and Y. Xiong*(熊宇杰), "*Spectroscopic Visualization of Reversible Hydrogen Spillover between Palladium and Metal-organic Frameworks toward Catalytic Semihydrogenation*", Nat. Commun. **15**, 2562 (2024).
- S. Liu, W.-H. Huang, S. Meng, K. Jiang, J. Han*(韓佳甲), Q. Zhang, Z. Hu, C.-W. Pao, H. Geng, X. Huang, C. Zhan, Q. Yun, Y. Xu*(徐雍), and X. Huang*(黃小青), "*3D Noble-metal Nanostructures Approaching Atomic Efficiency and Atomic Density Limits*", Adv. Mater. **36**, 2312140 (2024).
- S. Liu, C.-W. Pao, J.-L. Chen, S. Li, K. Chen, Z. Xuan, C. Song, J. J. Urban*, M. T. Swihart*, and C. Dun*, "*A General Flame Aerosol Route to High-entropy Nanoceramics*", Matter **7**, P3994 (2024).
- Z. Liu, Y. Bai, H. Sun, D. Guan, W. Li, W.-H. Huang, C.-W. Pao, Z. Hu, G. Yang*(楊廣明), Y. Zhu*(朱印龍), R. Ran, W. Zhou, and Z. Shao*(邵宗平), "*Synergistic Dual-phase Air Electrode Enables High and Durable Performance of Reversible Proton Ceramic Electrochemical Cells*", Nat. Commun. **15**, 472 (2024).
- L. Luo, T. Zhou, W. Li, X. Li, H. Yan, W. Chen, Q. Xu, S. Hu, C. Ma, J. Bao, C.-W. Pao, Z. Wang, H. Li, X. Ma*(馬新龍), L. Luo*(羅賴昊), and J. Zeng*(曾杰), "*Close Intimacy between PtIn Clusters and Zeolite Channels for Ultrastability toward Propane Dehydrogenation*", Nano Lett. **24**, 7236 (2024).
- L.-M. Lyu, H.-J. Li, R.-S. Tsai, C.-F. Chen, Y.-C. Chang, Y.-C. Chuang, C.-S. Li, J.-L. Chen, T.-W. Chiu*(邱德威), and C.-H. Kuo*(郭俊宏), "*In Operando X-ray Spectroscopic and DFT Studies Revealing Improved H_2 Evolution by the Synergistic Ni-Co Electron Effect in the Alkaline Condition*", ACS Appl. Mater. Interfaces **16**, 27329 (2024).
- T. T. Mamo, M. Qorbani*, A. G. Hailemariam, R. Putikam, C.-M. Chu, T.-R. Ko, A. Sabbah, C.-Y. Huang, S. Kholimatussadiah, T. Billo, M. K. Hussien, S.-Y. Chang, M.-C. Lin, W.-Y. Woon, H.-L. Wu*(吳恆良), K.-T. Wong, L.-C. Chen*(林麗瓊), and K.-H. Chen*(陳貴賢), "*Enhanced CO_2 Photoreduction to CH_4 via *COOH and *CHO Intermediates Stabilization by Synergistic Effect of Implanted P and S Vacancy in Thin-film SnS_2*", Nano Energy **128**, 109863 (2024).
- L. Merinda, F.-M. Wang*(王復民), N.-L. Wu*(吳乃立), R. A. Yuwono, C. Khotimah, U. Qonita, W.-H. Huang, L.-P. Wan, C.-K. Chang, P.-H. Hsu, C.-W. Pao, J.-L. Chen, C.-L. Chen, and T.-S. Chan, "*Carbonate Deprotonation on an Ni-rich Layered Cathode: Development of a New Cis-oligomer as an Organic Coverage*", J. Mater. Chem. A **12**, 28886 (2024).
- E. A. Moges, C.-Y. Chang, W.-H. Huang, F. T. Angerasa, K. Lakshmanan, T. M. Hagos, H. G. Edao, W. B. Dilebo, C.-W. Pao, M.-C. Tsai*(蔡孟哲), W.-N. Su*(蘇威年), and B. J. Hwang*(黃炳照), "*Heteroatom-coordinated Palladium Molecular Catalysts for Sustainable Electrochemical Production of Hydrogen Peroxide*", J. Am. Chem. Soc. **146**, 419 (2024).
- T. Natarajan, S. Arumugam, Y.-F. Tsai, A. Abou-taleb, and S. S.-F. Yu*(俞聖法), "*Unveiling the Enhanced Electrochemical CO_2 Conversion: The Role of 3D Porous BiOCl with Defects and CTAB-mediated Nanosheets*", J. CO2 Util. **85**, 102888 (2024).
- H. Niu, H. Liu, L. Yang, T. Kang, T. Shen, B. Jiang, W.-H. Huang, C.-C. Chang, Y. Pei*(裴艷中), G. Cao*(曹國忠), and C. Liu*(劉超峰), "*Impacts of Distorted Local Chemical Coordination on Electrochemical Performance in Hydrated Vanadium Pentoxide*", Nat. Commun. **15**, 9421 (2024).
- R. Patil, A. Rajput, B. M. Matsagar, N. C. R. Chen, M. Ujihara, R. R. Salunkhe, P. Yadav, K. C.-W. Wu, B. Chakraborty*, and S. Dutta*, "*Elevated Temperature-driven Coordinative Reconstruction of an Unsaturated Single-Ni-atom Structure with Low Valency on a Polymer-derived Matrix for the Electrolytic Oxygen Evolution Reaction*", Nanoscale **16**, 7467 (2024).
- A. Pei, P. Wang, S. Zhang, Q. Zhang, X. Jiang, Z. Chen, W. Zhou, Q. Qin, R. Liu, R. Du, Z. Li, Y. Qiu, K. Yan, L. Gu*(谷林), J. Ye, G. I. N. Waterhouse, W.-H. Huang, C.-L. Chen, Y. Zhao*(趙云), and G. Chen*(陳光需), "*Enhanced Electrocatalytic Biomass Oxidation at Low Voltage by Ni^{2+}-O-Pd Interfaces*", Nat. Commun. **15**, 5899 (2024).
- S.-M. Peng, S.-T. Chang, C.-C. Chang, Priyadarshini HN, C.-C. Chang*(張鈞智), K.-C. Wu, Y.-H. Huang, Y.-C. Chen, T.-R. Kuo, C.-W. Pao, J.-L. Chen, and D.-Y. Wang*(王迪彥), "*Boosted Urea Electrooxidation Activity by Dynamic Steady Blending CoOOH-Ni$(OH)_2$ Nanoclusters for H_2 Production in a pH-asymmetric Electrolyzer*", J. Mater. Chem. A **12**, 24126 (2024).
- Y. Pi, Z. Qiu, Y. Fan, Q. Mao, G. Zhang, X. Wang, H.-H. Chang, H.-J. Chen, T.-Y. Chen, H.-Y. Chen, S. Zhang, M. Shakouri, and H. Pang*(龐歡), "*Immobilization of Metal Nanoparticles to an Ultrathin Two-dimensional Conjugated Metal-organic Framework for Synergistic Electrocatalysis*", Nano Lett. **24**, 13760 (2024).
- Z.-X. Qian, C.-K. Peng, M.-F. Yue, L.-C. Hsu, J.-S. Zeng, D.-Y. Wei, Z.-Y. Du, G.-Y. Xu, Hua Zhang*(張華), J.-H. Tian, S.-Y. Chen, Y.-G. Lin*(林彥谷), and J.-F. Li*(李劍鋒), "*Direct Capturing and Regulating Key Intermediates for High-efficiency Oxygen Evolution Reactions*", Small Methods **8**, 2301504 (2024).
- Y. Qin, C.-H. Chuang, X. Liu, X. Liang, L. Xie, K. Wang, C.-W. Pao, Y.-R. Lu, Y. Liu, Y. Chen, Z. Lei*(雷占武), P. Yan, L. Wu, S. Jiao, Q. Li*(李箐), and R. Cao*(曹瑞國), "*DNA-anchored Single-molecule Iron Phthalocyanine As an Efficient Electrocatalyst for Alkaline Fuel Cells*", ACS Catalysis **14**, 7514 (2024).
- J. Quintal, C. McGuire, T. Shi, W.-H. Huang, D. Chow, C.-K. Hung, D.-T. Jiang, B. J. Hwang, and A. Chen*(陳愛成), "*Substrate-assisted Atomic Dispersion of Cobalt for Alkaline Water Electrolysis*", J. Phys. Chem. Lett. **15**, 9208 (2024).
- Veeramani Rajendran, C.-Y. Chang, M.-H. Huang, K.-C. Chen, W.-T. Huang, Mikołaj Kaminski, Tadeusz Lesniewski, Sebastian Mahlik*, Grzegorz Leniec*, K.-M. Lu, D.-H. Wei*(魏大華), Ho Chang*(張合), and R.-S. Liu*(劉如熹), "*Chromium Cluster Luminescence: Advancing Near-infrared Light-emitting Diode Design for Next-generation Broadband Compact Light Sources*", Adv. Opt. Mater. **12**, 2302645 (2024).
- M. Rinawati, Y.-S. Chiu, L.-Y. Chang, C.-Y. Chang, W.-N. Su, N. L. W. Septiani, B. Yuliarto, W.-H. Huang, J.-L. Chen, and M.-H. Yeh*(葉旻鑫), "*Evoking Dynamic Fe-N_x Active Sites through the Immobilization of Molecular Fe Catalysts on N-doped Graphene Quantum Dots for the Efficient Electroreduction of Nitrate to Ammonia*", J. Mater. Chem. A **12**, 22070 (2024).
- N. Runprapan, R. A. Yuwono, F.-M. Wang*(王復民), C.-C. Yuan*(袁九重), N.-L. Wu, A. Ramar, R. Foeng, C.-K. Chang, P.-H. Hsu, and J.-F. Lee, "*Auto-reduction of Au(III) on Fe-doped, Pyrrolic-N-modified Nanoporous Carbon Derived from ZIF-8 for the Electrochemical Immunosensing of CA-125*", Electrochim. Acta **498**, 144577 (2024).
- A. Satpathy, W.-T. Huang, T.-H. Liu, T.-Y. Su, W. Zhang, M. Kaminski, M. Grzegorczyk, J.-H. Chen, D.-H. Cherng, K.-M. Lu, X. Chen, S. Mahlik*, and R.-S. Liu*(劉如熹), "*Mini Light-emitting Diode Technology with High Quantum Efficient NIR-II Partially Inverse Spinel $MgGa_2O_4$: Cr^{3+},Ni^{2+} Nanophosphors*", Adv. Opt. Mater. **12**, 2400130 (2024).
- M. M. R. Singuru, J.-L. Chen, H.-Y. Chen, W.-C. Liao, Y.-Y. Chen, M.-C.

Chuang*(莊旻傑), "*Mercury^{II}-mediated Construction of DNA Capsules for Turn-on Fluorescence Detection of Melamine*", Microchim. Acta **191**, 658 (2024).

- R. Subramani, S.-Y. Hsu, Y.-C. Chuang, L.-C. Hsu, K.-T. Lu*(盧柱子), and J.-M. Chen*(陳錦明), "*Fe-MIL-101 Metal Organic Framework Integrated Solid Polymer Electrolytes for High-performance Solid-state Lithium Metal Batteries*", J. Mater. Chem. A **12**, 7132 (2024).
- L. Sun, H. Peng, F. Xue, S. Liu, Z. Hu, H. Geng, X. Liu, D. Su, Y. Xu*(徐勇), and X. Huang*(黃小青), "*Pd Single Atoms Cooperate with S Vacancies in $ZnIn_2S_4$ Nanosheets for Photocatalytic Pure-water Splitting*", Sci. China-Chem. **67**, 855 (2024).
- N. Sun, Z. Zheng, Z. Lai, J. Wang, P. Du, T. Ying*(應天平), H. Wang*(王海豐), J. Xu, R. Yu, Z. Hu, C.-W. Pao, W.-H. Huang, K. Bi, M. Lei*(雷鳴), and K. Huang*(黃凱), "*Augmented Electrochemical Oxygen Evolution by d-p Orbital Electron Coupling*", Adv. Mater. **36**, 2404772 (2024).
- N. Sun, Z. Lai, W. Ding, W. Li, T. Wang, Z. Zheng, B. Zhang, X. Dong, P. Wei, P. Du, Z. Hu, C.-W. Pao, W.-H. Huang, H. Wang*(王海豐), M. Lei, K. Huang*(黃凱), and R. Yu*(于潤澤), "*Alkali Metals Activated High Entropy Double Perovskites for Boosted Hydrogen Evolution Reaction*", Adv. Sci. **11**, 2406453 (2024).
- G.-H. Tan, H.-C. Lin, H.-C. Liang, C.-W. Pao, P.-Y. Chen, W.-T. Chuang, C.-A. Hsieh, D. M. Dorrah, M.-C. Li, L.-Y. Chen, H.-H. Chou, and H.-W. Lin* (林皓武), "*Highly Efficient Manganese Bromides with Reversible Luminescence Switching through Amorphous-crystalline Transition*", ACS Appl. Mater. Interfaces **16**, 55842 (2024).
- J. Tang, X. Liu, X. Xiong, Q. Zeng, Y. Ji, C. Liu, J. Li, H. Zeng, Y. Dai, X. Zhang, C. Li, H. Peng, Q. Jiang, T. Zheng, C.-W. Pao, and C. Xia*(夏川), "*Ruthenium Single-atom Modulated Protonated Iridium Oxide for Acidic Water Oxidation in Proton Exchange Membrane Electrolysers*", Adv. Mater. **36**, 2407394 (2024).
- P. Tangthuam, S. Wannapaiboon, P. Kidkhunthod, J.-L. Chen, C.-C. Chang, C. W. Pao, P. A. Zijdemans, T. Yonezawa, M. Suttipong*, and S. Kheawhom, "*Innovative pH-buffering Strategies for Enhanced Cycling Stability in Zinc-iodine Flow Batteries*", J. Mater. Chem. A **12**, 29513 (2024).
- T. M. Tekaligne, H. K. Bezabh, S. K. Merso, K. N. Shitaw, M. A. Weret, Y. Nikodimos, S.-K. Jiang, S.-C. Yang, C.-H. Wang, S.-H. Wu, W.-N. Su*(蘇威年), and B. J. Hwang*(黃炳照), "*Enhancing Aluminum Foil Performance in Aqueous and Organic Electrolytes: Dual-secure Passivation with Phthalocyanine as a Corrosion Inhibitor*", J. Mater. Chem. A **12**, 2157 (2024).
- N. Q. Thang, A. Sabbah*, C.-Y. Huang, N. H. Phuong, T.-Y. Lin, M. K. Hussien, H.-L. Wu, C.-I. Wu, N. N. T. Pham, P. V. Viet, C.-H. Lee, L.-C. Chen*(林麗瓊), and K.-H. Chen*(陳貴賢), "*Tailoring Atomically Dispersed Fe-induced Oxygen Vacancies for Highly Efficient Gas-phase Photocatalytic CO_2 Reduction and NO Removal with Diminished Noxious Byproducts*", J. Mater. Chem. A **12**, 31847 (2024).
- Y.-T. Tsai, T. Lesniewski, N. Majewska, M. Kaminski, J. Barzowska, E.-P. Liu, W.-T. Chen, S. Mahlik*, and M.-H. Fang*(方牧懷), "*Pressure/Temperature-assisted Crystallographic Engineering-A Strategy for Developing the Infrared Phosphors*", Chem. Eng. J. **490**, 151596 (2024).
- Y.-T. Tsai, P.-X. Chen, M. Kaminski, N. Majewska, S. Mahlik*, and M.-H. Fang*(方牧懷), "*Sharp-to-broad Band Energy Transfer in Lithium Aluminate and Gallate Phosphors for SWIR LED*", ACS Appl. Opt. Mater. **2**, 2401 (2024).
- B. Wang, J. Ma, K. Wang, D. Wang, G. Xu, X. Wang*(王曉剛), Z. Hu, C.-W. Pao, J.-L. Chen, L. Du, X. Du*(杜曉璠), and G. Cui*(崔光磊), "*High-entropy Phase Stabilization Engineering Enables High-performance Layered Cathode for Sodium-ion Batteries*", Adv. Energy Mater. **14**, 2401090 (2024).
- B. Wang, M. Wang, Z. Fan, C. Ma, S. Xi, L.-Y. Chang, M. Zhang, N. Ling, Z. Mi, S. Chen, W. R. Leow, J. Zhang, D. Wang, and Y. Lum*(林彥瑋), "*Nanocurvature-induced Field Effects Enable Control over the Activity of Single-atom Electrocatalysts*", Nat. Commun. **15**, 1719 (2024).
- J. Wang, Y. Zhu, X. Zhong, Z. Hu, W.-H. Huang, C.-W. Pao, H. Cheng* (程洪飛), N. Alonso-Vante*, and J. Ma*(馬吉偉), "*Universal Synthesis Strategy for Preparation of Transition Metal Oxide Electrocatalysts Doped with Noble Metal Single Atoms for Oxygen Evolution Reaction*", Energy Adv. **3**, 2002 (2024).
- J. Wang, S. Wang, Z. Wei, P. Wang, Y. Cao, Y. Huang, L. He*(何林), and A. Lei*(雷愛文), "*Synchronous Recognition of Amines in Oxidative Carbonylation toward Unsymmetrical Ureas*", Science **386**, 776 (2024).
- L. Wang, M. Ma, C. Zhang, H.-H. Chang, Y. Zhang, L. Li, H.-Y. Chen, and S. Peng*(彭生杰), "*Manipulating the Microenvironment of Single Atoms by Switching Support Crystallinity for Industrial Hydrogen Evolution*", Angew. Chem. Int. Edit. **63**, e202317220 (2024).
- L.-C. Wang, L.-C. Chang, H.-L. Huang, P.-Y. Chang, C.-W. Pao, Y.-F. Liu, K.-S. Huang, Y.-H. Chien*(簡儀欣), H.-S. Sheu*(許火順), W.-P. Su*(蘇文彬), C.-H. Yeh*(葉丞豪), and C.-S. Yeh*(葉晨聖), "*Synergistic ROS Generation via Core-shell Nanostructures with Increased Lattice Microstrain Combined with Single-atom Catalysis for Enhanced Tumor Suppression*", ACS Appl. Mater. Interfaces **16**, 45356 (2024).
- M. Wang, C. Tang, S. Geng, C. Zhan, L. Wang, W.-H. Huang, C.-W. Pao, Z. Hu, Y. Li, X. Huang, and L. Bu*(卜令正), "*Compressive Strain in Platinum-iridium-nickel Zigzag-like Nanowire Boosts Hydrogen Catalysis*", Small **20**, 2310036 (2024).
- Y. Wang, Z. Wang, K. Yang, J. Liu, Y. Song, J. Li, Z. Hu, M. J. Robson, Z. Zhang, Y. Tian, S. Xu, Y. Lu, H. M. Law, F. Liu, Q. Chen, Z. Yang*(楊志賓), and F. Ciucci*, "*Self-recoverable Symmetric Protonic Ceramic Fuel Cell with Smart Reversible Exsolution/Dissolution Electrode*", Adv. Funct. Mater. **34**, 2404846 (2024).
- L. Wei, N. Fang, F. Xue, S. Liu, W.-H. Huang, C.-W. Pao, Z. Hu, Y. Xu*(徐勇), H. Geng*(耿洪波), and X. Huang*(黃小青), "*Amorphous-crystalline RuTi Nanosheets Enhancing OH Species Adsorption for Efficient Hydrogen Oxidation Catalysis*", Chem. Sci. **15**, 3928 (2024).
- L. Wei, W. Yan, Z. Huang, R. Li, Q. Kong, W.-H. Huang, C.-W. Pao, Z. Hu, H. Lin, N. Chen, Y. Xu*(徐勇), H. Geng*(耿洪波), and X. Huang*(黃小青), "*Phase and Interface Engineering of a Ru-Sn Nanocatalyst for Enhanced Alkaline Hydrogen Oxidation Reaction*", Energ. Environ. Sci. **17**, 5922 (2024).
- C.-Y. Wu, Y.-C. Hsiao, Y. Chen, K.-H. Lin, T.-J. Lee, C.-C. Chi, J.-T. Lin, L.-C. Hsu, H.-J. Tsai, J.-Q. Gao, C.-W. Chang, I.-T. Kao, C.-Y. Wu, Y.-R. Lu, C.-W. Pao, S.-F. Hung, M.-Y. Lu, S. Zhou, and T.-H. Yang*(楊東翰), "*A Catalyst Family of High-entropy Alloy Atomic Layers with Square Atomic Arrangements Comprising Iron-and Platinum-group Metals*", Sci. Adv. **10**, eadl3693 (2024).
- W.-Y. Wu, W.-Y. Zheng, W.-T. Chen, F.-T. Tsai*(蔡富潯), M.-L. Tsai, C.-W. Pao, J.-L. Chen, and W.-F. Liaw*(廖文峯), "*Electronic Structure and Transformation of Dinitrosyl Iron Complexes (DNICs) Regulated by Redox Non-innocent Imino-substituted Phenoxide Ligand*", Inorg. Chem. **63**, 2431 (2024).
- W. Xu, H. Li, X. Zhang, T.-Y. Chen, H. Yang, H. Min, X. Shen, H.-Y. Chen, and J. Wang*(王瑾), "*Regulating Graphitic Microcrystalline and Single-atom Chemistry in Hard Carbon Enables High-performance Potassium Storage*", Adv. Funct. Mater. **34**, 2309509 (2024).
- F. Xue, C. Zhang, C. Cheng, X. Yan, F. Liu, X. Liu, B. Jiang, Q. Zhang, L. Sun, H. Peng, W.-H. Huang, C.-W. Pao, Z. Hu, M. Chen, D. Su, M. Liu*(劉茂昌), X. Huang*(黃小青), and Y. Xu*(徐勇), "*Selective Light-driven Methane Oxidation to Ethanol*", Nat. Commun. **15**, 10451 (2024).
- B. Yang, K. Liu, Y. Ma, J.-J. Ma, Y.-Y. Chen, M. Huang, C. Yang, Y. Hou, S.-F. Hung, J. C. Yu, J. Zhang*(張金水), and X. Wang*(王心晨), "*Incorporation of Pd Single-atom Sites in Perovskite with an Excellent Selectivity toward Photocatalytic Semihydrogenation of Alkynes*", Angew. Chem. Int. Edit. **63**, e202410394 (2024).
- J. Yang, L. Wang, J. Wan, F. El Gabaly, A. L. F. Cauduro, B. E. Mills, J.-L. Chen, L.-C. Hsu, D. Lee, X. Zhao, H. Zheng, M. Salmeron, C. Wang, Z. Dong, H. Lin, G. A. Somorjai, F. Rosner, H. Breunig, D. Prendergast, D.-E. Jiang*(江德恩), and S. Singh*, and J. Su*, "*Atomically Synergistic Zn-Cr Catalyst for Iso-stoichiometric Co-conversion of Ethane and CO_2 to Ethylene and CO*", Nat. Commun. **15**, 911 (2024).
- J. Yang, J. Zheng, C. Dun, L. J. Falling, Q. Zheng, J.-L. Chen, M. Zhang, N. R. Jaegers, C. Asokan, J. Guo, M. Salmeron, D. Prendergast, J. J. Urban*, G. A. Somorjai*, Y. Guo*(郭彥炳), and J. Su*, "*Unveiling Highly Sensitive Active Site in Atomically Dispersed Gold Catalysts for Enhanced Ethanol Dehydrogenation*", Angew. Chem. Int. Edit. **63**, e202408894 (2024).
- P.-T. Yang, Y.-H. Liang, D.-C. Lee, and S.-L. Wang*(王尚禮), "*Chemical Speciation and Rice Uptake of Soil Molybdenum-investigation with X-ray Absorption Spectroscopy and Isotope Fractionation*", Sci. Total Environ. **949**, 175141 (2024).
- Y. Yang, Y. Xiao, L. Zhang*(張林杰), H.-T. Wang, K.-H. Chen, W.-X. Lin, N. Jin, C. Sun, Y.-C. Shao, J.-L. Chen, J. Qian*(錢金杰), and L. Han* (韓麗麗), "*Encaging Co Nanoparticle in Atomic Co-N_4-dispersed Graphite Nanopocket Evokes High Oxygen Reduction Activity for Flexible Zn-air Battery*", Appl. Catal. B-Environ. **347**, 123792 (2024).
- C.-H. Yeh, J.-W. Kang, Y.-L. Chen, H.-J. Chen, H.-H. Chang, W.-H. Lu, S.-Y. Chen, H.-L. Chen, C.-W. Hu, L.-Y. Chueh, Y.-T. F. Pan, and H.-Y. Chen* (陳翰儀), "*Electrochemical Improvement of $Na_{0.62}K_{0.05}Mg_{2/9}Cu_{1/9}Mn_{2/3}O_2$ P2-type Layer-oxide Anionic Redox Cathodes of Sodium-ion Batteries via Incorporating K-doping*", ACS Sustain. Chem. Eng. **12**, 12795 (2024).
- S. Yin, L. Chen, J. Yang, X. Cheng, H. Zeng, Y. Hong, H. Huang, X. Kuai, Y.-G. Lin, R. Huang*(黃蕊), Y. Jiang*(姜豔霞), and S. Sun*(孫世剛), "*A Fe-NC Electrocatalyst Boosted by Trace Bromide Ions with High Performance in Proton Exchange Membrane Fuel Cells*", Nat. Commun. **15**, 7489 (2024).
- H. Yu, Y. Ji, C. Li, W. Zhu, Y. Wang, Z. Hu, J. Zhou, C.-W. Pao, W.-H. Huang, Y.

Li, X. Huang, and Q. Shao*(邵琪), "*Strain-triggered Distinct Oxygen Evolution Reaction Pathway in Two-dimensional Metastable Phase IrO_2 via CeO_2 Loading*", J. Am. Chem. Soc. **146**, 20251 (2024).

- Z. Yu, Y. Chen, J. Xia, Q. Yao, Z. Hu, W.-H. Huang, C.-W. Pao, W. Hu, X.-M. Meng, L.-M. Yang*(楊利明), and X. Huang*(黃小青), "*Amorphization Activated Multimetallic Pd Alloys for Boosting Oxygen Reduction Catalysis*", Nano Lett. **24**, 1205 (2024).
- Z. Yu, H. Deng, Q. Yao, L. Zhao, F. Xue, T. He, Z. Hu, W.-H. Huang, C.-W. Pao, L.-M. Yang*(楊利明), and X. Huang*(黃小青), "*Selective and Durable H_2O_2 Electrosynthesis Catalyst in Acid by Selenization Induced Straining and Phasing*", Nat. Commun. **15**, 9346 (2024).
- L. Zhang, X. Li, Y. Chen, H.-T. Wang, Y. Chen, K. H. Chen, Y.-C. Shao, W. Lin*, C.-W. Pao, H. Wang, W.-F. Pong, J. Luo, and L. Han*(韓麗麗), "*Strain-controlled Intermetallic PtZn Nanoparticles via N-doping Propel Highly Efficient Oxygen Reduction Electrocatalysis*", ACS Sustain. Chem. Eng. **12**, 405 (2024).
- L. Zhang, H. Hu, C. Sun, D. Xiao, H.-T. Wang, Y. Xiao, S. Zhao, K. H. Chen, W.-X. Lin, Y.-C. Shao, X. Wang, C.-W. Pao, and L. Han*(韓麗麗), "*Bimetallic Nanoalloys Planted on Super-hydrophilic Carbon Nanocages Featuring Tip-intensified Hydrogen Evolution Electrocatalysis*", Nat. Commun. **15**, 7179 (2024).
- S. Zhang, F. Zhao, H. Su, Y. Zhong, J. Liang, J. Chen, M. L. Zheng, J. Liu, L.-Y. Chang, J. Fu, S. H. Alahakoon, Y. Hu, Y. Liu, Y. Huang, J. Tu, T.-K. Sham, and X. Sun*(孫學良), "*Cubic Iodide Li_xYI_{3+x} Superionic Conductors through Defect Manipulation for All-solid-state Li Batteries*", Angew. Chem. Int. Edit. **63**, e202316360 (2024).
- S. Zhao, Y. Wang, Y. Hao, L. Yin, C.-H. Kuo, H.-Y. Chen, L. Li, and S. Peng* (彭生杰), "*Lewis Acid Driving Asymmetric Interfacial Electron Distribution to Stabilize Active Species for Efficient Neutral Water Oxidation*", Adv. Mater. **36**, 2308925 (2024).
- S. Zhao, S.-F. Hung, L. Deng, W.-J. Zeng, T. Xiao, S. Li, C.-H. Kuo, H.-Y. Chen, F. Hu, and S. Peng*(彭生杰), "*Constructing Regulable Supports via Nonstoichiometric Engineering to Stabilize Ruthenium Nanoparticles for Enhanced pH-universal Water Splitting*", Nat. Commun. **15**, 2728 (2024).
- S. Zheng, Y. He, J. Liu, W.-H. Huang, C.-W. Pao, Z. Hu, X. Huang*(黃小青), and Y. Li*(李雲華), "*Palladium-Tin Alloy Nanoparticles in Different Crystalline Phases for Direct Hydrogen Peroxide Synthesis*", ACS Appl. Nano Mater. **7**, 13603 (2024).
- W.-J. Zhong, M.-Y. Hung, Y.-T. Kuo, H.-K. Tian*(田弘康), C.-N. Tsai, C.-J. Wu, Y.-D. Lin, H.-C. Yu, Y.-G. Lin, and J.-J. Wu*(吳季珍), "*Dual-vacancy-engineered $ZnIn_2S_4$ Nanosheets for Harnessing Low-frequency Vibration Induced Piezoelectric Polarization Coupled with Static Dipole Field to Enhance Photocatalytic H_2 Evolution*", Adv. Mater. **36**, 2403228 (2024).
- X. Zhong, L. Sui, M. Yang, T. Koketsu, M. Klingenhof, S. Selve, K. G. Reeves, C. Ge, L. Zhuang, W. H. Kan, M. Avdeev, M. Shu, N.-A. Vante, J.-M. Chen, S.-C. Haw, C.-W. Pao, Y.-C. Chang, Y. Huang, Z. Hu*(胡志偉), P. Strasser*, and J. Ma*(馬吉偉), "*Stabilization of Layered Lithium-rich Manganese Oxide for Anion Exchange Membrane Fuel Cells and Water Electrolyzers*", Nat. Catal. **7**, 546 (2024).
- C. Zhou, X. Wang, D. Liu, M. Fei, J. Dai, D. Guan, Z. Hu, L. Zhang, Y. Wang, W. Wang, R. O'Hayre, S. P. Jiang, W. Zhou*(周蒐), M. Liu, and Z. Shao* (邵宗平), "*New Strategy for Boosting Cathodic Performance of Protonic Ceramic Fuel Cells Through Incorporating a Superior Hydronation Second Phase*", Energ. Environ. Mater. **7**, e12660 (2024).
- J. Zhu, L. An, X. Li, K. Iputera, R.-S. Liu*(劉如熹), J. Yang, D. Wang*(王得麗), and X. Zhao*(趙旭), "*Anchoring Isolated Pd Atoms on $Ti_3C_2T_x$ MXene with Boosted Kinetics for Alkaline Hydrogen Evolution*", Appl. Surf. Sci. **644**, 158809 (2024).
- W. Zhu, X. Zhu, J. Qi, J. Yao, Y. Shen*(沈炎賓), G. Cheng, X. Huang, S. Yang, H. Zhang, C.-L. Chiang, Y.-G. Lin, J. Bai, W. Yin, L. Gao*(高立軍), L. Chen, F. Wang, and J. Zhao*(趙建慶), "*Stabilizing High-Ni Cathodes with Gradient Surface Ti-enrichment*", Chem. Eng. J. **489**, 151208 (2024).
- Y. Zhu, M. Klingenhof, C. Gao, T. Koketsu, G. Weiser, Y. Pi, S. Liu, L. Sui, J. Hou, J. Li, H. Jiang, L. Xu, W.-H. Huang, C.-W. Pao, M. Yang*(楊孟昊), Z. Hu*(胡志偉), P. Strasser*, and J. Ma*(馬吉偉), "*Facilitating Alkaline Hydrogen Evolution Reaction on the Hetero-interfaced Ru/RuO_2 through Pt Single Atoms Doping*", Nat. Commun. **15**, 1447 (2024).

TPS 45A Submicron Soft X-ray Spectroscopy

- B. Faceira, S. S. Nayak, L. Teulé-Gay, C. Labrugère-Sarroste, H.-Y. Huang, Y.-C. Shao, C.-L. Dong, and A. Rougier*, "*Influence of Fe Doping on the Electrochromic Properties of Cosputtered V_2O_5 Thin Films*", ACS Appl. Energy Mater. **7**, 9882 (2024).
- D. S. Christovam*, A. Marino, J. Falke, C.-E. Liu, C.-F. Chang, C.-Y. Kuo, O. Stockert, S. Wirth, M. W. Haverkort, G. Zwicknagl, A. Severing, P. F. S. Rosa, A. M. Caffer, M. H. Carvalho, and P. G. Pagliuso, "*X-ray Spectroscopic Investigation of Crystal Fields in $Ce_2Rh_{1-x}Ir_xIn_8$ Heavy Fermions*", Phys. Rev. B **110**, 075161 (2024).
- J. Cui, Y. Zhang, Z. Hu, C.-Y. Kuo, C.-F. Chang, Y.-C. Ku, Z. Liu, Z. Xia, J. Zhu, J. Zhang, Y. He, J. Ma, A. Li, X. Lin, C.-T. Chen, G. Kim*(金建兌), J.-Q. Wang*(王建強), and L. Zhang*(張林娟), "*Suppressing Structure Delamination for Enhanced Electrochemical Performance of Solid Oxide Cells*", Small Methods **8**, 2400178 (2024).
- M. N. Duong, Y.-X. Chen, W.-Y. Tzeng, T. Amrillah, S. Yang, C.-E. Liu, D. Z. Dimitrov, S.-C. Haw, C.-H. Hsu, J.-M. Chen*(陳錦明), J.-Y. Lin, K.-H. Wu, C.-W. Luo, C.-T. Chen, C.-Y. Kuo*(郭昌洋), and J.-Y. Juang*(莊振益), "*Orbital Ordering and Ultrafast Carrier Dynamics Anisotropies in Orientation-engineered Orthorhombic $YMnO_3$ Films*", APL Mater. **12**, 021117 (2024).
- W.-E. Ke, J.-W. Chen, C.-E. Liu, Y.-C. Ku, C.-F. Chang, P. Shafer, S.-J. Lin, M.-W. Chu, Y.-C. Chen*(陳怡誠), J.-W. Yeh, C.-Y. Kuo*(郭昌洋), and Y.-H. Chu*(朱英豪), "*Crystalline Magnetic Anisotropy in High Entropy (Fe, Co, Ni, Cr, $Mn)_3O_4$ Oxide Driven by Single-element Orbital Anisotropy*", Adv. Funct. Mater. **34**, 2312856 (2024).
- C. E. Liu, C. N. Wu, J. Falke, C. F. Chang, C.-Y. Kuo, S. Yang, J. Y. Juang, C. Koz, U. Schwarz, C. T. Chen, L. H. Tjeng, and S. G. Altendorf*, "*In Situ X-ray Absorption and Photoelectron Spectroscopy on Epitaxial Fe_xTe Thin Films with a Wide Range of Fe/Te Compositions*", Phys. Rev. B **110**, 245139 (2024).
- Y.-C. Liu, B.-C. Chen, C.-C. Wei, S.-Z. Ho, Y.-D. Liou, P. Kaur, Rahul, Y.-C. Chen, and J.-C. Yang*(楊展其), "*Thickness-dependent Ferroelectricity in Freestanding $Hf_{0.5}Zr_{0.5}O_2$ Membranes*", ACS Appl. Electron. Mater. **6**, 8617 (2024).
- A. Marino, D. S. Christovam, D. Takegami, J. Falke, M. M. F. Carvalho, T. Okauchi, C.-F. Chang, S. G. Altendorf, A. Amorese, M. Sundermann, A. Gloskovskii, H. Gretarsson, B. Keimer, A. V. Andreev, L. Havela, A. Leithe-Jasper, A. Severing, J. Kuneš, L. H. Tjeng*(莊鎏豪), and A. Hariki* (播木敦), "*Quantifying the U 5f Covalence and Degree of Localization in U Intermetallics*", Phys. Rev. Res. **6**, 033068 (2024).
- A. Meléndez-Sans*, V. M. Pereira, C. F. Chang, C.-Y. Kuo, C. T. Chen, L. H. Tjeng, and S. G. Altendorf, "*Influence of Nitrogen Stoichiometry and the Role of Sm 5d States in SmN Thin Films*", Phys. Rev. B **110**, 045120 (2024).
- M. Stavinoha, C.-L. Huang, W. A. Phelan, A. M. Hallas, V. Loganathan, M. Michiardi, J. Falke, S. Zhdanovich, D. Takegami, C.-E. Liu, K. D. Tsuei, C. T. Chen, L. Qian, N. J. Ng, J. W. Lynn, Q. Huang, F. Weickert, V. Zapf, K. R. Larsen, P. D. Sparks, J. C. Eckert, A. B. Puthirath, H.-H. Kung, T. M. Pedersen, S. Gorovikov, A. Damascelli, L. H. Tjeng, C. Hooley, A. H. Nevidomskyy, and E. Morosan, "*Conductive Surface States and Kondo Exhaustion in Insulating $YbIr_3Si_7$*", Phys. Rev. B **109**, 035112 (2024).
- D. Takegami, K. Kawai, M. Ferreira-Carvalho, S. Rößler, C.-E. Liu, C.-Y. Kuo, C.-F. Chang, A. Minamida, T. Miyazaki, M. Okubo, L. H. Tjeng, and T. Mizokawa*(溝川貴司), "*Valence Study of $Li(Ni_{0.5}Mn_{0.5})_{1-x}Co_xO_2$ and $LiNi_{1-x}Co_xO_2$: The Role of Charge Transfer and Charge Disproportionation*", Phys. Rev. Mater. **8**, 055401 (2024).
- X. Wang*(王瀟), J. Zhang, Z. Pan, D. Lu, M. Pi, X. Ye, C. Dong, J. Chen, K. Chen, F. Radu, S. Francoual, S. Agrestini, Z. Hu, C.-F. Chang, A. Tanaka, K. Yamaura, Y. Shen*(沈瑶), and Y. Long*(龍有文), "*X-ray Absorption Spectroscopic Study of the Transition-metal-only Double Perovskite Oxide Mn_2CoReO_6*", J. Phys. Chem. C **128**, 15668 (2024).
- C. Zhou, L. Ma, Y. Feng, C.-Y. Kuo, Y.-C. Ku, C.-E. Liu, X. Cheng, J. Li, Y. Si, H. Huang, Y. Huang, H. Zhao, C.-F. Chang, S. Das, S. Liu*(劉仕), and Z. Chen*(陳祖煌), "*Enhanced Polarization Switching Characteristics of HfO_2 Ultrathin Films via Acceptor-donor Co-doping*", Nat. Commun. **15**, 2893 (2024).

TLS 01A1 SWLS – White X-ray (PRT 75%)

- S.-J. Tsou, M. Mazurkiewicz-Pawlicka, Y.-J. Chiou*(邱郁菁), and C.-K. Lin* (林中魁), "*Effect of Synchrotron X-ray Irradiation Time on the Particle Size and DFAFC Performance of Pd/CNT Catalysts*", Nanomaterials **14**, 162 (2024).

TLS 01B1 SWLS – X-ray Microscopy (PRT 75%)

- Y.-L. Cho, Y.-M. Tzou, A. Assakinah, N. A. T. Than, H. S. Yoon, S. I. Park, C.-C. Wang, Y.-C. Lee, L.-C. Hsu, P.-Y. Huang, S.-L. Liu, and Y.-T. Liu* (劉雨庭), "*Accumulation and Bio-oxidation of Arsenite Mediated by Thermoacidophilic Cyanidiales: Innate Potential Biomaterials toward Arsenic Remediation*", Bioresource Technol. **406**, 130912 (2024).
- J.-H. Huang, X.-F. Luo, T.-Y. Kuo, Y.-H. Lai, P. C. Rath, C.-W. Huang, M.-H. Lin, A.-Y. Hou, J. Li, Y.-S. Su, W.-W. Wu*(吳文偉), and J.-K. Chang*(張仍奎),

"*Dual-salt Aqueous Electrolyte for Enhancing Charge-storage Properties of VO_2 Polymorphic Cathodes for Zn-ion Batteries*", Chem. Eng. J. **497**, 154609 (2024).

- Y.-J. Huang*(黃逸仁), J.-H. Chang, S.-W. Chen, T.-C. Lin, C.-C. Wang, C.-J. Su, T.-N. Lam, and W.-C. Ko, "*Multiscale Insights into Electric Field Orientation Effects on Piezoelectric Strain and Crystallography in P(VDF–TrFE) and P(VDF–TrFE–CTFE) Fibers*", J. Mol. Struct. **1310**, 138391 (2024).
- T.-C. Su, S. Gull, W.-H. Lin, Y.-S. Huang, C.-S. Ni, C.-C. Wang, and H.-Y. Chen*(陳翰儀), "*3D Porous Reduced Graphene Oxide-coated Zinc Anodes for Highly-stable Aqueous Zinc-ion Capacitors via Electrostatic Spray Deposition*", Carbon **229**, 119467 (2024).
- C. Wen, H. Wang*(王華沛), Y.-M. Chou, C.-C. Wang, X. Chen, F. Han, J. Miao, Y. Ma, J. Liu, and J. A. Karson, "*Planetary Paleomagnetic Intensity Recording Fidelity Test Using a Synthetic Lava*", J. Geophys. Res. -Planets **129**, e2023JE008055 (2024).

TLS 01C1 SWLS – EXAFS

- D. B. Adam, W.-H. Huang, M.-C. Tsai*(蔡孟哲), W.-N. Su*(蘇威年), and B. J. Hwang*(黃炳照), "*Atomically Dispersed Ruthenium Single-atom Alloy Catalysts Enabling Efficient Iodide Oxidation Reaction Electrolysis in Acidic Media*", Int. J. Hydrogen Energ. **91**, 548 (2024).
- K. S. Bayikadi, S. Imam, W.-S. Tee, S. Kavirajan, C.-Y. Chang, A. Sabbah, F.-Y. Fu, T.-R. Liu, C.-Y. Chiang, D. Shukla, C.-T. Wu, L.-C. Chen, M.-Y. Chou, K.-H. Chen*(陳貴賢), and R. Sankar*, "*Ultra-low Lattice Thermal Conductivity Driven High Thermoelectric Figure of Merit in Sb/W Co-doped GeTe*", J. Mater. Chem. A **12**, 30892 (2024).
- A. Beniwal, D. Bhalothia, Y.-R. Chen, J.-C. Kao, C. Yan, N. Hiraoka, H. Ishii, M. Cheng, Y.-C. Lo, X. Tu, Y.-W. Chiang, C.-H. Kuo, J.-P. Chou, C.-H. Wang, and T.-Y. Chen*(陳燦耀), "*Incorporation of Atomic Fe-oxide Triggers a Quantum Leap in the CO_2 Methanation Performance of Ni-hydroxide*", Chem. Eng. J. **493**, 152834 (2024).
- D. Bhalothia, C. Yan, N. Hiraoka, H. Ishii, Y.F. Liao, S. Dai, P.-C. Chen*(陳柏均), and T.-Y. Chen*(陳燦耀), "*Iridium Single Atoms to Nanoparticles: Nurturing the Local Synergy with Cobalt-oxide Supported Palladium Nanoparticles for Oxygen Reduction Reaction*", Adv. Sci. **11**, 2404076 (2024).
- D. Bhalothia, A. Beniwal, C. Yan, K.-C. Wang, C.-H. Wang, and T.-Y. Chen* (陳燦耀), "*Potential Synergy Between Pt_2Ni_4 Atomic-clusters, Oxygen Vacancies and Adjacent Pd Nanoparticles Outperforms Commercial Pt Nanocatalyst in Alkaline Fuel Cells*", Chem. Eng. J. **483**, 149421 (2024).
- L. Cai, H. Bai, C.-W. Kao, K. Jiang, H. Pan, Y.-R. Lu*(盧英睿), and Y. Tan* (譚勇文), "*Platinum-ruthenium Dual-atomic Sites Dispersed in Nanoporous $Ni_{0.85}$ Se Enabling Ampere-level Current Density Hydrogen Production*", Small **20**, 2311178 (2024).
- Y.-M. Cai, Y.-H. Li, Y. Xiao, Q. Meyer, Q. Sun, W.-J. Lai, S.-W. Zhao, J. Li, L.-J. Zhang*(張林杰), H. Wang*(王晗), Z. Lin, J. Luo, and L.-L. Han*(韓麗麗), "*Synergistic Rare-earth Yttrium Single Atoms and Copper Phosphide Nanoparticles for High-selectivity Ammonia Electrosynthesis*", Rare Metals **43**, 5792 (2024).
- J.-M. Chang, T.-H. Lin, K.-C. Hsiao, K.-P. Chiang, Y.-H. Chang, and M.-C. Wu*(吳明忠), "*Gas-solid Phase Reaction Derived Silver Bismuth Iodide Rudorffite: Structural Insight and Exploring Photocatalytic Potential of CO_2 Reduction*", Adv. Sci. **11**, 2309526 (2024).
- S. Chen, T. Luo, X. Li, K. Chen, Q. Wang, J. Fu, K. Liu, C. Ma, Y.-R. Lu, H. Li, K. S. Menghrajani, C. Liu, S. A. Maier, T.-S. Chan*(詹丁山), and M. Liu* (劉敏), "*Design of Reaction-driven Active Configuration for Enhanced CO_2 Electroreduction*", Nano Energy **128**, 109873 (2024).
- S.-Y. Chen*(陳仕元), L.-Y. Wang, K.-C. Chen, C.-H. Yeh, W.-C. Hsiao, H.-Y. Chen, M. Nishi, M. Keller, C.-L. Chang, C.-N. Liao, T. Mochizuki, H.-Y. T. Chen*(陳馨怡), H.-H. Chou*(周鶴修), and C.-M. Yang*(楊家銘), "*Ammonia Synthesis Over Cesium-promoted Mesoporous-carbon-supported Ruthenium Catalysts: Impact of Graphitization Degree of the Carbon Support*", Appl. Catal. B-Environ. **346**, 123725 (2024).
- Y. Chen, C.-W. Kao, T. Luo, H. Zhang, Y. Long, J. Fu, Z. Lin, L. Chai, T.-S. Chan*(詹丁山), and M. Liu*(劉敏), "*Enhanced Surface Lewis Acidity of ZrO_2 by -HSO_4 for Efficient CF_4 Decomposition*", Environ. Sci.-Nano **11**, 881 (2024).
- C.-C. Cheng, Y.-C. Ting, F.-Y. Yen, G.-R. Li, C.-H. Lee, K.-A. Lee, S.-I. Chang, H.-Y. T. Chen*(陳馨怡), and S.-Y. Lu*(呂世源), "*Synergistic Mo and W Single Atoms Co-doped Surface Hydroxylated NiFe Oxide as Bifunctional Electrocatalysts for Overall Water Splitting*", Appl. Catal. B-Environ. **358**, 124356 (2024).
- C.-Y. Cheng, Y.-M. Shen, W.-H. Huang, C.-C. Chang, C.-C. Tsai, C.-J. Lin, Y.-G. Lin, Y.-R. Lu, C.-L. Dong, W.-N. Su, S.-Y. Chen, K. Kumar, H.-Y. Chen, C.-J. Tsai, and C.-L. Chen*(陳啟亮), "*Electronic and Atomic Structural Properties Associated with Enhanced Photodegradation Activity in Mo-doped TiO_2 Nanoparticles*", Langmuir **40**, 19506 (2024).
- T. Dey, A. Rajput, G. Jhaa, B. M. Matsagar, N. C.-R. Chen, N. Kumar, R. Salunkhe, K. C.-W. Wu, B. Chakraborty*, and S. Dutta*, "*Rapid Electronic Transport Channel of Co-P with Mo in a Heterostructure Embedded with P, N Dual Doped Porous Carbon for Electrocatalytic Oxygen and Hydrogen Evolution*", ChemNanoMat **10**, e202400089 (2024).
- W. B. Dilebo, M.-C. Tsai*(蔡孟哲), C.-Y. Chang, H. G. Edao, Y. Nikodimos, E. A. Moges, K. Lakshmanan, F. T. Angerasa, C. B. Guta, K. B. Ibrahim, Y. A. Awoke, T. Alamirew, W.-S. Liao, G. B. Desta, J.-L. Chen, W.-N. Su*(蘇威年), and B. J. Hwang*(黃炳照), "*Synergistic Interfacial Electronic Modulation of Topotactically Developed Bimetallic CoNiP on NiS Nanorods for Enhanced Alkaline Hydrogen Evolution Reaction*", Nanoscale **16**, 20701 (2024).
- C. B. Guta, H. G. Edao, W. B. Dilebo, C.-Y. Chang, F. T. Angerasa, E. A. Moges, Y. Nikodimos, K. Lakshmanan, M.-C. Tsai*(蔡孟哲), W.-N. Su*(蘇威年), and B. J. Hwang*(黃炳照), "*Novel Electrocatalyst with Abundant Oxygen Vacancies Enabling Efficient Two-electron Water Oxidation Reaction for H_2O_2 Synthesis*", Chem. Eng. J. **500**, 156418 (2024).
- H.-C. Hsieh, R.-C. Chen, Y.-K. Huang, H.-S. Sheu, Y.-C. Chuang, and C.-S. Lee*(李積琛), "*Enhancing Catalytic Performance in Oxidative Steam Reforming of Ethanol: The Role of Ruthenium ion Substitution in Layered Perovskite $La_2Ti_{2-x}Ru_xO_{7\pm\delta}$ Catalysts*", J. Phys. Chem. C **128**, 19570 (2024).
- X. Huang, J. Feng, S. Hu, B. Xu, M. Hao, X. Liu, Y. Wen, D. Su, Y. Ji, Y. Li, Y. Li, Y. Huang, T.-S. Chan, Z. Hu, N. Tian, Q. Shao*(邵琪), and X. Huang* (黃小青), "*Regioselective Epitaxial Growth of Metallic Heterostructures*", Nat. Nanotechnol. **19**, 1306 (2024).
- Z. Huang, S. Hu, M. Sun, Y. Xu*(徐雍), S. Liu, R. Ren, L. Zhuang, T.-S. Chan, Z. Hu, T. Ding, J. Zhou, L. Liu, M. Wang, Y.-C. Huang, N. Tian, L. Bu*(卜令正), B. Huang*(黃勃龍), and X. Huang*(黃小青), "*Implanting Oxophilic Metal in PtRu Nanowires for Hydrogen Oxidation Catalysis*", Nat. Commun. **15**, 1097 (2024).
- Z. Huang, Y. Wang, J. Xia, S. Hu, N. Chen, T. Ding, C. Zhan, C.-W. Pao, Z. Hu, W.-H. Huang, T. Shi, X. Meng, Y. Xu*(徐勇), L. Cao*(曹亮), and X. Huang* (黃小青), "*Atom-glue Stabilized Pt-based Intermetallic Nanoparticles*", Sci. Adv. **10**, eadq6727 (2024).
- Y. Jin*(金延超), Y. Qiu, R. Kumar, T. Chan, and L. Yan*(閻莉), "*Understanding the Goethite Role on Stibnite Oxidative Dissolution and Transformation: Spectroscopic and DFT Study*", Sci. Total Environ. **906**, 167823 (2024).
- B.-H. Kao, Y.-F. Zeng, Y.-C. Lee, C.-W. Pao, J.-L. Chen, Y.-C. Chuang, H.-S. Sheu, F.-T. Tsai*(蔡富潯), and W.-F. Liaw*(廖文峯), "*Unveiled the Structure-selectivity Relationship for Carbon Dioxide Reduction Triggered by Bi-doped Cu-based Nanocatalysts*", Small **20**, 2307910 (2024).
- J.-C. Kao, T.-Y. Teng, H.-W. Lin, F.-G. Tseng, L.-Y. Ting, D. Bhalothia, H.-H. Chou, Y.-C. Lo, J.-P. Chou*(周至品), and T.-Y. Chen*(陳燦耀), "*Single Atom Ag Bonding Between PF3T Nanocluster and TiO_2 Leads the Ultra-stable Visible-light-driven Photocatalytic H_2 Production*", Small **20**, 2403176 (2024).
- J. Lan, Z. Wang, C.-W. Kao, Y.-R. Lu, F. Xie, and Y. Tan*(譚勇文), "*Isolating Cu-Zn Active-sites in Ordered Intermetallics to Enhance Nitrite-to-ammonia Electroreduction*", Nat. Commun. **15**, 10173 (2024).
- J. Li, T. Chan, C. Jing, and J. Wang*(王錦), "*CO_2 Photoreduction with High Selectivity of C_2H_4 Production on Conjugated Microporous Polymer with Cu Single Atoms*", Fuel **357**, 130020 (2024).
- R. Li, C.-W. Tung, B. Zhu, Y. Lin, F.-Z. Tian, T. Liu, H. M. Chen*(陳浩銘), P. Kuang*(鄺攀勇), and J. Yu*(余家國), "*D-band Center Engineering of Single Cu Atom and Atomic Ni Clusters for Enhancing Electrochemical CO_2 Reduction to CO*", J. Colloid Interf. Sci. **674**, 326 (2024).
- W. Liao, J. Wang, G. Ni, K. Liu, C. Liu, S. Chen, Q. Wang, Y. Chen, T. Luo, X. Wang, Y. Wang, W. Li, T.-S. Chan, C. Ma, H. Li, Y. Liang, W. Liu, J. Fu*(傅俊偉), B. Xi*(席北斗), and M. Liu*(劉敏), "*Sustainable Conversion of Alkaline Nitrate to Ammonia at Activities Greater than 2A cm^{-2}*", Nat. Commun. **15**, 1264 (2024).
- M. Liu*(劉敏), Q. Wang*(王其憂), T. Luo, M. Herran, X. Cao, W. Liao, L. Zhu, H. Li, A. Stefancu, Y.-R. Lu, T.-S. Chan, E. Pensa, C. Ma, S. Zhang, R. Xiao*(肖睿洋), and E. Cortés*, "*Potential Alignment in Tandem Catalysts Enhances CO_2toC_2H_4 Conversion Efficiencies*", J. Am. Chem. Soc. **146**, 468 (2024).
- S. Ma, K.-M. Leung, C. Liao*(廖長忠), C.-K. Chang, Y. Zhou, S. Chen, X. Zhao, Q. Zhao, and K. Shih*(施凱閔), "*Green Conversion of Waste Alkaline Battery Material to Zeolitic Imidazolate Framework-8 and Its Iodine Capture Mechanism*", J. Hazard. Mater. **469**, 133612 (2024).
- T. Ma, R. Li, Y.-C. Huang, Y. Lu, L. Guo, M. Niu, X. Huang, R. A. Soomro, J. Ren, Q. Wang, B. Xu, C. Yang*(楊春明), F. Fu*(付峰), and D. Wang*

(王丹軍), "*Interfacial Chemical-bonded MoS_2/In-Bi_2MoO_6 Heterostructure for Enhanced Photocatalytic Nitrogen-to-ammonia Conversion*", ACS Catalysis **14**, 6292 (2024).

- L. Meng, C.-W. Kao, Z. Wang, J. Ma, P. Huang, N. Zhao, X. Zheng, M. Peng, Y.-R. Lu, and Y. Tan*(譚勇文), "*Alloying and Confinement Effects on Hierarchically Nanoporous CuAu for Efficient Electrocatalytic Semi-hydrogenation of Terminal Alkynes*", Nat. Commun. **15**, 5999 (2024).
- L. Merinda, F.-M. Wang*(王復民), N.-L. Wu*(吳乃立), R. A. Yuwono, C. Khotimah, U. Qonita, W.-H. Huang, L.-P. Wan, C.-K. Chang, P.-H. Hsu, C.-W. Pao, J.-L. Chen, C.-L. Chen, and T.-S. Chan, "*Carbonate Deprotonation on an Ni-rich Layered Cathode: Development of a New Cis-oligomer as an Organic Coverage*", J. Mater. Chem. A **12**, 28886 (2024).
- T. Natarajan, S. Arumugam, Y.-F. Tsai, A. Abou-taleb, and S. S.-F. Yu*(俞聖法), "*Unveiling the Enhanced Electrochemical CO_2 Conversion: The Role of 3D Porous BiOCl with Defects and CTAB-mediated Nanosheets*", J. CO2 Util. **85**, 102888 (2024).
- R. Patil, A. Rajput, B. M. Matsagar, N. C. R. Chen, M. Ujihara, R. R. Salunkhe, P. Yadav, K. C.-W. Wu, B. Chakraborty*, and S. Dutta*, "*Elevated Temperature-driven Coordinative Reconstruction of an Unsaturated Single-Ni-atom Structure with Low Valency on a Polymer-derived Matrix for the Electrolytic Oxygen Evolution Reaction*", Nanoscale **16**, 7467 (2024).
- Y. Qiao, M. Luo, L. Cai, C.-W. Kao, J. Lan, L. Meng, Y.-R. Lu, M. Peng, C. Ma, and Y. Tan*(譚勇文), "*Constructing Nanoporous Ir/Ta_2O_5 Interfaces on Metallic Glass for Durable Acidic Water Oxidation*", Small **20**, 2305479 (2024).
- X. She, L. Zhai, Y. Wang, P. Xiong, M.-M. Jung, T.-S. Wu, M. C. Wong, X. Guo, Z. Xu, H. Li, H. Xu*(許暉), Y. Zhu*(朱葉), S. C. E. Tsang*(曾適之), and S. P. Lau*(劉樹平), "*Pure-water-fed, Electrocatalytic CO_2 Reduction to Ethylene beyond 1,000 h Stability at 10 A*", Nano Energy **9**, 81 (2024).
- Z. Teng, H. Yang, Q. Zhang, W. Cai, Y.-R. Lu, K. Kato, Z. Zhang, J. Ding, H. Sun, S. Liu, C. Wang, P. Chen, A. Yamakata, T.-S. Chan, C. Su*(蘇陳良), T. Ohno*, and B. Liu*(劉彬), "*Atomically Dispersed Low-valent Au Boosts Photocatalytic Hydroxyl Radical Production*", Nat. Chem. **16**, 1250 (2024).
- Y.-C. Ting, C.-C. Cheng, F.-Y. Yen, G.-R. Li, S.-I. Chang, C.-H. Lee, H.-Y. T. Chen*(陳馨怡), and S.-Y. Lu*(呂世源), "*Highly Asymmetrically Configured Single Atoms Anchored on Flame-roasting Deposited Carbon Black as Cathode Catalysts for Ultrahigh Power Density Zn-air Batteries*", EnergyChem **6**, 100134 (2024).
- J. Wang*(王健), Y. Zhang, Y. Wang*(王瑩), J. Cho, T.-S. Chan, Y. Ha, S.-C. Haw, C.-W. Kao, Z. Wang, J. Lei, M. Ju, J. Tang, T. Liu, S. Zhao, Y. Dai, A.-B. Wiechec, F.-R. Chen, W. Wang, C. H. Choi, Z. Shao*(邵宗平), and M. Ni*(倪盟), "*Heterostructure Boosts a Noble-metal-free Oxygen-evolving Electrocatalyst in Acid*", Energ. Environ. Sci. **17**, 5972 (2024).
- L. Wang, W. Yan, Q. Yu, L. Liu, C.-W. Kao, Y.-C. Huang, T.-S. Chan, Z. Hu, H. Lin, D. Shen*(申大志), X. Huang*(黃小青), and Y. Li*(李雲華), "*Tuning Crystal Phase of Palladium-selenium Nanowires for Enhanced Ethylene Glycol Electrocatalytic Oxidation*", Small **20**, 2403448 (2024).
- L. Wang, C. Zhang, T. Lin, H. Chu, Y. Gao, Z. Hu, S.-C. Haw, C.-T. Chen, C.-Y. Kuo, X. Li, Y. Gai, Q. Guo, Y. Meng, H. Zhuang, X. Shen*(沈希), Z. Wang*(王兆翔), and R. Yu*(禹日成), "*Anti-siting for Stabilizing Structure and Modulating Cationic/Anionic Redox Reactions*", Energy Storage Mater. **70**, 103479 (2024).
- M. Wang, Z. Wang, Y. Zhang, Y. Shi, T.-S. Chan, S.-C. Haw, J. Wang, H. Wang, S. Wang, H. Fei, R. Liu, T. Liu, C.-F. Yan, and J. Wang*(王健), "*Regulating Reconstruction Activity of Cobalt Electrode for Optimized Water Oxidation*", ACS Energ. Lett. **9**, 5502 (2024).
- Q. Wang, Y. Gong, X. Zi, L. Gan, E. Pensa, Y. Liu, Y. Xiao, H. Li, K. Liu, J. Fu, J. Liu*(劉俊), A. Stefancu, C. Cai, S. Chen, S. Zhang, Y.-R. Lu, T.-S. Chan, C. Ma, X. Cao*(曹雪瑩), E. Cortés*, and M. Liu*(劉敏), "*Coupling Nano and Atomic Electric Field Confinement for Robust Alkaline Oxygen Evolution*", Angew. Chem. Int. Edit. **63**, e202405438 (2024).
- S. Wang, F. Li, J. Zhao, Y. Zeng, Y. Li, Z.-Y. Lin, T.-J. Lee, S. Liu, X. Ren, W. Wang, Y. Chen, S.-F. Hung, Y.-R. Lu, Y. Cui, X. Yang, X. Li*(李旭寧), Y. Huang*(黃延強), and B. Liu*(劉彬), "*Manipulating C-C Coupling Pathway in Electrochemical CO_2 Reduction for Selective Ethylene and Ethanol Production over Single-atom Alloy Catalyst*", Nat. Commun. **15**, 10247 (2024).
- C.-Y. Wu, Y.-C. Hsiao, Y. Chen, K.-H. Lin, T.-J. Lee, C.-C. Chi, J.-T. Lin, L.-C. Hsu, H.-J. Tsai, J.-Q. Gao, C.-W. Chang, I.-T. Kao, C.-Y. Wu, Y.-R. Lu, C.-W. Pao, S.-F. Hung, M.-Y. Lu, S. Zhou, and T.-H. Yang*(楊東翰), "*A Catalyst Family of High-entropy Alloy Atomic Layers with Square Atomic Arrangements Comprising Iron-and Platinum-group Metals*", Sci. Adv. **10**, eadl3693 (2024).
- Q. Xia, C. Jin, Y. L. Huang, Y. Zhai, W. Han, J. Wu, C. Xia, C. C. Lin*(林群哲), X. Zhao*(趙訓華), and X. Zhang*(張曉), "*Methanol-facilitated Surface Reconstruction Catalysts for Near 200% Faradaic Efficiency in a Coupled System*", Adv. Funct. Mater. **34**, 2314596 (2024).
- F. Xie, Z. Wang, C.-W. Kao, J. Lan, Y.-R. Lu, and Y. Tan*(譚勇文), "*Asymmetric Local Electric Field Induced by Dual Heteroatoms on Copper Boosts Efficient CO_2 Reduction Over Ultrawide Potential Window*", Angew. Chem. Int. Edit. **63**, e202407661 (2024).
- P. Xiong, Z. Xu, T.-S. Wu, T. Yang, Q. Lei, J. Li, G. Li, M. Yang, Y.-L. Soo, R. D. Bennett, S. P. Lau, S. C. E. Tsang*(曾適之), Y. Zhu*(朱葉), and M. M.-J. Li*(李孟蓉), "*Synthesis of Core@shell Catalysts Guided by Tammann Temperature*", Nat. Commun. **15**, 420 (2024).
- B. Xu, X. Huang, S. Liu, Z. Hu, C.-W. Kao, T.-S. Chan, H. Geng, Y. Zhang*(張應), and X. Huang*(黃小青), "*Antimony Oxides-protected Ultrathin Ir-Sb Nanowires as Bifunctional Hydrogen Electrocatalysts*", Nano Res. **17**, 1042 (2024).
- C. Xu, W. Orbell, G. Wang, B. Li, B. K. Y. Ng, T.-S. Wu, Y.-L. Soo, Z.-X. Luan, K. Tang, X.-P. Wu, S. C. E. Tsang*(曾適之), and P. Zhao*(趙朴), "*Direct Visualisation of Metal-defect Cooperative Catalysis in Ru-doped Defective MOF-808*", J. Mater. Chem. A **12**, 19018 (2024).
- Z. Xu, Z. Huang, H. Li, S. Zhu, Z. Lei, C. Liu*(劉承帥), F. Meng, J.-L. Chen, T.-Y. Chen, and C. Feng*(馮春華), "*Sulfidation-reoxidation Enhances Heavy Metal Immobilization by Vivianite*", Water Res. **263**, 122195 (2024).
- T. Yang, A. Beniwal, D. Bhalothia, C. Yan, C.-H. Wang, and T.-Y. Chen*(陳燦耀), "*Oxygen Vacancies Coupled with Surface Silicide Facilitate CO_2 Activation at Near-room Temperature for Efficient Methane Productivity on Ni-oxide Supported Pd Nanoparticles*", Sustain. Energy Fuels **8**, 3399 (2024).
- Z. Yao, H. Cheng, Y. Xu, X. Zhan, S. Hong, X. Tan*(譚心怡), T.-S. Wu, P. Xiong, Y.-L. Soo, M. M-J. Li, L. Hao, L. Xu, A. W. Robertson, B. Xu, M. Yang*(楊明), and Z. Sun*(孫振宇), "*Hydrogen Radical-boosted Electrocatalytic CO_2 Reduction Using Ni-partnered Heteroatomic Pairs*", Nat. Commun. **15**, 9881 (2024).
- H. Zhang, H.-C. Chen, S. Feizpoor, L. Li, X. Zhang, X. Xu, Z. Zhuang, Z. Li, W. Hu, R. Snyders, D. Wang*(王定勝), and C. Wang*(王春棟), "*Tailoring Oxygen Reduction Reaction Kinetics of Fe-N-C Catalyst via Spin Manipulation for Efficient Zinc-air Batteries*", Adv. Mater. **36**, 2400523 (2024).
- Y. Zhang, X.-G. Zhang*(張霞光), S. Yang, H. Peng, T. Fan, Z. Huang, F. Xue, T. Yang, S. Liu, Z. Chen, Q. Kong, Z. Hu, T.-S. Chan, X. Yi*(伊曉東), and X. Huang*(黃小青), "*Strong Synergy between Pd Single Atom and Zn Vacancy Boosts Photocatalytic Pure Water Splitting*", Solar RRL **8**, 2400194 (2024).
- J. Zhu, L. An, X. Li, K. Iputera, R.-S. Liu*(劉如熹), J. Yang, D. Wang*(王得麗), and X. Zhao*(趙旭), "*Anchoring Isolated Pd Atoms on $Ti_3C_2T_x$ MXene with Boosted Kinetics for Alkaline Hydrogen Evolution*", Appl. Surf. Sci. **644**, 158809 (2024).

TLS 01C2 SWLS – X-ray Powder Diffraction

- A. Beniwal, D. Bhalothia, Y.-R. Chen, J.-C. Kao, C. Yan, N. Hiraoka, H. Ishii, M. Cheng, Y.-C. Lo, X. Tu, Y.-W. Chiang, C.-H. Kuo, J.-P. Chou, C.-H. Wang, and T.-Y. Chen*(陳燦耀), "*Incorporation of Atomic Fe-oxide Triggers a Quantum Leap in the CO_2 Methanation Performance of Ni-hydroxide*", Chem. Eng. J. **493**, 152834 (2024).
- D. Bhalothia, H.-Y. Liu, S.-H. Chen, Y.-T. Tseng, W. Li, S. Dai, K.-W. Wang*(王冠文), and T.-Y. Chen*(陳燦耀), "*The Sub-nanometer In_2O Clusters on Ag Nanoparticles with Highly Selective Electrochemical CO_2 Reduction to Formate*", Chem. Eng. J. **481**, 148295 (2024).
- D. Bhalothia, C. Yan, N. Hiraoka, H. Ishii, Y.F. Liao, S. Dai, P.-C. Chen*(陳柏均), and T.-Y. Chen*(陳燦耀), "*Iridium Single Atoms to Nanoparticles: Nurturing the Local Synergy with Cobalt-oxide Supported Palladium Nanoparticles for Oxygen Reduction Reaction*", Adv. Sci. **11**, 2404076 (2024).
- D. Bhalothia, A. Beniwal, C. Yan, K.-C. Wang, C.-H. Wang, and T.-Y. Chen*(陳燦耀), "*Potential Synergy Between Pt_2Ni_4 Atomic-clusters, Oxygen Vacancies and Adjacent Pd Nanoparticles Outperforms Commercial Pt Nanocatalyst in Alkaline Fuel Cells*", Chem. Eng. J. **483**, 149421 (2024).
- C.-Y. Chang, M.-H. Huang, K.-C. Chen, W.-T. Huang, M. Kaminski, N. Majewska, T. Klimczuk, J.-H. Chen, D.-H. Cherng, K.-M. Lu, W. K. Pang, V. K. Peterson, S. Mahlik*, G. Leniec*, and R.-S. Liu*(劉如熹), "*Ultrahigh Quantum Efficiency Near-infrared-II Emission Achieved by Cr^{3+} Clusters to Ni^{2+} Energy Transfer*", Chem. Mater. **36**, 3941 (2024).
- C.-Y. Chen, Y. Chen, T.-Y. Chang, M.-T. Lee, S.-Y. Liu, Y.-C. Yu, Y.-H. Lin, C.-H. Lee, H.-L. Chen, K.-Y. Wu, W.-T. Chuang, and C.-L. Wang*(王建隆), "*Thermophilic Artificial Water Channels of a Lipid-like Dendron Stabilized by Water-containing Hydrogen-bonded Network*", Giant **17**, 100220 (2024).
- W.-H. Chen, Y.-T. Weng, Y.-C. Lu, H. Chen, P.-Y. Chang, H.-S. Sheu, S.-K. Parthasarathi*, and N.-L. Wu*(吳乃立), "*In-situ Formation of Spinel Protective Layer through Extremely Low K-doping for Enhanced Performance of Ni-rich Layered Cathodes*", J. Power Sources **623**, 235446 (2024).

- M. Cheng, D. Bhalothia, G.-H. Huang, P. K. Saravanan, Y. Wu, A. Beniwal, P.-C. Chen, X. Tu*, and T.-Y. Chen*(陳燦耀), "*Sub-millisecond Pulsed Laser Engineering of CuO_x-decorated Pd Nanoparticles for Enhanced Catalytic CO_2 Hydrogenation*", Catal. Today **441**, 114891 (2024).
- H.-H. Chiu, M.-K. Ho, T.-E. Hsu, S.-L. Yu, K. Manjunatha, C.-L. Cheng, T.-Y. Li, C.-K. Chang, S. Tummala, Y.-P. Ho, J. Angadi V, S. Matteppanavar, A. C. Gandhi*, and S. Y. Wu*(吳勝允), "*Manipulating and Investigating the Room-temperature Magnetic Memory Phenomenon: The Impact of Rare-earth Ion Doping on Nickel Oxide Nanoparticles*", Mater. Today Chem. **39**, 102190 (2024).
- C.-H. Chuang, Y.-H. Peng, C.-K. Chang, P.-Y. Chang, D.-Y. Kang*(康敦彥), and L.-H. Yeh*(葉禮賢), "*Crystal Orientation Control in Angstrom-scale Channel Membranes for Significantly Enhanced Blue Energy Harvesting*", Chem. Eng. J. **499**, 155934 (2024).
- T. T. K. Cuc, Y.-C. Tso, T.-C. Wu, P. Q. Nhien, T. M. Khang, B. T. B. Hue, W.-T. Chuang, and H.-C. Lin*(林宏洲), "*Ultrahigh Toughness of Stretchable Ratiometric Mechanofluorescent Polyurethane Elastomers Enhanced by Dual Slide-ring Motion of Polyrotaxane Cross-linkers and Daisy Chain Backbones*", J. Mater. Chem. C **12**, 14469 (2024).
- H.-C. Hsieh, R.-C. Chen, Y.-K. Huang, H.-S. Sheu, Y.-C. Chuang, and C.-S. Lee*(李積琛), "*Enhancing Catalytic Performance in Oxidative Steam Reforming of Ethanol: The Role of Ruthenium ion Substitution in Layered Perovskite $La_2Ti_{2-x}Ru_xO_{7\pm\delta}$ Catalysts*", J. Phys. Chem. C **128**, 19570 (2024).
- C.-W. Hsu, S.-K. Yu, M.-Y. Shen, Ender Ercan, Y.-J. Wang, B.-H. Lin, H.-C. Wu*(吳亘承), Y.-C. Lin*(林彥丞), C.-L. Liu*(劉振良), and W.-C. Chen*(陳文章), "*Spider Silk/Hemin Biobased Electrets for Organic Phototransistor Memory: a Comprehensive Study on Solution Process Engineering*", Adv. Funct. Mater. **34**, 2314907 (2024).
- P.-Y. Huang, Y.-Y. Zhang, P.-C. Tsai, R.-J. Chung, Y.-T. Tsai, M.-K. Leung, S.-Y. Lin*(林時彥), and M.-H. Fang*(方牧懷), "*Interfacial Engineering of Quantum Dots-metal-organic Framework Composite Toward Efficient Charge Transport for a Short-wave Infrared Photodetector*", Adv. Opt. Mater. **12**, 2302062 (2024).
- Y.-C. Huang, Y. Wu, Y.-R. Lu, J.-L. Chen, H.-J. Lin, C.-T. Chen, C.-L. Chen, C. Jing, J. Zhou, L. Zhang, Y. Wang, W.-C. Chou*(周武清), S. Wang*(王雙印), Z. Hu*(胡志偉), and C.-L. Dong*(董崇禮), "*Direct Identification of O-O Bond Formation through Three-step Oxidation During Water Splitting by Operando Soft X-ray Absorption Spectroscopy*", Adv. Sci. **11**, 2401236 (2024).
- B.-H. Kao, Y.-F. Zeng, Y.-C. Lee, C.-W. Pao, J.-L. Chen, Y.-C. Chuang, H.-S. Sheu, F.-T. Tsai*(蔡富潯), and W.-F. Liaw*(廖文峯), "*Unveiled the Structure-selectivity Relationship for Carbon Dioxide Reduction Triggered by Bi-doped Cu-based Nanocatalysts*", Small **20**, 2307910 (2024).
- J.-C. Kao, T.-Y. Teng, H.-W. Lin, F.-G. Tseng, L.-Y. Ting, D. Bhalothia, H.-H. Chou, Y.-C. Lo, J.-P. Chou*(周至品), and T.-Y. Chen*(陳燦耀), "*Single Atom Ag Bonding Between PF3T Nanocluster and TiO_2 Leads the Ultra-stable Visible-light-driven Photocatalytic H_2 Production*", Small **20**, 2403176 (2024).
- H.-Y. Lin, B.-J. Zhong, H.-J. Liu, Y.-K. Wu, C.-H. Peng, and C.-L. Wang*(王建隆), "*Optimal Compositions in the NDI: Pyrene Charge-transfer Complexes Revealed by Thermal Analysis and Structural Characterizations*", Cryst. Growth Des. **24**, 2833 (2024).
- Veeramani Rajendran, C.-Y. Chang, M.-H. Huang, K.-C. Chen, W.-T. Huang, Mikołaj Kaminski, Tadeusz Lesniewski, Sebastian Mahlik*, Grzegorz Leniec*, K.-M. Lu, D.-H. Wei*(魏大華), Ho Chang*(張合), and R.-S. Liu*(劉如熹), "*Chromium Cluster Luminescence: Advancing Near-infrared Light-emitting Diode Design for Next-generation Broadband Compact Light Sources*", Adv. Opt. Mater. **12**, 2302645 (2024).
- A. Sarkar, S.-Y. Huang, V. R. Dharmaraj, B. Bazri, K. Iputera, H.-H. Su, Y.-A. Chen, H.-C. Chen, Y.-P. Lin, R.-J. Chung*(鍾仁傑), D.-H. Wei*(魏大華), and R.-S. Liu*(劉如熹), "*Polyethylene Oxide-based Solid-state Polymer Electrolyte Hybridized with Liquid Catholyte for Semi-solid-state Rechargeable Mg-O_2 Batteries*", J. Mater. Chem. A **12**, 25968 (2024).
- R. Subramani, S.-Y. Hsu, Y.-C. Chuang, L.-C. Hsu, K.-T. Lu*(盧桂子), and J.-M. Chen*(陳錦明), "*Fe-MIL-101 Metal Organic Framework Integrated Solid Polymer Electrolytes for High-performance Solid-state Lithium Metal Batteries*", J. Mater. Chem. A **12**, 7132 (2024).
- G.-H. Tan, H.-C. Lin, H.-C. Liang, C.-W. Pao, P.-Y. Chen, W.-T. Chuang, C.-A. Hsieh, D. M. Dorrah, M.-C. Li, L.-Y. Chen, H.-H. Chou, and H.-W. Lin*(林皓武), "*Highly Efficient Manganese Bromides with Reversible Luminescence Switching through Amorphous-crystalline Transition*", ACS Appl. Mater. Interfaces **16**, 55842 (2024).
- Y.-T. Tsai, P.-X. Chen, M. Kaminski, N. Majewska, S. Mahlik*, and M.-H. Fang*(方牧懷), "*Sharp-to-broad Band Energy Transfer in Lithium Aluminate and Gallate Phosphors for SWIR LED*", ACS Appl. Opt. Mater. **2**, 2401 (2024).
- C.-C. Wang*(王志傑), Y.-C. Wu, Y.-C. Chung, E.-C. Yang*(楊恩哲), G.-H. Lee, S.-Y. Chien, P.-Y. Chang, and H.-S. Sheu, "*Synthesis, Structural Characterization, Water Ad-/De-sorption Isotherm, and CO_2 Uptakes of a 2D Cu(I) Metal Organic Framework with 1,3,5-tris(4-pyridylethynyl)Benzene (L) and Tricyanomethanide (tcm^-) Ligands*", J. Chin. Chem. Soc. **71**, 1464 (2024).
- J. Wang*(王健), Y. Zhang, Y. Wang*(王瑩), J. Cho, T.-S. Chan, Y. Ha, S.-C. Haw, C.-W. Kao, Z. Wang, J. Lei, M. Ju, J. Tang, T. Liu, S. Zhao, Y. Dai, A.-B. Wiechec, F.-R. Chen, W. Wang, C. H. Choi, Z. Shao*(邵宗平), and M. Ni*(倪盟), "*Heterostructure Boosts a Noble-metal-free Oxygen-evolving Electrocatalyst in Acid*", Energ. Environ. Sci. **17**, 5972 (2024).
- L.-C. Wang, L.-C. Chang, H.-L. Huang, P.-Y. Chang, C.-W. Pao, Y.-F. Liu, K.-S. Huang, Y.-H. Chien*(簡儀欣), H.-S. Sheu*(許火順), W.-P. Su*(蘇文彬), C.-H. Yeh*(葉丞豪), and C.-S. Yeh*(葉晨聖), "*Synergistic ROS Generation via Core-shell Nanostructures with Increased Lattice Microstrain Combined with Single-atom Catalysis for Enhanced Tumor Suppression*", ACS Appl. Mater. Interfaces **16**, 45356 (2024).
- P.-C. Wei*(魏百駿), C.-R. Hsing, C.-C. Yang, Y.-H. Tung, H.-J. Wu, W.-T. Yen, Y.-C. Lai, J.-J. Lee, C.-W. Wang, H.-C. Wu, H.-D. Yang, V. Singaravelu, X. Miao, A. Giugni, J.-K. Hu, J.-H. Fu, V. Tung, J. He, C.-M. Wei*(魏金明), and J.-H. He*(何志浩), "*Liquid-like Thermal Conductivity in Solid Materials: Dynamic Behavior of Silver Ions in Argyrodites*", Nano Energy **122**, 109324 (2024).
- E.-C. Yang*(楊恩哲), Y.-T. Tsai, P.-Y. Chang, M. Ozerov, J. Krzystek, S.-Y. Chien, J.-X. He, T.-S. Kuo, and H.-S. Sheu*(許火順), "*Cobalt(II) Single-Ion Magnet Coordinated by Double Deprotonation of 2,2'-bipyridine-6,6'-diol Ligands*", ACS Omega **9**, 26149 (2024).
- T. Yang, A. Beniwal, D. Bhalothia, C. Yan, C.-H. Wang, and T.-Y. Chen*(陳燦耀), "*Oxygen Vacancies Coupled with Surface Silicide Facilitate CO_2 Activation at Near-room Temperature for Efficient Methane Productivity on Ni-oxide Supported Pd Nanoparticles*", Sustain. Energy Fuels **8**, 3399 (2024).
- Y.-H. Yang, Y.-S. Chen, W.-T. Chuang, and J.-S. Yang*(楊吉水), "*Bifurcated Polymorphic Transition and Thermochromic Fluorescence of a Molecular Crystal Involving Three-dimensional Supramolecular Gear Rotation*", J. Am. Chem. Soc. **146**, 8131 (2024).
- C.-H. Yeh, J.-W. Kang, Y.-L. Chen, H.-J. Chen, H.-H. Chang, W.-H. Lu, S.-Y. Chen, H.-L. Chen, C.-W. Hu, L.-Y. Chueh, Y.-T. F. Pan, and H.-Y. Chen*(陳翰儀), "*Electrochemical Improvement of $Na_{0.62}K_{0.05}Mg_{2/9}Cu_{1/9}Mn_{2/3}O_2$ P2-type Layer-oxide Anionic Redox Cathodes of Sodium-ion Batteries via Incorporating K-doping*", ACS Sustain. Chem. Eng. **12**, 12795 (2024).
- R. A. Yuwono, C. Khotimah, F.-M. Wang*(王復民), N.-L. Wu*(吳乃立), A. C. Imawan, R. Foeng, P.-C. Huang, G.-Y. Liu, S.-C. Haw, and H.-S. Sheu, "*Investigations of an Organic Coverage to Ni-rich Cathode Materials: Effects on Deteriorated, Cathode Electrolyte Interphase, and Chemical Crossover*", J. Energy Storage **92**, 112184 (2024).
- W.-J. Zeng, J.-J. Ma, W.-Y. Huang, T.-J. Lee, Z.-Y. Lin, K.-S. Peng, N. Hiraoka, Y.-F. Liao, Y.-R. Lu, C.-W. Hu*(胡芝瑋), S.-H. Hsu*(徐韶徽), and S.-F. Hung*(洪嵚富), "*Leveraging Bifunctional Phosphide-based Catalysts in a Membrane-electrode-assembly to Achieve Industrial Hydrogen Production*", Mater. Today Sustain. **27**, 100820 (2024).

TLS 03A1 BM – (HF-CGM) Photoabsorption/ Photoluminescence

- S.-L. Chou, W.-J. Huang, C.-H. Chin, S.-Y. Lin, H.-F. Chen, and Y.-J. Wu*(吳宇中), "*Electronic Absorption Spectra of Aniline Cations in Solid Neon*", J. Mol. Struct. **1316**, 139051 (2024).
- W.-J. Huang, S.-L. Chou, S.-Y. Lin, H.-F. Chen, and Y.-J. Wu*(吳宇中), "*Direct UV Absorption Spectra of CO^+_2 in Solid Neon*", Low Temp. Phys. **50**, 733 (2024).
- S.-Y. Lin, S.-L. Chou, T.-P. Huang, M.-Y. Lin, H.-F. Chen, P. J. Sarre, C.-M. Tseng*(曾建銘), and Y.-J. Wu*(吳宇中), "*Blue Luminescence from N-doped Graphene*", Astrophys. J. **977**, 230 (2024).
- A. Motla, T. A. Kumaravelu, C.L. Dong, C.L. Chen, K. Asokan, and S. Annapoorni*, "*Role of Annealing Environments on the Local Electronic and Optical Properties of Zinc Oxide Films*", J. Mater. Sci.-Mater. Electron. **35**, 267 (2024).
- R. Ramachandran*, J. K. Meka, K. K. Rahul, W. Khan, J.-I. Lo, B.-M. Cheng, D. V. Mifsud, B. N. Rajasekhar, A. Das, H. Hill, P. Janardhan, A. Bhardwaj, N. J. Mason, and B. Sivaraman*, "*Ultraviolet Spectrum Reveals the Presence of Ozone on Jupiter's Moon Callisto*", Icarus **410**, 115896 (2024).
- R. Ramachandran*, A. Hazarika, S. Gupta, S. Nag, J. K. Meka, Tejender S. Thakur, S. Yashonath, G. Vishwakarma, S.-L. Chou, Y.-J. Wu, P. Janardhan, B. N. Rajasekhar, A. Bhardwaj, N. J. Mason, B. Sivaraman*, and P. K. Maiti*, "*Amorphous 1-propanol Interstellar Ice Beyond Its Melting Point*", Mon. Not. R. Astron. Soc. **530**, 1027 (2024).

- R. Ramachandran*, Milan Sil, Prasanta Gorai, J. K. Meka, S. Pavithraa, J.-I. -I., S.-L. Chou, Y.-J. Wu, P. Janardhan, B.-M. Cheng, Anil Bhardwaj, Vıctor M. Rivilla, N. J. Mason, B. Sivaraman*, and Ankan Das*, "*Experimental and Computational Study of Ethanolamine Ices under Astrochemical Conditions*", Astrophys. J. **975**, 181 (2024).
- C.-C. Wang and C.-H. Lee*(李志浩), "*Wafer-scale Epitaxial Molybdenum Disulfide Ultrathin Film on Sapphire Prepared by Low-energy Reactive Magnetron Sputtering*", Appl. Surf. Sci. **659**, 159889 (2024).

TLS 05A1 EPU – Inelastic Scattering

- S.-H. Hsieh, S. Ghosh, Y.-H. Liang, H.-T. Wang, C.-H. Du*(杜昭宏), J.-W. Chiou, C.-M. Wu, C.-W. Wang, Y.-C. Shao, J.-L. Chen, C.-W. Pao, H.-M. Tsai, T.-S. Chan, W.-B. Wu, H.-J. Lin, J.-F. Lee, A. Kandasami, and W.-F. Pong* (彭維鋒), "*Correlation Between Noncollinear Spin Orientation and Lattice Distortion in $Ni_{0.4}Mn_{0.6}TiO_3$*", Phys. Rev. Mater. **8**, 124410 (2024).

TLS 05B1 EPU – Soft X-ray Chemistry

- Y.-J. Chiang, W.-C. Huang, C.-H. Han, C.-L. Liu*(劉振霖), C.-C. Tsai, and W.-P. Hu*(胡維平), "*Near-edge X-ray Absorption Fine Structure Spectra and Specific Dissociation of Small Peptoid Molecules*", J. Chem. Phys. **160**, 074305 (2024).

TLS 05B2 EPU – PEEM

- L.-J. Liaw, P.-C. Chang, Y.-C. Wang, Z.-Q. Liu, P.-W. Chen, Y.-T. Liao, T.-H. Chuang, D.-H. Wei, M.-Y. Chern, F.-Y. Lo, and W.-C. Lin*(林文欽), "*Field-free Magnetic Rotation in FePd Alloy Films Controlled by Reversible Hydrogenation*", J. Alloy. Compd. **983**, 173754 (2024).

TLS 07A1 IASW – X-ray Scattering

- D. Bhalothia, C. Yan, N. Hiraoka, H. Ishii, Y.F. Liao, S. Dai, P.-C. Chen*(陳柏均), and T.-Y. Chen*(陳燦耀), "*Iridium Single Atoms to Nanoparticles: Nurturing the Local Synergy with Cobalt-oxide Supported Palladium Nanoparticles for Oxygen Reduction Reaction*", Adv. Sci. **11**, 2404076 (2024).
- S.-L. Chen, T.-S. Wu, H.-L. Huang, S.-F. Chen, Y.-L. Soo, H.-T. Jeng, and H.-H. Hung*(洪雪行), "*Polarized X-ray Diffraction Anomalous Near-edge Structure Study on the Orbital Physics of Thin WSe_2 Layers*", J. Appl. Crystallogr. **57**, 344 (2024).
- M. N. Duong, Y.-X. Chen, W.-Y. Tzeng, T. Amrillah, S. Yang, C.-E. Liu, D. Z. Dimitrov, S.-C. Haw, C.-H. Hsu, J.-M. Chen*(陳錦明), J.-Y. Lin, K.-H. Wu, C.-W. Luo, C.-T. Chen, C.-Y. Kuo*(郭昌洋), and J.-Y. Juang*(莊振益), "*Orbital Ordering and Ultrafast Carrier Dynamics Anisotropies in Orientation-engineered Orthorhombic $YMnO_3$ Films*", APL Mater. **12**, 021117 (2024).
- H.-J. Huang, C.-S. Hsu, J.-Y. Huang, S.-C. Haw, H.-Y. Chen, N. Hiraoka, Y.-F. Liao*(廖彥發), and C.-W. Hu*(胡芝瑋), "*Electronic Structure Evolution upon Lithiation: A Li K-edge Study of Silicon Oxide Anode through X-ray Raman Spectroscopy*", J. Power Sources Adv. **29**, 100155 (2024).
- Y.-C. Kao, H.-K. Peng, S.-W. Hsiao, K.-A. Wu, C.-M. Liu, S.-Y. Zheng, Y.-H. Wu*(巫勇賢), and P.-J. Wu*(吳品鈞), "*Investigation of Annealing Temperature Dependent Sub-cycling Behavior for $HfZrO_x$-based Ferroelectric Capacitor*", APL Mater. **12**, 051118 (2024).
- G. Li, P.-L. B. Ho, B. K. Y. Ng, T.-S. Wu, P. Rymarz, and S. C. E. Tsang* (曾適之), "*Structural Insight into Palladium-nickel Clusters over Mordenite Zeolite for Carbene-insertion Reaction*", Front. Chem. Sci. Eng. **18**, 104 (2024).
- X. Li, B. K. Y. Ng, P.-L. Ho, C. Jia, J. Shang, T. Yoskamtorn, X. Pan, Y. Li, G. Li, T.-S. Wu, Y.-L. Soo, H. He*(賀鶴勇), B. Yue*(岳斌), and S. C. E. Tsang* (曾適之), "*Stabilization of Ni-containing Keggin-type Polyoxometalates with Variable Oxidation States as Novel Catalysts for Electrochemical Water Oxidation*", Chem. Sci. **15**, 9201 (2024).
- Y.-H. Sun, S.-W. Chen*(陳世偉), Z.-H. Lai, S.-L. Lu, Y.-T. Lin, J.-F. Tu, and H.-W. Yen*(顏鴻威), "*Strain-hardening Resilience via the Cooperation of Geometrically Necessary Dislocations and Deformation Twins in a Strong and Ductile Lightweight High-entropy Steel*", Mater. Des. **244**, 113212 (2024).
- C. K. T. Wun, Z. Wang, S. Kawaguchi, S. Kobayashi, T.-S. Wu, T. Chen, C. Lin, C. C. Tang, J. Yin*(殷俊), and T. W. B. Lo*(勞子桓), "*Investigating Synergistic Cooperativity of Metal-brønsted Acid Site Pair in MFI-type Zeolites by Synchrotron X-ray Powder Diffraction*", J. Mater. Chem. A **12**, 25442 (2024).
- D. Ye, K. C. Leung, W. Niu, M. Duan, J. Li, P.-L. Ho, D. Szalay, T.-S. Wu, Y.-L. Soo, S. Wu, and S. C. E. Tsang*(曾適之), "*Active Nitrogen Sites on Nitrogen Doped Carbon for Highly Efficient Associative Ammonia Decomposition*", iScience **27**, 110571 (2024).
- M. Yi, Y. Ren, X. Zhang, Z. Zhu*(朱振業), and J. Zhang*(張嘉恒), "*Ionic Liquid-assisted Synthesis of N, F, and B Co-doped BiOBr/Bi_2Se_3 on Mo_2CT_x for Enhanced Performance in Hydrogen Evolution Reaction and Supercapacitors*", J. Colloid Interf. Sci. **658**, 334 (2024).
- X. Zhan, L. Zhang, J. Choi, X. Tan*(譚心怡), S. Hong, T.-S. Wu, P. Xiong, Y.-L. Soo, L. Hao, M.-M. Jung, L. Xu, A. W. Robertson, Y. Jung*, X. Sun*(孫曉甫), and Z. Sun*(孫振宇), "*A Universal Synthesis of Single-atom Catalysts via Operando Bond Formation Driven by Electricity*", Adv. Sci. **11**, 2401814 (2024).

TLS 08B1 BM – AGM

- W. Chang*(張薇), B. J. Lin, P.-J. Wu, J.-R. Shih, Y.-D. Chih, J. Chang, C. J. Lin, and Y.-C. King*(金雅琴), "*Nano-meter Resolution Line-offset Detector Arrays (LODAs) for Pattern Monitoring in EUV Lithography System*", IEEE T. Electron Dev. **71**, 6850 (2024).
- M.-Y. Kao, C.-H. Hsu, Y.-Q. Huang, Y.-C. Hsu, M.-J. Liu, C.-T. Chen, P.-C. Lai, M.-Y. Lu, P.-J. Wu*(吳品鈞), and Y.-L. Chueh*(闕郁倫), "*Effects of Extreme Ultraviolet Radiation on Transition Metal Dichalcogenides: Investigation of Physical and Electrical Properties*", ACS Appl. Electron. Mater. **6**, 5640 (2024).

TLS 09A1 U50 – SPEM

- C.-M. Chu, P.-Y. Chuang, S.-H. Hsieh, C.-M. Cheng, C.-H. Chen, H.-S. Tsai* (蔡勛升), and W.-Y. Woon*(溫偉源), "*Graphene as the Anti-oxidation Protective Layer: How Good or Bad Can It Be?*", Mater. Today Comm. **39**, 108752 (2024).
- D. Hao, W.-H. Chang, Y.-C. Chang, W.-T. Liu, S.-Z. Ho, C.-H. Lu, T. H. Yang, N. Kawakami, Y.-C. Chen, M.-H. Liu, C.-L. Lin*(林俊良), T.-H. Lu*(陸亭樺), Y.-W. Lan*(藍彥文), and N.-C. Yeh*(葉乃嘉), "*Magnetic Field-induced Polar Order in Monolayer Molybdenum Disulfide Transistors*", Adv. Mater. **36**, 2411393 (2024).
- Y.-J. Wang, Z.-L. Yang, J.-W. Chen, R. Zhu, S.-H. Hsieh, S.-H. Chang, H.-Y. Lin, C.-L. Lin, Y.-C. Chen, C.-H. Chen, B.-C. Huang, Y.-P. Chiu, C.-H. Yeh, P. Gao, P.-W. Chiu, Y.-C. Chen*(陳怡誠), and Y.-H. Chu*(朱英豪), "*Nonvolatile Modulation of Bi_2O_2Se/Pb(Zr,Ti)O_3 Heteroepitaxy*", ACS Appl. Mater. Interfaces **16**, 27523 (2024).
- T. H. Yang*(楊弘偉), B.-W. Liang, H.-C. Hu, F.-X. Chen, S.-Z. Ho, W.-H. Chang, Liu Yang, H.-C. Lo, T.-H. Kuo, J.-H. Chen, P.-Y. Lin, K. B. Simbulan, Z.-F. Luo, A. C. Chang, Y.-H. Kuo, Y.-S. Ku, Y.-C. Chen, Y.-J. Huang, Y.-C. Chang, Y.-F. Chiang, T.-H. Lu, M.-H. Lee, K.-S. Li, M. Wu, Y.-C. Chen, C.-L. Lin*(林俊良), and Y.-W. Lan*(藍彥文), "*Ferroelectric Transistors Based on Shear-transformation-mediated Rhombohedral-stacked Molybdenum Disulfide*", Nat. Electron. **7**, 29 (2024).

TLS 09A2 U50 – Spectroscopy

- P. F. Chan, M. Qin*(秦敏超), C.-J. Su, L. Ye, X. Wang, Y. Wang, X. Guan, Z. Lu, G. Li, T. Ngai, S. W. Tsang, N. Zhao, and X. Lu*(路新慧), "*iso-BAI Guided Surface Recrystallization for Over 14% Tin Halide Perovskite Solar Cells*", Adv. Sci. **11**, 2309668 (2024).
- W.-T. Chen, L.-C. Yu, J.-H. Lin, S. L. Cheng, H. W. Shiu, Y.-L. Lai, Y.-H. Chu, Y.-Y. Chin, J.-H. Wang*(王禎翰), and Y.-J. Hsu*(許瑤真), "*Unravelling the Strong Interplay for Interfacial Magnetic Switching in Metal-organic-based Spintronics*", J. Mater. Chem. C **12**, 3931 (2024).
- J.-W. Hsueh, L.-H. Kuo, P.-H. Chen, W.-H. Chen, C.-Y. Chuang, C.-N. Kuo, C.-S. Lue, Y.-L. Lai, B.-H. Liu, C.-H. Wang, Y.-J. Hsu, C.-L. Lin*(林俊良), J.-P. Chou*(周至品), and M.-F. Luo*(羅夢凡), "*Investigating the Role of Undercoordinated Pt Sites at the Surface of Layered $PtTe_2$ for Methanol Decomposition*", Nat. Commun. **15**, 653 (2024).

TLS 11A1 BM – (Dragon) MCD, XAS (PRT 75%)

- F. Abdelghafar, X. Xu*(許曉敏), D. Guan, Z. Lin, Z. Hu, M. Ni, H. Huang, T. Bhatelia, S. P. Jiang, and Z. Shao*(邵宗平), "*New Nanocomposites Derived from CationNonstoichiometric Ba_x(Co, Fe, Zr, Y)$O_{3-\delta}$ as Efficient Electrocatalysts for Water Oxidation in Alkaline Solution*", ACS Mater. Lett. **6**, 2985 (2024).
- W.-T. Chen, L.-C. Yu, J.-H. Lin, S. L. Cheng, H. W. Shiu, Y.-L. Lai, Y.-H. Chu, Y.-Y. Chin, J.-H. Wang*(王禎翰), and Y.-J. Hsu*(許瑤真), "*Unravelling the Strong Interplay for Interfacial Magnetic Switching in Metal-organic-based Spintronics*", J. Mater. Chem. C **12**, 3931 (2024).
- H. Chou*(周雄), S. J. Sun*(孫士傑), K.-S. Yang, G. D. Dwivedi, C.-H. Chen, S. L. Cheng, J. G. Lin*(林昭吟), J. W. Chiou, Y. Y. Chin, H. J. Lin, and V. I. Grebennikov*, "*Controllable Spin-triplet Superconductivity States and Enhanced Non-dissipation Spin-polarized Supercurrents in $YBa_2Cu_3O_7$/$La_{0.67}Sr_{0.33}MnO_3$ Interfaces*", Appl. Surf. Sci. **644**, 158739 (2024).
- J. Cui, Y. Zhang, Z. Liu, Z. Hu, H.-P. Wang, P.-Y. Cho, C.-Y. Kuo, Y.-Y. Chin, C.-T. Chen, J. Zhu, J. Zhou, G. Kim*(金建兌), J.-Q. Wang*(王建強), and L. Zhang*(張林娟), "*Key Roles of Initial Calcination Temperature in Accelerating*

the Performance in Proton Ceramic Fuel Cells via Regulating 3D Microstructure and Electronic Structure", Small Struct. **5**, 2300439 (2024).

- J. Dai, Y. Tong, L. Zhao, Z. Hu, C.-T. Chen, C.-Y. Kuo, G. Zhan, J. Wang, X. Zou, Q. Zheng, W. Hou, R. Wang, K. Wang, R. Zhao, X.-K. Gu*(顧向奎), Y. Yao*(么豔彩), and L. Zhang*(張禮知), "*Spin Polarized Fe1-Ti Pairs for Highly Efficient Electroreduction Nitrate to Ammonia*", Nat. Commun. **15**, 88 (2024).
- J. Dai, Z. Shen, Y. Chen, M. Li, V. K. Peterson, J. Tang, X. Wang, Y. Li, D. Guan, C. Zhou, H. Sun, Z. Hu, W.-H. Huang, C.-W. Pao, C.-T. Chen, Y. Zhu*(朱印龍), W. Zhou, and Z. Shao*(邵宗平), "*A Complex Oxide Containing Inherent Peroxide Ions for Catalyzing Oxygen Evolution Reactions in Acid*", J. Am. Chem. Soc. **146**, 33663 (2024).
- Y. Fan, C. Zhang, L. Zhang*(張倫勇), J. Zhou, Y. Li, Y.-C. Huang, J. Ma, T.-S. Chan, C.-T. Chen, C. Jing, E. Mijit, Z. Hu*(胡志偉), J.-Q. Wang*(王建強), and L. Zhang*(張林娟), "*Novel Mechanism of Fe^{4+}/Ni^{3+} Synergistic Effect via Exchange Energy Gain for Boosting Water Oxidation*", Chem Catalysis **4**, 100981 (2024).
- S.-H. Hsieh, S. Ghosh, Y.-H. Liang, H.-T. Wang, C.-H. Du*(杜昭宏), J.-W. Chiou, C.-M. Wu, C.-W. Wang, Y.-C. Shao, J.-L. Chen, C.-W. Pao, H.-M. Tsai, T.-S. Chan, W.-B. Wu, H.-J. Lin, J.-F. Lee, A. Kandasami, and W.-F. Pong*(彭維鋒), "*Correlation Between Noncollinear Spin Orientation and Lattice Distortion in $Ni_{0.4}Mn_{0.6}TiO_3$*", Phys. Rev. Mater. **8**, 124410 (2024).
- Y.-C. Huang, Y. Wu, Y.-R. Lu, J.-L. Chen, H.-J. Lin, C.-T. Chen, C.-L. Chen, C. Jing, J. Zhou, L. Zhang, Y. Wang, W.-C. Chou*(周武清), S. Wang*(王雙印), Z. Hu*(胡志偉), and C.-L. Dong*(董崇禮), "*Direct Identification of O-O Bond Formation through Three-step Oxidation During Water Splitting by Operando Soft X-ray Absorption Spectroscopy*", Adv. Sci. **11**, 2401236 (2024).
- C. Jing, L. Li, Y.-Y. Chin, C.-W. Pao, W.-H. Huang, M. Liu, J. Zhou, T. Yuan, X. Zhou, Y. Wang, C.-T. Chen, D.-W. Li*(李大偉), J.-Q. Wang, Z. Hu*(胡志偉), and L. Zhang*(張林娟), "*Balance Between Fe^{IV}–Ni^{IV} Synergy and Lattice Oxygen Contribution for Accelerating Water Oxidation*", ACS Nano **18**, 14496 (2024).
- A. Z. Laila, T. L. Nguyen, R. Furui, A. Shelke, F.-H. Chang, H.-J. Lin, C.-T. Chen, S. Hamamoto, A. Fujimori, T. Mizokawa, A. Chainani, and A. Yamamoto*(山本文子), "*Comparative Study of a High-entropy Metal Disulfide and Its Parent Compounds Using X-ray Absorption Spectroscopy*", Phys. Rev. B **109**, 195129 (2024).
- J. Li, L. Liu, J. Wu, Z. Hu, Y.-Y. Chin, H.-J. Lin, C.-T. Chen, X. Pan, Y. Deng, N. Alonso-Vante, L. Sui, Y. Xie*(謝禹), and J. Ma*(馬吉偉), "*Synergistic Effect to Unlock the Activity and Stability for Oxygen Evolution Reaction in Spinel $LiMn_2O_4$ via D-block Metal Substitution*", Appl. Catal. B-Environ. **357**, 124331 (2024).
- S. Liu, W.-H. Huang, S. Meng, K. Jiang, J. Han*(韓佳甲), Q. Zhang, Z. Hu, C.-W. Pao, H. Geng, X. Huang, C. Zhan, Q. Yun, Y. Xu*(徐雍), and X. Huang*(黃小青), "*3D Noble-metal Nanostructures Approaching Atomic Efficiency and Atomic Density Limits*", Adv. Mater. **36**, 2312140 (2024).
- S. Liu, X. Wang, Z. Deng, X. Ye, Z. Pan, D. Lu, H. Zhao, J. Zhang, M. Pi, Z. Hu, C.-T. Chen, C. Dong, Y. Shen, T. Cui, Y. Huang, J. Hong*(洪家旺), Z. Chi*(池振華), and Y. Long*(龍有文), "*Observation of Enhanced Long-range Ferromagnetic Order in B-site Ordered Double Perovskite Oxide Cd_2CrSbO_6*", Inorg. Chem. **63**, 19964 (2024).
- D. Lu, J. Zhang, H. Zhao, M. Pi, X. Ye, Z. Liu, X. Wang, X. Zhang, Z. Pan, S.-Y. Hsu, C.-K. Chang, J.-M. Chen, Z. Hu, and Y. Long*(龍有文), "*Robust Crystal Phase Separation with Distinct Charge, Orbital, and Spin Orders in $AgMn_7O_{12}$*", Inorg. Chem. **63**, 3191 (2024).
- D. Lu, J. Yang, J. Zhang, H. Zhao, M. Pi, X. Ye, X. Wang, Z. Pan, C. Dong, L. He, F. Shen, C.-Y. Kuo, C.-T. Chen, Z. Hu, P. Yu, Y. Shen*(沈瑤), and Y. Long*(龍有文), "*Giant Spin-induced Electric Polarization in Absence of Orbital Order in $(Bi_{0.5}Ag_{0.5})Mn_7O_{12}$*", Phys. Rev. B **109**, 174417 (2024).
- D. Lu, D. Sheptyakov, Y. Cao, H. Zhao, J. Zhang, M. Pi, X. Ye, Z. Liu, X. Zhang, Z. Pan, X. Jiang, Z. Hu, Y.-F. Yang, P. Yu, and Y. Long*(龍有文), "*Magnetic-field Controllable Displacement-type Ferroelectricity Driven by Off-center Fe^{2+} Ions in $CaFe_3Ti_4O_{12}$ Perovskite*", Adv. Funct. Mater. **34**, 2411133 (2024).
- T. L. Nguyen, T. Mazet, É. Gaudry, D. Malterre, F.-H. Chang, H.-J. Lin, C.-T. Chen, Y.-C. Tseng, and A. Chainani*(查里), "*Element-specific Curie Temperatures and Heisenberg Criticality in Ferrimagnetic $Gd_6(Mn_{1-x}Fe_x)_{23}$ via Kouvel-fisher Analysis*", Commun. Mater. **5**, 68 (2024).
- T. L. Nguyen, T. Mazet, F.-H. Chang, H.-J. Lin, C.-T. Chen, and A. Chainani*(查里), "*Ligand Field Calculations for Element-specific Spectroscopy of Rare Earth-transition Metal Ferrimagnetic Alloys*", J. Phys. Soc. JPN. **93**, 121006 (2024).
- W. Peng, H. Guo, W. Schmidt, A. Piovano, H. Luetkens, C.-T. Chen, Z. Hu, and A. C. Komarek*, "*Hour-glass Spectra Due to Oxygen Doping in Cobaltates*", Commun. Phys. **7**, 399 (2024).
- J. Su, Y. Ji, S. Geng, L. Li, D. Liu, H. Yu, B. Song, Y. Li, C.-W. Pao, Z. Hu, X. Huang*(黃小青), J. Lu*(路建美), and Q. Shao*(邵琪), "*Core-shell Design of Metastable Phase Catalyst Enables Highly-performance Selective Hydrogenation*", Adv. Mater. **36**, 2308839 (2024).
- C. W. Chuang*(莊茜雯), Y. Nakata*, K. Hori, S. Gupta, F. M. F. de Groot, A. Fujimori, T. P. T. Nguyen, K. Yamauchi, I. Rajput, A. Lakhani, F.-H. Chang, H.-J. Lin, C.-T. Chen, F. Matsukura, S. Souma, T. Takahashi, T. Sato, and A. Chainani, "*Indication of Exchange Interaction Induced Spin Splitting in Unoccupied Electronic States of the High-T_C Ferromagnet $(Cr_{0.35}Sb_{0.65})_2Te_3$*", Phys. Rev. B **109**, 195134 (2024).
- L. Wang, A. Mukherjee, C.-Y. Kuo, S. Chakrabarty, R. Yemini, A. A. Dameron, J. W. DuMont, S. H. Akella, A. Saha, S. Taragin, H. Aviv, D. Naveh, D. Sharon, T.-S. Chan, H.-J. Lin, J.-F. Lee, C.-T. Chen, B. Liu, X. Gao, S. Basu, Z. Hu*(胡志偉), D. Aurbach*, P. G. Bruce, and M. Noked*, "*High-energy All-solid-state Lithium Batteries Enabled by Co-free $LiNiO_2$ Cathodes with Robust Outside-in Structures*", Nat. Nanotechnol. **19**, 208 (2024).
- L. Wang, C. Zhang, T. Lin, H. Chu, Y. Gao, Z. Hu, S.-C. Haw, C.-T. Chen, C.-Y. Kuo, X. Li, Y. Gai, Q. Guo, Y. Meng, H. Zhuang, X. Shen*(沈希), Z. Wang*(王兆翔), and R. Yu*(禹日成), "*Anti-siting for Stabilizing Structure and Modulating Cationic/Anionic Redox Reactions*", Energy Storage Mater. **70**, 103479 (2024).
- Y. Yang, Q. Wang*(王勍), J. Hou, J. Liu, T. Sun, M. Tang, C.-T. Chen, C.-Y. Kuo, Z. Hu, T. Zheng, G. Yan, and J. Ma*(馬吉偉), "*Enhancing Reversibility and Kinetics of Anionic Redox in O3-$NaLi_{1/3}Mn_{2/3}O_2$ Through Controlled P2 Intergrowth*", Angew. Chem. Int. Edit. **63**, e202411059 (2024).
- Z. Yin, J. Zhao, D. Luo, Y.-Y. Chin, C.-T. Chen, H. Chen, W. Yin, Y. Tang, T. Yang, J. Ren, T. Li, K. M. Wiaderek, Q. Kong, J. Fan*(范俊), H. Zhu*(朱賀), Y. Ren, and Q. Liu*(劉奇), "*Regulating the Electron Distribution of Metal-oxygen for Enhanced Oxygen Stability in Li-rich Layered Cathodes*", Adv. Sci. **11**, 2307397 (2024).
- H. Yu, Y. Ji, C. Li, W. Zhu, Y. Wang, Z. Hu, J. Zhou, C.-W. Pao, W.-H. Huang, Y. Li, X. Huang, and Q. Shao*(邵琪), "*Strain-triggered Distinct Oxygen Evolution Reaction Pathway in Two-dimensional Metastable Phase IrO_2 via CeO_2 Loading*", J. Am. Chem. Soc. **146**, 20251 (2024).
- J. Zhang, Z. Liu, X. Ye, X. Wang, D. Lu, H. Zhao, M. Pi, C.-T. Chen, J.-L. Chen, C.-Y. Kuo, Z. Hu, X. Yu, X. Zhang, Z. Pan*(潘昭), and Y. Long*(龍有文), "*High-pressure Synthesis of Quadruple Perovskite Oxide $CaCu_3Cr_2Re_2O_{12}$ with a High Ferrimagnetic Curie Temperature*", Inorg. Chem. **63**, 3499 (2024).
- H. Zhao, Z. Pan, X. Shen, J. Zhao, D. Lu, J. Zhang, Z. Hu, C.-Y. Kuo, C.-T. Chen, T.-S. Chan, C. J. Sahle, C. Dong, T. Nishikubo, T. Koike, Z.-Y. Deng, J. Hong, R. Yu, P. Yu, M. Azuma, C. Jin, and Y. Long*(龍有文), "*Antiferroelectricity-induced Negative Thermal Expansion in Double Perovskite Pb_2CoMoO_6*", Small **20**, 2305219 (2024).
- H. Zhao, D. Lu, X. Wang, X. Ye, J. Zhang, M. Pi, Z. Pan, Y.-Y. Chin, C.-T. Chen, Z. Hu, and Y. Long*(龍有文), "*High-pressure Synthesis of Semiconducting $PbCu_3Mn_4O_{12}$ with Near-room-temperature Ferrimagnetic Order*", Inorg. Chem. **63**, 5924 (2024).
- C. Zhou, L. Ma, Y. Feng, C.-Y. Kuo, Y.-C. Ku, C.-E. Liu, X. Cheng, J. Li, Y. Si, H. Huang, Y. Huang, H. Zhao, C.-F. Chang, S. Das, S. Liu*(劉仕), and Z. Chen*(陳祖煌), "*Enhanced Polarization Switching Characteristics of HfO_2 Ultrathin Films via Acceptor-donor Co-doping*", Nat. Commun. **15**, 2893 (2024).
- M. Zhu, H. Xu, J. Dai, D. Guan*(管大秦), Z. Hu, S. She, C.-T. Chen, R. Ran*(冉然), W. Zhou, and Z. Shao*(邵宗平), "*A Dynamically Stable Self-assembled CoFe (oxy) Hydroxide-based Nanocatalyst with Boosted Electrocatalytic Performance for the Oxygenevolution Reaction*", J. Mater. Chem. A **12**, 24308 (2024).

TLS 13A1 SW60 – X-ray Scattering

- A.-C. Chang, Y.-S. Wu, W.-C. Chen, Y.-H. Weng, B.-H. Lin, C.-C. Chueh, Y.-C. Lin*(林彥丞), and W.-C. Chen*(陳文章), "*Modulating the Photoresponsivity of Perovskite Photodetectors through Interfacial Engineering of Self-assembled Monolayers*", Adv. Opt. Mater. **12**, 2301789 (2024).
- J.-M. Chang, T.-H. Lin, K.-C. Hsiao, K.-P. Chiang, Y.-H. Chang, and M.-C. Wu*(吳明忠), "*Gas-solid Phase Reaction Derived Silver Bismuth Iodide Rudorffite: Structural Insight and Exploring Photocatalytic Potential of CO_2 Reduction*", Adv. Sci. **11**, 2309526 (2024).
- S.-T. Chang, W.-C. Chen, C.-F. Lin, P.-Z. Yu, C.-H. Tsai, C.-J. Cho, Y.-C. Lin*(林彥丞), W.-C. Chen*(陳文章), and C.-C. Kuo*(郭霽慶), "*Quasi-2D Perovskite with Ligand Engineering to Improve the Stability of Phototransistor Memory with a Floating Gate*", Adv. Opt. Mater. **12**, 2400470 (2024).
- Y. Chang, Y.-H. Huang, P.-S. Lin, S.-H. Hong, S.-H. Tung, and C.-L. Liu*(劉振良), "*Enhanced Electrical Conductivity and Mechanical Properties of*

Stretchable Thermoelectric Generators Formed by Doped Semiconducting Polymer/Elastomer Blends", ACS Appl. Mater. Interfaces **16**, 3764 (2024).

- W.-C. Chen, Y.-C. Lin, Z.-S. Syu, Y.-S. Wu, K.-W. Lin, C.-L. Liu, C.-C. Kuo*(郭霽慶), and W.-C. Chen*(陳文章), "*Surface Ligand Engineering of Perovskite Quantum Dots for N-type and Stretchable Photosynaptic Transistor with an Ultralow Energy Consumption*", Chem. Eng. J. **494**, 152897 (2024).
- P.-H. Chiu, C.-T. Hu, S.-K. Chia, L.-Y. Su*(蘇莉芸), P.-T. Chen, Z.-Y. Liu, C.-Y. Lin, C.-C. Hsieh, C.-A. Dai*(戴子安), and L. Wang*(王立義), "*Synergistic Enhancement of Stability and Performance for Perovskite Solar Cells Using Fluorinated Benzoic Acids as Additives*", Solar RRL **8**, 2300902 (2024).
- C.-A. Chou, S.-C. Fang, P.-S. Lin, W.-N. Wu, S.-H. Hong, J.-M. Lin, K.-T. Wong*(汪根欉), and C.-L. Liu*(劉振良), "*Tuning Thermoelectric Performance with N-annulated Perylene-based Small Molecules and Single-walled Carbon Nanotube Nanocomposite Films*", Mater. Today Chem. **38**, 102129 (2024).
- S. Chuo, Y.-C. Peng, T. Puangniyom, Q.-G. Chen, C.-C. Chueh*(闕居振), and W.-Y. Lee*(李文亞), "*Enhancing Charge Transport in Isoindigo-based Donor-acceptor Copolymers by Combining Ionic Doping with Polar Alkoxy Side Chains*", RSC Appl. Interfaces **1**, 1012 (2024).
- M. N. Duong, Y.-X. Chen, W.-Y. Tzeng, T. Amrillah, S. Yang, C.-E. Liu, D. Z. Dimitrov, S.-C. Haw, C.-H. Hsu, J.-M. Chen*(陳錦明), J.-Y. Lin, K.-H. Wu, C.-W. Luo, C.-T. Chen, C.-Y. Kuo*(郭昌洋), and J.-Y. Juang*(莊振益), "*Orbital Ordering and Ultrafast Carrier Dynamics Anisotropies in Orientation-engineered Orthorhombic $YMnO_3$ Films*", APL Mater. **12**, 021117 (2024).
- C.-H. Huang, C. S. Gantepogu, P.-J. Chen, T.-H. Wu, W.-R. Liu, K.-H. Lin, C.-L. Chen, T.-K. Lee, M.-J. Wang*(王明杰), and M.-K. Wu, "*Substrate Charge Transfer Induced Ferromagnetism in MnSe/$SrTiO_3$ Ultrathin Films*", Nanomaterials **14**, 1355 (2024).
- C.-M. Hung, S.-F. Wang, W.-C. Chao, J.-L. Li, B.-H. Chen, C.-H. Lu, K.-Y. Tu, S.-D. Yang, W.-Y. Hung, Y. Chi*(季昀), and P.-T. Chou*(周必泰), "*High-performance Near-infrared OLEDs Maximized at 925 nm and 1022 nm through Interfacial Energy Transfer*", Nat. Commun. **15**, 4664 (2024).
- H.-A. Lin, Y.-H. Weng, T. Mulia, C.-L. Liu, Y.-C. Lin*(林彥丞), Y.-Y. Yu*(游洋雁), and W.-C. Chen*(陳文章), "*Electrical Double-layer Transistors Comprising Block Copolymer Electrolytes for Low-power-consumption Photodetectors*", ACS Appl. Mater. Interfaces **16**, 25042 (2024).
- Y. H. G. Lin, C. K. Cheng, L. B. Young, L. S. Chiang, W. S. Chen, K. H. Lai, S. P. Chiu, C. T. Wu, C. T. Liang, J. J. Lin, C. H. Hsu*(徐嘉鴻) Y. H. Lin*(林晏詳), J. Kwo*(郭瑞年), and M. Hong*(洪銘輝), "*Nanometer-thick Molecular Beam Epitaxy Al Films Capped with in Situ Deposited Al_2O_3-High-crystallinity, Morphology, and Superconductivity*", J. Appl. Phys. **136**, 074401 (2024).
- M. Liu, Y.-H. Shih, X. Yu, M.-H. Yu, X. Sun, C.-C. Chueh*(闕居振), and Z. Li*(李忠安)., "*High Mobility n-type Imide-based Semiconductor with Unusual Single-crystal Packing Structure in Solution-processed Thin Film*", Adv. Funct. Mater. **34**, 2405171 (2024).
- Y.-C. Neu, Y.-S. Lin, Y.-H. Weng, W.-C. Chen, C.-L. Liu, B.-H. Lin, Y.-C. Lin*(林彥丞), and W.-C. Chen*(陳文章), "*Reversible Molecular Conformation Transitions of Smectic Liquid Crystals for Light/Bias-gated Transistor Memory*", ACS Appl. Mater. Interfaces **16**, 7500 (2024).
- Y.-C. Neu, C.-W. Hsu, Y.-S. Wu, Y. Liu, C.-L. Liu, Y.-C. Lin*(林彥丞), and W.-C. Chen*(陳文章), "*Interfacial Charge Trap Engineering of Organic Semiconductors Using Reactive Oxygen Plasma for Enhanced Performance in Phototransistor Memory*", Mater. Today Chem. **42**, 102445 (2024).
- Y.-H. Shih, G.-L. Chen, P.-H. Liu, K.-W. Tseng, W.-Y. Lee, W.-C. Chen, L. Wang*(王立義), and C.-C. Chueh*(闕居振), "*Revealing the Effect of Branched Side Chain Length on Polymer Aggregation and Paracrystallinity for Improved Mobility-stretchability Properties*", ACS Appl. Electron. Mater. **6**, 1797 (2024).
- C.-Y. Sung, C.-Y. Lin, C.-C. Chueh, Y.-C. Lin*(林彥丞), and W.-C. Chen*(陳文章), "*Investigating the Mobility-compressibility Properties of Conjugated Polymers by the Contact Film Transfer Method with Prestrain*", Macromol. Rapid Comm. **45**, 2300058 (2024).
- C.-Y. Sung, W.-C. Chen, C.-L. Liu, B.-H. Lin, Y.-C. Lin*(林彥丞), and W.-C. Chen*(陳文章), "*Ultrafast Quasi-2D/3D Perovskite Photodetectors Conferred Using Interfacial Engineering of Self-assembled Monolayers*", Adv. Opt. Mater. **12**, 2303241 (2024).
- S. Y. Tsai, P.-H. Tseng, C. C. Chen, C.-M. Huang, H.-W. Yen, Y.-S. Chen, K.-L. Lin, R. Niu, Y.-S. Lai, and F.-H. Ko*(柯富祥), "*Lattice Boundary Enhancement on Thermoelectric Behaviors of Heavily Boron-doped Silicon for Energy Harvesting: Electrical versus Thermal Conductivity*", Adv. Mater. Interfaces **11**, 2400536 (2024).
- C.-C. Tseng, K.-C. Wang, P.-S. Lin, C. Chang, L.-L. Yeh, S.-H. Tung, C.-L. Liu*(劉振良), and Y.-J. Cheng*(鄭彥如), "*Intrinsically Stretchable Organic Thermoelectric Polymers Enabled by Incorporating Fused-ring Conjugated Breakers*", Small **20**, 2401966 (2024).
- P.-H. Tseng, Y.-S. Lai*(賴宇紳), M.-Y. Li, C.-M. Huang, S.-Y. Tsai, K. Y.-J. Hsu, and F.-H. Ko*(柯富祥), "*Sustainable Solar-powered Hydrogen Generation with a Silicon Nanopillar Device with a Low Carbon Footprint*", Int. J. Hydrogen Energ. **68**, 1322 (2024).
- Y.-C. Tseng, Q. Fan, C.-Y. Tsai, J.-F. Chang, M.-H. Yu, H.-Z. Tseng, H.-L. Yip, F. R. Lin*, A. K.-Y. Jen*(任廣禹), and C.-C. Chueh*(闕居振), "*Compatibilizer Effects of Strategically Designed Donor-acceptor Block Copolymers to Enhance the Performance, Stability, and Mechanical Durability of Inverted Organic Solar Cells*", Adv. Funct. Mater. **34**, 2408993 (2024).
- W.-L. Wei, C.-Y. Lin, T.-C. Huang, Y.-C. Li, Y.-H. Wu, C.-Y. Lee, B.-Y. Chen, G.-C. Yin, M.-T. Tang, W.-C. Chou, F.-Y. Lo*(駱芳鈺), and B.-H. Lin*(林碧軒), "*Structural and Optical Properties of Eu-doped ZnO Epitaxial Thin Films Grown by Pulsed-laser Deposition*", APL Mater. **12**, 111112 (2024).
- Y.-S. Wu, W.-C. Chen, Y.-S. Lin, C.-L. Liu, Y.-C. Lin*(林彥丞), and W.-C. Chen*(陳文章), "*Revealing the Effect of Crystalline Self-assembled Monolayer in Biomimetic Photosynapse with Ultraviolet Light Protection Capability*", ACS Appl. Mater. Interfaces **16**, 69645 (2024).
- H.-C. Yen, C.-Y. Sung, P.-H. Chen, Y.-C. Lin*(林彥丞), T. Higashihara*(東原知哉), and W.-C. Chen*(陳文章), "*Imparting Stretchable Semiconducting Polymers with Ambipolar Charge-transport Capability by Using a Lewis Base of Triazabicyclodecene*", ACS Appl. Polym. Mater. **6**, 2534 (2024).
- M.-H. Yu, Xingyu Liu, H.-W. Yu, S.-F. Kao, C.-H. Chen, Y.-C. Tseng, I.-C. Ni, B.-H. Lin, Yang Wang*(王漾), and C.-C. Chueh*(闕居振), "*Impact of Self-assembled Monolayer Structural Design on Perovskite Phase Regulation, Hole-selective Contact, and Energy Loss in Inverted Perovskite Solar Cells*", Nano Energy **132**, 110405 (2024).

TLS 13B1 SW60 – Protein Crystallography

- C.-H. Lai, K.-T. Ko, P.-J. Fan, T.-A. Yu, C.-F. Chang, P. Draczkowski, and S.-T. D. Hsu*(徐尚德), "*Structural Insight into the ZFAND1-p97 Interaction Involved in Stress Granule Clearance*", J. Biol. Chem. **300**, 107230 (2024).
- H.-Y. Li, H.-Y. Lin, S.-K. Chang, Y.-T. Chiu, C.-C. Hou, T.-P. Ko, K.-F. Huang, D.-M. Niu*(牛道明), and W.-C. Cheng*(鄭偉杰), "*Mechanistic Insights into Dibasic Iminosugars as pH-selective Pharmacological Chaperones to Stabilize Human α-galactosidase*", JACS Au **4**, 908 (2024).
- K. Ma, B. Xue, R. Chu, Y. Zheng, S. Sharma, L. Jiang, M. Hu, Y. Xie, Y. Hu, T. Tao, Y. Zhou, D. Liu, Z. Li, Q. Yang, Y. Chen, S. Wu, Y. Tong, R. C. Robinson, W. S. Yew, X. Jin, Y. Liu, H. Zhao, E. L. Ang, Y. Wei*, and Y. Zhang*(張雁), "*A Widespread Radical-mediated Glycolysis Pathway*", J. Am. Chem. Soc. **146**, 26187 (2024).
- M. K. Sriramoju, K.-T. Ko, and S.-T. D. Hsu*(徐尚德), "*Tying a True Topological Protein Knot by Cyclization*", Biochem. Biophy. Res. Co. **696**, 149470 (2024).
- S. Wang, C.-H. Huang, T.-S. Lin, Y.-Q. Yeh, Y.-S. Fan, S.-W. Wang, H.-C. Tseng, S.-J. Huang, Y.-Y. Chang, U.-S. Jeng, C.-I. Chang, and S.-R. Tzeng*(曾秀如), "*Structural Basis for Recruitment of Peptidoglycan Endopeptidase MepS by Lipoprotein NlpI*", Nat. Commun. **15**, 5461 (2024).
- C.-Y. Yang, C.-I. Lien, Y.-C. Tseng, Y.-F. Tu, A. W. Kulczyk, Y.-C. Lu, Y.-T. Wang, T.-W. Su, L.-C. Hsu*(徐立中), Y.-C. Lo*(羅玉枝), and S.-C. Lin*(林世昌), "*Deciphering DED Assembly Mechanisms in FADD-procaspase-8-cFLIP Complexes Regulating Apoptosis*", Nat. Commun. **15**, 3791 (2024).
- C.-Y. Yang, Y.-C. Tseng, Y.-F. Tu, B.-J. Kuo, L.-C. Hsu, C.-I. Lien, Y.-S. Lin, Y.-T. Wang, Y.-C. Lu, T.-W. Su, Y.-C. Lo*(羅玉枝), and S.-C. Lin*(林世昌), "*Reverse Hierarchical DED Assembly in the cFLIP-procaspase-8 and cFLIP-procaspase-8-FADD Complexes*", Nat. Commun. **15**, 8974 (2024).
- H.-W. Yeh, P.-P. Chen, T.-C. Yeh, S.-L. Lin, Y.-T. Chen, W.-P. Lin, Ting Chen, J. M. Pang, K.-T. Lin, L. H-C. Wang, Y.-C. Lin, O. Shih, U.-S. Jeng, K.-C. Hsia, and H.-C. Cheng*(鄭惠春), "*Cep57 Regulates Human Centrosomes through Multivalent Interactions*", P. Natl. Acad. Sci. USA **121**, e2305260121 (2024).

TLS 13B2 Beamline of Interdisciplinary Energy Researches

- Y.-A. Chen, Y. Nakayasu, Y.-C. Lin, J.-C. Kao, K.-C. Hsiao, Q.-T. Le, K.-D. Chang, M.-C. Wu, J.-P. Chou, C.-W. Pao, T.-F. M. Chang, M. Sone, C.-Y. Chen*(陳君怡), Y.-C. Lo*(羅友杰), Y.-G. Lin*(林彥谷), A. Yamakata*(山方啓), and Y.-J. Hsu*(徐雍鎏), "*Double-hollow Au@CdS Yolk@Shell Nanostructures as Superior Plasmonic Photocatalysts for Solar Hydrogen Production*", Adv. Funct. Mater. **34**, 2402392 (2024).
- R. Muruganantham, J.-Y. Huang, P.-J. Wu, L.-Y. Kuo, C.-C. Yang, Y.-G. Lin, J. Li, and W.-R. Liu*(劉偉仁), "*Nano-crystalline $Fe_3V_3O_8$ Material as an Efficient Advanced Anode for Energy Storage Applications*", J. Power Sources **613**, 234947

(2024).

- W.-J. Zhong, M.-Y. Hung, Y.-T. Kuo, H.-K. Tian*(田弘康), C.-N. Tsai, C.-J. Wu, Y.-D. Lin, H.-C. Yu, Y.-G. Lin, and J.-J. Wu*(吳季珍), "*Dual-vacancy-engineered $ZnIn_2S_4$ Nanosheets for Harnessing Low-frequency Vibration Induced Piezoelectric Polarization Coupled with Static Dipole Field to Enhance Photocatalytic H_2 Evolution*", Adv. Mater. **36**, 2403228 (2024).

TLS 13C1 SW60 – Protein Crystallography

- C.-C. Chen, Y.-R. Huang, Y. T. Chan, H.-Y. Lin, H.-J. Lin, C.-D. Hsiao, T.-P. Ko, T.-W. Lin, Y.-H. Lan, H.-Y. Lin, and H.-Y. Chang*(張欣暘), "*A Distinct Dimer Configuration of a Diatom Get3 Forming a Tetrameric Complex with Its Tail-anchored Membrane Cargo*", BMC Biol. **22**, 136 (2024).
- Y.-H. Huang and C.-Y. Huang*(黃晟洋), "*The Complexed Crystal Structure of Dihydropyrimidinase Reveals a Potential Interactive Link with the Neurotransmitter γ-aminobutyric Acid (GABA)*", Biochem. Biophy. Res. Co. **692**, 149351 (2024).
- S. Wang, C.-H. Huang, T.-S. Lin, Y.-Q. Yeh, Y.-S. Fan, S.-W. Wang, H.-C. Tseng, S.-J. Huang, Y.-Y. Chang, U.-S. Jeng, C.-I. Chang, and S.-R. Tzeng*(曾秀如), "*Structural Basis for Recruitment of Peptidoglycan Endopeptidase MepS by Lipoprotein NlpI*", Nat. Commun. **15**, 5461 (2024).

TLS 14A1 BM – IR Microscopy

- T. Agnihotri, S. A. Ahmed, E. B. Tamilarasan, R. Hasan, W.-N. Su*(蘇威年), and B. J. Hwang*(黃炳照), "*Transitioning Towards Asymmetric Gel Polymer Electrolytes for Lithium Batteries: Progress and Prospects*", Adv. Funct. Mater. **34**, 2311215 (2024).
- T. Agnihotri, S. A. Ahmed, E. B. Tamilarasan, R. Hasan, B. T. Hotasi, H. K. Bezabh, S. Suwito, Y. Nikodimos, S.-K. Jiang, K. N. Shitaw, Z. B. Muche, P. Y. Huang, Y.-C. Lee, W.-N. Su*(蘇威年), S.-H. Wu*(吳溪煌), and B. J. Hwang*(黃炳照), "*Anion-trapping Composite Gel Electrolyte for Safer and More Stable Anode-free Lithium-metal Batteries*", Chem. Eng. J. **484**, 149608 (2024).
- Y.-L. Cho, Y.-M. Tzou, A. Assakinah, N. A. T. Than, H. S. Yoon, S. I. Park, C.-C. Wang, Y.-C. Lee, L.-C. Hsu, P.-Y. Huang, S.-L. Liu, and Y.-T. Liu*(劉雨庭), "*Accumulation and Bio-oxidation of Arsenite Mediated by Thermoacidophilic Cyanidiales: Innate Potential Biomaterials toward Arsenic Remediation*", Bioresource Technol. **406**, 130912 (2024).
- B.-H. Kao, Y.-F. Zeng, Y.-C. Lee, C.-W. Pao, J.-L. Chen, Y.-C. Chuang, H.-S. Sheu, F.-T. Tsai*(蔡富潯), and W.-F. Liaw*(廖文峯), "*Unveiled the Structure-selectivity Relationship for Carbon Dioxide Reduction Triggered by Bi-doped Cu-based Nanocatalysts*", Small **20**, 2307910 (2024).
- C.-H. Kuan, Y.-C. Chen, S. Narra, C.-F. Chang, Y.-W. Tsai, J.-M. Lin, G.-R. Chen, and E. W.-G. Diau*(刁維光), "*Quadruple-cation Wide-bandgap Mixed-halide Tin Perovskite Solar Cells*", ACS Energ. Lett. **9**, 2351 (2024).
- K. Lakshmanan, W.-H. Huang, S. A. Chala, C.-Y. Chang, S. T. Saravanan, B. W. Taklu, E. A. Moges, Y. Nikodimos, B. D. Dandena, S.-C. Yang, J.-F. Lee, P.-Y. Huang, Y.-C. Lee, M.-C. Tsai*(蔡孟哲), W.-N. Su*(蘇威年), and B. J. Hwang*(黃炳照), "*Generating Multi-carbon Products by Electrochemical CO_2 Reduction via Catalytically Harmonious Ni/Cu Dual Active Sites*", Small **20**, 2307180 (2024).
- A. Windmüller*, K. Schaps, F. Zantis, A. Domgans, B. W. Taklu, T. Yang, C.-L. Tsai, R. Schierholz, S. Yu, H. Kungl, H. Tempel, R. E. Dunin-Borkowski, F. Hüning, B. J. Hwang, and R.-A. Eichel, "*Electrochemical Activation of $LiGaO_2$: Implications for Ga-doped Garnet Solid Electrolytes in Li-metal Batteries*", ACS Appl. Mater. Interfaces **16**, 39181 (2024).

TLS 15A1 Biopharmaceuticals Protein Crystallography

- H.-H. Chang, L.-C. Lee, Tsu Hsu, Y.-H. Peng, C.-H. Huang, T.-K. Yeh, C.-T. Lu, Z.-T. Huang, C.-C. Hsueh, F.-C. Kung, L.-M. Lin, Y.-C. Huang, Y.-H. Wang, L.-H. Li, Y.-C. Tang, L. Chang, C.-C. Hsieh, W.-T. Jiaang*(蔣維棠), C.-C. Kuo*(郭靜娟), and S.-Y. Wu*(伍素瑩), "*Development of Potent and Selective Inhibitors of Methylenetetrahydrofolate Dehydrogenase 2 for Targeting Acute Myeloid Leukemia: SAR, Structural Insights, and Biological Characterization*", J. Med. Chem. **67**, 21106 (2024).
- C.-C. Chen, Y.-R. Huang, Y. T. Chan, H.-Y. Lin, H.-J. Lin, C.-D. Hsiao, T.-P. Ko, T.-W. Lin, Y.-H. Lan, H.-Y. Lin, and H.-Y. Chang*(張欣暘), "*A Distinct Dimer Configuration of a Diatom Get3 Forming a Tetrameric Complex with Its Tail-anchored Membrane Cargo*", BMC Biol. **22**, 136 (2024).
- X. Chen, A. Mohapatra, H. T. V. Nguyen, L. Schimanski, T. K. Tan, P. Rijal, C.-P. Chen, S.-H. Cheng, W.-H. Lee, Y.-C. Chou, A. R. Townsend, C. Ma, and K.-Y. A. Huang*(黃冠穎), "*The Presence of Broadly Neutralizing Anti-SARS-CoV-2 RBD Antibodies Elicited by Primary Series and Booster Dose of COVID-19 Vaccine*", PLoS Pathog. **20**, e1012246 (2024).
- W. T. Chiang, Y.-K. Chang, W.-H. Hui, S.-W. Chang, C.-Y. Liao, Y.-C. Chang, C.-J. Chen, W.-C. Wang, C.-C. Lai, C.-H. Wang, S.-Y. Luo, Y.-P. Huang, S.-H. Chou, T.-L. Horng, M.-H. Hou, S. P. Muench, R.-S. Chen, M.-D. Tsai*(蔡明道), and N.-J. Hu*(胡念仁), "*Structural Basis and Synergism of ATP and Na^+ Activation in Bacterial K^+ Uptake System KtrAB*", Nat. Commun. **15**, 3850 (2024).
- C.-C. Cho, C.-Y. Fei, B.-C. Jiang, W.-Z. Yang, and H. S. Yuan*(袁小玲), "*Molecular Mechanisms for DNA Methylation Defects Induced by ICF Syndrome-linked Mutations in DNMT3B*", Protein Sci. **33**, e5131 (2024).
- C.-H. Chu, C.-T. Wu, M.-G. Lin, C.-Y. Yen, Y.-Z. Wu, C.-D. Hsiao*(蕭傳鐙), and Y.-J. Sun*(孫玉珠), "*Insights into the Molecular Mechanism of ParABS System in Chromosome Partition by HpParA and HpParB*", Nucleic Acids Res. **52**, 7321 (2024).
- Y.-C. Hsieh, H.-H. Guan, C.-C. Lin, T.-Y. Huang, P. Chuankhayan, N.-C. Chen, N.-H. Wang, P.-L. Hu, Y.-C. Tsai, Y.-C. Huang, M. Yoshimura, P.-J. Lin, Y.-H. Hsieh*(謝義簧), and C.-J. Chen*(陳俊榮), "*Structure-based High-efficiency Homogeneous Antibody Platform by Endoglycosidase Sz Provides Insights into Its Transglycosylation Mechanism*", JACS Au **4**, 2130 (2024).
- M.-F. Hsu, M. K. Sriramoju, C.-H. Lai, Y.-R. Chen, J.-S. Huang, T.-P. Ko, K.-F. Huang, and S.-T. D. Hsu*(徐尚德), "*Structure, Dynamics, and Stability of the Smallest and Most Complex 7_1 Protein Knot*", J. Biol. Chem. **300**, 105553 (2024).
- S.-C. Huang, C.-W. Chen, R. Satange, C.-C. Hsieh, C.-C. Chang, S.-C. Wang, C.-L. Peng, T.-L. Chen, M.-H. Chiang, Y.-C. Horng*(洪義盛), and M.-H. Hou*(侯明宏), "*Targeting DNA Junction Sites by Bis-intercalators Induces Topological Changes with Potent Antitumor Effects*", Nucleic Acids Res. **52**, 9303 (2024).
- B.-J. Kuo, S.-C. Lin, Y.-F. Tu, P.-H. Huang, and Y.-C. Lo*(羅玉枝), "*Study of Individual Domains Contributing to MALT1 Dimerization in BCL10-independent and Dependent Assembly*", Biochem. Biophy. Res. Co. **717**, 150029 (2024).
- C.-C. Lee*(李政忠), W.-C. Kuo, Y.-W. Chang, S.-F. Hsu, C.-H. Wu, Y.-W. Chen, J.-J. Chang*(張瑞仁), and A. H.-J. Wang*(王惠鈞), "*Structure-based Development of a Canine TNF-α-specific Antibody Using Adalimumab as a Template*", Protein Sci. **33**, e4873 (2024).
- H.-Y. Li, H.-Y. Lin, S.-K. Chang, Y.-T. Chiu, C.-C. Hou, T.-P. Ko, K.-F. Huang, D.-M. Niu*(牛道明), and W.-C. Cheng*(鄭偉杰), "*Mechanistic Insights into Dibasic Iminosugars as pH-selective Pharmacological Chaperones to Stabilize Human α-galactosidase*", JACS Au **4**, 908 (2024).
- S.-M. Lin, H.-T. Huang, P.-J. Fang, C.-F. Chang, R. Satange, C.-K. Chang, S.-H. Chou, S. Neidle*, and M.-H. Hou*(侯明宏), "*Structural Basis of Water-mediated cis Watson-cric k/Hoogsteen Base-pair Formation in Non-CpG Methylation*", Nucleic Acids Res. **52**, 8566 (2024).
- C.-Y. Liu, H.-P. Cheng, C.-P. Lin, Y.-T. Liao, T.-P. Ko, S.-J. Lin, S.-S. Lin*(林詩舜), and H.-C. Wang*(王皓青), "*Structural Insights into the Molecular Mechanism of Phytoplasma Immunodominant Membrane Protein*", IUCrJ **11**, 384 (2024).
- K.-T. Liu, S.-F. Chen, and N.-L. Chan*(詹迺立), "*Structural Insights into the Assembly of Type IIA Topoisomerase DNA Cleavage-relig ation Center*", Nucleic Acids Res. **52**, 9788 (2024).
- E. Y. C. Mao, H.-Y. Yen, and C.-C. Wu*(吳權娟), "*Structural Basis of How MGME1 Processes DNA 5′ Eends to Maintain Mitochondrial Genome Integrity*", Nucleic Acids Res. **52**, 4067 (2024).
- C. Y. Mok, H. Y. Chu, W. W. L. Lam, and S. W. N. Au*(區詠娥), "*Structural Insights into the Assembly Pathway of the Helicobacter Pylori CagT4SS Outer Membrane Core Complex*", Structure **32**, 1725 (2024).
- J.-C. Tsou, C.-J. Tsou, C.-H. Wang, A.-L. A. Ko, Y.-H. Wang, H.-H. Liang, J.-C. Sun, K.-F. Huang, T.-P. Ko, S.-Y. Lin, and Y.-S. Wang*(王彥士), "*Site-specific Histidine Aza-michael Addition in Proteins Enabled by a Ferritin-based Metalloenzyme*", J. Am. Chem. Soc. **146**, 33309 (2024).
- S. Wang, C.-H. Huang, T.-S. Lin, Y.-Q. Yeh, Y.-S. Fan, S.-W. Wang, H.-C. Tseng, S.-J. Huang, Y.-Y. Chang, U.-S. Jeng, C.-I. Chang, and S.-R. Tzeng*(曾秀如), "*Structural Basis for Recruitment of Peptidoglycan Endopeptidase MepS by Lipoprotein NlpI*", Nat. Commun. **15**, 5461 (2024).
- L.-C. Ye, S.-Y. Chow, S.-C. Chang, C.-H. Kuo, Y.-L. Wang, Y.-J. Wei, G.-C. Lee, S.-H. Liaw, W.-M. Chen*(陳文明), and S.-C. Chen*(陳勝嘉), "*Structural and Mutational Analyses of Trehalose Synthase from Deinococcus radiodurans Reveal the Interconversion of Maltose-trehalose Mechanism*", J. Agr. Food Chem. **72**, 18649 (2024).
- T.-J. Ye, K.-M. Fung, I.-M. Lee, T.-P. Ko, C.-Y. Lin, C.-L. Wong, I.-F. Tu, T.-Y. Huang, F.-L. Yang, Y.-P. Chang, J.-T. Wang, T.-L. Lin, K.-F. Huang*(黃開發), and S.-H. Wu*(吳世雄), "*Klebsiella Pneumoniae K2 Capsular Polysaccharide Degradation by a Bacteriophage Depolymerase Does Not Require Trimer Formation*", mBio **15**, 03519-23 (2024).

TLS 16A1 BM – Tender X-ray Absorption, Diffraction

- M. M. M. Ahmed, K.-Y. Chen, F.-Y. Tsao, Y.-C. Hsieh, Y.-T. Liu*(劉雨庭), and Y.-M. Tzou*(鄒裕民), "*Promotion of Phosphate Release from Humic Acid-iron Hydroxide Coprecipitates in the Presence of Citric Acid*", Environ. Res. **240**, 117517 (2024).
- A. Bandyopadhyay*, S. Lee, D. T. Adroja*, G. B. G. Stenning, A. Berlie, M. R. Lees, R. A. Saha, D. Takegami, A. Meléndez-Sans, G. Poelchen, M. Yoshimura, K. D. Tsuei, Z. Hu, C.-W. Kao, Y.-C. Huang, T.-S. Chan, and K.-Y. Choi, "*Quantum Spin Liquid Ground State in the Trimer Rhodate $Ba_4NbRh_3O_{12}$*", Phys. Rev. B **109**, 184403 (2024).
- A. Bandyopadhyay*, S. Lee, D. T. Adroja, M. R. Lees, G. B. G. Stenning, P. Aich, L. Tortora, C. Meneghini, G. Cibin, A. Berlie, R. A. Saha, D. Takegami, A. Meléndez-Sans, G. Poelchen, M. Yoshimura, K. D. Tsuei, Z. Hu, T.-S. Chan, S. Chattopadhyay, G. S. Thakur, and K.-Y. Choi, "*Gapless Dynamic Magnetic Ground State in the Charge-gapped Trimer Iridate $Ba_4NbIr_3O_{12}$*", Phys. Rev. Mater. **8**, 074405 (2024).
- D. Cao, Y. Mu, L. Liu, Z. Mou, S. Chen, W. Yan, H. Zhou, T.-S. Chan, L.-Y. Chang, L. Song, H.-J. Zhai*(翟華金), and X. Fan*(范修軍), "*Axially Modified Square-pyramidal CoN_4-F_1 Sites Enabling High-performance Zn-air Batteries*", ACS Nano **18**, 11474 (2024).
- P.-S. Chang, B.-H. Chen, Y.-C. Lin, W.-T. Dai, G. Kumar, Y.-G. Lin, and M. H. Huang*(黃暄益), "*Growth of Size-tunable Ag_2O Polyhedra and Revelation of Their Bulk and Surface Lattices*", Small **20**, 2401558 (2024).
- S. Chen, T. Luo, X. Li, K. Chen, Q. Wang, J. Fu, K. Liu, C. Ma, Y.-R. Lu, H. Li, K. S. Menghrajani, C. Liu, S. A. Maier, T.-S. Chan*(詹丁山), and M. Liu*(劉敏), "*Design of Reaction-driven Active Configuration for Enhanced CO_2 Electroreduction*", Nano Energy **128**, 109873 (2024).
- Y.-C. Chu, K.-H. Chen, C.-W. Tung, H.-C. Chen, J. Wang*(王佳麗), T.-R. Kuo*(郭聰榮), C.-S. Hsu, K.-H. Lin, L. D. Tsai, and H. M. Chen*(陳浩銘), "*Dynamic (Sub)surface-oxygen Enables Highly Efficient Carbonyl-coupling for Electrochemical Carbon Dioxide Reduction*", Adv. Mater. **36**, 2400640 (2024).
- L. Cui, S. Zhang, J. Ju*(朱佳偉), T. Liu, Y. Zheng, J. Xu, Y. Wang, J. Li, J. Zhao, J. Ma, J. Wang, G. Xu, T.-S. Chan, Y.-C. Huang, S.-C. Haw, J.-M. Chen, Z. Hu, and G. Cui*(崔光磊), "*A Cathode Homogenization Strategy for Enabling Long-cycle-life All-solid-state Lithium Batteries*", Nat. Energy **9**, 1084 (2024).
- B. D. Dandena, D.-S. Tsai, S.-H. Wu, W.-N. Su*(蘇威年), and B. J. Hwang*(黃炳照), "*Roles of Cation-doped Li-argyrodite Electrolytes on the Efficiency of All-solid-state-lithium Batteries*", Energy Storage Mater. **69**, 103305 (2024).
- W. B. Dilebo, M.-C. Tsai*(蔡孟哲), C.-Y. Chang, H. G. Edao, Y. Nikodimos, E. A. Moges, K. Lakshmanan, F. T. Angerasa, C. B. Guta, K. B. Ibrahim, Y. A. Awoke, T. Alamirew, W.-S. Liao, G. B. Desta, J.-L. Chen, W.-N. Su*(蘇威年), and B. J. Hwang*(黃炳照), "*Synergistic Interfacial Electronic Modulation of Topotactically Developed Bimetallic CoNiP on NiS Nanorods for Enhanced Alkaline Hydrogen Evolution Reaction*", Nanoscale **16**, 20701 (2024).
- Y. Fan, C. Zhang, L. Zhang*(張倫勇), J. Zhou, Y. Li, Y.-C. Huang, J. Ma, T.-S. Chan, C.-T. Chen, C. Jing, E. Mijit, Z. Hu*(胡志偉), J.-Q. Wang*(王建強), and L. Zhang*(張林娟), "*Novel Mechanism of Fe^{4+}/Ni^{3+} Synergistic Effect via Exchange Energy Gain for Boosting Water Oxidation*", Chem Catalysis **4**, 100981 (2024).
- A. G. Hailemariam, Z. Syum, T. T. Mamo, M. Qorbani*, C.-R. Hsing*(邢正蓉), A. Sabbah, S. Quadir, K. S. Bayikadi, H.-L. Wu*(吳恆良), C.-M. Wei, L.-C. Chen*(林麗瓊), and K.-H. Chen*(陳貴賢), "*Oxygen-incorporated Lithium-rich Iron Sulfide Cathodes for Li-ion Batteries with Boosted Material Stability and Electrochemical Performance*", Chem. Mater. **36**, 9370 (2024).
- C.-W. Hsieh, Z.-S. Chiou, C.-P. Lee*(李傳斌), S.-C. Tsai*(蔡世欽), W.-H. Tseng, Y.-H. Wang, Y.-T. Chen, C.-H. Kuo, and H.-M. Chiu, "*Enhancing Europium Adsorption Effect of Fe on Several Geological Materials by Applying XANES, EXAFS, and Wavelet Transform Techniques*", Toxics **12**, 706 (2024).
- H.-C. Hsieh, R.-C. Chen, Y.-K. Huang, H.-S. Sheu, Y.-C. Chuang, and C.-S. Lee*(李積琛), "*Enhancing Catalytic Performance in Oxidative Steam Reforming of Ethanol: The Role of Ruthenium ion Substitution in Layered Perovskite $La_2Ti_{2-x}Ru_xO_{7\pm\delta}$ Catalysts*", J. Phys. Chem. C **128**, 19570 (2024).
- S.-H. Hsieh, S. Ghosh, Y.-H. Liang, H.-T. Wang, C.-H. Du*(杜昭宏), J.-W. Chiou, C.-M. Wu, C.-W. Wang, Y.-C. Shao, J.-L. Chen, C.-W. Pao, H.-M. Tsai, T.-S. Chan, W.-B. Wu, H.-J. Lin, J.-F. Lee, A. Kandasami, and W.-F. Pong*(彭維鋒), "*Correlation Between Noncollinear Spin Orientation and Lattice Distortion in $Ni_{0.4}Mn_{0.6}TiO_3$*", Phys. Rev. Mater. **8**, 124410 (2024).
- N. Hu, Y.-H. Zhang, Y. Yang, H. Wu, Y. Liu, C. Hao, Y. Zheng, D. Sun, W. Li, J. Li, Z. Hu, T.-S. Chan, C.-W. Kao, Q. Kong, X. Wang, S.-C. Haw*(何樹智), J. Ma*(馬君), and G. Cui*(崔光磊), "*Unraveling the Spatial Asynchronous Activation Mechanism of Oxygen Redox-involved Cathode for High-voltage Solid-state Batteries*", Adv. Energy Mater. **14**, 2303797 (2024).
- Z. Huangfu, T. Yang, S. Ma, K. Wang, K. Shih, W. Yang, and C. Liao*(廖長忠), "*High Valency of Charge Compensator (Mo^{6+}) to Substitute Ti Site in REE Doped Zirconolite (REE=Nd, Sm, Gd, Ho and Yb): Solid Solubility, Phase Evolution and Structural Analysis*", Ceram. Int. **50**, 26351 (2024).
- B. Hubert, Y. Nikodimos, B. J. Hwang*(黃炳照), and J. P. Chu*(朱瑾), "*Ag-coated 3D Groove as a Study Platform in Evaluating the Throwing Power of Electrolytes for Li Metal Batteries*", J. Power Sources **589**, 233660 (2024).
- Jack S. Jarvis, Zhaofei Li, Zhiqiang Wang, Lijia Liu, L.-Y. Chang, Avinash Alagumalai, and Hua Song*(宋華), "*Inhibiting Platinum Sintering in Direct Ethane Dehydrogenation and Nonoxidative Methane Activation Reactions by Sequential Sulfide Layered Chemical Vapor Deposition*", Chem. Eng. J. **488**, 151080 (2024).
- Y. Jin*(金延超), Y. Qiu, R. Kumar, T. Chan, and L. Yan*(閻莉), "*Understanding the Goethite Role on Stibnite Oxidative Dissolution and Transformation: Spectroscopic and DFT Study*", Sci. Total Environ. **906**, 167823 (2024).
- S. G. Kim, D. Kim, J. Oh, Y. J. Son, S. Jeong, J. Kim, and S. J. Hwang*, "*Phosphorus-ligand Redox Cooperative Catalysis: Unraveling Four-electron Dioxygen Reduction Pathways and Reactive Intermediates*", J. Am. Chem. Soc. **146**, 11440 (2024).
- J.-H. Lu, A. M. G. Muchlis, C. Y. Lin, Y.-K. Huang, T.-S. Chan, and C. C. Lin*(林群哲), "*Plastic Identification by Using Energy Transfer Enhanced Broadband Short-wave Infrared Phosphor $Mg_3Ga_2GeO_8$: Cr^{3+}, Ni^{2+}*", ACS Appl. Opt. Mater. **2**, 2443 (2024).
- S. Ma, K.-M. Leung, C. Liao*(廖長忠), C.-K. Chang, Y. Zhou, S. Chen, X. Zhao, Q. Zhao, and K. Shih*(施凱閔), "*Green Conversion of Waste Alkaline Battery Material to Zeolitic Imidazolate Framework-8 and Its Iodine Capture Mechanism*", J. Hazard. Mater. **469**, 133612 (2024).
- T. T. Mamo, M. Qorbani*, A. G. Hailemariam, R. Putikam, C.-M. Chu, T.-R. Ko, A. Sabbah, C.-Y. Huang, S. Kholimatussadiah, T. Billo, M. K. Hussien, S.-Y. Chang, M.-C. Lin, W.-Y. Woon, H.-L. Wu*(吳恆良), K.-T. Wong, L.-C. Chen*(林麗瓊), and K.-H. Chen*(陳貴賢), "*Enhanced CO_2 Photoreduction to CH_4 via *COOH and *CHO Intermediates Stabilization by Synergistic Effect of Implanted P and S Vacancy in Thin-film SnS_2*", Nano Energy **128**, 109863 (2024).
- Z. Mou, Y. Mu, L. Liu, D. Cao, S. Chen, W. Yan, H. Zhou, T.-S. Chan, L.-Y. Chang, and X. Fan*(范修軍), "*In-plane Topological-defect-enriched Graphene as an Efficient Metal-free Catalyst for pH-universal H_2O_2 Electrosynthesis*", Small **20**, 2400564 (2024).
- Y.-C. Ting, C.-C. Cheng, F.-Y. Yen, G.-R. Li, S.-I. Chang, C.-H. Lee, H.-Y. T. Chen*(陳馨怡), and S.-Y. Lu*(呂世源), "*Highly Asymmetrically Configured Single Atoms Anchored on Flame-roasting Deposited Carbon Black as Cathode Catalysts for Ultrahigh Power Density Zn-air Batteries*", EnergyChem **6**, 100134 (2024).
- L. Wang, A. Mukherjee, C.-Y. Kuo, S. Chakrabarty, R. Yemini, A. A. Dameron, J. W. DuMont, S. H. Akella, A. Saha, S. Taragin, H. Aviv, D. Naveh, D. Sharon, T.-S. Chan, H.-J. Lin, J.-F. Lee, C.-T. Chen, B. Liu, X. Gao, S. Basu, Z. Hu*(胡志偉), D. Aurbach*, P. G. Bruce, and M. Noked*, "*High-energy All-solid-state Lithium Batteries Enabled by Co-free $LiNiO_2$ Cathodes with Robust Outside-in Structures*", Nat. Nanotechnol. **19**, 208 (2024).
- Q. Wang, Y. Gong, X. Zi, L. Gan, E. Pensa, Y. Liu, Y. Xiao, H. Li, K. Liu, J. Fu, J. Liu*(劉俊), A. Stefancu, C. Cai, S. Chen, S. Zhang, Y.-R. Lu, T.-S. Chan, C. Ma, X. Cao*(曹雪瑩), E. Cortés*, and M. Liu*(劉敏), "*Coupling Nano and Atomic Electric Field Confinement for Robust Alkaline Oxygen Evolution*", Angew. Chem. Int. Edit. **63**, e202405438 (2024).
- Z. Wang, Z. Luo, H. Xu, T. Zhu, D. Guan, Z. Lin, T.-S. Chan, Y.-C. Huang, Z. Hu, S. P. Jiang, and Z. Shao*(邵宗平), "*New Understanding and Improvement in Sintering Behavior of Cerium-rich Perovskite-type Protonic Electrolytes*", Adv. Funct. Mater. **34**, 2402716 (2024).
- P.-T. Yang, Y.-H. Liang, D.-C. Lee, and S.-L. Wang*(王尚禮), "*Chemical Speciation and Rice Uptake of Soil Molybdenum-investigation with X-ray Absorption Spectroscopy and Isotope Fractionation*", Sci. Total Environ. **949**, 175141 (2024).
- C. Yuan, L. Wang, P. Zeng*(曾攀), C. Cheng, H. Li, T. Yan, G. Liu, G. Zhao, X. Ma, T.-S. Chan, and L. Zhang*(張亮), "*Steering Sulfur Reduction Kinetics of Lithium-sulfur Batteries by Interfacial Microenvironment Modulation*", Energy Storage Mater. **71**, 103622 (2024).
- H. Zhao, Z. Pan, X. Shen, J. Zhao, D. Lu, J. Zhang, Z. Hu, C.-Y. Kuo, C.-T. Chen, T.-S. Chan, C. J. Sahle, C. Dong, T. Nishikubo, T. Koike, Z.-Y. Deng, J. Hong, R. Yu, P. Yu, M. Azuma, C. Jin, and Y. Long*(龍有文), "*Antiferroelectricity-induced Negative Thermal Expansion in Double Perovskite Pb_2CoMoO_6*", Small **20**, 2305219 (2024).
- E. Zhou, H. Jin, H. Lv, Y. Xie, Y. Lu, Y.-R. Lu, T.-S. Chan, C. Wang, W. Yan, J. Zhang, H. Ji*(季恒星), X. Wu*(武曉君), and X. Duan*(段鑲鋒), "*Solid-state Electrocatalysis in Heteroatom-doped Alloy Anode Enables Ultrafast Charge*

Lithium-ion Batteries", J. Am. Chem. Soc. **146**, 20700 (2024).

TLS 17A1 W200 – X-ray Powder Diffraction

- W.-T. Chen, L.-C. Yu, J.-H. Lin, S. L. Cheng, H. W. Shiu, Y.-L. Lai, Y.-H. Chu, Y.-Y. Chin, J.-H. Wang*(王禎翰), and Y.-J. Hsu*(許瑤真), "*Unravelling the Strong Interplay for Interfacial Magnetic Switching in Metal-organic-based Spintronics*", J. Mater. Chem. C **12**, 3931 (2024).
- P.-H. Chiu, C.-T. Hu, S.-K. Chia, L.-Y. Su*(蘇莉芸), P.-T. Chen, Z.-Y. Liu, C.-Y. Lin, C.-C. Hsieh, C.-A. Dai*(戴子安), and L. Wang*(王立義), "*Synergistic Enhancement of Stability and Performance for Perovskite Solar Cells Using Fluorinated Benzoic Acids as Additives*", Solar RRL **8**, 2300902 (2024).
- T. T. K. Cuc, C.-H. Hung, T.-C. Wu, P. Q. Nhien, T. M. Khang, B. T. B. Hue, W.-T. Chuang, and H.-C. Lin*(林宏洲), "*Force-activated Ratiometric Fluorescence Switching of Tensile Mechano-fluorophoric Polyurethane Elastomers with Enhanced Toughnesses Improved by Mechanically Interlocked [c2] Daisy Chain Rotaxanes*", Chem. Eng. J. **485**, 149694 (2024).
- J. R. Deka, D. Saikia, T.-H. Chang, S.-W. Wu, P.-I. Yen, H.-M. Kao*(高憲明), and Y.-C. Yang*(楊永欽), "*Bimetallic FeCo Nanoparticles Embedded N-rich Porous ZIF-derived Carbon as Highly Active Heterogeneous Fenton Catalyst for Degradation of Tetracycline and Organic Dyes*", J. Environ. Chem. Eng. **12**, 112414 (2024).
- C.-W. Hsieh, Z.-S. Chiou, C.-P. Lee*(李傳斌), S.-C. Tsai*(蔡世欽), W.-H. Tseng, Y.-H. Wang, Y.-T. Chen, C.-H. Kuo, and H.-M. Chiu, "*Enhancing Europium Adsorption Effect of Fe on Several Geological Materials by Applying XANES, EXAFS, and Wavelet Transform Techniques*", Toxics **12**, 706 (2024).
- W.-E. Ke, J.-W. Chen, C.-E. Liu, Y.-C. Ku, C.-F. Chang, P. Shafer, S.-J. Lin, M.-W. Chu, Y.-C. Chen*(陳怡誠), J.-W. Yeh, C.-Y. Kuo*(郭昌洋), and Y.-H. Chu*(朱英豪), "*Crystalline Magnetic Anisotropy in High Entropy (Fe, Co, Ni, Cr, Mn)$_3$O$_4$ Oxide Driven by Single-element Orbital Anisotropy*", Adv. Funct. Mater. **34**, 2312856 (2024).
- Y. Li, X. Zhu, Y. Su*(蘇岳鋒), L. Xu, L. Chen, D. Cao*(曹端云), N. Li*(李寧), and F. Wu, "*Enabling High-performance Layered Li-rich Oxide Cathodes by Regulating the Formation of Integrated Cation-disordered Domains*", Small **20**, 2307292 (2024).
- G.-B. Liao, J.-S. Wang, Z. Chong, C.-H. Ho, Y.-M. Shen*(沈祐民), P.-C. Huang, C.-C. Chang, D. R. Sahu*, and J.-L. Huang, "*Aluminum Doped Non-stoichiometric Titanium Dioxide as a Negative Electrode Material for Lithium-ion Battery: In-operando XRD Analysis*", J. Alloy. Compd. **1005**, 175876 (2024).
- I. M. A. Mekhemer, A. M. Elewa, M. M. Elsenety, M. M. Samy, M. G. Mohamed, A. F. Musa, T.-F. Huang, T.-C. Wei, S.-W. Kuo, B.-H. Chen, S.-D. Yang, and H.-H. Chou*(周鶴修), "*Self-condensation for Enhancing the Hydrophilicity of Covalent Organic Polymers and Photocatalytic Hydrogen Generation with Unprecedented Apparent Quantum Yield up to 500 nm*", Chem. Eng. J. **497**, 154280 (2024).
- M. M. Samy, M. G. Mohamed*, S. U Sharma, S. V Chaganti, J.-T. Lee, and S.-W. Kuo*(郭紹偉), "*An Ultrastable Tetrabenzonaphthalene-linked Conjugated Microporous Polymer Functioning as a High-performance Electrode for Supercapacitors*", J. Taiwan Inst. Chem. Eng. **158**, 104750 (2024).
- C.-C. Tseng, K.-C. Wang, P.-S. Lin, C. Chang, L.-L. Yeh, S.-H. Tung, C.-L. Liu*(劉振良), and Y.-J. Cheng*(鄭彥如), "*Intrinsically Stretchable Organic Thermoelectric Polymers Enabled by Incorporating Fused-ring Conjugated Breakers*", Small **20**, 2401966 (2024).
- P.-C. Wei*(魏百駿), C.-R. Hsing, C.-C. Yang, Y.-H. Tung, H.-J. Wu, W.-T. Yen, Y.-C. Lai, J.-J. Lee, C.-W. Wang, H.-C. Wu, H.-D. Yang, V. Singaravelu, X. Miao, A. Giugni, J.-K. Hu, J.-H. Fu, V. Tung, J. He, C.-M. Wei*(魏金明), and J.-H. He*(何志浩), "*Liquid-like Thermal Conductivity in Solid Materials: Dynamic Behavior of Silver Ions in Argyrodites*", Nano Energy **122**, 109324 (2024).
- Y.-S. Wu, C.-Y. Tsai, D. D. Thanh, Y.-H. Shih, H.-T. Cheng, T. Michinobu, W.-C. Chen, and C.-C. Chueh*(闕居振), "*Influence of Vinyl Bridging on Transistor Properties of Naphthalenediimide-based Dual-acceptor Copolymers*", ACS Appl. Polym. Mater. **6**, 5900 (2024).
- C. Yang, Y. Li, W. Su, X. Zhu, L. Hao, X. Wang, S. Wu, L. Chen, D. Cao, Y. Su*(蘇岳鋒), N. Li*(李寧), and F. Wu, "*Aluminium Doping in Single-crystal Nickel-rich Cathodes: Insights into Electrochemical Degradation and Enhancement*", J. Mater. Chem. A **12**, 20910 (2024).
- H.-C. Yang, Y.-S. Du, J.-J. Lee, C.-H. Yeh, M.-C. Tseng, Y.-C. Ho, H.-W. Kuo, H. Yoshida, A. Fujii, M. Ozaki, Y.-T. Tao, T. Akutagawg*, and H.-H. Chen*(陳秀慧), "*Morphology and Alignment Transition of Hexabenzocoronene (HBC) Mesogen Films by Bar Coating: Effect of Coating Speed*", Langmuir **40**, 16846 (2024).

TLS 17B1 W200 – X-ray Scattering

- S.-L. Chen, T.-S. Wu, H.-L. Huang, S.-F. Chen, Y.-L. Soo, H.-T. Jeng, and H.-H. Hung*(洪雪行), "*Polarized X-ray Diffraction Anomalous Near-edge Structure Study on the Orbital Physics of Thin WSe_2 Layers*", J. Appl. Crystallogr. **57**, 344 (2024).
- K.-W. Cheng, C.-H. Kung, J.-Y. Huang, C.-H. Ku, Q.-M. Huang, V. K. Ranganayakulu, Y.-Y. Chen, S.-J. Chiu, Y.-G. Lin, C.-M. Wang, and A. T. Wu*(吳子嘉), "*Preventing Degradation of Thermoelectric Property After Aging for Bi_2Te_3 Thin Film Module*", Mater. Chem. Phys. **318**, 129208 (2024).
- K. Dev*, V. R. Reddy, R. Medwal, S. Gupta, C. L. Dong, C. L. Chen, K. Asokan, and S. Annapoorni*, "*Magnetization Dynamics and Domain Reversal in Electrodeposited Permalloy Thin Films: Impact of Thickness and Annealing Treatment*", Phys. Scripta **99**, 075533 (2024).
- K. Dev*, A. Kadian, V. R. Reddy, R. Medwal, and S. Annapoorni*, "*Magnetization Switching Dynamics of Electrodeposited Fe-Ni Thin Films*", J. Supercond. Nov. Magn. **37**, 1243 (2024).
- M. N. Duong, Y.-X. Chen, W.-Y. Tzeng, T. Amrillah, S. Yang, C.-E. Liu, D. Z. Dimitrov, S.-C. Haw, C.-H. Hsu, J.-M. Chen*(陳錦明), J.-Y. Lin, K.-H. Wu, C.-W. Luo, C.-T. Chen, C.-Y. Kuo*(郭昌洋), and J.-Y. Juang*(莊振益), "*Orbital Ordering and Ultrafast Carrier Dynamics Anisotropies in Orientation-engineered Orthorhombic $YMnO_3$ Films*", APL Mater. **12**, 021117 (2024).
- C.-H. Kung, J.-Y. Huang, K.-W. Cheng, C.-H. Ku, Q.-M. Huang, V. K. Ranganayakulu, Y.-Y. Chen, Y.-G. Lin, S.-J. Chiu, and A. T. Wu*(吳子嘉), "*Enhancing Performance and Thermal Stability in GeTe Thermoelectric Joints with Cobalt Diffusion Barrier*", Mater. Chem. Phys. **323**, 129649 (2024).
- Y. H. G. Lin, C. K. Cheng, L. B. Young, L. S. Chiang, W. S. Chen, K. H. Lai, S. P. Chiu, C. T. Wu, C. T. Liang, J. J. Lin, C. H. Hsu*(徐嘉鴻) Y. H. Lin*(林晏詳), J. Kwo*(郭瑞年), and M. Hong*(洪銘輝), "*Nanometer-thick Molecular Beam Epitaxy Al Films Capped with in Situ Deposited Al_2O_3-High-crystallinity, Morphology, and Superconductivity*", J. Appl. Phys. **136**, 074401 (2024).
- Y.-C. Liu, B.-C. Chen, C.-C. Wei, S.-Z. Ho, Y.-D. Liou, P. Kaur, Rahul, Y.-C. Chen, and J.-C. Yang*(楊展其), "*Thickness-dependent Ferroelectricity in Freestanding $Hf_{0.5}Zr_{0.5}O_2$ Membranes*", ACS Appl. Electron. Mater. **6**, 8617 (2024).
- K.-H. Lu, W.-R. Wu, C.-J. Su, P.-W. Yang, N. L. Yamada, H.-J. Zhuo, S.-A. Chen, W.-T. Chuang, Y.-K. Lan, A.-C. Su*(蘇安仲), and U.-S. Jeng*(鄭有舜), "*Modulating Phase Segregation During Spin-casting of Fullerene-based Polymer Solar-cell Thin Films upon Minor Addition of a High-boiling Co-solvent*", J. Appl. Crystallogr. **57**, 1871 (2024).
- R. Muruganantham, J.-Y. Huang, P.-J. Wu, L.-Y. Kuo, C.-C. Yang, Y.-G. Lin, J. Li, and W.-R. Liu*(劉偉仁), "*Nano-crystalline $Fe_3V_3O_8$ Material as an Efficient Advanced Anode for Energy Storage Applications*", J. Power Sources **613**, 234947 (2024).
- B. Rehman, K. M. M. D. K. Kimbulapitiya, M. Date, C.-T. Chen, R.-H. Cyu, Y.-R. Peng, M. Chaudhary, F.-C. Chuang, and Y.-L. Chueh*(闕郁倫), "*Rational Design of Phase-engineered WS_2/WSe_2 Heterostructures by Low-temperature Plasma-assisted Sulfurization and Selenization toward Enhanced HER Performance*", ACS Appl. Mater. Interfaces **16**, 32490 (2024).
- S. Y. Tsai, P.-H. Tseng, C. C. Chen, C.-M. Huang, H.-W. Yen, Y.-S. Chen, K.-L. Lin, R. Niu, Y.-S. Lai, and F.-H. Ko*(柯富祥), "*Lattice Boundary Enhancement on Thermoelectric Behaviors of Heavily Boron-doped Silicon for Energy Harvesting: Electrical versus Thermal Conductivity*", Adv. Mater. Interfaces **11**, 2400536 (2024).
- C.-W. Tsao, S. Narra, J.-C. Kao, Y.-C. Lin, C.-Y. Chen, Y.-C. Chin, Z.-J. Huang, W.-H. Huang, C.-C. Huang, C.-W. Luo, J.-P. Chou, S. Ogata, M. Sone, M. H. Huang, T.-F. M. Chang*, Y.-C. Lo*(羅友杰), Y.-G. Lin*(林彥谷), E. W.-G. Diau*(刁維光), and Y.-J. Hsu*(徐雍鎂), "*Dual-plasmonic Au@Cu_7S_4 Yolk@shell Nanocrystals for Photocatalytic Hydrogen Production across Visible to Near Infrared Spectral Region*", Nat. Commun. **15**, 413 (2024).
- P.-H. Tseng, Y.-S. Lai*(賴宇紳), M.-Y. Li, C.-M. Huang, S.-Y. Tsai, K. Y.-J. Hsu, and F.-H. Ko*(柯富祥), "*Sustainable Solar-powered Hydrogen Generation with a Silicon Nanopillar Device with a Low Carbon Footprint*", Int. J. Hydrogen Energ. **68**, 1322 (2024).
- C.-C. Wang and C.-H. Lee*(李志浩), "*Wafer-scale Epitaxial Molybdenum Disulfide Ultrathin Film on Sapphire Prepared by Low-energy Reactive Magnetron Sputtering*", Appl. Surf. Sci. **659**, 159889 (2024).
- H. Wang, P.-H. Chen, C.-H. Kung, P.-K. Chang, S.-J. Chiu, Y.-G. Lin, C.-M. Wang, and A. T. Wu*(吳子嘉), "*Enhancement of Cu-to-Cu Bonding Property by Residual Stress in Cu Substrate*", Mater. Charact. **214**, 114107 (2024).
- M.-W. Zheng, C.-W. Lin, P.-H. Chou, C.-L. Chiang, Y.-G. Lin, and S.-H. Liu*(劉守恒), "*Highly Effective Degradation of Ibuprofen by Alkaline Metal-doped Copper Oxides via Peroxymonosulfate Activation: Mechanisms, Degradation Pathway and Toxicity Assessments*", J. Hazard. Mater. **462**, 132751 (2024).

TLS 17C1 W 200 – EXAFS

- M. M. M. Ahmed, K.-Y. Chen, F.-Y. Tsao, Y.-C. Hsieh, Y.-T. Liu*(劉雨庭), and Y.-M. Tzou*(鄒裕民), "*Promotion of Phosphate Release from Humic Acid-iron Hydroxide Coprecipitates in the Presence of Citric Acid*", Environ. Res. **240**, 117517 (2024).
- A. Beniwal, D. Bhalothia, Y.-R. Chen, J.-C. Kao, C. Yan, N. Hiraoka, H. Ishii, M. Cheng, Y.-C. Lo, X. Tu, Y.-W. Chiang, C.-H. Kuo, J.-P. Chou, C.-H. Wang, and T.-Y. Chen*(陳燦耀), "*Incorporation of Atomic Fe-oxide Triggers a Quantum Leap in the CO_2 Methanation Performance of Ni-hydroxide*", Chem. Eng. J. **493**, 152834 (2024).
- D. Bhalothia, C. Yan, N. Hiraoka, H. Ishii, Y.F. Liao, S. Dai, P.-C. Chen*(陳柏均), and T.-Y. Chen*(陳燦耀), "*Iridium Single Atoms to Nanoparticles: Nurturing the Local Synergy with Cobalt-oxide Supported Palladium Nanoparticles for Oxygen Reduction Reaction*", Adv. Sci. **11**, 2404076 (2024).
- D. Bhalothia, A. Beniwal, C. Yan, K.-C. Wang, C.-H. Wang, and T.-Y. Chen* (陳燦耀), "*Potential Synergy Between Pt_2Ni_4 Atomic-clusters, Oxygen Vacancies and Adjacent Pd Nanoparticles Outperforms Commercial Pt Nanocatalyst in Alkaline Fuel Cells*", Chem. Eng. J. **483**, 149421 (2024).
- B. Faceira, S. S. Nayak, L. Teulé-Gay, C. Labrugère-Sarroste, H.-Y. Huang, Y.-C. Shao, C.-L. Dong, and A. Rougier*, "*Influence of Fe Doping on the Electrochromic Properties of Cosputtered V_2O_5 Thin Films*", ACS Appl. Energy Mater. **7**, 9882 (2024).
- L. Cai, H. Bai, C.-W. Kao, K. Jiang, H. Pan, Y.-R. Lu*(盧英睿), and Y. Tan* (譚勇文), "*Platinum-ruthenium Dual-atomic Sites Dispersed in Nanoporous $Ni_{0.85}Se$ Enabling Ampere-level Current Density Hydrogen Production*", Small **20**, 2311178 (2024).
- C.-J. Chang*(張棋榕), S.-C. Hsieh, J. Chen, Y.-C. Wang, C.-L. Chiang, and Y.-G. Lin*(林彥谷), "*Electron-transfer Dynamics and Photocatalytic H_2-production Activity of PbS@Cu_2S Nanocomposites*", J. Taiwan Inst. Chem. Eng. **162**, 105587 (2024).
- C.-Y. Chang, W.-H. Huang, M.-C. Tsai, C.-W. Pao, M. Yoshimura, N. Hiraoka, C.-L. Chen*(陳啟亮), B. J. Hwang*(黃炳照), and W.-N. Su*(蘇威年), "*Turning Natural Copper Phthalocyanine into High-loading Single-atom Catalysts Using an Electrochemically-generated Template and Cationic Substitution*", Mater. Today Nano **25**, 100466 (2024).
- J.-M. Chang, T.-H. Lin, K.-C. Hsiao, K.-P. Chiang, Y.-H. Chang, and M.-C. Wu*(吳明忠), "*Gas-solid Phase Reaction Derived Silver Bismuth Iodide Rudorffite: Structural Insight and Exploring Photocatalytic Potential of CO_2 Reduction*", Adv. Sci. **11**, 2309526 (2024).
- L.-Y. Chang, M. Rinawati, Y.-T. Guo, Y.-C. Lin, C.-Y. Chang, W.-N. Su, H. Mizuguchi, W.-H. Huang, J.-L. Chen, and M.-H. Yeh*(葉旻鑫), "*Nitrogen-doped Graphene Quantum Dots Incorporated into MOF-derived NiCo Layered Double Hydroxides for Nonenzymatic Lactate Detection in Noninvasive Biosensors*", ACS Appl. Nano Mater. **7**, 14431 (2024).
- P.-W. Chen, C.-C. Cheng, Y.-C. Ting, T.-Y. Lin, F.-Y. Yen, G.-R. Li, and S.-Y. Lu*(呂世源), "*Single-atom Decorated Hollow Mesoporous Carbon Spheres Composited with Free-standing Carbon Cloth Supported Cobalt Sulfide Nanowire Arrays as High-performance Sulfur Host for Lithium-sulfur Batteries*", J. Taiwan Inst. Chem. Eng. **164**, 105699 (2024).
- S.-Y. Chen*(陳仕元), L.-Y. Wang, K.-C. Chen, C.-H. Yeh, W.-C. Hsiao, H.-Y. Chen, M. Nishi, M. Keller, C.-L. Chang, C.-N. Liao, T. Mochizuki, H.-Y. T. Chen*(陳馨怡), H.-H. Chou*(周鶴修), and C.-M. Yang*(楊家銘), "*Ammonia Synthesis Over Cesium-promoted Mesoporous-carbon-supported Ruthenium Catalysts: Impact of Graphitization Degree of the Carbon Support*", Appl. Catal. B-Environ. **346**, 123725 (2024).
- X. Chen, N. Yu, Y. Song, T. Liu, H. Xu, D. Guan, Z. Li, W.-H. Huang, Z. Shao, F. Ciucci*, and M. Ni*(倪萌), "*Synergistic Bulk and Surface Engineering for Expeditious and Durable Reversible Protonic Ceramic Electrochemical Cells Air Electrode*", Adv. Mater. **36**, 2403998 (2024).
- C.-C. Cheng, Y.-C. Ting, F.-Y. Yen, G.-R. Li, C.-H. Lee, K.-A. Lee, S.-I. Chang, H.-Y. T. Chen*(陳馨怡), and S.-Y. Lu*(呂世源), "*Synergistic Mo and W Single Atoms Co-doped Surface Hydroxylated NiFe Oxide as Bifunctional Electrocatalysts for Overall Water Splitting*", Appl. Catal. B-Environ. **358**, 124356 (2024).
- Y. Cheng, Y. Chen, J. Li*(李俊), Y. Chen, K. Ma, D. Chen, C.-Y. Li, H.-T. Wang, C.-W. Pao, J. Hu*(胡覺), and L. Han*(韓麗麗), "*Surmounting Scaling Relationship on Cu-base Diatomic Catalysts by Geminal-site-induced Synergistic Effect for High-selectivity CO_2 Electrochemical Reduction to CO*", Mater. Today Energy **46**, 101731 (2024).
- Y.-L. Cho, Y.-M. Tzou, A. Assakinah, N. A. T. Than, H. S. Yoon, S. I. Park, C.-C. Wang, Y.-C. Lee, L.-C. Hsu, P.-Y. Huang, S.-L. Liu, and Y.-T. Liu*(劉雨庭), "*Accumulation and Bio-oxidation of Arsenite Mediated by Thermoacidophilic Cyanidiales: Innate Potential Biomaterials toward Arsenic Remediation*", Bioresource Technol. **406**, 130912 (2024).
- A. Das*, M. Zajac, W.-H. Huang, C.-L. Chen, A. Kandasami, F. Delaunois, X. Noirfalise, and C. Bittencourt, "*Evolution of Structural Phase Transition from Hexagonal Wurtzite ZnO to Cubic Rocksalt NiO in Ni Doped ZnO Thin Films and Their Electronic Structures*", Phys. Scripta **99**, 015521 (2024).
- L. Deng, H. Chen, S.-F. Hung, Y. Zhang, H. Yu, H.-Y. Chen, L. Li, and S. Peng*(彭生杰), "*Lewis Acid-mediated Interfacial Water Supply for Sustainable Proton Exchange Membrane Water Electrolysis*", J. Am. Chem. Soc. **146**, 35438 (2024).
- L. Deng, S.-F. Hung, S. Liu, S. Zhao, Z.-Y. Lin, C. Zhang, Y. Zhang, A.-Y. Wang, H.-Y. Chen, J. Peng, R. Ma, L. Jiao, F. Hu, L. Li, and S. Peng*(彭生杰), "*Accelerated Proton Transfer in Asymmetric Active Units for Sustainable Acidic Oxygen Evolution Reaction*", J. Am. Chem. Soc. **146**, 23146 (2024).
- W. B. Dilebo, M.-C. Tsai*(蔡孟哲), C.-Y. Chang, H. G. Edao, Y. Nikodimos, E. A. Moges, K. Lakshmanan, F. T. Angerasa, C. B. Guta, K. B. Ibrahim, Y. A. Awoke, T. Alamirew, W.-S. Liao, G. B. Desta, J.-L. Chen, W.-N. Su*(蘇威年), and B. J. Hwang*(黃炳照), "*Synergistic Interfacial Electronic Modulation of Topotactically Developed Bimetallic CoNiP on NiS Nanorods for Enhanced Alkaline Hydrogen Evolution Reaction*", Nanoscale **16**, 20701 (2024).
- X. Duan, Q. Sha, P. Li, T. Li, G. Yang, W. Liu, E. Yu, D. Zhou, J. Fang, W. Chen, Y. Chen, L. Zheng, J. Liao, Z. Wang, Y. Li, H. Yang, G. Zhang, Z. Zhuang, S.-F. Hung, C. Jing, J. Luo, L. Bai, J. Dong, H. Xiao, W. Liu, Y. Kuang*(鄺允), B. Liu*(劉彬), and X. Sun*(孫曉明), "*Dynamic Chloride Ion Adsorption on Single Iridium Atom Boosts Seawater Oxidation Catalysis*", Nat. Commun. **15**, 1973 (2024).
- H. G. Edao, C.-Y. Chang, W. B. Dilebo, F. T. Angerasa, E. A. Moges, Y. Nikodimos, C. B. Guta, K. Lakshmanan, J.-L. Chen, M.-C. Tsai*(蔡孟哲), W.-N. Su*(蘇威年), and B. J. Hwang*(黃炳照), "*Nickel-iron Layered Double Hydroxides/Nickel Sulfide Heterostructured Electrocatalysts on Surface-modified Ti Foam for the Oxygen Evolution Reaction*", ACS Appl. Mater. Interfaces **16**, 50602 (2024).
- Z. C. Feng, J. Liu*(劉佳敏), D. Xie*(謝灯), M. T. Nafisa, C. Zhang, L. Wan, B. Jiang, H.-H. Lin, Z.-R. Qiu, W. Lu, B. Klein, I. T. Ferguson, and S. Liu, "*Optical, Structural, and Synchrotron X-ray Absorption Studies for GaN Thin Films Grown on Si by Molecular Beam Epitaxy*", Materials **17**, 2921 (2024).
- W.-X. Hong, W.-H. Wang, Y.-H. Chang, H. Pourzolfaghar, I.-H. Tseng, and Y.-Y. Li*(李元堯), "*A Ni-Fe Layered Double Hydroxide Anchored FeCo Nanoalloys and FeCo Dual Single-atom Electrocatalysts for Rechargeable and Flexible Zinc-air and Aluminum-air Batteries*", Nano Energy **121**, 109236 (2024).
- H.-C. Hsieh, R.-C. Chen, Y.-K. Huang, H.-S. Sheu, Y.-C. Chuang, and C.-S. Lee*(李積琛), "*Enhancing Catalytic Performance in Oxidative Steam Reforming of Ethanol: The Role of Ruthenium ion Substitution in Layered Perovskite $La_2Ti_{2-x}Ru_xO_{7\pm\delta}$ Catalysts*", J. Phys. Chem. C **128**, 19570 (2024).
- H. Hu, K. Ma, Y. Yang, N. Jin, L. Zhang*(張林杰), J. Qian, and L. Han*(韓麗麗), "*Ni Clusters Immobilized on Oxygen-rich Siloxene Nanosheets for Efficient Electrocatalytic Oxygen Reduction toward H_2O_2 Synthesis*", Dalton T. **53**, 4823 (2024).
- C.-C. Huang, Y.-H. Chen, C.-Y. Lee, Y.-S. Chen, and Y.-Y. Li*(李元堯), "*Single Iron Atom Embedded in Dual-size Nitrogen-doped Carbon Framework on Reduced Graphene Oxide: An Effective Catalyst for Proton Exchange Membrane Fuel Cells*", J. Power Sources **594**, 233963 (2024).
- C.-C. Huang, H. Pourzolfaghar, C.-L. Huang, C.-P. Liao, and Y.-Y. Li*(李元堯), "*FeNi Nanoalloy-carbon Nanotubes on Defected Graphene as an Excellent Electrocatalyst for Lithium-oxygen Batteries*", Carbon **222**, 118973 (2024).
- K. Huangmee, L.-C. Hsu, Y.-M. Tzou, Y.-L. Cho, C.-H. Liao, H. Y. Teah, and Y.-T. Liu*(劉雨庭), "*Thiol-functionalized Black Carbon as Effective and Economical Materials for Cr(VI) Removal: Simultaneous Sorption and Reduction*", J. Environ. Manage. **360**, 121074 (2024).
- B.-H. Kao, Y.-F. Zeng, Y.-C. Lee, C.-W. Pao, J.-L. Chen, Y.-C. Chuang, H.-S. Sheu, F.-T. Tsai*(蔡富浔), and W.-F. Liaw*(廖文峯), "*Unveiled the Structure-selectivity Relationship for Carbon Dioxide Reduction Triggered by Bi-doped Cu-based Nanocatalysts*", Small **20**, 2307910 (2024).
- K. Lakshmanan, W.-H. Huang, S. A. Chala, C.-Y. Chang, S. T. Saravanan, B. W. Taklu, E. A. Moges, Y. Nikodimos, B. D. Dandena, S.-C. Yang, J.-F. Lee, P.-Y. Huang, Y.-C. Lee, M.-C. Tsai*(蔡孟哲), W.-N. Su*(蘇威年), and B. J. Hwang*(黃炳照), "*Generating Multi-carbon Products by Electrochemical CO_2 Reduction via Catalytically Harmonious Ni/Cu Dual Active Sites*", Small **20**, 2307180 (2024).
- Y. Li, Q. Zhang, Y. Chong, W.-H. Huang, C.-L. Chen, X. Jin, G. Chen*(陳光需), Z. Fan*(范智勇), Y. Qiu*(丘勇才), and D. Ye, "*Efficient Photothermal Catalytic Oxidation Enabled by Three-dimensional Nanochannel Substrates*", Environ. Sci. Technol. **58**, 5153 (2024).
- Y. Li, W. Li, M. Zhang, Y. Zhuang, H. Li, Z. Pan, H. Min, T.-Y. Chen, H.-Y. Chen, H. Yang, and J. Wang*(王瑾), "*Electron-spin Regulation Driving*

Heterointerface Electron Distribution and Phase Transition toward Ultrafast and Durable Sodium Storage", Small **20**, 2405819 (2024).
- F.-J. Lin, C.-L. Huang, X.-Y. Jiang, J.-Q. Liao, and Y.-Y. Li*(李元堯), "*Cobalt Single Atoms Anchored on Nitrogen-doped Porous Carbon as an Interlayer for Capture and Catalysis of Polysulfides in Lithium-sulfur Batteries*", ACS Sustain. Chem. Eng. **12**, 3478 (2024).
- K.-S. Lin*(林錕松), A. Hussain, N. T. Thao*, J. Hussain, and C.-L. Chiang, "*Two-stage Conversion of CO_2 to Methanol and Dimethyl Ether Using CuO-ZnO-Al_2O_3/Protonated Y-type Zeolite Catalysts*", J. Environ. Chem. Eng. **12**, 111800 (2024).
- W.-S. Lin, M. Rinawati, W.-H. Huang, C.-Y. Chang, L.-Y. Chang*(張玲毓), Y.-S. Cheng, C.-C. Chang, J.-L. Chen, W.-N. Su*(蘇威年), and M.-H. Yeh* (葉旻鑫), "*Surface Restructuring Prussian Blue Analog-derived Bimetallic CoFe Phosphides by N-doped Graphene Quantum Dots for Electroactive Hydrogen Evolving Catalyst*", J. Colloid Interf. Sci. **654**, 677 (2024).
- Y.-C. Lin*(林裕川), S. Rajagopal, P.-T. Chou, P.-Y. Peng, Y.-R. Lu, C.-L. Chen, M.-H. Tsai, and C.-H. Wang, "*Crafting a Methanation-resistant, Reverse Water-gas Shift-active Nickel Catalyst with Significant Nanoparticle Dimensions Using the Molten Salt Approach*", ACS Sustain. Chem. Eng. **12**, 14771 (2024).
- D. Liu, F. Jiang, Q. Zhang, W.-H. Huang, Y. Zheng, M. Chen, L. Wu, R. Qin, M. Wang, S. Zhang, L. Chen, K. Yan, L. Zhou, Y. Zhao*(趙云), L. Gu*(谷林), and G. Chen*(陳光需), "*Pt-ZnO_x Interfacial Effect on the Performance of Propane Dehydrogenation and Mechanism Study*", ACS Nano **18**, 34671 (2024).
- H. Ma, S. Zhu*(朱世殊), Z. Huang, W. Zheng, C. Liu, F. Meng, J.-L. Chen, Y.-J. Lin, Z. Dang, and C. Feng*(馮春華), "*Photochemical Origins of Iron Flocculation in Acid Mine Drainage*", Environ. Sci. Technol. **58**, 16843 (2024).
- C. O. M. Mariano, R. H. Clemente, M.-H. Tsai, Y.-Y. Chin, J.-M. Chen, J.-F. Lee, Y.-J. Lu, C.-M. Chen, P.-T. Chen*(陳柏端), and C.-H. Chuang*(莊程豪), "*Operando X-ray and Mass Spectroscopy of Reduced Graphene Oxide (rGO)-mediated Cobalt Catalysts for Boosting the Hydrogen Evolution Reaction*", PRX Energy **3**, 033005 (2024).
- L. Merinda, F.-M. Wang*(王復民), N.-L. Wu*(吳乃立), R. A. Yuwono, C. Khotimah, U. Qonita, W.-H. Huang, L.-P. Wan, C.-K. Chang, P.-H. Hsu, C.-W. Pao, J.-L. Chen, C.-L. Chen, and T.-S. Chan, "*Carbonate Deprotonation on an Ni-rich Layered Cathode: Development of a New Cis-oligomer as an Organic Coverage*", J. Mater. Chem. A **12**, 28886 (2024).
- A. Motla, T. A. Kumaravelu, C.L. Dong, C.L. Chen, K. Asokan, and S. Annapoorni*, "*Role of Annealing Environments on the Local Electronic and Optical Properties of Zinc Oxide Films*", J. Mater. Sci.-Mater. Electron. **35**, 267 (2024).
- L. T. Ngo, W.-T. Huang, M.-H. Chan, T.-Y. Su, C.-H. Li, M. Hsiao*(蕭宏昇), and R.-S. Liu*(劉如熹), "*Comprehensive Neurotoxicity of Lead Halide Perovskite Nanocrystals in Nematode Caenorhabditis Elegans*", Small **20**, 2306020 (2024).
- K. Panneerselvam, A. R. Warrier, R. R. Mathiarasu, T. T. T. Nga, R. Ramya J, T. A. Kumaravelu*, W.-C. Chou, Y.-C. Huang, J.-L. Chen, C.-L. Chen, A. Kandasami, and C.-L. Dong*(董崇禮)., "*Enhancement in Supercapacitive Performance of Calcium Phosphate Nanoneedles through Ni-ion Incorporation: Insights into Atomic and Electronic Structures*", Mater. Today Sustain. **26**, 100769 (2024).
- M. Rinawati, L.-Y. Chang, C.-Y. Chang, C.-C. Chang, D. Kurniawan, W.-H. Chiang, W.-N. Su, B. Yuliarto, W.-H. Huang*(黃偉翔), and M.-H. Yeh* (葉旻鑫), "*Pioneering Molecularly-level Fe Sites Immobilized on Graphene Quantum Dots as a Key Activity Descriptor in Achieving Highly Efficient Oxygen Evolution Reaction*", Chem. Eng. J. **489**, 151436 (2024).
- M. Rinawati, Y.-S. Chiu, L.-Y. Chang, C.-Y. Chang, W.-N. Su, N. L. W. Septiani, B. Yuliarto, W.-H. Huang, J.-L. Chen, and M.-H. Yeh*(葉旻鑫), "*Evoking Dynamic Fe-N_x Active Sites through the Immobilization of Molecular Fe Catalysts on N-doped Graphene Quantum Dots for the Efficient Electroreduction of Nitrate to Ammonia*", J. Mater. Chem. A **12**, 22070 (2024).
- P. K. Saravanan, D. Bhalothia, A. Beniwal, C.-H. Tsai, P.-Y. Liu, T.-Y. Chen, H.-M. Ku*(辜鴻鳴), and P.-C. Chen*(陳柏均), "*Adjacent Reaction Sites of Atomic Mn_2O_3 and Oxygen Vacancies Facilitate CO_2 Activation for Enhanced CH_4 Production on Ti_o2-supported Nickel-hydroxide Nanoparticles*", Catalysts **14**, 410 (2024).
- W.-T. Shiu, V. Yoo, Y. Liu, L.-Y. Chang, T. Azizivahed, Y. Huang, P. J. Ragogna, and L. Liu*(劉儷佳), "*Small But Bright: Origin of the Enhanced Luminescence of Ultrasmall $ZnGa_2O_4$: Cr^{3+} in Mesoporous Silica Nanoparticles*", Phys. Chem. Chem. Phys. **26**, 17561 (2024).
- Y. J. Son, D. Kim, J. W. Park, K. Ko, Y. Yu, and S. J. Hwang*, "*Heteromultimetallic Platform for Enhanced C-H Bond Activation: Aluminum-incorporated Dicopper Complex Mimicking Cu-ZSM-5 Structure and Oxidative Reactivity*", J. Am. Chem. Soc. **146**, 29810 (2024).
- J. Su, Y. Ji, S. Geng, L. Li, D. Liu, H. Yu, B. Song, Y. Li, C.-W. Pao, Z. Hu, X. Huang*(黃小青), J. Lu*(路建美), and Q. Shao*(邵琪), "*Core-shell Design of Metastable Phase Catalyst Enables Highly-performance Selective Hydrogenation*", Adv. Mater. **36**, 2308839 (2024).
- R. Subramani, S.-Y. Hsu, Y.-C. Chuang, L.-C. Hsu, K.-T. Lu*(盧桂子), and J.-M. Chen*(陳錦明), "*Fe-MIL-101 Metal Organic Framework Integrated Solid Polymer Electrolytes for High-performance Solid-state Lithium Metal Batteries*", J. Mater. Chem. A **12**, 7132 (2024).
- W. Tanmathusorachai, S. Aulia, M. Rinawati, L.-Y. Chang, C.-Y. Chang, W.-H. Huang, M.-H. Lin, W.-N. Su, B. Yuliarto, and M.-H. Yeh*(葉旻鑫), "*High-entropy Prussian Blue Analogue Derived Heterostructure Nanoparticles as Bifunctional Oxygen Conversion Electrocatalysts for the Rechargeable Zinc-air Battery*", ACS Appl. Mater. Interfaces **16**, 62022 (2024).
- Yu Teng Wang, H.-Y. Lin, Y.-C. Chen, Y.-G. Lin, and Jyh Ming Wu*(吳忠明), "*Piezo-flexocatalysis of Single-atom Pt-loaded Graphitic Carbon Nitride*", Small Methods **8**, 2301287 (2024).
- N. Q. Thang, A. Sabbah*, C.-Y. Huang, N. H. Phuong, T.-Y. Lin, M. K. Hussien, H.-L. Wu, C.-I. Wu, N. N. T. Pham, P. V. Viet, C.-H. Lee, L.-C. Chen*(林麗瓊), and K.-H. Chen*(陳貴賢), "*Tailoring Atomically Dispersed Fe-induced Oxygen Vacancies for Highly Efficient Gas-phase Photocatalytic CO_2 Reduction and NO Removal with Diminished Noxious Byproducts*", J. Mater. Chem. A **12**, 31847 (2024).
- Y.-C. Ting, C.-C. Cheng, S.-H. Lin, T.-Y. Lin, P.-W. Chen, F.-Y. Yen, S.-I. Chang, C.-H. Lee, H.-Y. T. Chen, and S.-Y. Lu*(呂世源), "*Synergistic Fe and Co Binary Single Atoms Based Air Cathodes for High Performance and Ultra-stable Zn-air Batteries*", Energy Storage Mater. **67**, 103286 (2024).
- Y.-C. Ting, C.-C. Cheng, F.-Y. Yen, G.-R. Li, S.-I. Chang, C.-H. Lee, H.-Y. T. Chen*(陳馨怡), and S.-Y. Lu*(呂世源), "*Highly Asymmetrically Configured Single Atoms Anchored on Flame-roasting Deposited Carbon Black as Cathode Catalysts for Ultrahigh Power Density Zn-air Batteries*", EnergyChem **6**, 100134 (2024).
- C.-W. Tsao, S. Narra, J.-C. Kao, Y.-C. Lin, C.-Y. Chen, Y.-C. Chin, Z.-J. Huang, W.-H. Huang, C.-C. Huang, C.-W. Luo, J.-P. Chou, S. Ogata, M. Sone, M. H. Huang, T.-F. M. Chang*, Y.-C. Lo*(羅友杰), Y.-G. Lin*(林彥谷), E. W.-G. Diau*(刁維光), and Y.-J. Hsu*(徐雍鎏), "*Dual-plasmonic Au@Cu_7S_4 Yolk@shell Nanocrystals for Photocatalytic Hydrogen Production across Visible to Near Infrared Spectral Region*", Nat. Commun. **15**, 413 (2024).
- K.-C. Tso, T.-Y. Chan, T.-C. Yu, Y.-J. Tao, C.-Y. Chu, S.-Y. Chen, J.-F. Lee, J. Ohta, P.-C. Chen*(陳柏均), and P.-W. Wu*(吳樸偉), "*A Robust Bendable IrO_x Thin Film via Mild Alkaline Solution Process for Neuron Stimulating Electrodes*", Surf. Interfaces **44**, 103785 (2024).
- K.-C. Tso, C.-H. Chen, P.-C. Chen, S.-S. Li, J.-L. Chen, J. Ohta, and P.-W. Wu* (吳樸偉), "*Reuse of Sodium-doped Iridium Oxide Nanoparticles as a Bio-stimulating Electrode by a Chemical and Electrochemical Recovery Process*", Ceram. Int. **50**, 6220 (2024).
- G.-Z. Tu, J.-Y. Chen, Z.-X. Zhen, Y. Li, C.-W. Chang, W.-J. Chang, H. M. Chen, and C.-M. Jiang*(姜昌明), "*Elucidating the Epitaxial Growth Mechanisms of Solution-derived $BiVO_4$ Thin Films Utilizing Rapid Thermal Annealing*", ACS Appl. Electron. Mater. **6**, 1872 (2024).
- J. Wang, T. Y. Lai, H.-T. Lin, T.-R. Kuo*(郭聰榮), H.-C. Chen, C.-S. Tseng, C.-W. Tung*(童敬維), C.-Y. Chien, and H. M. Chen*(陳浩銘), "*Light-induced Dynamic Activation of Copper/Silicon Interface for Highly Selective Carbon Dioxide Reduction*", Angew. Chem. Int. Edit. **63**, e202403333 (2024).
- L. Wang, A. Mukherjee, C.-Y. Kuo, S. Chakrabarty, R. Yemini, A. A. Dameron, J. W. DuMont, S. H. Akella, A. Saha, S. Taragin, H. Aviv, D. Naveh, D. Sharon, T.-S. Chan, H.-J. Lin, J.-F. Lee, C.-T. Chen, B. Liu, X. Gao, S. Basu, Z. Hu* (胡志偉), D. Aurbach*, P. G. Bruce, and M. Noked*, "*High-energy All-solid-state Lithium Batteries Enabled by Co-free $LiNiO_2$ Cathodes with Robust Outside-in Structures*", Nat. Nanotechnol. **19**, 208 (2024).
- W.-H. Wang, C.-H. Han, W.-X. Hong, Y.-C. Chiu, I.-H. Tseng, Y.-H. Chang, H. Pourzolfaghar, and Y.-Y. Li*(李元堯), "*NiFe Layered Double Hydroxide (LDH) Anchored, Fe Single Atom and Nanoparticle Embedded on Nitrogen-doped Carbon-CNT (Carbon Nanotube) Framework as a Bifunctional Catalyst for Rechargeable Zinc-air Batteries*", J. Energy Storage **85**, 111058 (2024).
- Y.-T. Weng*(翁郁婷), T.-Y. Chen, J.-L. Chen, and N.-L. Wu*(吳乃立), "*Investigation on Pesudocapacitance Mechanism of Magnéli Oxide Ti_4O_7 in Aqueous Electrolyte*", Electrochemistry **92**, 074005 (2024).
- C.-Y. Wu, Y.-C. Hsiao, Y. Chen, K.-H. Lin, T.-J. Lee, C.-C. Chi, J.-T. Lin, L.-C. Hsu, H.-J. Tsai, J.-Q. Gao, C.-W. Chang, I.-T. Kao, C.-Y. Wu, Y.-R. Lu, C.-W. Pao, S.-F. Hung, M.-Y. Lu, S. Zhou, and T.-H. Yang*(楊東翰), "*A Catalyst Family of High-entropy Alloy Atomic Layers with Square Atomic Arrangements Comprising Iron-and Platinum-group Metals*", Sci. Adv. **10**, eadl3693 (2024).
- Q. Xia, C. Jin, Y. L. Huang, Y. Zhai, W. Han, J. Wu, C. Xia, C. C. Lin*(林群哲),

X. Zhao*(趙訓華), and X. Zhang*(張曉), "*Methanol-facilitated Surface Reconstruction Catalysts for Near 200% Faradaic Efficiency in a Coupled System*", Adv. Funct. Mater. **34**, 2314596 (2024).

- W. Xu, H. Li, X. Zhang, T.-Y. Chen, H. Yang, H. Min, X. Shen, H.-Y. Chen, and J. Wang*(王瑾), "*Regulating Graphitic Microcrystalline and Single-atom Chemistry in Hard Carbon Enables High-performance Potassium Storage*", Adv. Funct. Mater. **34**, 2309509 (2024).
- X. Xu, H.-C. Chen, L. Li, M. Humayun, X. Zhang, H. Sun, J. Jia, C. Xu, M. Bououdina, L. Sun, X. Wang*(王鑫), and C. Wang*(王春棟), "*Understanding the Role of Oxygen Vacancy Defects in Iridium-leveraged MOFs-type Catalyst*", Adv. Funct. Mater. **34**, 2408823 (2024).
- Z. Xu, Z. Huang, H. Li, S. Zhu, Z. Lei, C. Liu*(劉承帥), F. Meng, J.-L. Chen, T.-Y. Chen, and C. Feng*(馮春華), "*Sulfidation-reoxidation Enhances Heavy Metal Immobilization by Vivianite*", Water Res. **263**, 122195 (2024).
- T. Yang, A. Beniwal, D. Bhalothia, C. Yan, C.-H. Wang, and T.-Y. Chen*(陳燦耀), "*Oxygen Vacancies Coupled with Surface Silicide Facilitate CO_2 Activation at Near-room Temperature for Efficient Methane Productivity on Ni-oxide Supported Pd Nanoparticles*", Sustain. Energy Fuels **8**, 3399 (2024).
- W.-T. Yang, L. C. Kao*(高立誠), X.-T. Yu, C.-L. Dong, and S. Y. H. Liou*(劉雅瑄), "*Mechanistic Insights into Temperature Hysteresis in CO Oxidation on Cu-TiO_2 Mesosphere*", Appl. Catal. B-Environ. **352**, 124017 (2024).
- Y. Yang, Y. Xiao, L. Zhang*(張林杰), H.-T. Wang, K.-H. Chen, W.-X. Lin, N. Jin, C. Sun, Y.-C. Shao, J.-L. Chen, J. Qian*(錢金杰), and L. Han*(韓麗麗), "*Encaging Co Nanoparticle in Atomic Co-N_4-dispersed Graphite Nanopocket Evokes High Oxygen Reduction Activity for Flexible Zn-air Battery*", Appl. Catal. B-Environ. **347**, 123792 (2024).
- Y. Yang, Y. Wang, C. Xue, Y. Lin, J.-F. Lee, X. Yi*(易筱筠), and Z. Dang, "*Efficient Removal of Heavy Metals from Acid Mine Drainage by ε-MnO_2 Adsorption*", J. Clean. Prod. **452**, 141936 (2024).
- Yunduo Yao, Guangming Zhao, Xuyun Guo, Pei Xiong, Zhihang Xu, Longhai Zhang, Changsheng Chen, Chao Xu, T.-S. Wu, Y.-L. Soo, Zhiming Cui, M.-M. Jung, and Ye Zhu*(朱葉), "*Facet-dependent Surface Restructuring on Nickel (Oxy)hydroxides: A Self-activation Process for Enhanced Oxygen Evolution Reaction*", J. Am. Chem. Soc. **146**, 15219 (2024).
- ◦ C.-H. Yeh, J.-W. Kang, Y.-L. Chen, H.-J. Chen, H.-H. Chang, W.-H. Lu, S.-Y. Chen, H.-L. Chen, C.-W. Hu, L.-Y. Chueh, Y.-T. F. Pan, and H.-Y. Chen*(陳翰儀), "*Electrochemical Improvement of $Na_{0.62}K_{0.05}Mg_{2/9}Cu_{1/9}Mn_{2/3}O_2$ P2-type Layer-oxide Anionic Redox Cathodes of Sodium-ion Batteries via Incorporating K-doping*", ACS Sustain. Chem. Eng. **12**, 12795 (2024).
- H. Yu, Y. Ji, C. Li, W. Zhu, Y. Wang, Z. Hu, J. Zhou, C.-W. Pao, W.-H. Huang, Y. Li, X. Huang, and Q. Shao*(邵琪), "*Strain-triggered Distinct Oxygen Evolution Reaction Pathway in Two-dimensional Metastable Phase IrO_2 via CeO_2 Loading*", J. Am. Chem. Soc. **146**, 20251 (2024).
- W.-J. Zeng, J.-J. Ma, W.-Y. Huang, T.-J. Lee, Z.-Y. Lin, K.-S. Peng, N. Hiraoka, Y.-F. Liao, Y.-R. Lu, C.-W. Hu*(胡芝瑋), S.-H. Hsu*(徐韶徽), and S.-F. Hung*(洪崧富), "*Leveraging Bifunctional Phosphide-based Catalysts in a Membrane-electrode-assembly to Achieve Industrial Hydrogen Production*", Mater. Today Sustain. **27**, 100820 (2024).
- J. Zhang, Z. Liu, X. Ye, X. Wang, D. Lu, H. Zhao, M. Pi, C.-T. Chen, J.-L. Chen, C.-Y. Kuo, Z. Hu, X. Yu, X. Zhang, Z. Pan*(潘昭), and Y. Long*(龍有文), "*High-pressure Synthesis of Quadruple Perovskite Oxide $CaCu_3Cr_2Re_2O_{12}$ with a High Ferrimagnetic Curie Temperature*", Inorg. Chem. **63**, 3499 (2024).
- J. Zhao, Z. Deng*(鄧震), J. Zhang, Y. Peng, L. Shi, B. Min, L. Duan, W. Li, L. Cao, J.-L. Chen, Z. Hu, R. Yu, and C. Jin*(景傅勇), "*Anomalous Metallic Conductivity and Short-range Ferromagnetic Correlation in High-pressure Synthesized Pyrochlore $Hg_2Ir_2O_7$*", EPL **145**, 66001 (2024).
- S. Zhao, S.-F. Hung, L. Deng, W.-J. Zeng, T. Xiao, S. Li, C.-H. Kuo, H.-Y. Chen, F. Hu, and S. Peng*(彭生杰), "*Constructing Regulable Supports via Nonstoichiometric Engineering to Stabilize Ruthenium Nanoparticles for Enhanced pH-universal Water Splitting*", Nat. Commun. **15**, 2728 (2024).
- Y. Zhou, S. Ma, P. Lin, C. Liao, C.-W. Kao*(高振瑋), M. Chen, M. Su, and K. Shih*(施凱閔), "*Eco-friendly Synthesized Zeolitic Imidazolate Framework-8 Enables One-step Cerium Recovery from Water*", Chem. Eng. J. **500**, 157456 (2024).
- J. Zhu, L. An, X. Li, K. Iputera, R.-S. Liu*(劉如熹), J. Yang, D. Wang*(王得麗), and X. Zhao*(趙旭), "*Anchoring Isolated Pd Atoms on $Ti_3C_2T_x$ MXene with Boosted Kinetics for Alkaline Hydrogen Evolution*", Appl. Surf. Sci. **644**, 158809 (2024).

TLS 20A1 BM – (H-SGM) XAS

- D. Cao, Y. Mu, L. Liu, Z. Mou, S. Chen, W. Yan, H. Zhou, T.-S. Chan, L.-Y. Chang, L. Song, H.-J. Zhai*(翟華金), and X. Fan*(范修軍), "*Axially Modified Square-pyramidal CoN_4-F_1 Sites Enabling High-performance Zn-air Batteries*", ACS Nano **18**, 11474 (2024).
- C.-J. Chang*(張棋榕), S.-C. Hsieh, J. Chen, Y.-C. Wang, C.-L. Chiang, and Y.-G. Lin*(林彥谷), "*Electron-transfer Dynamics and Photocatalytic H_2-production Activity of PbS@Cu_2S Nanocomposites*", J. Taiwan Inst. Chem. Eng. **162**, 105587 (2024).
- P.-W. Chen, C.-C. Cheng, Y.-C. Ting, T.-Y. Lin, F.-Y. Yen, G.-R. Li, and S.-Y. Lu*(呂世源), "*Single-atom Decorated Hollow Mesoporous Carbon Spheres Composited with Free-standing Carbon Cloth Supported Cobalt Sulfide Nanowire Arrays as High-performance Sulfur Host for Lithium-sulfur Batteries*", J. Taiwan Inst. Chem. Eng. **164**, 105699 (2024).
- C.-C. Cheng, Y.-C. Ting, F.-Y. Yen, G.-R. Li, C.-H. Lee, K.-A. Lee, S.-I. Chang, H.-Y. T. Chen*(陳馨怡), and S.-Y. Lu*(呂世源), "*Synergistic Mo and W Single Atoms Co-doped Surface Hydroxylated NiFe Oxide as Bifunctional Electrocatalysts for Overall Water Splitting*", Appl. Catal. B-Environ. **358**, 124356 (2024).
- C.-Y. Cheng, Y.-M. Shen, W.-H. Huang, C.-C. Chang, C.-C. Tsai, C.-J. Lin, Y.-G. Lin, Y.-R. Lu, C.-L. Dong, W.-N. Su, S.-Y. Chen, K. Kumar, H.-Y. Chen, C.-J. Tsai, and C.-L. Chen*(陳啟亮), "*Electronic and Atomic Structural Properties Associated with Enhanced Photodegradation Activity in Mo-doped TiO_2 Nanoparticles*", Langmuir **40**, 19506 (2024).
- H.-H. Chiu, M.-K. Ho, T.-E. Hsu, S.-L. Yu, K. Manjunatha, C.-L. Cheng, T.-Y. Li, C.-K. Chang, S. Tummala, Y.-P. Ho, J. Angadi V, S. Matteppanavar, A. C. Gandhi*, and S. Y. Wu*(吳勝允), "*Manipulating and Investigating the Room-temperature Magnetic Memory Phenomenon: The Impact of Rare-earth Ion Doping on Nickel Oxide Nanoparticles*", Mater. Today Chem. **39**, 102190 (2024).
- Y.-S. Chiu, M. Rinawati, Y.-H. Chang, S. Aulia, C.-C. Chang, L.-Y. Chang*(張玲毓), W.-S. Hung, H. Mizuguchi, S.-C. Haw, and M.-H. Yeh*(葉旻鑫), "*Enhancing Self-induced Polarization of PVDF-based Triboelectric Film by P-doped g-C_3N_4 for Ultrasensitive Triboelectric Pressure Sensors*", Nano Energy **131**, 110207 (2024).
- S. Choi, S.-J. Kim, S. Han, J. Wang, J. Kim, B. Koo, A. A. Ryabin, S. Kunze, H. Hyun, J. Han, S.-C. Haw, K. H. Chae, C. H. Choi, H. Kim, and J. Lim*, "*Enhancing Oxygen Evolution Reaction via a Surface Reconstruction-induced Lattice Oxygen Mechanism*", ACS Catalysis **14**, 15096 (2024).
- L. Cui, S. Zhang, J. Ju*(朱佳偉), T. Liu, Y. Zheng, J. Xu, Y. Wang, J. Li, J. Zhao, J. Ma, J. Wang, G. Xu, T.-S. Chan, Y.-C. Huang, S.-C. Haw, J.-M. Chen, Z. Hu, and G. Cui*(崔光磊), "*A Cathode Homogenization Strategy for Enabling Long-cycle-life All-solid-state Lithium Batteries*", Nat. Energy **9**, 1084 (2024).
- A. Das*, M. Zajac, W.-H. Huang, C.-L. Chen, A. Kandasami, F. Delaunois, X. Noirfalise, and C. Bittencourt, "*Evolution of Structural Phase Transition from Hexagonal Wurtzite ZnO to Cubic Rocksalt NiO in Ni Doped ZnO Thin Films and Their Electronic Structures*", Phys. Scripta **99**, 015521 (2024).
- M. N. Duong, Y.-X. Chen, W.-Y. Tzeng, T. Amrillah, S. Yang, C.-E. Liu, D. Z. Dimitrov, S.-C. Haw, C.-H. Hsu, J.-M. Chen*(陳錦明), J.-Y. Lin, K.-H. Wu, C.-W. Luo, C.-T. Chen, C.-Y. Kuo*(郭昌洋), and J.-Y. Juang*(莊振益), "*Orbital Ordering and Ultrafast Carrier Dynamics Anisotropies in Orientation-engineered Orthorhombic $YMnO_3$ Films*", APL Mater. **12**, 021117 (2024).
- A. G. Hailemariam, Z. Syum, T. T. Mamo, M. Qorbani*, C.-R. Hsing*(邢正蓉), A. Sabbah, S. Quadir, K. S. Bayikadi, H.-L. Wu*(吳恆良), C.-M. Wei, L.-C. Chen*(林麗瓊), and K.-H. Chen*(陳貴賢), "*Oxygen-incorporated Lithium-rich Iron Sulfide Cathodes for Li-ion Batteries with Boosted Material Stability and Electrochemical Performance*", Chem. Mater. **36**, 9370 (2024).
- H.-C. Hsieh, R.-C. Chen, Y.-K. Huang, H.-S. Sheu, Y.-C. Chuang, and C.-S. Lee*(李積琛), "*Enhancing Catalytic Performance in Oxidative Steam Reforming of Ethanol: The Role of Ruthenium ion Substitution in Layered Perovskite $La_2Ti_{2-x}Ru_xO_{7\pm\delta}$ Catalysts*", J. Phys. Chem. C **128**, 19570 (2024).
- N. Hu, Y.-H. Zhang, Y. Yang, H. Wu, Y. Liu, C. Hao, Y. Zheng, D. Sun, W. Li, J. Li, Z. Hu, T.-S. Chan, C.-W. Kao, Q. Kong, X. Wang, S.-C. Haw*(何樹智), J. Ma*(馬君), and G. Cui*(崔光磊), "*Unraveling the Spatial Asynchronous Activation Mechanism of Oxygen Redox-involved Cathode for High-voltage Solid-state Batteries*", Adv. Energy Mater. **14**, 2303797 (2024).
- C.-H. Huang, C. S. Gantepogu, P.-J. Chen, T.-H. Wu, W.-R. Liu, K.-H. Lin, C.-L. Chen, T.-K. Lee, M.-J. Wang*(王明杰), and M.-K. Wu, "*Substrate Charge Transfer Induced Ferromagnetism in MnSe/$SrTiO_3$ Ultrathin Films*", Nanomaterials **14**, 1355 (2024).
- H.-J. Huang, C.-S. Hsu, J.-Y. Huang, S.-C. Haw, H.-Y. Chen, N. Hiraoka, Y.-F. Liao*(廖彥發), and C.-W. Hu*(胡芝瑋), "*Electronic Structure Evolution upon Lithiation: A Li K-edge Study of Silicon Oxide Anode through X-ray Raman Spectroscopy*", J. Power Sources Adv. **29**, 100155 (2024).
- ◦ C.-M. Hung, S.-F. Wang, W.-C. Chao, J.-L. Li, B.-H. Chen, C.-H. Lu, K.-Y. Tu, S.-D. Yang, W.-Y. Hung, Y. Chi*(季昀), and P.-T. Chou*(周必泰), "*High-performance Near-infrared OLEDs Maximized at 925 nm and 1022 nm through Interfacial Energy Transfer*", Nat. Commun. **15**, 4664 (2024).

- M. K. Hussien, A. Sabbah, M. Qorbani, R. Putikam, S. Kholimatussadiah, D.-L. M. Tzou, M. H. Elsayed, Y.-J. Lu, Y.-Y. Wang, X.-H. Lee, T.-Y. Lin, N. Q. Thang, H.-L. Wu, S.-C. Haw, K. C.-W. Wu, M.-C. Lin, K.-H. Chen*(陳貴賢), and L.-C. Chen*(林麗瓊), "*Constructing B-N-P Bonds in Ultrathin Holey g-C_3N_4 for Regulating the Local Chemical Environment in Photocatalytic CO_2 Reduction to CO*", Small **20**, 2400724 (2024).
- Ankit Kadian*, V. Manikandan, C. L. Chen, C. L. Dong, and S. Annapoorni*, "*Synergistically Enhanced Photocatalytic Properties of Co_3O_4-G/GO Nanocomposites: Unravelling Their Interactions and Charge-transfer Dynamics Using XAS*", Dalton T. **53**, 13550 (2024).
- D. C. Kakarla*, Y.-H. Ku, H. C. Wu, C. C. Chen, M. Y. Hsu, T. R. Hu, J.-Y. Lin, N. Puri, M.-J. Hsieh, C. W. Wang, W.-H. Li, Dhanasekhar C, A. Tiwari, C. H. Lu, K. J. You, T. W. Kuo, K. J. Fan, Y. C. Chang, and H. D. Yang*(楊弘敦), "*Exploring New Members of Magnetoelectric Materials in CuO-$CuCl_2$-SeO_2 System*", Mater. Today Phys. **46**, 101527 (2024).
- B.-H. Kao, Y.-F. Zeng, Y.-C. Lee, C.-W. Pao, J.-L. Chen, Y.-C. Chuang, H.-S. Sheu, F.-T. Tsai*(蔡富潯), and W.-F. Liaw*(廖文峯), "*Unveiled the Structure-selectivity Relationship for Carbon Dioxide Reduction Triggered by Bi-doped Cu-based Nanocatalysts*", Small **20**, 2307910 (2024).
- C. Khotimah, R. A. Yuwono, F.-M. Wang*(王復民), C.-C. Yang, N.-L. Wu, C. D. D. Sundari, A. C. Imawan, C.-K. Chang, P.-H. Hsu, P.-C. Huang, G.-Y. Liu, Y.-D. Tsai, S.-C. Haw, and F. Iskandar, "*Investigation of Space Group Effects of High-voltage Spinel $LiNi_{0.5}Mn_{1.5}O_4$: Unveiling the Influences of Fluorinate Benzimidazole Salt Additive*", Chem. Eng. J. **494**, 152988 (2024).
- J. Kim, S. Y. Lee, S.-J. Kim, B. Koo, J. Chung, D. Lee, S. Choi, J. Kim, S. Seo, C. Nam, K. A. Gandionco, G. Bak, S. Jo, N. Kim, H.-J. Shin, K. H. Chae, D. H. Won, M. A. Marcus, D. A. Shapiro, S.-C. Haw, D. H. Alsem, N. J. Salmon, B. K. Min, H. Kim*, Y. J. Hwang*, and J. Lim*, "*Spatiotemporal Active Phase Evolution for CO_2 Electrocatalysis*", Joule **8**, 3373 (2024).
- A. Krichene*, W. Boujelben, K. N. Rathod, K. Gadani, C.-L. Chen, A. Kandasami, N. A. Shah, and P. S. Solanki, "*Electronic Structure and Room Temperature Colossal Magnetodielectric Effect in $La_{0.4}Dy_{0.1}Ca_{0.5}MnO_3$ Manganite*", J. Alloy. Compd. **999**, 175022 (2024).
- S. Lee, S. Kang, Y. Choi, J. Kim, J. Yang, D. Han, K.-W. Nam, O. J. Borkiewicz, J. Zhang, and Y.-M. Kang*, "*Structural Disorder of a Layered Lithium Manganese Oxide Cathode Paving a Reversible Phase Transition Route toward Its Theoretical Capacity*", J. Am. Chem. Soc. **146**, 33845 (2024).
- C. Li, J. Wang*(王佳), J. Zhao, G. Gao, K.-H. Wu, B.-J. Su, J.-M. Chen, Y. Xi, Z. Huang, Y. Qiao, and F. Li*(李福偉), "*Construction of Synergistic Co/CoO Interface to Enhance Hydrogenation Activity of Ethyl Lactate to 1,2-propanediol*", Chem.-Asian J. **19**, e202301103 (2024).
- J. Lin, S. Zhao, J. Yang, W.-H. Huang, C.-L. Chen, T. Chen, Y. Zhao, G. Chen*(陳光需), Y. Qiu*(丘勇才), and L. Gu, "*Hydrogen Spillover Induced PtCo/CoO_x Interfaces with Enhanced Catalytic Activity for CO Oxidation at Low Temperatures in Humid Conditions*", Small **20**, 2309181 (2024).
- W.-S. Lin, M. Rinawati, W.-H. Huang, C.-Y. Chang, L.-Y. Chang*(張玲毓), Y.-S. Cheng, C.-C. Chang, J.-L. Chen, W.-N. Su*(蘇威年), and M.-H. Yeh*(葉旻鑫), "*Surface Restructuring Prussian Blue Analog-derived Bimetallic CoFe Phosphides by N-doped Graphene Quantum Dots for Electroactive Hydrogen Evolving Catalyst*", J. Colloid Interf. Sci. **654**, 677 (2024).
- H. Liu, H. Niu, W.-H. Huang, T. Shen, C. Li, C.-C. Chang, M. Yang, C. Gao, L. Yang, Q. Zong, Y. Pei, G. Cao*(曹國忠), and C. Liu*(劉超峰), "*Unveiling the Local Structure and the Ligand Field of Organic Cation Preintercalated Vanadate Cathode for Aqueous Zinc-ion Batteries*", ACS Energ. Lett. **9**, 5492 (2024).
- C. O. M. Mariano, R. H. Clemente, M.-H. Tsai, Y.-Y. Chin, J.-M. Chen, J.-F. Lee, Y.-J. Lu, C.-M. Chen, P.-T. Chen*(陳柏端), and C.-H. Chuang*(莊程豪), "*Operando X-ray and Mass Spectroscopy of Reduced Graphene Oxide (rGO)-mediated Cobalt Catalysts for Boosting the Hydrogen Evolution Reaction*", PRX Energy **3**, 033005 (2024).
- Z. Mou, Y. Mu, L. Liu, D. Cao, S. Chen, W. Yan, H. Zhou, T.-S. Chan, L.-Y. Chang, and X. Fan*(范修軍), "*In-plane Topological-defect-enriched Graphene as an Efficient Metal-free Catalyst for pH-universal H_2O_2 Electrosynthesis*", Small **20**, 2400564 (2024).
- Y. Nikodimos, S.-K. Jiang, S.-J. Huang, B. W. Taklu, W.-H. Huang, G. B. Desta, T. M. Tekaligne, Z. B. Muche, K. Lakshmanan, C.-Y. Chang, T. M. Hagos, K. N. Shitaw, S.-C. Yang, S.-H. Wu, W.-N. Su*(蘇威年), and B. J. Hwang*(黃炳照), "*Moisture Robustness of Li_6PS_5Cl Argyrodite Sulfide Solid Electrolyte Improved by Nano-level Treatment with Lewis Acid Additives*", ACS Energ. Lett. **9**, 1844 (2024).
- H. Niu, H. Liu, L. Yang, T. Kang, T. Shen, B. Jiang, W.-H. Huang, C.-C. Chang, Y. Pei*(裴艷中), G. Cao*(曹國忠), and C. Liu*(劉超峰), "*Impacts of Distorted Local Chemical Coordination on Electrochemical Performance in Hydrated Vanadium Pentoxide*", Nat. Commun. **15**, 9421 (2024).
- L. D. Palmer, W. Lee, C.-L. Dong, R.-S. Liu, N. Wu, and S. K. Cushing*, "*Determining Quasi-equilibrium Electron and Hole Distributions of Plasmonic Photocatalysts Using Photomodulated X-ray Absorption Spectroscopy*", ACS Nano **18**, 9344 (2024).
- M. Rinawati, L.-Y. Chang, C.-Y. Chang, C.-C. Chang, D. Kurniawan, W.-H. Chiang, W.-N. Su, B. Yuliarto, W.-H. Huang*(黃偉翔), and M.-H. Yeh*(葉旻鑫), "*Pioneering Molecularly-level Fe Sites Immobilized on Graphene Quantum Dots as a Key Activity Descriptor in Achieving Highly Efficient Oxygen Evolution Reaction*", Chem. Eng. J. **489**, 151436 (2024).
- M. Rinawati, Y.-S. Chiu, L.-Y. Chang, C.-Y. Chang, W.-N. Su, N. L. W. Septiani, B. Yuliarto, W.-H. Huang, J.-L. Chen, and M.-H. Yeh*(葉旻鑫), "*Evoking Dynamic Fe-N_x Active Sites through the Immobilization of Molecular Fe Catalysts on N-doped Graphene Quantum Dots for the Efficient Electroreduction of Nitrate to Ammonia*", J. Mater. Chem. A **12**, 22070 (2024).
- A. Sarkar, S.-Y. Huang, V. R. Dharmaraj, B. Bazri, K. Iputera, H.-H. Su, Y.-A. Chen, H.-C. Chen, Y.-P. Lin, R.-J. Chung*(鍾仁傑), D.-H. Wei*(魏大華), and R.-S. Liu*(劉如熹), "*Polyethylene Oxide-based Solid-state Polymer Electrolyte Hybridized with Liquid Catholyte for Semi-solid-state Rechargeable Mg-O_2 Batteries*", J. Mater. Chem. A **12**, 25968 (2024).
- W. Tanmathusorachai, S. Aulia, M. Rinawati, L.-Y. Chang, C.-Y. Chang, W.-H. Huang, M.-H. Lin, W.-N. Su, B. Yuliarto, and M.-H. Yeh*(葉旻鑫), "*High-entropy Prussian Blue Analogue Derived Heterostructure Nanoparticles as Bifunctional Oxygen Conversion Electrocatalysts for the Rechargeable Zinc-air Battery*", ACS Appl. Mater. Interfaces **16**, 62022 (2024).
- Y.-C. Ting, C.-C. Cheng, F.-Y. Yen, G.-R. Li, S.-I. Chang, C.-H. Lee, H.-Y. T. Chen*(陳馨怡), and S.-Y. Lu*(呂世源), "*Highly Asymmetrically Configured Single Atoms Anchored on Flame-roasting Deposited Carbon Black as Cathode Catalysts for Ultrahigh Power Density Zn-air Batteries*", EnergyChem **6**, 100134 (2024).
- C.-W. Tsao, S. Narra, J.-C. Kao, Y.-C. Lin, C.-Y. Chen, Y.-C. Chin, Z.-J. Huang, W.-H. Huang, C.-C. Huang, C.-W. Luo, J.-P. Chou, S. Ogata, M. Sone, M. H. Huang, T.-F. M. Chang*, Y.-C. Lo*(羅友杰), Y.-G. Lin*(林彥谷), E. W.-G. Diau*(刁維光), and Y.-J. Hsu*(徐雍鎏), "*Dual-plasmonic Au@Cu_7S_4 Yolk@shell Nanocrystals for Photocatalytic Hydrogen Production across Visible to Near Infrared Spectral Region*", Nat. Commun. **15**, 413 (2024).
- H.-C. Tu, Y.-L. Hsiao, Y.-D. Lin, Y.-G. Lin, D.-L. Liao, and K.-S. Ho*(何國賢), "*Multi-functional Hydrogen- and Oxygen-capturing FeCo-N-C Catalyst with Improved Hydrogenation of Nitroarenes and ORR Activity*", Chem. Eng. J. **487**, 150623 (2024).
- J. Wang*(王健), Y. Zhang, Y. Wang*(王瑩), J. Cho, T.-S. Chan, Y. Ha, S.-C. Haw, C.-W. Kao, Z. Wang, J. Lei, M. Ju, J. Tang, T. Liu, S. Zhao, Y. Dai, A.-B. Wiechec, F.-R. Chen, W. Wang, C. H. Choi, Z. Shao*(邵宗平), and M. Ni*(倪盟), "*Heterostructure Boosts a Noble-metal-free Oxygen-evolving Electrocatalyst in Acid*", Energ. Environ. Sci. **17**, 5972 (2024).
- L. Wang, C. Zhang, T. Lin, H. Chu, Y. Gao, Z. Hu, S.-C. Haw, C.-T. Chen, C.-Y. Kuo, X. Li, Y. Gai, Q. Guo, Y. Meng, H. Zhuang, X. Shen*(沈希), Z. Wang*(王兆翔), and R. Yu*(禹日成), "*Anti-siting for Stabilizing Structure and Modulating Cationic/Anionic Redox Reactions*", Energy Storage Mater. **70**, 103479 (2024).
- M. Wang, Z. Wang, Y. Zhang, Y. Shi, T.-S. Chan, S.-C. Haw, J. Wang, H. Wang, S. Wang, H. Fei, R. Liu, T. Liu, C.-F. Yan, and J. Wang*(王健), "*Regulating Reconstruction Activity of Cobalt Electrode for Optimized Water Oxidation*", ACS Energ. Lett. **9**, 5502 (2024).
- W.-T. Yang, L. C. Kao*(高立誠), X.-T. Yu, C.-L. Dong, and S. Y. H. Liou*(劉雅瑄), "*Mechanistic Insights into Temperature Hysteresis in CO Oxidation on Cu-TiO_2 Mesosphere*", Appl. Catal. B-Environ. **352**, 124017 (2024).
- R. A. Yuwono, C. Khotimah, F.-M. Wang*(王復民), N.-L. Wu*(吳乃立), A. C. Imawan, R. Foeng, P.-C. Huang, G.-Y. Liu, S.-C. Haw, and H.-S. Sheu, "*Investigations of an Organic Coverage to Ni-rich Cathode Materials: Effects on Deteriorated, Cathode Electrolyte Interphase, and Chemical Crossover*", J. Energy Storage **92**, 112184 (2024).
- C. Zhang, Y. Li, Y. Liu, X. Shen, Z. Hu, J.-M. Chen, H.-J. Lin, C.-T. Chen, Q. Kong, Y.-S. Hu, Y. Gao*(高玉瑞), S.-C. Haw*(何樹智), X. Wang*(王雪鋒), R. Yu*(禹日成), Z. Wang*(王兆翔), and L. Chen, "*Correlation Between Regulated Structure of Li-rich Layered Oxide and Low-potential TM Redox*", Nano Energy **121**, 109254 (2024).
- S.-D. Zhang, J. Wang, M.-Y. Qi, S.-J. Guo, H. Jin, H. Ji, Y.-R. Lu, T.-S. Chan, and A.-M. Cao*(曹安民), "*Recycling Spent $LiCoO_2$ for Improved 4.6 V Performance*", ACS Energ. Lett. **9**, 4976 (2024).
- M.-W. Zheng, C.-W. Lin, P.-H. Chou, C.-L. Chiang, Y.-G. Lin, and S.-H. Liu*(劉守恒), "*Highly Effective Degradation of Ibuprofen by Alkaline Metal-doped Copper Oxides via Peroxymonosulfate Activation: Mechanisms, Degradation*

Pathway and Toxicity Assessments", J. Hazard. Mater. **462**, 132751 (2024).
- X. Zhong, L. Sui, M. Yang, T. Koketsu, M. Klingenhof, S. Selve, K. G. Reeves, C. Ge, L. Zhuang, W. H. Kan, M. Avdeev, M. Shu, N.-A. Vante, J.-M. Chen, S.-C. Haw, C.-W. Pao, Y.-C. Chang, Y. Huang, Z. Hu*(胡志偉), P. Strasser*, and J. Ma*(馬吉偉), "*Stabilization of Layered Lithium-rich Manganese Oxide for Anion Exchange Membrane Fuel Cells and Water Electrolyzers*", Nat. Catal. **7**, 546 (2024).
- F. Zou, S. Lee, L. Lyu, J. Zhang, S. Kang, G. Kim, H. Lee, S. Park, G.-H. Lee, K.-W. Nam, and Y.-M. Kang*, "*Bulk-doped Heavy Element Mitigating the Ligand-to-metal Charge Transfer of $LiCoO_2$ Toward Its Robust High-voltage Charging Stability*", ACS Energ. Lett. **9**, 6011 (2024).

TLS 21A1 U90 – (White Light) Chemical Dynamics (PRT 75%)

- Y.-L. Sun, W.-J. Huang, and S.-H. Lee*(李世煌), "*Study on Formation of Interstellar C_7H from Reactions C_4+C_3H_2 and C_4H+C_3H*", J. Phys. Chem. A **128**, 456 (2024).
- Y.-L. Sun, W.-J. Huang, and S.-H. Lee*(李世煌), "*Formations of C_6H from Reactions C_3+C_3H_2 and C_3H+C_3H and of C_8H from Reactions C_4+C_4H_2 and C_4H+C_4H*", J. Chem. Phys. **160**, 044303 (2024).

TLS 21A2 U90 – (White Light) Photochemistry

- S.-Y. Lin, S.-L. Chou, T.-P. Huang, M.-Y. Lin, H.-F. Chen, P. J. Sarre, C.-M. Tseng*(曾建銘), and Y.-J. Wu*(吳宇中), "*Blue Luminescence from N-doped Graphene*", Astrophys. J. **977**, 230 (2024).

TLS 21B1 U90 – (CGM) Angle-resolved UPS

- C.-S. Cai, W.-Y. Lai, P.-H. Liu, T.-C. Chou, R.-Y. Liu, C.-M. Lin, S. Gwo, and W.-T. Hsu*(徐瑋廷), "*Ultralow Auger-assisted Interlayer Exciton Annihilation in WS_2/WSe_2 Moiré Heterobilayers*", Nano Lett. **24**, 2773 (2024).
- P.-Y. Cheng, M. Oudah, T.-L. Hung, C.-E. Hsu, C.-C. Chang, J.-Y. Haung, T.-C. Liu, C.-M. Cheng, M.-N. Ou, W.-T. Chen, L. Z. Deng, C.-C. Lee, Y.-Y. Chen, C.-N. Kuo, C.-S. Lue, J. Machts, K. M. Kojima, A. M. Hallas, and C.-L. Huang*(黃建龍), "*Physical Properties and Electronic Structure of the Two-gap Superconductor V_2Ga_5*", Phys. Rev. Res. **6**, 033253 (2024).
- H.-T. Chin, D.-C. Wang, D. P. Gulo, Y.-C. Yao, H.-C. Yeh, J. Muthu, D.-R. Chen, T.-C. Kao, M. Kalbác, P.-H. Lin, C.-M. Cheng, M. Hofmann, C.-T. Liang, H.-L. Liu, F.-C. Chuang, and Y.-P. Hsieh*(謝雅萍), "*Tungsten Nitride (W_3N6): An Ultraresilient 2D Semimetal*", Nano Lett. **24**, 67 (2024).
- C.-M. Chu, P.-Y. Chuang, S.-H. Hsieh, C.-M. Cheng, C.-H. Chen, H.-S. Tsai*(蔡勛升), and W.-Y. Woon*(溫偉源), "*Graphene as the Anti-oxidation Protective Layer: How Good or Bad Can It Be?*", Mater. Today Comm. **39**, 108752 (2024).
- V. Krishnamoorthy, H. K. Bangolla, C.-Y. Chen, Y.-T. Huang, C.-M. Cheng, R. K. Ulaganathan, R. Sankar, K.-Y. Lee, H.-Y. Du*(杜鶴芸), L.-C. Chen, K.-H. Chen, and R.-S. Chen*(陳瑞山), "*Efficient Hydrogen Evolution Reaction in 2H-MoS_2 Basal Planes Enhanced by Surface Electron Accumulation*", Catalysts **14**, 50 (2024).
- Y.-S. Lan, C.-J. Chen, S.-H. Kuo, Y.-H. Lin, A. Huang, J.-Y. Huang, P.-J. Hsu*(徐斌睿), C.-M. Cheng*(鄭澄懋), and H.-T. Jeng*(鄭弘泰), "*Dual Dirac Nodal Line in Nearly Freestanding Electronic Structure of β-Sn Monolayer*", ACS Nano **18**, 20990 (2024).
- M.-K. Lin*(林孟凱), J. A. Hlevyack, C. Zhao, P. Dudin, J. Avila, S.-K. Mo, C.-M. Cheng, P. Abbamonte, D. P. Shoemaker, and T.-C. Chiang*(江台章), "*Unconventional Spectral Gaps Induced by Charge Density Waves in the Weyl Semimetal $(TaSe_4)_2I$*", Nano Lett. **24**, 8778 (2024).
- N. N. Quyen, W.-Y. Tzeng, C.-E. Hsu, I.-A. Lin, W.-H. Chen, H.-H. Jia, S.-C. Wang, C.-E. Liu, Y.-S. Chen, W.-L. Chen, T.-L. Chou, I.-T. Wang, C.-N. Kuo, C.-L. Lin, C.-T. Wu, P.-H. Lin, S.-C. Weng, C.-M. Cheng, C.-Y. Kuo, C.-M. Tu, M.-W. Chu, Y.-M. Chang, C. S. Lue*(呂欽山), H.-C. Hsueh*(薛宏中), and C.-W. Luo*(羅志偉), "*Three-dimensional Ultrafast Charge-density-wave Dynamics in CuTe*", Nat. Commun. **15**, 2386 (2024).
- S. H. Su*(蘇書玄), T. T. Huang, B.-R. Pan, J.-C. Lee, Y. J. Qiu, P.-Y. Chuang, P. Gultom, C.-M. Cheng*(鄭澄懋), Y.-C. Chen, and J.-C. A. Huang*(黃榮俊), "*Large Tunable Spin-to-charge Conversion in $Ni_{80}Fe_{20}$/Molybdenum Disulfide by Cu Insertion*", ACS Appl. Mater. Interfaces **16**, 24122 (2024).
- I.-T. Wang, T.-L. Chou, C.-E. Hsu, Z. Lei, L.-M. Wang, P.-H. Lin, C.-W. Luo, C.-W. Chen, C.-N. Kuo, C. S. Lue, C.-H. Chen, H.-C. Hsueh*(薛宏中), and M.-W. Chu*(朱明文), "*The Growing Charge-density-wave Order in CuTe Lightens and Speeds up Electrons*", Nat. Commun. **15**, 9345 (2024).

TLS 21B2 U90 – Gas Phase

- C.-D. Li, T.-A. Lin, P.-H. Chen, T.-S. Gau, B.-J. Lin, P.-W. Chiu, and J.-H. Liu*(劉瑞雄), "*Synthesis of Pentameric Chlorotin Carboxylate Clusters for High Resolution EUV Photoresists Under Small Doses*", Nanoscale Adv. **6**, 2928 (2024).
- Y.-F. Tseng, P.-C. Liao, P.-H. Chen, T.-S. Gau, B.-J. Lin, P.-W. Chiu, and J.-H. Liu*(劉瑞雄), "*Highly Hydroxylated Hafnium Clusters are Accessible to High Resolution EUV Photoresists Under Small Energy Doses*", Nanoscale Adv. **6**, 197 (2024).

TLS 23A1 IASW – Small/Wide Angle X-ray Scattering

- K. S. Bayikadi, S. Imam, W.-S. Tee, S. Kavirajan, C.-Y. Chang, A. Sabbah, F.-Y. Fu, T.-R. Liu, C.-Y. Chiang, D. Shukla, C.-T. Wu, L.-C. Chen, M.-Y. Chou, K.-H. Chen*(陳貴賢), and R. Sankar*, "*Ultra-low Lattice Thermal Conductivity Driven High Thermoelectric Figure of Merit in Sb/W Co-doped GeTe*", J. Mater. Chem. A **12**, 30892 (2024).
- P. F. Chan, M. Qin*(秦敏超), C.-J. Su, L. Ye, X. Wang, Y. Wang, X. Guan, Z. Lu, G. Li, T. Ngai, S. W. Tsang, N. Zhao, and X. Lu*(路新慧), "*iso-BAI Guided Surface Recrystallization for Over 14% Tin Halide Perovskite Solar Cells*", Adv. Sci. **11**, 2309668 (2024).
- B. Chang, B.-H. Jiang, C.-P. Chen, K. Chen, B.-H. Chen, S. Tan, T.-C. Lu, C.-S. Tsao, Y.-W. Su, S.-D. Yang, C.-S. Chen, and K.-H. Wei*(韋光華), "*Achieving High Efficiency and Stability in Organic Photovoltaics with a Nanometer-scale Twin p-i-n Structured Active Layer*", ACS Appl. Mater. Interfaces **16**, 41244 (2024).
- C.-Y. Chang, G.-M. Manesi, W.-E. Wang, Y.-C. Hung, A. Avgeropoulos, and R.-M. Ho*(何榮銘), "*Frank-Kasper-like Network Phase from Self-assembly of High-χ star-block Copolymers*", Sci. Adv. **10**, eado4786 (2024).
- C.-Y. Chang, G.-M. Manesi, J. Xie, A.-C. Shi*(史安昌), T. Shastry, A. Avgeropoulos*, and R.-M. Ho*(何榮銘), "*Topology Effect on Order-disorder Transition of High-χ Block Copolymers*", Macromolecules **57**, 7087 (2024).
- C.-Y. Chang, Y.-H. Chen, and R.-M. Ho*(何榮銘), "*Metastable Network Phases from Controlled Self-assembly of High-χ Block Copolymers*", Phys. Rev. Mater. **8**, 030301 (2024).
- J.-W. Chang, K.-H. Su, C.-W. Pao, J.-J. Tsai, C.-J. Su, J.-L. Chen, L.-M. Lyu, C.-H. Kuo, A.-C. Su, H.-C. Yang*(楊小青), Y.-H. Lai*(賴英煌), and U.-S. Jeng*(鄭有舜), "*Arrayed Pt Single Atoms via Phosphotungstic Acids Intercalated in Silicate Nanochannels for Efficient Hydrogen Evolution Reactions*", ACS Nano **18**, 1611 (2024).
- Y.-J. Chang, K.-T. Lin, O. Shih, C.-H. Yang, C.-Y. Chuang, M.-H. Fang, W.-B. Lai, Y.-C. Lee, H.-C. Kuo, S.-C. Hung, C.-K. -K., U.-S. Jeng, and Y.-R. Chen*(陳韻如), "*Sulfated Disaccharide Protects Membrane and DNA Damages from Arginine-rich Dipeptide Repeats in ALS*", Sci. Adv. **10**, eadj0347 (2024).
- C.-C. Chen, Y.-R. Huang, Y. T. Chan, H.-Y. Lin, H.-J. Lin, C.-D. Hsiao, T.-P. Ko, T.-W. Lin, Y.-H. Lan, H.-Y. Lin, and H.-Y. Chang*(張欣暘), "*A Distinct Dimer Configuration of a Diatom Get3 Forming a Tetrameric Complex with Its Tail-anchored Membrane Cargo*", BMC Biol. **22**, 136 (2024).
- C.-H. Chen, M.-H. Yu, Y.-Y. Wang, Y.-C. Tseng, I.-H. Chao, I.-C. Ni, B.-H. Lin, Y.-J. Lu, and C.-C. Chueh*(闕居振), "*Enhancing the Performance of 2D Tin-based Pure Red Perovskite Light-emitting Diodes through the Synergistic Effect of Natural Antioxidants and Cyclic Molecular Additives*", Small **20**, 2307774 (2024).
- C.-Y. Chen, Y. Chen, T.-Y. Chang, M.-T. Lee, S.-Y. Liu, Y.-C. Yu, Y.-H. Lin, C.-H. Lee, H.-L. Chen, K.-Y. Wu, W.-T. Chuang, and C.-L. Wang*(王建隆), "*Thermophilic Artificial Water Channels of a Lipid-like Dendron Stabilized by Water-containing Hydrogen-bonded Network*", Giant **17**, 100220 (2024).
- L.-C. Chen, S.-A. Chen, K. Uma, C.-H. Chiang, J.-X. Xie, Z.-L. Tseng*(曾宗亮), and S.-W. Liu*(劉舜維), "*High-leakage-resistance and Low-turn-on-voltage Upconversion Devices Based on Perovskite Quantum Dots*", Adv. Funct. Mater. **34**, 2309589 (2024).
- T.-L. Chen, C.-Y. Huang, Y.-S. Lai, Y.-C. Chen, Y.-J. Yang, W.-L. Wang, and H.-Y. Hsueh*(薛涵宇), "*Fabrication of Stable Liquid-like Wetting Buckled Surfaces as Bioinspired Antibiofouling Coatings by Using Silicon-containing Block Copolymers*", ACS Appl. Mater. Interfaces **16**, 37212 (2024).
- P.-H. Chiu, C.-T. Hu, S.-K. Chia, L.-Y. Su*(蘇莉芸), P.-T. Chen, Z.-Y. Liu, C.-Y. Lin, C.-C. Hsieh, C.-A. Dai*(戴子安), and L. Wang*(王立義), "*Synergistic Enhancement of Stability and Performance for Perovskite Solar Cells Using Fluorinated Benzoic Acids as Additives*", Solar RRL **8**, 2300902 (2024).
- T.-C. Chou and S.-W. Kuo*(郭紹偉), "*Controllable Wet-brush Blending of Linear Diblock Copolymers with Phenolic/DDSQ Hybrids toward Mesoporous Structure Phase Diagram*", Macromolecules **57**, 5958 (2024).
- T. T. K. Cuc, Y.-C. Tso, T.-C. Wu, P. Q. Nhien, T. M. Khang, B. T. B. Hue,

W.-T. Chuang, and H.-C. Lin*(林宏洲), "*Ultrahigh Toughness of Stretchable Ratiometric Mechanofluorescent Polyurethane Elastomers Enhanced by Dual Slide-ring Motion of Polyrotaxane Cross-linkers and Daisy Chain Backbones*", J. Mater. Chem. C **12**, 14469 (2024).

- J.-F. Ding, G.-L. Chen, P.-H. Liu, K.-W. Tseng, W.-N. Wu, J.-M. Lin, S.-H. Tung, L. Wang*(王立義), and C.-L. Liu*(劉振良), "*Enhancing the Thermoelectric Performance of Donor-acceptor Conjugated Polymers through Dopant Miscibility: a Comparative Study of Fluorinated Substituents and Side-chain Lengths*", J. Mater. Chem. A **12**, 9806 (2024).
- D. D. Ejeta, Y.-S. Huang, J.-R. Hsu, M. Gurska, S.-W. Kuo, J. Kollar, J. Mosnacek, and C.-F. Huang*(黃智峯), "*Solution-state Self-assembly of Novel Poly(Carbamoyl Methacrylate)s Synthesized via Combining Passerini Three-component Reactions and Free Radical Polymerizations*", Eur. Polym. J. **218**, 113361 (2024).
- Y. Fu, L. Xu, Y. Li, E. J. Yang, Y. Guo, G. Cai, P. F. Chan, Y. Ke*(柯于斌), C.-J. Su, U.-S. Jeng, P. C. Y. Chow, J.-S. Kim, M.-C. Tang*(鄧敏聰), and X. Lu*(路新慧), "*Enhancing inter-domain Connectivity by Reducing Fractal Dimensions: the Key to Passivating Deep Traps in Organic Photovoltaics*", Energ. Environ. Sci. **17**, 8893 (2024).
- S. Hegde, V. Sridhar, R. S. Chen, and S. Chattopadhyay*(薛特), "*Gradient Dion-Jacobson Phase Stable Quasi-2D Perovskite@Graphene Hybrid for High Responsivity Photodetectors*", Adv. Opt. Mater. **12**, 2400232 (2024).
- S.-H. Hong, C.-C. Hsu, T.-H. Liu, T.-C. Lee, S.-H. Tung, H.-L. Chen, J. Yu*(游佳欣), and C.-L. Liu*(劉振良), "*Extremely Large Seebeck Coefficient of Gelatin Methacryloyl (GelMA)-based Thermogalvanic Cells by the Dual Effect of Ion-induced Crystallization and Nanochannel Control*", Mater. Today Energy **42**, 101546 (2024).
- Y.-J. Hsiao, Z.-E. Huang, A. Sahare, M.-Z. Chen, Y.-H. Lin, and H.-L. Chen*(陳信龍), "*Accessing the Frank-kasper Phase of Block Copolymer via Selective Incorporation of Metal Salt*", Macromolecules **57**, 10657 (2024).
- C.-C. Hsu, Y.-T. Lin, S.-H. Hong, U.-S. Jeng, H.-L. Chen, J. Yu, and C.-L. Liu*(劉振良), "*3D Printed Gelatin Methacrylate Hydrogel-based Wearable Thermoelectric Generators*", Adv. Sustain. Syst. **8**, 2400039 (2024).
- C.-H. Hsu, H.-Y. Liao, K. Wang, T.-W. Kuo, C.-C. Liu, J.-R. Shih, C.-J. Lin, C.-T. Chen, Y.-R. Peng, T.-Y. Yang, M.-Y. Kao, H.-F. Huang, H.-Y. Shen, Y.-C. King*(金雅琴), and Y.-L. Chueh*(闕郁倫), "*Design of Wireless Multiple Gases Complementary Architecture Sensors Based on $SnSe_2$ and $PtSe_2$ Layered Films and Oscillating Circuits*", Adv. Mater. Technol. **9**, 2301479 (2024).
- H.-F. Huang, Y.-H. Tsai, and C.-T. Lo*(羅介聰), "*Effects of Hard and Soft Confinement on Crystal Polymorphism and Crystal Development in Electrospun Core-sheath Fibers*", J. Polym. Sci. **62**, 4214 (2024).
- J.-H. Huang, X.-F. Luo, T.-Y. Kuo, Y.-H. Lai, P. C. Rath, C.-W. Huang, M.-H. Lin, A.-Y. Hou, J. Li, Y.-S. Su, W.-W. Wu*(吳文偉), and J.-K. Chang*(張仍奎), "*Dual-salt Aqueous Electrolyte for Enhancing Charge-storage Properties of VO_2 Polymorphic Cathodes for Zn-ion Batteries*", Chem. Eng. J. **497**, 154609 (2024).
- P.-Y. Huang, Y.-Y. Zhang, P.-C. Tsai, R.-J. Chung, Y.-T. Tsai, M.-K. Leung, S.-Y. Lin*(林時彥), and M.-H. Fang*(方牧懷), "*Interfacial Engineering of Quantum Dots-metal-organic Framework Composite Toward Efficient Charge Transport for a Short-wave Infrared Photodetector*", Adv. Opt. Mater. **12**, 2302062 (2024).
- Y.-J. Huang*(黃逸仁), J.-H. Chang, S.-W. Chen, T.-C. Lin, C.-C. Wang, C.-J. Su, T.-N. Lam, and W.-C. Ko, "*Multiscale Insights into Electric Field Orientation Effects on Piezoelectric Strain and Crystallography in P(VDF–TrFE) and P(VDF–TrFE–CTFE) Fibers*", J. Mol. Struct. **1310**, 138391 (2024).
- A.-T. Jhang, P.-C. Tsai, Y.-T. Tsai, S.-Y. Lin*(林時彥), and M.-H. Fan*(方牧懷), "*Quantum-dots-in-double-perovskite for High-gain Short-wave Infrared Photodetector*", Adv. Opt. Mater. **12**, 2401252 (2024).
- B.-H. Jiang, Y.-S. Chen, Y.-C. You, Y.-W. Su, C.-Y. Chang, H.-S. Shih, Z.-E. Shi, C.-P. Chen*(陳志平), and K.-T. Wong*(汪根欉), "*The Role of Unfused-ring-based Small-molecule Acceptors as the Third Component in Ternary Organic Photovoltaics*", J. Mater. Chem. C **12**, 12004 (2024).
- C. Lee, B. J. Ree, K. Chen, R. Komaki, S. Katsuhara, T. Yamamoto, R. Borsali, K. Tajima, H.-L. Chen*(陳信龍), T. Satoh*, and T. Isono*, "*Ultrasmall 3D Network Morphologies from Biobased Sugar-terpenoid Hybrid Block Co-oligomers in the Bulk and the Thin Film States*", Giant **17**, 100211 (2024).
- L.-C. Lee, K.-T. Huang, Y.-T. Lin, U.-S. Jeng, C.-H. Wang, S.-H. Tung, C.-J. Huang*(黃俊仁), and C.-L. Liu*(劉振良), "*A pH-sensitive Stretchable Zwitterionic Hydrogel with Bipolar Thermoelectricity*", Small **20**, 2311811 (2024).
- S.-H. Lien, P.-H. Lin, S.-W. Shao, P.-T. Chiu, C.-Y. Chang, Y.-C. Sung, J.-C. Tsai*(蔡敬誠), and R.-M. Ho*(何榮銘), "*Peculiar Transition between Chiral and Achiral Networks in Self-assembly of Chiral Block Copolymers*", Macromolecules **57**, 8734 (2024).
- C.-F. Lin, Y.-S. Wu, H.-C. Hsieh, W.-C. Chen, T. Isono, T. Satoh, Y.-C. Lin*(林彥丞), C.-C. Kuo*(郭霽慶), and W.-C. Chen*(陳文章), "*Enhanced Performance of Phototransistor Memory by Optimizing the Block Copolymer Architectures Comprising Polyfluorenes and Hydrogen-bonded Insulating Coils*", Polymer **295**, 126772 (2024).
- H.-A. Lin, Y.-H. Weng, T. Mulia, C.-L. Liu, Y.-C. Lin*(林彥丞), Y.-Y. Yu*(游洋雁), and W.-C. Chen*(陳文章), "*Electrical Double-layer Transistors Comprising Block Copolymer Electrolytes for Low-power-consumption Photodetectors*", ACS Appl. Mater. Interfaces **16**, 25042 (2024).
- H.-Y. Lin, B.-J. Zhong, H.-J. Liu, Y.-K. Wu, C.-H. Peng, and C.-L. Wang*(王建隆), "*Optimal Compositions in the NDI: Pyrene Charge-transfer Complexes Revealed by Thermal Analysis and Structural Characterizations*", Cryst. Growth Des. **24**, 2833 (2024).
- I.-M. Lin, C.-Y. Yang, Y.-M. Wang, W.-E. Wang, Y.-C. Hung, E. L. Thomas, and Y.-W. Chiang*(蔣酉旺), "*Flexible Block Copolymer Metamaterials Featuring Hollow Ordered Nanonetworks with Ultra-high Porosity and Surface-to-volume Ratio*", Small **20**, 2307487 (2024).
- Y.-L. Lin, S. Zheng, C.-C. Chang, L.-R. Lee, and J.-T. Chen*(陳俊太), "*Light-responsive MXenegel via Interfacial Host-guest Supramolecular Bridging*", Nat. Commun. **15**, 916 (2024).
- K.-P. Liu, A. S. Panda, W.-C. Huang, and R.-M. Ho*(何榮銘), "*Vacuum-driven Orientation of Nanostructured Polystyrene-block-poly(L-lactide) Block Copolymer Thin Films for Nanopatterning*", Giant **19**, 100303 (2024).
- K.-H. Lu, W.-R. Wu, C.-J. Su, P.-W. Yang, N. L. Yamada, H.-J. Zhuo, S.-A. Chen, W.-T. Chuang, Y.-K. Lan, A.-C. Su*(蘇安仲), and U.-S. Jeng*(鄭有舜), "*Modulating Phase Segregation During Spin-casting of Fullerene-based Polymer Solar-cell Thin Films upon Minor Addition of a High-boiling Co-solvent*", J. Appl. Crystallogr. **57**, 1871 (2024).
- T. Mulia, E. Ercan, M. Mumtaz, Y.-C. Lin*(林彥丞), R. Borsali*, and W.-C. Chen*(陳文章), "*Carbohydrate-based Block Copolymers with Sub-10 nm Face-centered Cubic Nanostructures for Low-power-consuming and Ultraviolet Light-triggered Synaptic Phototransistors*", Carbohydr. Polym. **344**, 122476 (2024).
- K. H. Ngai, X. Sun, X. Zou, K. Fan, Q. Wei, M. Li, S. Li, X. Lu, W. Meng, B. Wu, G. Zhou, M. Long*(龍明珠), and J. Xu*(許建斌), "*Charge Injection and Auger Recombination Modulation for Efficient and Stable Quasi-2D Perovskite Light-emitting Diodes*", Adv. Sci. **11**, 2309500 (2024).
- D. T. A. Nguyen, L. Wang, T. Imae*, C.-J. Su, U.-S. Jeng, and O. J. Rojas*, "*Nanoarchitectonics of Nanocellulose Filament Electrodes by Femtosecond Pulse Laser Deposition of ZnO and In Situ Conjugation of Conductive Polymers*", ACS Appl. Mater. Interfaces **16**, 22532 (2024).
- J. Park, H. Cho, J. Kim, Y.-C. Huang, N. Kim, S. Park, Y. Kim, S. Lee, J. Kwon, D. C. Lee*, and B. Shin*, "*Efficient and Spectrally Stable Pure Blue Light-emitting Diodes Enabled by Phosphonate Passivated $CsPbBr_3$ Nanoplatelets with Conjugated Polyelectrolyte-based Energy Transfer Layer*", EcoMat **6**, e12487 (2024).
- H. Sadek, S. K. Siddique, C. Chen, and R.-M. Ho*(何榮銘), "*Well-ordered Bicontinuous Nanohybrids from a Bottom-up Approach for Enhanced Strength and Toughness*", Nano Lett. **24**, 11020 (2024).
- S.-W. Shao, P. Puneet, M.-C. Li, T. Ikai, E. Yashima, and R.-M. Ho*(何榮銘), "*Chiral Luminophore Guided Self-assembly of Achiral Block Copolymers for the Amplification of Circularly Polarized Luminescence*", ACS Macro Lett. **13**, 734 (2024).
- T. Shastry, J. Xie, C.-H. Tung, T. Y. Lynn, A. S. Panda, A.-C. Shi, and R.-M. Ho*(何榮銘), "*Sequential Self-assembly of Polystyrene-block-polydimethylsiloxane for 3D Nanopatterning via Solvent Annealing*", ACS Appl. Mater. Interfaces **16**, 40263 (2024).
- C.-J. Shih, Y.-S. Chen, D. Luo, C.-W. Yu, K.-H. Chen, G. Murokinas, Y.-C. Huang, C.-F. Li, Y.-C. Huang*(黃裕清), and S.-W. Liu*(劉舜維), "*Exploring Buried Interface in All-vapor-deposited Perovskite Photovoltaics*", Sol. Energy **280**, 112872 (2024).
- V. Sridhar, M. Rameez, P. Selvarasu, D. S. Tomar, S. Hegde, R. S. Chen, C. T. Wu, C. H. Hung, and S. Chattopadhyay*(薛特), "*Mega Broadband Photoresponsivity in Degradation-controlled Super-halide PF_6 Substituted Perovskite@graphene Hybrid Photodetectors*", Mater. Today Phys. **40**, 101294 (2024).
- M. K. Sriramoju, K.-T. Ko, and S.-T. D. Hsu*(徐尚德), "*Tying a True Topological Protein Knot by Cyclization*", Biochem. Biophy. Res. Co. **696**, 149470 (2024).
- X. Sun, W. Meng, K. H. Ngai, Z. Nie, C. Luan, W. Zhang, S. Li, X. Lu, B. Wu, G. Zhou, M. Long*(龍明珠), and J. Xu*(許建斌), "*Regulating Surface-passivator Binding Priority for Efficient Perovskite Light-emitting Diodes*", Adv. Mater. **36**, 2400347 (2024).
- Y.-S. Sun*(孫亞賢), Y.-P. Liao, H.-H. Hung, P.-H. Chiang, and C.-J. Su, "*Molecular-weight Effects of a Homopolymer on the AB- and ABC-stacks of*

Perforations in Block Copolymer/Homopolymer Films", Soft Matter **20**, 609 (2024).

- Y.-C. Tseng, Q. Fan, C.-Y. Tsai, J.-F. Chang, M.-H. Yu, H.-Z. Tseng, H.-L. Yip, F. R. Lin*, A. K.-Y. Jen*(任廣禹), and C.-C. Chueh*(闕居振), "*Compatibilizer Effects of Strategically Designed Donor-acceptor Block Copolymers to Enhance the Performance, Stability, and Mechanical Durability of Inverted Organic Solar Cells*", Adv. Funct. Mater. **34**, 2408993 (2024).
- Z.-L. Tseng*(曾宗亮), S.-A. Chen, Kasimayan Uma, Y.-S. Chen, K.-Y. Ke, J.-X. Xie, and C.-Y. Chiang, "*All-solution-processed Perovskite-quantum-dot Light-emitting Diodes through Effective Synergistic Combination of Orthogonal Solvent and Electron Transport Material*", Alex. Eng. J. **97**, 256 (2024).
- K.-H. Wu, C.-P. Hsieh, and C.-T. Lo*(羅介聰), "*Compositional Asymmetry in a Crystalline-amorphous Block Copolymer Influences the Phase and Crystallization Behaviors of Its Blend with an Amorphous Block Copolymer*", Soft Matter **20**, 4308 (2024).
- Y. Xiang, W.-T. Chuang, and Y.-W. Chiang*(蔣酉旺), "*Synergistic Effects of Dry-brush Compatibility and Shear Stress on Rapid Alignment of Lamellar Microstructures for Block Copolymer Reflectors*", Giant **17**, 100225 (2024).
- Z.-L. Yan, H.-Y. Huang, J.-S. Benas, C.-W. Yang, C.-J. Su, F.-C. Liang, W.-C. Chen, H. Tsai*(蔡欣翰), R.-J. Jeng*(鄭如忠), and C.-C. Kuo*(郭霽慶), "*Optimizing Emission Stability in Blue Perovskite Light-emitting Diodes via Oxygen-plasma Treatment of Ni_xO_y Hole Transport Layer*", Adv. Opt. Mater. **12**, 2302358 (2024).
- C.-Y. Yang, C.-I. Lien, Y.-C. Tseng, Y.-F. Tu, A. W. Kulczyk, Y.-C. Lu, Y.-T. Wang, T.-W. Su, L.-C. Hsu*(徐立中), Y.-C. Lo*(羅玉枝), and S.-C. Lin*(林世昌), "*Deciphering DED Assembly Mechanisms in FADD-procaspase-8-cFLIP Complexes Regulating Apoptosis*", Nat. Commun. **15**, 3791 (2024).
- C.-Y. Yang, Y.-C. Tseng, Y.-F. Tu, B.-J. Kuo, L.-C. Hsu, C.-I. Lien, Y.-S. Lin, Y.-T. Wang, Y.-C. Lu, T.-W. Su, Y.-C. Lo*(羅玉枝), and S.-C. Lin*(林世昌), "*Reverse Hierarchical DED Assembly in the cFLIP-procaspase-8 and cFLIP-procaspase-8-FADD Complexes*", Nat. Commun. **15**, 8974 (2024).
- C.-W. Yeh, C.-J. Chen, C.-L. Tai, Y.-L. Yang, R. D. K. Misra, C.-N. Hsiao, C.-C. Chen, C.-S. Tsao, U. S. Jeng, H.-C. Lin, and T.-F. Chung*(鍾采甫), "*Pre-aged and Paint-baked Strengthening Response on the Prolonged Natural-aged Al-Mg-Si-Cu Aluminum Alloys*", J. Alloy. Compd. **1008**, 176677 (2024).

TLS 24A1 BM – (WR-SGM) XPS, UPS

- G. B. Adugna, K.-M. Lee*(李坤穆), H.-C. Hsieh*(謝孝基), S.-I. Lu*(呂世伊), C.-H. Lin, Y.-C. Hsieh, J. H. Yang, J.-M. Chiu, Y.-S. Liu, C.-W. Hu, W.-H. Chiu, S.-R. Li, K.-L. Liau, Y.-T. Tao, and Y.-D. Lin*(林彥多), "*Fluorination of Star-shaped Cyclopenta[2,1-b;3,4-b′] Dithiophene Derivatives and Its Application as Hole-transporting Materials in Scalable Perovskite Solar Cell Fabrication by Bar Coating*", Solar RRL **8**, 2300988 (2024).
- A. E. A. Aboubakr, M. K. Hussien, A. Sabbah, A. E. Hassan, M. H. Elsayed, Z. Wen*(溫珍海), K.-H. Chen, and C.-H. Hung*(洪政雄), "*Direct Z-scheme Heterostructure of In Situ Planted ZnO Nanorods on gC_3N_4 Thin Sheets Sprayed on TiO_2 Layer: A Strategy for Ternary-photoanode Engineering toward Enhanced Photoelectrochemical Water Splitting*", ACS Appl. Energy Mater. **7**, 906 (2024).
- D. B. Adam, W.-H. Huang, M.-C. Tsai*(蔡孟哲), W.-N. Su*(蘇威年), and B. J. Hwang*(黃炳照), "*Atomically Dispersed Ruthenium Single-atom Alloy Catalysts Enabling Efficient Iodide Oxidation Reaction Electrolysis in Acidic Media*", Int. J. Hydrogen Energ. **91**, 548 (2024).
- T. Agnihotri, T.-H. Chu, S.-K. Jiang, S. A. Ahmed, A. Ranjan, E. B. Tamilarasan, S.-C. Yang, T. M. Hagos, Z. B. Muche, J.-C. Jiang*(江志強), S.-H. Wu*(吳溪煌), W.-N. Su*(蘇威年), and B. J. Hwang*(黃炳照), "*Multifunctional Fluorinated Phosphonate-based Localized High Concentration Electrolytes for Safer and High-performance Lithium-based Batteries*", Energy Storage Mater. **73**, 103787 (2024).
- A. Beniwal, D. Bhalothia, Y.-R. Chen, J.-C. Kao, C. Yan, N. Hiraoka, H. Ishii, M. Cheng, Y.-C. Lo, X. Tu, Y.-W. Chiang, C.-H. Kuo, J.-P. Chou, C.-H. Wang, and T.-Y. Chen*(陳燦耀), "*Incorporation of Atomic Fe-oxide Triggers a Quantum Leap in the CO_2 Methanation Performance of Ni-hydroxide*", Chem. Eng. J. **493**, 152834 (2024).
- D. Bhalothia, A. Beniwal, C. Yan, K.-C. Wang, C.-H. Wang, and T.-Y. Chen* (陳燦耀), "*Potential Synergy Between Pt_2Ni_4 Atomic-clusters, Oxygen Vacancies and Adjacent Pd Nanoparticles Outperforms Commercial Pt Nanocatalyst in Alkaline Fuel Cells*", Chem. Eng. J. **483**, 149421 (2024).
- L.-Y. Chang, C.-C. Chang, M. Rinawati, Y.-H. Chang, Y.-S. Cheng, K.-C. Ho, C.-C. Chen, C.-H. Lin, C.-H. Wang, and M.-H. Yeh*(葉旻鑫), "*Near-infrared Photoelectrochromic Device with Graphene Quantum Dot Modified WO_3 Thin Film toward Fast-response Thermal Management for Self-powered Agrivoltaics*", Appl. Energy **361**, 122930 (2024).
- Y.-M. Chang, N. Yang, J. Min, F. Zheng, C.-W. Huang, J.-Y. Chen, Y. Zhang, P. Yang, C. Li, H.-Y. Liu, B. Ye, J.-B. Xu, H.-Y. Chen, Z. Luo, W.-W. Wu, K. Shih, J.-K. Huang, L.-J. Li*(李連忠), and Y. Wan*(萬怡), "*Atomically Thin Decoration Layers for Robust Orientation Control of 2D Transition Metal Dichalcogenides*", Adv. Funct. Mater. **34**, 2311387 (2024).
- S.-Y. Chen*(陳仕元), L.-Y. Wang, K.-C. Chen, C.-H. Yeh, W.-C. Hsiao, H.-Y. Chen, M. Nishi, M. Keller, C.-L. Chang, C.-N. Liao, T. Mochizuki, H.-Y. T. Chen*(陳馨怡), H.-H. Chou*(周鶴修), and C.-M. Yang*(楊家銘), "*Ammonia Synthesis Over Cesium-promoted Mesoporous-carbon-supported Ruthenium Catalysts: Impact of Graphitization Degree of the Carbon Support*", Appl. Catal. B-Environ. **346**, 123725 (2024).
- S.-H. Cheng, C.-H. Chang, J.-J. Velasco-Velez, and B.-H. Liu*(劉柏宏), "*Soft X-ray Induced Radiation Damage in Dip-and-pull Photon Absorption and Photoelectron Emission Experiments*", J. Phys. Chem. C **128**, 14381 (2024).
- C.-K. Fang, C.-H. Chuang, C.-W. Yang, Z.-R. Guo, W.-H. Hsu, C.-H. Wang, and I.-S. Hwang*(黃英碩), "*Formation of Highly Stable Interfacial Nitrogen Gas Hydrate Overlayers Under Ambient Conditions*", Surf. Interfaces **53**, 105002 (2024).
- C. B. Guta, H. G. Edao, W. B. Dilebo, C.-Y. Chang, F. T. Angerasa, E. A. Moges, Y. Nikodimos, K. Lakshmanan, M.-C. Tsai*(蔡孟哲), W.-N. Su*(蘇威年), and B. J. Hwang*(黃炳照), "*Novel Electrocatalyst with Abundant Oxygen Vacancies Enabling Efficient Two-electron Water Oxidation Reaction for H_2O_2 Synthesis*", Chem. Eng. J. **500**, 156418 (2024).
- L. Han*(韓麗麗), C. Sun, H.-T. Wang*(王孝祖), W.-X. Lin, J.-L. Chen, C.-W. Pao, Y.-C. Chuang, C.-H. Wang, J. Zhou, J. Wang, W.-F. Pong, and H. L. Xin* (忻獲麟), "*Interrogation of 3d Transition Bimetallic Nanocrystal Nucleation and Growth Using In Situ Electron Microscope and Synchrotron Xray Techniques*", Nano Lett. **24**, 7645 (2024).
- S. Hegde, V. Sridhar, R. S. Chen, and S. Chattopadhyay*(薛特), "*Gradient Dion-Jacobson Phase Stable Quasi-2D Perovskite@Graphene Hybrid for High Responsivity Photodetectors*", Adv. Opt. Mater. **12**, 2400232 (2024).
- J.-W. Hsueh, L.-H. Kuo, P.-H. Chen, W.-H. Chen, C.-Y. Chuang, C.-N. Kuo, C.-S. Lue, Y.-L. Lai, B.-H. Liu, C.-H. Wang, Y.-J. Hsu, C.-L. Lin*(林俊良), J.-P. Chou*(周至品), and M.-F. Luo*(羅夢凡), "*Investigating the Role of Undercoordinated Pt Sites at the Surface of Layered $PtTe_2$ for Methanol Decomposition*", Nat. Commun. **15**, 653 (2024).
- K. Iputera, C.-H. Yi, J.-Y. Huang, M. Nakayama, B.-H. Liu, C.-H. Wang, Y.-W. Yang, and R.-S. Liu*(劉如熹), "*In Situ Ambient Pressure X-ray Photoelectron Spectroscopy Study on O_2/H_2O-assisted Na-CO_2 Batteries*", J. Energy Storage **100**, 113467 (2024).
- Y.-C. Kao, H.-K. Peng, S.-W. Hsiao, K.-A. Wu, C.-M. Liu, S.-Y. Zheng, Y.-H. Wu*(巫勇賢), and P.-J. Wu*(吳品鈞), "*Investigation of Annealing Temperature Dependent Sub-cycling Behavior for $HfZrO_x$-based Ferroelectric Capacitor*", APL Mater. **12**, 051118 (2024).
- C.-H. Kuan, Y.-C. Chen, S. Narra, C.-F. Chang, Y.-W. Tsai, J.-M. Lin, G.-R. Chen, and E. W.-G. Diau*(刁維光), "*Quadruple-cation Wide-bandgap Mixed-halide Tin Perovskite Solar Cells*", ACS Energ. Lett. **9**, 2351 (2024).
- C.-H. Kuan, S. N. Afraj, Y.-L. Huang, A. Velusamy, C.-L. Liu, T.-Y. Su, X. Jiang, J.-M. Lin, M.-C. Chen*(陳銘洲), and E. W.-G. Diau*(刁維光), "*Functionalized Thienopyrazines on NiOx Film as Self-assembled Monolayer for Efficient Tin-perovskite Solar Cells Using a Two-step Method*", Angew. Chem. Int. Edit. **63**, e202407228 (2024).
- L.-C. Lee, K.-T. Huang, Y.-T. Lin, U.-S. Jeng, C.-H. Wang, S.-H. Tung, C.-J. Huang*(黃俊仁), and C.-L. Liu*(劉振良), "*A pH-sensitive Stretchable Zwitterionic Hydrogel with Bipolar Thermoelectricity*", Small **20**, 2311811 (2024).
- G.-J. Liao, W.-H. Hsueh, Y.-H. Yen, Y.-C. Shih, C.-H. Wang, J.-H. Wang*(王禎翰), and M.-F. Luo, "*Decomposition of Methanol-d_4 on Rh Nanoclusters Supported by Thin-film Al_2O_3/NiAl(100) under Near-ambient-pressure Conditions*", Phys. Chem. Chem. Phys. **26**, 5059 (2024).
- K.-W. Liao, H.-Y. Chen, W.-H. Wei, G.-C. Chen, I. Yamanaka, B.-T. Liu, T.-F. Hong, T.-C. Chiang, H.-C. Huang*(黃信智), and C.-H. Wang*(王丞浩), "*Novel Ruthenium-based Catalysts with Atomic Dispersion for Oxygen Evolution Reaction in Water Electrolysis*", Mater. Today Chem. **35**, 101857 (2024).
- S.-C. Lin, C.-W. Chang, M.-H. Tsai, C.-H. Chen, J.-T. Lin, C.-Y. Wu, I.-T. Kao, W.-Y. Jao, C.-H. Wang, W.-Y. Yu, C.-C. Hu, K.-H. Lin*(林昆翰), and T.-H. Yang*(楊東翰), "*Decreasing the O_2-to-H_2O_2 Kinetic Energy Barrier on Dilute Binary Alloy Surfaces with Controlled Configurations of Isolated Active Atoms*", Adv. Funct. Mater. **34**, 2314281 (2024).
- H.-T. Liu, W.-H. Chen, S.-J. Chang*(張書睿), C.-C. Yang, C.-H. Wang, W.-T. Liu, K.-Y. Chen, N. Kawakami, K.-B. Lin, C.-L. Lin*(林俊良), and C. Hu, "*Growth Behavior of Ni on Hydrogen-etched WS_2 Surface*", ACS Appl. Mater. Interfaces **16**, 56336 (2024).

- T. T. Mamo, M. Qorbani*, A. G. Hailemariam, R. Putikam, C.-M. Chu, T.-R. Ko, A. Sabbah, C.-Y. Huang, S. Kholimatussadiah, T. Billo, M. K. Hussien, S.-Y. Chang, M.-C. Lin, W.-Y. Woon, H.-L. Wu*(吳恆良), K.-T. Wong, L.-C. Chen*(林麗瓊), and K.-H. Chen*(陳貴賢), "*Enhanced CO_2 Photoreduction to CH_4 via *COOH and *CHO Intermediates Stabilization by Synergistic Effect of Implanted P and S Vacancy in Thin-film SnS_2*", Nano Energy **128**, 109863 (2024).
- S. K. Merso, T. M. Tekaligne, M. A. Weret, K. N. Shitaw, Y. Nikodimos, S.-C. Yang, Z. B. Muche, B. W. Taklu, B. T. Hotasi, C.-Y. Chang, S.-K. Jiang, G. Brunklaus, M. Winter, S.-H. Wu, W.-N. Su*(蘇威年), C.-Y. Mou*(牟中原), and B. J. Hwang*(黃炳照), "*Multiple Protective Layers for Suppressing Li Dendrite Growth and Improving the Cycle Life of Anode-free Lithium Metal Batteries*", Chem. Eng. J. **485**, 149547 (2024).
- T. L. Nguyen, C.-C. Yang, C.-H. Wang, Y.-W. Yang, T. Mazet, E. Gaudry, D. Malterre, M. Yoshimura, Y. F. Liao, H. Ishii, N. Hiraoka, H. J. Lin, Y. C. Tseng, and A. Chainani*(查里), "*Crucial Role of d-d Coulomb Correlations in the Magnetocaloric Ferrimagnets $Gd_6(Mn_{1-x}M_x)_{23}$ (M=Fe, Co)*", Phys. Rev. B **109**, 035102 (2024).
- M. Rinawati, L.-Y. Chang, C.-Y. Chang, C.-C. Chang, D. Kurniawan, W.-H. Chiang, W.-N. Su, B. Yuliarto, W.-H. Huang*(黃偉翔), and M.-H. Yeh*(葉旻鑫), "*Pioneering Molecularly-level Fe Sites Immobilized on Graphene Quantum Dots as a Key Activity Descriptor in Achieving Highly Efficient Oxygen Evolution Reaction*", Chem. Eng. J. **489**, 151436 (2024).
- P. K. Saravanan, D. Bhalothia, A. Beniwal, C.-H. Tsai, P.-Y. Liu, T.-Y. Chen, H.-M. Ku*(辜鴻鳴), and P.-C. Chen*(陳柏均), "*Adjacent Reaction Sites of Atomic Mn_2O_3 and Oxygen Vacancies Facilitate CO_2 Activation for Enhanced CH_4 Production on TiO_2-supported Nickel-hydroxide Nanoparticles*", Catalysts **14**, 410 (2024).
- G. G. Serbessa, B. W. Taklu, Y. Nikodimos, N. T. Temesgen, Z. B. Muche, S. K. Merso, T.-I. Yeh, Y.-J. Liu, W.-S. Liao, C.-H. Wang, S.-H. Wu*(吳溪煌), W.-N. Su*(蘇威年), C.-C. Yang*(楊純誠), and B. J. Hwang*(黃炳照), "*Boosting the Interfacial Stability of the Li_6PS_5Cl Electrolyte with a Li Anode via In Situ Formation of a LiF-rich SEI Layer and a Ductile Sulfide Composite Solid Electrolyte*", ACS Appl. Mater. Interfaces **16**, 10832 (2024).
- V. Sridhar, M. Rameez, P. Selvarasu, D. S. Tomar, S. Hegde, R. S. Chen, C. T. Wu, C. H. Hung, and S. Chattopadhyay*(薛特), "*Mega Broadband Photoresponsivity in Degradation-controlled Super-halide PF_6 Substituted Perovskite@graphene Hybrid Photodetectors*", Mater. Today Phys. **40**, 101294 (2024).
- S. H. Su*(蘇書玄), T. T. Huang, B.-R. Pan, J.-C. Lee, Y. J. Qiu, P.-Y. Chuang, P. Gultom, C.-M. Cheng*(鄭澄懋), Y.-C. Chen, and J.-C. A. Huang*(黃榮俊), "*Large Tunable Spin-to-charge Conversion in $Ni_{80}Fe_{20}$/Molybdenum Disulfide by Cu Insertion*", ACS Appl. Mater. Interfaces **16**, 24122 (2024).
- W. Tanmathusorachai, S. Aulia, M. Rinawati, L.-Y. Chang, C.-Y. Chang, W.-H. Huang, M.-H. Lin, W.-N. Su, B. Yuliarto, and M.-H. Yeh*(葉旻鑫), "*High-entropy Prussian Blue Analogue Derived Heterostructure Nanoparticles as Bifunctional Oxygen Conversion Electrocatalysts for the Rechargeable Zinc-air Battery*", ACS Appl. Mater. Interfaces **16**, 62022 (2024).
- T. M. Tekaligne, H. K. Bezabh, S. K. Merso, K. N. Shitaw, M. A. Weret, Y. Nikodimos, S.-K. Jiang, S.-C. Yang, C.-H. Wang, S.-H. Wu, W.-N. Su*(蘇威年), and B. J. Hwang*(黃炳照), "*Enhancing Aluminum Foil Performance in Aqueous and Organic Electrolytes: Dual-secure Passivation with Phthalocyanine as a Corrosion Inhibitor*", J. Mater. Chem. A **12**, 2157 (2024).
- Y.-C. Ting, C.-C. Cheng, F.-Y. Yen, G.-R. Li, S.-I. Chang, C.-H. Lee, H.-Y. T. Chen*(陳馨怡), and S.-Y. Lu*(呂世源), "*Highly Asymmetrically Configured Single Atoms Anchored on Flame-roasting Deposited Carbon Black as Cathode Catalysts for Ultrahigh Power Density Zn-air Batteries*", EnergyChem **6**, 100134 (2024).
- C.-C. Wang and C.-H. Lee*(李志浩), "*Wafer-scale Epitaxial Molybdenum Disulfide Ultrathin Film on Sapphire Prepared by Low-energy Reactive Magnetron Sputtering*", Appl. Surf. Sci. **659**, 159889 (2024).
- S.-K. Wu, H.-J. Wang, S.-W. Hsiao*(蕭聖偉), J.-S. Huang, W.-C. Chou*(周武清), C.-S. Yang*(楊祝壽), S.-J. Chang, C.-H. Wu, and Y.-C. Huang, "*Control of Lateral Epitaxial Nanothin β-In_2Se_3 Grown by Molecular Beam Epitaxy: Implications in Fabricating of Next-generation Transistors*", ACS Appl. Nano Mater. **7**, 20445 (2024).
- T. Yang, A. Beniwal, D. Bhalothia, C. Yan, C.-H. Wang, and T.-Y. Chen* (陳燦耀), "*Oxygen Vacancies Coupled with Surface Silicide Facilitate CO_2 Activation at Near-room Temperature for Efficient Methane Productivity on Ni-oxide Supported Pd Nanoparticles*", Sustain. Energy Fuels **8**, 3399 (2024).
- E. Zhao, J. Shan, P. Yin, W. Wang, K. Du, C.-C. Yang, J. Guo, J. Mao, Z. Peng*(彭振), C.-H. Wang*(王嘉興), and T. Ling*(凌濤), "*Breaking Oxygen Evolution Limits on Metal Chalcogenide Photocatalysts for Visible-light-driven Overall Water-splitting*", ACS Catalysis **14**, 14711 (2024).

SP 12B1 BM – Materials X-ray Study

- D. Bhalothia, A. Beniwal, C. Yan, K.-C. Wang, C.-H. Wang, and T.-Y. Chen* (陳燦耀), "*Potential Synergy Between Pt_2Ni_4 Atomic-clusters, Oxygen Vacancies and Adjacent Pd Nanoparticles Outperforms Commercial Pt Nanocatalyst in Alkaline Fuel Cells*", Chem. Eng. J. **483**, 149421 (2024).
- B. Faceira, S. S. Nayak, L. Teulé-Gay, C. Labrugère-Sarroste, H.-Y. Huang, Y.-C. Shao, C.-L. Dong, and A. Rougier*, "*Influence of Fe Doping on the Electrochromic Properties of Cosputtered V_2O_5 Thin Films*", ACS Appl. Energy Mater. **7**, 9882 (2024).
- Y.-M. Cai, Y.-H. Li, Y. Xiao, Q. Meyer, Q. Sun, W.-J. Lai, S.-W. Zhao, J. Li, L.-J. Zhang*(張林杰), H. Wang*(王晗), Z. Lin, J. Luo, and L.-L. Han*(韓麗麗), "*Synergistic Rare-earth Yttrium Single Atoms and Copper Phosphide Nanoparticles for High-selectivity Ammonia Electrosynthesis*", Rare Metals **43**, 5792 (2024).
- D. Chen, T. Gao, Z. Wei, M. Wang, Y. Ma, D. Xiao*(肖東東), C. Cao, C.-Y. Lee, P. Liu, D. Wang, S. Zhao, H.-T. Wang*(王孝祖), and L. Han*(韓麗麗), "*WS_2 Moiré Superlattices Supporting Au Nanoclusters and Isolated Ru to Boost Hydrogen Production*", Adv. Mater. **36**, 2410537 (2024).
- H.-C. Chen*(陳劾謙), A. Shabir, K.-H. Tu, C. M. Tan*(陳始明), W.-H. Chiu, R.-C. Fan, and N. A. Baruah, "*Additive-free Electroless Deposition on Graphene/Copper Foil: Photo-induced and Defect-assisted Approach for Environmentally Friendly Plating*", J. Environ. Chem. Eng. **12**, 111741 (2024).
- Y.-C. Chu, K.-H. Chen, C.-W. Tung, H.-C. Chen, J. Wang*(王佳麗), T.-R. Kuo*(郭聰榮), C.-S. Hsu, K.-H. Lin, L. D. Tsai, and H. M. Chen*(陳浩銘), "*Dynamic (Sub)surface-oxygen Enables Highly Efficient Carbonyl-coupling for Electrochemical Carbon Dioxide Reduction*", Adv. Mater. **36**, 2400640 (2024).
- L. Deng, H. Chen, S.-F. Hung, Y. Zhang, H. Yu, H.-Y. Chen, L. Li, and S. Peng*(彭生杰), "*Lewis Acid-mediated Interfacial Water Supply for Sustainable Proton Exchange Membrane Water Electrolysis*", J. Am. Chem. Soc. **146**, 35438 (2024).
- L. Deng, S.-F. Hung, S. Liu, S. Zhao, Z.-Y. Lin, C. Zhang, Y. Zhang, A.-Y. Wang, H.-Y. Chen, J. Peng, R. Ma, L. Jiao, F. Hu, L. Li, and S. Peng*(彭生杰), "*Accelerated Proton Transfer in Asymmetric Active Units for Sustainable Acidic Oxygen Evolution Reaction*", J. Am. Chem. Soc. **146**, 23146 (2024).
- Y. Ishiwata*(石渡洋一), G. Kawahara, K. Akase, T. Tominaga, H. Miyazaki, H. Ishii, A. Matsuo, K. Kindo, Y. Inagaki, K. Akashi, T. Kawae, T. Kida, S. Suehiro, M. Nantoh, and K. Ishibashi, "*Invariable Simultaneous Emergence of Antiferromagnetic Order and Tetragonal Deformation in CoO Nanocrystals*", J. Phys. Soc. JPN. **93**, 044603 (2024).
- F.-H. Liao, S.-P. Chen, C.-N. Yao, T.-H. Wu, M.-T. Liu, C.-S. Hsu, H. M. Chen* (陳浩銘), and S.-Y. Lin*(林淑宜), "*Oxygen-binding Sites of Enriched Gold Nanoclusters for Capturing Mitochondrial Reverse Electrons*", Nano Lett. **24**, 11202 (2024).
- T.-Y. Lin*(林姿瑩), C.-F. Hsieh, A. Kanai, T. Yashiro, W.-J. Zeng, J.-J. Ma, S.-F. Hung, and M. Sugiyama, "*Radiation Resistant Chalcopyrite CIGS Solar Cells: Proton Damage Shielding with Cs Treatment and Defect Healing via Heat-light Soaking*", J. Mater. Chem. A **12**, 7536 (2024).
- J.-J. Ma, Y.-T. Chueh, Y.-Y. Chen, Y.-H. Hsu, Y.-C. Liu, K.-S. Peng, C.-W. Hu, Y.-R. Lu, Y.-C. Shao, S.-H. Hsu, and S.-F. Hung*(洪嵩富), "*Robust iron-doped Nickel Phosphides in Membrane-electrode Assembly for Industrial Water Electrolysis*", Electrochim. Acta **500**, 144744 (2024).
- H. Sun, H.-C. Chen, M. Humayun, Y. Qiu, J. Ju, Y. Zhang, M. Bououdina, X. Xue, Q. Liu, Y. Pang, and C. Wang*(王春棟), "*Unlocking the Catalytic Potential of Platinum Single Atoms for Industry-level Current Density Chlorine Tolerance Hydrogen Generation*", Adv. Funct. Mater. **34**, 2408872 (2024).
- Y. Tezuka*(手塚泰久), H. Im, T. Watanabe, H. Ishii, N. Hiraoka, Y. Ishiwata, and H. Yamaoka, "*Pressure-dependent Electronic Structure of the A-site Ordered Perovskite $CaCu_3Ti_4O_{12}$ via X-ray Raman Scattering*", Phys. Rev. B **109**, 035132 (2024).
- H.-C. Tu, Y.-L. Hsiao, Y.-D. Lin, Y.-G. Lin, D.-L. Liao, and K.-S. Ho*(何國賢), "*Multi-functional Hydrogen- and Oxygen-capturing FeCo-N-C Catalyst with Improved Hydrogenation of Nitroarenes and ORR Activity*", Chem. Eng. J. **487**, 150623 (2024).
- M. Wang, G. Sun, J. Li, H.-C. Chen*(陳劾謙), B. Liu, Y. Chai, and Y. Pan* (潘原), "*Construction of Rh-N_4 Single Atoms and Rh Clusters Dual-active Sites for Synergistic Heterogeneous Hydroformylation of Olefins with Ultra-high Turnover Frequency*", Chem. Eng. J. **479**, 147505 (2024).
- M. Wang, C. Feng, W. Mi, M. Guo, Z. Guan, M. Li, H.-C. Chen*(陳劾謙), Y. Liu*(柳雲騏), and Y. Pan*(潘原), "*Defect-induced Electron Redistribution between Pt-N_3S_1 Single Atomic Sites and Pt Clusters for Synergistic Electrocatalytic Hydrogen Production with Ultra-high Mass Activity*", Adv. Funct. Mater. **34**, 2309474 (2024).
- X. Xu, L. Li, H.-C. Chen, X. Zhang, Y. Huang, M. Humayun, Y. A. Attia, Y. Pang, D. Wang, X. Wang*(王鑫), and C. Wang*(王春棟), "*Ru-enriched Metal-*

organic Framework Enabling a Self-powered Hydrogen Production System", ACS Catalysis **14**, 12051 (2024).

- X. Xu, H.-C. Chen, L. Li, M. Humayun, X. Zhang, H. Sun, J. Jia, C. Xu, M. Bououdina, L. Sun, X. Wang*(王鑫), and C. Wang*(王春棟), "*Understanding the Role of Oxygen Vacancy Defects in Iridium-leveraged MOFs-type Catalyst*", Adv. Funct. Mater. **34**, 2408823 (2024).
- H. Yamaoka*(山岡人志), A. Ohmura*(大村彩子), N. Tsujii, H. Ishii, N. Hiraoka, H. Sato, and M. Sawada, "*Pressure-induced Large Valence Transitions in Yb-Cu Binary Intermetallic Systems*", Phys. Rev. B **109**, 155147 (2024).
- H. Yamaoka*(山岡人志), Y. Michiue, Y. Yamamoto, N. Tsujii*(辻井直人), M. Arita, H. Sato, M. Sawada, H. Ishii, N. Hiraoka, and J. Mizuki, "*Valence Instability and Crystal Structures in $YbCu_xGa_{2-x}$ Studied by X-ray Absorption Spectroscopy and X-ray Diffraction*", Phys. Rev. B **110**, 205129 (2024).
- W.-T. Yang, L. C. Kao*(高立誠), X.-T. Yu, C.-L. Dong, and S. Y. H. Liou*(劉雅瑄), "*Mechanistic Insights into Temperature Hysteresis in CO Oxidation on Cu-TiO_2 Mesosphere*", Appl. Catal. B-Environ. **352**, 124017 (2024).
- W.-J. Zeng, J.-J. Ma, W.-Y. Huang, T.-J. Lee, Z.-Y. Lin, K.-S. Peng, N. Hiraoka, Y.-F. Liao, Y.-R. Lu, C.-W. Hu*(胡芝瑋), S.-H. Hsu*(徐韶徽), and S.-F. Hung*(洪崧富), "*Leveraging Bifunctional Phosphide-based Catalysts in a Membrane-electrode-assembly to Achieve Industrial Hydrogen Production*", Mater. Today Sustain. **27**, 100820 (2024).
- G. Zhang, Y. Lu, Y. Yang, H. Yang, Z. Yang, S. Wang, W. Li, Y. Sun, J. Huang, Y. Luo, H.-Y. Chen, Y.-F. Liao, H. Ishii, S. Gull, M. Shakouri, H.-G. Xue, Y. Hu, and H. Pang*(龐歡), "*Dynamic Phase Transformations of Prussian Blue Analogue Crystals in Hydrotherms*", J. Am. Chem. Soc. **146**, 16659 (2024).
- J. Zhang, F. Li, W. Liu, Q. Wang, X. Li, S.-F. Hung*(洪崧富), H. Yang*(楊鴻斌), and B. Liu*(劉彬), "*Modulating Spin of Atomic Manganese Center for High-performance Oxygen Reduction Reaction*", Angew. Chem. Int. Edit. **63**, e202412245 (2024).
- L. Zhang, H. Hu, C. Sun, D. Xiao, H.-T. Wang, Y. Xiao, S. Zhao, K. H. Chen, W.-X. Lin, Y.-C. Shao, X. Wang, C.-W. Pao, and L. Han*(韓麗麗), "*Bimetallic Nanoalloys Planted on Super-hydrophilic Carbon Nanocages Featuring Tip-intensified Hydrogen Evolution Electrocatalysis*", Nat. Commun. **15**, 7179 (2024).
- P. Zhang, H.-C. Chen, H. Zhu, K. Chen, T. Li, Y. Zhao, J. Li, R. Hu, S. Huang, W. Zhu, Y. Liu*(柳云騏), and Y. Pan*(潘原), "*Inter-site Structural Heterogeneity Induction of Single Atom Fe Catalysts for Robust Oxygen Reduction*", Nat. Commun. **15**, 2062 (2024).
- Z. Zhang, M. Ikeda, M. Utsumi, Y. Yamamoto, H. Goto, R. Eguchi, Y.-F. Liao, H. Ishii, Y. Takabayashi, K. Hayashi, R. Kondo, T. C. Kobayashi, and Y. Kubozono*(久保園芳博), "*Pressure Dependence of the Structural and Superconducting Properties of the Bi-based Superconductor $Bi_2Pd_3Se_2$*", Inorg. Chem. **63**, 2553 (2024).
- Z. Zhang, W. Pan, M. Utsumi, Y. Yamamoto, H. Goto, R. Kondo, T. Yokoya, R. Goban, T. Higashikawa, R. Eguchi, Y. Takabayashi, K. Hayashi, H. Ishii, T. C. Kobayashi, and Y. Kubozono*(久保園芳博), "*Structural and Superconducting Properties of $Bi_2Rh_3(Se_{1-x}S_x)_2$ (x=0–1.0)*", Inorg. Chem. **63**, 21531 (2024).
- S. Zhao, S.-F. Hung, L. Deng, W.-J. Zeng, T. Xiao, S. Li, C.-H. Kuo, H.-Y. Chen, F. Hu, and S. Peng*(彭生杰), "*Constructing Regulable Supports via Nonstoichiometric Engineering to Stabilize Ruthenium Nanoparticles for Enhanced pH-universal Water Splitting*", Nat. Commun. **15**, 2728 (2024).
- Yilin Zhao, H.-C. Chen, Xuelu Ma, Jiaye Li, Qing Yuan, Peng Zhang, Minmin Wang, Junxi Li, Min Li, Shifu Wang, Han Guo, Ruanbo Hu, K.-H. Tu, Wei Zhu, Xuning Li, Xuan Yang, and Yuan Pan*(潘原), "*Vacancy Defects Inductive Effect of Asymmetrically Coordinated Single-atom Fe-N_3S_1 Active Sites for Robust Electrocatalytic Oxygen Reduction with High Turnover Frequency and Mass Activity*", Adv. Mater. **36**, 2308243 (2024).

SP 12B2 BM – Protein X-ray Crystallography

- T.-J. Ye, K.-M. Fung, I.-M. Lee, T.-P. Ko, C.-Y. Lin, C.-L. Wong, I.-F. Tu, T.-Y. Huang, F.-L. Yang, Y.-P. Chang, J.-T. Wang, T.-L. Lin, K.-F. Huang*(黃開發), and S.-H. Wu*(吳世雄), "*Klebsiella Pneumoniae K2 Capsular Polysaccharide Degradation by a Bacteriophage Depolymerase Does Not Require Trimer Formation*", mBio **15**, 03519-23 (2024).

SP 12U1 U32 – Inelastic X-ray Scattering

- A. Bandyopadhyay*, S. Lee, D. T. Adroja*, G. B. G. Stenning, A. Berlie, M. R. Lees, R. A. Saha, D. Takegami, A. Meléndez-Sans, G. Poelchen, M. Yoshimura, K. D. Tsuei, Z. Hu, C.-W. Kao, Y.-C. Huang, T.-S. Chan, and K.-Y. Choi, "*Quantum Spin Liquid Ground State in the Trimer Rhodate $Ba_4NbRh_3O_{12}$*", Phys. Rev. B **109**, 184403 (2024).
- A. Bandyopadhyay*, S. Lee, D. T. Adroja, M. R. Lees, G. B. G. Stenning, P. Aich, L. Tortora, C. Meneghini, G. Cibin, A. Berlie, R. A. Saha, D. Takegami, A. Meléndez-Sans, G. Poelchen, M. Yoshimura, K. D. Tsuei, Z. Hu, T.-S. Chan, S. Chattopadhyay, G. S. Thakur, and K.-Y. Choi, "*Gapless Dynamic Magnetic Ground State in the Charge-gapped Trimer Iridate $Ba_4NbIr_3O_{12}$*", Phys. Rev. Mater. **8**, 074405 (2024).
- A. Beniwal, D. Bhalothia, Y.-R. Chen, J.-C. Kao, C. Yan, N. Hiraoka, H. Ishii, M. Cheng, Y.-C. Lo, X. Tu, Y.-W. Chiang, C.-H. Kuo, J.-P. Chou, C.-H. Wang, and T.-Y. Chen*(陳燦耀), "*Incorporation of Atomic Fe-oxide Triggers a Quantum Leap in the CO_2 Methanation Performance of Ni-hydroxide*", Chem. Eng. J. **493**, 152834 (2024).
- D. Bhalothia, C. Yan, N. Hiraoka, H. Ishii, Y.F. Liao, S. Dai, P.-C. Chen*(陳柏均), and T.-Y. Chen*(陳燦耀), "*Iridium Single Atoms to Nanoparticles: Nurturing the Local Synergy with Cobalt-oxide Supported Palladium Nanoparticles for Oxygen Reduction Reaction*", Adv. Sci. **11**, 2404076 (2024).
- C.-Y. Chang, W.-H. Huang, M.-C. Tsai, C.-W. Pao, M. Yoshimura, N. Hiraoka, C.-L. Chen*(陳啟亮), B. J. Hwang*(黃炳照), and W.-N. Su*(蘇威年), "*Turning Natural Copper Phthalocyanine into High-loading Single-atom Catalysts Using an Electrochemically-generated Template and Cationic Substitution*", Mater. Today Nano **25**, 100466 (2024).
- D. S. Christovam*, M. FFerreira-Carvalho, A. Marino, M. Sundermann, D. Takegami, A. Melendez-Sans, K. D. Tsuei, Z. Hu, S. Rößler, M. Valvidares, M. W. Haverkort, Y. Liu, E. D. Bauer, L. H. Tjeng, G. Zwicknagl, and A. Severing*, "*Spectroscopic Evidence of Kondo-induced Quasiquartet in $CeRh_2As_2$*", Phys. Rev. Lett. **132**, 046401 (2024).
- K. Fujinuma, D. Takegami*, T. Higo, A.-M. Sans, G. Poelchen, M. Yoshimura, K.-D. Tsuei, S. Nakatsuji, L. H. Tjeng, and T. Mizokawa, "*Bulk Mott Gap and S 3s/3p Spectral Distribution in Pyrite-type NiS_2 Revealed by Hard X-ray Photoemission Spectroscopy*", Phys. Rev. B **110**, 125136 (2024).
- H.-J. Huang, C.-S. Hsu, J.-Y. Huang, S.-C. Haw, H.-Y. Chen, N. Hiraoka, Y.-F. Liao*(廖彦發), and C.-W. Hu*(胡芝瑋), "*Electronic Structure Evolution upon Lithiation: A Li K-edge Study of Silicon Oxide Anode through X-ray Raman Spectroscopy*", J. Power Sources Adv. **29**, 100155 (2024).
- Y.-C. Kao, H.-K. Peng, S.-W. Hsiao, K.-A. Wu, C.-M. Liu, S.-Y. Zheng, Y.-H. Wu*(巫勇賢), and P.-J. Wu*(吳品鈞), "*Investigation of Annealing Temperature Dependent Sub-cycling Behavior for $HfZrO_x$-based Ferroelectric Capacitor*", APL Mater. **12**, 051118 (2024).
- R. Nakamura, D. Takegami, A. Melendez-Sans, L. H. Tjeng, T. Miyoshino, K. Iwamoto, W. Sekino, M. Yoshimura, K.-D. Tsuei, T. Katsufuji, and T. Mizokawa*(溝川貴司), "*Interplay Between Strongly Localized Eu 4f and Weakly Localized Nb 4d Electrons in $Eu_3Nb_5O_{15}$*", Phys. Rev. B **109**, 165148 (2024).
- R. Nakamura, D. Takegami, K. Fujinuma, M. Nakamura, M. Ferreira-Carvalho, A. Melendez-Sans, M. Yoshimura, K.-D. Tsuei, Y. Haraguchi, H. Aruga Katori, L. H. Tjeng*(莊鎏豪), and T. Mizokawa*(溝川貴司), "*Charge Fluctuations in a Cluster Mott State: Hard X-ray Photoemission Study on a Breathing Kagome Magnet Nb_3Cl_8*", Phys. Rev. B **110**, L081109 (2024).
- T. L. Nguyen, C.-C. Yang, C.-H. Wang, Y.-W. Yang, T. Mazet, E. Gaudry, D. Malterre, M. Yoshimura, Y. F. Liao, H. Ishii, N. Hiraoka, H. J. Lin, Y. C. Tseng, and A. Chainani*(查里), "*Crucial Role of d-d Coulomb Correlations in the Magnetocaloric Ferrimagnets $Gd_6(Mn_{1-x}M_x)_{23}$ (M=Fe, Co)*", Phys. Rev. B **109**, 035102 (2024).
- T. L. Nguyen, T. Mazet, F.-H. Chang, H.-J. Lin, C.-T. Chen, and A. Chainani*(查里), "*Ligand Field Calculations for Element-specific Spectroscopy of Rare Earth-transition Metal Ferrimagnetic Alloys*", J. Phys. Soc. JPN. **93**, 121006 (2024).
- M. Stavinoha, C.-L. Huang, W. A. Phelan, A. M. Hallas, V. Loganathan, M. Michiardi, J. Falke, S. Zhdanovich, D. Takegami, C.-E. Liu, K. D. Tsuei, C. T. Chen, L. Qian, N. J. Ng, J. W. Lynn, Q. Huang, F. Weickert, V. Zapf, K. R. Larsen, P. D. Sparks, J. C. Eckert, A. B. Puthirath, H.-H. Kung, T. M. Pedersen, S. Gorovikov, A. Damascelli, L. H. Tjeng, C. Hooley, A. H. Nevidomskyy, and E. Morosan, "*Conductive Surface States and Kondo Exhaustion in Insulating $YbIr_3Si_7$*", Phys. Rev. B **109**, 035112 (2024).
- D. Takegami*, K. Fujinuma, R. Nakamura, M. Yoshimura, K.-D. Tsuei, G. Wang, N. N. Wang, J.-G. Cheng, Y. Uwatoko, and T. Mizokawa, "*Absence of Ni^{2+}/Ni^{3+} Charge Disproportionation and Possible Roles of O 2p Holes in $La_3Ni_2O_{7-\delta}$ Revealed by Hard X-ray Photoemission Spectroscopy*", Phys. Rev. B **109**, 125119 (2024).
- D. Takegami*, K. Fujinuma, R. Nakamura, M. Yoshimura, K.-D. Tsuei, N. L. Saini, Zhiwei Wang, J.-X. Yin, and T. Mizokawa, "*Bulk Electronic Structure of AV_3Sb_5 (A=K, Cs) Studied by Hard X-ray Photoemission Spectroscopy: Possibility of Bond Order without Charge Disproportionation*", Phys. Rev. B **109**, 155108 (2024).
- D. Takegami*, M. Nakamura, A.-M. Sans, K. Fujinuma, R. Nakamura, M.

Yoshimura, K.-D. Tsuei, A. Tanaka, M. Gen, Y. Tokunaga, S. Ishiwata, and T. Mizokawa, "*Negative Charge-transfer Energy in $SrFeO_3$ Revisited with Hard X-ray Photoemission Spectroscopy*", Phys. Rev. B **109**, 235138 (2024).
- Y. Tezuka*(手塚泰久), H. Im, T. Watanabe, H. Ishii, N. Hiraoka, Y. Ishiwata, and H. Yamaoka, "*Pressure-dependent Electronic Structure of the A-site Ordered Perovskite $CaCu_3Ti_4O_{12}$ via X-ray Raman Scattering*", Phys. Rev. B **109**, 035132 (2024).
- H. Yamaoka*(山岡人志), A. Ohmura*(大村彩子), N. Tsujii, H. Ishii, N. Hiraoka, H. Sato, and M. Sawada, "*Pressure-induced Large Valence Transitions in Yb-Cu Binary Intermetallic Systems*", Phys. Rev. B **109**, 155147 (2024).
- H. Yamaoka*(山岡人志), Y. Michiue, Y. Yamamoto, N. Tsujii*(辻井直人), M. Arita, H. Sato, M. Sawada, H. Ishii, N. Hiraoka, and J. Mizuki, "*Valence Instability and Crystal Structures in $YbCu_xGa_{2-x}$ Studied by X-ray Absorption Spectroscopy and X-ray Diffraction*", Phys. Rev. B **110**, 205129 (2024).
- W.-J. Zeng, J.-J. Ma, W.-Y. Huang, T.-J. Lee, Z.-Y. Lin, K.-S. Peng, N. Hiraoka, Y.-F. Liao, Y.-R. Lu, C.-W. Hu*(胡芝瑋), S.-H. Hsu*(徐韶徽), and S.-F. Hung*(洪崧富), "*Leveraging Bifunctional Phosphide-based Catalysts in a Membrane-electrode-assembly to Achieve Industrial Hydrogen Production*", Mater. Today Sustain. **27**, 100820 (2024).

SP 44XU U32 – Macromolecular Assemblies (International Collaboration)

- H.-H. Chang, L.-C. Lee, Tsu Hsu, Y.-H. Peng, C.-H. Huang, T.-K. Yeh, C.-T. Lu, Z.-T. Huang, C.-C. Hsueh, F.-C. Kung, L.-M. Lin, Y.-C. Huang, Y.-H. Wang, L.-H. Li, Y.-C. Tang, L. Chang, C.-C. Hsieh, W.-T. Jiaang*(蔣維棠), C.-C. Kuo*(郭靜娟), and S.-Y. Wu*(伍素瑩), "*Development of Potent and Selective Inhibitors of Methylenetetrahydrofolate Dehydrogenase 2 for Targeting Acute Myeloid Leukemia: SAR, Structural Insights, and Biological Characterization*", J. Med. Chem. **67**, 21106 (2024).
- Y.-C. Hsieh, H.-H. Guan, C.-C. Lin, T.-Y. Huang, P. Chuankhayan, N.-C. Chen, N.-H. Wang, P.-L. Hu, Y.-C. Tsai, Y.-C. Huang, M. Yoshimura, P.-J. Lin, Y.-H. Hsieh*(謝義簧), and C.-J. Chen*(陳俊榮), "*Structure-based High-efficiency Homogeneous Antibody Platform by Endoglycosidase Sz Provides Insights into Its Transglycosylation Mechanism*", JACS Au **4**, 2130 (2024).

Beamline/Endstation Instrumentation

- C.-H. Chiang, C.-K. Chou, C.-C. Tseng, Y.-H. Chen, Y.-C. Liu, C.-Y. Huang, C.-H. Chao, and C.-H. Huang*(黃駿翔), "*Biopharmaceutical Beamline TLS 15A1 for Macromolecular Crystallography at the National Synchrotron Radiation Research Center*", J. Chin. Chem. Soc. **71**, 721 (2024).

Accelerator Facility

- F.-Y. Chang*(張富毓), Z.-K. Liu, M.-S. Yeh, C.-H. Lo, F.-T. Chung, L.-J. Chen, M.-H. Chang, M.-C. Lin, S.-W. Chang, Y.-T. Li, and C. Wang, "*Tuner Loop Based on FPGA for PETRA Cavity at TPS Booster Ring*", J. Phys.-Conf. Ser. **2687**, 072035 (2024).
- J. C. Chang*(張瑞麒), T. Y. Hsieh, and W. S. Chan, "*Numerical Analysis on a modified Air Conditioning System of the Experimental Hall at TPS*", International Particle Accelerator Conference (IPAC), 3861 Nashville,USA (2024).
- J.-C. Chang*(張瑞麒) and W.-S. Chan, "*Numerical Analysis on the Air Conditioning System of the Experimental Hall at TPS*", J. Phys.-Conf. Ser. **2687**, 022024 (2024).
- M. H. Chang*(張美霞), C. H. Lo, T. C. Yu, Z. K. Liu, F. T. Chung, F. Y. Chang, S. W. Chang, L. J. Chen, Y. T. Li, M. S. Yeh, C. Wang, and M. C. Lin, "*Status and Upgrades of Radio Frequency System at Taiwan Photon Source*", J. Phys.-Conf. Ser. **2687**, 082008 (2024).
- B. Y. Chen*(陳伯毅), C. C. Chang, C. K. Chan, Y. C. Yang, W. Y. Lai, C. M. Cheng, C. Shueh, and J. H. Kang, "*Modification of TPS Arc-Cell Vacuum System for Installation of EPU66*", International Particle Accelerator Conference (IPAC), 1572 Nashville,USA (2024).
- C. W. Chen*(陳智偉), C. S. Yang, H. Chen, C. K. Yang, and J. C. Huang, "*Integrated Hall Probe and Stretched Wire Measurement System for an In-vacuum Undulator*", International Particle Accelerator Conference (IPAC), 1398 Nashville,USA (2024).
- C.-W. Chen*(陳智偉), C.-H. Chang, H. Chen, Y.-L. Chu, F.-Y. Lin, C.-K. Yang, and J.-C. Huang, "*Pulsed Wire Magnetic-field Measurement System on Permanent Magnet Quadrupoles*", IEEE T. Appl. Supercon. **34**, 9001704 (2024).
- J. Chen*(陳秀珍), C. Y. Liao, C. Y. Wu, Y. S. Cheng, J. K. Liao, K. T. Hsu, and K. H. Hu, "*New Injection Controls Environment for the Taiwan Light Source*", J. Phys.-Conf. Ser. **2687**, 072024 (2024).
- C. M. Cheng*(鄭家沐), Y. T. Cheng, Y. C. Liu, B. Y. Chen, C. Shueh, Y. C. Yang, C. C. Chang, and C. K. Chan, "*The Status of the X-ray Beam Positon Monitor in the TPS Front End*", International Particle Accelerator Conference (IPAC), 1327 Nashville, USA (2024).
- Y. S. Cheng, S. H. Lee*(李淑華), C. Y. Wu, C. Y. Liao, J. K. Liao, J. Chen, K. H. Hu, and K. T. Hsu, "*New Digital Low-level RF Controls Based on the Red Pitaya Stemlab for the TLS Linac System*", J. Phys.-Conf. Ser. **2687**, 072023 (2024).
- C.-W. Chiang, M.-C. Chou, A.-P. Lee, Y.-Q. Wang, J.-J. Wang, M.-W. Lin, W.-K. Lau, and S.-W. Chou*(周紹暐), "*Cross-facility Absolute Charge Calibration of Scintillating Screens for Laser Wakefield Accelerated Beam Diagnostics*", Rev. Sci. Instrum. **95**, 123306 (2024).
- M. S. Chiu*(邱茂森), F. H. Tseng, H. W. Luo, N. Y. Huang, H. J. Tsai, T. Y. Lee, W. Y. Lin, T. W. Hsu, B. Y. Huang, C. Y. Hung, and P. J. Chou, "*Tune Feedback System in the Taiwan Photon Source*", International Particle Accelerator Conference (IPAC), 3258 Nashville, USA (2024).
- P. C. Chiu*(邱斐珍), C. H. Huang, C. Y. Wu, K. T. Hsu, J. Chen, D. Lee, Y. S. Cheng, C. Y. Liao, and K. H. Hu, "*TLS Fast Orbit Feedback Upgrade*", J. Phys.-Conf. Ser. **2687**, 072012 (2024).
- P. C. Chiu*(邱斐珍), C. H. Huang, C. Y. Wu, K. T. Hsu, C. Y. Liao, Y. S. Cheng, and K. H. Hu, "*TPS Fast Orbit Feedback Upgrade*", J. Phys.-Conf. Ser. **2687**, 072013 (2024).
- Y. L. Chu*(朱耘諒), Y. Y. Hsu, J. C. Jan, H. Chen, C. K. Yang, C. W. Chen, C. S. Yang, and J. C. Huang, "*Design of Permanent Dipole Magnet in TPS Transport Line*", International Particle Accelerator Conference (IPAC), 1537 Nashville, USA (2024).
- T.-Y. Chung*(鍾廷翊), C.-H. Chang, H. Chen, H.-H. Chen, and C.-S. Hwang, "*From Design and Construction to Operation of the APPLE Undulator at TPS*", J. Instrum. **19**, P03004 (2024).
- G. Y. Hsiung*(熊高鈺), C. M. Cheng, and R. Valizadeh, "*Measurement of the Photoelectron Yield from the Synchrotron Radiation for the NEG-coated Tubes*", J. Phys.-Conf. Ser. **2687**, 082027 (2024).
- G.-Y. Hsiung*(熊高鈺), Y.-C. Yang, F.-Y. Chang, C.-C. Chang, and C.-K. Chan, "*Setup of Goubau Line System for Impedance-measurement of Vacuum Components at the NSRRC* ", International Particle Accelerator Conference (IPAC), 1578 Nashville, USA (2024).
- K.-H. Hsu*(許耿豪), C.-K. Kuan, C.-S. Huang, H.-C. Ho, and W.-Y. Lai, "*Assembly Process and Inspection Results for W100*", International Particle Accelerator Conference (IPAC), 3788 Nashville, USA (2024).
- C. H. Huang*(黃至賢), K. T. Hsu, K. H. Hu, P. C. Chiu, J. Chen, D. Lee, J. K. Liao, and Y. S. Cheng, "*The Study of Single Bunch Instability at the Taiwan Photon Source*", International Particle Accelerator Conference (IPAC), 2371 Nashville, USA (2024).
- C. S. Huang*(黃春憲), W. Y. Lai, B. Y. Chen, C. J. Lin, C. K. Kuan, and T. C. Tseng, "*Improving the Uniformity of Magnetron Sputtering Titanium Film for Nonlinear Injection Kicker*", International Particle Accelerator Conference (IPAC), 3791 Nashville, USA (2024).
- C.-H. Huang, F.-T. Chung*(鍾福財), F.-Y. Chang, M.-S. Yeh, L.-J. Chen, Z.-K. Liu, M.-H. Chang, C.-H. Lo, Y.-T. Li, S.-W. Chang, C. Wang, and M.-C. Lin, "*Development of a Quality Test Platform for Solid-state Power Amplifiers in NSRRC*", International Particle Accelerator Conference (IPAC), 3707 Nashville, USA (2024).
- C.-H. Huang*(黃至賢), K.-T. Hsu, C.-Y. Liao, P.-C. Chiu, Y.-S. Cheng, J.-K. Liao, and K.-H. Hu, "*Bunch-by-bunch Transverse Position Measurement during Injection*", J. Phys.-Conf. Ser. **2687**, 072014 (2024).
- J.-C. Huang*(黃睿哲), C.-S. Yang, P.-S. Chuang, and C.-L. Chen, "*Cryogenic Permanent Magnet Undulator at High Beam Currents*", International Particle Accelerator Conference (IPAC), 3794 Nashville, USA (2024).
- J.-C. Huang*(黃睿哲), H. Kitamura, C.-S. Yang, C.-K. Yang, C.-W. Chen, and Y.-C. Chuang, "*Performance Investigation of Conduction-cooled Cryogenic Permanent Magnet Undulator at High Beam Currents*", Phys. Rev. Accel. Beams **27**, 023501 (2024).
- N. Y. Huang*(黃暖雅), M. S. Chiu, H. W. Luo, P. J. Chou, G. H. Luo, F. H. Tseng, and H. J. Tsai, "*Study of an Upgraded Lattice for Taiwan Photon Source*", International Particle Accelerator Conference (IPAC), 1324 Nashville, USA (2024).
- J. C. Jan*(詹智全), C. C. Tsai, C. Y. Wang, and F. Y. Lin, "*Design of 2G High-temperature Superconducting Undulator Structure and Winding Method*", IEEE T. Appl. Supercon. **34**, 4100604 (2024).
- J. C. Jan*(詹智全), F. Y. Lin, Y. L. Chu, C. K. Yang, and J. C. Huang, "*Optimizing the Magnetic Circuit of HTSU Through REBCO Tape Selection*", International Particle Accelerator Conference (IPAC), 2895 Nashville, USA (2024).
- S. P. Kao*(高小萍), Y. C. Lin, and P. J. Wen, "*Cryogenic Oxygen Deficiency Hazard Assessment at the National Synchrotron Radiation Research Center*", J.

Phys.-Conf. Ser. **2687**, 092011 (2024).
- C.-Y. Kuo, T.-Y. Chung*(鍾廷翊), C.-H. Chang, and C.-H. Chang, "*Experimental Verification of a Permanent Undulator for a Strong Helical Field*", IEEE T. Electron Dev. **71**, 5686 (2024).
- W.-Y. Lai*(賴惟揚), H.-S. Wang, K.-H. Hsu, C.-J. Lin, C.-S. Huang, D.-G. Huang, T.-C. Tseng, and C.-K. Kuan, "*Design and Fabrication of the Automation System in TLS BL07A End Station*", International Particle Accelerator Conference (IPAC), 3785 Nashville, USA (2024).
- C. Y. Liao*(廖志裕), C. Y. Wu, Y. S. Cheng, J. Chen, D. Lee, K. H. Hu, and K. T. Hsu, "*New Controls for White Circuits Power Supplies for the Booster Synchrotron of Taiwan Light Source*", J. Phys.-Conf. Ser. **2687**, 072021 (2024).
- J. K. Liao*(廖晉坤), D. Lee, Y. S. Cheng, C. Y. Wu, K. H. Hu, and K. T. Hsu, "*Novel Clock and Trigger Solutions with Ultra-high Precision Delay to Support Time-resolved Experiments at TPS*", International Particle Accelerator Conference (IPAC), 3305 Nashville, USA (2024).
- J. K. Liao, D. Lee*(李淑華), Y. S. Cheng, C. Y. Wu, K. H. Hu, and K. T. Hsu, "*Development of a New Control Interface for the Electron Gun Pulser of TLS Linac*", J. Phys.-Conf. Ser. **2687**, 072022 (2024).
- J. K. Liao*(廖晉坤), Y. S. Cheng, L. P. Hsu, J. Chen, K. H. Hu, and K. T. Hsu, "*Implementation and Performance Estimation of New Archive System for the TLS Control System*", J. Phys.-Conf. Ser. **2687**, 072020 (2024).
- S. Y. Lin*(林思妤), P. J. Wen, and J. C. Liu, "*Information Display Board System to Enhance Safety Management at the National Synchrotron Radiation Research Center*", International Particle Accelerator Conference (IPAC), 3701 Nashville, USA (2024).
- W. Y. Lin*(林威佑), H. J. Tsai, T. Y. Hsu, T. Y. Lee, C. Y. Hung, and B. Y. Huang, "*TPS Booster Power Supply Performance Experiment and Monitoring Program*", International Particle Accelerator Conference (IPAC), 3261 Nashville, USA (2024).
- Y. C. Lin*(林郁堉), P. J. Wen, C. R. Chen, and A. Y. Chen, "*Assessment of the Ratios of Radiation Sources and Total Electron Loss at the Injection Section of the Taiwan Photon Source Facility and Total Electron Loss by Using Neutron Measurements*", International Particle Accelerator Conference (IPAC), 3359 Nashville, USA (2024).
- Y.-J. Lin*(林揚蓁), M.-C. Chou, W.-Y. Chiang, W.-K. Lau, and A.-P. Lee, "*Dark Current Reduction for NSRRC Photoinjector System by Collimator*", International Particle Accelerator Conference (IPAC), 2112 Nashville, USA (2024).
- C.-Y. Liu*(柳振堯), B.-S. Wang, Y.-S. Wong, J.-C. Huang, and K.-B. Liu, "*Analysis of the Bi-bridge Topology and Power Device Circuit of the TPS Booster Dipole Power Supply*", J. Phys.-Conf. Ser. **2687**, 082020 (2024).
- Z.-K. Liu*(劉宗凱), F.-Y. Chang, M.-H. Chang, S.-W. Chang, L.-J. Chen, F.-T. Chung, C.-H. Huang, Y.-T. Li, M.-C. Lin, C.-H. Lo, C. Wang, and M.-S. Yeh, "*Operation of TPS 300 kW Solid-state Amplifier*", International Particle Accelerator Conference (IPAC), 1492 Nashville, USA (2024).
- H.-W. Luo*(羅皓文), M.-S. Chiu, N.-Y. Huang, and P.-J. Chou, "*Evaluation of Top-up Injection by a Single Nonlinear Kicker in Taiwan Photon Source*", International Particle Accelerator Conference (IPAC), 3254 Nashville, USA (2024).
- C. Shueh*(薛秦), Y. T. Cheng, J. Y. Chuang, C. K. Chan, C. C. Chang, C. M. Cheng, I. T. Huang, and Y. C. Yang, "*Investigation of Reduced Baking Time on Dynamic Pressure in a Taiwan Photon Source Front End System*", International Particle Accelerator Conference (IPAC), 1575 Nashville, USA (2024).
- H. H. Tsai*(蔡黃修), F. Z. Hsiao, P. S. Chuang, H. C. Li, W. R. Liao, W. S. Chiou, and S. H. Chang, "*The Study and Improvement of Pressure Degradation of Helium Cryogenic System at NSRRC*", IOP Conf. Series: Materials Science and Engineering, **1301**, 012122 Honolulu, USA (2024).
- B. Wang*(王寶勝), K. Liu, Y. Wong, and C. Liu, "*Develop an Automated Data Acquisition System for TPS Correction Magnet Power Supply*", J. Instrum. **19**, T03001 (2024).
- B. Wang*(王寶勝), K. Liu, and Y. Wong, "*Development of Bipolar High-current Correction Magnet Power Supply for TPS Facility*", J. Instrum. **19**, T05004 (2024).
- B. S. Wang*(王寶勝), Kuobin Liu, and Yongseng Wong, "*Realization of Modularized Corrector Magnet Power Supply with N+1 Redundancy for TPS Facilities*", J. Instrum. **19**, T07007 (2024).
- B. S. Wang*(王寶勝), K. B. Liu, and Y. S. Wong, "*Development of Linear Power Operational Amplifier for TPS Correction Magnet Power Supply*", International Particle Accelerator Conference (IPAC), 3742 Nashville, USA (2024).
- B. S. Wang*(王寶勝), K. B. Liu, and Y. S. Wong, "*Development of High-current Correction Magnet Power Supply for TPS Facilities*", International Particle Accelerator Conference (IPAC), 3745 Nashville, USA (2024).
- B.-S. Wang*(王寶勝), K.-B. Liu, C.-Y. Liu, and Y.-S. Wong, "*Optimization stability and performance of the TPS storage ring dipole magnet power supply*", J. Instrum. **19**, T05015 (2024).
- P. J. Wen*(溫博鈞), Y. C. Lin, S. Y. Lin, and M. H. Chang, "*Electrical Fire Safety Assessment of the Synchrotron Accelerator Experimental Station in NSRRC*", International Particle Accelerator Conference (IPAC), 3704 Nashville, USA (2024).
- P. J. Wen*(溫博鈞), Y. C. Lin, S. Y. Lin, and M. H. Chang, "*Measurement of Ozone Concentration at the BL-02A Beamline Hutch in the Taiwan Photon Source for Ensuring Personnel Safety*", International Particle Accelerator Conference (IPAC), 3758 Nashville, USA (2024).
- P. J. Wen*(溫博鈞), S. P. Kao, Y. C. Lin, S. Y. Lin, and M. H. Chang, "*Respiratory Protective Equipment Fit Tests for Researchers at the National Synchrotron Radiation Research Center*", J. Phys.-Conf. Ser. **2687**, 092010 (2024).
- Y.-S. Wong*(黃永信), K.-B. Liu, C.-Y. Liu, B.-S. Wang, and J.-C. Huang, "*A Novel Generation Design Dipole Magnet Power Supply of Booster to Storage Ring Transport Line in NSRRC*", J. Instrum. **19**, T06001 (2024).
- C. Y. Wu, C. Y. Liao(廖志裕)*J. Chen, D. Lee, Y. S. Cheng, K. H. Hu, and K. T. Hsu, "*New Event Based Timing System for the Taiwan Light Source*", J. Phys.-Conf. Ser. **2687**, 072033 (2024).
- C.-Y. Wu, C.-Y. Liao*(廖志裕), J. Chen, D. Lee, Y.-S. Cheng, K.-H. Hu, K.-T. Hsu, and C.-K. Yang, "*Control System for a Cryogenic Permanent Magnet Undulator With Taper Option at the Taiwan Photon Source*", IEEE T. Appl. Supercon. **34**, 4100405 (2024).
- Z. Q. Wu*(吳子琦), C. Y. Liao, C. Y. Wu, and J. K. Liao, "*Implementation of EPU56 Control System at the Taiwan Photon Source*", International Particle Accelerator Conference (IPAC), 3301 Nashville, USA (2024).
- C. K. Yang*(楊謹綱), F. Y. Lin, H. Chen, H. H. Chen, and Y. L. Chu, "*Development of a Non-linear Injection Kicker for the TPS Storage Ring*", International Particle Accelerator Conference (IPAC), 3264 Nashville, USA (2024).
- C.-K. Yang*(楊謹綱), C.-H. Chang, C.-W. Chen, F.-Y. Lin, J.-C. Jan, and J.-C. Huang, "*Development of Permanent Magnet Quadrupoles at NSRRC*", IEEE T. Appl. Supercon. **34**, 4001005 (2024).

Others

(Publications of the underlined author(s) affiliated with the NSRRC but not using the NSRRC facilities listed above)

- Y.-J. Chen*, T.-H. Chuang, J.-P. Hanke, Y. Mokrousov, S. Blugel, C. M. Schneider, and C. Tusche*, "*Magnons in a Two-dimensional Weyl Magnet*", Appl. Phys. Lett. **124**, 093105 (2024).
- A. Fujimori, "*Ligand Field and Charge Transfer in Transition-metal Compounds*", J. Phys. Soc. JPN. **93**, 121002 (2024).
- Y.-S. Hsiao, L.-Y. Weng, T.-H. Cheng, T.-Y. Huang, Y.-J. Wu, J.-H. Huang, N.-J. Wu, S.-C. Hsu*(許世杰), H. C. Weng*(翁輝竹), and C.-P. Chen*(陳志平), "*Construction of Core-shell $TiNb_2O_7$/$Li_4Ti_5O_{12}$ Composites with Improved Lithium Storage for Lithium-ion Batteries*", J. Energy Storage **77**, 109860 (2024).
- B. Hsieh, L.-C. Wu, and Arnaud Grosjean*(葛阿諾), "*FleX: a Computer Vision Program to Evaluate Strain in Flexible Crystals*", J. Appl. Crystallogr. **57**, 552 (2024).
- C.-K. Hu, J.-X. Lin, H.-A. Liu, W.-H. Chang, W.-B. Wu, J.-S. Lee, C.-R. Lin, S. Mangin, J. Chen*(陳駿), and H.-S. Hsu*(許華書), "*Manipulation of Energy-resolved Magneto-optical Effect in Yttrium Iron Garnet Films Achieved by Covering with Nonmagnetic Metals*", Chinese J. Phys. **90**, 717 (2024).
- M. D.-S. Hua, S. K. Rajendran, K.-W. Yeh, and C.-H. Yeh*(葉靖輝), "*Transcriptional Regulation of BZR1/PIF4 is Involved in High Temperature-induced early Fowering Process in Oncidium Grower Ramsay*", Plant Growth Regul. **104**, 1133 (2024).
- H. Ito*, R. Watanabe, T. Saito, K. Makino, H.-K. Wei, C.-W. Luo, K. Misawa, and S. Honma, "*Modulation and Real-time Monitoring of the Carrier-envelope Phase of Terahertz Pulses Based on Shaping of Near-infrared Femtosecond Pulses*", Opt. Lett. **49**, 5055 (2024).
- B. Jeevanantham, M. K. Shobana*, W.-N. Su*(蘇威年), and B. J. Hwang*(黃炳照), "*Surface Engineering of $TiSiO_4$ Nano-coating for High-voltage Nickel-rich Ternary Cathodes: An Approach to Improve Cyclic Performance*", J. Energy Storage **100**, 113546 (2024).
- B. Jeevanantham, M. K. Shobana*, Shadab Ali Ahmed, Y.-P. Fu, W.-N. Su*(蘇威年), and B. J. Hwang*(黃炳照), "*Improving High-voltage Cycling and Stabilizing the Electrode-electrolyte Interface of Nickel-rich Layered Cathodes by Magnesium Doping*", J. Phys. Chem. Solids **195**, 112296 (2024).
- A. Karthika, N. Hemavathy, M. Amala, S. Rajamanikandan, M. Veerapandian, D. Prabhu, U. Vetrivel, C. J. Chen, C. J. Pandian, and J. Jeyakanthan*, "*Structural and Functional Characterization of 6-phosphogluconate Dehydrogenase in Plasmodium Falciparum (3D7) and Identification of Its*

Potent Inhibitors", J. Biomol. Struct. Dyn. **42**, 2058 (2024).

- P. H. Le*, L. T. C. Tuyen, N. N. Quyen, C.-W. Luo*(羅志偉), J.-Y. Lin, and J. Leu*(呂志鵬), "*Weak Antilocalization and Gigahertz Acoustic Phonons in Bi_2Se_2Te and Bi_3Se_2Te-dominated Thin Films Grown Using Pulsed Laser Deposition*", Thin Solid Films **791**, 140241 (2024).
- P. H. Le*, L. T. C. Tuyen, N. N. Quyen, S.-R. Jian*(簡勝瑞), J.-W. Lee, C.-W. Luo*(羅志偉), J.-Y. Juang, and J.-Y. Lin, "*Thickness-dependent Magnetotransport and Ultrafast Dynamic Properties of Epitaxial Bi_2Se_3/InP(111) Thin Films Grown Using Pulsed Laser Deposition*", Chinese J. Phys. **91**, 857 (2024).
- P. T. Leung, C.-W. Chen, and H.-P. Chiang*(江海邦), "*Electric Response of a Composite of Topological Insulator Nanoparticles*", Chinese J. Phys. **89**, 1883 (2024).
- K.-Y. Lin, R.-T. Kuo, T. Miyazaki, B. J. Hwang, and J.-C. Jiang*(江志強), "*Unveiling Dendrite-suppressing Potential of Alkali Metal-based Alloys in Lithium Metal Batteries*", J. Energy Storage **88**, 111674 (2024).
- Benjamin Martinez, C.-H. Kuo*(郭俊宏), and M.-H. Chiang*(江明錫), "*Spray-pyrolysis Synthesis of $CuMnO_2$ with the Potential for Photoelectrocatalysis*", J. Chin. Chem. Soc. **71**, 1203 (2024).
- A. Mathimaran, H. Nagarajan, A. Mathimaran, Y.-C. Huang, C.-J. Chen, U. Vetrivel, and J. Jeyaraman*, "*Deciphering the pH-dependent Oligomerization of Aspartate Semialdehyde Dehydrogenase from Wolbachia Endosymbiont of Brugia Malayi: An in Vitro and in Silico Approaches*", Int. J. Biol. Macromol. **276**, 133977 (2024).
- E. A. Moges, K. Lakshmanan, C.-Y. Chang, W.-S. Liao, F. T. Angerasa, W. B. Dilebo, H. G. Edao, K. T. Tadele, D. D. Alemayehu, B. D. Bejena, C. B. Guta, C.-C. Chang, M.-C. Tsai, W.-N. Su*(蘇威年), and B. J. Hwang*(黃炳照), "*Materials of Value-added Electrolysis for Green Hydrogen Production*", ACS Mater. Lett. **6**, 4932 (2024).
- B. N. Olana, S.-H. Pan, B.-J. Hwang, H. Althues, J.-C. Jiang, and S. D. Lin*(林昇佃), "*Understanding the Formation Chemistry of Native Solid Electrolyte Interphase Over Lithium Anode and Its Implications Using a LiTFSI/TME-TTE Electrolyte and Polysulfide Additive*", J. Mater. Chem. A **12**, 3659 (2024).
- A. S. Rasal*, H. M. Chen*(陳浩銘), and W.-Y. Yu*(游文岳), "*Electronic Structure Engineering of Electrocatalyst for Efficient Urea Oxidation Reaction*", Nano Energy **121**, 109183 (2024).
- G. Vashisht*, A. C. Gandhi, V. Kumar, A. J. Mathew, C.-L. Dong, C.-L. Chen, K. Asokan, S. Y. Wu, Y. Fukuma, and S. Annapoorni, "*Peculiar Spin Glass Phase Emerging in FeCo/FePt Driven via Nanoconfined Crystallographic Distortions*", J. Phys. D- Appl. Phys. **57**, 465304 (2024).
- L.-T. Wu, Y.-T. Zhan, Z.-L. Li, P.-T. Chen, B. J. Hwang, and J.-C. Jiang*(江志強), "*Rational Electrolyte Design for Li-metal Batteries Operated under Extreme Conditions: a Combined DFT, COSMO-RS, and Machine Learning Study*", J. Mater. Chem. A **12**, 15792 (2024).
- Y.-C. Wu, T. Liu, C.-N. Liu, C.-Y. Kuo, Y.-H. Ting, C.-A. Wu, X.-L. Shen, H.-C. Wang, C.-J. Chen, P. P. Renta, Y.-L. Chen, M.-C. Hung, and Y.-M. Chen*(陳逸民), "*Transcriptional, Post-transcriptional, and Post-translational Regulation of Polyunsaturated Fatty Acid Synthase Genes in Aurantiochytrium limacinum Strain BL10: Responses to Nitrogen Starvation*", Int. J. Biol. Macromol. **274**, 133177 (2024).
- Y.-S. Hsiao, Y.-T. Lin, Y.-L. Chen, H.-S. Tseng, T.-Y. Huang, N.-J. Wu, J.-H. Huang, H.-C. Weng*(翁輝竹), S.-C. Hsu*(許世杰), T.-H. Cheng, and C.-P. Chen*(陳志平), "*Gold-decorated Laser-induced Graphene for Wearable Biosensing and Joule Heating Applications*", J. Taiwan Inst. Chem. Eng. **154**, 104979 (2024).

Neutron Project

(Supported by the NSRRC and NSTC 113-2112-M-213-010 "Cultivation and Promotion of Taiwan Neutron Research at ANSTO")

- S. S. Dwitya, K.-S. Lin*(林錕松), M.-T. Weng*(翁孟慈), N. V. Mdlovu, W.-C. Tsai, and C.-M. Wu, "*Synthesis and Characterization of pH-triggered Doxorubicin-conjugated Polydopamine-coated Cobalt Ferrite Nanoparticles for In-vitro/In-vivo Studies in Liver Cancer Therapy*", J. Ind. Eng. Chem. **129**, 499 (2024).
- H. Y. Hao, W. Q. Wang*(王文全), W. D. Hutchison, J. Y. Li, C. W. Wang, Q. F. Gu, S. J. Campbell, Z. X. Cheng*(程振祥), and J. L. Wang*(王建立), "*Enhanced Magnetocaloric Effect Accompanying Successive Magnetic Transitions in $TbMn_2Si_{2-x}Ge$ Compounds*", J. Magn. Magn. Mater. **590**, 171654 (2024).
- P. Athira, A. Tiwari, M.-J. Hsieh, J.-Y. Lin, N. Puri, C. W. Wang, C. H. Prashanth, C. Dhanasekhar, C. L. Huang, H.D. Yang*(楊弘敦), K. Jyothinagaram*, and D. C. Kakarla*, "*Hidden Magnetism, Nonlinear Magnetodielectric Coupling, and Large Multicaloric Effect in Multiferroic L-type $Fe_2(MoO_4)_3$*", Phys. Rev. Appl. **21**, 054025 (2024).
- H. Chae, E.-W. Huang*(黃爾文), J. Jain, D.-H. Lee, S. Harjo, T. Kawasaki, and S. Y. Lee*, "*Mechanical Stability of Retained Austenite and Texture Evolution in Additively Manufactured Stainless Steel*", Met. Mater. Int. **30**, 1321 (2024).
- Y. H. Chang, A. Pal*, P. T. W. Yen, C. W. Wang, S. Giri, G. R. Blake, J. Gainza, M.-J. Hsieh, J.-Y. Lin, C. Y. Huang, Y. J. Chen, T. W. Kuo, A. Tiwari, D. C. Kakarla, and H. D. Yang*(楊弘敦), "*Field-induced Transformation of Complex Spin Ordering and Magnetodielectric and Magnetoelastic Coupling in $MnGeTeO_6$*", Phys. Rev. B **110**, 064405 (2024).
- R. Curvello, V. S. Raghuwanshi, C.-M. Wu, J. Mata, and G. Garnier*, "*Nano- and Microstructures of Collagen-nanocellulose Hydrogels as Engineered Extracellular Matrices*", ACS Appl. Mater. Interfaces **16**, 1370 (2024).
- F. Gao, W. Ren*(任衛軍), C.-W. Wang*(王進威), S. Yano, S. Calder, Q. Zhang, H. Wu, M. An, Y. Jing, B. Li*(李喬), and Z. Zhang, "*High-order Harmonics and the Reverse of the Squaring Up Process in the Triangular-lattice Magnet $HoPdAl_4Ge_2$*", Phys. Rev. B **109**, 134407 (2024).
- S.-H. Hsieh, S. Ghosh, Y.-H. Liang, H.-T. Wang, C.-H. Du*(杜昭宏), J.-W. Chiou, C.-M. Wu, C.-W. Wang, Y.-C. Shao, J.-L. Chen, C.-W. Pao, H.-M. Tsai, T.-S. Chan, W.-B. Wu, H.-J. Lin, J.-F. Lee, A. Kandasami, and W.-F. Pong*(彭維鋒), "*Correlation Between Noncollinear Spin Orientation and Lattice Distortion in $Ni_{0.4}Mn_{0.6}TiO_3$*", Phys. Rev. Mater. **8**, 124410 (2024).
- T.-Y. Huang*(黃子晏), A. P. Le Brun, B. Sochor, C.-M. Wu, Y. Bulut, P.-M. Buschbaum, S. V. Roth, and Y.-L. Yang*(楊延齡), "*Nanometer-thick ITIC Bulk Heterojunction Films as Non-fullerene Acceptors in Organic Solar Cells*", ACS Appl. Nano Mater. **7**, 17588 (2024).
- D. C. Kakarla*, Y.-H. Ku, H. C. Wu, C. C. Chen, M. Y. Hsu, T. R. Hu, J.-Y. Lin, N. Puri, M.-J. Hsieh, C. W. Wang, W.-H. Li, Dhanasekhar C, A. Tiwari, C. H. Lu, K. J. You, T. W. Kuo, K. J. Fan, Y. C. Chang, and H. D. Yang*(楊弘敦), "*Exploring New Members of Magnetoelectric Materials in CuO-$CuCl_2$-SeO_2 System*", Mater. Today Phys. **46**, 101527 (2024).
- Y. S. Kim, M.-Y. Luo, D. Yu, K. An, Y. Chen, I.-H. Oh, E. Shin, W. Woo, H. Chae, Y.-S. Na, Peter K. Liaw, J. Jain, J. H. Han, E.-W. Huang*(黃爾文), and S. Y. Lee*, "*Enhancing the Fatigue Resistance of High and Medium Entropy Alloys by Manufacturing-driven Microstructural Developments*", Addit. Manuf. **91**, 104332 (2024).
- C.-H. Lai, C.-W. Wang, H.-C. Wu, Y.-H. Liang, A. J. Studer, W.-T. Chen*(陳威廷), and C.-H. Du*(杜昭宏), "*Tunable Magnetic Structures in the Helimagnet $YBa(Cu_{1-x}Fe_x)_2O_5$*", Phys. Rev. Mater. **8**, 054404 (2024).
- J. Li, K. Lin*(林鯤), H. Xu, W. Yang, Q. Zhang, C. Yu, Q. Zhang, J. Chen, C.-W. Wang, K. Kato, S. Kawaguchi, L. You, Y. Cao, Q. Li, X. Chen, J. Miao, J. Deng, and X. Xing, "*High-entropy Magnet Enabling Distinctive Thermal Expansions in Intermetallic Compounds*", J. Am. Chem. Soc. **146**, 30380 (2024).
- X. Liu*(劉新智), Y. Yuan, X. Ma, S. Meng, C.-W. Wang, L. Hao, H. Wang*(王洪亮), K. Sun, and D. Chen, "*Multiple Magnetic Transitions Induced by Mn-doping in Orthochromite $HoCrO_3$*", J. Alloy. Compd. **970**, 172586 (2024).
- N. V. Mdlovu, K.-S. Lin*(林錕松), M.-T. Weng*(翁孟慈), C.-M. Wu, S. S. Dwitya, and Y.-S. Lin, "*Preparation of Stimuli-responsive Mesoporous Composites for In-vitro/In-vivo Studies Against Liver Cancer*", J. Ind. Eng. Chem. **135**, 444 (2024).
- S.-Y. Park, S.-H. Do*, K.-Y. Choi, D. Jang, T.-H. Jang, J. Scheffer, C.-M. Wu, J. S. Gardner, J. M. S. Park, J.-H. Park*, and S. Ji*, "*Emergence of the Isotropic Kitaev Honeycomb Lattice α–$RuCl_3$ and Its Magnetic Properties*", J. Phys.-Condens. Mat. **36**, 215803 (2024).
- V. K. Ranganayakulu, T.-H. Wang, C.-L. Chen*(陳正龍), A. Huang, M.-H. Ma, C.-M. Wu, W.-H. Tsai, T.-L. Hung, M.-N. Ou, H.-T. Jeng*(鄭弘泰), C.-H. Lee, K.-H. Chen, W.-H. Li, M. K. Brod, G. J. Snyder, and Y.-Y. Chen*(陳洋元), "*Ultrahigh zT from Strong Electron-phonon Interactions and a Low-dimensional Fermi Surface*", Energ. Environ. Sci. **17**, 1904 (2024).
- S.-I. Shamoto*, H. Yamauchi, K. Iida, K. Ikeuchi, K. Kaneko, Y.-S. Chen, S.-I. Yano, P.-T. Hsu, M. K. Lee, A. E. Hall, G. Balakrishnan, and L.-J. Chang*(張烈錚), "*Magnetic Excitation in the Hyperkagome Antiferromagnet Mn_3RhSi*", Phys. Rev. Res. **6**, 033303 (2024).
- K. Sun, Y. Zhu, S. Yano, Q. Zhao, M. Su, G. Xu, R. Zheng, Y. E. Fu, and H.-F. Li*(李海峰), "*Structure and Magnetic Properties of a $La_{0.75}Sr_{0.25}Cr_{0.90}O_{3-\delta}$ Single Crystal*", Physica B **678**, 415776 (2024).
- S. Sun, X. Li*(李曉寧), C. Zhang, X. Wang, J. Wang, C.-W. Wang, Z. J. Xu, Z. Cheng*(程振祥), and Y. Bai*(白瑩), "*Magnetic Field-induced Disordered Phase of Spinel Oxides for High Battery Performance*", Adv. Mater. **36**, 2405876 (2024).
- P.-C. Wei*(魏百駿), C.-R. Hsing, C.-C. Yang, Y.-H. Tung, H.-J. Wu, W.-T. Yen, Y.-C. Lai, J.-J. Lee, C.-W. Wang, H.-C. Wu, H.-D. Yang, V. Singaravelu, X. Miao, A. Giugni, J.-K. Hu, J.-H. Fu, V. Tung, J. He, C.-M. Wei*(魏金明), and J.-H. He*(何志浩), "*Liquid-like Thermal Conductivity in Solid Materials: Dynamic*

Behavior of Silver Ions in Argyrodites", Nano Energy **122**, 109324 (2024).
- X. Wu, X. Mi, L. Zhang, C.-W. Wang, N. Maraytta, X. Zhou, M. He*(何明全), M. Merz*, Y. Chai*(柴一晟), and A. Wang*(王愛峰), "*Annealing-tunable Charge Density Wave in the Magnetic Kagome Material FeGe*", Phys. Rev. Lett. **132**, 256501 (2024).
- H. Y. Hao, J. Y. Li, W. D. Hutchison, C. C. Hu, C. W. Wang, Q. F. Gu, S. J. Campbell, W. Q. Wang*(王文全), Z. X. Cheng*(程振祥), and J. L. Wang*(王建立), "*Effects of Fe Substitution for Mn on Structural, Magnetic and Magnetocaloric Properties of $TbMn_{2-x}Fe_xSi_2$*", J. Alloy. Compd. **1003**, 175560 (2024).
- S. Yano*(矢野真一郎), Junjie Yang, Kazuki Iida, C.-W. Wang, Andrew G. Manning, Daichi Ueta, and Shinichi Itoh, "*Spin Reorientation and Interplanar Interactions of the Two-dimensional Triangular-lattice Heisenberg Antiferromagnets h-(Lu,Y)MnO_3 and h-(Lu,Sc)FeO_3*", Phys. Rev. B **110**, 134444 (2024).
- H. Zhou, Y. Cao*(曹宜力), S. Khmelevskyi, Q. Zhang, S. Hu, M. Avdeev, C.-W. Wang, R. Zhou, C. Yu, X. Chen, Q. Li, J. Miao, Q. Li, K. Lin, and X. Xing*(邢獻然), "*Colossal Zero-field-cooled Exchange Bias via Tuning Compensated Ferrimagnetic in Kagome Metals*", J. Am. Chem. Soc. **146**, 20770 (2024).
- H. Zhou, Y. Cao*(曹宜力), W. Yang, M. Avdeev, C.-W. Wang, Y. Sun, C. Yu, K. Lin, and X. Xing*(邢獻然), "*Axial Zero Thermal Expansion with Good Mechanical Strength in the Ni-doped Kagome Ho_2Fe_{17} Magnets*", ACS Appl. Mater. Interfaces **16**, 69548 (2024).
- J. Zhu, Q. Ren*(任清勇), C. Chen, C. Wang, M. Shu, M. He, C. Zhang, M. D. Le, S. Torri, C.-W. Wang, J. Wang, Z. Cheng, L. Li, G. Wang, Y. Jiang, M. Wu, Z. Qu, X. Tong*(童欣), Y. Chen*(陳岳), Q. Zhang*(張倩), and J. Ma*(馬杰), "*Vacancies Tailoring Lattice Anharmonicity of Zintl-type Thermoelectrics*", Nat. Commun. **15**, 2618 (2024).

Student Dissertations

Doctorate

- H. R. H. Ahmed, Advisor Prof. C.-C. Chang (張家靖), Dept. of Biol. Sci. & Tech., Natl. Yang Ming Chiao Tung Univ., *"Studying VP28 Refolding, Assembly Mechanism and Its Application as a Drug Nanocarrier"* (2024).
- J.-H. Chang (張仁豪), Advisor Prof. Y.-J. Huang (黃逸仁), Dept of Fiber & Composite Mater., Feng Chia Univ., *"Exploring the Physical Behavior of Using Auxetic Structures on Enhancing the Performance of Polymeric Piezoelectric Films and the Piezoelectric Effect of Composite Laminar Structures"* (2024).
- Y.-J. Chang (張育仁), Advisor Prof. Y.-R. Chen (陳韻如), Genomics Research Center, Academia Sinica, *"Investigating Toxicity Mechanisms and Potential Therapeutics of Arginine-rich Dipeptide Repeats in Amyotrophic Lateral Sclerosis"* (2024).
- S.-L. Chen (陳仕倫), Advisor Prof. M.-T. Tang (湯茂竹) & Y.-L. Soo (蘇雲良), Dept. of Phys., Natl. Tsing Hua Univ., *"Grazing-incidence X-ray Back Diffraction: Optical Characteristics and Applications"* (2024).
- T.-Y. Chen (陳則元), Advisor Prof. L.-W. Kuo (郭力維), Dept. of Earth Sci., Natl. Central Univ., *"The Formation and Alteration of Lightning Fossil - A Case Study of Fulgurite on Granitic Gneiss in Kinmen"* (2024).
- K.-C. Chiu (邱冠嘉), Advisor Prof. M.-T. Lin (林敏聰), Dept. of Phys., Natl. Taiwan Univ., *"Investigation of Spin Dynamics and Magnetoresistance Effects in Pt/Py Heterostructure with Underlying Bulk WSe_2"* (2024).
- P. Deetanya, Advisor Prof. K. Wangkanont, Dept. of Biochem., Chulalongkorn Univ., *"Structure and Properties of Recombinant Durio Zibethinus Seed Protease Inhibitors"* (2024).
- M. N. Duong (楊美玉), Advisor Prof. J.-Y. Juang (莊振益), Dept. of Electrophys., Natl. Yang Ming Chiao Tung Univ., *"The Intricate Interplay between Strain, Crystal Structure, Electronic Structure, and Magnetic Order in Orthorhombic and Hexagonal $YMnO_3$ Thin Films"* (2024).
- J. Falke, Advisor Prof. L.-H. Tjeng, Inst. for Chem. Phys. of Solids, Max-Planck-Gesellschaft, *"Bulk Electronic Structure of Single-crystal Perovskite Oxides Studied by Soft X-ray Angle-resolved Photoemission"*(2024).
- K.-J. Hsueh (薛坤仁), Advisor Prof. M.-T. Lin (林敏聰), Dept. of Phys., National Taiwan Univ., *"The Hydrogenation and Thickness Modulated Magnetic Anisotropy on CoPd and FePd Alloy/Co/$[Pt/Co]_4$/Pt Multilayer"* (2024).
- W.-T. Huang (黃文澤), Advisor Prof. R.-S. Liu (劉如熹), Dept. of Chem., Natl. Taiwan Univ., *"Near-infrared Light and Nanotechnology in Plants and Animals"* (2024).
- C. Khotimah, Advisor Prof. F.-M. Wang (王復民), Grad. Inst. of Appl. Sci. & Tech., Natl. Taiwan Univ. of Sci. & Tech., *"Synthesis and Characterization of Benzimidazole-based Salt Additive Electrolyte for High Voltage Cathode: Spinel $LiNi_{0.5}Mn_{1.5}O_4$"* (2024).
- L.-N. Ko, (柯齡甯), Advisor Prof. C.-S. Yang (楊啟伸), Dept. of Biochem. Sci. & Tech., Natl. Taiwan Univ., *"Structural and Optical Properties Perspectives on a Magnesium Transporting Middle Rhodopsin"* (2024).
- C.-H. Lai (賴君豪), Advisor Prof. C.-H. Du (杜昭宏), Dept. of Phys., Tamkang Univ., *"Study of the Spin Ordering in the Helimagnets $YBaCuFeO_5$ and CuB_2O_4"* (2024).
- T.-W. Lee, (李定偉), Advisor Prof. C.-Y. Chen (陳佳吟), Dept. of Environ. Engr., Natl. Chung Hsing Univ., *"Fate and Toxicity of Two-dimensional Molybdenum Disulfide Nanosheets in Aquatic Systems"* (2024).
- Y.-H. Liang (梁喻惠), Advisor Prof. C.-H. Du (杜昭宏), Dept. of Phys, Tamkang Univ., *"Exploring Spin and Charge Ordering in Materials Using Neutron and X-ray Scattering"* (2024).
- G. Lim, Advisor Prof. J. Hong, Energy mater. center, Korea Inst. of Sci. & Tech., *"Study of the Degradation Reaction at the Cathode-electrolyte Interface in Mn-rich and High-energy Lithium-ion Battery Cathodes"* (2024).
- Y.-S. Lin (林穎聖), Advisor Prof. Y.- J. Chang (張源杰), Dept. of Chem., Tunghai Univ., *"Novel Hole Transport Materials/Passivators Enhances Hole Mobility and Efficiency of Perovskite Solar Cells"* (2024).
- C.-Y. Liu (劉昌邑), Advisor Prof. H.-C. Wang (王皓青), The Ph.D. Program for Translational Med., Taipei Med. Univ., *"Structural and Functional Analysis of Component Proteins of Vaccinia Viral Fusion Complex"* (2024).
- A. Marino, Advisor Prof. L.-H. Tjeng, Max Planck Inst. for Chem. Phys. of Solids, Max-Planck-Gesellschaft, *"Correlation Effects in the 5f States of Uranium Intermetallics Probed with X-ray Spectroscopies"* (2024).
- M. Rinawati, Advisor Prof. M.-H. Yeh (葉旻鑫), Dept. of Chem. Engr., Natl. Taiwan Univ. of Sci. & Tech., "*Advances in Structural Modulation of Heterogeneous Molecular Catalyst on Carbon Support for Efficient Electrochemical Energy Conversions"* (2024).
- Y.-M. Tian (田園夢), Advisor Prof. J. Shang (尚進), School of Energy & Environ., City Univ. of Hong Kong, *"Thermosensitive Gating Effect for Selective Gas Adsorption in Ionic Metal-organic Frameworks"* (2024).
- S.-J. Tsou (鄒盛榮), Advisor Prof. Y.-J. Chiou (邱郁青), Dept. of Chem. Engr., Tatung Univ., *"Investigation of Optimal Preparation of Anodic Pd Catalyst for Direct Formic Acid Fuel Cell"* (2024).
- S. Wang (王紳), Advisor Prof. S.-R. Tzeng (曾秀如), Inst. of Biochem. & Molecular Biol., Natl. Taiwan Univ., *"Structural Studies of Peptidoglycan Endopeptidases in Complex with Substrate Adaptor NlpI"* (2024).
- Y.-S. Wang (王奕翔), Advisor Prof. S.-R. Tzeng (曾秀如), Inst. of Biochem. & Molecular Biol., Natl. Taiwan Univ., *"Structural and Biophysical Studies of Human Transthyretin A97S Variant"* (2024).
- S.-Y. Wei (魏詩晏), Advisor Prof. Y.-C. Chen (陳盈潔), Dept. of Mater. Sci. & Engr., Natl. Tsing Hua Univ., *"Engineering Large-sized Vascularized Nerve Tissue in Collagen Hydrogels for Volumetric Muscle Loss Repair"* (2024).
- C.-Y. Wu (伍政宇), Advisor Prof. T.-H. Yang (楊東翰), Dept. of Chem. Engr., Natl. Tsing Hua Univ., *"A Catalyst Family of High-entropy Alloy Atomic Layers with Square Atomic Arrangements Comprising Iron- and Platinum-Group Metals"* (2024).
- P. Xiong (熊佩), Advisor Prof. M.-J. Li (李孟蓉), Dept. of Appl. Phys., The Hong Kong Polytechnic Univ., *"Tammann Temperature-guided Synthesis of Efficient and Stable Core@Shell Ruthenium-free Catalysts for Ammonia Decomposition"* (2024).
- L.-T. Yen (嚴莉婷), Advisor Prof. Y.-T. Lin (林耀東), Dept. of Soil Environ. Sci., Natl. Chung Hsing Univ., *"Interactions between Nano/Micro-sized Particles and Microbes for Agricultural and Environmental Applications"* (2024).
- Y.-S. Yu (余祐陞), Advisor Prof. C.-W. Wu (吳嘉文), Dept. of Chem. Engr.,

Natl. Taiwan Univ., *"Downsizing and Functionalization of Interpenetrated Metal-organic Frameworks for Combined Photothermal and Radiation Cancer Therapy"* (2024).
- R. A. Yuwono, Advisor Prof. F.-M. Wang (王復民), Grad. Inst. of Appl. Sci. & Tech., Natl. Taiwan Univ. of Sci. & Tech., *"Study on the Surface of Layered Ni-rich Cathode for Lithium-ion Batteries"* (2024).

Master's Degree

- C. Chandit, Advisor Prof. K. Wangkanont, Dept of Biochem., Chulalongkorn Univ., *"Structural Characterization and Activity of a Dihydrofolate Reductase-like Enzyme from Leptospira Interrogans"* (2024).
- C.-H. Chang (張志瑄), Advisor Prof. C.-Y. Kuo (郭昌洋), Dept of Electrophys., Natl. Yang Ming Chiao Tung Univ., *"Explore the Resistance Anisotropic from the Orbital Polarization"* (2024).
- C.-K. Chang (張景凱), Advisor Prof. F.-M. Wang (王復民), Grad. Inst. of Appl. Sci. & Tech., Natl. Taiwan Univ. of Sci. & Tech., *"Recovery of Transition Metals from Waste Lithium-ion Batteries Using Oxalic Acid: Mechanism Investigation"* (2024).
- H. Chang (張翔), Advisor Prof. S.-M. Lin (林士鳴), Dept. of Biotech. & Bioindustry Sci., Natl. Cheng Kung Univ., *"Biochemical Characterization and Structural Analysis Reveal the Calcium Binding Sites in Vibrio Campbellii α-hemolysin"* (2024).
- K.-P. Chang (張凱評), Advisor Prof. S.-M. Lin (林士鳴), Dept. of Biotech. & Bioindustry Sci., Natl. Cheng Kung Univ., *"Structural and Biochemical Investigation of Shiftless in Suppressing -1 Programmed Ribosomal Frameshifting"* (2024).
- L.-C. Chang (張立婕), Advisor Prof. Y.-Y. Lai (賴育英), Inst. of Polymer Sci. & Engr., Natl. Taiwan Univ., *"Editing of Isoindigo-based Molecules and Polymers: Reconstruction and Degradation"* (2024).
- S.-T. Chang (張舒婷), Advisor Prof. D.-Y. Wang (王迪彥), & Y.-H. Lai (賴英煌), Dept. of Chem., Tunghai Univ., *"Amorphous CoNiFe Hydroxide Film as Highly Active Electrocatalysts for Oxygen Evolution Reaction and Urea Oxidation Reaction"* (2024).
- Y.-H. Chang (張友豪), Advisor Prof. Y.-Y. Li (李元堯), Dept of Chem. Engr., Natl. Chung Cheng Univ., *"Tailoring Synergistic Effects of Fe-Co dual Single Atoms and Co Nanoparticles Bifunctional Catalysts for Superior Longevity of Rechargeable Zn-Air Battery"*(2024).
- B.-W. Chen (陳柏維), Advisor Prof. M. Huang (黃暄益), Dept. of Chem., Natl. Tsing Hua Univ., *"$BaZrO_3$ Nanocrystals Revealing Size- and Facet-Dependent Optical and Photocatalytic Properties"* (2024).
- C. Chen (陳禎), Advisor Prof. D.-Y. Wang (王迪彥) & Y.-H. Lai (賴英煌), Dept. of Chem., Tunghai Univ., *"Studies on the Plating and Stripping of Aluminum Metal in Mixed Electrolytes"* (2024).
- C.-C. Chen (陳佳琪), Advisor Prof. S.-W. Kuo (郭紹偉), Dept. of Mater. & Optoelectron. Engr., Natl. Sun Yat-sen Univ. *"Construction of Benzoxazine-linked Porous Organic Polymer and Their Application Potential"* (2024).
- C.-C. Chen (陳俊吉), Advisor Prof. Y.-C. Lin (林彥丞), Dept. of Chem. Engr., Natl. Cheng Kung Univ., *"Imapct of Side-chain Modification on Conjugated Polymer's Physical Properties and Sorting Efficiency to Semiconducting Carbon Nanotubes"* (2024).
- G.-L. Chen (陳冠霖), Advisor Prof. S.-F. Hung (洪崧富), Dept. of Appl. Chem., Natl. Yang Ming Chiao Tung Univ., *"Silver-modified Cu_2O Nanocavities for Electrocatalytic CO_2 Reduction to C_{2+} Products"* (2024).
- H.-C. Chen (陳惠娟), Advisor Prof. J.-M. Ting (丁志明), Dept. of Mater. Sci. & Engr., Natl. Cheng Kung Univ., *"Ligand-modified Bimetallic Metal-organic Frameworks as Electrocatalysts for Urea Oxidation Reaction"* (2024).
- J.-H. Chen (陳建樺), Advisor Prof. C.-F. Huang (黃智峯), Dept. Chem. Engr., Natl. Chung Hsing Univ., *"Synthesis of Crosslinkers via Atom Transfer Radical Addition (ATRA) Containing Strong Electron-withdrawing Groups at the α-position for the Development of Catalyst-free Dynamic Covalent Bonding Epoxy Vitrimers"* (2024).
- K.-C. Chen (陳凱均), Advisor Prof. C.-M. Yang (楊家銘), Dept. of Chem., Natl. Tsing Hua Univ., *"Catalytic Study of Ammonia Synthesis over Mesoporous Carbon Supported Ru Based Bimetallic Catalysts"* (2024).
- L.-P. Chen (陳樂平), Advisor Prof. E-W. Huang (黃爾文), Dept. of Mater. Sci. & Engr., Natl. Yang Ming Chiao Tung Univ., *"Effects of Doping ZnO Nanoparticles and Process Optimization on the β-phase Content of P (VDF-TrFE) and P (VDF-TrFE-CTFE) Electrospun Nanofibers and the Circuit Improvements for Enhancing Piezoelectric Performance"* (2024).
- L.-T. Chen (陳亮彤), Advisor Prof. C.-L. Wang (王建隆), Dept. of Appl. Chem., Natl. Yang Ming Chiao Tung Univ., *"Characterization of the Supramolecular Structures between NDI: Pyrene Giant Tetrahedrons"* (2024).
- N.-H. Chen (陳乃華), Advisor Prof. Y.-J. Chang (張源杰), Dept. of Chem., Tunghai Univ., "*Novel Passivator of Spiro-based Structure with Lewis Base Functional Group Enhances the Efficiency of Perovskite Solar Cells"* (2024).
- P.-X. Chen (陳姵璇), Advisor Prof. M.-H. Fang (方牧懷), Inst. of Appl. Sci., Academia Sinica, *"Sharp-to-Broad Band Energy Transfer in Lithium Aluminate and Gallate Phosphors for SWIR LED"* (2024).
- P.-H. Chen (陳品宏), Advisor Prof. Y.-C. Lin (林彥丞), Dept. of Chem. Engr., Natl. Cheng Kung Univ., *"Diketopyrrolopyrrole-based Conjugated Polymer with Diastereomeric Conjugation Break Spacers for Intrinsically Stretchable Field-effect Transistor Application"* (2024).
- P.-Y. Chen (陳品瑜), Advisor Prof. C.-T. Lo (羅介聰), Dept. of Chem. Engr., Natl. Cheng Kung Univ., *"Photoresponsive Behaviors and Fluorescent Properties of Azobenzene-containing Amphiphilic Diblock Copolymer mPEG-b-PDMA-Azo under Visible Light Irradiation"* (2024).
- P.-Y. Chen (陳伯瑜), Advisor Prof. Y.-C. Chen (陳盈潔), Dept. of Mater. Sci. & Engr., Natl. Tsing Hua Univ., *"Impact of Controlled Vascularized Collagen Gel Scaffolds on Volume Restoration and Functional Recovery in Mouse Muscle Defects"* (2024).
- S.-Y. Chen (陳尚淵), Advisor Prof. P.-C. Lyu (呂平江), Inst. of Bioinform. & Struct. Biol., Natl. Tsing Hua Univ., *"Using Circular Permutation Technique to Explore the Key Structural Switch Controlling the Activity of Dual-specificity Phosphatase 26"* (2024).
- S.-Y. Chen (陳詩芸), Advisor Prof. S.-W. Kuo (郭紹偉), Dept. of Mater. & Optoelectron. Engr., Natl. Sun Yat-sen Univ., *"CO_2/Epoxy Cyclohexene Copolymerization for the Preparation of Mesoporous Carbons with High CO_2 Adsorption Capacity"* (2024).
- S.-C. Chen (陳嵩啓), Advisor Prof. H.-W. Chang (張漢威) & Y.-R. Lu (盧英睿) & C.-J. Chen (陳致融), Dept. of Chem. Engr., Natl. United Univ., *"Utilizing a Stable Co@PC800 Cathode Efficiently Synthesizes Hydrogen Peroxide to Achieve the Degradation of Phenol by Electro-fenton Process"* (2024).
- W.-L. Chen (陳威綸), Advisor Prof. L. Lo (羅立), Dept. of Geol., Natl. Taiwan Univ., *"Morphometric Characteristic of Planktonic Foraminifera Using μ-computed Tomographic Data"* (2024).
- Y.-Y. Chen (陳彥妤), Advisor Prof. C.-H. Lee (李志浩), Inst. of Nuclear Engr. & Sci., Natl. Tsing Hua Univ., *"Comparision of Hydrogen Annealing and Gd Doped Molybdenum Disulfide Nanoflower as Nitrogen Dioxide Gas Sensor with Mangetic Field"* (2024).
- Y.-E. Chen (陳穎兒), Advisor Prof. A.-S. Chiang (江安世) & Y.-K. Hwu (胡宇光), Inst. of Systems Neurosci., Natl. Tsing Hua Univ., *"Advancement of Heavy Metal Staining Techniques for Mapping the Entire Drosophila Connectome Using X-ray Synchrotron"* (2024).
- Y.-D. Chen (陳鈺典), Advisor Prof. D.-Y. Wang (王迪彥) & Y.-H. Lai (賴英煌), Dept. of Chem., Tunghai Univ., *"Copper Element-doped $CsPbBr_3$ Nanocrystals for Photocatalytic CO_2 Reduction Reaction"* (2024).
- R.-Y. Chen (陳韻如), Advisor Prof. B.-Q. Liang (梁碧清) & T.-R. Yang (楊子睿), Dept. of Earth Sci., Natl. Cheng Kung Univ., *"Preservation and Taphonomy of Taiwanese Fossil Resins and Burmese Feather-included Amber Revealed by Spectroscopy and Imaging Approaches"* (2024).
- P.-Y. Cheng (鄭博元), Advisor Prof. C.-L. Huang (黃建龍), Dept. of Phys., Natl. Cheng Kung Univ., *"Physical Properties and Electronic Structure of the Two-gap Superconductor V_2Ga_5"* (2024).
- C.-C. Li (李丞鈞), Advisor Prof. N.-J. Hu (胡念仁), Dept. of Biochem., Natl. Chung Hsing Univ., *"Probing the Structural Impacts and Regulatory Mechanisms of ATP and Cyclic-di-AMP on Streptococcus Pyogenes KtrA, a Regulatory Protein of Bacterial K^+ Channel KtrB"* (2024).
- L.-S. Chiang (江立生), Advisor Prof. T.-I Yang (楊大毅), Dept. of Chem. Engr., Chung Yuan Christian Univ., *"Exploring the Properties of Titanium Dioxide Photocatalyst/Bagworm Silk Fibroin Composite Material"* (2024).
- C.-Y. Chiu (邱兆妤), Advisor Prof. C.-H. Lin (林嘉和) & C.-Y. Tsai (蔡振彥), Dept. of Chem., Natl. Taiwan Normal Univ., *"The Study of NNO-2Ni-NU-1000(Zr) Applied in CO_2 Cycloaddition and Copolymerization of Anhydride with Oxide"* (2024).
- Y.-S. Chiu (邱彥碩), Advisor Prof. M.-H. Yeh (葉旻鑫), Dept. of Chem. Engr., Natl. Taiwan Univ. of Sci. & Tech., *"Developing Surface-modified g-C_3N_4/PVDF Composite Film to Enhance Self-polarized β-phase Induction for Ultrasensitive Triboelectric Pressure Sensor"* (2024).
- Y.-H. Chiu (邱奕豪), Advisor Prof. M.-H. Yeh (葉旻鑫), Dept. of Chem. Engr., Natl. Taiwan Univ. of Sci. & Tech., *"Development of Quantum Dot Modification Strategies to Enhance the Electrochemical Detection Sensitivity and Stability of Non-invasive Sweat Glucose Sensors"* (2024).
- Z. Chong (鍾震), Advisor Prof. J.-L. Huang (黃肇瑞) & Y.-M. Shen (沈祐民), Hierarchical Green-Energy Mater. Research Center, Natl. Cheng Kung Univ., *"The In Situ Analytical Techniques Assisted Study of Pre-lithiated MoOx@TiO_2 as the Anode Material of Lithium Ion Batteries"* (2024).

- P.-Y. Chou (周柏宇), Advisor Prof. E-W. Huang (黃爾文), Dept. of Mater. Sci. & Engr., Natl. Yang Ming Chiao Tung Univ., *"Carbon Black Characteristics on Absorption Performance and Additive Manufacturing of X-band Metamaterial Absorbers"* (2024).
- W.-L. Chou (周玟伶), Advisor Prof. W.-T. Chen (陳威廷), Center for Condensed Matter Sci., Natl. Taiwan Univ., *"The Synthesis and Magnetic Properties of Rare Earth Doped Pyrochlore and Double-perovskite Single-ion Magnets"* (2024).
- Y.-H. Chou (周祐賢), Advisor Prof. S.-H. Tung (童世煌), Inst. of Polymer Sci. & Engr., Natl. Taiwan Univ., *"Fluorine Rubber/Carbon Fillers/Ionic Liquids Composites for Flexible Thermoelectric Generator"* (2024).
- T.-C. Chuang (莊才俊), Advisor Prof. H.-M. Kao (高憲明), Dept. of Chem., Natl. Central Univ., *"Application of 2D MXene Combined with Molybdenum Disulfide / Manganese Sulfide and Bimetallic Zinc Manganese Oxide $ZnMn_2O_4$ as Anode Materials for Lithium (Sodium) Ion Batteries"* (2024).
- Y.-J. Chuang (莊雅茹), Advisor Prof. M. Huang (黃暄益), Dept. of Chem., Natl. Tsing Hua Univ., *"Synthesis of $PbZrTiO_3$ Nanocrystals Exhibiting Structure-dependent Piezoelectric Properties"* (2024).
- M.-C. Chung (鍾旻潔), Advisor Prof. S.-H. Tung (童世煌), Inst. of Polymer Sci. & Engr., Natl. Taiwan Univ., *"Investigating the Influence of Modification Through Compounding and Solid-state Polymerization on the Rheological Properties of Thermoplastic Polyester Elastomer"* (2024).
- Y.-C. Chung (鍾雅淇), Advisor Prof. H.-F. Hsu (徐秀福), Dept. of Chem., Tamkang Univ., *"Platinum-catalyzed Annulation of 4-Methyl-2,3,5,6-Tetrakis (phenylethynyl) -1,1'-biphenyl: Synthesis, Structural Analysis and Properties of Acephenanthrylene Derivatives"* (2024).
- T.-J. Fan (范添然), Advisor Prof. H.-L. Chen (陳信龍), Dept of Chem. Engr., Natl. Tsing Hua Univ., *"Crystallization Behavior and Morphology of Poly (decamethylene terephthalamide) and Its Copolymers"* (2024).
- Y.-C. Fan (范宜臻), Advisor Prof. C.-H. Lin (林嘉和), Dept. of Chem., Natl. Taiwan Normal Univ., *"Rapid Solvent-induced Lattice Rearrangement from One- to Three-Dimensional Cu (II) Metal - Organic Framework"* (2024).
- D.-W. Feng (馮大維), Advisor Prof. Y.-J. Sun (孫玉珠), Inst. of Bioinform. & Struct. Biol., Natl. Tsing Hua Univ., *"Study on the Expression, Purification, and Biological Functions of the Cytoplasmic Domain of Human Phosphate Transporter"* (2024).
- H.-X. Guo (郭弘翔), Advisor Prof. Y.-J. Chiou (邱郁菁), Dept. of Chem. Engr., Tatung Univ., *"Effect of Fast Solidifying Solution for $(Ta_2O_5)_{100-x}(BaTiO_3)_x$ Novel Dental Filling Materials"* (2024).
- J.-S. Guo (郭昭顯), Advisor Prof. N.-F. Chiu (邱南福), Inst. & Undergrad. Program of Electro-Optical Engr., Natl. Taiwan Normal Univ., *"Development of Sulfur-doped Graphene Quantum Dots-peptide-based Surface Plasmon Resonance Biosensors in Spiked Artificial Saliva to Detect Recombinant Human Cytokeratin 19 His Protein (NBP2)"* (2024).
- C.-H. Ho (何政勳), Advisor Prof. J.-L. Huang (黃肇瑞) & Y.-M. Shen (沈祐民), Dept. of Mater. Sci. & Engr., Natl. Cheng Kung Univ., *"The Research on SnO_2 Modified TiO_2 as Anode Material in Lithium-ion Battery"* (2024).
- Q.-A. Hong (洪祈安), Advisor Prof. Y.-C. Chiu (邱昱誠), Dept. of Chem. Engr., Natl. Taiwan Univ. of Sci. & Tech., *"Crosslinkable Elastomer-polymer Semiconductor Blends for Soft Organic Field-effect Transistor"* (2024).
- C.-T. Hsiao (蕭芷潞), Advisor Prof. B.-J. Hwang (黃炳照) & W.-N. Su (蘇威年), Grad. Inst. of Appl. Sci. & Tech., Natl. Taiwan Univ. of Sci. & Tech., *"Application of Modified Layers on Current Collectors in Anode-free Batteries"* (2024).
- J.-H. Hsiao (蕭人豪), Advisor Prof. C.-Y. Wang (王誠佑), Dept. of Mater. Sci. & Engr, Natl. Yang Ming Chiao Tung Univ., *"Hydrogen Spillover-driven High-entropy Alloy Nanoparticles from MOF for Ammonia Borane Hydrolysis"* (2024).
- T.-J. Hsiao (蕭慈蓉), Advisor Prof. Y.-Y. Lai (賴育英), Inst. of Polymer Sci. & Engr, Natl. Taiwan Univ., *"Application of Metal Oxides in the Photodegradation of Polystyrene"* (2024).
- Y.-H. Hsiao (蕭宇軒), Advisor Prof. R.-S. Liu (劉如熹), Dept. of Chem., Natl. Taiwan Univ., *"Tetravalent Chromium-doped Garnet Fluorescence Material for Application in Broadband Near-infrared Fiber Amplifiers"* (2024).
- W.-Y. Hsieh (謝文鈺), Advisor Prof. C.-H. Du (杜昭宏) & W.-T. Chen (陳威廷), Center for Condensed Matter Sci., Natl. Taiwan Univ., *"Study of Crystal and Magnetic Structure of Double-layered Perovskite YBa $(Mn_{1-x}Fe_x)_2O_5$"* (2024).
- Z.-J. Hsieh (謝宗哲), Advisor Prof. C.-H. Chuang (莊程豪), Dept of Phys., Tamkang Univ., *"Water Permeability and Storage Study of the Graphene Oxide Membrane"* (2024).
- C.-C. Hsu (許鈞荃), Advisor Prof. F.-M. Wang (王復民), Dept. of Chem. Engr, Natl. Taiwan Univ. of Sci. & Tech., *"Study of Lithium Polysiloxane as a Solid Electrolyte and Investigation of Its Application for Interface Modification in Nickel-rich Cathode Materials"* (2024).
- F.-E. Hsu (徐逢恩), Advisor Prof. B.-J. Hwang (黃炳照) & W.-N. Su (蘇威年), Dept. of Chem. Engr., Natl. Taiwan Univ. of Sci. & Tech., *"Optimizing Dry Process for Preparing Coin and Pouch Type All Solid State Lithium Batteries with Halide-sulfide Bilayer Electrolytes"* (2024).
- P.-Y. Hsu (許伯瑜), Advisor Prof. Y.-Y. Hsiao (蕭育源), Dept. of Biol. Sci. & Tech., Natl. Yang Ming Chiao Tung Univ., *"Unraveling the Mechanisms of Tardigrade DNA Protection Related Dsup Disorder-to-order Transition"* (2024).
- T.-W. Hsu (許庭維), Advisor Prof. B.-Q. Liang (梁碧清), Dept. of Earth Sci., Natl. Cheng Kung Univ., *"The Mechanism and Application of Short Range Order Nano-sized Iron and Titanium -containing Minerals to Promote Photocatalytic Degradation of Organic Carbon and Fluoride Pollutants"* (2024).
- Y.-Y. Hsu (徐衍裕), Advisor Prof. Y.-J. Chen (陳俞融), Dept. of Phys., Natl. Central Univ., *"Temperature Dependence of Effective Sites in Water Ice and Carbonaceous Dust Interactions"* (2024).
- J.-K. Hu (胡家愷), Advisor Prof. P.-C. Wei (魏百駿), Dept. of Mater. Sci. & Engr., Natl. Cheng Kung Univ., *"Structural, Optical, and Thermal Properties of $(MA/FA)PbX_3$ (X=Cl, Br, I) Organic-inorganic Halide Perovskite Single Crystals"* (2024).
- B.-R. Huang (黃柏睿), Advisor Prof. C.-F. Huang (黃智峯), Dept. Chem. Engr., Natl. Chung Hsing Univ., *"Synthesis of Crosslinkers via Atom Transfer Radical Addition (ATRA) Containing Strong Electron-withdrawing Groups at the α-position for the Development of Catalyst-free Dynamic Covalent Bonding Epoxy Vitrimers"* (2024).
- C.-C. Huang (黃竣琦), Advisor Prof. Y.-J. Chen (陳俞融), Dept. of Phys., Natl. Central Univ. *"Spectrally Resolved VUV Photoinduced Energy Transfer in Layered Ices"* (2024).
- C.-T. Huang (黃浚泰), Advisor Prof. R.-S. Liu (劉瑞雄), Dept. of Chem., Natl. Tsing Hua Univ., *"Base-treated 6-Sn and 6-Hf Metal Clusters and Their Hybrid Materials for Electron Beam Lithography Applications"* (2024).
- D.-J. Huang (黃鼎鈞), Advisor Prof. K.-W. Wang (王冠文), Inst. of Mater. Sci. & Engr, Natl. Central Univ., *"The Effects of Hydrogen Content and Iridium Addition on the Hydrogen Evolution Reaction Performance of Palladium in Acidic and Alkaline Seawater Media"* (2024).
- L.-X. Huang (黃立欣), Advisor Prof. T.-E. Lin (林子恩), Inst. of Biomed. Engr., Natl. Yang Ming Chiao Tung Univ., *"Finite Element Analysis and Auxetic Graphics in Developing a Liquid Metal-embedded Triboelectric Nanogenerator for Wearable Motion Sensor"* (2024).
- M.-H. Huang (黃敏瑄), Advisor Prof. R.-S. Liu (劉如熹), Dept. of Chem., Natl. Taiwan Univ., *"Tuning the Structural and Near-infrared Luminescent Properties of Spinel-type Phosphors"* (2024).
- S.-Y. Huang (黃尚洋), Advisor Prof. R.-S. Liu (劉如熹), Dept. of Chem., Natl. Taiwan Univ., *"Quasi-solid-state Magnesium Oxygen Battery with Polymer Electrolytes"* (2024).
- S.-Y. Huang (黃紹瑜), Advisor Prof. C.-H. Lin (林嘉和), Dept. of Chem., Natl. Taiwan Normal Univ., *"Hydrophobic Modification of Al-metal-organic Frameworks by Silane Coupling Reaction for CO_2 Capture"* (2024).
- S.-Y. Huang (黃仕堯), Advisor Prof. Y.-H. Liu (劉沂欣), Dept. of Chem., Natl. Taiwan Normal Univ., *"Influence of Defects in Two-dimensional Hybrid Organic-inorganic Halide Lead Perovskites"* (2024).
- K. Iputera (莫誠康), Advisor Prof. R.-S. Liu (劉如熹), Inst. for Chem. Research, Kyoto Univ., *"The Mechanism and Recycle of Metal-air Batteries"* (2024).
- J.-K. Jhang (張智凱), Advisor Prof. C.-H. Du (杜昭宏), Dep.t of Phys., Tamkang Univ., *"Studies of Structural and Magnetic Analysis of Inverse Rutile Material $(Fe_{1-x}Mn_x)_2TeO_6$"* (2024).
- J.-H. Jhang (張家華), Advisor Prof. Y.-C. Tseng (曾院介), Dept. of Mater. Sci. & Engr., Natl. Yang Ming Chiao Tung Univ., *"Thickness Reduction of $Hf_{1-x}Zr_xO_2$ Achieved Through Electrodes Optimization and In-situ Plasma Treatment"* (2024).
- K.-S. Jhang (張凱翔), Advisor Prof. H.-Y. Tuan (段興宇), Dept. of Chem. Engr., Natl. Tsing Hua Univ., *"Dual Atom Doped Chalcogenide Electrode for High-performance Potassium Ion Storage Devices"* (2024).
- Y.-T. Jian (簡宜婷), Advisor Prof. K.-W. Wang (王冠文), Inst. of Mater. Sci. & Engr., Natl. Central Univ., *"Ruthenium-boride Based Electrocatalysts for Efficient Hydrogen Evolution Reaction in both Acidic and Alkaline Seawater Media"* (2024).
- G.-H. Jiang (江國豪), Advisor Prof. Y.-C. Lin (林彥丞), Dept. of Chem. Engr., Natl. Cheng Kung Univ., *"Investigation of Conjugated Polymers with Asymmetric Side Chains in Organic Electrochemical Transistors"* (2024).
- Y.-Z. Jiang (江奕臻), Advisor Prof. C.-H. Lin (林嘉和), Dept. of Chem., Natl. Taiwan Normal Univ., *"Rapid Disorder to Crystalline Transition and Adsorption Separation of Trace Benzene from Cyclohexane of Tetracarboxylate Based Metal-*

organic Frameworks" (2024).

- P.-Y. Kao (高珮芸), Advisor Prof. F.-M. Wang (王復民), Grad. Inst. of Appl. Sci. & Tech., Natl. Taiwan Univ. of Sci. & Tech., *"Chemically Bonded Au Nano Particle on Carbon Nanotube as a Composite Material for CA125 Detection"* (2024).
- S.-M. Kuo (郭昇珉), Advisor Prof. Y.-Y. Chin (秦伊瑩), Dept. of Phys., Natl. Chung Cheng Univ., *"Oxygen Reduction Reactivity of Ruthenium-silver as Core and Palladium-platinum as Shell (RuxAgy@PdPtz) catalysts"* (2024).
- T.-W. Kuo (郭庭維), Advisor Prof. K.-W. Wang (王冠文), Inst. of Mater. Sci. & Engr., Natl. Central Univ., *"Enhancing the Selectivity and Stability of Cu in Electrocatalytic CO_2 Reduction to C_2H_4 Through ZnO Addition and PVP Modification"* (2024).
- C.-Y. Lai (賴倢玗), Advisor Prof. T.-Y. Lin (林姿瑩), Dept. of Mater. Sci. & Engr., Natl. Tsing Hua Univ., *"Effects of Co-evaporated Alkali Metal in the $Cu(In,Ga)(S,Se)_2$ Solar Cells and the Application Potential in Photo-charging System"* (2024).
- M.-R. Lai (賴玫如), Advisor Prof. B.-J. Hwang (黃炳照) & S.-H. Wu (吳溪煌) & W.-N. Su (蘇威年), Grad. Inst. of Appl. Sci. & Tech., Natl. Taiwan Univ. of Sci. & Tech., *"A Combined Experimental and Theoretical Study on the Design of High-voltage Dual-salt Localized High-concentration Electrolytes for Anode-free Lithium Metal Batteries"* (2024).
- K.-H. Lee (李冠賢), Advisor Prof. W.-N. Su (蘇威年) & B.-J. Hwang (黃炳照) & S.-H. Wu (吳溪煌), Grad. Inst. of Appl. Sci. & Tech., Natl. Taiwan Univ. of Sci. & Tech., *"Process and Performance Optimization of Pouch Cell for Anode-free Lithium Metal Batteries"* (2024).
- T.-Y. Lee (李庭瑀), Advisor Prof. S. L. I. Chan (陳立業), Dept. of Chem. & Mater. Engr., Natl. Central Univ., *"A study on the Electrical and Thermal Dissipation Properties of Carbon Nanotube/Graphene Composite Papers"* (2024).
- B.-W. Li (李柏緯), Advisor Prof. W. Kaveevivitchai (柯碧蓮), Dept. of Chem. Engr., Natl. Cheng Kung Univ., *"Iron-benzoquinoid Coordination Polymers as Cathode Materials for Lithium-ion Batteries"* (2024).
- C.-Y. Li (李佳穎), Advisor Prof. Y.-C. Lin (林彥丞), Dept. of Chem. Engr., Natl. Cheng Kung Univ., *"Improving the Performance of Polythiophene-based Conjugated Polymer in Organic Electrochemical Transistors with Block Architecture and Nonofibrillar Morphology Design"* (2024).
- G.-R. Li (李冠儒), Advisor Prof. S.-Y. Lu (呂世源), Dept. of Chem. Engr., Natl. Tsing Hua Univ., *"Iron Single-atom Decorated Hollow Porous Carbon Spheres of Brain-fold-like Surfaces Composited with Manganese Dioxide Nanowires as Sulfur Host Materials for Positive Electrodes of Lithium-sulfur Batteries"* (2024).
- J.-W. Li (李浚瑋), Advisor Prof. Y.-J. Chiou (邱郁菁), Dept. of Chem. Engr., Tatung Univ., *"Synthesis of PdCu/MWCNTs Electrocatalysts via Different Methods for Formic Acid Oxidation"* (2024).
- C.-H. Liao (廖政豪), Advisor Prof. S.-H. Tung (童世煌), Inst. of Polymer Sci. & Engr., Natl. Taiwan Univ., *"Recombinant Spider Silk as an Effective Additive in PEO-based Electrolytes for High-performance Solid Lithium-ion Batteries"* (2024).
- H.-T. Liao (廖小慈), Advisor Prof. C.-Y. Chang (張晉源), Dept. of Biol. Sci. & Tech., Natl. Yang Ming Chiao Tung Univ., *"Biochemical Characterization and Structural Determination of CmnI Involved in Capreomycin Biosynthesis"* (2024).
- M.-H. Liao (廖明軒), Advisor Prof. C.-C. Yang (楊仲準), Dept. of Phys., Chung Yuan Christian Univ., *"Study on the Interaction of Magnetism, Spin Gap, and Structure in Spinel Material $Fe_{1.49}V_{1.39}O_4$"* (2024).
- W.-Y. Liao (廖婉宜), Advisor Prof. N.-J. Hu (胡念仁), Dept. of Birchem., Natl. Chung Hsing Univ., "*Crystal Structure of Staphylococcus aureus ScdA and Biochemical Studies Reveal Oligomerization upon Redox Reactions"* (2024).
- Y.-W. Liao (廖弈瑋), Advisor Prof. C.-M. Yang (楊家銘), Dept. of Chem., Natl. Tsing Hua Univ., *"Preparation of Novel Nickel/Ceria/Silica Nanocatalysts for Hydrogenation of Carbon Dioxide"* (2024).
- Y.-K. Lien (連翊凱), Advisor Prof. S. L. I. Chan (陳立業), Dept. of Chem. & Mater. Engr., Natl. Central Univ., *"Study on the Cost-effective High-entropy Alloys for Efficient Hydrogen Storage"* (2024).
- C.-W. Lin (林宸葳), Advisor Prof. T.-I Yang (楊大毅), Dept. of Chem. Engr., Chung Yuan Christian Univ., *"Preparation of Silk Fibroin Graphene Composite Films Using 3D Printing Technology and Electrochemical Assistance System"* (2024).
- P.-H. Lin (林沛璇), Advisor Prof. B.-J. Hwang (黃炳照) & W.-N. Su (蘇威年) & S.-H. Wu (吳溪煌), Dept. of Chem. Engr., Natl. Taiwan Univ. of Sci. & Tech., *"Development of Supported Composite Sulfide Solid Electrolyte Membrane with Superb Tensile Strength"* (2024).
- T.-C. Lin (林子淇), Advisor Prof. H.-Y. Tuan (段興宇), Dept. of Chem. Engr., Natl. Tsing Hua Univ., *"Fe-single-atom Decorated Porous Carbon Nanofiber as Dentrite-free Anode For Potassium-metal Battery"* (2024).
- W.-C. Lin (林韋志), Advisor Prof. T.-Y. Lin (林姿瑩), Dept. of Mater. Sci. & Engr., Natl. Tsing Hua Univ., *"Interface Effect of Silver Incorporation in $Cu(In,Ga)(S,Se)_2$ Solar Cells and Application in Photoelectrochemical Water Splitting"* (2024).
- Y.-T. Lin (林彥廷), Advisor Prof. R.-S. Liu (劉如熹), Dept. of Mater. Sci. & Engr., Natl. Taiwan Univ., *"Co-doped Halide-type Solid-state Electrolyte for Lithium-ion Batteries"* (2024).
- Y.-Y. Lin (林彥妘), Advisor Prof. W.-W. Hu (胡威文), Dept. of Chem. & Mater. Engr., Natl. Central Univ., *"The Effects of Phospholipids on the Self-assembly and Gene Delivery of Stearylated Indolicidin"* (2024).
- Y.-C. Lin (林易辰), Advisor Prof. S.-F. Yu (俞聖法), Inst. of Chem., Academia Sinica, *"Preparation of Nano-manganese Oxide-multiwall Carbon Nanotube Composite Catalysts on Carbon Electrodes for Electrocatalytic Methane Oxidation to Methanol"* (2024).
- Y.-S. Lin (林育伸), Advisor Prof. W.-F. Liaw (廖文峰), Dept. of Chem., Natl. Tsing Hua Univ., *"Hydrolysis and Disproportionation of Dinitrosyl Iron Complex Forming Low Fe_0 Component of $Fe@Fe_xO_y$ toward Assemble $Fe@Fe_3O_4$ Carbonaceous Composite Material by Photo Induced Xanthene Dye Degradation"* (2024).
- Y.-C. Lin (林昱均), Advisor Prof. C.-C. Chang (張家靖), Dept. of Biol. Sci. & Tech., Natl. Yang Ming Chiao Tung Univ., *"Ni-DNA-based Thin-film Device Development and Pilot Study"* (2024).
- Y.-C. Lin (林昀築), Advisor Prof. H.-M. Kao (高憲明), Dept. of Chem., Natl. Central Univ., *"Application of Mn_3O_4 and Metal Organic Framework-derived CoS_2 Modified Pumpkin-derived Carbon Materials as Anode Materials for Lithium (Sodium) Ion Battery"* (2024).
- Y.-S. Lin (林毓珊), Advisor Prof. C.-H. Lin (林嘉和), Dept. of Chem., Natl. Taiwan Normal Univ., *"Metal-organic Frameworks Construction with Rhodium Based Metal-organic Cuboctahedra via Rigid Linker Insertion"* (2024).
- Y.-H. Lin (林育賢), Advisor Prof. C.-C. Yang (楊仲準), Dept. of Phys., Chung Yuan Christian Univ., *"Study on the Interaction of Magnetism and Structure in Corundum Material $Cr_{0.93}V_{0.87}O_3$"* (2024).
- Y.-Y. Ling (凌韻雅), Advisor Prof. L.-W. Kuo (郭力維), Dept. of Earth Sci., Natl. Central Univ., *"Fault-zone Characteristics of the Milun Fault, Taiwan, and Their Implications: In the Case of MiDAS Borehole Cores"* (2024).
- J.-Y. Liou (劉家佑), Advisor Prof. D.-I Yang (楊大毅), Dept. of Chem. Engr., Chung Yuan Christian Univ., *"Study on the Self-healing Properties of Silk/ Silica Composite Protein Membrane with Plant Surface Microstructure"* (2024).
- G.-X. Liu (劉冠賢), Advisor Prof. H.-H. Chen (陳秀慧), Dept. of Molecular Sci. & Engr. & Inst. of Organic & Polymeric Mater., Natl. Taipei Univ. of Tech., *"Development and Property Investigation of Room Temperature Unsymmetrical Photochromic Dithienylcyclopentene Carrying Fluorine Side Chain Liquid Crystalline Derivatives"* (2024).
- H.-Y. Liu (劉欣岳), Advisor Prof. B.-J. Hwang (黃炳照) & W.-N. Su (蘇威年) & S.-H. Wu (吳溪煌), Dept. of Chem. Engr., Natl. Taiwan Univ. of Sci. & Tech., *"Investigation of Lithium Dendrite Growth Mechanism Through Microscopic Observation and Analysis"* (2024).
- S.-Y. Liu (劉書佑), Advisor Prof. W.-F. Liaw (廖文峰), Dept. of Chem., Natl. Tsing Hua Univ., *"Optimization of Surface Electronic Structure for the Improved C_2 Selectivity in CO_2RR Using B-doped Cu-based Nanocatalysts"* (2024).
- Z.-Y. Liu (劉哲宇), Advisor Prof. C.-A. Dai (戴子安) & L.-Y. Wang (王立義), Dept. of Chem. Engr., Natl. Taiwan Univ., *"Development of Commercial Perovskite Solar Cell: High Efficiency, Large Area, and Indoore Light Application"* (2024).
- C.-Y. Lo (羅佳筠), Advisor Prof. C.-L. Wang (王建隆), Dept. of Appl. Chem., Natl. Yang Ming Chiao Tung Univ., *"Characterization of Supramolecular Amphiphiles Through Charge Transfer Interactions"* (2024).
- H.-C. Lo (羅漢傑), Advisor Prof. Y.-W. Lan (藍彥文), Dept. of Phys., Natl. Taiwan Normal Univ., *"Angle-dependent Conductivity in MoS_2 Field-effect Transistors with Bi Contacts"* (2024).
- J.-Y. Luo (羅振于), Advisor Prof. C.-A. Dai (戴子安), Dept. of Chem. Engr., Natl. Taiwan Univ., *"Development of Gradient Refractive Index (GRIN) Organic/ Inorganic Hybrid Materials for Novel Extended Depth-of Focus Intraocular Lens"* (2024).
- C.-C. Lu (呂家齊), Advisor Prof. C.-C. Yang (楊仲準), Dept. of Phys., Chung Yuan Christian Univ., *"Study on the Interaction of Magnetism, Structure, and Charge Transfer in Spinel Material $Fe_{1.495}V_{1.505}O_4$"* (2024).
- P.-J. Lu (呂沛儒), Advisor Prof. C.-H. Lin (林嘉和), Dept. of Chem., Natl. Taiwan Normal Univ., *"Research on Revealing the Crystalline State Transformation of Al-based Metal Organic Frameworks Under Treatments of Acidic and Basic Solutions"* (2024).
- J.-C. Luo (羅靖淳), Advisor Prof. C.-Y. Wang (王誠佑), Dept. of Mater. Sci. &

Engr., Natl. Yang Ming Chiao Tung Univ., *"High Entropy Alloy MgCoNiCuZn/SiO_2 Derived from ZIF as Catalysts for P-nitrophenol Hydrogenation"* (2024).

- T.-L. Ma (馬滋翎), Advisor Prof. S.-W. Kuo (郭紹偉), Dept. of Mater. & Optoelectron. Engr., Natl. Sun Yat-sen Univ., *"Mediating Hydrogen Bonding Interactions to Prepare Self-assembled Polymeric Micelles and Hollow Sphere"* (2024).
- Y.-X. Peng (彭奕翔), Advisor Prof. Y.-J. Chen (陳俞融), Dept. of Phys., Natl. Central Univ., *"VUV Photolysis of Methane Ice in N_2-rich Environment"* (2024).
- W.-L. Su (蘇暐倫), Advisor Prof. M.-H. Fang (方牧懷), Inst. of Appl. Sci., Academia Sinica, *"Structural Evolution and Octahedral-coordination Control in $Cs_2Ag_{1-x}Pb_{2x}Bi_{1-x}Br_6$ Double Perovskite Materials"* (2024).
- K.-X. Tang (湯可庠), Advisor Prof. C.-H. Lee (李志浩), Dept. of Engr. & System Sci., Natl. Tsing Hua Univ., *"Effect of Rare Earth Element Gadolinium Doped Molybdenum Disulfide Magnetic Catalyst on Hydrogen Evolution Reaction Under Magnetic Field"* (2024).
- Q.-X. Tang (湯騏勳), Advisor Prof. Y.-H. Liu (劉沂欣), Dept. of Chem., Natl. Taiwan Normal Univ., *"Using Mesoporous Graphene Oxide Nanoparticles in Combination with a Microarray for Surface-assisted Laser Desorption/Ionization Detection of Drug Abuse"* (2024).
- G. Tangkanont, Advisor Prof. K. Wangkanont, Dept. of Biochem., Chulalongkorn Univ., *"Structure Determination and Kinetic Properties of ATP Sulfurylase from Durian Durio Zibethinus"* (2024).
- W. Tanmathusorachai, Advisor Prof. M.-H. Yeh (葉旻鑫), Dept. of Chem. Engr., Natl. Taiwan Univ. of Sci. & Tech., *"Revealing the Metallic States and the Cyanide Coordinations of High-entropy Prussian Blue Analogues for an Efficient Bifunctional Oxygen Conversion Electrocatalyst in Rechargeable Zinc-air Batteries"* (2024).
- C.-H. Tsai (蔡正浩), Advisor Prof. E-W. Huang (黃爾文), Dept. of Mater. Sci. & Engr., Natl. Yang Ming Chiao Tung Univ. *"Effects of SiC Reinforced Particles Addition on Cast A356 Aluminum Alloy"* (2024).
- C.-Y. Tsai (蔡政諺), Advisor Prof. S.-C. Su (蘇士哲), Inst. of Bioinformatics & Structural Biol., Natl. Tsing Hua Univ., *"Modulating LT-ll2b-B5 GDIa Binding Ability Through Backbone Rearrangement"* (2024).
- C.-H. Tsai (蔡芷瑄), Advisor Prof. P.-W. Chung (鍾博文), Inst. of Chem., Academia Sinica, *"Understanding the Saccharides Adsorption Dynamics Using Hydrotalcite-derived Oxide"* (2024).
- H.-C. Tsai (蔡皓程), Advisor Prof. C.-C. Hsieh (謝之真), Dept. of Chem. Engr., Natl. Taiwan Univ., *"Research on the Effects of Replacing Silane with Surfactants on the Performance of Silica-filled Tread Compounds"* (2024).
- M.-S. Tsai (蔡鳴聲), Advisor Prof. C.-A. Dai (戴子安), Dept. of Chem. Engr., Natl. Taiwan Univ., *"Investigation of Gradient Latex Nanoparticles as Lithium Battery Anode Binders with Ionic Channels and Their Effects on Battery Performance"* (2024).
- W.-C. Tsai (蔡瑋晉), Advisor Prof. K.-S. Lin (林錕松), Dept. of Chem. Engr. & Mater. Sci., Yuan Ze Univ., *"Preparation and Characterization of pH-sensitive Graphene Quantum Dots-loaded Functional Metal Organic Frameworks for Drug Release and In-vitro Fluorescence Imaging"* (2024).
- Y.-H. Tsai (蔡奕昕), Advisor Prof. C.-T. Lo (羅介聰), Dept. of Chem. Engr., Natl. Cheng Kung Univ., *"Studies of Morphology and Crystallization Behavior of Poly(Butylene Succinate) / Poly(L-Lactic Acid) Coaxial Electrospun Fibers"* (2024).
- Y.-T. Tsai (蔡依庭), Advisor Prof. C.-C. Shih (石健忠), Dept. of Chem. & Mater. Engr., Natl. Yunlin Univ. of Sci. & Tech., *"Development of Novel Ultralow Bandgap Conjugated Polymers for Short-wave Infrared Organic Photodetectors Through Main Chain Engineering"* (2024).
- H.-K. Tseng (曾暄凱), Advisor Prof. T.-Y. Lin (林姿瑩), Dept. of Mater. Sci. & Engr., Natl. Tsing Hua Univ., *"Combining Recycled Silicon Waste with Novel Three-dimensional Cross-linked Adhesive for High-performance Lithium-ion Battery Anodes"* (2024).
- K.-W. Tseng (曾楷崴), Advisor Prof. Y.-W. Lan (藍彥文), Program for Nanoengr. & Nanosci., Natl. Taiwan Univ., *"High Performance of Dual-gated Molybdenum Disulfide Field Effect Transistor Enabled by Van der Waals High-κ Dielectric Material"* (2024).
- L.-C. Tseng (曾莉珈), Advisor Prof. P.-C. Lyu (呂平江), Inst. of Bioinform. & Struct. Biol., Natl. Tsing Hua Univ., *"The Study on the Structure-activity Relationship of Dual-specificity Phosphatase 22 (DUSP22) Gene Variants from Systemic Lupus Erythematosus (SLE) Patients"* (2024).
- Y.-Y. Tseng (曾彥揚), Advisor Prof. H.-Y. Tuan (段興宇), Dept. of Chem. Engr., Natl. Tsing Hua Univ., *"Multi-functional Coordination Engineering of Single Iron Atoms for The Enhanced Dendrite-free Potassium Ion Storage"* (2024).
- C.-M. Wang (王傑民), Advisor Prof. Y.-H. Luo (羅月霞), Dept. of Life Sci., Natl. Central Univ., *"ER Targeting Agent L-selenocystine Sabotages Proteostasis and Induces Immunogenic Cell Death in Colorectal Carcinoma"* (2024).
- K.-J. Wang (王凱巨), Advisor Prof. W. Kaveevivitchai (柯碧蓮), Dept. of Chem. Engr., Natl. Cheng Kung Univ., *"One-dimensional Coordination Polymers with Non-redox-active Metal Nodes as Cathode Materials for Lithium-ion Batteries"* (2024).
- S.-Y. Wang (王少妘), Advisor Prof. Y.-H. Liu (劉沂欣), Dept. of Chem., Natl. Taiwan Normal Univ., *"Effects of Atmospheric Oxygen and Water Adsorbed on the Surface of Mesoporous Graphene Oxide Nanoparticles on the Spectrum and Their Applications"* (2024).
- S.-X. Wang (王聖心), Advisor Prof. R.-N. Kwo (郭瑞年) & M.-H. Hong (洪銘輝), Dept. of Phys., Natl. Tsing Hua Univ., *"Off-axis Sputtering Growth of Ferrimagnetic Insulator EuropiumIron Garnet Films with Tunable Magnetic Properties"* (2024).
- Y.-T. Wang (王意婷), Advisor Prof. Y.-H. Lai (賴英煌), Dept. of Chem., Tunghai Univ., *"Low Amounts of Iridium Deposition on Dendritic Gold Surfaces: A Strategy for Efficient Oxygen Evolution Catalysis"* (2024).
- Y.-K. Wang (王昱凱), Advisor Prof. C.-T. Lo (羅介聰), Dept. of Chem. Engr., Natl. Cheng Kung Univ., *"Synthesis of Azobenzene-containing Diblock Copolymers Using PDMAEMA-Br as an Initiator and Study of Their Photoresponsive Behavior and Fluorescent Properties"* (2024).
- Y. Wei (魏瑜), Advisor Prof. C.-C. Hua (華繼中), Dept. of Chem. Engr., Natl. Chung Cheng Univ., *"Structural Investigations of Sodium Alginate Solution and Sodium Alginate - Ca^{2+} Gels"* (2024).
- H.-C. Weng (翁彗慈), Advisor Prof. E-W. Huang (黃爾文), Inst. of NanoTech., Natl. Yang Ming Chiao Tung Univ., *"Additive Manufacturing of Orthotropic Porous (OP) Structures with Varied Sizes and Distributions for Ti-6Al-4V Alloy and Their Mechanical Properties at High Temperatures"* (2024).
- Y.-C. Weng (翁于晴), Advisor Prof. C.-C. Shih (石健忠), Dept. of Chem. & Mater. Engr., Natl. Yunlin Univ. of Sci. & Tech., *"Boosting Performance in Stretchable Transistors Through the Use of Lewis Acid Doping Agents"* (2024).
- C.-W. Wu (吳季薇), Advisor Prof. M.-H. Fang (方牧懷), Inst. of Appl. Sci., Academia Sinica, *"Si-Al-Ox Enveloped Ag_2S Quantum Dot for Smart Textile"* (2024).
- G.-W. Wu (吳冠緯), Advisor Prof. J.-R. Huang (黃介嶸), Inst. of Biochem. & Molecular Biol., Natl. Yang Ming Chiao Tung Univ., *"Investigating TDP-43 Amyloidogenesis in LLPS-independent Pathway"* (2024).
- S.-W. Wu (吳聲維), Advisor Prof. H.-M. Kao (高憲明), Dept. of Chem., Natl. Central Univ., *"Preparation of Mesoporous Silica Materials with Acidic Functional Groups and Biomass-derived Carbon Materials for the Catalytic Organic Reaction"* (2024).
- S.-H. Wu (吳思慧), Advisor Prof. P.-L. Liu (劉博倫), Grad. Inst. of Med., Kaohsiung Med. Univ., *"Magnolol Induces Oxidative Stress in Lung Cancer Cells and Inhibits the Activation of the KEAP1/NRF2 Signaling Pathway, Promoting Mitochondrial Dysfunction and Oxeiptosis"* (2024).
- D.-Y. Xiao (蕭浔雍), Advisor Prof. Y.-H. Liu (劉沂欣), Dept. of Chem., Natl. Taiwan Normal Univ., *"Comprehensive Study on Sulfurization Kinetics and Adsorption of Transition Metal Ions to Enhance the HER Performance of $CdSe(en)_{0.5}$ Nanosheets: In-depth Analysis of Mesoporous Structural Changes and Radical Formation"* (2024).
- Y.-H. Yang (楊育昕), Advisor Prof. C.-M. Yang (楊家銘), Dept. of Chem., Natl. Tsing Hua Univ., *"Highly Dispersed Ruthenium Nanocatalysts Supported on Nanosheet-based Hierarchical MFI for CO_2 Methanation"* (2024).
- J.-H. Yang (楊柔歆), Advisor Prof. M. Huang (黃暄益), Dept. of Chem., Natl. Tsing Hua Univ., *"Formation of Magnetite (Fe_3O_4) Truncated Nanocubes to Rhombic Dodecahedra Revealing Facet-dependent Optical and Magnetic Behaviors"* (2024).
- S.-C. Yang (楊書承), Advisor Prof. M. Huang (黃暄益), Dept. of Chem., Natl. Tsing Hua Univ., *"Synthesis of Size-controlled $NiSe_2$ Octahedra of Ni-Zn Batteries and Electrical Hydrogen Evolution"* (2024).
- Y.-T. Yang (楊雅婷), Advisor Prof. M. Huang (黃暄益), Dept. of Chem., Natl. Tsing Hua Univ., *"Synthesis of $CaTiO_3$ Cubes and Cuboids: Implications for Photocatalytic Properties"* (2024).
- Z.-L. Yang (楊政霖), Advisor Prof. Y.-C. Tseng (曾院介), Dept. of Mater. Sci. & Engr., Natl. Yang Ming Chiao Tung Univ., *"Seed Layer Effects on the Ferroelectrical Properties of $Hf_{1-x}Zr_xO_2$ Thin Films"* (2024).
- C.-L. Yeh (葉俊良), Advisor Prof. H.-F. Hsu (徐秀福), Dept. of Chem., Tamkang Univ., *"Synthesis and Properties of Highly Substituted Acenaphthylene Derivatives with Fluorine and Alkoxy Groups Synthesis and Characterization of Twisted Helicenes from 1,2,4- and 1,2,4,5-(o-terphenyl)benzenes"* (2024).
- C.-W. Yeh (葉靜玟), Advisor Prof. T.-F. Chung (鍾采甫), Dept. of Mater. Sci. & Engr., Natl. Yang Ming Chiao Tung Univ., *"Impact of Pre-ageing on the Precipitation Evolution and Mechanical Properties of AA6061 (Al-Mg-Si-Cu) Aluminum Alloys"* (2024).

- F.-Y. Yen (顏范渝), Advisor Prof. S.-Y. Lu (呂世源), Dept. of Chem. Engr., Natl. Tsing Hua Univ., *"Nitrogen-doped Carbon-supported MnFeCoNi Alloy/CrOx Heterostructure as Bifunctional Positive Electrode Catalyst for Rechargeable Zinc-air Batteries"* (2024).
- P.-I Yen (顏姵宜), Advisor Prof. H.-M. Kao (高憲明), Dept. of Chem., Natl. Central Univ., *"Synthesis of Hollow Pt Nanospheres Using Amino Group Functionalized Mesoporous Silica SBA-1 as a Support and Its Use as Catalyst for Hydrogen Generation from Hydrolysis of Ammonia Borane and Sulfonic Acid Functionalized Mesoporous Silica Aupported Ag Nanoparticles as Catalyst for Dye Degradations"* (2024).
- Y.-S. Yen (顏煜昇), Advisor Prof. H.-Y. Hsu (許馨云), Dept. of Appl. Chem., Natl. Yang Ming Chiao Tung Univ., *"Structural Investigation of Acid-mediated Guanosine Monophosphate Self-assembled Hydrogel"* (2024).
- Y.-C. Huang (黃翊宸), Advisor Prof. J.-C. Chen (陳志堅), Dept. of Mater. Sci. & Engr., Natl. Taiwan Univ. of Sci. & Tech., *"Modified Soluble Polybenzimidazole Membranes for Vanadium Redox Flow Batteries"* (2024).
- P.-X. Yu (余芃萱), Advisor Prof. F.-M. Wang (王復民), Grad. Inst. of Appl. Sci. & Tech., Natl. Taiwan Univ. of Sci. & Tech., *"Study the Electrodeposition Effects of Lithium Ions in an Anode-free Lithium-ion Battery and Investigate the Mechanisms for Enhancing Lithium-ion Nucleation"* (2024).
- S.-C. Yu (游善竹), Advisor Prof. T.-E. Lin (林子恩), Inst. of Biomed. Engr., Natl. Yang Ming Chiao Tung Univ., *"MXene-cellulose Composite Materials in Environmentally-friendly Biomedical Sensors"* (2024).
- S.-H. Yu (游士賢), Advisor Prof. H.-H. Chen (陳秀慧), Dept. of Molecular Sci. & Engr. & Inst. of Organic & Polymeric Mater., Natl. Taipei Univ. of Tech., *"Synthesis and Property Study of Novel Photo-induced Liquid Crystalline Materials"* (2024).
- Y.-F. Zeng (曾榆芳), Advisor Prof. W.-F. Liaw (廖文峰), Dept. of Chem., Natl. Tsing Hua Univ., *"Modulation of Surface Property and Electronic Structure of Cu Nanocatalyst by F/Al^{3+} Dopants for CO_2-to-C_2 Electro-Selectivity"* (2024).
- D.-X. Zhang (張迪翔), Advisor Prof. W.-F. Liaw (廖文峰), Dept. of Chem., Natl. Tsing Hua Univ., *"Cation-doped FeCoNi-based Nanoparticles for Electro-selective Oxygen Evolution and Mechanism Investigation in Simulated Alkaline Seawater"* (2024).
- D.-C. Zhou (周鼎智), Advisor Prof. S.-W. Kuo (郭紹偉), Dept. of Mater. & Optoelectron. Engr., Natl. Sun Yat-sen Univ., *"Conducting the Tunable Wet-brush Blending of Phenolic/DDSQ Based Nanocomposite and Diblock Copolymer to Prepare the Mesoporous Materials with Frank-Kasper Phases"* (2024).

NSRRC Activity Report 2024
Editorial Committee


Der-Hsin Wei


Cheng-Maw Cheng

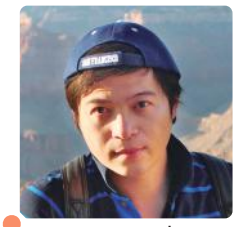
Hao Ming Chen

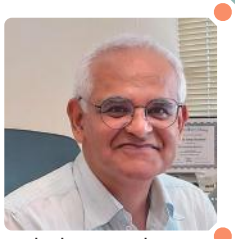
Ashish Atma Chainani


Chi-Liang Chen


Mau-Sen Chiu


Shih-Chun Chung


Chun-Hsiang Huang


Bi-Hsuan Lin


Orion Shih


Chun-Chieh Wang


Yu-Jong Wu

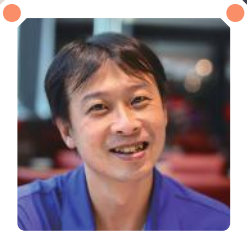
Chin-Kang Yang

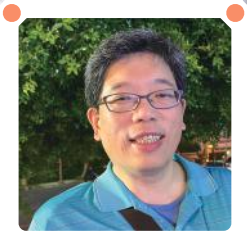
Gung-Chian Yin

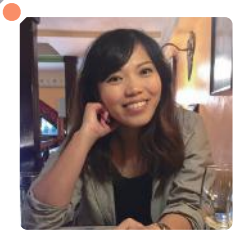
Elsa Shih

Activity Report 2024 ©NSRRC, April 2025

Publisher: National Synchrotron Radiation Research Center

Editorial Committee: Der-Hsin Wei (Editor in Chief), Cheng-Maw Cheng (Deputy Editor in Chief), Hao Ming Chen (2024 UEC Chair), Ashish Atma Chainani, Chi-Liang Chen, Mau-Sen Chiu, Shih-Chun Chung, Chun-Hsiang Huang, Bi-Hsuan Lin, Orion Shih, Chun-Chieh Wang, Yu-Jong Wu, Chin-Kang Yang, Gung-Chian Yin

Executive Editor: Elsa Shih

Our thanks to the authors and all colleagues who contributed to this publication.

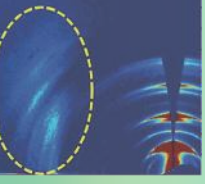

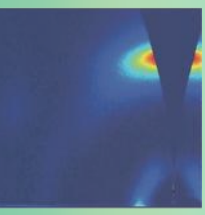

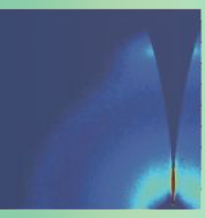

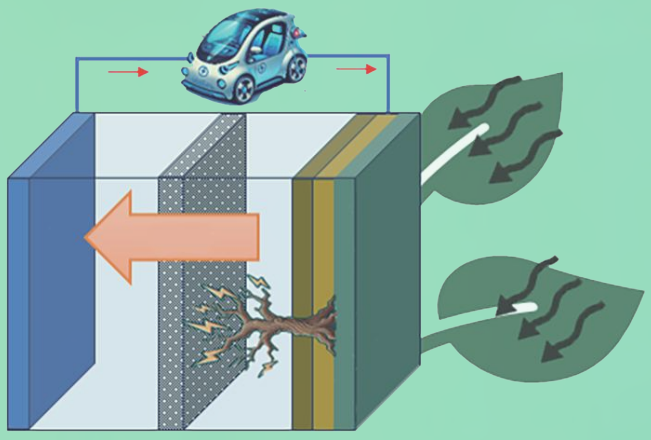

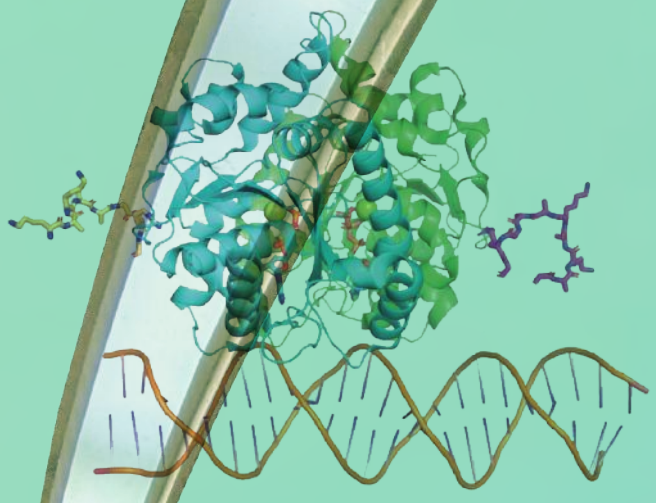

國家同步輻射研究中心
National Synchrotron Radiation Research Center
101 Hsin-Ann Road, Hsinchu Science Park, Hsinchu 300092, Taiwan
Tel: +886-3-578-0281 Fax: +886-3-578-9816 https://www.nsrrc.org.tw